PHY

Volume

Information for Contributors

Manuscripts

Send manuscripts [illegible] Editor, Department of Physics, Univ[illegible] apolis 14, Minnesota.

Each article submitted for publication in general should consist of (a) textual material which is to be set in type, (b) drawings or photographs from which [illegible] or copper halftones will be made, (c) material will consist of an abstract, [illegible] paper, tabular material, [illegible] captions. All of this material must be [illegible], typewritten (except mathematical [illegible]) double-spaced with wide margins, [illegible] instructions to the printer) on a [illegible] paper, preferably letter size. The [illegible], not the carbon, should be submitted.

For general style, [illegible] abbreviations, and form, recent issues of the journal should be consulted.

The prime requisite is that the copy shall be clear to the typesetter, who is neither a physicist nor a mathematician.

Abstracts

An abstract is required with each article. It should be adequate to [illegible] and as a summary. As an index it should give all subjects, major and minor, concerning which new information is presented. As a summary it should give the conclusions of the [illegible] and all numerical results of general importance.

Mathematical Expressions

All but the simplest mathematical expressions should be carefully [illegible] by hand. Be sure to distinguish between capital and small letters. Indicate clearly superiors and subscripts by inverted carets and [illegible] respectively. Avoid complicated superiors and subscripts. Avoid repetition of a complicated expression by representing it by some [illegible] symbol. Identify in the margin Greek [illegible] and unusual symbols. Use fractional exponents instead of root signs. Use the solidus (/) [illegible] wherever its use will save vertical space.

References

References should be [illegible] footnotes, numbered consecutively, [illegible] arranged thus:

[1] A. B. Smith, Phys. [illegible] (1910).

[2] T. Lamb, *Hydrodynamics*, [illegible] University Press, Teddington, England), [illegible] pp. 573, 645.

Tables

All but the simplest tabular material should be organized in tables [illegible] rather than as a part of the running text. Tables may be written on sheets separate from the text with indications in the margin of the text where the table is to be inserted. Each table should have a caption which will make the data in the table intelligible without reference to the text. Avoid complicated column headings; if necessary, use symbols which are explained in the table caption.

Figures

Wherever possible figures should be [illegible] for the width of a column of the *Physical Review* (3 inches). A convenient reduction ratio is [illegible] 2:1 or 3:1. The original drawings or photographs should therefore be in general about 6 inches wide and the lettering and symbols should be large enough on the original that when reduced they shall not be less than about 1/16 in. (2 mm). If the reduction is 3:1, the original lettering should be not less than 1/8 in. high.

The process of making zinc etchings for halftones is a black and white photography. Therefore line drawings must be in [illegible] white paper or tracing cloth. Coordinates are not desirable but if used must be blue [illegible] the coordinate lines which are to show [illegible] inked over.

Photographs should have maximum [illegible] white contrast.

Plan figures to use space efficiently. Avoid wasting space, particularly at the top or [illegible].

Identify on the black or other suitable [illegible] each original drawing or photograph with author's name and the figure number. [illegible] should be numbered consecutively and their approximate position indicated in the margin of the running text. Figure captions should be typed and included with the manuscript (not on [illegible] of the figure).

Avoid round and oval photographs.

Alterations

Take great care that each manuscript is [illegible] graphically accurate. A limited number of alterations in proof are unavoidable, but the cost of making extensive alterations after the article has been set in type will be charged to the author.

Proof and all correspondence concerning [illegible] in the process of publication should be addressed to the Publication Manager, American Institute of Physics, 57 East 55 Street, New York 22, New York.

THE PHYSICAL REVIEW

A journal of experimental and theoretical physics established by E. L. Nichols in 1893

VOLUME 81

Second Series

JANUARY 1–MARCH 15, 1951

Published for the

AMERICAN PHYSICAL SOCIETY

by the

AMERICAN INSTITUTE OF PHYSICS

Incorporated

THE PHYSICAL REVIEW

A journal of experimental and theoretical physics established by E. L. Nichols in 1893

Published by the American Institute of Physics for the

AMERICAN PHYSICAL SOCIETY

Officers

President

I. I. RABI
Columbia University
New York, New York

Vice-President

C. C. LAURITSEN
California Institute of Technology
Pasadena, California

Secretary

K. K. DARROW
Bell Telephone Laboratories
Office:
Columbia University
New York 27, New York

Treasurer

G. B. PEGRAM
Columbia University
New York 27, New York

Local Secretary for the Pacific Coast

J. KAPLAN
University of California at Los Angeles
Los Angeles, California

Managing Editor

E. L. HILL
University of Minnesota
Minneapolis, Minnesota

BOARD OF EDITORS

Editor

E. L. HILL

Assistant Editor

J. W. BUCHTA

Associate Editors

S. A. GOUDSMIT — W. E. LAMB, JR. — HARVEY BROOKS
E. M. PURCELL — R. G. HERB — R. F. CHRISTY
V. F. WEISSKOPF — J. BARDEEN — BRUNO ROSSI

Manuscripts for publication should be submitted to E. L. HILL, University of Minnesota, Minneapolis, Minnesota. The authors' institutions are requested to pay a publication charge of $8 per page which, if honored, entitles them to 100 free reprints. Instructions will be sent with galley proofs.

Proof and all correspondence concerning papers in the process of publication should be addressed to the Publication Manager, American Institute of Physics, 57 East 55 Street, New York 22, New York.

Subscription Price

United States and Canada $25.00
Elsewhere $27.00

Back Numbers [1]

Yearly back number rate when complete year is available:
Prior to 1949: **$20.00**
Thereafter: **$27.00**
Single copies: **$2.00** each, prior to July, 1929;
$1.00 each, July, 1929–December, 1941;
$2.00 each, January, 1942–December, 1946;
$1.00 each, January, 1947–December, 1948;
$1.25 each, thereafter.
General index, 1893–1920: **$4.00.**

Subscriptions, renewals, and orders for back numbers should be addressed to the American Institute of Physics, 57 East 55 Street, New York 22, New York.

Changes of address in the case of members of the American Physical Society should be addressed to the Treasurer; in the case of other subscribers to the American Institute of Physics.

[1] For Series I inquire of Physics Department, Cornell University, Ithaca, New York.

The Physical Review is published semi-monthly at Prince and Lemon Streets, Lancaster, Pennsylvania.

Entered as second-class matter March 6, 1947, at the Post Office at Lancaster, Pennsylvania, under the Act of March 3, 1879.

Acceptance for mailing at special rate of postage provided for in paragraph (d-2), section 34.40, P. L. & R. of 1948, authorized January 27, 1933.

THE
PHYSICAL REVIEW

A journal of experimental and theoretical physics established by E. L. Nichols in 1893

SECOND SERIES, VOL. 81, NO. 1 JANUARY 1, 1951

On the Tritium HFS and the Anomalous Magnetic Moment of the Triton*

EDWARD N. ADAMS, II†‡
Department of Physics, University of Wisconsin, Madison, Wisconsin
(Received August 11, 1950)

The hfs of tritium is studied using the model of A. Bohr according to which the electron centers on the proton at small electron-nuclear separations. The hfs effects due to this recentering of the electron are calculated for three theories of the origin of the triton moment anomaly: the spin-orbital moment theory of Avery and Sachs, the phenomenological interaction moment theory of Blanchard, Avery, and Sachs, and the meson exchange moment theory of Villars. In addition the hfs contributions due to relativistic effects of internal nuclear motion are calculated for deuterium, and the result is used to estimate the uncertainty in the tritium hfs coming from this source. It is found that in each case considered the hfs effects may be classified as either "Bohr effect," proportional to the size of the nucleus, or "orbital effect," proportional to the size of the region of centering of the electron. On each of the three theories the total hfs effect is of the order of magnitude of the present experimental uncertainty in the determination of the hfs. While the effect is large enough so that it could be observed with only a small improvement of the experimental precision, it is about the same for each theory considered and would not, therefore, serve as a possible means of distinguishing among the several theoretical accounts of the triton moment anomaly.

I. INTRODUCTION

ACCORDING to the simplest theory of the H^3 nucleus the triton magnetic moment should be equal to, or slightly less than, one proton moment, whereas the experimental value of μ_T is greater than μ_P by about $0.2\mu_0$, μ_0 being the nuclear magneton $e\hbar/2Mc$. A detailed consideration of the matter[1] has shown that one cannot account for the observed triton moment as simply the sum of spin and orbital moments of individual nucleons unless one abandons the assumption that the triton ground state is the predominantly S-state expected on the usual theories of nuclear forces. A number of suggestions have been made as to the source of the excess triton moment, each requiring special assumptions about the nature of the triton ground state and/or the nature of nuclear forces. Consequently, an experiment which can serve as a test of these theories of the triton moment is of some interest in the study of nuclear forces. That the precision determination of the tritium hfs is such an experiment was suggested by a recent theoretical study[2] of the deuterium hfs.

The observed value[3] of the deuterium hfs is somewhat larger than the value calculated for a point deuteron having the observed deuteron moment.[4] A. Bohr has shown[2] that a discrepancy of this sort arises because the hfs contribution of the neutron spin is reduced when the electron is within the nucleus. An essential part of Bohr's demonstration was the assumption that at small electron-nuclear separations the electron wave function centers on the proton position rather than the deuteron center of mass. This recentering leads in addition to a reduction of the proton orbital hfs.[5,6] A detailed calculation shows[5] that the sum of these two theoretical corrections to the hfs is in good agreement with the value of the observed discrepancy for deuterium, so that it is probable that Bohr's assumption is basically correct.

A similar recentering of the electron wave function must occur for tritium, so that some such discrepancy[6a] might be expected for the tritium hfs. In the following, estimates of this discrepancy, which is due to both the Bohr effect and the orbital effect, will be made on the basis of each of several theories of the triton moment.

* Work supported partly by the AEC and partly by the Wisconsin Alumni Research Foundation.
† AEC Predoctoral Fellow.
‡ Now at Institute for Nuclear Studies, University of Chicago.
[1] R. Avery and R. G. Sachs, Phys. Rev. **74**, 1320 (1948).
[2] A. Bohr, Phys. Rev. **73**, 1109 (1948).
[3] J. E. Nafe and E. B. Nelson, Phys. Rev. **73**, 718 (1948).
[4] Bloch, Levinthal, and Packard, Phys. Rev. **72**, 1125 (1947).
[5] F. Low, Phys. Rev. **77**, 361 (1950).
[6] E. N. Adams II, Phys. Rev. **77**, 755 (1950).
[6a] The hfs discrepancy is defined as the amount by which the hfs differs from that calculated for a point nucleus which has the observed nuclear moment.

These theories will be referred to as: A. Spin and orbital moment (SOM) theory. B. Phenomenological interaction moment (PIM) theory. C. Meson exchange moment (MEM) theory.

Previous estimates[1,7] of the Bohr effect for the tritium hfs have indicated that it is much smaller than that for the deuterium hfs, and is of the order, in fact of the present experimental uncertainty in the determination of the hfs. It was found in the present work that the *total* hfs effect probably exceeds the present experimental uncertainty in only one of the cases considered. While a moderate improvement of the experimental precision would permit this one case, which occurs on the PIM theory, to be definitely distinguished from the others, it appears that because of theoretical uncertainties no further distinctions would be possible.

The hfs effects considered here are so small that it was thought necessary to examine the role of relativistic contributions to the nuclear moment in the hfs of the centered electron. Since the relativistic contributions to the deuteron moment have been discussed previously,[8,9] it was simpler to study the effects in question for the deuterium hfs rather than for the tritium hfs. However, on the basis of the deuterium results one can easily estimate how much the relativistic effects contribute to the uncertainty in the interpretation of the tritium hfs effects. The uncertainty from this source is found to be unimportant.

II. THE ELECTRON WAVE FUNCTION AND THE MAGNETIC FIELD DUE TO THE ELECTRON

Of the theories of the triton moment which are to be considered here, no one of them is complete in the sense that it is a part of a more comprehensive theory which has been shown to give a satisfactory account of the triton binding energy and of the known properties of the deuteron. For this reason it did not appear to be feasible to make such a detailed treatment of the triton wave function as would be required in order to carry through a second-order perturbation method analogous to that used by Low[6] for the calculation of the deuterium hfs effects. Instead, the hfs was computed in first order only, on Bohr's original assumption that for large electron-nuclear separations the electron wave function is the *ls* Coulomb function centered on the nuclear center of mass, while for electron-nuclear separations smaller than a critical length D, it is the same *ls* function centered on the proton. As a means of improving the quantitative validity of the results obtained in Bohr's approximation, the value of D was taken as a free parameter which was then fixed by the requirement that the method used here gave the same value for the deuterium hfs effect as is given by Low's more accurate method.

For the present purpose it is convenient to regard the hfs as due to the interaction of the nucleus with the electromagnetic field arising from the electron current. The value of the vector potential at a point $\mathbf{r}$ in the nucleus is, then:

$$\mathbf{A}(\mathbf{r})=-e\langle\boldsymbol{\alpha}_e/|\mathbf{r}-\mathbf{r}_e|\rangle, \tag{1}$$

in which the angular brackets denote the electronic expectation value.

In evaluating Eq. (1) it is sufficiently accurate to use the well known approximation in which the electron large function is replaced by the nonrelativistic *ls* Coulomb function. The *ls* function must be modified so that it centers on the proton for distances smaller than D. Using such a wave function and making use of the relations $r\ll a$, $r\ll D$, $D\ll a$, one finds for $\mathbf{A}(\mathbf{r})$:

$$\begin{aligned}
&\mathbf{A}=\mathbf{A}_1+\mathbf{A}_2+\mathbf{A}_3\\
&\mathbf{A}_1(\mathbf{r})=-(8\pi/3)\mu_B\psi_{(0)}^2[\boldsymbol{\sigma}_e\times\mathbf{r}/2](1-2D/a)\\
&\mathbf{A}_2(\mathbf{r})=-(8\pi/3)\mu_B\psi_{(0)}^2[\boldsymbol{\sigma}_e\times(\mathbf{r}-\mathbf{r}_\pi)/2](2D/a)\\
&\mathbf{A}_3(\mathbf{r})=-(8\pi/3)\mu_B\psi_{(0)}^2[-(3|\mathbf{r}-\mathbf{r}_\pi|/2a)\boldsymbol{\sigma}_e\\
&\qquad\qquad\times(\mathbf{r}-\mathbf{r}_\pi)/2],
\end{aligned} \tag{2}$$

in which $\psi_{(0)}$ denotes the value at the origin of the nonrelativistic *ls* Coulomb function, $\boldsymbol{\sigma}_e$ is twice the expectation value of the electron spin angular momentum, a is the Bohr radius, and the label π is used to denote the proton coordinate. All vectors are measured from the center of mass. The magnetic field derived from the potential $\mathbf{A}(\mathbf{r})$ can be written as the sum of three terms:

$$\begin{aligned}
&\mathbf{H}_1(\mathbf{r})=-(8\pi/3)\mu_B\psi_{(0)}^2\boldsymbol{\sigma}_e\\
&\mathbf{H}_2(\mathbf{r})=-(8\pi/3)\mu_B\psi_{(0)}^2(-2|\mathbf{r}-\mathbf{r}_\pi|/a)\boldsymbol{\sigma}_e\\
&\mathbf{H}_3(\mathbf{r})=-(8\pi/3)\mu_B\psi_{(0)}^2\\
&\qquad\times\left[\frac{|\mathbf{r}-\mathbf{r}_\pi|}{4a}\left\{\frac{3(\boldsymbol{\sigma}_e\cdot[\mathbf{r}-\mathbf{r}_\pi])(\mathbf{r}-\mathbf{r}_\pi)}{|\mathbf{r}-\mathbf{r}_\pi|^2}-\boldsymbol{\sigma}_e\right\}\right].
\end{aligned} \tag{3}$$

The notation is *not* intended to imply that $\mathbf{H}_1=\mathrm{curl}\mathbf{A}_1$.

The interaction of the nucleus with the field provides for the atom an additional energy $E(\mathbf{A})$ given by:

$$\begin{aligned}
E(\mathbf{A})=&-\mu_P\langle\boldsymbol{\sigma}_\pi\cdot\mathbf{H}(\mathbf{r}_\pi)\rangle\\
&-\mu_N\sum_\nu\langle\boldsymbol{\sigma}_\nu\cdot\mathbf{H}(\mathbf{r}_\nu)\rangle-\frac{1}{c}\left\langle\int d^3\mathbf{r}(\mathbf{A}\cdot\mathbf{S})\right\rangle,
\end{aligned} \tag{4}$$

in which the sum of ν is a sum over neutrons, $\mathbf{S}(\mathbf{r})$ is a nuclear operator the expectation value of which gives the density of the nuclear electric current, and the angular brackets denote the nuclear expectation value. The hfs energy is the difference between the values of $E(\mathbf{A})$ for the $F=I+\frac{1}{2}$ and $F=I-\frac{1}{2}$ states of the atom. It is well known that the difference is proportional to the value of $E(\mathbf{A})$ for the $F=I+\frac{1}{2}$ state, so this value of $E(\mathbf{A})$, which is denoted as U, will be referred to as the hfs energy.

[7] E. Fermi and E. Teller, conference at Pocono Manor (1948).
[8] R. G. Sachs, Phys. Rev. **72**, 91 (1947).
[9] G. Breit and I. Bloch, Phys. Rev. **72**, 135 (1947).

III. THE MAGNETIC STRUCTURE EFFECTS ON THE HFS

The terms in Eq. (4) which involve $\mathbf{H}_1$ give the neutron and proton spin hfs as calculated for a point nucleus, while the terms in $\mathbf{H}_2$, $\mathbf{H}_3$ give the corrections to the spin hfs for the finite space extension of the nucleus and for the recentering of the electron wave function. The proton spin hfs is "normal," i.e., the same as it would be for a point nucleus, as is evidenced by the vanishing of $\mathbf{H}_2(\mathbf{r})$ and $\mathbf{H}_3(\mathbf{r})$ at the proton. The neutron hfs is changed by an amount:

$$\delta U_N = -(8\pi/3)\mu_B\mu_N\psi_{(0)}^2\sum_\tau\left\langle(2r_{\pi\tau}/a)(\boldsymbol{\sigma}_e\cdot\boldsymbol{\sigma}_\tau)\right.$$

$$\left.-(r_{\pi\tau}/4a)\left\{\frac{3(\boldsymbol{\sigma}_e\cdot\mathbf{r}_{\pi\tau})(\boldsymbol{\sigma}_\tau\cdot\mathbf{r}_{\pi\tau})}{r_{\pi\tau}^2}-(\boldsymbol{\sigma}_e\cdot\boldsymbol{\sigma}_\tau)\right\}\right\rangle. \quad (5)$$

The hfs effect given by Eq. (5) is the Bohr effect. Since the first term is by far the larger, the Bohr effect is just a reduction of the neutron hfs by the relative amount $2\bar{r}_{\pi\tau}/a$.

The proton orbital hfs can be obtained from the third term on the right-hand side of Eq. (4) by inserting for the current density operator $\mathbf{S}(\mathbf{r})=(e/M)\delta(\mathbf{r}-\mathbf{r}_\tau)\mathbf{p}_\tau$. Then

$$U_{\mathrm{ORB}}=-\frac{1}{c}\left\langle\int d^3\mathbf{r}[\mathbf{A}(\mathbf{r})\cdot\mathbf{S}(\mathbf{r})]\right\rangle$$

$$=\left(\frac{8\pi}{3}\right)\mu_B\mu_0\psi_{(0)}^2\langle(\boldsymbol{\sigma}_e\cdot\mathbf{L}_\tau)\rangle(1-2D/a). \quad (6)$$

The orbital hfs comes entirely from $\mathbf{A}_1$, since $\mathbf{A}_2$ and $\mathbf{A}_3$ vanish at the proton. Except for the factor $(1-2D/a)$, Eq. (6) gives the normal hfs contribution of the orbital moment; from the occurrence of that factor one sees that the orbital hfs is reduced by the relative amount $2D/a$. Such a reduction, which results from the vanishing of the contribution to the orbital hfs from the entire region of centering, is to be expected on semiclassical considerations.[5,6]

It will be seen that there are, in addition, magnetic structure effects on the hfs contributions of exchange moments and of the interaction moments which arise as a consequence of the velocity dependence of the nuclear interactions; these effects may be analogous to either the Bohr effect or the orbital effect. A "Bohr effect" (effect proportional to $\bar{r}_{\pi\tau}/a$) in such a case is just caused by a weakening of the interaction between the electron and the current distribution when the electron is within the distribution. An "orbital effect" (effect proportional to D/a) results if the magnetic moment is not a translational invariant, since, in effect, the recentered electron interacts with the moment of the currents about the proton rather than the moment about the center of mass.

IV. EFFECTS ON THE HFS CONTRIBUTION OF THE TRITON MOMENT ANOMALY

Fermi-Teller Effect

Before discussing the hfs effects which are peculiar to the individual theories a discussion will be given of the Bohr effect for the triton ^2S state, since it must be taken into account in computing the total hfs effect in each of the three cases. The effect is not entirely analogous to the Bohr effect on the deuterium hfs. The ^2S state of the triton is predominantly a space symmetric ^2S_s state in which the neutron spins are paired, and for this state there is no neutron spin hfs and no Bohr effect on the hfs. However, it was pointed out by Fermi and Teller[7] that because of the spin dependence of nuclear forces the ^2S_s state has admixed into it a small amount of ^2S_a state, antisymmetric in the neutron space coordinates, in which the neutron spins are parallel. They showed that this admixture of states has the property that the proton spin is partially aligned with the spin of whichever neutron is closer to it. Although the neutron spins still contribute almost nothing to the total magnetic moment, there is within the nucleus an average neutron spin distribution which is parallel to the proton spin at short distances from the proton and antiparallel to the proton spin at larger distances. The electron penetrates the outer part of the spin distribution more often than it does the inner part, so there is a slight net contribution to the hfs from the inner part. Because the neutron moment is negative, the result is a decrease of the tritium hfs.

On any of the theories to be considered here the ^2S_a admixture must be taken to be very small. It was considered adequate for the present purpose to assume simply that $|^2S_a|^2\sim 0.01|^2S_s|^2$. On this basis the Fermi-Teller effect was estimated to be:

$$\frac{\delta_{F-T}U}{U}=-\frac{4}{3}|^2S_a\,{}^2S_s|\frac{|\mu_N|}{\mu_T}$$

$$\times\left(\frac{2\bar{r}_{\pi\tau}}{a}\right)\sim -0.08|^2S|^2(2\bar{r}_{\pi\tau}/a). \quad (7)$$

SOM Theory

In order to account for the observed value of the triton moment as simply the sum of spin and orbital moments of individual nucleons (SOM theory) it is necessary to abandon the assumption that the triton ground state is a predominantly S state. Assuming the triton ground state to be an arbitrary admixture of all possible states of $I=\frac{1}{2}$ and even parity, Sachs[10] and Avery and Sachs[1] have investigated the possibility of fitting the observed triton moment on a SOM theory. They found that an additional condition which is imposed on the triton wave function by the observed value of the He^3 moment is extremely restrictive, so

[10] R. G. Sachs, Phys. Rev. 73, 312 (1947).

that there is no possibility of satisfying it except with a wave function which has a P state admixture of from 40 to 100 percent, the remainder of the wave function being ^2S state. According to present ideas it seems unlikely that this is a good description of the triton wave function; however, in order to find out what the hfs effect would be on a SOM theory, the hfs was calculated using the triton wave function which Avery and Sachs found to offer the best prospect of accounting for the observed moments. It was somewhat surprising to find that despite the large P state admixture the orbital moment is very small; the triton moment is increased for the P state admixture chiefly because the neutron spins are no longer paired.

The total hfs effect is given by:

$$(\delta U/U)=-(\mu_0/9\mu_T)[2|^2P|^2-|^4P|^2](2D/a) -0.08|^2S|^2(2\bar{r}_{pp}/a)-(|\mu_N|/9\mu_T) \times[4|^2P|^2+8\sqrt{2}|^2P^4P|-10|^4P|^2](2\bar{r}_{pp}/a). \quad (8)$$

The size of the effect varies *inversely* as the amount of P state admixture; for the two extreme cases it was found to be:

40 percent P state ($|^2P|^2\approx 0.18$; $|^4P|^2=0.20$) (8a)

$$(\delta U/U)\sim -0.11(2\bar{r}_{pp}/a)-0.006(2D/a);$$

100 percent P state ($|^2P|^2\approx 0.38$; $|^4P|^2\approx 0.61$) (8b)

$$(\delta U/U)\sim -0.06(2\bar{r}_{pp}/a)-0.002(2D/a).$$

PIM Theory

The triton wave function which is required by the SOM theory is quite different from that found by a study of the triton binding energy. In order to account for the triton binding energy using current phenomenological two-body interactions the triton wave function should be taken to be a ^2S function with a few percent of ^4D admixture.[11] If the ^4D admixture is taken to be about four percent, such a wave function also gives agreement[1] with the sum of the observed values of the H^3 and He^3 moments, although not, of course, with the values of the H^3 and He^3 moments individually. The agreement can be understood if it is assumed that both nuclei have, in addition to the nucleon spin and orbital moments, other moments which arise as a consequence of the nucleon-nucleon interaction, the "interaction moments" of the two nuclei being of equal magnitude and opposite sign.

It can be shown that interaction moments of this sort are to be expected, even on a phenomenological theory of nuclear forces, when the nucleon-nucleon interaction involves either explicit velocity dependence[12] (direct $L-S$ coupling) or implicit velocity dependence[13] (space exchange). The existence of an interaction moment is inferred as follows: in the presence of an externally arising electromagnetic field the nuclear Hamiltonian is modified by replacing $\mathbf{p}_j\rightarrow\mathbf{p}_j-(e_j/c)\mathbf{A}(\mathbf{r}_j)$ wherever the nucleon momentum $\mathbf{p}_j$ occurs in the Hamiltonian; interactions involving space exchange are included in the scheme by expressing the exchange operator as a power series in the nucleon momenta. As a consequence of this replacement the Hamiltonian includes terms in which the vector potential of the external field occurs together with the nuclear interaction. Such terms represent a magnetic energy depending directly on the nucleon-nucleon interaction, and a nucleus for which this energy does not vanish has a non-zero interaction moment.

For the case of pure space exchange Sachs[13] has derived an explicit expression for the exchange current which gives rise to the interaction moment. His expression may be rewritten in terms of an operator $\mathbf{S}_X(\mathbf{r})$, which is defined so that its nuclear expectation value gives the exchange current density at an arbitrary point $\mathbf{r}$.

$$\mathbf{S}_X(\mathbf{r})=(ie/\hbar)\sum_\tau \mathbf{r}_{\tau\tau}\left\{\int_0^1 d\alpha\delta(\mathbf{r}-\mathbf{r}_\tau-\alpha\mathbf{r}_{\tau\tau})\right\}J_{\tau\tau}P_{\tau\tau}^X, \quad (9)$$

in which $J_{\tau\tau}$ describes the spin and space dependence of the neutron-proton interaction. From Eq. (9) the energy of interaction between the exchange currents and the external field may readily be obtained.

In the case of the explicitly velocity dependent interactions the magnetic energy terms may take a variety of forms, according to the precise manner in which the interactions depend on the nucleon momenta. Only two interactions will be considered here, *viz.*, the interactions (5) and (6) of Blanchard, Avery, and Sachs, which were found to lead to suitable interaction moments for H^3 and He^3. Interaction (6) differs from interaction (5) only by a space exchange operator; however, the magnetic energy terms in the two cases differ somewhat more, being given, for our purpose, by:

$$E^{(5)}=(e/\hbar c)\sum_\tau J_{\tau\tau}{}^{(5)}(\boldsymbol{\sigma}_{\tau\tau}\times\mathbf{r}_{\tau\tau}\cdot\mathbf{A}_\tau), \quad (10a)$$

$$E^{(6)}=(e/2\hbar c)\sum_\tau J_{\tau\tau}{}^{(6)}(\boldsymbol{\sigma}_{\tau\tau}\times\mathbf{r}_{\tau\tau}\cdot\mathbf{A}_{\tau\tau}). \quad (10b)$$

The exchange moment which arises from the currents Eq. (9) has been found[14] to contribute only about $0.016\mu_0$ to the triton moment. Thus if the H^3 moment anomaly of $0.2\mu_0$ is to be accounted for on a PIM theory, it must be assumed that the neutron-proton interaction includes an interaction of either type (5) or type (6) and that this interaction has a strength adequate to provide the required interaction moment. (Although a linear combination of interactions (5) and (6) would do just as well for this purpose, only the two pure cases need be considered in computing the hfs effect.)

The hfs contribution of the exchange currents Eq. (9) may be obtained directly from Eq. (4) using the vector potential Eq. (2). The appearance of the δ-function in

[11] H. Feshbach and W. Rarita, Phys. Rev. **75**, 1384 (1949); R. E. Clapp, Phys. Rev. **76**, 873 (1949).
[12] Blanchard, Avery, and Sachs, Phys. Rev. **78**, 292 (1950).
[13] R. G. Sachs, Phys. Rev. **74**, 433 (1948); **76**, 1605 (1949).
[14] R. Avery and E. N. Adams II, Phys. Rev. **75**, 1106 (1949).

the operator $\mathbf{S}_X(\mathbf{r})$ has the result that the exchange current vanishes except on straight line filaments connecting the neutrons to the proton, the current having the direction $\mathbf{r}-\mathbf{r}_\tau$ at points on the filament. Since $\mathbf{A}_2(\mathbf{r})$ and $\mathbf{A}_3(\mathbf{r})$ are perpendicular to $\mathbf{r}-\mathbf{r}_\tau$ at all points, it is clear that the scalar products $\mathbf{A}_2\cdot\mathbf{S}_X$ and $\mathbf{A}_3\cdot\mathbf{S}_X$ vanish, and the entire hfs comes from the term in $\mathbf{A}_1\cdot\mathbf{S}_X$. It follows that the hfs contribution of the exchange moment is reduced by the factor $(1-2D/a)$, which is characteristic of the orbital effect. The hfs contribution of the interaction moment arising from interaction (5) also shows an "orbital effect," as can be seen by using the vector potential Eq. (2) in Eq. (10a) and noting that $\mathbf{A}_2(\mathbf{r})$ and $\mathbf{A}_3(\mathbf{r})$ vanish for $\mathbf{r}=\mathbf{r}_\tau$. In the case of interaction (6), however, all three terms in the vector potential make a nonvanishing contribution to the hfs and it is found that for this interaction moment the hfs effect is a "Bohr effect." From Eq. (10b) it is clear that the "Bohr effect" is in this case proportional to r_0/a rather than $\hbar_{\tau\tau}/a$, r_0 being the range of the interaction $J_{\tau\tau}$[6].

Choosing the interaction moment as $0.25\mu_0$, as is required to fit the triton moment for the case of four percent ^4D state, and taking into account the F-T effect, and the Bohr effect and orbital effect caused by the ^4D state admixture, one finds for the hfs effect: (a) assuming interactions (5) (velocity dependence without space exchange)

$$\frac{\delta U}{U}=-0.27\frac{\mu_0}{\mu_T}\left(\frac{2D}{a}\right)-\frac{2}{3}\frac{|\mu_N|}{\mu_T}|{}^4D|^2\left(\frac{2\hbar_{\tau\tau}}{a}\right)$$
$$-\frac{1}{3}\frac{\mu_0}{\mu_T}|{}^4D|^2\left(\frac{2D}{a}\right)-0.08|{}^2S|^2\left(\frac{2\hbar_{\tau\tau}}{a}\right)$$
$$\sim-0.1(2\hbar_{\tau\tau}/a)-0.09(2D/a), \quad (11a)$$

(b) assuming interaction (6) (velocity dependence with space exchange)

$$\frac{\delta U}{U}=-0.25\frac{\mu_0}{\mu_T}\left(\frac{3r_0}{2a}\right)-0.016\frac{\mu_0}{\mu_T}\left(\frac{2D}{a}\right)$$
$$-\frac{2}{3}\frac{|\mu_N|}{\mu_T}|{}^4D|^2(2\hbar_{\tau\tau}/a)-\frac{1}{3}\frac{\mu_0}{\mu_T}|{}^4D|^2(2D/a)$$
$$-0.08|{}^2S|^2(2\hbar_{\tau\tau}/a). \quad (11b)$$

If a mixture of the two interactions is considered, the hfs effect is just the weighted mean.

MEM Theory

If nuclear forces result from the exchange of charged mesons between nuclear particles, then there must exist exchange currents in the nucleus, and these exchange currents can make a nonvanishing contribution to the nuclear magnetic moment. Villars[15] and Thellung and Villars[16] have investigated such exchange moments in special cases and have found that the pseudoscalar theory appears likely to lead to an exchange moment of the right sign and size to account for the triton moment anomaly. Using the pseudoscalar theory Villars[15] found a MEM operator which is equivalent to the operator:

$$\mathbf{M}_X=\mathbf{M}_{X1}+\mathbf{M}_{X2}$$
$$\mathbf{M}_{X1}=-(ie/\hbar c)(f_K)^2$$
$$\times\sum_\tau\frac{1}{\kappa}\left\{\mathbf{r}_{\tau\tau}\frac{(\boldsymbol{\sigma}_\tau\times\boldsymbol{\sigma}_\tau\cdot\mathbf{r}_{\tau\tau})}{r_{\tau\tau}^2}\left(1+\frac{1}{\kappa r_{\tau\tau}}\right)\right.$$
$$\left.-(\boldsymbol{\sigma}_\tau\times\boldsymbol{\sigma}_\tau)\right\}e^{-\kappa r_{\tau\tau}}P_{\tau\tau}{}^\sigma P_{\tau\tau}{}^\tau$$
$$M_{X2}=(ie/\hbar c)\sum_\tau[\mathbf{r}_\tau\times\mathbf{r}_\tau]U_{\tau\tau}P_{\tau\tau}{}^\sigma P_{\tau\tau}{}^\tau, \quad (12)$$

in which $U_{\tau\tau}$ is the (improper) neutron-proton static interaction of the pseudoscalar theory.

The explicit expression for the current operator which gives rise to the magnetic moment Eq. (12) was used in Eq. (4) together with the vector potential Eq. (2) in order to compute the contribution of the exchange moment to the tritium hfs. It was found that the contribution of the moment $\mathbf{M}_{X1}$ shows a "Bohr effect," while that of $\mathbf{M}_{X2}$ shows an "orbital effect."

For the numerical evaluation of the total hfs effect on the MEM theory the triton wave function was again taken to be 96 percent ^2S state, four percent ^4D state. The moment $\mathbf{M}_{X2}$ vanishes for the triton ^2S state, but it does make a contribution through $S-D$ interference, since $U_{\tau\tau}$ includes a tensor interaction. Because the ^4D state amplitude is small, however, $\mathbf{M}_{X2}$ is much smaller than $\mathbf{M}_{X1}$, which does not vanish in the ^2S state. For the magnitude of $\mathbf{M}_{X2}$ the estimate $0.016\mu_0$ was used.[14] The magnitude of $\mathbf{M}_{X1}$ was then taken to be $0.25\mu_0$ as required for the theory to give the observed triton moment. Equation (12) shows that the exchange currents extend only a distance r_0 from the proton, r_0 being the range of the nuclear interaction. Accordingly, the estimate $\hbar_{\tau\tau}\sim r_0$ was used in evaluating the "Bohr effect" for $\mathbf{M}_{X1}$. The total hfs effect, including the F-T effect, and the ^4D state effects, was found to be:

$$\frac{\delta U}{U}=-0.25\frac{\mu_0}{\mu_T}\left(\frac{3}{2}\frac{r_0}{a}\right)-0.016\frac{\mu_0}{\mu_T}\left(\frac{2D}{a}\right)$$
$$-\frac{2}{3}\frac{|\mu_N|}{\mu_T}|{}^4D|^2\left(\frac{2\hbar_{\tau\tau}}{a}\right)-\frac{1}{3}\frac{\mu_0}{\mu_T}|{}^4D|^2\left(\frac{2D}{a}\right)$$
$$-0.08|{}^2S|^2\left(\frac{2\hbar_{\tau\tau}}{a}\right)\sim-0.06\left(\frac{2r_0}{a}\right)$$
$$-0.01\left(\frac{2D}{a}\right)-0.1\left(\frac{2\hbar_{\tau\tau}}{a}\right). \quad (13)$$

[15] F. Villars, Helv. Phys. Acta **20**, 476 (1946).

[16] A. Thellung and F. Villars, Phys. Rev. **73**, 924 (1948).

V. THE HFS EFFECT FOR THE RELATIVISTIC CORRECTION TO THE NUCLEAR MOMENT

In order to give an accurate theoretical interpretation of a nuclear magnetic moment one must take account of certain relativistic corrections to the moment which are a result of the rapid motion of the nucleon under nuclear forces. Even for the deuteron the relativistic correction is of the order of one percent of the total deuteron moment, and it is just because the sign of the relativistic correction is unknown that the amount of ^3D state admixture in the deuteron ground state cannot be fixed from the observed value of the deuteron moment. The hfs contribution of the relativistic correction is of the order of 10^3 times the present experimental uncertainty in the hfs, so it can be seen that if the experimental precision were much improved, it would be necessary to consider the effect which the electron recentering has on the hfs contribution of the relativistic correction. For this reason the hfs contribution of the relativistic correction was considered in some detail.

Because the relativistic corrections have already been discussed extensively for the deuteron, it was simpler to do the detailed calculations for deuterium. The nuclear Hamiltonian which was used is that given by Breit[17] for a neutron-proton interaction which transforms like a scalar. In order to include hfs effects of order $(v/c)^2$ in the nucleon the well-known expression[18] for the magnetic interaction of two Dirac particles was used to obtain the proton Dirac moment hfs and a corresponding approximation[19] to obtain the Pauli moment hfs of the neutron and proton. The method of handling the nuclear wave function was the same as that of Breit and Bloch.[9] The procedure was to calculate the contributions to the hfs which are of order $(v/c)^2$ in the nucleons and to compare these with the relativistic correction to the magnetic moment of the deuteron, which is given by:[20]

$$\Delta_R\mu_D=-\mu_N\langle\sigma_z T/6Mc^2\rangle-(\mu_P-\mu_0)\langle\sigma_z T/6MC^2\rangle$$
$$-\mu_0\left\langle\sigma_z\frac{[2E_D-T]}{2Mc^2}\right\rangle-\mu_0\left\langle\sigma_z\frac{r_{nn}}{12MC^2}\frac{\partial V_{nn}}{\partial r_{nn}}\right\rangle, \quad (14)$$

in which T is the internal kinetic energy of the deuteron, V_{nn} is the (central) neutron-proton interaction potential, E_D is the energy of the deuteron ground state, and the angular bracket denotes expectation value in the deuteron ground state.

The following effects were found to result from the recentering of the electron:

(a) The hfs contribution of the relativistic correction to the neutron Pauli moment (first term on the right-hand side of Eq. (14) shows a somewhat complicated "Bohr effect."

(b) The hfs contributions of the corrections given by the second and third terms of Eq. (14) are normal, i.e., unaffected by the recentering.

(c) The hfs contributions of the fourth term of Eq. (14) shows an "orbital effect."

In the hfs calculation there arise certain divergent integrals which contribute an uncertainty in the hfs of the relative order $\alpha^2(m/M)\ln(b/a)$ in which b is the "proton radius." These integrals have been discussed in the case of the H^1 hfs[21] and are thought to be small. In any case they should be about the same for H^1, H^2, and H^3, since most of the contribution to such integrals is from distances much smaller than the region of centering. It may be expected, therefore, that in the observed H^1-H^3 hfs ratio these effects just cancel, so they do not need to be considered in estimating the uncertainty in the tritium hfs due to the relativistic correction.

On the basis of the deuterium hfs calculation it is possible to estimate the size of the tritium hfs effect. For this purpose the triton wave function may be taken to be simply a ^2S state. The bulk of the hfs comes from the proton spin moment, so all of the relativistic correction contributes normally to the hfs with the exception of the part corresponding to the fourth term in the deuteron moment correction Eq. (14). This correction to the deuteron moment resembles the Thomas correction to the hydrogen fine structure; it may be thought of as resulting from a precession of the proton spin due to the acceleration of the proton by the nuclear forces. From this point of view the orbital effect for its hfs contribution results because there is no acceleration of the proton relative to the recentered electron.

By the virial theorem the correction in question may be written:

$$-\mu_0\left\langle\sigma_z\frac{r_{nn}}{12MC^2}\frac{\partial V_{nn}}{\partial r_{nn}}\right\rangle=-\mu_0\left\langle\sigma_z\frac{T}{6MC^2}\right\rangle \quad (15)$$
$$=-\mu_0\left\langle\sigma_z\frac{T_z}{3MC^2}\right\rangle.$$

The hfs effect can now be estimated for tritium by assuming Eq. (15) to give the corresponding correction to the triton moment. Before making a numerical estimate, however, it should be noted that if a vector, instead of a scalar potential had been assumed then: (a) the correction given in Eq. (15) would have been of the opposite sign, and (b) there would be an additional correction to the magnetic moment arising from the second-order correction to the Hamiltonian,[9] and the hfs contribution of this correction would also show an

[17] G. Breit, Phys. Rev. **51**, 248 (1937).
[18] G. Breit, Phys. Rev. **34**, 553 (1929).
[19] See the magnetic interaction used by J. Schwinger, Phys. Rev. **78**, 135 (1950).
[20] The correction given by Eq. (14) agrees with that given by Sachs (reference 8) rather than that given by Breit and Bloch (reference 9). Professor Breit has been kind enough to check this part of the calculations and has informed us that Eq. (14) is correct.
[21] Breit and Meyerott, Phys. Rev. **72**, 1023 (1947); Breit, Brown, and Arfken, Phys. Rev. **76**, 1299 (1949).

"orbital effect." Taking into account this last source of uncertainty and using $(T_\pi/Mc^2)\sim 0.01$ it was estimated that the uncertainty in the hfs contribution due to the relativistic correction is of the order of:

$$(\delta_R U/U)=\pm 0.01(\mu_0/\mu_T)(2D/a). \quad (16)$$

VI. RESULTS AND CONCLUSIONS

In order to obtain numerical values of the tritium hfs effects one requires values of r_0, $\bar{r}_{\pi\pi}$ and $(D/\bar{r}_{\pi\pi})$. For the purpose of illustrating the relative magnitudes of the effects expected in the various cases it is sufficient to use the estimates $r_0\sim 1\times 10^{-13}$ cm, $\bar{r}_{\pi\pi}\sim 2\times 10^{-13}$ cm, $(D/\bar{r}_{\pi\pi})\sim 2.5$. This last estimate was obtained from Low's detailed deuterium calculations[5] on the following basis. According to a semiclassical interpretation, the recentering of the electron wave function occurs in that region of space for which the ratio of electron velocity to proton velocity exceeds a certain critical value. This critical ratio, which should be the same for deuterium and tritium, is proportional to $(\bar{r}_{\pi\pi}/D)$. The numerical value of the ratio was determined by requiring that the orbital effect on the deuterium hfs as given by Eq. (6) agree with Low's value. The calculation[22] led to a value $(D/\bar{r}_{\pi\pi})\sim 2.5\pm 1$.

The hfs discrepancy δU is defined as the amount by which the observed tritium hfs differs from that calculated for a point triton having the observed triton moment. With presently attained experimental precision there is no statistically meaningful discrepancy, the data giving:[23,24]

$$(\delta U/U)\approx -[0.06\pm 0.25](2\bar{r}_{\pi\pi}/a). \quad (17)$$

The uncertainty given in Eq. (17) is the sum of the quoted experimental uncertainties in the measurement of the hfs and in the direct measurement of the magnetic moment. In Table I the experimental discrepancy is compared with the discrepancy predicted on each of the theories of the triton moment which were discussed in Sec. IV.

The amount by which the theoretical values in Table I are uncertain is large. The greatest uncertainty comes from the crudeness of the electron wave function which was used to obtain the magnetic field at the nucleus.

TABLE I. The hfs discrepancy $(\delta U/U)$ in units of $(2\bar{r}_{\pi\pi}/a)$.

Observed	-0.06 ± 0.25
SOM: 40 percent P state	-0.1
100 percent P state	-0.06
PIM: velocity dependence—nonexchange	-0.3
exchange	-0.1
MEM	-0.1
Relativistic correction	± 0.01

The other chief source of uncertainty is that, since the radial dependences of the several triton states are unknown, $\bar{r}_{\pi\pi}$ cannot be calculated for each case separately. Other sources of uncertainty seem likely to be relatively unimportant. It has already been seen that the relativistic effects of internal nuclear motion are not large enough to spoil the interpretation of the hfs effects. Effects due to the possible spatial extension of the proton moment, which have been discussed by Bohr and Low for the case of the deuterium hfs, can be ignored in interpreting the tritium hfs, since such effects should be the same for H^1 and H^3 and would not, therefore, affect the tritium-hydrogen hfs ratio. Finally, the hfs uncertainties depending on the cutoff of the Coulomb field at the "proton radius" should be unimportant as was asserted in Sec. V.

Within the present experimental uncertainties the predicted hfs effect is consistent with experiment no matter which theory of the triton moment is considered. In order to observe effects of the size predicted it would be necessary to increase the experimental precision by at least a factor of 2 but preferably by a factor of 4 or 5. Unfortunately, the hfs effect is not theory sensitive, and the size of the effect on any one theory can be calculated only very approximately. Only in the case of the PIM theory (velocity dependence without space exchange) is the effect sufficiently different to be distinctive. While an increase of experimental precision might permit a test of the suitability of that particular theory, it is quite possible that the evidence would remain ambiguous because of the permissability, mentioned in Sec. IV, of a mixture of the two kinds of PIM theory. It is necessary to conclude therefore, that the tritium hfs is likely to furnish only meager information about the magnetic structure of the triton, since it is improbable that the information which could be obtained from the hfs would afford any insight into the process which leads to the existence of the triton magnetic moment anomaly.

The writer would like to acknowledge his indebtedness to Professor R. G. Sachs for numerous helpful suggestions and criticisms and to Dr. Francis Low for communicating and discussing his results before publication.

[22] As a check the Bohr effect for the deuterium ^3S state was recomputed taking into account the fact that there is a small, but non-zero, probability for the occurrence of $r_{\pi\pi}>D$. The value for the Bohr effect found by this calculation differs from that given in Eq. (6) by about 15 percent, the correction depending sensitively on the value of D. The value of the correction agrees with that of a similar correction given by Low if $(D/\bar{r}_{\pi\pi})\sim 2$, in agreement with the value found from the orbital effect.

[23] E. B. Nelson and J. E. Nafe, Phys. Rev. 75, 1194 (1949).

[24] Bloch, Graves, Packard, and Spence, Phys. Rev. 71, 551 (1947).

New Neutron-Deficient Radioactive Isotopes of the Light Rare-Earth Region*†

BETSY JONES STOVER
Radiation Laboratory and Department of Chemistry, University of California, Berkeley, California
(Received August 18, 1950)

In the light rare-earth region, seven new neutron-deficient radioactive isotopes have been produced by proton bombardment in the 184-in. cyclotron and the linear accelerator; their radiations have been studied by absorption curve and magnetic counter methods. The new isotopes and their half-lives are La^{134}, 6.5±0.25 min; Ce^{133}, 6.30±0.1 hr; Ce^{134}, 72.0±0.5 hr; Pr^{133}, 120±5 min; Pr^{139}, 4.50±0.2 hr; Nd^{138}, 22±2 min; Nd^{139}, 5.50±0.2 hr. Additional data have been obtained for the isotopes, Ce^{135} and Ce^{137}.

I. INTRODUCTION

A MAJOR part of the previous work of synthesis and characterization of neutron-deficient radioactive isotopes in the rare earth region has been done in this laboratory using the 19-Mev deuterons and the 38-Mev helium ions of the 60-in. cyclotron. Thus the conversion of the 184-in. cyclotron to protons and the availability of the proton linear accelerator for bombardment work offer the possibility of producing new activities by (p,xn) reactions. With the two accelerators approximate maximum proton energies of from 10 to 80 Mev were used to obtain different mixtures of reaction products.

End-on type Geiger-Müller counters were used throughout. The radiations were characterized by absorption curve and magnetic counter data. The results are summarized in Tables I and II.

II. LANTHANUM AND CERIUM ISOTOPES

Lanthanum oxide prepared by Dr. F. H. Spedding served as target material. Spectrographic analysis revealed no other rare earths within the limits of detection, i.e., less than 0.1 percent.

The bombarded material was dissolved in nitric acid and cerous carrier and barium hold-back carrier were added. The material was then subjected to fluoride hydroxide cycles. This consists in precipitating the fluoride from warm nitric acid solution, dissolving the fluoride with 8*N* nitric acid saturated with boric acid, precipitating the hydroxide with ammonium hydroxide, dissolving in nitric acid, and repeating to obtain sufficient purity. The chemistry is specific for rare earths and yttrium.

TABLE I. New isotopes.

Isotope	Radiations	Half-life	Energies in Mev: Particles	Energies in Mev: γ-rays	Produced by
$_{57}La^{134}$	β^+, K	6.5±0.25 min	2.7	no γ	Ce^{134} decay
$_{58}Ce^{133}$	β^+, K, γ	6.30±0.1 hr	1.3	1.8	La(p,7n)
$_{58}Ce^{134}$	K	72.0±0.5 hr		no γ	La(p,5n)
$_{59}Pr^{133}$	ϵ^-, β^+, K, γ	120±5 min	0.24(ϵ^-), 1.4(β^+)	0.16, 1.3	Ce(p,3n)
$_{59}Pr^{139}$	β^+, K, γ	4.50±0.2 hr	1.0	1.0	Ce(p,2n)
$_{60}Nd^{138}$	β^+, K	22±2 min	2.4		Pr(p,4n)
$_{60}Nd^{139}$	ϵ^-, β^+, K, γ	5.50±0.2 hr	0.28(ϵ^-), 3.1(β^+)	1.1	Pr(p,3n)

To the purified lanthanum and cerium in nitric acid cooled to 0°C were added first potassium bromate to oxidize the cerium and then iodic acid to precipitate ceric iodate. The coprecipitation of lanthanum is less than two percent by spectrographic analysis, and two reprecipitations of the ceric iodate were sufficient to remove those lanthanum activities which did not grow in rapidly.

Separation of the lanthanum daughter activities was affected by precipitation of the fluoride from the ceric solution. Additional purification was obtained by methods similar to the above.

Proton energies of 50, 60, 70, and 80 Mev were used in the lanthanum (La^{139}, 99.911 percent abundance) bombardments. The 36-hr Ce^{137} observed by Chubbuck[1] was produced in all bombardments, as was Ce^{135}, of estimated 16-hr half-life,[1] which has been shown to be a positron emitter and the parent of the 19.5-hr La^{135}. A 72-hr activity appeared at 60 Mev and in larger amounts at 70 and 80 Mev. At 70 and 80 Mev a 6.3-hr activity was formed. The 72-hr and 6.3-hr periods have been assigned to Ce^{134} and Ce^{133}, respectively.

Ce^{137}

Since this isotope was formed in all lanthanum bombardments, and since its conversion electron is of comparatively high abundance, it was necessary to verify Chubbuck's measurements. The only discrepancy was in the energy of the electron. Magnetic counter measurements and beryllium absorption data both give 0.24 Mev. Decay of the electron through about eight half-lives showed it to be the correct one. A re-examination of Chubbuck's data revealed similar results with an interpretive error on his part.

Ce^{135}

This isotope had been identified as a positron emitter and shown to be the parent of the 19.5-hr La^{135}. A half-life estimate of 16 hr was made by considering the

TABLE II. Revised values.

$_{58}Ce^{135}$	22 hr	0.80 β^+ 0.24 ϵ^-	La(p,5n) La(p,3n)

* This research was done under the auspices of the AEC.
† Portion of dissertation submitted in partial fulfillment of the requirements for the Ph.D. degree at the University of California.

[1] J. B. Chubbuck and I. Perlman, Phys. Rev. 74, 982 (1948).

areas under the curves from positron sweeps on the magnetic counter. An unusually large cross section for formation of Ce^{137} was offered as explanation for the fact that no 16-hr period could be resolved from decay curves of Ce^{135} and Ce^{137}. However, a more satisfactory explanation is the very low β^+/electron-capture branching ratio for Ce^{135} and the fact that the growth of La^{135} gives an apparent slope of about 36 hr for Ce^{135}.

The cerium fraction from a lanthanum plus 50-Mev proton bombardment, which contained only Ce^{135} and Ce^{137}, was analyzed on the magnetic counter and found to have a 0.81-Mev ($H\rho$=4060 gauss-cm) positron which decayed with a 22-hr half-life.

A beryllium absorption gave a range of 300 mg Be/cm² by Feather analysis for the Ce^{135} positron, and 60 mg/cm²=0.24 Mev for the Ce^{137} conversion electron. Since an unambiguous resolution of decay curves could not be made, no quantitative analysis of Ce^{135} radiations can be offered except that the positron branching is less than one percent.

Lanthanum fractions showed only the 19.5-hr La^{135} and the very long La^{137} which confirms the mass assignment.

Ce^{134} and La^{134}

In all bombardments with protons of 60- to 80-Mev energy, a 72.0-hr cerium activity remained after the other cerium activities had decayed out and their daughter activities had decayed or had been removed by chemical means. Chemical separation of the lanthanum daughter gave a 6.5-min activity.

The La^{133} (4 hr) and La^{135} (19.5 hr) mass assignments have been confirmed mass spectrographically.[2] Since La^{134} is an odd-odd type nucleus, and since La^{136} has a half-life of 10 min,[2] a value of approximately 5 min was anticipated for La^{134}. This evidence plus the approximate threshold energy of 60 Mev for the 72.0-hr cerium constitute the basis for the mass assignment of this pair of isotopes.

A beryllium absorption of Ce^{134} and La^{134} in equilibrium revealed a particle of range 1340 mg Be/cm² =2.7 Mev. The magnetic counter proved it to be a positron of maximum energy 2.7 Mev; an end point of $1.06 \cdot 10^4$ gauss-cm, and positron decay through ten half-lives gave a 72.0-hr half-life. Analysis of the electromagnetic radiation by lead absorption gave only K x-rays and annihilation radiation. The absorption curve data gave the following ratios for the radiations of the two isotopes in equilibrium:

2.7 Mev β^+: K x-rays: 0.5 Mev γ = 0.44 : 1.56 : 0.44.

The L x-rays being of only a few kilovolts energy escape detection by these methods, which constitutes a major error in the radiation analysis.

That the La^{134} daughter emitted the positrons was verified by following the decay of a separated La^{134} sample on the magnetic counter. This was also shown by beryllium absorption (Fig. 1) which was done on the chemically separated daughter. Since the necessarily quick chemistry did not remove all the parent, the beryllium absorption was repeated on the sample as soon as the 6.5-min activity decayed out, and a point-by-point resolution of the absorption curve was made. This method was found to give reproducible results in obtaining absorption data for short-lived activities.

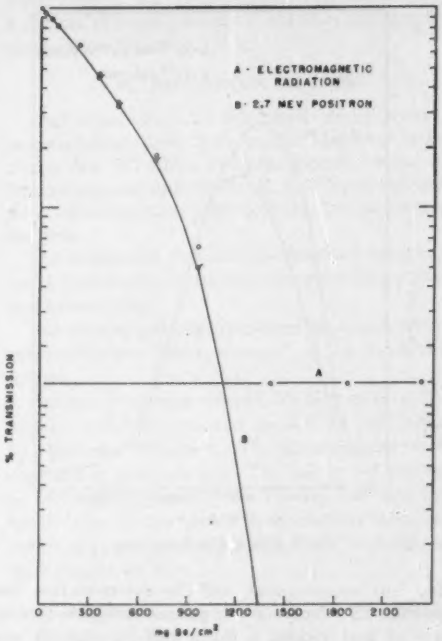

FIG. 1. La^{134} 2.7 Mev positron.

The assumption that, since La^{134} is a positron-emitter, it emits all the positrons, and hence the 0.5-Mev gamma-rays, coupled with the absorption data, allows the following ratios for the La^{134} radiations to be calculated:

2.7 Mev β^+: K x-rays: 0.5 Mev γ = 0.4 : 0.6 : 0.4.

From the above data it can be postulated that the 72.0-hr Ce^{134} decays entirely by orbital electron capture, and that the 6.5-min La^{134} decays 44 percent by positron-emission and 56 percent by electron capture. There are no conversion electrons, and the only gamma is the annihilation radiation.

Ce^{133}

In the bombardments with 70- and 80-Mev protons a cerium activity of shorter half-life which emitted a hard gamma was formed. Since Ce^{134}, Ce^{135}, and Ce^{137} have no gamma-radiation of energy greater than 0.8

[2] Naumann, Reynolds, and Perlman, Phys. Rev. 77, 398 (1950).

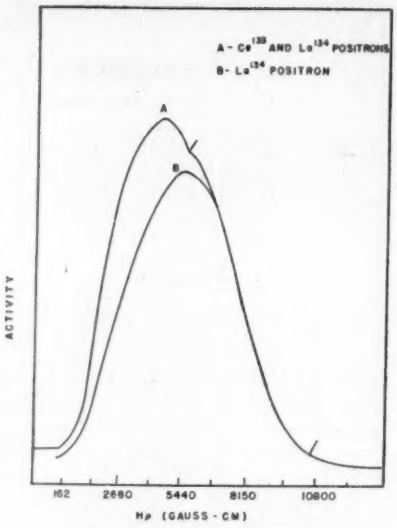

FIG. 2. Ce^{133} and La^{134} positrons.

Mev, an unambiguous half-life determination was possible. The decay of the gamma-radiation through 20 g of lead yielded a 6.3-hr half-life through nine half-lives with a 36-hr tail from the 0.75-Mev gamma of Ce^{137}.

The mass number of the 6.3-hr cerium activity was determined by separating its lanthanum daughter. The 4.0-hr La^{133}, which has been run on the mass spectrograph, was shown to grow in only during the decay of the 6.3-hr activity which must then be Ce^{133}. The approximate threshold of 70 Mev for its formation is also compatible with this assignment.

A satisfactory analysis of the relative abundances of Ce^{133} radiations was not obtained, since the data are complicated by the presence of four cerium activities and the growth of their four daughter activities.

The decay of positrons on the magnetic counter had two components, the 72.0-hr Ce^{134} and an approximately 6-hr one. The positron spectrum indicated two particles as shown in Fig. 2, where curve A was obtained when both activities were present and curve B is the distribution of the 72.0-hr component only. The estimated end point of the 6.3-hr positron is $H\rho = 5680$ gauss-cm $= 1.3$ Mev. The energy was confirmed by beryllium absorption which showed a particle of range 600 mg $Be/cm^2 = 1.3$ Mev in addition to the La^{134} positron and the Ce^{137} 0.24-Mev electron. The data also indicate a conversion electron of about the same energy as the Ce^{137} electron, but this was not unambiguously demonstrated.

The above mentioned hard gamma had a half-thickness in lead of 15 g/cm^2 which corresponds to 1.8 Mev.

Thus the 6.30-hr Ce^{133} decays by orbital electron capture and positron-emission and emits gamma-rays of 1.8-Mev energy.

III. PRAESEODYMIUM ISOTOPES

Cerium metal of 10-mil thickness prepared by Dr. F. H. Spedding was found to be the most satisfactory target material for the study of light praeseodymium isotopes. Traces of calcium and iron were the only impurities detected by spectrographic analysis. An air-tight wrapping of aluminum foil minimized oxidation so that the reaction $O^{18}(p, n)F^{18}$ was not detectable, as it was with the oxide.

The bombarded metal was dissolved in dilute hydrochloric acid, lanthanum carrier for the praeseodymium was added, and then the hydroxides were precipitated with ammonium hydroxide. After dissolving these with concentrated nitric acid and adding potassium bromate, the bulk of the cerium was precipitated as ceric iodate. The lanthanum carrier was then subjected to fluoride hydroxide cycles, and the final step of purification consisted of adding inactive cerium and precipitating to remove the remaining traces of active cerium.

The cerium bombardments were made on the linear accelerator using 10-, 20-, and 32-Mev protons for (p,n), $(p,2n)$, and $(p,3n)$ reactions. Even though cerium has an even atomic number, its isotopic abundances are suitable. The relative abundances are Ce^{142}, 11.07; Ce^{140}, 88.48; Ce^{138}, 0.250; Ce^{136}, 0.193. The contributions of the last two are negligible, and (p,n) on Ce^{142} gives the well-known[3] 19.5-hr Pr^{142}, $(p,2n)$ gives stable Pr^{141}. Thus the reactions of the abundant Ce^{140} can be used to study the neutron deficient praeseodymiums.

At 10 Mev the 19.5-hr Pr^{142} and a 3.5-min period were observed. The 3.5-min half-life has previously been reported[4] for Pr^{140}. At 20 Mev a 4.50-hr, the 19.5-hr, and the 3.5-min activities were formed. A 120-min half-life was seen at 32 Mev only. The 4.50-hr and the 120-min activities have been assigned to Pr^{139} and Pr^{138}, respectively.

Pr^{140}

Pool and Quill[4] reported a 3.5-min positron-emitter from the reaction $Pr^{141}(n,2n)Pr^{140}$. Since a short Pr^{139} was suspected from the decay of Nd^{139}, it was necessary to verify this value. Cerium plus 10-Mev protons gave a 3.5-min half-life through many half-lives as did cerium plus 20-Mev protons.

Pr^{139}

The 4.50-hr praeseodymium activity was formed in bombardments of 20- and 32-Mev protons on cerium but did not appear at 10 Mev. It was thus assigned to Pr^{139} as the product of a $(p,2n)$ reaction on Ce^{140}.

Confirmation of the mass assignment was made by

[3] DeWire, Pool, and Kurbatov, Phys. Rev. **61**, 564 (1942).
[4] M. L. Pool and L. L. Quill, Phys. Rev. **53**, 437 (1938).

showing it to be the parent of the 140-day Ce^{139}. The proton beam of the linear accelerator is much too small to produce sufficient 4.50-hr activity to determine the growth curve of a 140-day activity. A solution containing mainly the 4.50-hr Pr^{139} and a very small amount of the 19.5-hr Pr^{142}, was purified and then allowed to decay for approximately 20 hr. A cerium fraction was then precipitated in which the only cerium activity appearing was Ce^{139}, which must necessarily have grown in from the 4.50-hr activity.

A beryllium absorption showed one particle of range 400 mg Be/cm² which corresponds to 1.0 Mev. The Feather range was found to be the same. This was verified by a magnetic counter sweep which gave a positron of maximum energy 1.0 Mev = 4750 gauss-cm.

In addition to the expected K x-rays and annihilation radiation, a 1.0-Mev gamma-ray appeared in the lead absorption.

From absorption data, the relative abundances of these radiations are as follows: 1.0-Mev β^+:K x-rays: 0.5-Mev γ:1.0-Mev γ = 0.06:1:0.06:0.04. Since no conversion electrons were observed, it can be assumed that each quantum of K x-radiation represents one disintegration by orbital electron capture. And from the above data it can be postulated that Pr^{139} decays mainly by orbital electron capture with approximately six percent positron branching.

Pr^{138}

In the bombardments with 32-Mev protons a 120-min praeseodymium activity appeared in higher yield than the 4.50-hr Pr^{139}. On the basis of the approximate threshold of 30 Mev, it was allocated to Pr^{138} as the product of a $(p,3n)$ reaction on Ce^{140}.

Decay through 16 g of lead of the abundant hard gamma-ray allowed the 120-min activity to be observed through six half-lives before the amount of Pr^{139} 1.0-Mev gamma became significant.

This isotope emits both a positron and a conversion electron as shown by beryllium absorption, and the magnetic counter. The range of the positron is 625 mg Be/cm², which was verified by Feather analysis, and the visual end point of the magnetic counter sweep is 6140 gauss-cm, both of which correspond to a maximum energy of 1.4 Mev. The values 50 mg Be/cm² and 1740 gauss-cm show the energy of the conversion electron to be 0.22 Mev.

Gamma-rays of half-thicknesses 0.275, 4.5, and 12.0 g Pb/cm², corresponding to 0.16, 0.5, and 1.3 Mev, and K x-radiation appeared in the lead absorption. From absorption data the relative abundances of the radiations are as follows: 0.22-Mev ϵ^-:1.4-Mev β^+: K x-rays:0.5-Mev γ:1.3-Mev γ = 0.04:0.14:1:0.22:0.36:0.75.

If it is assumed that four percent of the K x-radiation arises from the process of conversion, an approximate branching ratio of positron-emission to electron capture of 0.13:1 is obtained for the decay of Pr^{138}. The high abundance of the 0.5-Mev gamma-radiation indicates a gamma of approximately 0.5 Mev in addition to the annihilation radiation.

IV. NEODYMIUM ISOTOPES

The target material for these experiments was praeseodymium oxide from Johnson Matthey Company, sample No. 547 which had been further purified on an ion exchange column by Mr. R. C. Lilly of this laboratory. No impurities were detected by spectrographic analysis.

The bombarded material was dissolved in nitric acid and a pure rare-earth fraction was obtained by fluoride hydroxide cycles.

The neodymium activities were separated from the praeseodymium target material of an ion-exchange column.

Protons of energies 40 and 50 Mev gave a 22-min activity, a 5.50-hr one, and the 3.3-day Nd^{140} reported by Hicks and Wilkinson.[5] The 145-min Nd^{141} was[5] not observed at these energies. The 5.50-hr Nd was shown to be the grandparent of the 140-day Ce^{139} and thus is Nd^{139}. The 22-min period is tentatively assigned to Nd^{138}, since its yield relative to Nd^{139} is greater at 50 Mev than at 40 Mev.

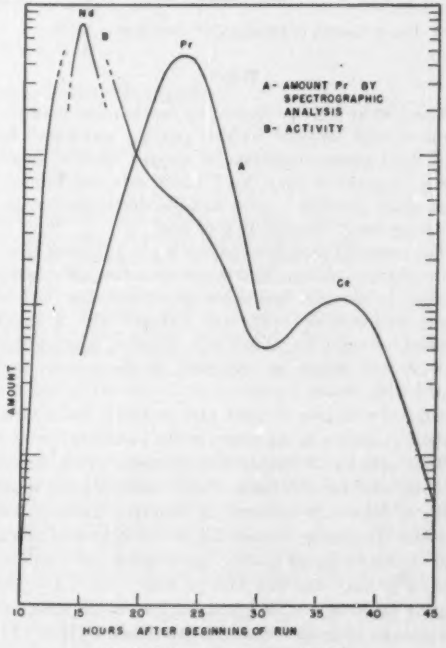

FIG 3. Column separation of Nd^{138}.

[5] H. G. Hicks and G. Wilkinson, Phys. Rev. 75, 1687 (1949).

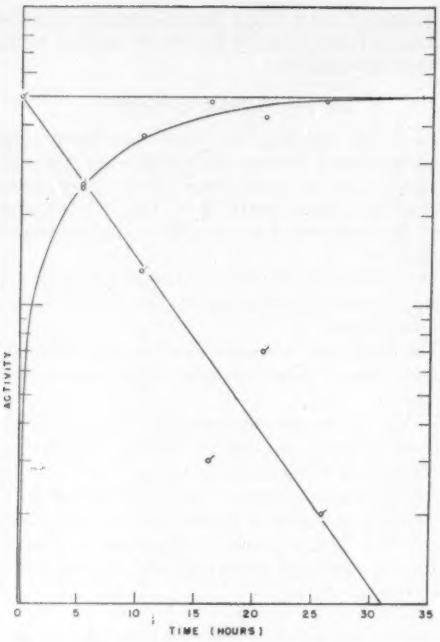

FIG. 4. Growth of 140-day Ce^{139} from 5.50-hr Nd^{139}.

Nd^{139}

The 5.50-hr activity formed by bombarding praseodymium with 40- and 50-Mev protons was found to emit hard gamma-radiation of greater relative abundance than the 3.3-day Nd^{140} which was also formed. This made possible a good half-life determination by following decay through 16 g of lead.

The chemical identification was made by means of an ion exchange column. The target material, after being purified by fluoride hydroxide cycles and dissolved in dilute hydrochloric acid, was warmed with a small amount of resin for about five minutes, after which time it was placed on the resin in the column and eluted with citrate.

Since the elution of light rare earths is quite slow, a short column was necessary in the identification of a 5.50-hr activity. A length of 4 cm and a cross section of 0.317 cm^2 for the resin, which was the ammonium form of Dowex-50 spheres, an aromatic hydrocarbon polymer containing nuclear sulfonic acid groups as the only active exchange groups,[6] gave satisfactory separation. The flow rate was 0.06 ml min^{-1} cm^{-2}, and the eluting agent was 0.5M citric acid to which sufficient ammonium hydroxide was added to obtain a pH of 3.15.

[6] W. C. Bauman and J. Eichhorn, J. Am. Chem. Soc. **69**, 2830 (1947).

The elution curve is shown in Fig. 3. Curve A shows the position of the target material and was determined by spectrographic analysis. Curve B represents the elution of the activity. It is not an accurate representation of the shape of the curve, since it was not corrected for decay. However, it is an accurate representation of the position of the peak, since decay of samples taken at the peak and on both sides of it when extrapolated to an arbitrary time showed a constant ratio of 5.50-hr activity to 3.3-day Nd^{140}. This proves that the 5.50-hr activity is neodymium.

The broad shoulder of curve B under curve A is in part the 4.50-hr Pr^{139} daughter, but the elution time is too long relative to the time for growth and decay to detect any distinct separation with the similarity of half-lives. After many hours the 140-day Ce^{139} granddaughter appeared.

The mass number was confirmed by separating Ce^{139} from an approximately equilibrium mixture of Nd^{139} and Pr^{139}. The 140-day Ce^{139} was found to grow in with a 5.50-hr half-life (Fig. 4).

In the analysis of the Nd^{139} radiations an uncertainty was introduced by the presence of a small but unknown amount of Pr^{139} daughter. In short bombardments a (p,p) reaction to give the 3.5-min Pr^{140} was detected at 50 Mev but not at 40 Mev. From this it was assumed that the amount of (p,pn) reaction to give Pr^{139} was

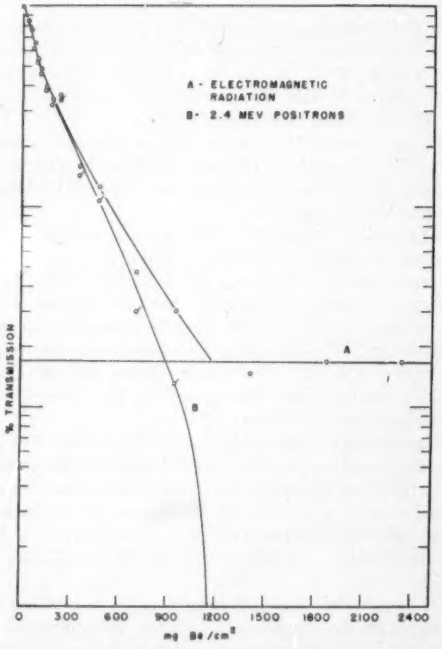

FIG. 5. Be absorption of 22-min Nd^{128}.

negligible at 40 Mev. The absorption data were obtained as soon after bombardment as possible when a minimum of Pr^{139} was present.

Beryllium absorption showed two particles of ranges 70 and 1560 mg Be/cm² corresponding to 0.28 and 3.1 Mev, respectively. These were shown to be a conversion electron and a positron on the magnetic counter, and the energies were verified, for the conversion electron, $H\rho = 2010$ gauss-cm $= 0.28$ Mev, and for the positron, $H\rho = 1.19 \cdot 10^4 = 3.1$ Mev. The sweeps were taken a number of hours after bombardment and the curious shape of curve B results from the 1.0-Mev Pr^{139} positron which had grown in, the presence of which in no way affects the determination of the Nd^{139} positron end point.

In addition to the K x-rays and the annihilation radiation, a gamma-ray of half-thickness 12.5 g Pb/cm² = 1.3 Mev was detected by lead absorption.

The relative abundances of these radiations, subject to the uncertainty introduced by daughter growth, are as follows: 0.28-Mev e^-: 3.1-Mev β^+: K x-rays: 0.5-Mev γ: 1.3-Mev $\gamma = 0.03 : 0.11 : 1 : 0.11 : 0.10$.

From these ratios it can be postulated that Ne^{139} decays mainly by electron capture, and, assuming that each K x-ray quantum represents one disintegration by electron capture, the positron branching is approximately 10 percent.

Nd^{128}

A 22-min activity was formed in the bombardments of praseodymium with 40- and 50-Mev protons, and appeared in greater yield relative to Nd^{139} at 50 Mev. It was shown to be a rare earth by fluoride hydroxide cycles, and, since Nd^{139}, Pr^{139}, and Pr^{138} have been identified, the 22-min activity is tentatively assigned to Nd^{138}.

A beryllium absorption was taken of the 22-min activity, and, after it was gone, the absorption was repeated on the Nd^{139}. A point-by-point resolution shows a particle of approximate range 1160 mg Be/cm² corresponding to a maximum energy of 2.4 Mev (Fig. 5). It undoubtedly is a positron, and the shape of the curve indicates that there may also be a conversion electron.

I wish to thank Dr. B. B. Cunningham under whose direction the work was done, Mr. J. T. Vale and the crew of the 184-in. cyclotron, Mr. R. D. Watt and the crew of the linear accelerator, Mr. J. Conway and Mr. M. Moore of the spectrographic laboratory, and Dr. LeRoy Eyring who participated in the study of Nd^{139}.

PHYSICAL REVIEW VOLUME 81, NUMBER 1 JANUARY 1, 1951

Energy Degeneration of Cosmic-Ray Primaries*

F. J. MILFORD† AND L. L. FOLDY
Case Institute of Technology, Cleveland, Ohio

(Received August 16, 1950)

Under the assumptions that a meson-producing collision between two nucleons with relativistic energies is completely inelastic and that the collision cross-section is independent of energy, one can calculate the energy degeneration of the primary cosmic rays (assumed to be nucleons) and the energy spectrum of high energy nucleons as a function of depth in the atmosphere for any primary spectrum. While this model is highly restricted, it is of considerable interest for comparison with experimental results, since it leads to the maximum possible rate of energy degeneration for nucleons. Binding of nucleons into nuclei is neglected (except for the "packing effect" on the mean-free-path for collision) and the results are further limited to energies greater than 1 Bev where energy loss due to ionization is negligible and the velocity of the nucleons may be taken to be the velocity of light. Analytic solutions are obtained for the energy spectrum at any depth for monoenergetic and power-law primary spectra. The effect of the geomagnetic cut-off on a primary power-law spectrum is also investigated.

I. INTRODUCTION

RECENT cosmic-ray investigations,[1] particularly those at high altitudes, have accumulated a body of experimental evidence favoring a coherent interpretation of cosmic-ray phenomena in terms of the identification of the majority of cosmic-ray primaries as *nucleons* (either free (protons) or bound in nuclei[2]) and for meson-producing collisions (or, more generally, nuclear interactions) as the principal agency for their rapid absorption in the atmosphere. The variety of

* Part of the work herein contained formed a portion of a thesis submitted by one of the authors (F.J.M.) in partial fulfillment of the requirements for the degree of Bachelor of Science in Physics. A preliminary report on this work was made at the semi-centennial meeting of the American Physical Society, Cambridge, Massachusetts, June 16–18, 1949.

† Present address: Department of Physics, Massachusetts Institute of Technology, Cambridge, Massachusetts.

[1] See, for example, W. Heisenberg, Ed., *Cosmic Radiation* (Dover Publications, 1946); B. Rossi, Rev. Mod. Phys. **20**, 537 (1948); Proceedings of the Symposium on Cosmic Rays at the California Institute of Technology, June 21–25, 1948, Rev. Mod. Phys. **21** (1949).

[2] Freier, Lofgren, Ney, Oppenheimer, Bradt, and Peters, Phys. Rev. **74**, 213 (1948); Freier, Lofgren, Ney, and Oppenheimer, Phys. Rev. **74**, 1818 (1948); H. L. Bradt and B. Peters, Phys. Rev. **74**, 1828 (1948).

cosmic-ray phenomena at lower altitudes are then to be interpreted as arising from the numerous progeny through several generations of the primary particles. If this picture is correct, it is of interest to investigate the energy degeneration of these primaries as they pass through the atmosphere and the consequent variation of the energy spectrum of high energy nucleons with atmospheric depth. A detailed theoretical discussion of this process is made difficult by the lack of any thoroughly satisfactory theory of meson production in collisions of high energy nucleons.[3] Experimental observations bearing on this problem, because of difficulties and ambiguities in the interpretation of the experimental results, have not yet yielded a very clear or coherent picture of the meson production process, itself, at high energies. There appears, however, to be general agreement that the primary cosmic-ray particles, as a result of meson-producing collisions, are approximately exponentially absorbed in the atmosphere[4] with an absorption mean-free-path of the order of 120 g/cm², and that mesons are produced multiply[5] in such collisions with a multiplicity which probably increases with energy.

In view of the lack of more detailed information, it might be considered premature to attempt a theoretical investigation of the proposed problem at the present time; on the other hand, an investigation of this problem, even on the basis of a highly oversimplified model of the meson production process, may have considerable value as a basis on which to analyze forthcoming experimental results. In the spirit of this latter view we have investigated theoretically the energy degeneration process on the simplest model of meson-producing collisions consistent with the experimental evidence presented above. In particular, this model may have considerable value from the point of view of an interpretion of the experimental results, since it represents an extreme limiting case in which the energy degeneration process occurs at the maximum possible rate.

The features of this model are:

(1) The cross section for a meson-producing collision between two nucleons is assumed to be independent of energy from 1 Bev to the highest energies encountered in the cosmic rays.

(2) The collision of two high energy nucleons resulting in meson production is assumed to be a completely inelastic collision in which all of the available energy in the frame in which the total momentum of the two nucleons is zero goes into the production of mesons.

The first of these assumptions is probably not unreasonable and perhaps quite close to the truth. The second is dictated more by tractability of the theory than by physical arguments. The principal objection which may be raised to it is that the theoretical results, especially at ultra-relativistic energies, may depend critically upon it. As will be seen in the next section, there is a considerable difference between a totally inelastic collision and one which is say 99 percent inelastic. In defense of the second assumption, the only evidence presently available is very indirect. The application of this assumption by Wouthuysen[6] to the study of the production of cosmic-ray stars by the primary cosmic radiation at high altitudes (95,000 feet) has made possible the explanation of the experimental curve of number of stars of given prong number *versus* prong number up to prong numbers of the order of 10. Evidence of this character is, of course, far from conclusive.

The convenience of the second assumption lies in the fact that the energy of the two nucleons after a collision (in the laboratory frame) is uniquely determined by the primary energy, independently of any further details of the process, and the two nucleons emerge from the collision with equal energies. This is not true for partially inelastic collisions, since the energy distribution between the residual nucleons then depends on the angle of emergence of the nucleons from the collision relative to their initial direction in the reference frame in which the total momentum is zero.

In the present work we shall be concerned only with nucleons of relativistic energies (specifically, kinetic energies greater than 1 Bev) for which the assumptions above might be expected to have some validity and for which there is in addition further simplification of the theory. When a nucleon of such kinetic energy (whether free or bound in a primary nucleus) strikes a nucleus, it is reasonable to assume that the binding forces in both the incident and target nuclei play no part in the collision and that the collisions may be considered to take place between effectively free nucleons. Hence, all effects of binding of nucleons into nuclei will be neglected.[7]

[3] Reference should be made, however, to the following work: Lewis, Oppenheimer, and Wouthuysen, Phys. Rev. **73**, 127 (1948); Hamilton, Heitler, and Peng, Phys. Rev. **64**, 78 (1943); Heitler and Peng, Proc. Ir. Ac. **49**, 101 (1944); W. Heitler and P. Walsh, Rev. Mod. Phys. **17**, 252 (1945); L. Janossy, **64**, 345 (1943); R. P. Feynman and H. A. Bethe, Phys. Rev. **70**, 786 (1946); see also, G. Wataghin, Phys. Rev. **70**, 787 (1946); **74**, 975 (1948); **75**, 693 (1949).

[4] See for example, B. Rossi, Rev. Mod. Phys. **20**, 537 (1948).

[5] See reference 1. There is still considerable controversy as to whether the meson production is truly multiple or "plural." For a discussion of the latter interpretation see the papers of Heitler and his co-workers under reference 3 as well as L. Jánossy, *Cosmic Rays* (Oxford University Press, 1948) and references contained therein. Criticisms of the theoretical foundations of the work of Hamilton, Heitler, and Peng (reference 3) are presented in H. A. Bethe, Phys. Rev. **70**, 785 (1946). Recent photographic evidence favoring truly multiple production (with co-existent plural production) is presented in Kaplon, Peters, and Bradt, Phys. Rev. **76**, 1735 (1949). The model of the meson production process employed in this paper assumes the existence of true multiple production of mesons in an elementary collision between nucleons.

[6] S. A. Wouthuysen, unpublished work.

[7] If either the target nucleons or the incident nucleons are bound into nuclei instead of being uniformly distributed in space, the collision mean-free-path will be increased. This "packing

A picture of the energy degeneration process on the basis of the above assumptions may be formulated in the following way. An incident nucleon of total energy E makes a collision with a nucleon at rest. If the collision is completely inelastic, then in the frame in which the total momentum is zero the two nucleons are at rest after the collision. Transforming to the terrestrial frame, one then has two nucleons travelling in the direction of the incident primary, each with a total energy which one can easily calculate to be

$$\bar{E}=[Mc^2(E+Mc^2)/2]^{\frac{1}{2}}. \tag{1}$$

These two nucleons can then make further collisions of the same character with consequent multiplication of the number of nucleons but with degradation of their energies according to the relation (1) at each step. This process continues until energies at which our assumptions surely break down are reached. The meson-producing proclivities of the nucleons are then reduced and other processes, such as ionization energy loss, nuclear excitation, etc., complete the absorption of the nucleons. At energies above 1 Bev, energy loss by ionization of a proton is negligible compared to the energy loss entailed in meson-producing collisions (see Fig. 1) and so can be safely neglected.

In the following, after a brief discussion of the collision between two nucleons, we derive the equation for the change in the differential energy spectrum of high energy nucleons with thickness of matter traversed. Various solutions to this equation are then examined: (1) solutions for which the energy spectrum does not change with depth, (2) the solution corresponding to an initially monoenergetic flux of nucleons incident on the matter, (3) by application of the preceding result, solutions corresponding to incident energy spectra of the form of a power law in both total energy and kinetic energy, and (4) solutions for an incident energy spectrum corresponding to a geomagnetic cut-off at the lower end of a power law initial spectrum.

One general result of these calculations may be readily anticipated. If the incident spectrum of nucleons falls off monotonically with increasing energy at a sufficiently rapid rate, then there exists for every thickness of the material traversed an energy E_d above which the original spectral distribution is maintained but exponentially absorbed. This is a consequence simply of the fact that the number of particles leaving some small energy interval by collisions is proportional to the number present in this interval, while the number entering this interval as a result of collisions of higher energy particles is small compared with the number leaving because of the relative scarcity of particles of higher energy. Below the indicated energy E_d there are deviations of the lower energy intervals. This latter effect is responsible, then, for a difference between the mean-free-path for collision and the mean-free-path for absorption of the lower energy nucleons. The dividing energy E_d increases with increasing depth at a rate which depends on the initial energy spectrum.

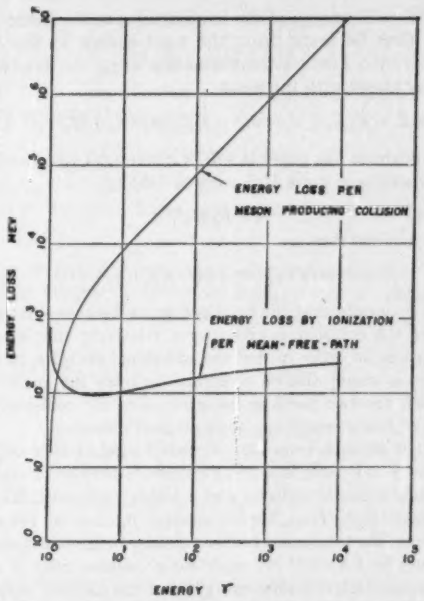

FIG. 1. Energy loss per meson-producing collision and energy loss by ionization per mean-free-path as functions of energy γ.

II. RELATIVISTIC COLLISION OF TWO NUCLEONS

Consider a collision between two nucleons, each of mass M, one of the nucleons being initially at rest and the other having a total energy E_1 and momentum p_1. Let the frame of reference in which this situation holds be denoted by S, and let the reference frame in which the total momentum is zero be denoted by S'. One finds readily that the velocity of S' relative to S is given by

$$v=c^2p_1/(E_1+Mc^2).$$

The energies and momenta of the nucleons before the collision in the frame S' will be denoted by $E_1'=E_2'$ and $p_1'=-p_2'$. Using bars to denote the corresponding quantities after the collision, we can define a parameter K to measure the elasticity of the collision by

$$K=(\bar{E}_1'+\bar{E}_2'-2Mc^2)/(E_1'+E_2'-2Mc^2), \tag{2}$$

where $K=1$ for a completely elastic collision and $K=0$ for a completely inelastic collision. Since in the frame S', $\bar{E}_1'=\bar{E}_2'$, it follows from the last equation that

$$\bar{E}_1'=\bar{E}_2'=KE_1'+(1-K)Mc^2.$$

effect" on the mean-free-path can be taken into account in our calculations simply by employing the effective mean-free-path for a collision in all of the formulas we develop.

The total energy of the two nucleons in the frame S can then be found from the total energy in the S' frame by a Lorentz transformation using the velocity found above with the result

$$\bar{E}_1+\bar{E}_2=K(E_1+Mc^2)+(1-K)[2Mc^2(E_1+Mc^2)]^{\frac{1}{2}}. \quad (3)$$

Throughout this paper it will be convenient to measure all energies in units Mc^2, whence defining

$$\gamma=E/Mc^2,$$

Eq. (3) becomes

$$\bar{\gamma}_1+\bar{\gamma}_2=K(\gamma_1+1)+(1-K)[2(\gamma_1+1)]^{\frac{1}{2}}. \quad (4)$$

We may note that the total energy of the two particles after the collision is given by a relatively simple expression; in order to find the individual energies, however, it would also be necessary to know the angle at which the two particles emerged after the collision in the S' frame relative to their original direction.

It is obvious from Eq. (4) that for relativistic collisions $\gamma_1 \gg 1$ there is a great difference between a completely inelastic collision and a highly, but not totally, inelastic one. Thus, for an incident nucleon of 10^{15}-ev energy, the total energy after a totally inelastic collision would be 1.4×10^{12} ev, while for a collision with K as small as 0.01, the total energy after the collision would be 10^{13} ev. The great simplicity of the completely inelastic case lies not only in the fact that the angle of scattering need not be known but also in the fact that the two particles after the collision each have the same energy given by

$$\gamma=[(\gamma_1+1)/2]^{\frac{1}{2}}. \quad (5)$$

It should also be pointed out that if the actual collisions are not completely inelastic, there is no reason to believe that the quantity K is independent of the energy.

III. THE EQUATION FOR THE ENERGY DISTRIBUTION FUNCTION

We now derive the equation for the variation of the energy spectrum of nucleons as they penetrate matter, under the assumption of completely inelastic collisions and a collision cross-section independent of energy. As a consequence of the latter assumption, the mean-free-path for collisions will also be independent of energy and we may use the mean-free-path as the unit of distance in the material. Let $n(\gamma, t)d\gamma$ be the number of nucleons per unit volume at a depth t (measured in mean-free-paths) in the material having an energy lying between γ and $\gamma+d\gamma$. The flux of nucleons in this energy range per unit area at a depth t in the material is then given by

$$n(\gamma, t)v(\gamma)d\gamma,$$

where v is the velocity corresponding to the energy γ. The flux at a depth $t+dt$ is then given by

$$n(\gamma, t+dt)v(\gamma)d\gamma=n(\gamma, t)v(\gamma)d\gamma-n(\gamma, t)v(\gamma)d\gamma dt +2n(\gamma_1, t)v(\gamma_1)d\gamma_1 dt, \quad (6)$$

that is, the flux at a depth t minus the number leaving the energy range under consideration as a result of collisions plus the number entering the energy range under consideration as a result of collisions in the thickness dt. The energy γ_1 is related to the energy γ by

$$\gamma_1=2\gamma^2-1, \quad (5')$$

and the factor 2 in the last term in Eq. (6) comes from the fact that each collision of a nucleon of energy γ_1 yields 2 nucleons of energy γ. From Eq. (6) follows

$$\partial n(\gamma, t)/\partial t=2n(\gamma_1, t)[v(\gamma_1)d\gamma_1/v(\gamma)d\gamma]-n(\gamma, t) \quad (7)$$

and using Eq. (5′) together with the relation

$$v(\gamma_1)/v(\gamma)=[2\gamma^2/(2\gamma^2-1)]^{\frac{1}{2}},$$

one obtains the desired equation

$$\partial n(\gamma, t)/\partial t=8\gamma[2\gamma^2/(2\gamma^2-1)]^{\frac{1}{2}}n(2\gamma^2-1, t) -n(\gamma, t). \quad (7')$$

While we could attempt to solve this equation, it is doubtful whether our assumptions have any validity for nucleons with kinetic energies less than 1 Bev, that is, $\gamma=2$. For values of γ greater than this, we can replace $2\gamma^2-1$ by $2\gamma^2$ with only small error. This simplifies the equation to

$$\partial n(\gamma, t)/\partial t=8\gamma n(2\gamma^2, t)-n(\gamma, t). \quad (8)$$

The remainder of our work then consists of finding suitable solutions of this functional-differential equation.

IV. STATIONARY ENERGY SPECTRA

It is rather interesting that Eq. (8) possesses solutions in which the energy spectrum of the nucleons, apart from an over-all exponential absorption, does not change as the nucleons penetrate matter. These solutions exist as a consequence of the fact that the variables in the equation can be separated. By writing

$$n(\gamma, t)=T(t)G(\gamma), \quad (9)$$

we obtain the two equations

$$dT/Tdt=k \quad (10a)$$

$$8\gamma^2G(2\gamma^2)/G(\gamma)=k+1. \quad (10b)$$

The solution of the first is simply

$$T=e^{kt}.$$

The second is a functional equation of a sufficiently simple form that it can be solved by inspection:

$$G(\gamma)=\frac{w(\gamma)}{\gamma}\exp\left\{\left[\frac{\ln(k+1)}{\ln 2}-2\right]\ln\ln 2\gamma\right\}, \quad (11)$$

where $w(\gamma)$ is an arbitrary function satisfying the functional equation $w(2\gamma^2)=w(\gamma)$. k is an arbitrary constant which may be complex. The solution is to be taken as the real part of the product $T(t)G(\gamma)$. Actually,

however, none of these solutions can be realized physically. k must be real and greater than -1 if the spectrum is to be positive definite. For $k>1$, the solutions are unbounded in the number of particles at high energies. For all values of k the total energy carried by the particles is unbounded at high energies.

V. SOLUTION FOR MONOENERGETIC INITIAL SPECTRUM

It is obvious that by finding the solution of Eq. (8) for a monoenergetic initial spectrum of nucleons one can readily obtain the solution for an arbitrary initial spectrum by superposition. Hence, we first derive the solution of Eq. (8) which corresponds to the initial condition

$$n(\gamma, 0)=\delta(\gamma-\gamma_0), \tag{12}$$

where δ is Dirac's δ-function.

To accomplish this we first make a Laplace transformation on the variable t:

$$n(\gamma, t)=(1/2\pi i)\int_C \nu(\gamma, \alpha)e^{\alpha t}d\alpha,$$

where C is an as yet undetermined contour; this transformation reduces Eq. (8) to the functional equation

$$\nu(2\gamma^2, \alpha)=(1+\alpha)\nu(\gamma, \alpha)/8\gamma. \tag{13}$$

The solution of this equation can be obtained by inspection and has the form

$$\nu(\gamma, \alpha)=[g(\gamma, \alpha)/\gamma \ln^2 2\gamma] \times\exp\{[\ln 2\gamma/\ln 2]\ln(1+\alpha)\}, \tag{14}$$

where $g(\gamma, \alpha)$ is an arbitrary function of its arguments which satisfies the condition

$$g(2\gamma^2 \alpha)=g(\gamma, \alpha). \tag{15}$$

The solution of the original equation is therefore

$$n(\gamma, t)=(1/2\pi i)\int_C [g(\gamma, \alpha)/\gamma \ln^2 2\gamma] \times\exp\{(\ln 2\gamma/\ln 2)\ln(1+\alpha)+\alpha t\}d\alpha. \tag{16}$$

To impose the initial condition, we make the change of variable $\alpha=e^\beta-1$ and let

$$g(\gamma, \alpha)=\rho(\gamma, \beta)\exp\{-\beta[(\ln 2\gamma_0/\ln 2)+1]\} \tag{17}$$
$$\rho(2\gamma^2, \beta)=\rho(\gamma, \beta).$$

The solution then becomes

$$n(\gamma, t)=(1/2\pi i)\int_{C'} [\rho(\gamma, \beta)/\gamma \ln^2 2\gamma] \times\exp\{\beta[(\ln \ln 2\gamma-\ln \ln 2\gamma_0)/\ln 2]+(e^\beta-1)t\}d\beta,$$

where C' is the mapping of C on the β-plane. Setting $t=0$, we see that the initial condition will be satisfied if C' is chosen to lie along the axis of imaginaries from $-i\infty$ to $i\infty$ and ρ is chosen as the constant

$$\rho(\gamma, \beta)=\ln(2\gamma_0)/\ln 2.$$

Hence, the desired solution is given in the form of a contour integral by

$$n(\gamma, t)=(e^{-t}\ln 2\gamma_0/\rho \ln 2 \ln^2 2\gamma)(1/2\pi i) \times\int_{C'} \exp\{\beta[(\ln \ln 2\gamma-\ln \ln 2\gamma_0)/\ln 2]+te^\beta\}d\beta. \tag{18}$$

If the integrand is now expanded in a power series in t and the integration performed term by term we obtain a series form of the solution:

$$n(\gamma, t)=\frac{e^{-t}\ln 2\gamma_0}{\gamma \ln 2 \ln^2 2\gamma}\sum_{n=0}^{\infty}\frac{t^n}{n!}\frac{1}{2\pi i} \times\int_{C'} \exp\left\{\beta\left[\frac{\ln \ln 2\gamma}{\ln 2}-\frac{\ln \ln 2\gamma_0}{\ln 2}\right]+n\right\}d\beta$$
$$=\frac{e^{-t}\ln 2\gamma_0}{\gamma \ln 2 \ln^2 2\gamma}\sum_{n=0}^{\infty}\frac{t^n}{n!}\delta\left(\frac{\ln \ln 2\gamma}{\ln 2}-\frac{\ln \ln 2\gamma_0}{\ln 2}+n\right). \tag{19}$$

We see that an energy spectrum in the form of discrete lines is obtained, the sequence of energies being just those which follow from the sequence of energy degeneration steps generated by the law (5).

VI. INITIAL POWER LAW ENERGY SPECTRUM

From the solution obtained in the last section one can now obtain the solution corresponding to an arbitrary initial energy spectrum $n(\gamma, 0)=f(\gamma)$ by integration:

$$n_f(\gamma, t)=\int f(\gamma_0)n(\gamma, t, \gamma_0)d\gamma_0. \tag{20}$$

The cases of greatest interest are those in which the initial spectrum has the form of an inverse power law in either the total energy or the kinetic energy. Considering the former first, we have

$$f(\gamma_0)=\gamma_0^{-s} \quad (s>1). \tag{21}$$

The integrations can be readily executed and the result is

$$n_s(\gamma, t)=\int \gamma_0^{-s}n(\gamma, t, \gamma_0)d\gamma_0$$
$$=\frac{e^{-t}2^{s-1}}{\gamma}\sum_{n=0}^{\infty}\frac{(4t)^n}{n!}\exp\{-2^n(s-1)\ln 2\gamma\}. \tag{22}$$

We note that the result has the form of a series of inverse power spectra with increasingly negative exponents. The solution can also be obtained by using the contour integral representation (18) instead of the series solution, giving the result in the form of the

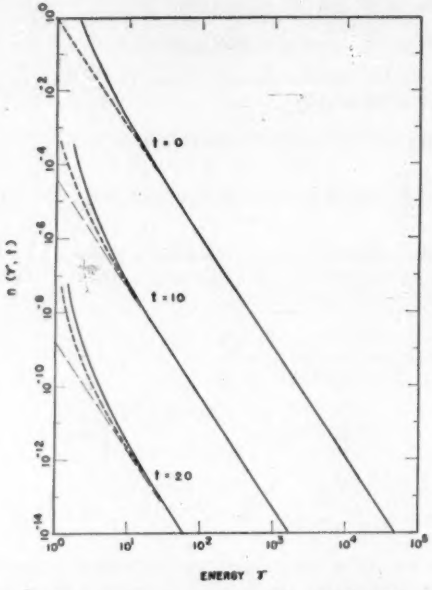

FIG. 2. Energy spectrum $n_s(\gamma, t)$ at various depths t. The solid curve is for an initial power law kinetic energy spectrum and the dashed curve for an initial power law total energy spectrum.

following contour integral:

$$n_s(\gamma, t) = [e^{-t} 2^{s-1}/(s-1)^2 \gamma \ln 2 \ln^2 2\gamma][1/2\pi i] \times \int_{C'} \exp\{\beta[(\ln \ln 2\gamma - \ln \ln 2\gamma_0)/\ln 2] + te^{\beta}\} \times \Gamma(2-\beta/\ln 2) d\beta. \quad (23)$$

For large t, this integral can be evaluated by the method of steepest descents, but the result is complicated and appears to be inferior for calculation to the rapidly converging series (22) even for relatively high values of t.

In the case where the initial spectrum is an inverse power law in the kinetic energy $f(\gamma_0) = (\gamma_0 - 1)^{-s}$, the calculations are similar and the result obtained is

$$n_s' = \frac{e^{-t} 2^{s-1}}{\gamma} \sum_{n=0}^{\infty} \frac{(4t)^n}{n!} [(2\gamma)^{2n} - 2]^{-s} (2\gamma)^{2n}. \quad (24)$$

Graphs of the energy spectra at various depths are shown in Fig. 2 for both total energy and kinetic energy power law distributions with exponent $s = 3$. It will be noted from these that at high energies, except for the change in normalization, the original power law character of the spectrum is preserved with the same exponent but that deviations toward higher populations occur for the lower energies. This behavior may be anticipated from our solutions (22) and (24), for by a comparison of successive terms in the series one finds that for energies

$$\gamma \gg 2^{(3-s)/(s-1)} t^{1/(s-1)}$$

the functions are accurately represented by the first term in each series. This behavior was anticipated on the basis of physical arguments in the introduction.

The above results allow one to calculate immediately a differential absorption coefficient which we define as $(-dn_s/n_s dt)$. This quantity is plotted in Fig. 3 as a function of t for various values of γ. If the absorption and collision mean-free-paths were equal, the differential absorption coefficient would simply be equal to unity. The curves here show the increase in absorption mean-free-path over collision mean-free-path as a result of the production of secondaries in the collisions.

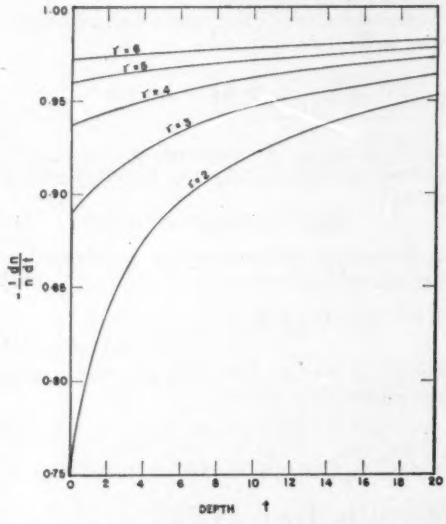

FIG. 3. Absorption coefficient for initial power law total energy spectrum as a function of depth for various energies ($s = 3$).

VII. GEOMAGNETIC CUT-OFF

The effect of the earth's magnetic field on the primary energy spectrum can easily be included in our calculation for a power law spectrum by modifying the initial spectrum to the form

$$n(\gamma_0, 0) = \begin{cases} (\gamma_0 - 1)^{-s} & \gamma_0 > \gamma_c \\ 0 & \gamma_0 < \gamma_c \end{cases}.$$

This spectrum approximates the more gradual geomagnetic cut-off on a power law spectrum by a sharp cut-off at a critical energy γ_c. For energies greater than this critical energy, there is no change in the results. However, for energies smaller than the critical energy, certain of the terms in the sum in Eq. (24) are absent.

The result may be written in the same form as Eq. (24), except that the sum on n goes only from $n=n_1$ to infinity, where

$$n_1=\begin{cases}\text{smallest integer}>(\ln \ln 2\gamma_c-\ln \ln 2\gamma)/\ln 2 & \gamma<\gamma_c\\ 0 & \gamma>\gamma_c.\end{cases}$$

This spectrum, as would be anticipated from solution in δ-functions, contains a series of steps occurring at the critical energy γ_c, and at the energies to which nucleons of energy γ_c are successively degraded.

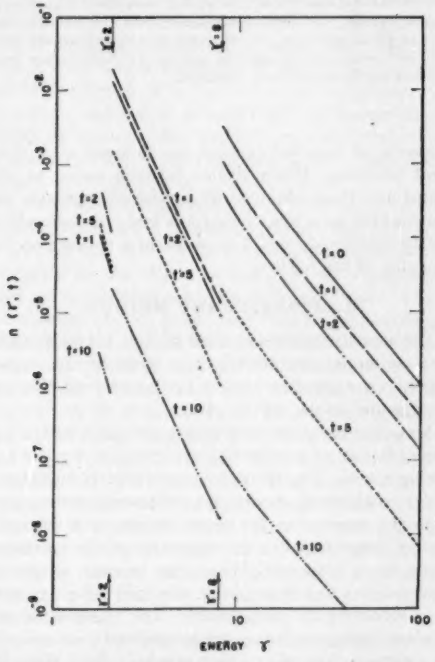

FIG. 4. Energy spectrum for initial power law total energy spectrum cut-off at $\gamma=8$ as a function of energy γ at various depths.

Graphs of this spectrum are shown in Fig. 4 for the exponent $s=3$. The critical energy has been taken to be 7 Bev, which corresponds to the energy above which

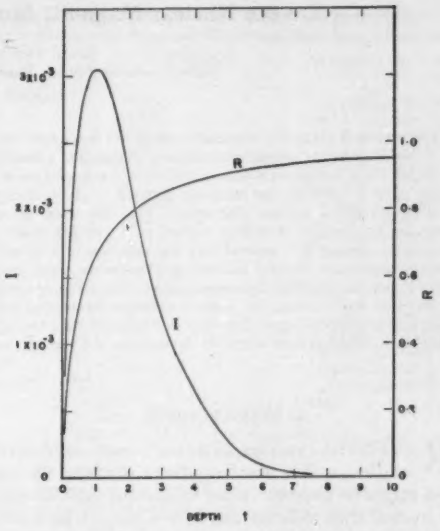

FIG. 5. $I=\int_2^8 n(\gamma, t)d\gamma$, $R=\int_2^8 n(\gamma, t)d\gamma/\int_2^\infty n(\gamma, t)d\gamma$ for initial cut-off power law kinetic energy spectrum as a function of depth.

all protons reach the earth at a geomagnetic latitude of about 40°. As the nucleons penetrate the atmosphere, the originally empty energy interval from $\gamma=2$ to $\gamma=8$ is filled in by nucleons from higher energies. This filling-in process is shown in Fig. 5, where the total number of nucleons in this energy interval, as well as the ratio of this number to the total number of nucleons with energies greater than $\gamma=2$, is plotted as a function of depth in the atmosphere. These two curves are closely approximated by the functions $2te^{-t}$ and $2t/(2t+1)$, respectively. The close similarity of this behavior with the growth and decay of a radioactive daughter nucleus whose half-life is the same as its parent nucleus may be noted; the extra factor of 2 results simply from the fact that two secondaries are produced in each collision.

This work has been supported by the Atomic Energy Commission and by a grant-in-aid of the Scientific Research Society of America to one of the authors (L.L.F.).

On the Nuclear Magnetic Moments of Several Stable Isotopes*

W. G. PROCTOR† AND F. C. YU
Department of Physics, Stanford University, Stanford, California
(Received August 28, 1950)

The nuclear induction spectrometer which has previously been described was used to measure the magnetic moments of a number of nuclei. These values are without corrections of any kind and are based upon a value for the magnetic moment of the proton of (2.79348±0.00034) nuclear magnetons. The experience gained from the observation of a large variety of nuclei has made it possible to discuss in a general way the selection of a suitable sample compound. Various interesting phenomena which have turned up in the course of these measurements are discussed; some of these are the following. (a) Nuclear resonance frequencies have been found to depend upon the compound used for the sample in some cases. This has been noted for the isotopes of Cl and N, and for Co, the latter having resonances over a region as large as 1.3 percent. This effect has been demonstrated to be of molecular rather than nuclear origin, and it is responsible for our listing the chemical compounds used for each measurement. (b) The magnetic moments of both In^{113} and In^{115} have been found to be 0.64 percent greater than their respective atomic beam values, a discrepancy very similar to that noted for Ga^{69} and Ga^{71}. (c) An hfs anomaly for the isotopes of chlorine has been observed, which is notable, because the atomic beam experiments deal with the $P_{3/2}$ state of atomic chlorine. (d) An unusual structure for the Sb^{121} and Sb^{123} resonances in aqueous solution of $NaSbF_6$ has been observed and is qualitatively explained.

I. INTRODUCTION

RECENTLY various authors[1–3] have emphasized the importance of information concerning the spin and magnetic moment values toward the establishment of nuclear shell theories, and indeed the precise knowledge of nuclear magnetic moments have always played an important role in the development of nuclear theory. In this paper we shall give a detailed report on a series of measurements by which the magnetic moments of nuclei of several stable isotopes were determined. The measurements were made with a nuclear induction spectrometer described in an earlier paper.[4] The results are summarized in Table I; brief reports of these results have been made from time to time.[5]

While in principle nuclear magnetic moments can be compared with the same accuracy with which the ratio of their respective resonance frequencies can be determined, it was recently found that the nuclear magnetic resonance frequency is somewhat different for different molecules containing the nucleus.[6] Relative shifts of the resonance frequency of as much as 1.3 percent have been observed for Co^{59} in various octahedral cobalt complexes. Such shifts, which are at this time not well understood, greatly impair the precision of the values of the magnetic moments obtained. However, certain measurements described in Sec. III, which have been done with different isotopes of nitrogen and chlorine in the same molecular form, indicate that these shifts are characteristic of the molecule itself rather than of the nucleus in question. Therefore, it can be contended at the present time that at least the ratio of the magnetic moments of two isotopes can be obtained with very great precision. Discrepancies between ratios so obtained and those obtained by precise hfs methods are contributing to a new, important body of data which can be interpreted in terms of features concerning the structure of the nucleus.[7]

II. APPARATUS AND METHOD

The measurements described in Sec. III were made with an apparatus described in detail in an earlier paper.[4] Consequently, only a brief review of this apparatus and its use will be given.

A nuclear induction instrument of typical design has been adapted as a recording spectrometer by the following means. The static magnetic field is modulated with a small sweep, so that the component of the signal from the receiver at the sweep frequency is approximately proportional to the derivative of the resonance mode being observed. When the receiver output is detected by a lock-in amplifier, this derivative is plotted by a recording dc milliammeter. The transmitter and receiver tuning condensers are gauged and their common frequency is changed at a slow rate by a clock drive. By using changeable radiofrequency parts, a frequency range of 2.2 to 9.0 Mc is available. The record from the milliammeter is divided into 10- (or 25-) kc intervals by the markers which occur as the transmitter is tuned through the harmonics of a 10- (or 25-) kc commercial multivibrator. Only a single sample is accommodated at a time, and different samples are always located in the same position in the magnetic field.

The electromagnet is supplied with electronically regulated current; its pole-faces are $7\frac{13}{16}$ in. in diameter and spaced $1\frac{3}{4}$ in. A current of two amp produces a field intensity of nearly 12,000 gauss. The homogeneity is such that the variation of the magnetic field over the region occupied by a typical sample is about 0.003 percent.

* Assisted by the joint program of the AEC and ONR.
† Now at the Department of Physics, University of Basle, Switzerland.
[1] E. Feenberg and K. C. Hammack, Phys. Rev. **75**, 1877 (1949).
[2] L. W. Nordheim, Phys. Rev. **75**, 1894 (1949).
[3] M. G. Mayer, Phys. Rev. **78**, 16 (1950).
[4] W. G. Proctor, Phys. Rev. **79**, 35 (1950).
[5] (a) W. G. Proctor and F. C. Yu, Phys. Rev. **76**, 1728 (1949); (b) **77**, 716 (1950); (c) **78**, 471 (1950).
[6] W. G. Proctor and F. C. Yu, Phys. Rev. **77**, 717 (1950); W. C. Dickinson, Phys. Rev. **77**, 736 (1950).
[7] A. Bohr and V. F. Weisskopf, Phys. Rev. **77**, 94 (1950).

The first task in the process of measuring the gyromagnetic ratio of a nucleus is that of locating the resonance in a suitable material, and its choice is determined by various factors. First, we have chosen, with the exception of Xe, to work with aqueous solutions or liquids, since it is often possible, by the additional dissolution of paramagnetic salts, to control the thermal relaxation time[8] and since sharp lines can be expected.[9] Further, sample substances have been used of such solubilities that signals sufficiently large to be observed could be expected; the choice of the compound was frequently restricted by the condition that it must be mutually soluble with a paramagnetic salt. Finally, we avoided molecules containing unpaired electrons and attempted to choose molecules or ions containing the nucleus in question in a position of high symmetry, if the nucleus was known or anticipated to have a large quadrupole moment; these precautions were dictated by the desire to avoid excessive broadening due to molecular magnetic and inhomogeneous electric fields.

Previous spectroscopic or other measurements of the magnetic moment and spin of a nucleus, which indicate the approximate value of the gyromagnetic ratio, serve as a guide for the region of frequency to be explored with a given magnetic field. Suitable magnitudes of the field intensity H_0, the modulating field and the exciting radiofrequency field are chosen in view of the consideration given in other papers.[4,8,10] After the resonance has once been located, the exact gyromagnetic ratio of a nucleus can be measured by comparing, in the same field, its resonance frequency with that of another nucleus, the gyromagnetic ratio of which is known. On the recording chart each resonance is enclosed between frequency markers and the frequency of resonance can be read by interpolation. Since we cannot measure the frequencies of two resonances at the same time, it is necessary to measure the resonances three or four times in turn in order to allow for corrections arising from drifts of the field.

The use of a separate receiver coil perpendicular to the exciting radiofrequency coil makes it possible to infer the sign of a magnetic moment from the phase of the induced r-f voltage. Relative signs of two nuclear magnetic moments can be determined by comparison of the signs of the detected audiofrequency output voltages from the two respective resonances, provided that some care is taken not to disturb the phase of the r-f homodyning voltage with which the r-f nuclear induction signal voltage is detected.

To determine spin values, the magnitudes of two signals are compared, one of which originates from nuclei of known spin. From the expression for the absorption mode observed in slow passage[10] it can be shown that the maximum derivative of the signal amplitude is proportional to $nI(I+1)\gamma^3T_2^2$, where n is the number of resonating nuclei of spin I and gyromagnetic ratio γ, and T_2 is the transverse relaxation time. By measurement of the line widths under slow passage conditions and a knowledge of relative concentrations and gyromagnetic ratios, the quantity $I(I+1)$ is experimentally determined. For nuclei with odd mass number the experimental value can be expected to lie near one of the numbers 3/4, 15/4, 35/4, 63/4, $\cdots$ which makes it an easy matter to distinguish between the lower spin values. However, for spins of 5/2 or greater, small errors in the determination of n, T_2 and the recorded signal maxima for both resonances make a spin determination less certain. Furthermore, it has been observed that T_2 may depend on the state of dissociation in water of the salt being used in a sample. This case occurs for such nuclei and compounds where the relaxation time is largely determined by electric interaction between the quadrupole moment of the nucleus and its molecular surrounding. Hence a given resonance may consist of two or more superimposed lines and can give rise to a complex line shape which invalidates the above relationship used for the determination of spin values.

TABLE I. Magnetic moments and magnetic moment ratios.*

Nucleus	Compound used	Magnetic moment in nuclear magnetons
N^{14}	NHO_3	0.40369±0.00006
N^{15}	HNO_3	−0.28312±0.00004
Cl^{35}	HCl	0.8211 ±0.0001
Cl^{37}	HCl	0.6835 ±0.0001
Sc^{45}	$Sc(NO_3)_3$	4.7497 ±0.0008
V^{51}	V_2O_5	+5.1408 ±0.0008
Mn^{55}	$LiMnO_4$	3.4624 ±0.0006
Co^{59}	$K_3Co(CN)_6$	4.6399 ±0.0009
Mo^{95}	K_2MoO_4	−0.9098 ±0.0002
Mo^{97}	K_2MoO_4	−0.9289 ±0.0002
In^{113}	$In(NO_3)_3$	5.4972 ±0.0010
In^{115}	$In(NO_3)_3$	5.5088 ±0.0010
Sb^{121}	$NaSbF_6$	3.3427 ±0.0006
Sb^{123}	$NaSbF_6$	2.5341 ±0.0004
Xe^{129}	Xe	−0.7726 ±0.0001
Pt^{195}	H_2PtCl_6	0.6005 ±0.0001
Hg^{199}	$Hg_2(NO_3)_2$	0.4994 ±0.0001
Bi^{209}	$Bi(NO_3)_3$	4.0400 ±0.0007
$\mu(N^{15})/\mu(N^{14}) = -0.7013\pm0.00007$		
$\mu(Cl^{35})/\mu(Cl^{37}) = 1.2014\pm0.0001$		
$\mu(Mo^{97})/\mu(Mo^{95}) = 1.0210\pm0.0001$		
$\mu(In^{115})/\mu(In^{113}) = 1.0021\pm0.0001$		
$\mu(Sb^{121})/\mu(Sb^{123}) = 1.3191\pm0.0001$		

* With the exception of xenon all samples are aqueous solutions.

III. EXPERIMENTAL RESULTS

In order to compute the magnetic moments as listed in Table I, we have used only the measured frequency ratios, known spins, and the known magnetic moments of the nuclei used as standards. In view of the observed dependence of a nuclear magnetic resonance frequency upon the compound used in a sample,[6] it is evident that corrections of a new kind must be applied in many cases before magnetic moments can be listed with good accuracy. Since corrections cannot be made at this time, the results quoted in Table I are without corrections of any kind. The compound which has been

[8] Bloch, Hansen and Packard, Phys. Rev. **70**, 474 (1946).
[9] Bloembergen, Purcell, and Pound, Phys. Rev. **71**, 466 (1947).
[10] F. Bloch, Phys. Rev. **70**, 460 (1946).

TABLE II. Dependence of frequency on the compound.

Compounds compared	Separation at 3.3 Mc	Separation at 2.1 Mc	Ratio
NH_4^+ and NO_3^- from 7.5-molar NH_4NO_3 in 2.0-molar $MnSO_4$	1.6 kc	0.9 kc	0.58
HNO_3 and $NH_4C_2H_3O_2$	1.0	0.7	0.70
HNO_3 and $(NH_2)_2CO$	1.0	0.6	0.60
NO_3^- and NH_3 from sample (a)	1.2	0.7	0.58

used in each measurement is also listed; the compound used for the standard nucleus may be found by reference to the pertinent paragraph below.

For the purpose of computation, we have used the value $\mu(H^1)=(2.79348\pm0.00034)\mu_N$ for the magnetic moment of the proton. This value follows from that given by Taub and Kusch[11] when the uncertainty of the ratio of m_e/M_p equal to 1.1×10^{-2} percent is included and when the calculated diamagnetic correction, without error, of 1.8×10^{-3} percent is removed; hence the above value is a completely experimental number. We have further used the value $\nu(Na^{23})/\nu(H^1)=0.26450\times(1\pm10^{-4})$ given by Bitter[12] to compute $\mu(Na^{23})=(2.21663\pm0.00035)\mu_N$ and the value $\nu(D^2)/\nu(H^1)=0.3070117\pm0.0000015$ given by Levinthal[13] to compute $\mu(D^2)=(0.857631\pm0.00011)\mu_N$. The uncertainties in the final value for a magnetic moment is then the rms value of our experimental frequency ratio error and that of the nucleus which has been used as a standard.

The sign of the nuclear magnetic moment[14] was ascertained in all cases, while the determination of spin values was not carried out unless specific mention is made.

We shall now proceed to describe the measurements on the various nuclei in the order of their atomic number.

1. Nitrogen

From the study of the band spectra of N_2 the spins of the isotopes N^{14} and N^{15}, with natural abundances of 99.62 and 0.38 percent, respectively, were given to be[15,16] 1 and[17] 1/2. The magnetic moment of N^{14} was determined by the molecular beam method[18] to be $0.402\mu_N$, while that of N^{15} was given[19] as $(0.280\pm0.003)\mu_N$, its sign being uncertain. We sought to observe the resonances of these isotopes in order to improve the values of the magnetic moments and to establish the sign of $\mu(N^{15})$.

In the first part of these measurements, dealing with N^{14}, we observed for the first time an effect of the chemical compound on the resonance frequency;[6] at the same time Dickinson[6] found a similar, although somewhat smaller, effect with F^{19}. We used the following sample, which for the purpose of reference we shall designate as sample (a): 5 cc of liquid NH_3, enriched to 7.5 percent in N^{15}, containing 1.18 g of NH_4NO_3 and 1.25 g of $Cr(NO_3)_3\cdot9H_2O$ in solution. One weak resonance, apparently arising from the N^{14} in the NO_3^- radical appeared at a frequency of 3.3 Mc, about 1 kc higher than the frequency of a strong resonance, presumably from the N^{14} in the NH_3 and the NH_4^- ion. We associated these resonances with these radicals, because samples of $NH_4C_2H_3O_2$, NH_4NO_3, and NH_4Cl on the one hand and samples of HNO_3, NH_4NO_3, and $Cu(NO_3)_2$ on the other separately gave resonances having frequencies in agreement with those above. Below we shall discuss subsequent observations which show that the resonance frequencies of Cl^{35}, Cl^{37}, and Co^{59} likewise depend upon the chemical compound used in the sample; the effect is particularly large for cobalt, where frequencies differing from one another by as much as 1.3 percent have been found.

With a resolution of 0.1 kc the N^{14} resonances from the above ammonium samples, from the liquid NH_3 as well as NH_4OH, and from KCN in water were found respectively at frequencies 1.0 kc, 1.2 kc, and 0.2 kc lower than that from HNO_3.

The frequency separations for four pairs of compounds were measured at 3.3 Mc and at 2.1 Mc to determine whether or not they were dependent of the applied field intensity; the samples used and the separations measured are given in Table II. They were found, within the resolution of the apparatus, to be proportional to the field, since the ratios of the separations are in agreement with the frequency ratio 2.1/3.3 = 0.64.

The cause of this effect must evidently be sought in the rearrangement of the electrons which takes place in chemical binding. The fact that the atomic electrons can affect nuclear resonance frequencies has been recognized for a considerable time and has been taken into account in the so-called "diamagnetic corrections" which refer to the shielding of the external field by the electrons; this shielding can indeed be expected to be somewhat modified by the chemical binding and the consequent change in the distribution of electrons. The observed differences in the resonance frequencies of nitrogen are almost twice as large as the total computed shielding effect of the atom; and it does not, therefore, seem possible that they can be explained by a mere modification of this effect, particularly since the inner electrons which contribute mostly to the shielding are hardly affected by the chemical binding. It must be pointed out, however, that in the case of polyatomic molecules there exists another mechanism through which the effective magnetic field, acting upon the nucleus, can be modified by the electrons, and which also affects the susceptibility where it leads to a temperature-independent "induced" paramagnetism, super-

[11] H. Taub and P. Kusch, Phys. Rev. **75**, 1481 (1949).
[12] F. Bitter, Phys. Rev. **75**, 1326 (1949).
[13] E. C. Levinthal, Phys. Rev. **78**, 204 (1950).
[14] A positive moment is written without the plus sign.
[15] R. Kronig, Naturwiss. **16**, 335 (1928).
[16] L. S. Ornstein and W. R. van Wijk, Z. Physik **49**, 315 (1928).
[17] R. W. Wood and G. H. Dieke, J. Chem. Phys. **6**, 908 (1938).
[18] Kusch, Millman, and Rabi, Phys. Rev. **55**, 1176 (1939).
[19] J. R. Zacharias and J. M. B. Kellogg, Phys. Rev. **57**, 570 (1940).

imposed upon the normal diamagnetism.[20] The need of taking this mechanism into account in the measurements of resonance frequencies has recently been pointed out by Ramsey[21] who was able, by comparison with the rotational moments, to calculate its magnitude for the H_2 molecule. Unfortunately, a similar numerical evaluation is not possible, at present, for other more complicated molecules and it must suffice here to point out that this induced paramagnetic effect can be considerable, particularly in cases where excited electronic states lie relatively close to the ground state of the molecule. Like the diamagnetic corrections, these induced paramagnetic corrections must be proportional to the external field and the above-mentioned observed proportionalities are in agreement with this expectation.

Nevertheless, the assumption that the observed chemical effects are to be ascribed to a modification of the field acting upon the nucleus requires further corroboration. It seemed particularly important to us to verify that they are indeed of molecular origin and not connected with questions concerning nuclear structure and to show that they do not affect the determination of ratios, where one deals with the magnetic moments of isotopes of the same element.

For this purpose we investigated the resonances of both N^{14} and N^{15} in two different compounds. Since the two isotopes have different spins and widely different moments, one would expect a different result for the ratio of their resonance frequencies, measured in different compounds, if one assumes the effect to be of nuclear origin. If, however, the effect can be understood as a modification of the external field by the molecular electrons, this ratio can be expected to be independent of the compound, since the field modification would affect both isotopes equally.

We used the above-mentioned sample (a) for the measurement of $\nu(N^{15})/\nu(N^{14})$ in NH_3 and a sample (b), composed of a 6.2-molar aqueous solution of $NaNO_3$, enriched to 31.4 percent in N^{15} and containing $MnSO_4$ to 1.0-molar concentration, for the measurement of the same ratio in NO_3^- group. We found for sample (a)

$$\nu(N^{15})/\nu(N^{14})=1.4026\pm0.0001 \tag{1}$$

and for sample (b)

$$\nu(N^{15})/\nu(N^{14})=1.4027\pm0.0001 \tag{2}$$

so that within our accuracy agreement between the two values was established. This agreement must be considered as significant, since it was ascertained with an error of only about 15 percent of the observed chemical shifts.

Arbitrarily choosing HNO_3 as a standard, we measured

$$\nu(N^{14})/\nu(D^2)=0.47070\pm0.00005, \tag{3}$$

using a General Radio, Model 271, frequency meter. The D^2 resonance was obtained from a 0.6-molar aqueous solution of $MnSO_4$ in 85 percent D_2O. The value (3) corresponds to

$$\mu(N^{14})=(0.40369\pm0.00006)\mu_N, \tag{4}$$

and by applying the average of (1) and (2) leads to

$$\mu(N^{15})=-(0.28312\pm0.00004)\mu_N. \tag{5}$$

As indicated here, the sign of the magnetic moment of N^{15} was observed to be negative. The values (4) and (5) are in good agreement with the molecular beam values. The value (5) is different by 1 part in 2800 from that reported earlier[5b] for $\mu(N^{15})$; this is because (5) was measured relative to the N^{14} resonance in NO_3^- and the earlier value was obtained with NH_3 from sample (a).

2. Chlorine

Kusch and Millman,[22] using the molecular beam method, determined the magnetic moments of the two stable odd chlorine isotopes to be

$$\mu(Cl^{35})=(0.819\pm0.003)\mu_N$$

and

$$\mu(Cl^{37})=(0.683\pm0.003)\mu_N,$$

assuming the present known[23] spin value of 3/2. Bitter found a more accurate value of $(0.8213\pm0.0003)\mu_N$ for the former, using the nuclear induction method; we have here observed the resonances of both isotopes. The resonance of the more abundant isotope Cl^{35} (75.4 percent) from a sample of concentrated hydrochloric acid was observed directly on the oscilloscope, and its frequency was compared with a General Radio, Model 271, frequency meter to that of D^2, obtained from a sample of 0.6-molar $MnSO_4$ in 85 percent D_2O. The resonance was near 4.5 Mc, when the field intensity was in the neighborhood of 11 kilogauss. For the ratio of the resonance frequencies we found

$$\nu(Cl^{35})/\nu(D^2)=0.63827\pm0.00006. \tag{6}$$

The resonance of the less abundant isotope Cl^{37} (24.6 percent) was compared with that of $Cl,^{35}$ using the same sample of concentrated hydrochloric acid, but making measurement on the recorded signals, with the result:

$$\nu(Cl^{35})/\nu(Cl^{37})=1.2014\pm0.0001. \tag{7}$$

The ratio (7) is the ratio of the nuclear magnetic moments, since both isotopes have the same spin 3/2. The values (6) and (7) lead directly to

$$\mu(Cl^{35})=(0.8211\pm0.0001)\mu_N, \tag{8}$$

$$\mu(Cl^{37})=(0.6835\pm0.0001)\mu_N. \tag{9}$$

The ratio of the magnetic dipole interaction constants a_{35}/a_{37}, for the two chlorine isotopes in their $^2P_{3/2}$ ground

[20] J. H. Van Vleck, *Electric and Magnetic Susceptibilities* (Oxford University Press, London, 1932). The mechanism is contained here in the so-called "high frequency terms" in the formula (11), Chapter X.

[21] N. F. Ramsey, Phys. Rev. **77**, 567 (1950); **78**, 699 (1950).

[22] P. Kusch and S. Millman, Phys. Rev. **56**, 527 (1939).

[23] Townes, Holden, Bardeen, and Merritt, Phys. Rev. **71**, 644 (1947).

states has been measured by Davis, Feld, Zabel, and Zacharias[24] and found to be 1.20272±0.00009. The ratio should ordinarily be expected to be equal to the ratio of the magnetic moments of these two isotopes, since the spins are the same and the reduced electron mass corrections are negligible. However, the above value is in disagreement with the ratio (7) by (0.11±0.02) percent. Bitter[25] has suggested that such anomalies may be due to the difference in the distribution of magnetism over the nuclear volumes of the isotopes, since in one case the magnetic field intensity is given by the electron density over the nuclear volume and in the other by the homogeneous applied field. Bohr and Weisskopf[7] have considered this effect for the nuclei of heavy atoms whose electronic configuration is of the type $s_{1/2}$ or $p_{1/2}$ and it has been applied with success to the isotopes of potassium and rubidium. This explanation does not apply, however, to the $p_{3/2}$ ground state with which one has to deal in the atom of chlorine and where the effect of nuclear structure on the hyperfine structure should be very small. A satisfactory explanation of the observed discrepancy between the ratio (7) and that of the corresponding hfs separation has not yet been given.

A shift toward a higher frequency for the same applied field was observed for Cl^{35} and Cl^{37} in solution of $Ba(ClO_4)_2$ and of $HClO_4$, compared to the resonance frequencies of the same isotopes in HCl. Measurements showed that

$$\nu(Cl^{35} \text{ in } HClO_4)/\nu(Cl^{35} \text{ in HCl}) = 1.0009 \pm 0.0001, \quad (10a)$$

$$\frac{\nu(Cl^{35} \text{ in } HClO_4)}{\nu(Cl^{35} \text{ in HCl})} \Big/ \frac{\nu(Cl^{37} \text{ in } HClO_4)}{\nu(Cl^{37} \text{ in HCl})} = 1.0000 \pm 0.0001. \quad (10b)$$

The assumption that the chemical shift is of molecular origin is supported by the result given in (10b). Because of the similarity of the nuclei Cl^{35} and Cl^{37} this evidence, however, cannot be considered to be as strong as that reported above for the two very different nuclei N^{14} and N^{15}.

3. Scandium

Scandium occurs entirely as the isotope Sc^{45}. Kopfermann and Rasmussen[26] determined its spin as 7/2 and gave a good estimate of its magnetic moment; Kopfermann and Wittke[27] later measured the magnetic moment as 4.8 nuclear magnetons. By dissolving Sc_2O_3 in dilute nitric acid we prepared a 0.65-molar solution of $Sc(NO_3)_3$ which gave a large signal at 7.6 Mc, using a magnetic field of 7.4 kgauss. Its frequency was compared to that of Na^{23} from a saturated aqueous solution of NaCl with 0.5-molar of $MnSO_4$ by means of a General Radio, Model 271, frequency meter. We found

$$\nu(Sc^{45})/\nu(Na^{23}) = 0.9183 \pm 0.0001. \quad (11)$$

Taking for the spin the value 7/2, this leads to a value for the magnetic moment

$$\mu(Sc^{45}) = (4.7497 \pm 0.0008)\mu_N \quad (12)$$

in excellent agreement with the spectroscopically determined value. The sign was confirmed to be positive, but no attempt was made to check the spin, since we could not be certain about the degree of dissociation of the molecules in the solution and about the effect of dissociation upon the signal amplitude.

4. Vanadium

The spin of V^{51} (100 percent) has been unequivocally determined as 7/2 by Kopfermann and Rasmussen,[28] while the magnetic moment was measured by Knight and Cohen,[29] using the nuclear induction method. We observed the V^{51} resonance in order to establish the sign of the magnetic moment, although no exceptions are known to the rule that all odd-proton nuclei with spin greater than 1/2 have positive moments. The sign was indeed found to be the same as that of Na^{23}, that is positive. The value, given in brackets in Table I, is that obtained by Knight and Cohen, but we have explicitly indicated the positive sign, since it represents a new result. Our sample was an aqueous solution of $NaVO_3$.

5. Manganese

Manganese occurs only as the isotope Mn^{55}; it is paramagnetic in most compounds because of the unpaired spin of $3d$ electrons. The negative permanganate ion, MnO_4^-, however, is known to possess electrons with paired spins and the very soluble compound $LiMnO_4$ is only slightly paramagnetic. Being guided by the spectroscopic spin value 5/2 obtained by White and Ritschl[30] and the magnetic moment value of 3.0 nuclear magnetons by Fisher and Peck,[31] we found the resonance near 8.3 Mc at a field of 7.9 kgauss, using a 2.0-molar aqueous solution of $LiMnO_4$ as sample. With a General Radio, Model 271, frequency meter we measured the ratio

$$\nu(Mn^{55})/\nu(Na^{23}) = 0.9372 \pm 0.0001. \quad (13)$$

This gives

$$\mu(Mn^{55}) = (3.4624 \pm 0.0006)\mu_N. \quad (14)$$

Since the compound $LiMnO_4$ is slightly paramagnetic, there is the possibility that our value for the magnetic moment is too high. However, a frequency dependence upon the temperature, such as that shown by cobalt

[24] Davis, Feld, Zabel, and Zacharias, Phys. Rev. **76**, 1076 (1949).
[25] F. Bitter, Phys. Rev. **76**, 150 (1949).
[26] H. Kopfermann and E. Rasmussen, Z. Physik **92**, 82 (1934).
[27] H. Kopfermann and H. Wittke, Z. Physik **105**, 16 (1937).
[28] H. Kopfermann and E. Rasmussen, Z. Physik **98**, 624 (1936).
[29] W. D. Knight and V. W. Cohen, Phys. Rev. **76**, 1421 (1949).
[30] H. E. White and R. Ritschl, Phys. Rev. **35**, 208 (1930).
[31] R. A. Fisher and E. R. Peck, Phys. Rev. **55**, 270 (1939).

salts and mentioned below, was not observed for this sample.

6. Cobalt

Cobalt occurs in nature only as the isotope Co^{59}. Its spin was determined by the optical hfs method as 7/2 by Kopfermann and Rasmussen.[32] More[33] confirmed this spin value and gave the magnetic moment as 2.7 nuclear magnetons, although Kopfermann and Rasmussen[34] later showed reason to believe that it is larger.

We have restricted our investigations of the cobalt resonances to those compounds which contain cobalt in essentially covalent octahedral complexes. From simple consideration these compounds should be expected to be only feebly paramagnetic.[30,35]

We first observed the resonance of Co^{59} in a 1.0-molar aqueous solution of $K_3Co(CN)_6$ and obtained the frequency ratio

$$\nu(Co^{59})/\nu(Na^{23}) = 0.89709 \pm 0.00009. \qquad (15)$$

The resonances of Co^{59} in other compounds were subsequently observed and it was found that the resonance frequency is strongly dependent upon the compound. Table III presents data showing the compounds used and the frequencies of Co^{59} resonances relative to the value (15). It will be noted that the frequencies of these resonances spread over a range as large as 1.3 percent. It is indicated in Table III that $Na_3Co(NO_2)_6$ was observed to manifest two resonances; these two lines may be due to the simultaneous existence of two isomeric forms of this compound. The line widths of both of these lines are the same, 0.72 gauss, and the resonance at the lower frequency is about 16 times more intense than the other. We have searched in the neighborhood of the resonance for each of the other compounds and found no other resonances.

Measurements made on the two lines of $Na_3Co(NO_2)_6$ at four different field values, ranging from 4400 gauss to 7900 gauss, showed that the ratios given in Table III were independent of the field strength to one part in 10,000, suggesting a similar origin of the chemical shift as mentioned above for nitrogen.

As a possible explanation of the large chemical effect observed in cobalt one may assume that it likewise is due to the mechanism of induced paramagnetism as discussed in connection with the measurements on nitrogen. One must then postulate the existence of electronic energy levels very close to that of the ground state and is hence led to the expectation of the dependence of the resonance frequency upon the temperature. The fact that such a dependence exists was indeed demonstrated by the following experiment. Those samples which would not decompose were heated by placing them in boiling water; the resonance frequency of each was compared to that of a like sample at room temperature by exchanging one sample for the other in quick succession and observing the shift of the resonance upon the oscilloscope screen. The compounds, $K_3Co(CN)_6$, $Co(C_2H_4(NH_2)_2)_3Cl_3$, and $Co(NH_3)_6Cl_3$, for which the experiment was performed, showed the same temperature dependence. For about 20 percent increase in temperature, that is, from 20°C to 80°C, the frequency increased by 0.015 percent or about 1 kc out of 7000 kc. Although this small increase is not much greater than the usual experimental error (about 0.006 percent), it is quite certain that there is such a slight temperature-dependence of the Co^{59} resonance, because similar experiments were carried out with NaCl and $LiMnO_4$ and gave no observable shift of Na^{23} and Mn^{55} resonances. It is also interesting to note that the N^{14} resonances in the various compounds listed in Table III showed no unusual frequency shifts, thus indicating that the mechanism, suggested above to explain the shift of the Co^{59} resonance, is mostly concerned with its $3d$ electrons.

TABLE III. Frequencies of Co^{59} resonances in various compounds.

Compound	Relative frequency
$K_3Co(CN)_6$	1.0000
$Co(C_2H_4(NH_2)_2)_3Cl_3$	1.0073±0.0001
	1.0074±0.0001
$Na_3Co(NO_2)_6$	1.0081±0.0001
$Co(NH_3)_6Cl_3$	1.0083±0.0001
$K_3Co(C_2O_4)_3$	1.0130±0.0001

If the value (15) is used, we obtain

$$\mu(Co^{59}) = (4.6399 \pm 0.0009)\mu_N. \qquad (16)$$

The sign was observed to be positive. The value (16) is very much larger than the value $2.7\mu_N$ given by More[33] and provides the widest discrepancy known to us between the values of nuclear moments determined from hyperfine structure and from nuclear magnetic resonance. This new higher value agrees with the assumption that the odd proton is in an $f_{7/2}$ orbit as proposed by Mayer;[3] the hfs value indicated an orbit $g_{7/2}$ in disagreement with her single-particle model of the nucleus. Uncertainties in the value (16) of the order of one percent, which arise from the chemical effect, are of course not large enough to affect this assignment.

7. Molybdenum

Molybdenum has two odd isotopes, Mo^{95} and Mo^{97}, which occur naturally to 16.1 percent and 9.6 percent, respectively. The spins of these isotopes have recently been given[36] a probable value 5/2. Mack,[37] from hfs studies, has reported that the ratio of the magnetic moments is 1.07±0.05 with the hfs separation for Mo^{97} definitely larger than that for Mo^{95}. Using a saturated

[32] H. Kopfermann and E. Rasmussen, Naturwiss. **22**, 291 (1934).
[33] K. R. More, Phys. Rev. **47**, 256 (1935).
[34] H. Kopfermann and E. Rasmussen, Z. Physik **94**, 58 (1935).
[35] L. Pauling, *Nature of the Chemical Bond* (Cornell University Press, Ithaca, 1948), second edition.
[36] J. E. Mack, Rev. Modern Phys. **22**, 64 (1950).
[37] J. E. Mack, private communication.

aqueous solution of K_2MoO_4 as sample, two resonances were found near 3.1 Mc at a magnetic field of 11 kgauss. We obtained

$$\nu(Mo^{97})/\nu(N^{14})=0.9208\pm0.0001 \quad (17)$$

and

$$\nu(Mo^{97})/\nu(Mo^{95})=1.0210\pm0.0001, \quad (18)$$

where we have used the identification made by Mack. The N^{14} resonance was obtained from HNO_3.

The signs were observed to be negative. The single-particle model of Mayer[3] predicts, for nuclei with 53 and 55 neutrons, that, if the spin is 5/2, the single particle orbit is $d_{5/2}$ leading to a magnetic moment with a negative sign; on the other hand, spins of 3/2 and 7/2 would correspond to positive moments. This argument gives weight to the assumption of spin 5/2 for both isotopes. Using this value and the value for $\mu(N^{15})$ given in (4), we calculated

$$\mu(Mo^{97})=-(0.9289\pm0.0002)\mu_N, \quad (19)$$

$$\mu(Mo^{95})=-(0.9098\pm0.0002)\mu_N. \quad (20)$$

These moments have roughly the same magnitude as others for odd-neutron nuclei of spin 5/2. With the assumption of equal spin for both isotopes, the ratio of their magnetic moments is accurately given by (18).

In the ion MoO_4^- the Mo atom is probably contained in the center of a regular tetrahedron of O atoms which together form a shell about the Mo atom and keep it at a certain minimum distance from the solvent water molecules. Since the gyromagnetic ratio of the Mo nuclei is relatively small, it is quite safe to assume that T_1, the thermal relaxation time, is entirely determined by the quadrupole coupling of the nucleus to the electric field gradients at its position. For quadrupole relaxation T_1 goes as Q^{-2}; since in our case T_2 is determined by field inhomogeneities, it is the same for both isotopes. We were not able to measure the relaxation times T_1 for the two isotopes, because they were too long for us to achieve slow passage conditions. We did observe, however, that the intensities of the exciting radio-frequency fields, for which maximum signals in the absorption mode were obtained, were strikingly different for the two isotopes, i.e., greater for Mo^{97} than for Mo^{95}. Since this "saturation intensity" gives a measure for the longitudinal relaxation time T_1 and since we assume this quantity is determined by quadrupole relaxation, we may conclude $|Q(Mo^{97})|>|Q(Mo^{95})|$ for the relative order of magnitude of the quadrupole moments of Mo^{97} and Mo^{95}. It was not possible, under our experimental conditions to identify the two isotopes by their signal magnitude and we have therefore used the identification by Mack.[37]

8. Indium

The gyromagnetic ratio of the indium isotopes, In^{113} (4.5 percent) and In^{115} (95.5 percent), were measured with a sample of 0.38-molar $In(NO_3)_3$, which was prepared by dissolving In metal in dilute nitric acid; as will be discussed below, this concentration gave approximately optimum signal conditions. The frequency measurements were first undertaken to find whether a hfs anomaly exists, since a precise measurement of the dipole interaction constants was known.[38] The results of the measurements were

$$\nu(In^{115})/\nu(Na^{23})=0.82841\pm0.00008, \quad (21)$$

$$\nu(In^{113})/\nu(Na^{23})=0.82667\pm0.00008, \quad (22)$$

$$\nu(In^{115})/\nu(In^{113})=1.0021\pm0.0001. \quad (23)$$

The Na^{23} resonance was obtained from a 0.25-molar solution of NaCl with 0.5-molar of $MnSO_4$. The measurements were carried out at a magnetic field of 6600 gauss with radiofrequencies near 6 Mc.

The ratio (24) is in close agreement with the ratio

$$a_{115}/a_{113}=1.00224\pm0.00010 \quad (24)$$

determined by Hardy and Millman,[38] so that no hfs anomaly is found here.

Using spin 9/2 for both isotopes,[38] we calculated

$$\mu(In^{115})=(5.5088\pm0.0010)\mu_N, \quad (25)$$

$$\mu(In^{113})=(5.4972\pm0.0010)\mu_N. \quad (26)$$

On the other hand, the diamagnetically uncorrected atomic beam values taken from Taub and Kusch[11] are

$$\mu(In^{115})=(5.474\pm0.003)\mu_N \quad (27)$$

and

$$\mu(In^{113})=(5.463\pm0.003)\mu_N. \quad (28)$$

One notes that the resonance values are each 0.6 percent higher than the atomic beam values. A similar discrepancy has already been noted for the isotopes Ga^{69} and Ga^{71} for which the nuclear induction values are 0.7 percent higher than the atomic beam hfs values.[39] Since our measurements were made in rather dilute solution in which the compound $In(NO_3)_3$ can be expected to dissociate, it is not likely that this discrepancy is of the same origin as the observed frequency shifts for N, Cl, and Co. The frequency ratios (21), (22), and (23) were also measured at a field of 3500 gauss and found to be the same.

It was found that a highly concentrated solution of $In(NO_3)_3$ was unfavorable, insofar as it caused an undesirable broadening of the line. To show that this effect was caused by an insufficient degree of dissociation, we performed the following experiment. Solutions of $In(NO_3)_3$, with a constant molarity 0.55 M/l, but with increasing concentration of HNO_3, were compared for line widths, the object being that the presence of the common ion NO_3^- would suppress the dissociation of the salt to a different degree in each sample. It was found that as the NO_3^- concentration was increased, the

[38] T. C. Hardy and S. Millman, Phys. Rev. 61, 459 (1942).
[39] R. V. Pound, Phys. Rev. 73, 1112 (1948); G. Becker and P. Kusch, Phys. Rev. 73, 584 (1948); see also reference 11.

In^{115} resonance line indeed became broader, achieving a maximum width for 8-molar HNO_3, while a further increase of HNO_3 had no effect. It is reasonable to assume, because of the large quadrupole moment of the In^{115} nucleus, that the line width is given by quadrupole relaxation. Making this assumption, our observation led to the conclusion that the quadrupole interaction with its surroundings is greater for In bound in the molecule $In(NO_3)_3$ than for the dissociated In ion. The maximum observed line width corresponds to a thermal relaxation time of about 10^{-4} sec, while the minimum width leads to a value of about 10^{-3} sec. At intermediate concentrations intermediate widths were of course observed. Viscosity changes were inadequate to account for these differences of the relaxation time.

9. Antimony

Antimony has two odd isotopes, Sb^{121} (56.0 percent) with a spin[40] 5/2 and Sb^{123} (44.0 percent) with a spin 7/2. Spectroscopically Crawford and Bateson[41] have measured their magnetic moments as $3.7\mu_N$ and $2.8\mu_N$, respectively, with a ratio 1.30 ± 0.02. These nuclei are known to have relatively large quadrupole moments[42] and we chose the compound $NaSbF_6$ in aqueous solution as a sample, because in the ion SbF_6^- the Sb nucleus is at the center of a regular octahedron formed by the six fluorine atoms. As a result, the gradient of the electric field to which it is subjected must vanish for symmetry reasons and an excess quadrupole broadening of the line is consequently avoided. The resonance of Sb^{121} was located near 6.7 Mc at a field of 6600 gauss and the resonance of Sb^{123} was found near 6.0 Mc at a field of 11000 gauss. We obtained

$$\nu(Sb^{121})/\nu(Na^{23})=0.90480\pm0.00009, \quad (29)$$

$$\nu(Sb^{123})/\nu(D^2)=0.84423\pm0.00008. \quad (30)$$

The Na^{23} signal was provided from a 0.25-molar solution of NaCl with 0.5-molar of $MnSO_4$ and the D^2 signal was provided from 1.8-molar solution of $MnSO_4$ in 25 percent D_2O. The ratios (29) and (30) give

$$\mu(Sb^{121})=(3.3427\pm0.0006)\mu_N, \quad (31)$$

$$\mu(Sb^{123})=(2.5341\pm0.0004)\mu_N, \quad (32)$$

and

$$\mu(Sb^{121})/\mu(Sb^{123})=1.3191\pm0.0001, \quad (33)$$

all of which are in good agreement with the work of Crawford and Bateson. The recorded signals of both Sb^{121} and Sb^{123}, representing the derivative of the absorption mode, showed an interesting structure which is reproduced in Fig. 1. Each resonance is composed of five lines separated by 1.90 gauss. For reasons presented below we believe that they are caused by the magnetic dipole interaction of the Sb nucleus with the

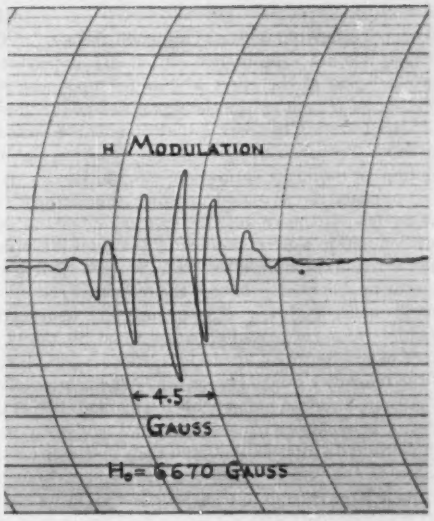

FIG. 1. The experimental derivative of Sb^{121} absorption line in aqueous solution of $NaSbF_6$ and HF.

surrounding fluorine nuclei. It follows from this explanation of the structure that the frequency of the central line is unaffected and we have used this line for our frequency measurements.

The features of the shape of the lines from the $NaSbF_6$ solution are qualitatively understood. The Sb atom is contained in the center of an octahedron formed by the six fluorine atoms. For any given orientation of the ion SbF_6^- the magnetic moments of the fluorine nuclei are either parallel or anti-parallel to the external field H_0. This alignment gives rise to a finite number of field perturbations H' at the Sb nucleus. In particular,

$$H'=\sum_i 2M_i\mu(F^{19})(3\cos^2\theta_i-1)/r^3, \quad (34)$$

where M_i is the nuclear magnetic quantum number of the ith fluorine nucleus, θ_i its polar angle with respect to the Sb nucleus with the direction of the external field chosen as polar axis, and r the internuclear distance for the Sb−F bond, equal to 1.95×10^{-8} cm.[43] The contribution of one fluorine nucleus to this sum may be as large as $2\mu(F^{19})/r^3=3.54$ gauss. Resonance from Sb nuclei from a large number of molecular ions with the same orientation will give rise to resonance lines at the field values H_0+H', the different values H' corresponding to the values $\pm1/2$ which the quantum number M_i can independently assume. If the molecules are considered to have a stationary but random orientation, one obtains a distribution function for the values H' which shows five lines, separated from each other by $2\mu(F^{19})/r^3$ gauss. The orientation of the molecules in the

[40] J. S. Badami, Z. Physik **79**, 206 (1932).
[41] M. F. Crawford and S. Bateson, Can. J. Research **10A**, 693 (1934).
[42] K. Murakawa and S. Suwa, Phys. Rev. **76**, 433 (1949).
[43] N. Schrewelius, Z. anorg. u. allgem. Chem. **238**, 241 (1938).

solution is, of course, not stationary but actually undergoes a random rotation; although this step in the analysis has not been carried out, it can be expected that inclusion of the effect of rotation upon the distribution of H' will reduce the separation of the lines.[44]

It is interesting to observe that one cannot measure the thermal relaxation time of the Sb nucleus in $NaSbF_6$ solution by ordinary saturation procedures. To show this, consider the situation in which the frequency of the r-f field is chosen such as to cause resonance absorption within a narrow range of the total line structure. While irradiation takes place, reorientation of the fluorine moments may destroy the resonance conditions for Sb nuclei originally at resonance and temporarily establish resonance conditions for some Sb nuclei of other molecules which would otherwise remain outside of the resonance range. Hence, while one is attempting to saturate a certain group of nuclei, reorientation of the fluorine moments exchanges these for a new group with equilibrium distribution between their magnetic energy states. In the present apparatus the r-f field could not be made large enough to test this effect experimentally, but measurements with higher r-f field are in progress.

10. Xenon

Xenon has two odd isotopes, Xe^{129} (26.2 percent) and Xe^{131} (21.2 percent). Kopfermann and Rindal[45] have determined from hfs measurements that the former has a spin 1/2 and the latter a spin 3/2. Bethe and Bacher,[46] from the work of Kopfermann and Rindal and that of Jones,[47] found that

$$\mu(Xe^{129}) = -0.9\mu_N, \tag{35}$$

$$\mu(Xe^{129})/\mu(Xe^{131}) = -1.11. \tag{36}$$

Being a monatomic gas, pure Xe must be expected to have an exceedingly long thermal relaxation time and it is therefore necessary to provide a paramagnetic catalyst. While the admixture of oxygen could be used in principle for this purpose,[10] calculations indicate that an excessive pressure of O_2 would be necessary. Instead, following a suggestion made by Bloch,[48] we filled the sample volume with powdered Fe_2O_3, so that the impacts of the Xe atoms on the surfaces of the paramagnetic particles could provide the necessary relaxation mechanism. Using a pressure of 12 atmos of Xe and a magnetic field of 5400 gauss, the resonance of Xe^{129} was located near 6.4 Mc with a signal-to-noise ratio of about four. The isotope was identified by the reasonably good agreement of its gyromagnetic ratio with the spectroscopic value. We obtained

$$\nu(Xe^{129})/\nu(Na^{23}) = 1.0457 \pm 0.0001, \tag{37}$$

which leads to

$$\mu(Xe^{129}) = -(0.7726 \pm 0.0001)\mu_N. \tag{38}$$

The sodium resonance was obtained from a 0.25-molar solution of NaCl with 0.5-molar of $MnSO_4$.

The fact that the observed resonance was indeed due to xenon and not to some impurities contained in the Fe_2O_3, was verified, since a sample containing only the powdered Fe_2O_3 gave no resonance. Two other powdered paramagnetic compounds, $CuCl_2$ and Cr_2O_3, were used, but without success. An experiment was also made to see whether, by any unanticipated means, the thermal relaxation time could have been sufficiently short to observe a resonance in the pure xenon gas; as expected, no resonance was observed. In view of its lower gyromagnetic ratio an observable resonance of Xe^{131} cannot be expected from our present samples. If we use the spectroscopic value (36) for the ratio of the magnetic moments, we obtain

$$\mu(Xe^{131}) = 0.696\mu_N. \tag{39}$$

11. Platinum

Platinum has only one stable isotope of odd mass number, Pt^{195}, occurring with an abundance of 35.3 percent. Its spin is known[49] to be 1/2 and its magnetic moment has been determined[50] spectroscopically to be $0.6\mu_N$.

Using a magnetic field of 6600 gauss, the resonance of Pt^{195} was located in the neighborhood of 5.9 Mc. We compared its frequency with that of Na^{23} and found

$$\nu(Pt^{195})/\nu(Na^{23}) = 0.81273 \pm 0.00008, \tag{40}$$

which leads to

$$\mu(Pt^{195}) = (0.6005 \pm 0.0001)\mu_N. \tag{41}$$

The sign of the magnetic moment is positive in agreement with the determination by Schmidt and the signal amplitude is consistent with a spin 1/2. Our sample was prepared by dissolving platinum metal in aqua regia, forming H_2PtCl_6 to 1.0-molar concentration, to which 0.5-molar concentration of $MnCl_2$ was added. The Na^{23} sample was a 0.2-molar aqueous solution of NaCl with 0.2-molar $MnSO_4$. No attempt to observe the Pt^{195} resonance in any other chemical form was made.

12. Mercury

Mercury has two isotopes of odd mass number, Hg^{199} (17.0 percent) and Hg^{201} (13.2 percent), the former having a spin 1/2 and the latter[51] a spin 3/2. The magnetic moment of Hg^{199} was measured spectroscopically by Mrozowski[52] as

$$\mu(Hg^{199}) = (0.547 \pm 0.002)\mu_N. \tag{42}$$

[44] H. S. Gutowsky and G. E. Pake, J. Chem. Phys. **18**, 162 (1950).
[45] H. Kopfermann and E. Rindal, Z. Physik **87**, 460 (1934).
[46] H. Bethe and R. F. Bacher, Revs. Modern Phys. **8**, 82 (1936).
[47] E. G. Jones, Proc. Roy. Soc. **A144**, 587 (1934).
[48] F. Bloch, to be published.
[49] B. Jaeckel and H. Kopfermann, Z. Physik **99**, 492 (1936); B. Jaeckel, Z. Physik **100**, 513 (1936).
[50] T. Schmidt, Z. Physik **101**, 486 (1936).
[51] H. Schüler and J. E. Keyston, Z. Physik **72**, 423 (1931).
[52] S. Mrozowski, Phys. Rev. **57**, 207 (1940).

The ratio of the magnetic moments

$$\mu(Hg^{199})/\mu(Hg^{201}) = -0.9018, \quad (43)$$

given by Schüler and Schmidt,[53] was used by Mrozowski to obtain the value

$$\mu(Hg^{201}) = -(0.607 \pm 0.003)\mu_N. \quad (44)$$

We used a sample containing a 3.5-molar concentration of $Hg_2(NO_3)_2$, prepared by dissolving mercury in dilute nitric acid and a 0.2-molar concentration of $Mn(NO_3)_2$. The resonance of Hg^{199} was found in the neighborhood of 6.8 Mc with a magnetic field of 8900 gauss. Comparison of the frequency with that of D^2 from a 1.8-molar aqueous solution of $MnSO_4$ containing 25 percent D_2O yields

$$\nu(Hg^{199})/\nu(D^2) = 1.1647 \pm 0.0001. \quad (45)$$

Taking for the spin the value 1/2, we have

$$\mu(Hg^{199}) = (0.4994 \pm 0.0001)\mu_N. \quad (46)$$

The positive sign was confirmed and the spin was verified to be 1/2.

Computations indicated that for our sample, making even favorable assumption about the relaxation time, the resonance of Hg^{201} could not be observed. However, if (43) is used, we obtain from (46)

$$\mu(Hg^{201}) = -0.5538\mu_N. \quad (47)$$

13. Bismuth

Bismuth is composed entirely of one isotope Bi^{209}. From hfs work Back and Goudsmit[54] first concluded that the spin of Bi^{209} is 9/2; Mack,[36] reporting upon hfs work from a variety of sources, concluded that the magnetic moment is equal to 4.1 nuclear magnetons. The nuclear resonance of Bi^{209} was found with a 0.69-molar aqueous solution of $Bi(NO_3)_3$, the quadrupole relaxation providing a satisfactory short thermal relaxation time. The magnetic field used was near 10 kgauss and the radiofrequency near 7.0 Mc. The frequency of resonance was compared with that of D^2 in an aqueous solution of 1.8-molar $MnSO_4$ with 25 percent D_2O. We found

$$\nu(Bi^{209})/\nu(D^2) = 1.0468 \pm 0.0001, \quad (48)$$

which leads to the value

$$\mu(Bi^{209}) = (4.0400 \pm 0.0007)\mu_N \quad (49)$$

in good agreement with the spectroscopic value given above.

IV. SUMMARY

The magnetic moments which were obtained from the measurements described in Sec. III are summarized in Table I. It was pointed out in the introduction that the discovery of chemical effects on the resonance frequency introduces an element of uncertainty into the determination of the values of the magnetic moments. In the present state of knowledge of these effects it is sometimes difficult to say to what extent they affect the experimental accuracy. With the exception of Co, where they introduce an error of at least one percent, it seems safe to estimate from the observed magnitude of these effects that the error thus committed is usually well below one percent. However, rather than trying to estimate the error, we felt that the results are presented on a firmer experimental basis if they are given with their full experimental accuracy. The fact that different results may be expected in different compounds is taken into cognizance in Table I by listing the chemical compound used for the sample from which the particular value was derived.

TABLE IV. Diamagnetic corrections.

Element	Diamagnetic correction in percent
Nitrogen	0.03
Chlorine	0.11
Scandium	0.15
Manganese	0.19
Cobalt	0.21
Molybdenum	0.40
Indium	0.49
Antimony	0.52
Xenon	0.56
Platinum	0.93
Mercury	0.96
Bismuth	1.04

Diamagnetic corrections have been totally omitted in Table I, although there is no doubt concerning their existence. Their application, however, would be clearly illusory in the cases like N and Co, while for heavier elements they are large enough to justify their inclusion. For the isolated atom the magnitude of the diamagnetic corrections is closely calculable and in Table IV we list for completeness' sake appropriate diamagnetic corrections for the neutral atom of each element under discussion in this paper. In computing these values we have consistently made use of the following exact expression:[55]

$$-\Delta H/H = (e/3mc^2)V, \quad (50)$$

where $-\Delta H/H$ is the fractional decrease in field intensity at a nucleus which is at a potential $-V$ produced by the atomic electrons, and where the other symbols have their usual meaning. Eight values for V, determined from Hartree field calculations for different atoms, are conveniently listed by Lamb.[55] We have chosen to use values for V which are linearly interpolated or extrapolated between the given points. Calculations of an independent kind, using hydrogen-like wave functions and the empirical shielding constants proposed by Slater,[56] give values for V which agree with

[53] H. Schüler and T. Schmidt, Z. Physik **98**, 239 (1935).
[54] E. Back and S. Goudsmit, Z. Physik **47**, 174 (1928).
[55] W. E. Lamb, Jr., Phys. Rev. **60**, 817 (1941).
[56] J. C. Slater, Phys. Rev. **36**, 57 (1930).

the above Hartree points to within two percent. The diamagnetic corrections listed in Table IV agree closely with other presentations of the same information.[56,57]

Very small corrections to these results may still be necessary because of the addition of paramagnetic salts to our samples[55] and have likewise been omitted in Table I. Systematic errors of various instrumental kinds have been examined and found to be negligible.[4]

The authors wish to take this opportunity to express their appreciation for the stimulation and guidance of a year's association with Professor Felix Bloch whose contributions to this work are too manifold to detail. We wish also to thank Dr. F. Alder for his assistance during the period of the measurements upon the isotopes of indium and molybdenum.

[57] Properties of Atomic Nuclei, Publication BNL 26 (T-10), Brookhaven National Laboratories, October 1, 1949.
[56] N. Bloembergen and W. C. Dickinson, Phys. Rev. 79, 179 (1950).

PHYSICAL REVIEW VOLUME 81, NUMBER 1 JANUARY 1, 1951

The Disintegration of Rb^{88}*

M. E. Bunker, L. M. Langer,† and R. J. D. Moffat†
Los Alamos Scientific Laboratory, Los Alamos, New Mexico
(Received September 8, 1950)

The radioactive disintegration of Rb^{88} (17.8 min) has been investigated in a magnetic lens spectrometer. Three beta-ray groups are observed having maximum energies of 5.13±0.03, 3.29±0.10, and 2.04±0.15 Mev, with intensities of 66, 19, and 15 percent, respectively. The 5.13 Mev group has a forbidden shape indicating a spin change of 2 units and a parity change. Gamma-rays are found with energies of 0.90, 1.86, and 2.8 Mev. A unique decay scheme is presented giving levels in Sr^{88} at 1.86 and 2.8 Mev. These levels are substantiated by a previous investigation of the disintegration of Y^{88} to Sr^{88}. Spins and parities of Rb^{88}, Sr^{88}, and Y^{88} are discussed in the light of the one particle shell model.

I. INTRODUCTION

THE radioactivity of Rb^{88} has been studied by various investigators. Glasoe and Steigman[1] have identified a 17.8-min. beta-activity with Rb^{88} and have measured the beta-ray end point as 4.6 Mev by absorption in aluminum. G. L. Weil,[2] by cloud chamber measurements, observed two beta-ray groups with energies of 5.0 and 2.5 Mev. The period was measured as 17.5 min. Thus logft for the high energy group was determined as ~7.0, suggesting a forbidden transition.

The gamma-rays of the product nucleus Sr^{88} have been investigated by several groups.[3–7] There is general agreement on gamma-ray energies of approximately 0.908, 1.86, and 2.8 Mev. These investigators have used sources of Y^{88}, which decays to Sr^{88} by positron emission and K electron capture with a half-life of 108 days.

A further investigation of the Rb^{88} beta-radiation employing higher resolution seemed desirable, since the previous work indicated complexity of the spectrum and the possibility of a unique shape.

II. EXPERIMENTAL METHOD

The investigation of the beta- and gamma-radiation from Rb^{88} (17.8 min) was performed with the aid of a large magnetic lens spectrometer.[8] An end-window Geiger tube with a 3.6-mg/cm² mica window and 0.5-inch diameter aperture was employed as a detector. This aperture, together with sources of similar diameter, yielded 6-percent resolution.

Two circular beta-ray sources were prepared from finely powdered Rb_2SO_4. The first was 26 mg/cm² on a 0.0002-inch Al backing and covered with a thin Zapon film. The second source was 30 mg/cm² on a backing of 0.7-mg/cm² nylon, which had been coated with Aquadag to maintain it at ground potential. A thin Zapon cover was again employed.

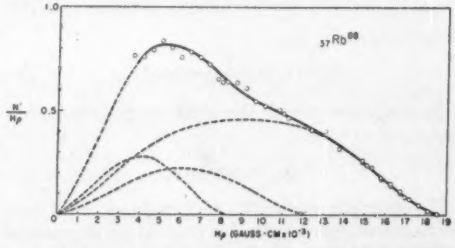

FIG. 1. Beta-spectra of Rb^{88}. The partial spectra are determined from the Fermi plot analysis.

* This document is based on work performed under government contract for the Los Alamos Scientific Laboratory of the University of California.
† Indiana University, Bloomington, Indiana.
[1] G. N. Glasoe and J. Steigman, Phys. Rev. 58, 1 (1940).
[2] G. L. Weil, Phys. Rev. 62, 229 (1942).
[3] G. S. Goldhaber, Phys. Rev. 59, 937 (1941).
[4] J. R. Richardson, Phys. Rev. 60, 188 (1941).
[5] Downing, Deutsch, and Roberts, Phys. Rev. 60, 470 (1941).
[6] G. R. Gamertsfelder, Phys. Rev. 66, 288 (1944).
[7] W. C. Peacock and J. W. Jones, Plut. Proj. Rep. CNL-14, February, 1948, unpublished.
[8] L. M. Langer, Phys. Rev. 77, 50 (1950).

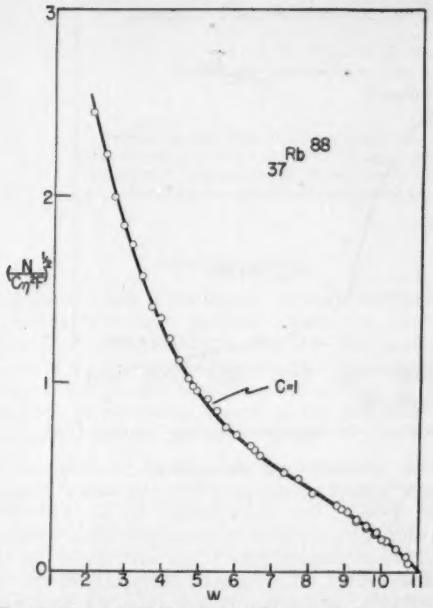

FIG. 2. Conventional Fermi plot. The curve is bent towards the energy axis as it approaches the end point. Values of F were determined from the tables of Moszkowski.

For study of the gamma-radiation, a strong $RbNO_3$ source was irradiated and enclosed in a 0.125-inch walled copper cylinder which stopped all primary beta-radiation. A 0.75-inch diameter, 56-mg/cm² uranium radiator covered the front end of the cylinder.

The sources were irradiated with slow neutrons from a nuclear reactor. Times of irradiation and of the spectrometer runs were chosen so that there resulted no interference from other activities. The radioactive decay of a dummy source was monitored during the spectrometer runs, and the decay period was checked in the spectrometer at various energies. The half-life was measured as 17.8±0.2 min.

III. RESULTS

Figure 1 is a momentum plot of the electron spectrum or Rb^{88}. The obviously complex shape has been resolved into three beta-ray groups on the basis of a Fermi analysis of the data. Figure 2 shows the conventional Fermi plot. In addition to the rise at low energy, there is at high energies a distinct deviation from the straight line characteristic of an allowed transition. The forbidden factor $a=W^2-1+(W_0-W)^2$, applicable to once forbidden transitions with spin change of two units, has been applied to the data and yields the straight line shown in Fig. 3. By appropriate subtractions, the spectrum has been resolved into three groups. The two inner groups are assumed to have the allowed shape. This analysis results in maximum beta-ray energies of 5.13±0.03, 3.29±0.10, and 2.04±0.15 Mev, with corresponding intensities of 66, 19, and 15 percent. The resulting momentum distributions are shown in Fig. 1. The comparative half-lives for the transitions are respectively $\log ft=7.3$, 7.0, and 6.2. It is of interest to note that f, the integral of the *allowed* transition probability over the energy, must here be modified by the factor $a=W^2-1+(W_0-W)^2$. The product $(W_0^2-1)ft$ is then a better indication of the comparative half-life[9] and for transitions with a parity change and spin change of two units should have a value 10^{10}. For the high energy group from Rb^{88}, $(W_0^2-1)ft=0.24\times10^{10}$. Figure 4 shows the observed distribution of photo- and Compton electrons from the uranium radiator. There is evidence of a K photo peak corresponding to a gamma-ray of 0.90 Mev. In addition, a gamma-ray energy of 1.85 Mev is determined by means of the second photo peak and also from the Compton edge. The high energy Compton tail gives a gamma-ray energy of 2.8 Mev.

IV. CONCLUSIONS

The three beta-ray groups of 5.13, 3.29, and 2.04 Mev, together with the observed gamma-ray energies of 0.90, 1.86, and 2.8 Mev, suggest the decay scheme shown in Fig. 5. The 1.86-Mev gamma-ray fits well the energy difference between the two highest energy beta-groups. The level in Sr^{88} indicated by the 2.04-Mev beta-ray is somewhat higher than the gamma-rays of 0.90 and 2.80 Mev would substantiate. Levels in Sr^{88} have been determined by Peacock and Jones[7] in studying the decay of Y^{88} by K capture and positron emission. They

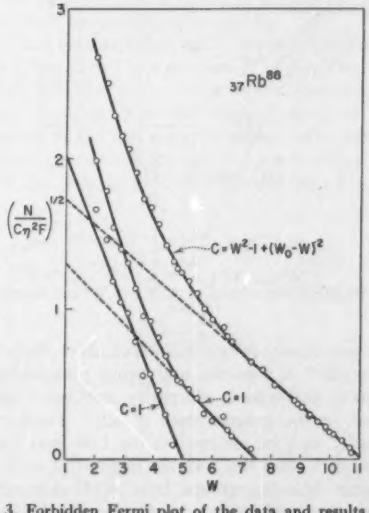

FIG. 3. Forbidden Fermi plot of the data and results of two successive subtractions. It is assumed that the spectra of the inner groups are of the allowed form.

[9] F. B. Shull and E. Feenberg, Phys. Rev. **75**, 1768 (1949).

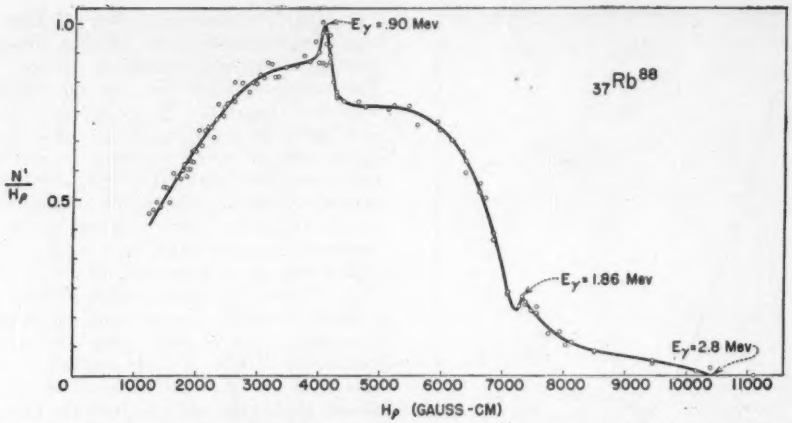

FIG. 4. Compton and photo-electrons ejected from a uranium radiator by the gamma-rays following the decay of Rb^{88}.

found gamma-rays at 0.908, 1.853, and 2.76 Mev. These values are in excellent agreement with the gamma-rays from Rb^{88}. Since the value of 2.04 Mev is the result of two subtractions in the Fermi analysis, it is possible that the error is greater than 0.15 Mev and that the softest beta-ray group actually feeds the 2.8-Mev level. A search for a gamma-ray of about 0.3 Mev which would bridge the energy difference gave negative results.

The spectrum shape of the high energy beta-ray group indicates that the transition is once forbidden

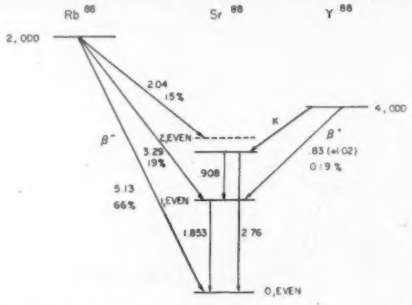

FIG. 5. Disintegration scheme of Rb^{88} and Y^{88} and energy levels of Sr^{88}.

with a spin change of two units; and, since the product nucleus $_{38}Sr^{88}$ is *even-even* and hence presumably has *even* parity and spin 0, *odd* parity and spin 2 may be assigned to the ground state of Rb^{88}. Furthermore, *even* parity may be assigned to the 1.86- and 2.8-Mev levels in Sr^{88}, since the ft values ($\log ft = 7.0, 6.2$) of the two inner beta-ray groups from Rb^{88} suggest once forbiddenness and hence a parity change. Assignment of *even* parity to these levels contradicts the parity assignments made by Peacock and Jones[7] on the basis of internal conversion coefficients. However, more recent calculations of the internal conversion coefficients[10] permit a reinterpretation of the data of Peacock and Jones. Their measurement of the 1.853-Mev gamma-ray is consistent with magnetic dipole radiation and would indicate spin 1 and even parity for the 1.8-Mev level. The reported conversion of the Y^{88} 0.908-Mev gamma-ray is less than the theoretical electric dipole value and must be assumed to be in error. Peacock and Jones' assignment of spin 2 for the 2.8-Mev level in Sr^{88} is still justified on grounds of the relative intensities of positron emission and K electron capture in Y^{88}.

Consideration of the one-particle spin-orbit coupling model,[11] extended to odd-odd nuclei,[12] suggests a spin of 4 and odd parity for the ground state of Y^{88}. This is the result of $p_{1/2}$ for the 39th proton and $g_{9/2}$ for the 49th neutron. These assignments agree both with the order of energy levels obtained theoretically and with the measured spins of Y^{89} and Sr^{87}, for which Z and N respectively are the same as for Y^{88}.

The shell model prediction for the ground state of Rb^{88} is less certain. The 37th proton and 51st neutron are predicted as $p_{3/2}$ and $g_{7/2}$ respectively. The spin of Rb^{87} with 37 protons and Sb^{122} with 51 protons have been measured and substantiate these assignments. However, Rb^{85} and Zn^{67} exhibit $f_{5/2}$ for the 37th nucleon while Sb^{121} and Zr^{91} show $d_{5/2}$ for the 51st nucleon. Thus four possible combinations result in odd parity and *permit* a spin of two units. The $p_{3/2}-g_{7/2}$ combination predicts odd parity and spin 2 uniquely and seems most probable.

The authors wish to express their gratitude to Dr. J. D. Knight for chemical preparation of the source material and to Mr. R. E. Carter for help with some of the measurements. The entire staff at this laboratory has been most cooperative during this investigation.

[10] M. E. Rose, tables privately circulated.
[11] M. G. Mayer, Phys. Rev. **78**, 16 (1950).
[12] L. W. Nordheim, Phys. Rev. **78**, 294 (1950).

Angular Distribution of 14-Mev Neutrons Scattered by Tritons*

J. H. Coon, C. K. Bockelman, and H. H. Barschall
University of California, Los Alamos Scientific Laboratory, Los Alamos, New Mexico
(Received September 5, 1950)

Tritons recoiling from 14-Mev neutrons were observed in a coincidence counter telescope. The angular distribution of neutrons scattered through angles between 180° and 90° in the center-of-mass system was investigated. Absolute differential scattering cross sections were obtained by comparison with hydrogen. No evidence for the presence of disintegration protons or deuterons was found.

I. INTRODUCTION

In continuation of the survey of the interactions of tritons with light particles carried out at this laboratory[1] the angular distribution of 14-Mev neutrons scattered by tritons was investigated. The technique used in the present experiments is similar to that described previously in reports on the scattering of neutrons by protons[2] and by deuterons.[3]

II. PROCEDURE

Neutrons were obtained from the $T(d,n)He^4$ reaction as described previously.[2] Use was made of the neutrons emitted in a direction making an angle of 77° with the direction of the deuteron beam. The energy of the neutrons is calculated to be 14.3 Mev with a maximum energy spread of about ±0.2 Mev. Their number was monitored by counting the alpha-particles from the same reaction.

Interaction of the neutrons with tritons was studied by observing triton recoils originating in a small gas cell and entering the counter telescope shown in Fig. 1. Argon mixed with about 3 percent CO_2 was used for the counter gas. Triple coincidences between the first three counters and quadruple coincidences between all four counters were observed.

The cross section for neutron-triton scattering was measured relative to the known cross section of hydrogen. For this comparison, the gas cell was filled alternately with 4.9 atmos of tritium gas and with the same pressure of normal hydrogen, and the number of recoiling tritons and protons was determined for the two fillings. Gas cell and counter telescope were joined by a 7/16-inch diameter aperture in which was mounted a 1-mil Dural window of stopping power equivalent to 5.0 cm of air.

In order to minimize the number of background coincidence counts produced by disintegration products originating in the wall of the cell, it was lined with clean 20-mil thick platinum sheet. The number of coincidence counts which were not produced by recoiling particles originating in the gas cell was determined by inserting the 20-mil thick platinum shutter shown in Fig. 1 between the gas cell and counter telescope. This shutter could be moved by means of a magnet placed outside the cell. A piece of 1-mil Dural foil, similar to that separating the gas cell and the counter, covered the platinum shutter to account for background particles originating in the Dural window.

The center of the gas cell was located at a distance of 11.3 cm from the neutron source. As a result of the finite sizes of the neutron source, of the gas cell, and of counter apertures, spreads $\Delta\theta$ (see Fig. 1) in the acceptance angle of recoiling particles were introduced as follows: for an angle setting of $\theta=0°$, $\Delta\theta=\pm 9.5°$ for triple coincidences and $\pm 8.0°$ for quadruples; for an angle setting of $\theta=45°$, $\Delta\theta=\pm 12°$ for triples and $\pm 10°$ for quadruples.

To facilitate handling the tritium sample, a small stainless steel tube containing uranium was attached to the gas cell. Whenever it was desirable to empty the cell, the uranium was allowed to absorb the tritium, which could be re-evolved by heating.

For the measurements with normal hydrogen the counters were filled to a pressure of 63 cm. The counter telescope was first set to detect protons recoiling in the forward direction. Since the energy loss of the recoils is smallest in the first counter, a bias curve was taken by observing coincidence counts as a function of the bias of the pulse-height discriminator which received

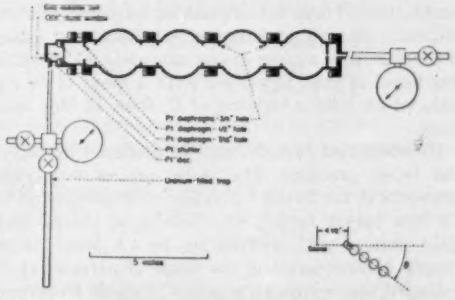

FIG. 1. Section through the axis of the counter telescope, consisting of four cylindrical counters. The telescope was rotated about the center of the gas radiator cell to measure particles recoiling at angles θ, as shown in the lower right-hand corner.

* Work done under the auspices of the AEC.

[1] E. Bretscher and A. P. French, Phys. Rev. **75**, 1154 (1949); Taschek, Jarvis, Hemmendinger, Everhart, and Gittings, Phys. Rev. **75**, 1361 (1949); Hemmendinger, Jarvis, and Taschek, Phys. Rev. **76**, 1137 (1949); Argo, Gittings, Hemmendinger, Jarvis, and Taschek, Phys. Rev. **78**, 691 (1950).

[2] H. H. Barschall and R. F. Taschek, Phys. Rev. **75**, 1819 (1949).

[3] J. H. Coon and R. F. Taschek, Phys. Rev. **76**, 710 (1949).

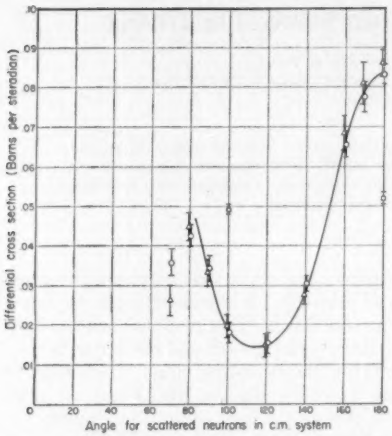

FIG. 2. Angular distribution data obtained by observing triple (circles) and quadruple (triangles) coincidence counts produced by recoil tritons. The squares are observations of recoil protons under similar conditions.

pulses from this counter. It was found that the coincidence counting rate was independent of bias over a wide range of biases. For the final determination of the number of recoil protons, biases on all four counters were set corresponding to the middle of the bias plateau of the first counter. Subsequently the number of proton recoils at 40° was determined, the bias settings for these data being the same as for the observations at 0°.

Since the tritium available for the present measurements contained about 35 percent hydrogen, and since it was desired to detect any products of the disintegration of tritium, it was necessary to establish the identity of the particles producing coincidence counts. For this purpose, the ranges and differences in specific ionization of the particles were used. Range determinations were carried out by varying the argon pressure in the counters.

With tritium in the gas cell, the axis of the counter telescope was set to detect particles at 0°, and the biases adjusted to detect all particles, including protons, deuterons (if any), and tritons. A predominant group of particles with a range of approximately 60 cm of air was found in good agreement with a range of 58 cm deduced for tritons recoiling at 0° from 14-Mev neutrons.

Disintegration particles may be produced by $(n,2n)$ and $(n,3n)$ processes. The $(n,2n)$ process may yield deuterons in the forward direction with energies up to 7.8 Mev (44-cm range), while the $(n,3n)$ process may yield protons with energies up to 4.8 Mev (32-cm range). Measurements of the range of particles at 0° indicated that within an accuracy of about 10 percent there were no particles with ranges between 55 cm and 9 cm, the lower limit of detection. Nine cm is the range of 2.3-Mev protons and 3.0-Mev deuterons. Therefore, these measurements do not indicate the presence of any disintegration particles, though they do not exclude disintegration processes producing mostly particles with ranges of less than 9 cm.

From the range measurement, the hydrogen impurity in the tritium sample could be determined, since with high pressure in the counters only the recoil protons had sufficient range to cause coincidence counts. A comparison with the number of counts observed when the gas cell contained normal hydrogen indicated a percent impurity of 35 ± 4.

With tritium in the gas cell, angular distribution measurements were made using 15-cm pressure in the counters. Since the foregoing measurements indicated that there were few, if any, detectable disintegration particles, adjustments were determined for measuring the angular distribution of the triton recoils over as great an angular range as possible. Tritons recoiling at 55° with respect to the incident neutrons in the laboratory system had barely enough range to reach the third counter and cause a triple coincidence count. When the angular resolutions given above are taken into account, it is found that at angle settings greater than 43° some of the recoiling tritons would be missed. Bias curves were taken at 0° and at 50° in the manner described for the case when the gas cell was filled with hydrogen. The energy loss of recoil tritons and recoil protons in the first counter for different angle settings is such that it is desirable to change the bias (in channel 1) with angle if one wants to be sure of detecting all the tritons but none of the protons. This bias change was made on the basis of the measured bias curves and the calculated change in energy loss with angle.

III. RESULTS

The results of the angular distribution measurements are shown in Fig. 2. Differential cross sections $\sigma(\phi)$ in barns/steradian are plotted in the center-of-mass system against the scattering angle ϕ of the neutron. Since, for the data taken with tritium in the gas cell, the biases were set so as to count all recoil tritons but no recoil protons, and since the results of the range measurements indicate that there is no measurable number of disintegration protons, the curve in Fig. 2 represents the angular distribution of $n-T$ scattering. Data obtained with hydrogen in the gas cell are also shown. For deducing the absolute value of the cross section, 0.050 barn/steradian was used for the differential cross section for scattering of neutrons by protons through 180° in the center-of-mass system.[2] Errors indicated in Fig. 2 are the standard errors arising from counting statistics. The average ratio of the observed triple coincidence count to the quadruple count was 1.98, in good agreement with the geometric solid angle ratio of 1.96.

The error in the scale of absolute values of $\sigma(\phi)$ is estimated to be ±20 percent. This estimate allows for a 10 percent uncertainty in the neutron-proton scat-

tering cross section, 6 percent uncertainty in the purity of the tritium sample, and 5 percent statistical error. Errors introduced by Rutherford scattering are estimated to be negligible. The finite angular resolution will cause some broadening of the peak in the angular distribution at $\phi=180°$.

For the $n-T$ angular distribution measurements the background count observed with the platinum shutter in place averaged 30 percent for triple coincidences and 20 percent for quadruples. Accidental coincidences were calculated to contribute a background of less than one part in 10^4. For the data with hydrogen in the gas cell the corresponding backgrounds were about 20 percent and 10 percent. These backgrounds were lower because the higher counter gas pressure (63 cm instead of 15 cm) did not allow short range background particles to traverse all counters.

Integration of $\sigma(\phi)$ as plotted in Fig. 2 from 90° to 180° gives a value of 0.17 barn. If, as might be expected, the total cross section of tritium is greater than that of hydrogen (0.64 barn), there must either be a large peak in the angular distribution curve for scattering in the region from 0° to 90°, or a disintegration process which contributes a large fraction to the total cross section.

It is a pleasure to acknowledge helpful discussions with Dr. R. F. Taschek and to thank Mr. R. W. Davis for taking much of the data.

PHYSICAL REVIEW VOLUME 81, NUMBER 1 JANUARY 1, 1951

Velocity Dependent Interactions and Nuclear Shells*

C. H. BLANCHARD† AND R. AVERY‡
University of Wisconsin, Madison, Wisconsin
(Received August 30, 1950)

An investigation is made of the energy splitting of the two possible j values, $l\pm\frac{1}{2}$, of a single nucleon outside a closed shell resulting from the assumption of certain velocity dependent terms in the nucleon-nucleon interaction.

I. INTRODUCTION

THE modification[1] by Mayer of the nuclear shell model demands spin-orbit coupling such that the single nucleon state with $j=l+\frac{1}{2}$ is displaced in energy well below the state with $j=l-\frac{1}{2}$. It was suggested in a previous communication[2] that the splitting might be accounted for by terms in the nucleon-nucleon interaction which are linear in the nucleon momenta.

II. THEORY

We have considered the system of a single nucleon outside a nuclear core consisting of a closed shell of nucleons, and have investigated the splitting between the two possible j values which results from the velocity dependent interaction of the outside nucleon with the closed shell. The following notation is used for the quantum numbers involved:

k=orbital angular momentum of each of the $4(2k+1)$ nucleons in the closed shell (two neutrons and two protons in each of the $2k+1$ states).

l=orbital angular momentum of the outside nucleon.

$j=l\pm\frac{1}{2}$=total angular momentum of the outside nucleon, and hence, of the entire system.

Let $U(k,l,j)$ be the average velocity dependent interaction energy of the outside nucleon with the closed shell. The difference

$$\Delta U(k,l)=U(k,l,l+\tfrac{1}{2})-U(k,l,l-\tfrac{1}{2})$$

gives the first-order splitting. Neither central nor tensor static forces can contribute to the splitting in first order.

It follows from the fact that the average velocity dependent interaction energy of an *entire* k shell with the l shell must vanish because of the transformation properties of the interactions, and from the ratio of the degeneracies of the $j=l+\frac{1}{2}$ and $j=l-\frac{1}{2}$ states, that

$$(l+1)U(k,l,l+\tfrac{1}{2})=-lU(k,l,l-\tfrac{1}{2}).$$

Thus

$$\Delta U(k,l)=[(2l+1)/l]U(k,l,l+\tfrac{1}{2})$$

and only the case $j=l+\frac{1}{2}$ need be evaluated.

The velocity dependent forces may be enumerated as

TABLE I. Energy splitting due to velocity dependent interactions.

n	$S_{\alpha\beta}{}^{(n)}T_{\alpha\beta}{}^{(n)}$	$\Delta U(k,l)$
1	$(\sigma_\alpha+\sigma_\beta)\frac{1}{2}(\tau_{\alpha z}+\tau_{\beta z})$	$Q(A-B)$
2	$(\sigma_\alpha+\sigma_\beta)\frac{1}{2}(1+\tau_{\alpha z}\tau_{\beta z})$	$A-B$
3	$(\sigma_\alpha+\sigma_\beta)\frac{1}{2}(3+\tau_\alpha\cdot\tau_\beta)$	$\frac{1}{2}(A-B)$
4	$(\sigma_\alpha+\sigma_\beta)\frac{1}{2}(1-\tau_{\alpha z}\tau_{\beta z})$	A
5	$(\sigma_\alpha-\sigma_\beta)\frac{1}{2}(\tau_{\alpha z}-\tau_{\beta z})$	QA
6	$[\sigma_\alpha\times\sigma_\beta]_z\frac{1}{2}[\tau_\alpha\times\tau_\beta]_z$	QB

* This work was supported in part by the AEC.
† Now at National Bureau of Standards, Washington, D. C.
‡ Now at Argonne National Laboratory, Chicago, Illinois.
[1] M. G. Mayer, Phys. Rev. 78, 16 (1950).
[2] Blanchard, Avery, and Sachs, Phys. Rev. 78, 292 (1950).

TABLE II. Values of A and B for particular values of k and l.

k	l	A/V_0	B/V_0
0	1	0.25	−0.25
	2	0.18	−0.06
	3	0.11	−0.01
	4	0.06	−0.003
	5	0.03	−0.0008
1	2	0.28	−0.11
	3	0.22	−0.06
	4	0.14	−0.02
2	3	0.20	−0.04

in reference 2:

$$V_{\alpha\beta}^{(n)}=J(|\mathbf{r}_\alpha-\mathbf{r}_\beta|)[(\mathbf{r}_\alpha-\mathbf{r}_\beta)\times(\mathbf{p}_\alpha-\mathbf{p}_\beta)]\cdot\mathbf{S}_{\alpha\beta}^{(n)}T_{\alpha\beta}^{(n)}$$

with n running from 1 to 6. The results of the calculation of the splitting are summarized in Tables I and II.

In Table I, $Q=+1$ if the outside nucleon is a neutron and -1 if it is a proton. A and B are the following integrals over all space:

$$A=\frac{2(2k+1)(2l+1)\hbar}{(4\pi)^2}\int\int[f(r_1)]^2[g(r_2)]^2\times J(|\mathbf{r}_1-\mathbf{r}_2|)\left\{1-\frac{r_1}{r_2}\mu\right\}d^3r_1d^3r_2,$$

$$B=\frac{2(2k+1)(2l+1)\hbar}{l(l+1)(4\pi)^2}\int\int f(r_1)g(r_2)J(|\mathbf{r}_1-\mathbf{r}_2|)\times\left\{l(l+1)\left(1-\frac{r_1}{r_2}\mu\right)P_k(\mu)P_l(\mu)+(1-\mu^2)\left(1-\frac{r_1}{r_2}\mu\right)P_k'(\mu)P_l'(\mu)-\frac{r_1}{r_2}(1-\mu^2)P_k(\mu)P_l'(\mu)+r_1r_2(1-\mu^2)P_k(\mu)P_l'(\mu)\times\left[\frac{1}{r_2}\frac{\partial}{\partial r_2}-\frac{1}{r_1}\frac{\partial}{\partial r_1}\right]\right\}f(r_2)g(r_1)d^3r_1d^3r_2,$$

where $\mu=(\mathbf{r}_1\cdot\mathbf{r}_2)/r_1r_2$; $f(r)$, $g(r)$ are the normalized radial wave functions for the k orbits and l orbit, respectively; P_m is the Legendre polynomial of degree m, and P_m' its derivative.

The integrals A and B were evaluated for a few low values of k and l. In order to do so, it is of course necessary to assign definite radial dependences to the wave functions and to the interaction. The choice made was:

$$f(r)\sim r^k e^{-ar};\quad g(r)\sim r^l e^{-ar};\quad J(r)=V_0e^{-br}/\hbar br,$$

where V_0 has the dimensions of energy; $a/b=1$.

With this choice of parameters, the numerical results obtained are given in Table II.

The results given in Table II depend on a and b only through their ratio, but they are extremely sensitive to the choice made, the splitting decreasing very rapidly if a/b is decreased.

If the strength, V_0, of the velocity dependent interaction is taken to be comparable to that of the usually assumed static forces, then splittings of the order of magnitude of those hypothesized for the spin-orbit coupling shell model can be expected. For the interactions $V^{(2)}$, $V^{(3)}$, $V^{(4)}$, V_0 must be negative if the state $j=l+\frac{1}{2}$ is to lie lower. For $V^{(1)}$, $V^{(5)}$, $V^{(6)}$, however, the presence of the factor Q has the following consequence. With a definite sign for V_0, the total angular momentum state that is lowest depends on whether the outside nucleon is a neutron or a proton. Since no such charge-dependent doublet inversion has been observed experimentally,[3] this argues strongly against $V^{(1)}$, $V^{(5)}$, $V^{(6)}$ as possible interaction functions.

Since $V^{(4)}$ can be discarded by the considerations of reference 2, the only velocity dependent interactions which remain with no serious shortcomings are $V^{(2)}$ and $V^{(3)}$. $V^{(2)}$ is charge dependent, giving the same forces for the neutron-neutron and proton-proton interactions but no forces in the neutron-proton interaction. $V^{(3)}$ is charge independent; $\mathbf{S}_{\alpha\beta}^{(3)}T_{\alpha\beta}^{(3)}$ can be written as $(\boldsymbol{\sigma}_\alpha+\boldsymbol{\sigma}_\beta)(1-P_{\alpha\beta}^X)$, where $P_{\alpha\beta}^X$ is the space exchange operator. It is interesting that $V^{(3)}$ is just the interaction inferred from high energy scattering data by Case and Pais.[4]

It is to be noted that rejection of $V^{(5)}$ and $V^{(6)}$ would weaken one of the arguments of reference 2 for the introduction of velocity dependent interactions: the possibility of resolving the magnetic moment anomalies of H^3 and He^3 through interaction moments. It was found that only $V^{(5)}$ and $V^{(6)}$ allowed such a possibility.

The suggestions and advice of Professor R. G. Sachs have been of value throughout the course of this work.

[3] $V^{(1)}$ gives a clearcut contradiction with observation, since it gives interactions only between like nucleons. Thus, for a particular choice of V_0, if the next neutron added after a closed shell of neutrons went into the $j=l+\frac{1}{2}$ state, then the corresponding proton state would be $j=l-\frac{1}{2}$, and neutron and proton magic numbers would not coincide. $V^{(5)}$ and $V^{(6)}$, on the other hand, give interactions only between unlike nucleons. Accordingly, we compare the spins of two nuclei: (N_1, Z_1) and (N_2, Z_2), where $Z_1=N_2$, and N_1 and Z_2 correspond to closed shells in the sense of the present calculation. Only one applicable case has been found. $Sb^{121}(I=5/2)$ and $Zr^{91}(I=5/2)$. This case certainly gives no indication of charge dependent doublet inversion. For purposes of interpretation, it does not seem to be necessary to have closed shells in the strict sense of the calculation, since the splittings found are proportional to the size of the core. Thus we conclude that $V^{(5)}$ and $V^{(6)}$ would actually give effects like those of $V^{(1)}$, and can be excluded.

[4] K. M. Case and A. Pais, Phys. Rev. **80**, 203 (1950).

Deuteron-Proton Scattering at 10.0 Mev by a Coincidence Method*

H. J. KARR,† R. O. BONDELID,† AND K. B. MATHER‡
Physics Department, Washington University, St. Louis, Missouri
(Received July 3, 1950)

A description is given of a scattering chamber possessing several novel features. This chamber was applied to the determination of absolute cross sections for elastic scattering of 10.0-Mev deuterons by protons, over a range of angles from 45° to 160° in the center-of-mass system. Two independently movable proportional counters were connected in coincidence and set at appropriate angles with respect to the incident beam so that coincidences were recorded between deuterons entering one counter and their recoil protons entering the other. The advantages and disadvantages of this system are made clear. The scattering media were thin Nylon and polyethylene-terephthalate foils. The relative cross sections reported here are believed to be accurate to ±3.5 percent and the absolute values to ±5 percent. Some comparison is made with the *mhbw* theory of Buckingham and Massey. Agreement is excellent over a considerable range of angles; but the theoretical curve is shallower than the experimental, and considerable anomaly appears at large angles. The experimental curve rises very steeply beyond about 120° in the center-of-mass system.

I. INTRODUCTION

THIS is the first of a series of articles reporting experiments on the scattering of charged nuclear particles. The scattering project at Washington University was commenced early in 1947 and entailed the construction of two independent scattering chambers, (1) detecting both scattered and recoil particles with proportional counters connected in coincidence,[1] (2) using photographic plates[2] to record tracks of scattered particles. The present article describes the coincidence chamber and auxiliary equipment together with the complete results obtained on the scattering of 10-Mev deuterons by protons. *P-d* scattering has been examined previously at 830 kev,[3] at 200–300 kev,[4] at 4.2 Mev[5] and very extensively and accurately at a set of energies from 1.5–3.5 Mev.[6] The present work extends *p-d* scattering to 5.0 Mev. The experiment was carried out as *d-p* at 10 Mev, which is equivalent to *p-d* at 5 Mev.

II. METHOD

The coincidence technique consisted in counting the number of electrical coincidences between two proportional counters which were set at such angles with respect to each other and to the incident beam that each scattered particle entering one counter resulted in the recoil particle *from the same collision* entering the other counter. One of the collision particles entered a proportional counter through a small slit, the size of which determined the counting rate and angular resolution. Its dimensions therefore had to be known accurately. It will be referred to as the *defining slit* and that counter as the *defining counter*. In *d-p* scattering either the deuterons or protons may be defined, but for consistency in this section reference will always be to the case of deuteron definition.

Associated with every scattered deuteron in the *d-p* scattering process there is a recoil proton referred to here as the conjugate proton. Moreover, there is a definite angular relationship between the path of an incident deuteron, a scattered deuteron, and a conjugate proton (Sec. III). In order to record a coincidence for every deuteron that entered the defining counter, it was imperative that every conjugate proton should enter the other counter. The *conjugate slit* had to be large enough to permit this entrance. It was merely a problem of geometry to calculate the conjugate paths of protons corresponding to every conceivable path by which a deuteron could enter the defining slit. The contour at the conjugate counter which would embrace all of these paths will be called the "geometrical conjugate pattern." The conjugate slit had to be larger than this pattern by a safety factor to allow for slight imperfections of machining and alignment, etc., and also because a certain "magnification" of the pattern

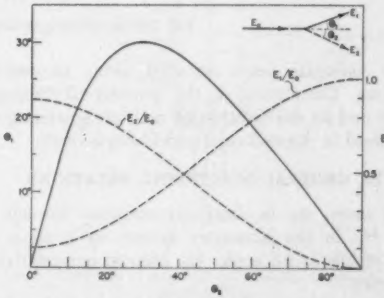

FIG. 1. Angle of deuteron scattering, Θ_1, *versus* angle of proton recoil, Θ_2, in laboratory coordinates. Also, variation of relative energy of deuteron, E_1/E_0, and of proton, E_2/E_0, with Θ_2.

* Assisted by the joint program of the ONR and the AEC.
† Now at Los Alamos, New Mexico.
‡ Now at Birmingham University, Birmingham, England.
[1] R. R. Wilson and E. C. Creutz published the first scattering data obtained by this technique (*p-p* scattering), Phys. Rev. **59**, 916 (1940); also Phys. Rev. **71**, 339 (1947), and subsequent papers.
[2] To be published.
[3] Tuve, Heydenberg, and Hafstad, Phys. Rev. **50**, 806 (1936).
[4] R. F. Taschek, Phys. Rev. **61**, 13 (1942).
[5] Heitler, May, and Powell, Proc. Roy. Soc. **190A**, 180 (1947).
[6] Sherr, Blair, Kratz, Bailey, and Taschek, Phys. Rev. **72**, 662 (1947).

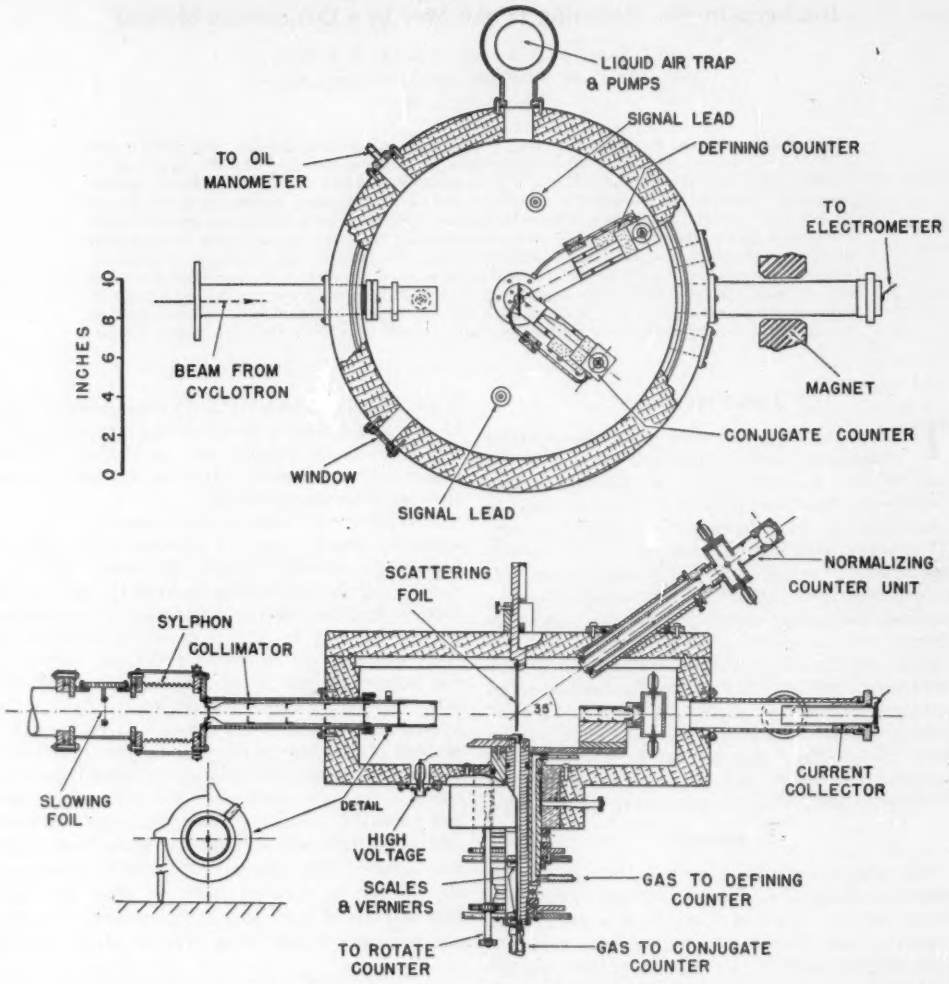

FIG. 2. Plan and side elevation of coincidence scattering chamber.

of the conjugate beam occurred owing to multiple scattering. Calculation of the geometrical conjugate pattern and its modification by multiple scattering will be outlined in Appendices I and II respectively.

III. GENERAL SCATTERING RELATIONS

If a mass, m_1, is elastically scattered through an angle, Θ_1, in the laboratory system by a mass, m_2, which recoils at an angle, Θ_2, then in non-relativistic mechanics

$$m_1/m_2=\sin(2\Theta_2+\Theta_1)/\sin\Theta_1,$$

or

$$\tan\Theta_1=\sin 2\Theta_2/[(m_1/m_2)-\cos 2\Theta_2].$$

Θ_1 is graphed against Θ_2 in Fig. 1. For a given mass ratio a specification of Θ_2 uniquely determines Θ_1. If E_0 is the energy of m_1 before collision, E_1, its energy after collision, and E_2, the recoil energy of m_2, then

$$E_2=4E_0m_1m_2\cos^2\Theta_2/(m_1+m_2)^2=(8/9)E_0\cos^2\Theta_2,$$
$$E_1=E_0-E_2=E_0\{1-(m_1/m_2)[\sin\Theta_1/\sin(\Theta_2+\Theta_1)]^2\}.$$

Calculations show that for 10-Mev deuterons ($\beta\sim 0.1$) the relativistic correction to these equations is very small. Its effect was taken into account in reconciling deuteron-defined with proton-defined data.

IV. DESCRIPTION OF THE APPARATUS

A. Cyclotron and Slit System

The source of deuterons was the Washington University 45-inch cyclotron. The primary beam had considerable energy spread at the target chamber, probably about 1 Mev. However, in the scattering experiment a narrow strip of the beam was extracted by a 5-mm slit at the target chamber. The particles passing through this slit in the correct direction could pass down a 2½-inch tube made in several sections connected by sylphons, the whole being about 270 cm long. The fringing field of the cyclotron dispersed the beam into curved trajectories of slightly different radii of curvature, the tube being curved to accommodate the deflection which totalled approximately 9°. At the far end of the tube a portion of the dispersed beam was selected by a second slit. A small section of this beam then entered the collimator of the scattering chamber. The slit system described served the dual purpose of providing a very well collimated beam and of rendering the beam reasonably monoenergetic (~1 percent).

B. Slowing Foil and Sylphon

A brass box and sylphon were inserted between the last tube section of the slit system and the flange of the collimator. The box mounted a ring to which aluminum foils could be clamped. This arrangement was for slowing the 10-Mev beam for the study of scattering at lower energies (not reported here). The sylphon served as a flexible connector for aligning the chamber with the beam.

C. Collimator

A semi-schematic illustration of the scattering chamber[7] is shown in Fig. 2. The collimator comprised two concentric brass tubes, the inner of which could slide and rotate in the outer. The inner tube mounted two defining slits (the first and next to last in Fig. 2) 10.0 inches apart. The other slits in the collimator were essentially baffles intended to reduce the effect of slit scattering which occurred at the edges of both defining slits. The most important baffle was the last one, which controlled the size of the cone of particles which sprayed from the second defining slit. For the collimator arrangement of the December and April runs the maximum angle of spray[8] measured from the axis of the beam was about 3°.

The collimator and defining slits used for the December and April runs were rectangular[9] in shape and for the September run they were circular.

The dimensions of the beam at the scattering foil entered into calculations of the geometrical conjugate pattern and in application of a correction, if necessary, for loss of counts when the conjugate slit size was inadequate. It was difficult to calculate the cross section of the beam at the scattering foil because of uncertainty as to the state of collimation of the particles reaching the chamber from the cyclotron. As this was important, it was measured. A photographic plate of the Nuclear Research kind was placed at the center of the chamber in the normal position of the foil. A very short exposure was given with the cyclotron, and the plate was withdrawn, developed, and scanned. The numbers of deuteron tracks per unit area were counted over the area of exposure. This observation established the beam pattern including penumbra effects. The maximum dimensions were 0.110 cm×0.241 cm. The dimensions of the collimator slits were 0.103 cm×0.208 cm.

The collimator slits had one dimension considerably greater than the other for a purpose. At certain angles the height of the beam had to be small while the width was relatively unimportant, and *vice versa* at some other angles. Hence, by rotation of the collimator through 90° the more favorable condition for the pair of angles being studied was available. A device was attached to the collimator to assist in making this change accurately (see detail, Fig. 2). It consisted of a ring with two projecting teeth whose faces were on perpendicular diameters of the ring. This was fastened to the inner tube of the collimator so that when one face was horizontal the slit was horizontal also. To facilitate

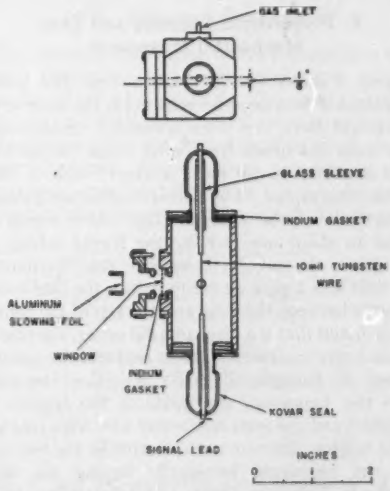

FIG. 3. Schematic of proportional counter, and mount for slowing foils.

[7] Our design was influenced to some extent by the Los Alamos scattering chamber, the details of which were made available to us late in 1946.

[8] This observation considers single scattering only. Particles can be doubly scattered and emerge with virtually any angle less than 90°.

[9] From the considerations of Appendix I it can be seen that the conjugate slit size and shape are dependent on the size and shape of the collimator and defining slits. For a given counting rate (i.e., solid angle $d\Omega$) the rectangular slits permit a more efficient use of the available conjugate area.

setting either face horizontal a post was machined to a length equal to the height of the axis of the collimator from the floor of the chamber.

D. Chamber

The chamber was turned from a solid aluminum forging. The external diameter was 20 inches, internal diameter 16.5 inches, and internal depth 5.5 inches. The lid was located by a tongue and groove and sealed with a rubber gasket. Seven holes were bored in the cylindrical wall of the chamber for attachment of various devices needed or potentially needed. High precision was demanded in the machining of the chamber. In particular, the axis of the collimator had to intersect and be perpendicular to the axis of rotation of the counters. The tolerance on this was ± 0.001 inch.

E. Current Collector

After traversing the chamber the beam was collected by a Faraday cup insulated from the supporting tube by a polystyrene ring. The far end of the cup was covered by nickel gauze and a glass disk painted with a mixture of willemite and clear Glyptal. The painted glass fluoresced under bombardment and aided alignment of the chamber. The Faraday cup was connected by a coaxial line to the integrator (Sec. VI). A permanent magnet ($\sim$500 gauss) was mounted over the current collector to avoid errors in charge measurement from secondary electron effects. (Apparently any effect was negligible, since removing the magnet did not affect the rate of integration.)

F. Proportional Counters and Their Mechanical Movement

Figure 3 shows one of the counters. The internal dimensions of both counters were made the same so that they would have the same operating characteristics. They were machined from solid brass blocks to an inside diameter of 1.0 inch. A center wire of 10-mil tungsten was supported by Kovar-to-glass seals soldered to the ends of the counter. The active region was limited to about one inch by the Kovar tubing projecting into the counter from each seal. Surrounding each tube was a glass sleeve to reduce the likelihood of discharge between the tube and the top of the counter. (It was found that if a discharge did occur, the counters became hypersensitive to gamma-rays and the enormous increase in background made operation impossible. When this happened, the inside of the counter was repolished and the seals and center wire were renewed.)

The window size was not the same in the two counters, the conjugate necessarily having the larger. Aluminum, Formvar, Nylon, and polyethylene-terephthalate (referred to subsequently as p.e.t.) windows were used at various times; but the p.e.t. proved most reliable. As the conjugate counter window was 0.55 inch in diameter and the counter pressure about 20 cm Hg, the window material required considerable tensile strength. P.e.t., initially 0.25 mil thick, was stretched to about 0.1 mil for the defining counter and to about 0.2 mil for the conjugate. (Neither figure was known accurately.) Gas-tight windows were obtained by sealing the p.e.t. between indium gaskets. Provision was made for the insertion of aluminum slowing foils in front of the windows. A number of small cylinders were prepared, each mounting an aluminum foil of known thickness (see Fig. 3). These could be plugged into the counter aperture so that the foil was close to the window. The counters operated at about 20 cm pressure with a mixture of argon and 5 percent CO_2. The counters were pumped and refilled several times per 24 hours. The walls of the counters were at high potential (-1000 v) and the center wire at signal level. With this system, disturbances produced by high voltage leakage in cables and decoupling condensers were minimized, since the high voltage circuit was connected to the amplifier input only via the small interelectrode capacitance of the counter. Also, this system permitted direct coupling of the center wire to the amplifier grid input without a coupling condenser. High potential and signal leads to the counters were brought into the chamber via Kovar seals through three ports in the bottom (Fig. 2). Within the chamber, flexible insulated leads connected these Kovar seals to the counters. The flexible leads proved highly satisfactory.

A slit system was set into a brass block in front of each counter. Only the defining slit immediately in front of the defining counter was critical. The area, ΔA, of this slit, together with its distance, R, from the center of the scattering foil, determined the solid angle $\Delta\Omega = \Delta A/R^2$ to which the counting rate was directly proportional. The shape of the defining slit had to be determined by the same considerations that applied to the collimator slits. At certain angles it was necessary to have a small slit height, while at other angles the slit width had to be curtailed (Appendix I). The defining slit was made rectangular, 0.2582 ± 0.0005 cm $\times 0.1036 \pm 0.0005$. The length, R, was 15.40 ± 0.05 cm. Hence $\Delta\Omega$ was $1.128 \pm 0.015 \times 10^{-4}$ steradian. The defining slit also determined the angular resolution[10] ($2\Delta\alpha$ in the notation of Appendix I). With foil scattering the resolution was not constant, since the width of foil seen by the counter decreased as $\cos\alpha$ with increasing angle α of the defining counter from the beam. In the worst case (collimator and defining slits horizontal and α small) $2\Delta\alpha \simeq 1.8°$. In general it was considerably less. Both slits were vertical for all the proton-defined data ($2\Delta\alpha \simeq 0.8°$). The conjugate slit was rectangular (1.01

[10] A small error was caused by the finite slit width at certain angles where the cross section was changing rapidly. At angles $\alpha = \alpha^*$, where the effect was not negligible, a small correction (usually about 1 percent) was applied by multiplying by the ratio $n(\alpha^*)2\Delta\alpha / \int_{\alpha^*-\Delta\alpha}^{\alpha^*+\Delta\alpha} n(\alpha)d\alpha$. The correction was required only in the region of small angles so $n(\alpha)$ was given the Rutherford form.

cm×0.85 cm) and 10.08 cm from the foil. All other slits in front of the two counters were merely baffles to shield the counters from collimator slit scattering.

As the counter walls were at high potential, the counters had to be supported on plastic insulators. Likewise, gas leads to the counters, introduced through the rotary joint at the bottom, were broken and joined by plastic sleeves with O-ring vacuum joints.

The two counters had to be capable of independent rotation about the cylindrical axis of the chamber. In the present design this rotation was achieved by means of two concentric brass shafts passing through the bronze bushing in the hub at the bottom of the chamber. An arm was attached to the top of each shaft and a brass block containing the slits and supporting the counter was seated on each arm. Vacuum seals where the shafts passed through the bushing were made with O-rings. These were quite satisfactory. A five-inch gear wheel and a calibrated angle scale were mounted on each shaft. Angles could be read to 0.1° by the scales and verniers.

G. Foil Holder

A 0.75-inch diameter solid brass rod passed through the center of the lid of the chamber. An O-ring seal in the lid allowed the rod to slide and rotate freely without influencing the vacuum. Foils were attached by clear Glyptal to a 2-inch×2-inch brass frame mounted on the lower end of the rod. The foil holder was calibrated for vertical positioning and orientation with respect to the beam direction. While this defined an area vastly greater than was actually traversed by the beam, it was desirable to keep the frame itself as far from the path of the beam as possible.

H. Normalizing Counter Unit

The counters shown in Fig. 2 mounted on the chamber lid were intended to provide a normalizing count to be used as a supplement to the current collector as a measure of the incident particle flux. Probably because of unsuitable design of the counters themselves, leading to poor pulse-height characteristics, this arrangement was not actually used for any of the data reported in this paper.

I. Vacuum System

The chamber was evacuated by a Distillation Products oil diffusion pump backed by a Duo Seal mechanical pump. During operation the gate valve in the slit system was open, and the scattering chamber was directly connected to the main vacuum of the cyclotron. The operating pressure was 10^{-4} mm Hg. The counters were pumped by opening them to the main vacuum of the chamber. Design of the vacuum system of this chamber owed much to the versatility of O-ring seals.[11]

[11] An excellent description of O-ring seals was given by F. N. D. Kurie, Rev. Sci. Instr. 19, 485 (1948).

J. Checking and Alignment of the Scattering Chamber

Numerous checks were made on the accuracy of machining and assembly of the equipment, but the following were the most significant. A mandril was turned so that one end fitted the ports for the collimator and current collector and the other end fitted the blocks in which the counter slit systems were inserted. Each counter arm was swung round in turn to align with the collimator port and the mandril pushed through the port into the slit block. For this operation to be possible the slit block had to be at the correct height. At the same time the angle scale for that counter was set at 180.0°. The same procedure was repeated at the current collector port. If the collimator and current collector ports were diametrically opposite, the angle scales should then have read zero. Satisfactory checks were obtained (±0.05°).

The chamber was aligned by centering the fluorescent spot caused by the impact of the deuteron beam on the painted glass plate of the current collector. Centering was facilitated by placing a cap with a 0.25-inch central hole over the end of the current collector and centering with respect to the hole. The alignment was done remotely with a mirror and telescope system. Centering was probably correct to within 0.03 inch at the end of the current collector, which corresponded to 0.015 inch at the foil. Vertical alignment was somewhat more critical than horizontal. A vertical error could cause some of the conjugate paths to lie too high or too low for acceptance by the conjugate slit.

K. Electronic Equipment

The counters were connected to preamplifiers which, during operation, sat directly under the scattering chamber to permit short leads. The preamplifiers were connected by 150 feet of coaxial cable stretching from the cyclotron pit to the control room in which the main linear amplifiers, discriminators, coincidence circuit, and scalers were located. Figure 4 is a block diagram of the electronic equipment. Design of the preamplifier

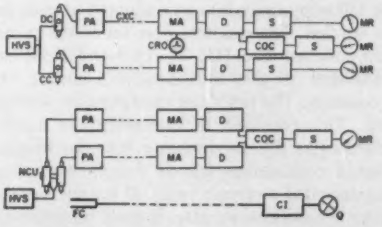

FIG. 4. Block diagram of basic electronic equipment. Abbreviations are as follows: DC-defining counter, CC-conjugate counter, NCU-normalizing counter unit, HVS-high voltage supply, PA-preamplifier, CXC-150 feet of coaxial cable, MA-main linear amplifier, D-discriminator, S-scaler, MR-mechanical register, CRO-cathode-ray oscilloscope, COC-coincidence circuit, FC-Faraday cup, CI-current integrator, Q-quadrant electrometer.

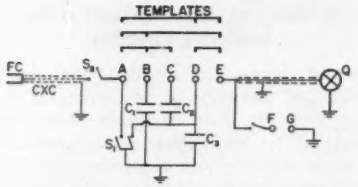

FIG. 5. Current integrator circuit. Connecting terminals ABCDE with the various templates shown above, resulted in different rates of deflection. Nominal values of the condensers were $C_1=1$ μf, $C_2=0.01$ μf, and $C_3=0.1$ μf. When the electrometer was calibrated, the potentiometer was applied at FG. S_1 and S_2 were switches. All switch contacts were platinum to avoid contact potentials. FC-Faraday cup, Q-quadrant electrometer, and CXC-coaxial cable.

and amplifier was due to Elmore, coincidence circuit to Sands, and discriminator and scale of 64 to Higginbotham.

During a run the amplifier operation was monitored with an oscilloscope. Normal cyclotron operation caused no electrical disturbances, whereas faulty operation such as parasitic oscillations were picked up by the amplifiers. The electronic equipment was checked daily by connecting a pulser to the preamplifiers. The output of the amplifiers was checked with a synchroscope. In this way a change in the amplification could be detected. The scalers and coincidence circuit were checked by comparison of the number of counts recorded by each scaler when operated simultaneously. All three scalers should give the same result. The dead time and resolving time of the circuit were measured with a sliding pulser (see Sec. VIII). The resolving time was also measured by placing the counters at an "off coincidence" position; that is, Θ_1 and Θ_2 were not corresponding angles for a 2:1 mass ratio and were sufficiently far from being so that any coincidences observed were the result of chance.[12] The resolving time was computed from $n=2n_1n_2\tau$, where n was the accidental coincidence rate observed, n_1 and n_2 the individual counting rates, and τ the resolving time. τ was $\sim 3\times 10^{-6}$ sec.

V. PROCEDURE FOR OBTAINING SCATTERING DATA

The following procedure was adopted at each pair of angles studied. The counters were set at the calculated angular positions (Sec. III). The cyclotron beam current was adjusted to give a reasonable counting rate in both counters. The optimum discriminator setting was located. This consisted in measuring the number of coincidences as the discriminator bias was raised. The number of coincidences fell off sharply when the bias setting exceeded a certain value. If raising the bias did not alter the coincidence rate, it could be assumed that all the scattering events were being recorded. This check was made on both counters at every angle. When a discriminator check was obtained, the discriminator was advanced as far as had been found to be safe, in order to reduce accidental coincidences to a minimum.

At certain angles, in particular those at which the particles had maximum energy, the discriminator check could not be obtained, owing to the fact that some of the pulses had too nearly the background height. The situation was eased by placing aluminum foils in front of the counter to slow the particles and increase their pulse heights so that a discriminator check could be obtained. Actually, doubts sometimes existed regarding the interpretation of the results obtained with slowing foils. It was found that as the thickness of aluminum increased the number of coincidences first increased but then decreased. This behavior was interpreted as caused by scattering from the slowing foil. Hence, unless a number of different thicknesses of aluminum were tested at each angle and a flat plateau established, there was no guarantee that the maximum coincidence rate observed corresponded to counting of all the scattered particles. Unfortunately, to insert a variety of foils was very time-consuming with the present design because the chamber had to be opened each time a change was made.

The correct angular position of the conjugate counter corresponding to a selected setting of the defining counter was always found by rotating it through several degrees on each side of the calculated conjugate position and recording the coincidence rates. Besides locating accurately the conjugate position, this procedure provided a valuable check on the conjugate beam width. If the slit width was more than sufficient to accept all the particles, the peak was flat; if the peak was sharp, the slit width was too small.

The setting of the conjugate counter having been established, long runs were made to obtain good counting statistics. This was done on each of several foil positions (see Sec. VII) to average over irregularities in the foil. The number of counts obtained at each angle varied from 1000 to 10,000.

VI. CHARGE MEASUREMENT

The charge collected during each run had to be measured for two reasons: (a) successive runs were normalized according to the charge collected during

TABLE I. Capacitance values.

Nominal capacitance	Current	Apparent capacitance
0.1 μf	9.65×10^{-10} amp	0.1057 μf
	1.271×10^{-11}	0.1075
1.0	1.021×10^{-9}	1.122
	4.000×10^{-9}	1.100

Final voltage = 0.850 percent
Limit of error = $\pm$0.5 percent
Short discharge time error = -2 percent

[12] There are processes by which true coincidences could be obtained under such conditions, e.g., as a result of products of nuclear reactions occurring in the foil; but these have negligible probability by comparison with the chance rate.

each; (b) to calculate absolute cross sections it was necessary to know the total number of particles traversing the chamber. The beam current through the chamber was actually about 10^{-8} to 10^{-9} amp.

The Faraday cup of the current collector was connected by coaxial cable to a network of three condensers, whose nominal capacitances were $C_1=1.0$, $C_2=0.01$, and $C_3=0.1$ μf, arranged as in Fig. 5. The capacitances of these condensers were measured by the Bureau of Standards under conditions as nearly as possible resembling those used in the actual scattering operations. These conditions were that the condensers were charged to a potential of 0.8 volt in an interval ranging from 200 to 900 seconds. The capacitances reported differed appreciably from the labeled values, and were subject to even further correction if discharge times of less than 15 minutes were employed. The values are listed in Table I.

The potential developed was applied to a calibrated Compton electrometer. Operation of the integrator comprised the following steps: (a) Faraday cup grounded by closing switch S_1, and the electrometer brought to zero, (b) switch S_2 closed to connect cup to network, (c) S_1 opened allowing integration to commence, (d) at the end of run S_2 opened, stopping integration. The electrometer reading was then noted. Operation of S_1 and S_2 automatically turned the scalers on and off simultaneously. The electrometer was calibrated at regular intervals by means of a Leeds and Northrup potentiometer standardized against a Weston cell calibrated by the Bureau of Standards.

Several sources of error had to be reckoned with such as (1) leakage of charge from the integrator system, cable, etc. This was measured by charging the system to a definite potential and observing the change in deflection of the electrometer as a function of time after the source of potential was removed. The leakage resistance, R, was calculated from $V=V_0\exp(t/RC)$. It varied slightly with the seasons but kept within the range 5×10^{10} to 10^{11} ohms. The correction for leakage was applied to observed electrometer deflections as follows:

$$D_{\text{true}}=D_{\text{obs}}(1+T/2RC),$$

where T was the total running time. The correction rarely exceeded two percent. No variation of leakage rate was observed when the cyclotron was operating. (2) The capacitance of the 150 feet of coaxial line was appreciable when the charge was applied to the 0.1-μfd condenser. It amounted to ~10 $\mu\mu$f per foot, and hence the total capacitance was 0.0015 μf. This capacitance was included in the calculation of total charge collected. (3) Production of secondary electrons in the Faraday cup was guarded against by providing a magnetic field across the current collector. (4) Ionization currents in the residual air in the collector were negligible at the operating pressures used and with 10-Mev particles. (5) To determine whether the neutron and gamma-ray flux in the cyclotron room affected the rate of integration of charge, the gate valve in the slit system was closed and the electrometer connected. No measurable deflection was detected when the cyclotron was turned on.

Charge measurement errors from all sources during the April run were believed to be $\lesssim0.5$ percent.

VII. SCATTERING FOILS

To satisfy the requirements of the experiment it was only necessary to use as scattering material any hydrogenous foil. To reduce the relative accidental coincidence rate it was desirable to choose a material having a high proton content. Nylon ($C_{12}H_{23}N_2O_2$), 0.2 mil thick, was used in the September run (H content ~10 percent). Nylon suffered from two defects. (1) It stretched too readily. In order for a smooth foil to be obtained, stuck to the holder, the Nylon had to be stretched taut by hand. It was difficult to keep the foils uniformly thick over the 2-inch by 2-inch holder. Each foil was examined by means of a Michelson interferometer, and only those foils whose interference patterns seemed satisfactory were used; but the accuracy of this control was not high. (2) Nylon foils changed their characteristics considerably under bombardment, confirming the experience of R. R. Wilson *et al.*[1]

During the December and April runs, 0.25-mil p.e.t. foils were substituted. Du Pont gave the formula $C_{10}O_4H_8$, corresponding to a hydrogen content of greater than 4 percent. However, p.e.t. proved far superior in spite of its lower hydrogen content.

After completion of each scattering run an accurately known area of each foil was removed (18.90 cm^2), weighed on a microbalance, and analyzed for hydrogen. Foils were stored in vacuum until analyzed. Analyses were carried out by burning in dry oxygen and weighing the water of combustion. The number of H atoms per cm^2 was obtained by substitution in the equation, $N_a=fmN/sA$, where m was the mass of the scattering foil, f, its fraction H content, N, Avogadro's number (6.025×10^{23}), s, the area of foil, and A, the atomic weight of H (1.0081). Resulting N_a values used in the calculations of cross sections were as follows:

December 1948,
Foil 3: $(1.86\pm0.09)\times10^{19}$ H atoms cm^{-2}
April 1949, Foil 4: $(1.41\pm0.07)\times10^{19}$
Foil 5: $(1.68\pm0.08)\times10^{19}$.

The September foils were not analyzed. The large errors quoted were contributed almost wholly by uncertainty in f (±4 or 5 percent). The value of m may be ±0.025 percent in error and of s about ±0.1 percent. Moreover, it should be realized that the actual error may be even larger than this. These errors do not include (a) non-uniformity of the foil. Scattering was measured only from the area of foil actually traversed by the beam in the course of a run, comprising about

1 percent of the whole area of the foil, whereas N_a values were derived from the entire foil. Some idea of the importance of this circumstance was conveyed by the fact that the counting rate varied from one position to another by as much as 10 percent. (b) Foil change under bombardment. This was eliminated as completely as possible by using certain areas of the foil infrequently, thereby preserving them as "standards" with which the more bombarded areas of the foil could be compared from time to time. This procedure guarded against errors in relative cross sections at different angles due to any progressive foil change.

VIII. CORRECTIONS ARISING FROM COINCIDENCE CIRCUIT

A. Accidental Background

Individual counters responded to deuterons scattered by the carbon and oxygen present in the foil. Hence, the individual counting rates were much greater than the coincidence rate. By chance it was possible for two particles not related to the same nuclear collision to activate the two counters during a time interval less than the resolving time of the coincidence circuit. A coincidence was then recorded. When data was taken, the total number of counts recorded in each counter was noted, n_1 and n_2 respectively, as well as the number of coincidences. The resolving time of the coincidence circuit, τ, which was about 3×10^{-6} sec, and the total running time T being known, the number of chance coincidences, n', was calculated from the formula $n'=2n_1n_2\tau/T$ and was subtracted from the observed number of coincidences, n_c. Accidentals rarely exceeded a few percent.

B. Dead Time of Coincidence Circuit

A certain fraction of true coincidences was lost because the coincidence circuit was inoperative for an interval, τ', following each count ($\tau'=26\times10^{-6}$ sec). Any further counts arriving before the circuit had recovered could not be recorded. This meant that during a running time, T, the coincidence circuit was dead for a time $(n_1+n_2)\tau'$, leading to an additive correction of the type $n''=n_c(n_1+n_2)\tau'/T$, where n'' was the number of coincidences lost which were to be added to the number actually recorded, n_c. This correction amounted to several percent at some angles. Both of the above corrections involved T^{-1}. Therefore, both corrections were diminished relative to true coincidences by using small beam currents and slow counting rates. On the other hand, longer times increased the electrometer leakage correction. Owing to the prolific scattering of deuterons from C and O at small angles, corrections for both accidentals and dead time were always worst there. It was preferable to use the defining counter with its much smaller aperture at the smaller angle of the conjugate pair; e.g., near $\Theta_1=17.9°$,

TABLE II. Complete tabulation of differential cross section measurements. Cross sections, $\sigma(\theta)$, and angles, θ, refer to center-of-mass coordinates. Data from five foils are listed separately. Laboratory angle pairs, Θ_1 and Θ_2, are included. Uncertainties after each measurement are standard deviations based on the number of coincidences. Symbols at the head of each column of cross sections are used to represent the column in Fig. 6. The next-to-last column lists average $\sigma(\theta)$ values. The last column lists some ratios of observed to Rutherford-Darwin cross sections.

Run			September 1948[a]		December 1948		April 1949			
Foil number			1	2	3	4	4	5	Weighted	
Defining			Deut.	Deut.	Deut.	Deut.	Prot.	Deut.	average	
Scattering foil			Nylon	Nylon	P.e.t.	P.e.t.	P.e.t.	P.e.t.	$\sigma^a(\theta)$	
Symbol (Fig. 6)			×	●	△	⊡	⊙	+	$\times10^{28}$	
Θ_1	Θ_2	θ	$\sigma(\theta)\times10^{28}$ cm² steradian^{-1}						[b]	$\frac{\sigma(\theta)_{av.}}{\sigma(\theta)_{R-D}}$
14.63	67.5	45			1.75±0.02 c	1.51±0.02 m		1.59±0.02 m	1.79	
16.17	65.0	50			1.71±0.02				1.66	45
17.65	62.5	55				1.43±0.02		1.52±0.02	1.56	
19.10	60.0	60			1.48±0.01		1.51±0.04		1.44	
20.52	57.5	65					1.37±0.03		1.32	
21.87	55.0	70	1.12±0.02	1.13±0.03	1.21±0.01		1.19±0.03		1.21	110
23.15	52.5	75				1.06±0.01	1.11±0.02	1.08±0.01	1.10	
24.37	50.0	80	0.99±0.02	0.92±0.02	0.98±0.01		1.03±0.02		0.99	
25.52	47.5	85					0.94±0.02		0.89	
26.57	45.0	90	0.78±0.02	0.77±0.01	0.77±0.01		0.82±0.02		0.79	170
27.50	42.5	95					0.79±0.02		0.71	
28.33	40.0	100	0.63±0.02	0.65±0.01		0.61±0.01	0.71±0.02		0.63	
29.02	37.5	105		0.58±0.01		0.59±0.01	0.61±0.02		0.59	
29.53	35.0	110					0.59±0.01		0.57	220
29.88	32.5	115					0.60±0.02 d		0.57	
30.00	30.0	120					0.63±0.02 d		0.61	
29.87	27.5	125					0.69±0.02 d		0.68	
29.43	25.0	130				0.75±0.01	0.80±0.02		0.79	450
28.67	22.5	135		1.03±0.02		0.91±0.02	0.98±0.02		0.97	
27.52	20.0	140	1.06±0.05	1.26±0.02		1.17±0.02	1.23±0.02		1.22	
25.92	17.5	145		1.50±0.04		1.60±0.04	1.43±0.03		1.47	
23.78	15.0	150		1.87±0.04		1.92±0.05	1.75±0.03		1.79	1300
21.13	12.5	155				2.24±0.22	2.09±0.03		2.12	
17.87	10.0	160					2.40±0.03 m		2.43	1900

[a] Relative values only.

[b] Final results of experiment.

$\Theta_2 = 10.0°$ defining the protons at Θ_2 was more suitable, whereas near $\Theta_1 = 16.2°$, $\Theta_2 = 65.0°$, it was somewhat preferable to define the deuterons at Θ_1.

Another factor contributing to the individual counting rates was the neutron and gamma-ray background in the cyclotron room (the neutrons presumably coming from (dn) and $(d,2n)$ reactions[13] on the copper dees and target plate). For the same coincidence rate the individual counting rates were noted to vary haphazardly. This effect was reduced during the April run when the equipment was surrounded by a 16-inch concrete wall.

IX. MEASUREMENT OF BEAM ENERGY

The mean energy of the beam and its half-width at the end of the slit system were obtained by measuring lengths of deuteron tracks in Ilford C2 Nuclear Research Emulsions. A convenient number of tracks was obtained by scattering the deuterons from 0.1-mil platinum foil through an angle of 20°. Deuterons entered the emulsions at ~3°, and track lengths were measured with a Leitz microscope and calibrated eyepiece micrometer. A check on the range-energy curve for C2 emulsions was made by measuring tracks of UI and UII in a plate from the same batch loaded with uranium. This checked the curve only at much lower energies but was useful in verifying that the emulsions did not change their characteristics appreciably. The range-energy curve published by Lattes *et al.*[14] formed the basis of the energy measurements.

Two independent measurements of the beam energy were made by the photographic method. Mean ranges of the deuterons, after correction, corresponded to 9.95±0.10 Mev and 9.85±0.10 Mev respectively. Corrections were made for loss of energy in traversing the Pt foil and energy transferred to the Pt nucleus in elastic collision. An independent check was made by Mr. J. Miskel, who measured the activation of Al foils behind various thicknesses of Al absorber. This gave 10.1±0.2 Mev. Plates exposed in the photographic scattering chamber yielded 10.1±0.1 Mev. This range of variation was well within the uncertainty of the range-energy relationship for the emulsion. However, as no attempt to control the beam energy was made during the course of the runs, each of which extended over several weeks, it probably varied slightly with the deflector voltage and exact location of the arc structure.

The stopping power relative to air of the p.e.t. foil was calculated to be 1000. Scattering foils were $\sim 6 \times 10^{-4}$ cm thick, corresponding to a mean energy loss before collision (half-thickness) of about 30 kev. This correction was negligible. The beam energy to which the present data correspond may conservatively be taken as 10.0±0.2 Mev. The half-width of beam energy distribution after correction for straggling in the emulsion was approximately 70 kev.

[13] J. C. Grosskreutz, Phys. Rev. **76**, 482 (1949).
[14] Lattes, Fowler, and Cuer, Proc. Phys. Soc. London **59**, 883 (1947).

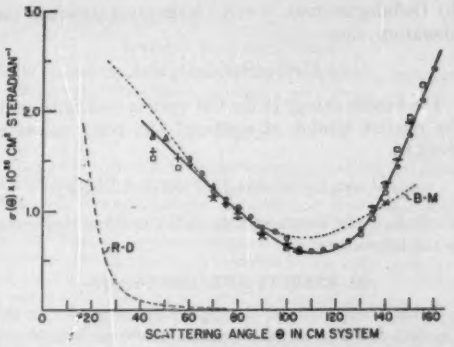

FIG. 6. Differential d-p cross sections in the center-of-mass system, in units of 10^{-24} cm² steradian^{-1}. All values listed in Table II are plotted with the symbols of Table II. The smooth curve is considered to be the best fit to the data after the worth of each point is estimated. The dotted curve *R–D* was calculated from the Rutherford-Darwin formula and the dotted curve *B–M* is based on data supplied by Buckingham and Massey (theoretical).

The purity of the deuteron beam was checked by setting the counter at 90° with respect to each other and then measuring the coincidence rate. It was no greater than the usual background rate, indicating that there were no appreciable number of protons in the beam (<1 percent).

X. REDUCTION OF DATA

If $\sigma(\alpha)$ is the cross section in the laboratory for scattering (or recoil) into unit solid angle at angle α (measured from the incident beam), N_i, the number of incident particles, N_a, the number of scattering centers per cm³, $n(\alpha)$, the number of scattered (or recoil) particles entering the defining counter, and $\Delta\Omega$, the solid angle subtended by the defining slit at the center of the foil, then

$$\sigma(\alpha) = n(\alpha)/N_a N_i \Delta\Omega.$$

When defining deuterons, $\alpha = \Theta_1$, and when defining protons, $\alpha = \Theta_2$. For any one electrometer deflection, to obtain $\sigma(\alpha)$ it was necessary to know $n(\alpha)$, N_i, N_a, and $\Delta\Omega$. Determination of each of these has been described in previous sections.

Conversion to Center of Mass

The data obtained were reduced from laboratory coordinates to a center-of-mass (CM) coordinate system as follows:

(a) Defining deuterons: if $\sigma(\Theta_1)$ is the measured cross section in the laboratory, then $\sigma(\theta)$, the cross section in CM, relates to the angle of scattering, Θ_1, in the laboratory and θ in CM as follows:

$$\sigma(\theta) = \sigma(\Theta_1)(\sin\Theta_1/\sin\theta)^2 \cos(\theta - \Theta_1).$$

The angles are related by $\theta = \pi - 2\Theta_2$.

(b) Defining protons: if $\sigma(\Theta_2)$ is the cross section in the laboratory, then

$$\sigma(\theta)=\tfrac{1}{2}\sigma(\Theta_2)(\sin\Theta_2/\sin\theta).$$

The kinetic energy in the *CM* system associated with the relative motion of scattered and recoil nuclei is given by

$$E_0'=m_2E_0/(m_1+m_2)=1/3E_0=3.3 \text{ Mev},$$

where E_0 is the kinetic energy of the incident deuterons in the laboratory.

XI. RESULTS AND DISCUSSION

Table II summarizes the experimental results on the angular dependence of *d-p* cross sections. Values are given for the five foils studied during the three runs. Only three points were taken on Foil 5, enough to give an additional check on absolute cross sections. Owing to accidental loss of Foils 1 and 2 before the chemical analysis had been carried out, only relative values were obtained from the September run. The absolute values quoted were obtained by fitting the data to the December and April runs.

All data are shown in Fig. 6 as $\sigma(\theta)$ *versus* θ. The smooth curve is considered to be the best fit. Table II also includes average values for $\sigma(\theta)$ as read from the smooth curve. Values marked "*m*" in Table II were open to suspicion because of multiple scattering and should be treated as lower limits. Values "*c*" were corrected for multiple scattering, corrections being based on the data obtained when the scattering foil was rotated (see Appendix II). At these angles some loss may have occurred because of failure of some protons to penetrate the conjugate counter window. A similar situation occurred for the deuterons at $\theta=160°$ in the proton-defined data. Here $E_1=1.4$ Mev, corresponding to a range in air of 2.7 cm. The air equivalent of the longest path through the scattering foil plus the conjugate window was 1.2 cm, and allowance also had to be made for range straggling within the window itself. Even so, window effects were small at these angles, and these were the worst cases.

Between $\theta=115°$ and 125° (indicated by "*d*" in Table II) cross sections were too high owing to "double counting" and should be regarded as upper limits. This "double counting" refers to the fact that when both counters were near 30° in the laboratory system, besides the *bona fide* coincidences from protons entering the defining counter and deuterons entering the conjugate counter, it was possible to record some spurious coincidences from deuterons entering the defining counter and protons entering the conjugate counter.

The limits of error given after each value in Table II are standard deviations based solely on the number of coincidences contributing to the value. They should be regarded as lower limits to the actual errors. Taking account of all sources of uncertainty, the extreme limits of error are considered to lie within ±3.5 percent for the relative cross sections and ±5 percent for the absolute cross sections. However, it must be remarked that in any experiment as complex as this, small systematic errors can easily remain concealed.

As a matter of general interest some Rutherford-Darwin cross sections have been computed and are included in Fig. 6 (dotted curve *R–D*). The ratio of experimental to *R–D* cross sections has been tabulated in the last column of Table II for certain angles. The magnitude of these is of interest merely to emphasize the dominance of specifically nuclear forces at this energy.

The most extensive theoretical treatment[15] of *n-d* and *p-d* scattering is the work of Buckingham and Massey. They assumed an interaction energy between the nucleons,

$$V(r)=A(mM+hH+bMH+w)e^{-2r/a}.$$

M is the Majorana operator, *H* the Heisenberg operator; various assumptions were made concerning the constants *mhbw*, and cross sections derived in each case. Comparison of these cross sections with experiment has been made in three ways. (a) Total *n-d* cross sections at a variety of energies. (b) Differential *n-d* cross sections. Both of these strongly support exchange type (symmetrical) rather than ordinary (neutral) forces. (c) Differential *p-d* cross sections. Here comparison has previously been made[16] for a proton energy of 1.85 Mev. Cross sections based on ordinary forces were too large at all angles by a large factor (~60 percent) while exchange forces showed reasonable agreement over most angles, being somewhat too small at large angles, e.g., by about 20 percent at $\theta=150°$.

The present results, corresponding to 5-Mev *p-d* scattering, are of special interest at large angles. The Buckingham and Massey 5-Mev data are included in Fig. 6 (dotted curve *B–M*). Agreement between experimental and theoretical values is remarkably good for $\theta\lesssim 90°$, but thereafter the theoretical curve is too shallow; e.g., at $\theta=150°$ the discrepancy is around 33 percent and increases rapidly with angle. The steep rise in cross sections beyond $\theta=120°$ has been confirmed[17] and now appears to present a new aspect of the *p-d* interaction.

On quite general grounds one might expect anomalies to develop at large angles (presumably associated with small approach parameters). It is not obvious at present whether the large angle anomaly arises solely from neglect, in the theory, of polarization of the deuteron or indicates that even the extremely general potential

[15] For the *n-d* case see R. A. Buckingham and H. S. W. Massey, Proc. Roy. Soc. **A 179**, 133 (1941); Phys. Rev. **71**, 558 (1947). Treatment of the *p-d* interaction along the same lines has been completed recently. We are indebted to Professor Massey for sending us theoretical cross sections in advance of publication.

[16] H. S. W. Massey and R. A. Buckingham, Phys. Rev. **73**, 260 (1948).

[17] Communication from Los Alamos Scientific Laboratory, Los Alamos, N. M.; also confirmatory work in this laboratory using a photographic scattering chamber.

assumed by Buckingham and Massey is inadequate, in which case the cause of the anomaly may be fundamental. One would expect polarization effects to vanish at sufficiently high energy, whereas the discrepancy evidently increases with energy.

It is a pleasure to acknowledge the interest of Professors R. N. Varney and A. L. Hughes in the progress of the experiment. The excellent performance of the mechanical equipment reflects the skill of Mr. O. Retzloff and his workshop staff. We wish to thank the crew of the cyclotron under Mr. A. A. Schulke for co-operation throughout, Mr. J. C. Grosskreutz who worked with us on the beam energy determinations, Du Pont de Nemours for providing the foil materials, Miss Dorothy Kuene of the Chemistry Department for analyzing the foils, and Mr. P. Bohlman who assisted in the taking of data. One of us (KBM) acknowledges his Studentship from Science and Industry Endowment Fund, Commonwealth of Australia.

APPENDIX I. CALCULATION OF GEOMETRICAL CONJUGATE PATTERN

A. Height

Figure 7 is a projection on a plane perpendicular to the beam of paths of scattered and recoil particles. Here a is the vertical height of beam where it strikes the foil, h_1, the height of the defining slit, h_2, the height of the geometrical conjugate pattern (g.c.p.) corresponding to h_1, L_1, the distance between center of scattering foil and defining slit, L_2, the distance between scattering foil and conjugate slit, α, the angle at which the defining counter is set, and β, the conjugate angle. The incident beam, path of the scattered particle, and path of the recoil particle must be coplanar. Extreme paths of scattered and recoil particles are shown in Fig. 7. These determine the height of the g.c.p., h_2.

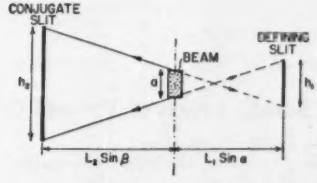

FIG. 7. Relationship between heights of defining and conjugate slits. Extreme paths of particles scattered from the top and bottom of the beam are illustrated.

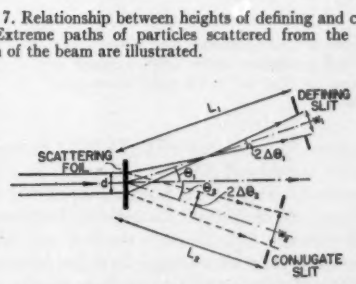

FIG. 8. Relationship between width of defining and conjugate slits. Extreme paths of deuterons entering the defining slit and recoil protons entering the conjugate slit are shown for the case $\Theta_2<30°$. Extreme rays for other cases were similar but not identical.

It follows from the geometry that

$$h_2=a+(h_1+a)L_2\sin\beta/L_1\sin\alpha.$$

In the present experiment $L_2/L_1=0.65$. When defining deuterons, $\alpha=\Theta_1$, $\beta=\Theta_2$. When defining protons, $\alpha=\Theta_2$, $\beta=\Theta_1$.

B. Width

Figure 8 is a projection on a horizontal plane of extreme paths of scattered and recoil particles. Here, also, it is necessary to distinguish between deuteron definition and proton definition. It is also necessary to distinguish the treatment for $\Theta_2<30°$ and $\Theta_2>30°$. Figure 8 applies to deuteron definition, $\alpha=\Theta_1$, $\beta=\Theta_2$, when $\Theta_2<30°$. The treatment is similar for the other cases, but not identical. w_1 is the width of the defining slit, w_2, the corresponding width of the g.c.p., and d, the width of the beam where it strikes the foil. $2\Delta\Theta_1$ is the angle between extreme rays entering the defining slit (corresponding to angles $\Theta_1^*=\Theta_1+\Delta\Theta_1$ and $\Theta_1^{**}=\Theta_1-\Delta\Theta_1$), and $2\Delta\Theta_2$ is the angle between corresponding recoil protons, i.e., $\Theta_2^*-\Theta_2^{**}$. To compute w_2 from w_1, the procedure is as follows: obtain $\Delta\Theta_1=(w_1+d\cos\Theta_1)/2L_1$, then calculate Θ_2^* and Θ_2^{**} corresponding to Θ_1^* and Θ_1^{**} using $\sin(2\Theta_2+\Theta_1)/\sin\Theta_1=2$, and hence get $2\Delta\Theta_2$, and then compute $w_2=(d\cos\Theta_2+L_2 2\Delta\Theta_2)$. It is possible to obtain w_2 explicitly, but the above proved to be more convenient.

It has been assumed in the above that the deuterons traversing the chamber were all perfectly collimated. The presence of small transverse components would increase the width of the g.c.p. slightly.

APPENDIX II. MULTIPLE SCATTERING

Figure 9 represents the scattering process occurring within the foil. Deuterons have full energy from A to B and reduced energy after collision from B to C. Protons recoil along BD. Multiple scattering occurs along AB, BC, and BD; and the effect is to spread the cones of scattered and recoil particles. The spread at C and D may be represented by a Gaussian distribution. Suppose that deuterons are being defined. Coincidences can be lost by (1) deuterons being multiply scattered so as to miss the defining slit. This is most probable where the deuterons have low energy. The order of magnitude of this effect can be found by calculating the rms angle of scattering using Williams' formula.[18] The probability that a particle undergoes a resultant deflection ϕ (projected deflection on a plane) into an angular range $d\phi$ is

$$P(\phi)d\phi=(2/\pi\cdot\langle\bar{\phi}^2\rangle)^{\frac{1}{2}}\exp[-\phi^2/2\langle\bar{\phi}^2\rangle]\cdot d\phi,$$

where $\langle\bar{\phi}^2\rangle$ is the mean square angle of scattering,

$$\langle\bar{\phi}^2\rangle=\frac{\pi}{2}\left(\frac{Ze^2}{E}\right)^2 N_v\frac{4}{9}t\ln\left[\frac{Z^{4/3}N_v t\hbar^2 M}{4\pi m^2 E}\right],$$

and Z is the mean atomic number of the foil. For p.e.t. $Z_{av.}\simeq 4.5$, e is the electronic charge, E, the energy of the particle, N_v, the number of nuclei per $cm^3=N\rho\nu/\bar{M}$, where N is Avogadro's number, $\bar{M}$, the gram-molecular weight of p.e.t.$=192$, ρ, the density of p.e.t.~ 1.1 g cm^{-3}, and ν, the number of nuclei per molecule$=22$, whence $N_v\simeq 7.6\times 10^{23}$. t is the maximum path

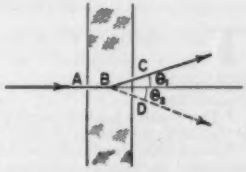

FIG. 9. Scattering within a foil. Deuteron enters at A and collides at B. Deuteron leaves at C and proton at D.

[18] E. J. Williams, Proc. Roy. Soc. **A 169**, 521 (1938); Phys. Rev. **58**, 292 (1940); Revs. Modern. Phys. **17**, 217 (1945).

length[10] and $\frac{4}{9}\cdot t$ the effective path length. The foil was ~0.25 mil. h is Planck's constant, M, the mass of the deuteron, and m, the mass of the electron. The combined rms value $\langle\bar{\phi}^2\rangle^{\frac{1}{2}}$ due to AB and BC must be calculated assuming the foil to be normal to the incident beam. For AB, $E_0=10$ Mev, and $\langle\bar{\phi}^2\rangle^{\frac{1}{2}}\simeq 0.048°$, which is negligible. For BC, ($\Theta_1=21.1°$, $\Theta_2=12.5°$), $E_1\simeq 1.5$ Mev, $\langle\bar{\phi}^2\rangle^{\frac{1}{2}}\simeq 0.39$. The angles subtended at the foil by the defining slit were 0.38° and 0.95° (vertical and horizontal dimensions respectively); therefore, the rms angle of scattering was comparable in size to the angles subtended by the slit. On this basis a gross loss of counts would be anticipated at this angle. However, there was a compensating mechanism. Deuterons which would have just missed the defining slit can be multiply scattered into it and will cause a coincidence if their conjugate protons can also enter the conjugate slit. Effectiveness of compensation, therefore, depends on conjugate slit size. We can estimate how much it needs to be increased beyond the g.c.p. to provide practically complete compensation by calculating the conjugate angle $\delta\Theta_2$ corresponding to $\langle\bar{\phi}^2\rangle^{\frac{1}{2}}$. At $\Theta_2=12.5°$, $\partial\Theta_2/\partial\Theta_1\sim 1$, therefore, $\delta\Theta_2\simeq 0.39$; $L_2=10.1$ cm, hence $\delta w_2\simeq 0.07$ cm. Similarly, $\partial h_2/\partial h_1\simeq 0.4$, $\delta h_1\simeq 0.1$ cm, whence $\delta h_2\simeq 0.04$ cm; i.e., a margin of ~0.07 cm at each side and ~0.04 cm at top and bottom are required to compensate for rms scattering. The g.c.p. at this angle is height 0.46 cm and width 0.28 cm. The actual size was 1.01 cm×0.85 cm, so there was ample margin for complete compensation. Actually, the situation was more complicated because there were several baffles which may have interfered with compensation, and it is almost impossible to estimate their effect. The best criterion for this and similar cases is a comparison of deuteron-defined with proton-defined data for the same angle pair. (2) Coincidences can also be lost by protons being multiply scattered so as to miss the conjugate slit. For this there is no compensating process. It can be prevented only by making the slits sufficiently large to collect effectively all protons in spite of multiple scattering. (Notice that in both (1) and (2) it is the size of the conjugate slit which must be increased because of multiple scattering—in (2) to catch all the proper coincidences and in (1) to catch the necessary compensating coincidences.) When defining deuterons (2) is worst when Θ_2 is large. For $\Theta_2=67.5°$, t is increased 2.6 times, $E_2\simeq 1.3$ Mev, $\langle\bar{\phi}^2\rangle^{\frac{1}{2}}\simeq 0.67°$, whence the g.c.p. must be increased on all sides by a strip 0.12 cm. The required g.c.p. size is 0.66 cm ×0.43 cm. Allowing for non-uniform distribution of particles across the g.c.p., a margin of two "rms distances" would be adequate, requiring the slit to be 1.04 cm×0.91 cm. Evidently some counts were lost at this angle. Moreover, the chamber was certainly not exactly aligned, and there was in any case some uncertainty in the g.c.p. owing to diffuse edges of the beam. It was, therefore, impossible to calculate any meaningful correction. Instead, an experimental check on multiple scattering was made at $\Theta_2=65°$ and 67.5° by rotating the scattering foil away from the normal to the beam in such a direction that the low energy proton could escape more readily. However, at the same time this process rapidly increased the path length of the deuteron ($\Theta_1=14.6°$); and although its energy was 8.6 Mev, its value of $\langle\bar{\phi}^2\rangle^{\frac{1}{2}}$ soon became significant and made excessive demands on the compensating mechanism (especially as regards height of the conjugate slit because of $\partial h_2/\partial h_1$ being 2.4 at this angle). It was indeed observed that the coincidence rate (reduced) initially increased as the foil was rotated, but reached a maximum and then declined with continued rotation, indicating the presence of multiple scattering and confirming the above reasoning. A correction was applied to the data at $\Theta_2=67.5°$ and 65° of the December run based on these observations.

Between about $\Theta_2=25°$ and 35° there is danger of losing coincidences, when defining deuterons, owing to inadequate conjugate slit width ($\partial\Theta_2/\partial\Theta_1\gg 1$). In general we did not take data closer than 22.5° and 37.5° for this reason (both these angles being safe even allowing for spread due to multiple scattering).

Similar considerations apply to proton-defined data; but it is found that multiple scattering losses are less serious here, a difference which is one advantage of defining protons. Width requirements for the conjugate slit are very easily met; but height requirements are worst when Θ_2 is small; e.g., $\Theta_2=10.0°$, $\Theta_1=17.9°$, $E_1=1.4$ Mev. Calculation of $\langle\bar{\phi}^2\rangle^{\frac{1}{2}}$ indicates that some coincidences were probably lost here (of the order of a few percent). At $\Theta_2=12.5°$ there was no loss from multiple scattering.

[10] The factor 4/9 appears with t because particles can have all lengths in the foil from 0 to t with equal probability and the average of t^3 is $\left[\left(\frac{4}{9}\right)t\right]^3$.

PHYSICAL REVIEW VOLUME 81, NUMBER 1 JANUARY 1, 1951

The (p,n) Reaction on Scandium and Vanadium: Energy Levels of Ti^{46} and Cr^{52}*

W. D. Baker,† J. S. Howell,† Clark Goodman, and W. M. Preston
Laboratory for Nuclear Science and Engineering, Massachusetts Institute of Technology, Cambridge, Massachusetts

(Received August 25, 1950)

Thin targets of the monoisotopic elements vanadium and scandium were bombarded with magnetically resolved protons at energies up to about 4 Mev. The neutron and gamma-ray yields were measured as functions of the proton energy. In each case a number of maxima are observed in the yield curves, presumably corresponding to excited states in the compound nucleus.

I. INTRODUCTION

THE reactions $V^{51}(p,n)Cr^{51}$ and $Sc^{45}(p,n)Ti^{45}$ have been mentioned by Hanson, Taschek, and Williams[1] as useful monoenergetic neutron sources at low energies. As compared with the $Li^7(p,n)$ reaction, the greater weights of V^{51} and Sc^{45} result in a much lower neutron energy at the reaction threshold‡ and a smaller variation of energy with angle in the laboratory frame of reference. In addition, a study of the variation of the neutron yield with energy furnishes information about the energy levels of two medium weight nuclei, Ti^{46} and Cr^{52}, in the excitation range above particle

* This research has been partially supported by a joint program of the ONR, the Bureau of Ships, and the AEC.

† Lieutenant Commander and Lieutenant, U.S.N., respectively. Submitted in partial fulfillment of the requirements for the degree of Master of Science in Physics under the Naval Postgraduate Training Program.

[1] Hanson, Taschek, and Williams, Rev. Modern Phys. **21**, 635 (1949).

‡ The neutron energies at zero degrees and at the (p,n) threshold are 29, 1.37, and 0.57 kev for the $Li^7(p,n)$, $Sc^{45}(p,n)$, and the $V^{51}(p,n)$ reactions, respectively.

binding energies. The reaction $Sc^{45}(p,n)Ti^{45}$ was studied by Allen, Pool, Kurbatov, and Quill.[2] At 5-Mev proton bombarding energy, a 3.0-hour positron activity was produced which was shown to come from Ti^{45}. Hanson, Taschek, and Williams[1] state that the threshold lies at 2.9 Mev. They measured the thick target yield up to a proton energy, $E_p = 3.5$ Mev.

By bombarding V^{51} with 6.5-Mev protons, Bradt *et al.*[3] confirmed the existence of 36.5-day Cr^{51}. The $V^{51}(p,n)$ threshold was accurately measured by Smith and Richards[4] as 1.566 Mev. Hanson, Taschek, and Williams[1] measured the thin target yield up to 2.9 Mev without finding any resonances.

II. EXPERIMENTAL PROCEDURE

The Rockefeller electrostatic generator at M.I.T. furnishes several microamperes of magnetically resolved protons at energies up to approximately 4 Mev. The voltage is measured by a generating voltmeter which is calibrated by the $Li^7(p,n)$ threshold, 1.882 Mev for protons and 3.764 Mev for the H_2^+ beam. Within this range, the scale appears to be linear to within ± 20 kev.

A vanadium target was prepared without special difficulty by evaporating vanadium metal from a tungsten helix in vacuum. The vanadium contained 10 percent iron, with only traces of other impurities.

TABLE I. Proton energies (in Mev) at which maxima occur in the neutron and gamma-yield curves of scandium and vanadium. A qualitative evaluation of the definiteness of the resonance peaks is indicated by the letters *A*, *B*, *C* in the order of decreasing certainty.

Scandium				Vanadium			
Neutron		Gamma		Neutron		Gamma	
Below		1.46	*B*	2.13	*B*	?	
(p,n)		1.51	*C*	2.19	*C*	—	—
threshold		1.62	*C*	2.22	*B*	2.21	*A*
		1.70	*A*	2.29	*C*	—	—
		1.85	*B*	2.34	*A*	2.34	*A*
		1.91	*B*	2.44	*A*	2.45	*A*
		2.17	*A*	—	—	2.50	*A*
		2.32	*A*	2.58	*A*	2.59	*A*
		2.52	*C*	2.[illegible]	*A*	2.66	*C*
		2.57	*C*	Aus. K	*A*	—	—
		2.78	*A*	t by	*A*	2.79	*C*
3.00	*A*	2.97	*A*		*A*	2.87	*A*
3.08	*A*	—	—	ents up	—	2.97	*B*
3.13	*C*	3.11	*A*	eavier	*A*	3.02	*C*
3.17	*A*	3.16	*A*		*B*	—	—
—	—	3.21	*A*		*A*	3.12	*A*
3.32	*A*	3.32	*B*	3.22	*A*	3.22	*A*
3.37	*A*	3.36	*B*	3.31	*A*	3.31	*A*
3.43	*A*	3.42	*C*	—	—	3.36	*B*
3.50	*A*	3.48	*A*	3.40	*A*	3.40	*B*
3.57	*A*	3.58	*A*	3.46	*A*	3.46	*A*
—	—	3.63	*A*	3.56	*A*	—	—
—	—	3.71	*A*	—	—	3.60	*A*
				3.64	*A*	3.65	*C*
				3.68	*A*	3.69	*A*
				3.75	*C*	3.76	*A*

[2] Allen, Pool, Kurbatov, and Quill, Phys. Rev. **60**, 425 (1941).
[3] Bradt, Gugelot, Huber, Medicus, Preiswerk, and Scherrer, Helv. Phys. Acta **18**, 259 (1945).
[4] R. V. Smith and H. T. Richards, Phys. Rev. **74**, 1257 (1948).

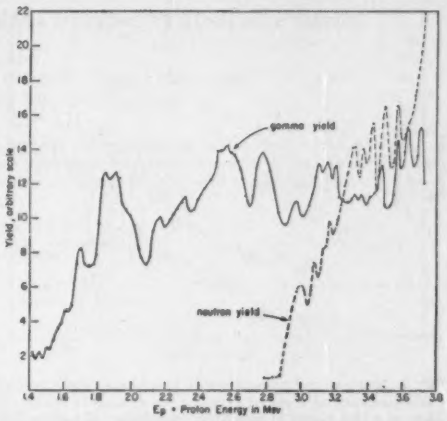

FIG. 1. Neutron and gamma yields in arbitrary units (counts per microcoulomb of incident protons) for protons of energy E_p in Mev on a thin target of scandium.

The thickness was estimated to be about 17 kev at $E_p = 1.5$ Mev.

"Spectroscopically standardized" scandium, in the form of the oxide, was obtained from Matthey and Company, Ltd., of London. The material is very refractory and could not be evaporated from a tungsten wire, but a simple method was found which proved successful. A spectroscopic-grade graphite rod, 1/4-inch diameter, was tapered down to a 1.5-mm square section near the center. A small groove was cut in one face of the small section and packed with the scandium oxide. With a heating current in vacuum of about 200 amperes through the graphite rod, the oxide was reduced and the metal evaporated onto the usual 10-mil tantalum backing.

Neutrons were detected by means of a BF_3 counter embedded in an 8-inch diameter paraffin cylinder, the whole forming a "long counter" as described by Hanson and McKibben.[5] The total gamma-ray yield was measured by means of a Victoreen 1B85 Thyrode Counter Tube with aluminum walls.

III. RESULTS

A. Scandium

Figure 1 shows the thin target neutron and gamma-ray yield curves, in terms of counts/microcoulomb (arbitrary scale). Except near the threshold, the statistical error of each point shown is about one percent. The front face of the "long counter" neutron detector was 16 cm from the target, on the axis of the beam; the G-M tube was 12 cm from the target.

A number of maxima are evident in the yield curves, and these are assumed to represent excited states in the compound nucleus Ti^{46}. The energies E_p at which

[5] A. O. Hanson and J. L. McKibben, Phys. Rev. **72**, 673 (1947).

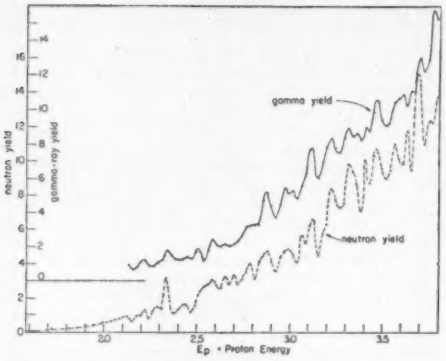

FIG. 2. Neutron and gamma yields in arbitrary units (counts per microcoulomb of incident protons) for protons of energy E_p in Mev on a thin target of vanadium (containing 10 percent iron as impurity).

the maxima occur are listed in Table I. The code letter A indicates a definite peak; B, one less well resolved; C, one whose existence is doubtful, from the present data.

Below the (p,n) threshold at $E_p=2.9$ Mev, the gammas probably come from $S^{45}(p,\gamma)Ti^{46}$ or from $Sc^{45}(p,p'\gamma)Sc^{45}$. Above the threshold, most neutron and gamma-yield peaks coincide within the uncertainty of measurement of about ± 20 kev; the apparent exceptions are indicated. The corresponding energy levels in Ti^{46} can be computed from the relation $E_L=8.3+45/46E_p$, where E_p is the proton energy at a resonance. (The energy equivalent to the mass difference $Sc^{45}+p-Ti^{46}=8.3$ Mev is known only roughly.)

B. Vanadium

Figure 2 shows the thin target yields from vanadium. The long counter face was 53 cm from the target, the G-M counter was 29 cm. The yields near the threshold at 1.55 Mev are small because of the Coulomb barrier.

TABLE II. Estimates of the Q-values of (p,n) reactions in the isotopes of iron contained as an impurity (10 percent) in vanadium. These Q-values are based on known disintegration schemes of the corresponding isobars of cobalt.

Isotope	Abundance	Q for (p,n) reaction
Fe^{54}	5.81	?
Fe^{56}	91.64	-5.39[a]
Fe^{57}	2.21	-2.06[b]
Fe^{58}	0.34	-3.08[a]

[a] A. C. G. Mitchell, Rev. Modern Phys. **22**, 36 (1950).
[b] G. T. Seaborg and I. Perlman, Rev. Modern Phys. **20**, 585 (1948).

The positions of the observed maxima are listed in Table I. As in the case of scandium, the gamma and neutron peaks coincide in most cases within experimental error. The energy levels of Cr^{52} can be computed from $E_L=9.1+51/52E_p$, but the error in the energy equivalent of $V^{51}+p-Cr^{52}=9.1$ Mev may be several hundred kilovolts.

The vanadium used as target material contained 10 percent iron as an impurity. We are not aware of any measurements of the (p,n) thresholds of the isotopes of iron, but these can be estimated when the positron disintegration scheme of the corresponding isobars of cobalt are known. For example,

$$Fe^{56}+p\rightarrow Co^{56}+n+Q_1$$
$$Co^{56}\rightarrow Fe^{56}+\beta^++\beta^-+Q_2$$
$$-Q_1=(n-p)+2m_0c^2+Q_2.$$

The Q_1 of the (p,n) reaction is equal to the energy equivalent of the neutron-proton mass difference, plus twice the self-energy of an electron, plus Q_2. Q_2 is the sum of the energy of the positron spectrum end point and any succeeding gamma-rays. The results are shown in Table II.

In the case of Fe^{57}, the Q listed is a minimum value; it is not known whether the observed gamma-rays follow positron emission from Co^{57}. $Fe^{54}(p,n)Co^{54}$ probably has a high negative Q because Co^{54} is likely to be less stable than Co^{56}. Since the two isotopes with (p,n) thresholds in the range we are interested in are of small abundance and higher atomic number than vanadium, it is unlikely that they contribute appreciably to the observed neutron yield.

IV. CONCLUSIONS

A number of resonances are found in the neutron and gamma-ray yields of scandium and vanadium bombarded by protons. Above the (p,n) threshold energy, the peaks coincide in most cases within the experimental error of ± 20 kev. The observed half-widths of some of the resonances are [illegible] small as the available energy resolution. It must be emphasized that considerably better resolution [illegible] required to confirm the existences of peaks [illegible]e bombar[illegible]l as "C" in Table I and to determine the tr[illegible]na-ray yi[illegible] widths. Very tentatively, we infer a level spacing [illegible]d i[illegible] of ~130 kev in the excitation range of 9.7 to 11.0 Mev and of ~65 kev between 11.2 and 11.9 Mev; in Cr^{52}, the average spacing is ~65 kev from 11.2 to 12.8 Mev.

The authors are deeply indebted to the generator operations crew, Donald Thompson, Gene Slawson, Vincent Yaras, and Edward Jansen, for their continued helpfulness.

Neutron Spectra from Nuclear Reactions Induced by 16-Mev Protons*

P. C. GUGELOT
Palmer Physical Laboratory, Princeton University, Princeton, New Jersey
(Received August 7, 1950)

The form of neutron spectra from (p,n) reactions has been studied by measuring proton recoil tracks in photographic emulsions which were exposed to neutrons produced by bombardment of 1-Mev thick targets of several elements with 16-Mev protons. The number of emitted neutrons with energy ϵ can be represented by

$$n d\epsilon = \text{const}\ \epsilon \cdot \exp(-\epsilon/T) d\epsilon \quad \text{for } \epsilon > 2 \text{ Mev}.$$

The values of T for different elements is found to be as follows:

Be:	$T=2.3\pm0.3$ Mev	for $\epsilon>4$ Mev,
	$T=0.9\pm0.1$ Mev	for $1<\epsilon<4$ Mev,
Al:	$T=1.3\pm0.1$ Mev,	
Fe:	$T=0.95\pm0.1$ Mev,	
Rh:	$T=0.85\pm0.1$ Mev,	
Au:	$T=0.8\pm0.1$ Mev,	
Tl:	$T=0.78\pm0.1$ Mev.	

From these results the relative level density for the residual nucleus is calculated and compared with other experimental data and with theoretical predictions. The values for T_{exp} are lower than those predicted by Weisskopf's statistical model.

I. INTRODUCTION

CONSIDERABLE experimental data have been collected on the level structures of light nuclei.[1] However, a theoretical interpretation of these data is difficult in general. For the heavier elements several attempts have been made to calculate energy levels on the basis of statistical models,[2–10] but little experimental information is available except for the lowest states excited by β- and γ-transitions. To obtain information concerning the level structure at high excitation it is possible to observe excited states in the compound nucleus by the resonance scattering of slow neutrons and protons. These very accurate experiments, however, allow the detection of levels only as long as the level spacing is large compared to the level width; i.e., levels can be found only over a relatively small range of energy. Another method, the analysis of the particle emission spectra from nuclear reactions, yields the states in the residual nucleus. Recent experiments by the Yale group show that by this method level structure is observed in elements up to argon.[11,12] The statistical treatment for the heavier elements ($A>50$) predicts a level spacing, above a few Mev excitation energy, which is so small that the peaks in the emission spectra cannot be resolved with ordinary instruments. The average level spacing of the residual nucleus at an excitation energy $E=\epsilon_{max}-\epsilon$ can be inferred from the emission probability of the outgoing particles of energy, ϵ, where ϵ_{max} is the maximum possible kinetic energy of the outgoing particle. It will be of interest to compare the average level spacing obtained from the emission probability and the observed level spacing from the peaks in the emission spectra for the range of elements where a statistical treatment is possible and the levels of the residual nucleus can be resolved.

On the basis of Bohr's compound nucleus hypothesis, Weisskopf and Ewing[13] developed a theory which yields cross sections for nuclear reactions in heavy elements ($A>60$). These cross sections depend on the level density of the residual nucleus. It is assumed that the level density of the nucleus R at an energy of excitation E is $\omega_R(E)=C\exp(aE)^{\frac{1}{2}}$. C is calculated from the observed level density at very low excitation and a is obtained from the levels found by slow neutron resonance experiments.[14]

Experimental cross sections for several reactions are in qualitative agreement with this theory.[15–17] Only the reactions induced by γ-rays show a large discrepancy. Hirzel and Wäffler[18] measured the ratio of the cross section $\sigma(\gamma,p)/\sigma(\gamma,n)$ and found that the (γ,p) reaction is by a factor 1000 more probable than the statistical

* This work was assisted in part by the joint program of the ONR and AEC.
[1] T. Lauritsen, *Energy Levels of Light Nuclei*, Nuclear Science Series (Nat. Research Council, Washington, D. C.).
[2] J. Frenkel, Physik. Z. Sowjetunion **9**, 533 (1936).
[3] J. R. Oppenheimer and R. Serber, Phys. Rev. **50**, 391 (1936).
[4] H. A. Bethe, Phys. Rev. **50**, 332 (1936); H. A. Bethe, Rev. Mod. Phys. **9**, 69 (1937).
[5] J. Bardeen, Phys. Rev. **51**, 799 (1937).
[6] V. F. Weisskopf, Phys. Rev. **52**, 295 (1937).
[7] C. V. Lier and G. E. Uhlenbeck, Physica **4**, 531 (1937).
[8] N. Bohr and F. Kalckar, Kgl. Danske Videnskab. Selskab. Mat.-fys. Medd. **14**, No. 10 (1937).
[9] J. Bardeen and E. Feenberg, Phys. Rev. **54**, 809 (1938).
[10] H. Wergeland, Fysik. Verden, 223 (1945).
[11] V. L. Sailor, Phys. Rev. **75**, 1836 (1949).
[12] Davison, Buchanan, and Pollard, Phys. Rev. **76**, 890 (1949).
[13] V. F. Weisskopf and D. H. Ewing, Phys. Rev. **57**, 472 (1940).
[14] V. F. Weisskopf, *Lecture Series in Nuclear Physics* (U. S. Govt. Printing Office, Washington, D. C., 1947) p. 107.
[15] H. L. Bradt and D. J. Tendam, Phys. Rev. **72**, 1117 (1947).
[16] G. M. Temmer, Phys. Rev. **76**, 424 (1949).
[17] H. Wäffler, Helv. Phys. Acta **23**, 239 (1950).
[18] O. Hirzel and H. Wäffler, Helv. Phys. Acta **20**, 373 (1947).

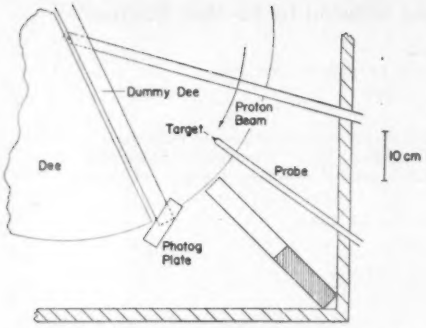

FIG. 1. Section of the cyclotron chamber showing the position of the target and photographic plate.

theory predicts. An explanation was given by Schiff.[19] He assumed that not all of the states in the residual nucleus are excited because of special modes of vibration of the compound nucleus formed by γ-ray absorption.[20] Levinger and Bethe[21] explain (γ,p) reactions by an α-particle model. The γ-ray interacts with one of the protons of the nuclear α-particles. In some of the reactions a proton might escape from the nucleus without sharing its energy with the other nuclear constituents. If this is the case, the energy spectrum of emitted nucleons should show a markedly different form as compared to the spectrum from a heavy particle induced reaction.

To obtain more direct information about the level spacing in various nuclei, it is of interest to study the energy distribution of particles emitted in nuclear reactions.

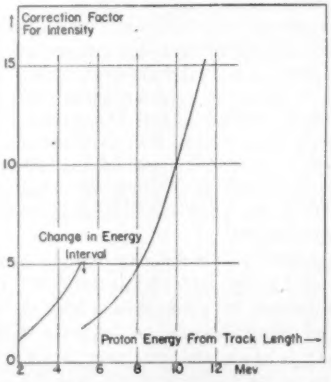

FIG. 2. The correction factor to transform the number of observed proton recoil tracks per unit range interval into number of neutrons per unit energy interval is plotted as a function of proton recoil energy. This correction includes the escape of tracks out of an emulsion of finite thickness.

[19] L. I. Schiff, Phys. Rev. **73**, 1311 (1948).
[20] M. Goldhaber and E. Teller, Phys. Rev. **74**, 1046 (1948).
[21] J. S. Levinger and H. A. Bethe, Phys. Rev. **78**, 115 (1950).

Arguments based on the principle of detailed balancing[6] give the energy distribution of particles a emitted from a compound nucleus C leaving a residual nucleus R:

$$n_a d\epsilon = [m_a g \omega_R(\epsilon_{\max}-\epsilon)/2\pi^2\hbar^3\omega_c(E_c)]\xi\sigma_a(\epsilon)\epsilon d\epsilon,$$

where m_a is the mass of particle a; $\omega_c(E_c)$ is the level density of compound nucleus C at an excitation energy E_c; $\omega_R(\epsilon_{\max}-\epsilon)$ is the level density of residual nucleus at an excitation $E_R=(\epsilon_{\max}-\epsilon)$; $\epsilon_{\max}$ is the maximum energy available for a; $\sigma_a(\epsilon)$ is the geometrical cross section for the formation of a compound nucleus C with excitation E_c if the nucleus R is in a state with excitation energy E_R and the entering nucleon a has kinetic energy ϵ; g is the statistical weight factor, depending on spin of a; and ξ is the "sticking probability." The sticking probability is usually assumed to be a constant (≈ 1) for high energy particles.[4,6] However, Muto and Nogami[22] find from neutron transmission experiments that ξ varies rapidly with neutron energy ($2.25<\epsilon_n<3$ Mev). Because no other data are available, ξ will be assumed to be constant. The cross section $\sigma_a(\epsilon)$ depends not only on the energy of the escaping particle, but also on the angular momentum of a (for charged particles σ_a will involve the penetration of the Coulomb barrier). In order to calculate the spectral distribution of neutrons, the penetration through the centrifugal barrier must be computed. It can be shown that the cross section σ_n for the penetration of the centrifugal barrier in Al, summed over all possible angular momenta, varies by approximately 30 percent for a change in neutron energy from 2 to 9 Mev. The effect of this correction would be to increase the level density at high excitation energy of the residual nucleus.

With the approximations for $\sigma_n=\text{const}$ and $\xi=\text{const}$, in the energy range considered here, ω_R can be calculated from the observed spectrum:

$$\omega_R(\epsilon_{\max}-\epsilon)=\text{const}n/\epsilon$$

(n is the number of neutrons per unit energy range).

II. EXPERIMENTAL PROCEDURE

The neutrons produced by the bombardment of several different targets with 16-Mev protons were detected by measuring proton recoil tracks in 100-μ thick Ilford C2 photographic emulsions. The geometrical setup for the exposure of the plates is shown in Fig. 1. The targets and photographic plates were mounted inside the vacuum chamber of the cyclotron. The plates wrapped in thin lead sheet were placed at a distance of 20 cm from the target in the forward direction of the proton beam. The thickness of the targets was so chosen that the 16-Mev protons from the cyclotron lost approximately one Mev in traversing them. The actual energy loss might have been somewhat larger because protons which were not seriously scat-

[22] T. Muto and M. Nogami, J. Phys. Soc. Japan **2**, 138 (1947).

tered during a traversal might penetrate the target again after one revolution in the magnetic field of the cyclotron. The beam currents recorded with these targets were smaller by a factor 50 to 100 than with targets in which protons were stopped. The residual current probably originated from secondary emission and very slow protons circulating in the chamber.

The position of the photographic plates was just at the edge of the dee. With this geometry the neutrons produced in the dee structure will enter the emulsion at approximately 90° to the direction in which the proton recoil tracks were selected. Hence, only very slow proton recoils will be observed from these "background neutrons."

The plates were examined with a Spencer binocular microscope with 95× oil immersion objective and 6× eyepieces. A specially designed object stage[22a] made it possible to move the plate by means of a micrometer screw in order to obtain the length of a track in microns and by turning the micrometer back to zero to return

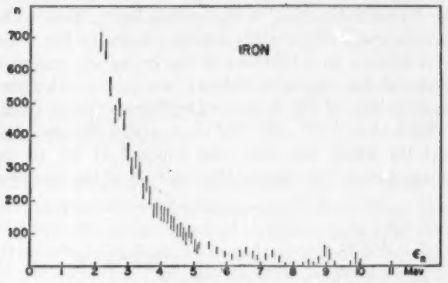

FIG. 3. Neutron spectrum from Fe+p.

to the field in which the track started. In this way one can make certain that no tracks are lost in one field.

The following criteria for the selection of the tracks were used. They had to be within ±15° of the forward direction of the proton beam in the unprocessed emulsion, and both endpoints of the track had to be inside the emulsion. The shrinkage factor of the emulsion was measured to be 2.3. An eyepiece reticule ruled in squares and so aligned that one side was parallel to the forward direction enabled one to define the maximum angle criterion in terms of the minimum length of track which had to stay between two parallel lines of the reticule. In the vertical direction the angle of 15° was obtained from the minimum length over which the track had to appear in focus. Both limits were not defined completely sharply, and for this reason it was assumed to be necessary to check the method by measurement of the tracks for one spectrum (Li+p−neutron spectrum) precisely at all angles. This was done and the agreement between the two methods was found to be good; the first method showed some loss in resolving power, which is not essential for these experiments.

[22a] This stage was designed by R. J. Britten.

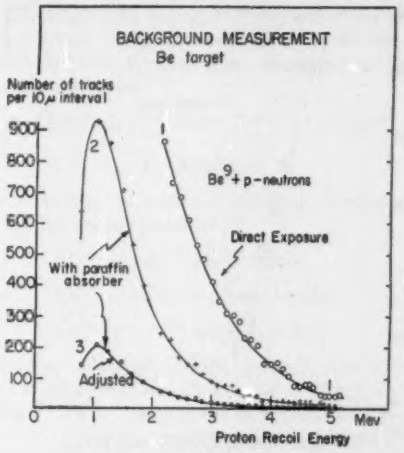

FIG. 4. Results of a measurement to estimate the number of neutrons which do not originate from the target. Curve 1: number of proton recoils observed from the Be+p reaction; curve 2: number of proton recoil tracks observed by bombarding the same target, but by interposing a 20-cm long paraffin rod in between target and photographic plate; curve 3: curve 2 adjusted on the same scale as curve 1, showing that the background is 7 percent at 2-Mev proton recoil energy.

The plates were so exposed that on the average approximately one measurable track appeared per field. About 3000 tracks were counted for each spectrum.

After the count was completed, two overlapping histograms were made up with 10μ-intervals for tracks between 30 and 180μ, and with 30μ-intervals for tracks longer than 180μ. The number of tracks in each interval was then corrected for the (n,p) scattering cross section, the escape of tracks out of a layer of finite thickness,[23] and for the change in energy interval. The range-energy relation for the proton tracks in the

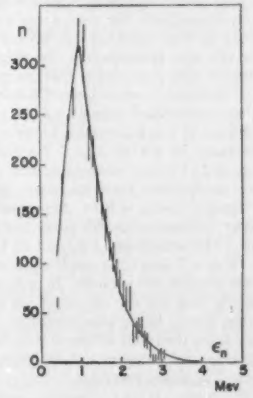

FIG. 5. Background observed in an exposure for which the proton beam was not stopped by a target. Of 1240 tracks one was observed with energy of 4.1 Mev.

[23] H. T. Richards, Phys. Rev. 59, 796 (1941).

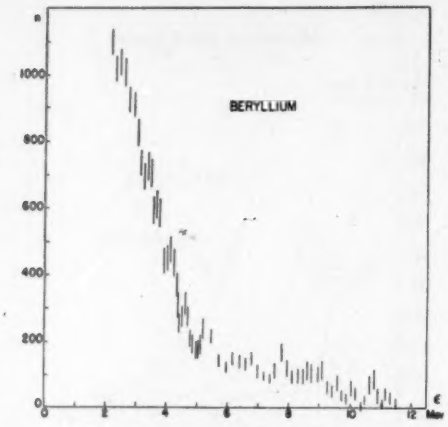

FIG. 6. Neutron spectrum from Be^9+p.

emulsion was taken from Lattes, Fowler, and Cuer.[24] The applied total correction factor is plotted in Fig. 2. Figure 3 shows a typical spectrum obtained for the neutrons from $Fe+p$.

Because all of the exposures were made inside the vacuum chamber, it was very difficult to measure the background of neutrons which were not produced in the target. Of several measurements to estimate this background flux, the following two are the most conclusive.

(1) A Be target was bombarded with 16-Mev protons and one plate exposed in the normal geometry described above. Then a second plate was exposed with the same target, but with a paraffin rod interposed between target and plate. The rod was 20-cm long and 2-cm high; and its width tapered from 0.5 cm at the target to a width of 2.5 cm, equal to the width of the photographic plate, at the other end. Figure 4 shows the results of these measurements. Curve 1 represents the number of proton recoils obtained from the direct exposure. Curve 2 shows the data with the paraffin rod in place. Because no absolute measurement of the beam intensity is available, the two curves must be normalized to be comparable. The tracks between 9.5 and 11.5 Mev are certainly proton recoils from neutrons from the target. In the unshielded plate 51 tracks were measured in this energy interval, in the shielded one 41 tracks in the same range. Of 51 neutrons, 8.9 should be able to pass unscattered through such a paraffin absorber. This means that curve 1 is comparable to curve 2 modified by multiplying its ordinate by 8.9/41. Curve 2 adjusted in this way is shown as curve 3. The low energy tracks in curve 3 are practically all due to background neutrons, since the paraffin rod is essentially "opaque" below 4 Mev. A comparison of curves 1 and 3 shows that the background for curve 1 is 7 percent at a neutron energy of 2 Mev and about 2 percent at 4 Mev.

Figure 5 shows the result of an exposure for which the beam is not stopped by a target. In this case, the beam blows up and finally hits the dee structure. All the proton recoils counted are then due to background neutrons. The observed recoil spectrum confirms the result obtained with the Be target, namely, that the background increases rapidly below approximately 3 Mev, but is small at higher energies.

[24] Lattes, Fowler, and Cuer, Proc. Phys. Soc. London 59, 883 (1947).

(2) Another method of checking background consisted of using two Al targets of different thicknesses; here the result obtained is that with increasing target thickness the number of neutrons produced in the target increases relative to the neutrons produced elsewhere. The spectrum obtained with a 2-Mev thick target yielded the same result as the spectrum obtained with a 0.2-Mev thick target, showing that the form of the spectra is not seriously changed by background.

No corrections for the background *in* the emulsions were made. Some neutrons produce (n,p) reactions in the elements of which the emulsion is composed. However, the probability for these reactions is small compared with the probability for (n,p) scattering in the emulsion.

III. RESULTS

A. Beryllium

The Be^9 nucleus cannot give any support for the statistical description of nuclei; however, it is still of interest to study the change in level density with excitation energy. Because of the low mass of this nucleus, the data shown in Fig. 6, which are taken in the forward direction of the proton beam, have to be transformed in the center-of-mass system. In Fig. 7 the level density as a function of the excitation energy is given; of the two curves shown, curve 1 is calculated from the data of Fig. 6; curve 2 represents the data from a measurement (of which the fluctuations are smoothed out) for which the plate was exposed at 90° to the proton beam. The assumption that all of the observed

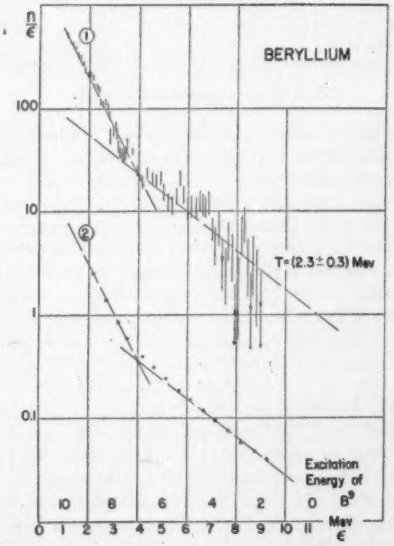

FIG. 7. Relative level density of B^9 *vs* neutron energy in c.m. system and excitation energy of B^9. Curve 1: shows the data from a measurement for which the photographic plate was exposed in the forward direction of the proton beam; curve 2: represents a measurement at 90° to the proton beam. The fluctuations are smoothed out.

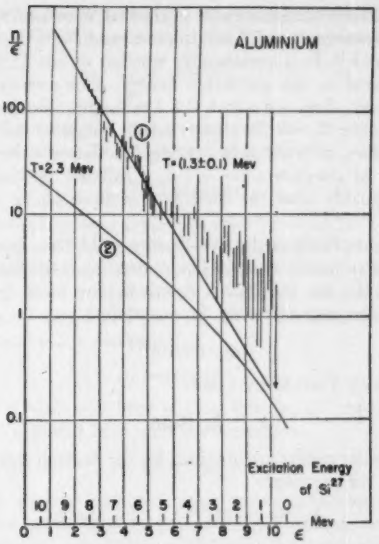

FIG. 8. Level density of Si^{27}. Curve 1: relative level density *vs* neutron energy and excitation energy of Si^{27} obtained from the neutron spectrum; curve 2: level density calculated by Bardeen and Feenberg (reference 9).

neutrons originated from a (p,n) reaction may be valid only at low excitation energy. It is therefore possible that the apparent rapid increase of the level density above 7 Mev results from the total disintegration of Be^9. The level density in the assumed residual nucleus B^9 may then be represented by

$$\omega_B = \text{const} e^{E/T},$$

in which $T=2.3\pm0.3$ Mev for an excitation energy $E<7$ Mev and $T=0.9$ Mev for $E>7$ Mev.

B. Aluminum

For Al two measurements with different target thickness (0.2 Mev and 2.0 Mev) gave the same result within the limits of error. The thin target spectrum, however, showed considerably greater fluctuations in the neutron intensity than the thick target spectrum; this may be attributed to a level structure in the residual nucleus Si^{27}. The level density (Fig. 8, curve 1) can be approximated by

$$\omega_{Si}(E) = \text{const} e^{E/T},$$

in which $T=1.3\pm0.1$ Mev. The proton energy was assumed to be 16 Mev. The reaction energy of $Al^{27}(p,n)Si^{27}$ is -5.4 Mev.

C. Iron

Natural iron has 4 isotopes of which Fe^{56} has an abundance of 92 percent. It is assumed that the neutrons are produced in the reaction[25] $Fe^{56}(p,n)Co^{56}$ for which $Q=-5.5$ Mev. Again, the level density of the residual nucleus Co^{56} (Fig. 9, curve 1) can be represented by an exponential function

$$\omega_{Co}(E) = \text{const} e^{E/T}, \text{ where } T=0.95\pm0.1 \text{ Mev}.$$

D. Rhodium

With 16-Mev protons the following neutron producing reactions are possible:[26,27]

$$Rh^{103}+p = Pd^{103}+n-2.0 \text{ Mev}, \quad (1)$$

$$Rh^{103}+p = Rh^{102}+p+n-9.4 \text{ Mev}, \quad (2)$$

$$Rh^{103}+p = Pd^{102}+2n-11.2 \text{ Mev}. \quad (3)$$

Very few neutrons with energy >2 Mev will be observed from reaction (2) because of the Coulomb barrier of 9.6 Mev through which the protons have to penetrate. However, neutrons will be observed from reaction (3) for which the maximum neutron energy is 4.8 Mev for a proton bombarding energy of 16.0 Mev. Therefore, the observed neutron spectrum (Fig. 3) below 4.8 Mev includes neutrons from this reaction. The following method was developed to account for the presence of neutrons from this source:

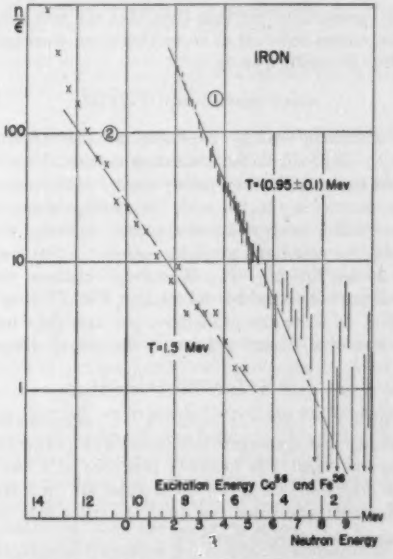

FIG. 9. Relative level density of Co^{56} and Fe^{56}. Curve 1: represents the relative level density for Co^{56} obtained from the neutron spectrum; curve 2: shows the relative level density of Fe^{56} as observed from the inelastic scattering of 16-Mev protons by iron (reference 38).

[25] L. G. Elliot and M. Deutsch, Phys. Rev. **64**, 321 (1942).
[26] Q value calculated: E. Feenberg, Revs. Modern Phys. **19**, 239 (1947).
[27] N. Hole, Arkiv. Mat. Astron. Fysik **52**, No. 3A (1946).

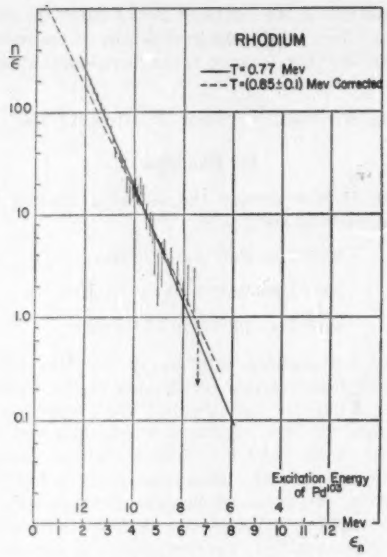

FIG. 10. Relative level density of Pd^{103}.

The probability per unit time that the first neutron in the energy interval $d\epsilon$ is emitted from a compound nucleus is assumed to be

$$n_1 d\epsilon = \text{const} \cdot \epsilon \cdot \exp(-\epsilon/T_1) d\epsilon.$$

The maximum energy available for this neutron is $E_1 = E_c - E_{b1}$. (E_c is the excitation energy of the compound nucleus, E_{b1} the binding energy of the neutron.) This neutron is emitted with the average energy $2T_1$. The binding energy for the second neutron is E_{b2}. Hence, the maximum available energy for this neutron will be $\epsilon_2 = E_1 - 2T_1 - E_{b2}$. Weisskopf[14] assumes that T and E are connected by the relation $E = bT^2$. It is then possible to write the probability per unit time for the emission of a second neutron in the energy range $d\epsilon$:

$$n_2 d\epsilon = C_2 \epsilon \exp(-\epsilon/T_2) d\epsilon,$$

in which $T_2 = [(E_1 - 2T_1 - E_{b2})/b]^{\frac{1}{2}}$. C_2 is calculated by assuming that if energetically possible two neutrons are always emitted. The intensity observed at ϵ has then to be multiplied by $1/(1+K)$ in order for the intensity of the neutrons from the (p,n) reaction only to be obtained, where K is given by

$$K = p^2 \exp(-\epsilon(p-1)/T_1); \quad p^2 = E_1/(E_1 - E_{b2} - 2T_1).$$

A different method of calculation, which assumes a level density for the final nucleus $\omega = C \exp(E/T_2)$ in which T_2 does not change appreciably with excitation energy, yields for K:

$$K = (T_1/T_2)^2 \exp[-\epsilon(T_1 - T_2)/T_1 T_2].$$

K will have the same value as above if Weisskopf's relation between E and T is introduced and $T_2 = [(E_1 - 2T_1 - E_{b2})/b]^{\frac{1}{2}}$. It is questionable whether or not T^2 is proportional to the excitation energy. This assumption, however, does not affect the final result, because the difference $T_1 - T_2$ is always small compared with T; therefore, K is a slowly varying function of ϵ, and the slope of the curves for n/ϵ *vs* ϵ will not be changed appreciably after the correction outlined above is applied.

Figure 10 shows the level density of Pd^{103} as a function of the excitation energy. The dotted line is the function corrected for the $(p,2n)$ reaction. The level density increases approximately exponentially:

$$\omega_{Pd} = \text{const} e^{E/T},$$

in which $T = 0.85 \pm 0.1$ Mev.

E. Gold

Similar results are obtained for the neutron spectrum from the reaction

$$Au^{197} + p = Hg^{197} + n - 1.4 \text{ Mev}^{26}. \quad (4)$$

Other possible reactions are

$$Au^{197} + p = Au^{196} + p + n - 8.00 \text{ Mev},^{28} \quad (5)$$

$$Au^{197} + p = Hg^{196} + 2n - 9.3 \text{ Mev}^{26,29}. \quad (6)$$

A small correction in the observed spectrum is necessary for reaction (6). The resultant level density

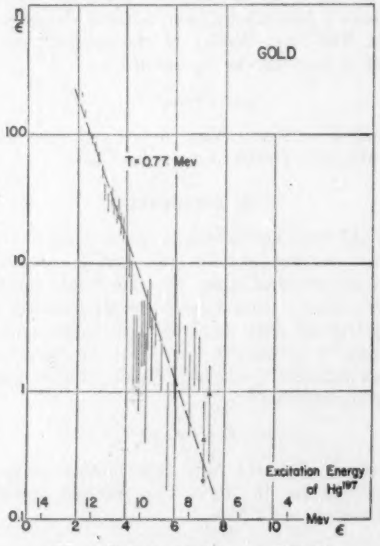

FIG. 11. Relative level density of Hg^{197}.

[28] Hanson, Duffield, Knight, Diven and Palevsky, Phys. Rev. 76, 578 (1949).
[29] Steffen, Huber, and Humbel, Helv. Phys. Acta. 22, 167 (1949).

of Hg^{197} is plotted in Fig. 11. The distribution after the $(p,2n)$ correction has been applied is approximated by

$$\omega_{Hg} = \text{const} e^{E/T},$$

where $T = 0.8 \pm 0.1$ Mev.

In this case, the plates were analyzed by two different observers,[29a] and their results agreed.

F. Thallium

Thallium consists of two isotopes: Tl^{203} and Tl^{205}. The following reaction energies are estimated[26] for the most abundant isotope Tl^{205}: $Q(p,n) = -1.7$ Mev, $Q(p,2n) = -8.2$ Mev. A small correction is again necessary for the $(p,2n)$ reaction. Figure 12 shows the level density obtained by this method:

$$\omega_{Pb} = \text{const} e^{E/T},$$

where $T = 0.7 \pm 0.1$ Mev without the $(p,2n)$ correction or $T = 0.78 \pm 0.1$ Mev with the correction.

IV. DISCUSSION

The results obtained from these measurements indicate in the first place that a rapid increase of the level density takes place with increasing excitation of the nucleus. This is in general agreement with the predictions of the statistical model. The relatively poor statistics of the measurements and some uncertain factors (e.g., background from neutrons which are not produced in the target) may cause some uncertainty about the nuclear "temperature" T. It is not expected,

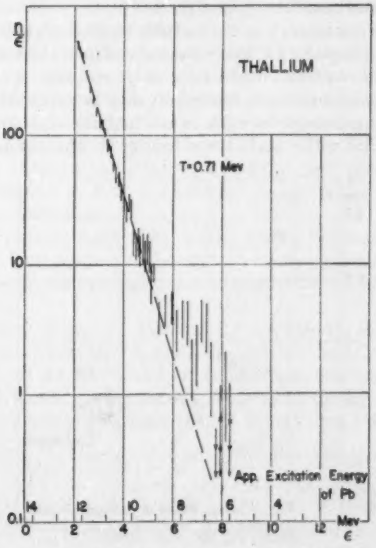

FIG. 12. Relative level density of Pb.

[29a] We thank Mrs. L. Anderson for her cooperation in carrying out these measurements.

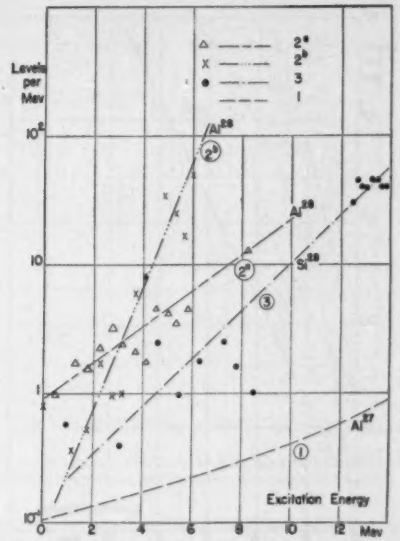

FIG. 13. Level density of Al and Si. Curve 1: relative level density calculated from the inelastic scattering of 30 Mev protons by Al^{27}; curve 2a: level density of Al^{28} computed from the known levels of Al^{28}. The level density is approximated by: $\omega = \text{const}$ $\exp(E/2.9)$; curve 2b: relative level density of Al^{28} calculated from the proton spectrum emitted in the reaction $Al^{27}(d,p)Al^{28}$. The increase in level density can be represented by $\omega = \text{const}$ $\exp(E/1)$; curve 3: level density of Si^{29} computed from the known levels of Si^{29}; $\omega = \text{const} \exp(E/2.6)$.

however, that uncertainties from these causes are so large as to have an appreciable effect on $T(A)$.

Some data are available with which these measurements may be compared.

Peck[30] showed that the neutron spectrum from Al bombarded by 3.68-Mev deuterons and observed at 90° to the deuteron beam can be approximated by $nd\epsilon = \text{const} \epsilon \exp(-\epsilon/T)d\epsilon$. In this case T is approximately 1.5 Mev.

Levinthal, Martinelli, and Silverman[31] measured the spectrum of protons inelastically scattered by Al at 90° to an incoming beam of 30-Mev protons. The level density for Al^{27} calculated from these measurements shows a completely different form as compared with the results from the neutron spectra (Fig. 13, curve 1). The spectrum contains too large a number of fast protons. The increase of the level density is even slower than that calculated from the observed levels.

Pollard *et al.*[32] studied the energy distribution of the protons produced in the reaction $Al^{27}(d,p)Al^{28}$. The deuteron energy was 3.78 Mev and the angle of observation 90°. Several levels of Al^{28} are detected. Their results are plotted in Fig. 13, curve 2a. The level density

[30] R. A. Peck, Phys. Rev. **76**, 1279 (1949).

[31] Levinthal, Martinelli, and Silverman, Phys. Rev. **78**, 199 (1950).

[32] Pollard, Sailor, and Wyly, Phys. Rev. **75**, 727 (1949).

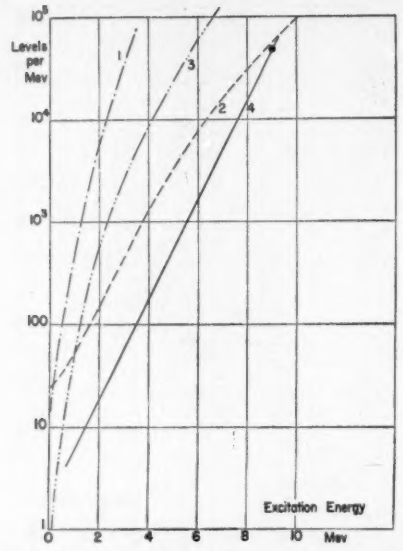

FIG. 14. Level density of a nucleus of atomic weight 100 *vs* its excitation energy according to different models. Curve 1: v. Lier and Uhlenbeck (reference 7); curve 2: Wergeland (reference 10); curve 3: Weisskopf (reference 14); curve 4: observed for Pd^{105} and adjusted at the neutron dissociation energy. The level density at 9 Mev is estimated from the resonance observed by slow neutron scattering experiments with Rh^{103}.

is taken to be $1/D$, in which D is the distance between two observed levels. At 8 Mev, Seagondollar and Barschall[33] observed 10 levels with an average spacing of 50 kev. The change in level density with excitation energy for Al^{28} can be approximated as

$$\omega = \text{const} \exp(E/2.9).$$

A similar result is obtained for Si^{28} (Fig. 13, curve 3). Shoemaker, Faulkner, Kaufmann, and Bouricius[34] observed a large number of resonances by bombarding Al^{27} with low energy protons. Some other levels at low excitation of Si^{28} are found by Peck.[30] The level density obtained from these data increases approximately as $\exp(E/T)$, where T is of the order of 2.6 Mev.

The increase in level density with excitation energy for Al^{28} and Si^{28}, as shown in Fig. 13, is apparently not as fast as that calculated for Si^{27} from the neutron intensity distribution. In order to calculate the level density from the neutron intensity distribution, it is assumed that each nondegenerate state in the residual nucleus is weighted equally; degenerate states are given weights equal to the degree of degeneracy. However, the data obtained from a listing of the peaks in the spectra do not take account of different transition probabilities. An intense group of particles is given in this case the same weight factor as is a weak and narrow peak.

Pollard's data from $Al^{27}(d,p)Si^{28}$ are suitable for a comparison of the two methods of measuring the level density. The surface area of each of the observed peaks is corrected for the proton barrier penetration. (The barrier penetration factor is calculated by the W.K.B. method and averaged over different possible angular momenta.) The result is shown in curve 2*b* of Fig. 13. The level density defined in this way shows approximately the exponential increase with $T \approx 1$ Mev, in fair agreement with our result.

The disagreement between the two kinds of measurements of the level density is apparently caused by the different ways in which ω is defined. In our experiments the "level densities" are actually proportional to the product of the number of levels per unit energy range times the oscillator strength of each level. The other method gives only the number of states per unit energy range, without taking account of the intensities of the particle groups. Consequently, this discrepancy may be explained by a high degree of degeneracy of the highly excited states. This would mean that several nuclear constituents are excited with the same energy just above their individual particle ground states. It has been observed by different experimenters that in nuclear reactions with light elements the transition of the compound nucleus to a highly excited state in the residual nucleus is often more probable than the transition to a low lying state.[34] This means that very seldom is only one nuclear constituent highly excited above its individual particle ground state.

The discrepancy in the inelastic scattering at 30 Mev may be explained if the protons are able to traverse the nucleus without interacting very strongly; i.e., no compound nucleus is formed. It may be expected that similar effects occur even in the inelastic scattering of particles with much lower energy.[35] The compound

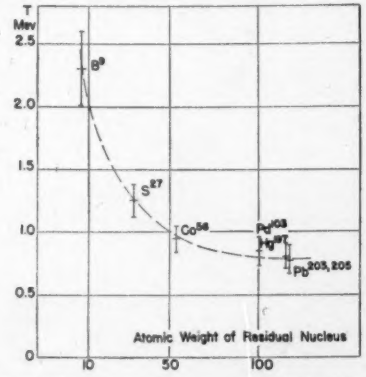

FIG. 15. "Nuclear temperature" *vs.* atomic weight of the residual nucleus.

[33] L. W. Seagondollar and H. H. Barschall, Phys. Rev. **72**, 439 (1947).

[34] Shoemaker, Faulkner, Kaufmann, and Bouricius, Phys. Rev. **79**, 228 (1950).

[35] V. F. Weisskopf, Helv. Phys. Acta **23**, 187 (1950).

nucleus picture still holds if it is possible to excite the *whole* nucleus to very high energies. Cosmic-ray data from Harding, Lattimore, and Perkins,[36] as interpreted by Le Couteur,[37] show that if the nucleus is excited to about 600 Mev, the resultant star can be explained by the evaporation of nucleons with the assumption of reasonable level spacing.

In curve 2 of Fig. 8 the level density of Si^{27} is shown as calculated by Bardeen and Feenberg.[9] The increase in level density according to this model seems to be better represented by a value of $T=2.4$ Mev at an excitation energy of 8 Mev. This agrees with the increase of the level density computed from the observed levels.

The spectrum of inelastically scattered protons of 16 Mev by Fe was observed by Fulbright and Milton.[38] The level density calculated from their results corrected for the barrier penetration is plotted in Fig. 9, curve 2. Between 5-Mev and 11-Mev excitation energy for Fe^{56}, ω can be represented by $\omega=\text{const}\exp(E/1.5)$. The value for T is larger than $T=0.95$ Mev observed from the (p,n) reaction for Co^{56}.

Grosskreutz[39] observed the neutrons from $Cu(d,n)Zn$. The neutrons were measured at an angle of 90° with the 9.93-Mev deuteron beam. The spectrum can be represented fairly well by

$$nd\epsilon=\text{const}\epsilon\cdot\exp(-\epsilon/T)d\epsilon \text{ with } T=1 \text{ Mev}.$$

Bradt and Tendam[18] obtained T for In by measuring the excitation functions for the reactions $Ag(\alpha,n)In$ and $Ag(\alpha,2n)In$; they find $T=1.8$ Mev. Recent measurements on these reactions[40] indicate that T may be lower and approximately 1.5 Mev.

Figure 14 compares the level densities obtained from several models for $A=100$. Van Lier and Uhlenbeck's level density, curve 1, increases much more rapidly with excitation energy than is observed experimentally. It can be concluded from the measurements of Borst, Ulrich, Osborne, and Hasbrouck[41] and Meyer[42] that the level density at 9-Mev excitation energy is approximately 5.10^6/Mev.

Wergeland's liquid drop model (curve 2) gives the correct level spacing at the neutron binding energy. At low energy the level density is probably somewhat too large.

Curve 3 shows the level density assumed by Weisskopf, $\omega=C\cdot\exp(aE)^{\frac{1}{2}}$ in which $a=26$ Mev^{-1} and $C=0.2$ Mev^{-1} for $A=100$. The level density near the ground level is of the right order. The density at the neutron dissociation energy seems to be too large. Curve 4 is the

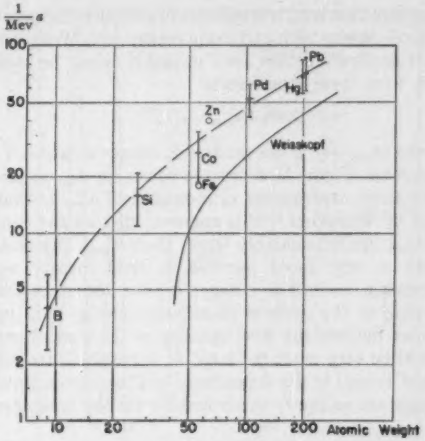

FIG. 16. a as a function of atomic weight; the experimental values are larger than those estimated by Weisskopf ($a=4E/T^2$).

experimentally observed level distribution. This curve is only relative and may be adjusted to give the right level spacing at the neutron dissociation energy. With this adjustment, the right level spacing is obtained near the ground state. This seems to contrast with the situation for aluminum, where the level density at high excitation energy gives values much larger than that observed experimentally. The level spacing for various elements found by slow neutron scattering experiments changes abruptly above $A\approx 50$. This change seems not to be reflected in the values of T for the spectra observed here.

V. CONCLUSIONS

The values of T obtained from the observed neutron spectra are shown as a function of the atomic weight of the residual nucleus in Fig. 15. This graph does not take into account any change in T caused by the different excitations of the various compound nuclei. It assumes that T is independent of, or a very slow varying function of, E. This means an infinite heat capacity for the nucleus in terms of the thermodynamic model, which would be in contradiction to some general viewpoints and in disagreement with the f-sum rule.[43] It is probable that the simple exponential increase of the level density with excitation energy as shown here is only an approximation. The observed spectra may be distorted at high neutron energy by neutrons which can escape after a collision with the entering proton without sharing its energy with other nuclear constituents. At the low energy side of the observed spectrum the $(p,2n)$ reaction introduces too many slow neutrons.

If it is assumed that part of the observed spectra is due to neutrons emitted in a (p,n) reaction from a

[36] Harding, Lattimore, and Perkins, Proc. Roy. Soc. London **A196**, 325 (1949).
[37] K. J. Le Couteur, Proc. Phys. Soc. London **A63**, 259 (1950).
[38] We thank Dr. H. W. Fulbright and Mr. J. C. D. Milton for submitting their results prior to publication.
[39] J. C. Grosskreutz, Phys. Rev. **76**, 482 (1949).
[40] E. Bleuler, private communication.
[41] Borst, Ulrich, Osborne, and Hasbrouck, Phys. Rev. **70**, 557 (1946).
[42] R. R. Meyer, Phys. Rev. **75**, 773 (1949).
[43] E. P. Wigner and T. Teichmann, unpublished.

compound nucleus, it is possible to compare the increase in level density with excitation energy with Weisskopf's level density function $\omega = C \exp(aE)^{\frac{1}{2}}$. a can be evaluated from these experiments:

$$a = 4(\epsilon_{max} - \epsilon)/T^2,$$

where $(\epsilon_{max} - \epsilon)$ is the excitation energy at which T is computed. Figure 16 shows the values for a_{exp} obtained from these experiments as compared to a_{theo} as evaluated by Weisskopf.[14] It is apparent that all the values for a_{exp} are considerably larger than a_{theo}. This would mean a very rapid increase in level density with increasing excitation energy; or, for the right level spacing at the neutron dissociation energy of a particular nucleus the level spacing at the ground state would be very much too large. It is possible that additional terms for the dependence of T on the excitation energy are necessary to account for the low lying levels which are not explainable by a statistical model. The experimental curves for ω show little tendency to be concave as would be expected from Weisskopf's density function. Otherwise, one might assume that high energy neutrons escape before the compound nucleus is formed. The number of neutrons necessary to account for the deviation from Weisskopf's function need only to be in the order of about 1 percent of the total number of neutrons emitted if their energy is larger than 6 Mev. These small effects are within the precision of our experiments.

The author would like to express his gratitude to Mrs. D. Lynn who carried out the microscopic measurements and to Dr. M. G. White for his continued interest and stimulating discussions during the course of this investigation. We are also indebted to Mr. F. Feiner for his assistance in computing some Coulomb and centrifugal barrier penetration functions.

PHYSICAL REVIEW VOLUME 81, NUMBER 1 JANUARY 1, 1951

Proton Groups from the Deuteron Bombardment of F^{19} and P^{31}

ROBERT C. ALLEN AND WALDO RALL
Sloane Physics Laboratory, Yale University, New Haven, Connecticut*
(Received August 28, 1950)

The $F^{19}(d, p)F^{20}$ and $P^{31}(d, p)P^{32}$ reactions were studied with 3.76-Mev cyclotron deuterons. The $F^{19}(d, p)F^{20}$ ground-state Q-value was found to be 4.16±0.08 Mev, giving 1.00211±0.00010 MU for the $F^{20}-F^{19}$ mass difference and 20.00660±0.00012 MU for the mass of F^{20}. Excited states of F^{20} were found at 0.64, 0.97, 1.31, 1.91, 2.52, 2.83, 3.45, and 4.01 Mev. The $P^{31}(d, p)P^{32}$ ground-state Q-value was found to be 5.52±0.10 Mev, giving 1.00065±0.00011 MU for the $P^{32}-P^{31}$ mass difference, and 30.98286±0.00021 MU for the mass of P^{31}. Excited states of P^{32} were found at 0.50, 1.10, 1.36, 1.71, 2.22, 2.72, and 3.27 Mev.

I. INTRODUCTION

A SURVEY of the light elements through oxygen indicates that, in general, the separation of the energy levels is 1 Mev or greater. Bower and Burcham,[1] studying the $F^{19}(d, p)F^{20}$ reaction with 800-kev deuterons showed that the F^{20} nucleus has four excited states under 2-Mev excitation. The present work was undertaken to determine whether the comparatively high density of levels exists in states of energy greater than 2 Mev. The reaction is also of interest in that a more accurate knowledge of the mass difference, $F^{20}-F^{19}$, is desirable.

The $P^{31}(d, p)P^{32}$ reaction was studied since very little has been done on the energy levels of P^{32}.

TABLE I. Energy levels in F^{20}.

	Energy levels	Q	Q-values of Bower and Burcham
Q_0	0 Mev	4.16 Mev	4.3 Mev
Q_1	0.64±0.03	3.52	3.6
Q_2	0.97±0.05	3.19	3.3
Q_3	1.31±0.05	2.85	2.95
Q_4	1.91±0.04	2.25	2.4
Q_5	2.52±0.04	1.64	
Q_6	2.83±0.04	1.33	
Q_7	3.45±0.03	0.71	
Q_8	4.01±0.15	0.15	

II. FLUORINE

Lead fluoride and beryllium fluoride targets of 1 to 2 mm air equivalent range were prepared by vacuum evaporation on thin gold foils. The targets were bombarded with deuterons of 3.76-Mev mean energy. The protons, emitted at 90° with the incident beam, were detected by a highly biased proportional counter. The proton ranges were determined by means of the interposition of aluminum foils and a variable pressure absorption cell. A composite curve of the proton groups observed with the lead fluoride targets is shown in Fig. 1. This curve has been resolved into nine groups, as indicated by the dotted lines.

Since the 24-cm and 34-cm groups corresponded to possible oxygen contaminants, further work was neces-

* Assisted by the Joint Program of the ONR and AEC.
[1] J. C. Bower and W. E. Burcham, Proc. Roy. Soc. (London) 173, 379 (1939).

TABLE II. Energy levels of P^{32}.

	Energy levels	Q	Q-Pollard
Q_0	0 Mev	5.52 Mev	5.9±0.3 Mev
Q_1	0.50±0.05	5.02	
Q_2	1.10±0.03	4.42	
Q_3	1.36±0.05	4.16	
Q_4	1.71±0.04	3.81	
Q_5	2.22±0.04	3.30	
Q_6	2.72±0.03	2.82	
Q_7	3.27±0.04	2.25	

sary to justify their inclusion as fluorine groups. Pollard and Davison[3] have investigated the relative intensities of the two oxygen groups with a bombarding energy of 3.76 Mev and found them to be about equal. Therefore, because of the large yield of the 24-cm group relative to the 34-cm group, the shorter range group was attributed to fluorine. To check the 34-cm protons, it was decided to use a different fluorine compound in order to change the oxygen content. Beryllium fluoride was chosen, since studies of beryllium[3,4] indicated that no proton group would mask the 34-cm group in question. In the beryllium fluoride runs, the 34-cm group appeared with the same yield relative to the other fluorine groups, and thus it was ascribed to fluorine.

Table I lists the results as calculated from the proton yield curve. Corrections have been applied for range and

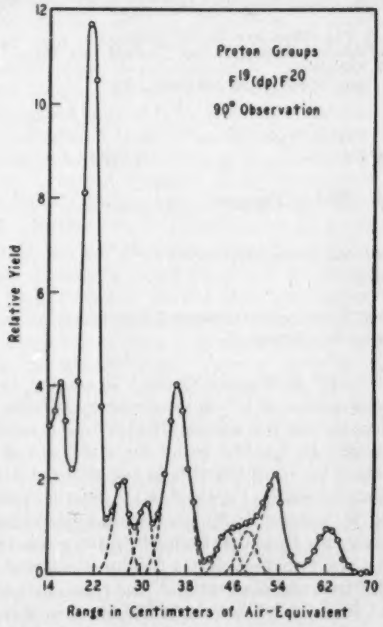

FIG. 1. Proton yield *versus* proton range.

[3] E. Pollard and P. W. Davison, Phys. Rev. **72**, 736 (1947).
[3] E. Pollard, Phys. Rev. **57**, 241 (1940).
[4] W. W. Buechner and E. N. Strait, Phys. Rev. **76**, 1547 (1949).

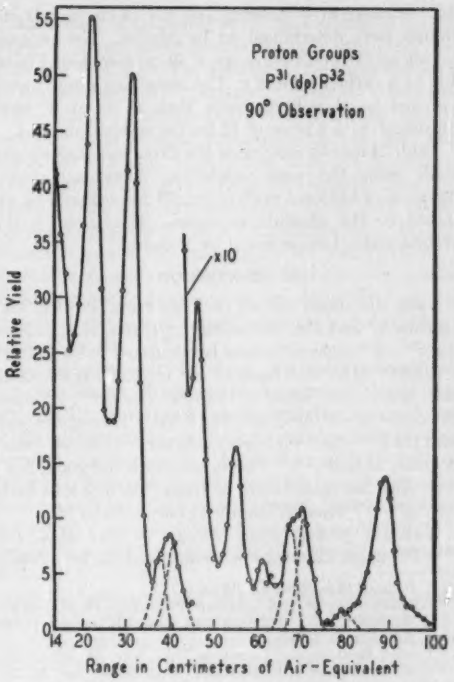

FIG. 2. Proton yield *versus* proton range.

angle straggling, beam inhomogeneity, and counter bias.[5,6] The errors quoted in Table I are relative errors and are stated with the energy levels. An additional error of ±0.05 Mev must be assigned to the absolute Q-values. The Q-values found by Bower and Burcham are also listed.

III. PHOSPHORUS

For the phosphorus reaction, the targets used were vacuum evaporated, 1 to 2 mm air equivalent, red phosphorus. The methods of detection and range measurement of the protons were the same as those used for fluorine.

In the case of phosphorus it was easier to rule out groups from contaminants because of the larger mass differences between phosphorus and the standard high yield, light element impurities. The group structure was observed at 90° and 0° with respect to the incident beam, so that from energy and momentum considerations, the shifts in the range of the groups for the two observations could be used to determine the approximate masses of nuclei giving rise to the groups.

Figure 2 shows the results for 90° observation. By the

[5] M. S. Livingston and H. A. Bethe, Rev. Modern Phys. **9**, 245 (1937).
[6] R. F. Humphreys and H. T. Mots, Phys. Rev. **74**, 1232 (1948).

shift in range at 0° observation, the 24-cm and 34-cm groups were determined to be oxygen. The protons having an extrapolated range of 40 cm were found to be due to a carbon impurity. The remaining groups were assigned to phosphorus since their shifts at 0° were consistent with a mass of 32 for the residual nucleus.

Table II lists an analysis of the data. The analysis was made using the same corrections mentioned above. Again, an additional error of ±0.05 Mev should be assigned to the absolute Q values. Also listed is the ground-state Q value found by Pollard.[7]

IV. DISCUSSION

Using the mass values of Tollestrup, Fowler, and Lauritsen,[8] and the ground-state Q-value of 4.16 Mev the $F^{20}-F^{19}$ mass difference is calculated to be 1.00211 ±0.00010 MU. The mass of F^{20} is 20.00660±0.00012 MU. With a Ne^{20} mass[9] of 19.99890, the $Ne^{20}-F^{20}$ mass difference is −0.00770±0.00015 MU. This agrees well with the $F^{20}\rightarrow Ne^{20}+\beta^-$-decay scheme (−0.00784) found by many authors.[1,10,11] The agreement is not good, however, with the recent work of Jelley,[12] in which he finds the $Ne^{20}-F^{20}$ mass difference to be −0.00716 MU.

With the ground state Q-value of 5.52 Mev, the $P^{32}-P^{31}$ mass difference is determined to be 1.00065 ±0.00011 MU. Using the Mattauch and Flammersfeld[9] P^{32} mass, the P^{31} mass is 30.98286±0.00021.

The reactions[13–15]

$$Cl^{35}(d,\alpha)S^{33} \quad Q_0=9.1 \text{ Mev}$$
$$S^{32}(d,p)S^{34} \quad Q_0=8.7 \text{ Mev}$$
$$P^{31}(\alpha,p)S^{34} \quad Q_0=1.3 \text{ Mev}$$

give the $Cl^{35}-P^{31}$ mass difference as 3.99609. The Cl^{35} mass[16] of 34.97903 leads to a P^{31} mass of 30.9829, in excellent agreement with the above value.

With the Mattauch and Flammersfeld aluminum and silicon mass values, the reactions[17,18]

$$Al^{27}(\alpha,n)P^{30} \quad Q_0=-2.93 \text{ Mev}$$
$$P^{31}(\gamma,n)P^{30} \quad Q_0=-12.4 \text{ Mev}$$

give a P^{31} mass of 30.98448 and[17,19]

$$Si^{30}(d,n)P^{31} \quad Q_0=4.56 \text{ Mev}$$
$$Si^{28}(\alpha,p)P^{31} \quad Q_0=-2.23 \text{ Mev}$$

give 30.98392 and 30.98361, respectively. These values do not agree with the present work.

The authors wish to express their appreciation to Professor E. C. Pollard who suggested these problems and generously gave encouragement and advice.

[7] E. Pollard, Phys. Rev. **57**, 1086A (1940).
[8] Tollestrup, Fowler, and Lauritsen, Phys. Rev. **78**, 372 (1950).
[9] J. Mattauch and A. Flammersfeld, "Isotopic report" Verlag der Z. Naturforsch. (1949).
[10] Fowler, Delsasso, and Lauritsen, Phys. Rev. **49**, 561 (1936).
[11] S. C. Curran and J. E. Strothers, Proc. Camb. Soc. **36**, 252 (1940).
[12] J. V. Jelley, Proc. Phys. Soc. (London) **63**, 538 (1950).
[13] E. F. Shrader and E. Pollard, Phys. Rev. **59**, 277 (1941).
[14] P. W. Davison, Phys. Rev. **75**, 757 (1949).
[15] O. Meerhaut, Physik. Z. **41**, 528 (1940).
[16] Okuda, Ogata, Aoki, and Sugawara, Phys. Rev. **58**, 578 (1940).
[17] R. A. Peck, Phys. Rev. **73**, 947 (1948).
[18] McElhinney, Hanson, Becker, Duffield, and Diven, Phys. Rev. **75**, 542 (1949).
[19] O. Haxel, Physik. Z. **36**, 804 (1935).

PHYSICAL REVIEW VOLUME 81, NUMBER 1 JANUARY 1, 1951

A Note Concerning the $C^{14}-N^{14}$ β-Decay

E. GERJUOY
Department of Physics, University of Southern California, Los Angeles, California
(Received July 3, 1950)

The possibility that the parities of the ground states of C^{14} and N^{14} are opposite is discussed. Experiments which would determine or assist in determining the parity change are suggested.

THE spins of C^{14} and N^{14} are known to be 0 and 1, respectively. The sheli model predicts that C^{14} and N^{14} both have even parity. However, the $C^{14}-N^{14}$ beta-decay is forbidden. The value of ft is 8×10^8, implying a second-forbidden transition or possibly a highly unfavored first-forbidden transition, but certainly not an allowed transition. Nonetheless, it has been argued that the $C^{14}-N^{14}$ transition does not disagree with the shell model predictions.[1] The large ft value is explained on the hypothesis that the ground state of N^{14} is almost entirely $^3D_1$.

The ft value normally to be expected in this transition is about 6×10^9. This is the value of ft in the N^{13} and O^{15} decays, both of which are favored in Wigner's sense, as is $C^{14}-N^{14}$ in Wigner's theory.[2] To account for the observed ft-value of C^{14} on the above hypothesis, it is therefore necessary to assume that $[c(^3S_1)]^2$ is not more than about 10^{-5}, $c(^3S_1)$ being the coefficient of the normalized $^3S_1$ wave function in the ground states of N^{14}. Simultaneously, $[c(^5D_0)]^2$ in C^{14} must be approximately 10^{-5}, since $^5D_0$ to $^3D_1$ transitions are allowed. Moreover, the transition from O^{14} to the ground state of N^{14} is also forbidden, with a ft-value which is at least 2.4×10^6 from the observations[3] that transitions to the ground state of N^{14} have a probability less than five percent of that for transitions to the excited level in N^{14}. It follows that $[c(^5D_0)]^2$ in O^{14} also is small if O^{14},

[1] E. Feenberg and K. C. Hammack, Phys. Rev. **75**, 1877 (1949).
[2] E. J. Konopinski, Rev. Mod. Phys. **15**, 209 (1943).
[3] Sherr, Muether, and White, Phys. Rev. **75**, 282 (1949).

like its mirror nucleus, has spin zero and even parity. It is true that $^5D_0$ does not occur in the p^2 configuration equivalent to the configuration of C^{14} and O^{14}. However, it is improbable that the quantum numbers of the individual nucleons and the total L and S should be so nearly constant in these three nuclei.

An alternative hypothesis is the assumption that the shell model fails in one or more of these nuclei. The simplest assumption is that it fails to predict the parity of N^{14}. If N^{14} is assumed to have odd parity, the C^{14} and O^{14} transitions would each be first forbidden. The ft value would then be expected to be about 5×10^6, making the observed value of 8×10^8 in C^{14} much more readily explainable on the grounds, supported by the known magnetic moment,[1] that the ground state of N^{14} is 90 percent $^3D_1$. It is to be noted that $^1S_0$ to $^3D_1$ transitions do not occur in the first-forbidden approximation of the beta-decay theory,[2] and that the $^5D_0$ admixture in O^{14} and C^{14} may be expected to be ten percent or less if the shell model configuration assignments are approximately valid.

The remark that a different parity assignment to N^{14} can explain the observed C^{14} and O^{14} decays is not original. We wish to call attention to the fact that there exists experimental information bearing on the parity change in the C^{14} decay, and that further information can probably be obtained. The gamma-ray intensities in the reaction $N^{14}(n,\gamma)$ have been measured.[4] An excited level of N^{15} whose parity must be the same as the parity of the ground state of N^{14} is formed by slow neutron capture. The 10.82-Mev γ-ray from this level to the ground state of N^{15} is only one-fourth as intense as a competing 5.55-Mev line. If the 10.8-Mev line is assumed to be electric dipole, it is difficult to account for the observed intensity ratio, no matter what assumption is made concerning the multipole character of the 5.55-Mev line. The observations can be fitted by assuming the 10.8-Mev line either magnetic dipole or electric quadrupole. Since the spin of the excited level of N^{15} is at most 3/2, the 10.8-Mev line is either dipole or quadrupole. Magnetic quadrupole radiation is negligible compared to electric dipole. So if the 10.8-Mev line is not electric dipole, there is surely no parity change in this line, and the parity of the ground state of N^{14} is the same as the parity of the ground state of N^{15}. Accepting the shell model for N^{15}, this would mean that the parity of N^{14} is odd. On the other hand, the large radiation width of the 8.1-Mev line in $C^{13}(p,\gamma)$ suggests that this line is electric dipole and therefore, as explained below, that the parity of the ground states of N^{14} and C^{13} are opposite, in agreement with the shell model.

These speculations could be confirmed or disproved in a number of ways:

(1) By measuring the polarization-direction correlation of successive quanta in the transition from the excited level of N^{15} down to the ground state.[5] The measurement is complicated by the presence of several pairs of gamma-rays,[4] competing with each other and with the 10.8-Mev line. However, the mere existence or non-existence of a polarization-direction correlation unambiguously determines the over-all parity change, provided there is some angular correlation[6] and provided the efficiency of detection does not depend on which gamma-ray goes to the polarization detector.[6] There will be angular correlation[7] unless each of the intermediate levels in the N^{15} transitions have $J=1/2$. Since the gamma-ray energies are not too different, it should be possible to make the detection efficiencies equal. Consequently, despite the complexity of the transition, determination of the over-all parity change appears hopeful.

(2) By measuring, as above, the polarization-direction correlation of successive quanta in the reaction, $C^{13}(p,\gamma)N^{14}$. Because of the large proton width of this reaction, it is almost certainly formed by capture of an s-proton. Consequently the 8.1-Mev excited state of N^{14} which is formed is almost certain to have the same parity as C^{13}, odd on the shell model. That the excited state of N^{14} is formed by s-protons is consistent with measurements of the angular distribution of the gamma-radiation.[8]

(3) By measuring the internal pair creation coefficient. This provides a useful means of determining the multipole character of gamma-radiation in high energy transitions in light nuclei.[9] Calculations of this coefficient have been made for electric dipole and quadrupole transitions, and for magnetic dipole transitions.[10] Both the 10.8-Mev line of N^{15} and the 8.1-Mev line of N^{14} discussed above at most can be quadrupole transitions. Thus, comparison of theory and experiment can determine unambiguously the parity change in these transitions. Since a multiplicity of lines are observed in these transitions and the coefficients are not very strongly energy dependent at these energies, the experiment may prove to be difficult. An alternative is measurement of this coefficient in the 2.3-Mev line which follows the positron decay of O^{14}. Since the O^{14} decay is obviously allowed,[3] hypothesizing the spin of O^{14} to be zero, we infer that the excited state of N^{14} at 2.3 Mev has at most spin 1 and has the same parity as the ground state of O^{14}. The 2.3-Mev line is therefore at most a quadrupole transition, and measurement of its internal pair creation coefficient should give the parity change between the ground state of O^{14} and the ground state of N^{14}.

It is, of course, necessary to examine each of these proposed experiments more closely before experimental feasibility is assured.

I wish to thank Professor Robert Christy for his comments.

[4] Kinsey, Bartholomew, and Walker, Phys. Rev. **77**, 723 (1950).
[5] F. Metzger and M. Deutsch, Phys. Rev. **78**, 551 (1950).
[6] D. R. Hamilton, Phys. Rev. **74**, 782 (1948).
[7] D. R. Hamilton, Phys. Rev. **58**, 122 (1940).
[8] S. Devons and M. G. N. Hine, Proc. Roy. Soc. **A199**, 56, 73 (1949).
[9] E. R. Rae, Phil. Mag. **40**, 1155 (1949).
[10] M. E. Rose, Phys. Rev. **76**, 678 (1949).

World-Wide Distribution of Natural Radiocarbon*

E. C. ANDERSON† AND W. F. LIBBY
Institute for Nuclear Studies and Department of Chemistry, University of Chicago, Chicago, Illinois
(Received May 31, 1950)

The natural radiocarbon content of biological materials collected from locations widely scattered over the earth's surface have shown no evidence of the latitudinal variation which would be expected were the turnover time for the biosphere comparable with the mean life of radiocarbon. The strong dependence of the intensity of the cosmic-ray neutrons, which produce the natural radiocarbon, on latitude would be expected to cause this effect. Since it is expected, however, on geochemical evidence that the turnover time for the biosphere would be very short compared to the mean life of radiocarbon, the observed uniformity is not surprising.

The observed mean assay of carbon in equilibrium with the biosphere is 16.1±0.5 dpm/g C. Consideration of the amounts of the various types of carbon in equilibrium with the biosphere, of which the most abundant is the inorganic carbonate and bicarbonate ions dissolved in sea water, gives 8.3 grams per cm² of the earth's surface. A direct comparison with observed cosmic-ray neutron intensity is made by taking the observed thermal intensity and correcting according to standard formulas for the epithermal production of radiocarbon, to give a total of 156±30 neutrons/cm² of earth's surface/minute on the average. Therefore, one expects that the mean specific activity of carbon in equilibrium with the biosphere would be the ratio of 156 to 8.3, or 18.8±5 dpm/g. The agreement between the predicted and observed specific activity is gratifying, but owing to the considerable uncertainties in our knowledge of the cosmic-ray intensity and the amount of diluting carbon, it may be that it is somewhat fortuitous. It does appear to indicate, however, that no considerable variation in cosmic-ray intensity over the past several thousand years has occurred. The fact that the principal part of the diluting reservoir is inorganic material in the sea water serves to make any large variation in the amount of carbon in this reservoir unlikely.

I. INTRODUCTION

THE occurrence of radiocarbon in nature because of cosmic-ray action on the atmosphere[1–5] and its use for archaeological and geological dating[6,7] raise several points of general interest. One of these is the world-wide distribution of radiocarbon and the balance between the cosmic radiation intensity and the observed specific radioactivity of living matter.[1,4,6]

The cosmic-ray primaries produce neutron secondaries in the intensity $\bar{Q}$ (neutrons/cm²/sec) as averaged over the earth's surface. Since no other process for neutron absorption in air is likely to utilize more than 2 or 3 percent as many neutrons as the $N^{14}(n,p)C^{14}$ reaction to produce radiocarbon, we immediately conclude that the terrestrial inventory of radiocarbon must be such as to insure a disintegration rate of $5.1\times10^{18}\bar{Q}$, where 5.1×10^{18} is the area of the earth in cm². This assumes that the process has been occurring at a steady value of $\bar{Q}$ for several half-lives, or sometime over 20,000 years, so that a steady-state condition has been established in which the rates of formation and disintegration are equal.

The steady-state inventory must be $(5.1\times10^{18}\bar{Q}\times14)/(6\times10^{23}\lambda)$ grams, where λ is the disintegration rate corresponding to the half-life of 5568±30 years.[8–12] The measured value of $\bar{Q}$ appears to be close to 2.6 neutrons/cm²/sec, as we shall see later. These figures correspond to an inventory of 80 metric tons of radiocarbon and an annual production rate of 9.8 kg.

The questions of the world-wide distribution of radiocarbon and the expected average specific radioactivity for the various forms of terrestial carbon involve two principal considerations. First, the neutrons are absorbed at high altitudes,[13] so the source of radiocarbon can be considered to be at 30,000 ft or higher and the newly born carbon atoms will probably burn to CO_2 before reaching the earth. Therefore, we are led to expect all plant life to be radioactive, since the atmospheric CO_2 on which it lives is radioactive and the animals living off plants must possess the same radioactivity. In addition we see that inorganic carbon such as CO_3^{--}, HCO_3^-, and H_2CO_3 in the sea which exchange with CO_2 will be radioactive. This last category proves to constitute the main part of the diluting carbon inventory.

The second major consideration is whether the mixing is likely to be adequate in the lifetime of the average radiocarbon atom (8033 years, average life). The mixing times for the atmosphere and the biosphere seem certain to be short as compared with 8033 years,

* Submitted by E. C. Anderson in partial fulfillment of the requirements for the degree of Doctor of Philosophy in the Graduate School, Division of Physical Sciences, University of Chicago. This research was supported in part by a grant from the Viking Fund, Inc., for which the authors express their gratitude.

† DuPont Fellow in Chemistry, 1948–49. Now at Los Alamos Scientific Laboratory.

[1] W. F. Libby, Phys. Rev. **69**, 671 (1946).
[2] Anderson, Libby, Weinhouse, Reid, Kirshenbaum, and Grosse, Science **105**, 576 (1947).
[3] A. V. Grosse and W. F. Libby, Science **106**, 88 (1947).
[4] Anderson, Libby, Weinhouse, Reid, Kirshenbaum, and Grosse, Phys. Rev. **72**, 931 (1947).
[5] E. C. Anderson, Doctoral Thesis, University of Chicago, 1949.
[6] Libby, Anderson, and Arnold, Science **109**, 227 (1949).
[7] J. R. Arnold and W. F. Libby, Science **110**, 678 (1949).
[8] Engelkemeir, Hamill, Inghram, and Libby, Phys. Rev. **75**, 1825 (1949).
[9] W. M. Jones, Phys. Rev. **76**, 885 (1949).
[10] Miller, Ballentine, Bernstein, Friedman, Nier, and Evans, Phys. Rev. **77**, 714 (1950).
[11] Engelkemeir and Libby, Rev. Sci. Instr. **21**, 550 (1950).
Note added in proof: The 5568 year half-life is derived from a correction[11] on our earlier value of 5720[8] and an averaging with other published values.
[12] Hawkings, Hunter, Mann, and Stevens, Can. J. Research, **27**, 545 (1949).
[13] For example, L. C. L. Yuan, Phys. Rev. **77**, 728 (1950).

but the status of ocean mixing is less certain. It seems likely, however, that this probably is essentially complete also.

The experimental values for the inventory are given in Table I.

The experimental value for the specific radioactivity of living (biospheric and organic) material is 15.3±0.5 disintegrations per minute per gram of carbon; for inorganic carbonate carbon, 16.2±0.5; to give 16.1±0.5 for the average carbon in the inventory, which weighs 8.3 g/cm². Multiplying, we have 134 dpm/cm² *vs.* 156±30 cosmic-ray neutrons/cm²-min., the rate expected for a complete steady-state balance. Since the data are hardly more accurate than twenty percent, the check seems satisfactory. In addition, no significant variation with latitude, longitude, altitude, or depth in the sea has been found, so the mixing seems to be essentially complete.

II. NEUTRON PRODUCTION RATE, Q

The distribution of neutrons[12–18] in the atmosphere is exponential up to about 40,000 feet with a half-thickness of about one meter of water equivalent. Above 40,000 feet a maximum is reached followed by a rapid decrease indicating the secondary nature of the neutrons. In addition to the altitude dependence, the neutron intensity shows a strong dependence on geomagnetic latitude,[14,17] the intensity at high latitudes being about four times that at the magnetic equator. This variation must be considered, of course, in calculating the world-wide average intensity, $\bar{Q}$.

The measurements on neutron intensity which we use for our calculations of total intensity have been on the thermal component as defined by cadmium absorption for a boron detector. We shall take this to mean that that fraction of the neutron spectrum lying below 0.4 ev has been measured, and in order to calculate Q and its world-wide average $\bar{Q}$, we must determine theoretically the probable ratio of the total intensity to the thermal intensity. Bethe, Korff, and Placzek[19] and Placzek[20] have considered the problem in detail. Following their treatment and using the later data of Melkonian,[21] together with the data collected in the M.I.T. Volume,[22] we shall assume that in the range 0.4 ev to 0.5 Mev the total cross section in units of 10^{-24} cm² for air is given by

$$\sigma_t = 8.56 + (0.266/E^{\frac{1}{2}}),$$

and that the capture cross section is given by

$$\sigma_c = 0.266/E^{\frac{1}{2}}.$$

The expression for the ratio of the total number of neutrons generated to the number which reach the thermal range is e^y, where y is given by

$$y = (2/0.248)\int_{0.4}^{5\times10^5} \sigma_c dE/\sigma_t E,$$

where the number 0.248 is the fractional energy loss in elastic collision with the nitrogen atom, the bond strength being neglected. Integration and substitution give 0.79 for the integral and the calculated ratio of total production to thermal population of 2.20. It is clear, however, that one must consider the effect of the very strong bonds in the nitrogen and oxygen molecules on the cooling process. Study of the analogous problem of the effect of binding on the neutron elastic and inelastic cross sections for hydrogen[23] leads us to expect that no large error is made in neglecting the binding for cooling down to the Cd cut-off of 0.4 ev, which is 1.5 vibrational quanta for the average air molecule.

It is necessary to make a correction for the absorption above 0.5 Mev. It has been shown by Barschall and Battat[24] and others[22] that resonance production of radiocarbon occurs in this range at cross sections rising to maxima of 0.1×10^{-24} cm² and falling to about 0.01×10^{-24} cm² in the range 0.5 Mev to 2 Mev. To obtain a probable upper limit for the capture contribution in this high energy range, we assume that only elastic scattering occurs and an average capture cross section of 0.035×10^{-24} cm² applies throughout the high energy interval. This gives an additional contribution of 7 percent to the ratio of total to thermal neutron population. The corrected ratio is 2.36.

The value of Q is now to be obtained at any given latitude by multiplying the observed thermal intensity Q by the number 2.36. For this purpose we choose the data of Yuan and Ladenberg[13–15] obtained at Princeton, New Jersey, which give 1.9 as the number of slow cosmic-ray neutrons absorbed per sec per cm² of earth's surface at that latitude (we are very obliged to Professor Ladenberg for making this result available to us before publication). Using Simpson's data for the variation of Q with latitude and integrating over the surface of the earth, we find for the average thermal flux, 1.1 thermal cosmic-ray neutrons/cm²-sec. Finally, multiplying by the ratio of total production to thermal neutron population, we obtain 2.6 as the most likely value for $\bar{Q}$, the

TABLE I. Carbon inventory.

Source	Amount
Ocean "carbonate"	7.25 g/cm²
Ocean, dissolved organic	0.59
Biosphere	0.33
Atmosphere	0.12
Total	8.3 g/cm²

[12] L. C. L. Yuan, Phys. Rev. **76**, 1267, 1268 (1949).
[13] L. C. L. Yuan and R. Ladenburg, Bull. Am. Phys. Soc. **23**, No. 2, 21 (1948).
[14] L. C. L. Yuan, Phys. Rev. **74**, 504 (1948).
[17] J. A. Simpson, Jr., Phys. Rev. **73**, 1389 (1948).
[15] Agnew, Bright, and Froman, Phys. Rev. **72**, 203 (1947). (This paper contains references to many earlier measurements.)
[19] Bethe, Korff, and Placzek, Phys. Rev. **57**, 573 (1940).
[20] G. Placzek, Phys. Rev. **69**, 423 (1946).
[21] E. Melkonian, Phys. Rev. **76**, 1750 (1949).
[22] *Science and Engineering of Nuclear Power* (Addison-Wesley Press, Inc., 1947), Vol. 1, pp. 408–411.
[23] H. A. Bethe, Revs. Modern Phys. **9**, 122–127 (1937).
[24] H. H. Barschall and M. E. Battat, Phys. Rev. **70**, 245 (1946).

average total production of cosmic-ray neutrons per cm^2 of earth's surface per sec. Considering the various sources of error in this figure, it seems that it probably is good to about 20 percent, though there is, of course, considerable possibility that the error is somewhat larger or smaller than this.

III. EXPECTED TERRESTRIAL DISTRIBUTION AND SPECIFIC ACTIVITY OF LIVING MATTER

Turning now from the production of radiocarbon to the process of dilution, we consider the geochemical fate of the C^{14} produced by the cosmic-ray neutrons. It is clear that it will be rapidly converted to carbon dioxide and therefore will be diluted by all carbon dioxide in the air. It then follows, of course, that all plant life and all animal life on earth must contain radiocarbon, and that the carbonate dissolved in the sea, which will exchange with atmospheric carbon dioxide, will also be radioactive. We shall find that the largest part of the diluting material is the carbonate dissolved in the sea.

In order to estimate the amount of dissolved carbonate in the sea one needs to know the alkalinity and the pH$[-\log(H^+)]$ of the ocean water. The alkalinity is the excess of positive ions over the anions of strong acids, and is made up by the ionization of weak acids, of which carbonic acid is the principal one in the ocean. The average value of the alkalinity is well established at 2.43 milliequivalents per liter.[25] This must be reduced to 2.37 for the boric acid in the water. The total amount of dissolved inorganic carbon in the sea is not uniquely determined by the alkalinity, owing to the possibility of its existence as H_2CO_3, HCO_3^-, and $CO_3^=$. The ratio of the amounts in these various forms is determined by the pH.

The values of the dissociation constants for H_2CO_3 and HCO_3^- have been carefully measured by a number of investigators[26–28] as functions of pH, salinity, temperature, and pressure in both natural and artificial sea water. The results appear to be very reliable. Using standard data we find for average ocean water $K_1 = 1.26 \times 10^{-6}$ and $K_2 = 7.4 \times 10^{-10}$. The variation in the pH of the ocean is surprisingly small, the average value[29] being 8.0 and the total variation less than 0.1 pH unit. The application of these numbers gives 26.2 mg of carbon per kg of sea water, or 7.25 g/cm^2 of the earth's surface, corresponding to a total mass of 3.7×10^{19} grams. The error in this figure may be as large as 10 percent, arising mainly from the small but significant observed variation of the pH and the scatter in the values for the alkalinity as reported by various observers.

The remaining items in the inventory of exchangeable carbon are the dissolved organic carbon in the sea, the atmospheric carbon dioxide, and the biosphere. For the first of these the best figure[30] appears to be 2 mg/liter, corresponding to 0.59 g/cm^2.

Atmospheric carbon dioxide has been determined by several people. The values are: Buch,[31] 0.12 (polar) to 0.13 (tropical and continental); Paneth,[32] 0.12; and Vernadsky,[33] 0.12. We will use 0.12 g/cm^{-2} for the amount of carbon in atmospheric carbon dioxide. This is equivalent to CO_2 partial pressure of 0.21 mm Hg, or a concentration of 0.028 percent.

The amount of carbon in living matter is difficult to estimate and appears to have been grossly overestimated by some writers in the past. We base our estimate on the rate of fixation of carbon by photosynthesis, a quantity which appears to be fairly well established.[34] Fortunately it can be shown that biosphere carbon is small compared with ocean carbonate, and therefore an error in its estimation will not be of great importance.

The total rate of fixation of carbon by land plants has been investigated by Schroeder[35] who concluded that the average annual fixation by this source is 1.63×10^{16} grams or 3.2 mg/cm^{-2}. Riley[36] made an investigation of the fixation by ocean plankton and arrived at a figure of 30.5 mg/cm^{-2} for the average annual rate. Rabinowitch[37] estimates that on the basis of the solar energy flux, reflection losses, and photosynthetic efficiency, not more than 60 mg/cm^{-2} could be fixed annually, indicating that Riley's figure cannot be too low by any large factor. We shall use the sum of the values given by Schroeder and Riley as the total annual rate of fixation of carbon, namely 33 mg/cm^{-2}. The total amount of carbon contained in the biosphere at any time will be given by the fixation rate times the average "life" of a carbon atom in the biosphere, if a steady state exists. Estimation of this life is somewhat easier than might appear on first glance since 90 percent of the fixation is by ocean plankton, which are minute organisms of very short life. Furthermore, even the carbon contained in longer-lived organisms does not in general have a "life" equal to that of the organism, but rather the material of the organism is replaced a number of times during its life. A maximum average "life" of a carbon atom of not more than a few years is indicated by these considerations. Since biocarbon is such a small fraction of the total reservoir, a more exact treatment appears unnecessary. Taking 10 years for the average carbon life, our calculated biosphere holdup

[25] Sverdrup, Johnson, and Fleming, *The Oceans* (Prentice-Hall, Inc., 1946), p. 208.
[26] Moberg, Greenberg, Revelle, and Allen, Bull. Scripps Inst. of Oceanography, Univ. of Cal. Tech. Series 3, 231 (1934).
[27] K. Buch, Acta Acad. Aboensis, Math. et Phys. 11, no. 5 (1938).
[28] Reference 25, p. 250.
[29] Reference 25, p. 191.
[30] Reference 25, p. 250.
[31] K. Buch, Acta Acad. Abonensis, Math. et Phys. 11, no. 12 (1939).
[32] F. Paneth, quoted by G. Kuiper, *The Atmospheres of the Earth and Planets* (University of Chicago Press, Chicago, 1949), p. 1.
[33] W. J. Vernadsky, *Geochemie in Ausgewahlten Kapiteln* (Akademische Verlagsgesellschaft, Leipzig, 1930).
[34] E. Rabinowitch, *Photosynthesis and Related Processes* (Interscience Publishers, Inc., New York, 1945), Chapter I.
[35] G. Schroeder, Naturwiss. 7, 8 (1919); 7, 976 (1919).
[36] J. Riley, Bull. Bingham Oceanographic Coll. 1, 1 (1941), quoted by Rabinowitch, reference 34, p. 6.
[37] Reference 34, p. 6.

will be taken as 0.33 g/cm^{-2}, which will prove to be only 4 percent of the total.

The only way of appreciably increasing the hold-up of the biosphere is by the assumption that a considerable portion of this material spends many years in slow decay as humus or ocean sediments before it is recycled. The available evidence seems to be that the major part of the dead material is dissolved during the settling process and that little of it ever reaches the ocean floor.[38] The possibility of appreciable hold-up in humus can be eliminated on the basis of the comparatively small amount of carbon involved in the terrestrial cycle.

In addition to the dilution of cosmic radiocarbon by the carbon of the exchange reservoir, some is being removed constantly by incorporation in sedimentary rocks as they form. This rate of loss of radiocarbon will be estimated. The rates of deposition of calcium carbonate in the sea are not at all well established. Various estimates can be made on the basis of the total amount of calcium carbonate that has been deposited, the bicarbonate contents of rivers emptying into the sea, and the direct observation of the rate of formation of ocean sediments. For example, Brown[39] has calculated the following inventory of carbon in the sedimentary rocks: in shale, 5.45×10^{21} grams; in sandstone, 0.20×10^{21} grams; and in limestone, 3.67×10^{21} grams; for a total of 9.3×10^{21} grams of carbon. If we assume uniform deposition over a two-billion-year period, we have a yearly loss rate of 5×10^{12} grams, which would remove only 6 grams of the 9800 grams of radiocarbon made each year. This may be low because recycling may be important, and the other methods give somewhat higher figures; but it seems likely that the total removal by the formation of sedimentary deposits is not likely to exceed about 3 percent.

We may now consider the question as to whether or not the various portions of the exchange reservoir are sufficiently well mixed so that they are 100 percent efficient in the dilution process. The uniform distribution of C^{14} throughout the reservoir will result only if the various mixing processes are complete in a time short compared with the average life of C^{14}. From the estimated photo-synthetic fixation rate given above and the total material in the exchange reservoir, it can be calculated that 250 years would suffice to turn over all the carbon through the biosphere. This insures that the thin layer of the reservoir at the surface of the earth and of the ocean will be well mixed. The main question is whether or not the depths of the oceans and the upper reaches of the atmosphere are mixed.

Considering the latter first, we note that Yuan's data indicated that the maximum in the neutron flux intensity occurs at about 40,000 feet and that it has fallen off considerably by 70,000 feet. At this altitude the air pressure is 3.5 mm Hg. Excellent and rapid mixing is well established in the troposphere, the adiabatic portion of the atmosphere in which most weather phenomena occur. In the meteorological "standard atmosphere" the tropopause, or boundary between the adiabatic troposphere and the isothermal stratosphere, is assumed to be[40] at 10.8 km (36,000 feet). However, the height of the tropopause varies considerably with the season and with latitude, reaching 18 km (58,000 feet) in the winter at 40° N latitude while in summer it may be found at 16 km (52,000 feet) as far north as 60° N geomagnetic latitude.[41] Thus the tropopause is actually above the altitude of maximum neutron intensity some of the time each year. Even the isothermal stratosphere is not without vertical mixing.[42]

The situation with regard to oceanic mixing is much less obvious. Very little indeed is known concerning the quantitative rates of convective mixing of the deep ocean basins. (Diffusive mixing is of course so extremely slow as to be out of the question.)

From the limited data available on ocean circulation at moderate depths (*ca.* 4000 meters), one can estimate that mixing in the Atlantic Ocean, for example, may occur on a time scale of the order of 10^3 years, but this estimate is a crude one and not applicable to deep basins.

Another argument in favor of complete mixing of the ocean basins may be based on the following considerations. It is known that heat is being liberated from the earth's crust at the rate[43] of about 30 cal/cm^2-yr. Presumably the evolution of heat from the bottom of the ocean is of a similar magnitude,[44,45] and one might expect regions of temperature inversion to develop near the ocean bottom for this reason, especially in areas of poor circulation. To transfer this amount of heat by molecular conduction would require a thermal gradient of 8×10^{-4} deg/cm (if the conductivity of water is assumed to be 0.0013). If a layer of 1,000-meters thickness at the bottom were cooled by molecular conduction only, a temperature difference of 80°C would be required. Naturally, turbulent eddy circulation patterns would be set up at much lower gradients, and the more effective mechanism of eddy conductivity would operate to remove the heat. Such eddy circulation would be equally efficacious in the transfer of dissolved carbonate, and a very efficient method of maintaining the C^{14} equilibrium would arise. It can be calculated, for example, that a temperature gradient of 1.6×10^{-6} deg/cm would require a coefficient of eddy conduction some 500 times the molecular coefficient for the transfer of the postulated amount of heat. (This is quite small as eddy coefficients go, since they often range up to 10^5 or more times the molecular coefficients.) Such an

[38] Reference 25, p. 1012.
[39] H. S. Brown, private communication.
[40] H. R. Byers, *General Meteorology* (McGraw-Hill Book Company, New York, 1944), p. 171.
[41] C. G. Rossby in *The Atmospheres of the Earth and Planets*, Ed. G. Kuiper (University of Chicago Press, Chicago, 1949), p. 21.
[42] L. Spitzer, Jr., reference 41, p. 221.
[43] E. C. Bullard, Nature **156**, 35 (1945).
[44] H. Pettersson, Nature **164**, 468 (1949).
[45] A. E. Benfield, Nature **165**, 445 (1950).

eddy circulation operating at depths below 4,000 meters can be shown[46] to be adequate to mix the ocean depths sufficiently so that the assay of C^{14} at 6000 meters would be 90 percent of normal with an integrated effect of only 1.4 percent on the mean specific activity.

Few cases of temperature inversion in the deep ocean have been established. The inversion gradient chosen in the above calculation is that observed in the Mindanao Trench[47] and is almost exactly equal to the gradient which would be produced by adiabatic compression (i.e., there is no density inversion, the density of the water being constant with depth, as is also the potential temperature). However, the smaller the thermal gradient the larger the coefficient of eddy conduction required to transport the heat. Without specifying the nature or source of the circulation, we merely point out that if 30 cal/cm^{-2}-yr are being evolved from the ocean floor, a certain minimum rate of circulation must exist in order to prevent the development of large thermal gradients. The above arguments are of necessity qualitative, since turbulent eddy circulation is not amenable to calculation. However, if the assumption of the specified heat evolution is correct, the absence of appreciable thermal inversions near the ocean bottom would seem to indicate that the mixing is very good indeed on our time scale.

It has not been possible to obtain samples of dissolved carbon from the very deep ocean, so that experimental evidence on the mixing time is not at hand. It would appear that measurements of this kind might be of considerable oceanographic interest and might shed some light on the problem of circulation in the deep basins.

We arrive finally, therefore, at 8.3 g/cm^2 for the value of the diluting inventory, distributed as indicated in Table I through the exchange reservoir. The uncertainty in this value we place at about 15 percent, most of this error being in the estimated uncertainty in the value for ocean carbonate. Combining with the value of 156±30 for the neutron intensity/cm^2-min. we calculate an expected specific activity of 18.8±5 per minute per gram of carbon.

IV. EXPERIMENTAL TECHNIQUE

The measurement technique employed the screen wall counter[48,49] with a sample consisting of elementary carbon and the shielding accomplished by a combination of several inches of lead and iron and a surrounding layer of anticoincidence counters.[50] The sample was disposed on a movable cylinder so that the background could be measured by sliding it to one end of the counters away from the sensitive volume.

The preparation of the sample consisted in direct combustion (or in the addition of acid in the case of carbonates) to produce carbon dioxide, which was then purified by precipitation as calcium carbonate, reaction of this carbonate with acid to form carbon dioxide a second time, and reduction of the purified carbon dioxide with hot magnesium metal.

The samples were washed frequently with dilute acid prior to combustion in order to remove any occluded calcium carbonate which might be decomposed during the combustion. These cleansing precautions were found to be necessary in certain instances and were instituted as a standard step in the procedure in nearly all cases.

The elementary carbon sample (8.5 g) was moistened with 20 cc of 0.15 percent agar-agar solution plus about 30 cc of distilled water to make a paste, which was spread smoothly over the inside of the sample cylinder, dried in a warm air stream until the paste was no longer fluid, placed in the counter which was then evacuated for several hours during which the remaining water was pumped off, and then filled with 0.6 cm of ethylene and 10 cm of argon.

A standard run consisted of 48 hours with alternations of the sample cylinder every 4 to 8 hours between the "sample" and the "background" positions. The relative time spent on the sample and background depended on the difference between them, and the intervals were taken as the square roots of the ratios of the absolute counts under the two different conditions.

The observed difference between the sample and the background together with the Poisson statistical error for both were used to calculate the activity of the sample, together with the error in it. The absolute activity of the sample was determined by a separate calibration of the counter.

For the calibration of the counter, carbon dioxide which had been assayed absolutely in a gas counter[8] was used to prepare a carbon sample, which then was counted in the usual manner; and the percent response was used to determine the absolute efficiency. The result was 5.46±0.03 percent for 8 grams of carbon spread over 400 cm^2.

V. EXPERIMENTAL RESULTS. THE DISTRIBUTION AND MEAN SPECIFIC ACTIVITY

It was planned to select samples from widely scattered points over the earth's surface so that any latitudinal variation caused by the known variation in the neutron component of the cosmic radiation would be revealed. The material chosen for the majority of the samples was wood. This choice was made because wood was thought to be the material most likely to be encountered in the program of archaeological age measurements to which the present research was fundamental. A second point was that wood is widely distributed through great extremes of latitude and altitude, and is readily available from museum collections. The final point was that

[46] The authors are indebted to Dr. Henry Kierstead of the Institute for Nuclear Studies for his interest in this question and for his assistance in the calculations.
[47] Reference 25, p. 739.
[48] W. F. Libby, Phys. Rev. **46**, 196 (1934).
[49] W. F. Libby and D. D. Lee, Phys. Rev. **55**, 245 (1939).
[50] Detailed blueprints may be obtained from the authors.

TABLE II. Activity of terrestrial biosphere samples.

Source	Geomagnetic latitude	Absolute specific activity (dpm/g)
White spruce, Yukon (Frederick Johnson)	60° N	14.84±0.30
Norwegian spruce, Sweden (Donald Collier, CNH Museum)	55° N	15.37±0.54
Elm wood, Chicago (Authors)	53° N	14.72±0.54
Fraximus excelsior, Switzerland (Donald Collier)	49° N	15.16±0.30
Honeysuckle leaves, Oak Ridge, Tenn. (C. H. Perry, Clinton Laboratory)	47° N	14.60±0.30
Pine twigs and needles (12,000 ft alt.), Mount Wheeler, New Mexico (Robert Fryxell)	44° N	15.82±0.47
North African briar (John Hudson Moore, Inc.)	40° N	14.47±0.44
Oak, Sherafut, Palestine (Donald Collier)	34° N	15.19±0.40
Unidentified wood, Teheran, Iran (M. Hessaby)	28° N	15.57±0.31
Fraximus Mandshurica, Japan (Donald Collier)	26° N	14.84±0.30
Unidentified wood, Panama (John Simpson)	20° N	15.94±0.51
Chlorophora excelsa, Liberia (Donald Collier)	11° N	15.08±0.34
Sterculia excelsa, Copacabana, Bolivia (9000 ft alt.) (Donald Collier)	1° N	15.47±0.50
Ironwood, Majoro, Marshall Islands (Donald Collier)	0°	14.53±0.60
Unidentified wood, Ceylon (Donald Collier)	2° S	15.29±0.67
Beech wood, Tierra del Fuego (Junius Bird)	45° S	15.37±0.49
Eucalyptus, New South Wales, Australia (Donald Collier)	45° S	16.31±0.43
Seal oil from seal meat from Antarctic (Byrd Expedition *via* H. J. Deason)	65° S	15.69±0.30
Average		15.3 ±0.1[a]

[a] Error of calibration of counter raises error on absolute assay to 0.5.

it seems from a chemical point of view that cellulose and lignin should be relatively free from any danger of exchanging their carbon with other materials after the death of the tree, and samples from museum collections could be used even though they had been collected several years ago. Carbonate samples were regarded with suspicion because it was feared that exchange between crystalline calcium carbonate and carbon dioxide might occur in moist air. Only a few measurements of contemporaneous ocean carbonate were made to confirm the expected fractionation of the isotopes.

One group of samples was concentrated near the geomagnetic equator where the neutron flux is a minimum, and another in high latitudes where the neutron flux is a maximum. Some consideration was given to the archaeological importance of the region with the thought that, if no uniformity were demonstrated, these data might be utilized for the age measurement research. Two samples from high altitudes were measured, but the height of the timber line was of course very small indeed compared with the altitudes at which radiocarbon production occurs.

Experimental results are given in Tables II and III, which record the type of material measured, its geographical source, and the observed specific activity in absolute disintegrations per minute per gram of carbon. The associated error is the standard deviation calculated from the counting statistics only.

The average specific activity of all of the biosphere samples is found[51] to be 15.3±0.5 absolute dpm/g. The data seem to show no scatter other than the expected statistical fluctuations, indicating that the samples involved did indeed have specific activities identical within the error of measurement, and that the variation over the earth's surface is within the experimental error of the radioactivity measurement of about 2 percent, also. The data presented in Table III for shell reveal that shell is definitely more radioactive than organic material. This difference is to be expected, since it has been shown[52,53] that fractionation of the stable isotopes of carbon, C^{12} and C^{13}, occurs in these systems. The ratio of the C^{14} content of carbonate to that of organic material which is found here is 1.09±0.03. On the basis of the fractionation factor of 1.03 found for C^{13} against C^{12}, one would expect a value of 1.06 for C^{14}. The difference between this value and the one found in the present investigation is not outside of the present experimental error, and since the accuracy of the estimation of the fractionation factor is better than the precision of our measurements of the shell activity, we take the observed value to be 16.2±0.5, derived by multiplication of the mean of the organic specific activity by 1.06. It seems that a further investigation of the fractionation factor would be worth while.

TABLE III. Activity of contemporaneous shell samples.

Source	Assay
Murex shell, Florida West Coast	17.1±0.5
Freshly deposited ocean sediments, 1150-meters depth, Bermuda (J. Lawrence Kulp)	17.4±0.6
Oyster shells, Chesapeake Bay	15.1±0.5[a]
Average	16.5±0.5

[a] This sample had a high ash (22 percent), so the number is less reliable than the counting error indicated.

In order to calculate the mean world-wide specific activity of carbon in the exchange reservoir, we take the weighted mean using 1.0 g/cm² as the total amount of organic material in the reservoir and 7.3 g/cm² for the carbonate carbon. The result is 16.1±0.5. The agreement of this value with the expected value of 18.8±5 is very gratifying and suggests that no major factors contributing to the situation have been overlooked, although it does seem likely that the agreement may be in some part due to cancellation of errors.

[51] Earlier publications have given 12.5 for this number. The counters have been recalibrated for absolute efficiency since, and the new figure is derived from the old one by correction for the more accurately determined efficiency.

[52] A. O. Nier and E. A. Gulbranson, J. Am. Chem. Soc. **61**, 697 (1939).

[53] B. F. Murphy and A. O. Nier, Phys. Rev. **59**, 771 (1941).

A New Evaluation of h/e by X-Rays*

J. A. Bearden, F. T. Johnson, and H. M. Watts
Johns Hopkins University, Baltimore, Maryland
(Received August 2, 1950)

In previous evaluations of h/e by x-rays the correction for the work function of the cathode has been the principal source of error. New experiments have been performed with a technique which eliminates this error and proves conclusively that in the usual x-ray method a correction for the cathode work function must be made. It is also shown that the separation of the fine structure peaks from the cut off point of the high frequency limit is a function of the voltage applied to the x-ray tube. The value of h/e computed with the new velocity of light is $(1.37928\pm0.00004)\times10^{-17}$ erg sec esu^{-1}.

I. INTRODUCTION

In a recent paper,[1] the fundamental ratio h/e has been re-evaluated by the x-ray method. In that work, the principal factors which prevented a more precise evaluation of h/e were the indefiniteness of the proper work function that should be assumed for the particular oxide cathode used, and a small error which arose in locating the exact limit of the continuous spectrum. The sharpness of the fine structure observed with some targets, notably tungsten, suggested that both of the above difficulties could be eliminated by measuring the wavelength separation of the fine structure peaks for two widely separated voltages. This was found to be impossible, but h/e was measured at two very different frequencies using a unipotential tungsten emitter and a tungsten target, thus eliminating the uncertainty due to the cathode work function.

II. EXPERIMENTAL PROCEDURE

The apparatus and the experimental procedure used in the present work were the same as described by Bearden and Schwarz[1] with only two modifications. Instead of plotting the high frequency limits with a fixed x-ray wavelength and varying the voltage applied to the x-ray tube, we have maintained a constant potential and varied the x-ray wavelength by rotation of the second crystal of the double crystal spectrometer. This method, which was described in the above-mentioned work, but used only to a limited extent, has the advantage of eliminating the use of a potentiometer and its associated inaccuracies. The second, and more important modification of the equipment has been the introduction of a technique used in thermionic emission work.[2] This technique permits the use of a pure tungsten filament as a unipotential emitter. The block diagram of the apparatus is shown in Fig. 1. The precision megohm resistor[3] (number 1427) was divided into ten 10^5 ohm sections, and by a proper choice of high voltage and the number of 10^5 ohm sections used, a constant voltage drop was maintained across the 100-ohm standard resistor[3] (number 649482) which was exactly balanced by the voltage of a standard cell[3] (number 968). A switching arrangement made it possible to keep the standard cell out of the circuit while preliminary adjustments were being made. The x-ray intensity near the high frequency limit dropped so rapidly with voltage that it was found to be impracticable to use much less than 6000 volts with the x-ray spectrometer in air. The resolving power of the perfect crystals was such that little is gained by the use of potentials in excess of 10,000 volts. Therefore these were the voltages used in all of the present work.

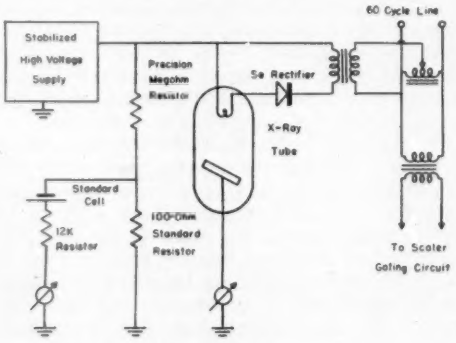

FIG. 1. Block diagram of apparatus.

In part of the present measurements, the unipotential cathode previously described[1] was used. In most of the work, however, a new technique was employed which permitted a pure tungsten filament to be used as a unipotential emitter. This was accomplished by heating the filament with half-wave rectified 60-cycle current as shown in Fig. 1 and applying a gate to the Geiger counter scaler from the same 60-cycle source, so that counts were registered only during the half-cycle when

* We acknowledge the assistance of the Bureau of Ordnance, U.S.N. which made this work possible.

[1] J. A. Bearden and G. Schwarz, Phys. Rev. **79**, 674 (1950). (The value of h/e quoted later from this paper has been corrected for the new velocity of light.)

[2] G. E. Moore and H. W. Allison, Phys. Rev. **77**, 246 (1950).

[3] For National Bureau of Standards calibration of these resistors and standard cell, see reference 1. All of the present measurements have been made as described in the above reference. Correction for temperature of spectrometer crystals has also been made as above, and all auxiliary constants are the same except the velocity of light. We have adopted the value $C=299{,}790.0$ km/sec as derived in the following paper.

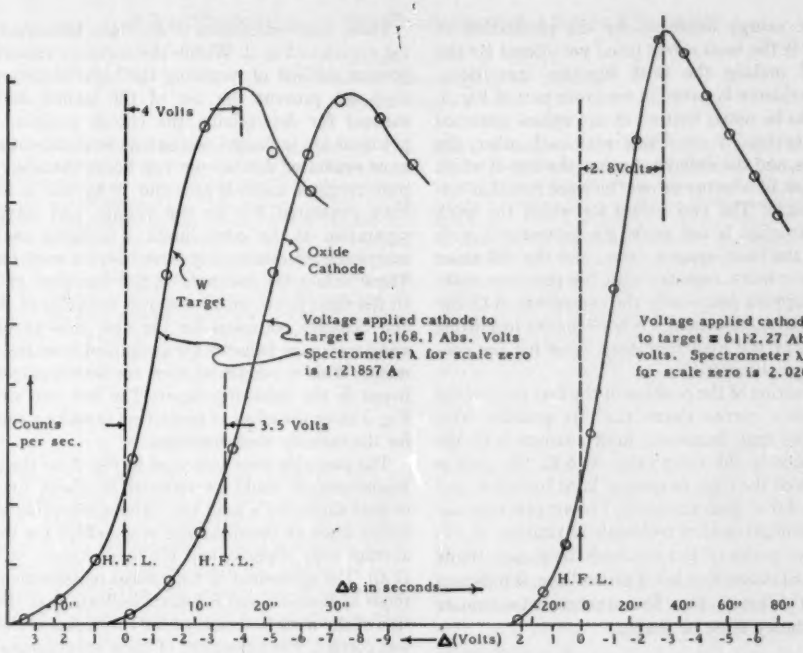
4 Volts
2.8Volts
Oxide Cathode
W Target
Voltage applied cathode to target = 10;168.1 Abs. Volts Spectrometer λ for scale zero is 1.21857 A
Voltage applied cathode to target = 6112.27 Abs. volts. Spectrometer λ for scale zero is 2.02652 A
Counts per sec.
3.5 Volts
H. F. L.
H. F. L.
H. F. L.
Δθ in seconds
Δ(Volts)

FIG. 2. Average intensity curves for three high frequency limits.

no heating current was flowing through the filament. Hence during the time the counting was taking place the filament was a unipotential surface. The x-ray tube current dropped about 20 percent during this half-cycle, but this introduced no difficulty, since the regulation of the power supply was sufficiently good to prevent the high voltage applied to the x-ray tube from changing during this current change. An oscilloscope study of the voltage variation across the tube occurring during the nonheating half of the cycle showed it to be less than 0.15 volt peak to peak, and over the entire cycle was less than 0.25 volt. The effect of the gating circuit on the scalar was tested by observing the counting rate for photons from a gamma-ray source with and without the gate at rates from 0.5 to 40 counts per second. The ratio of the counting rate with the gate to the counting rate without the gate was constant over this range, which included all the rates used in the x-ray measurements. This would not have been the case if the gate had introduced spurious counts.

III. RESULTS

The recording and averaging of the data was exactly the same as that in the previous work. Figure 2 shows the final average intensity curves for three high frequency limits taken with: (1) a tungsten target and tungsten cathode at 10 kv, (2) a tungsten target and a barium oxide on nickel cathode at 10 kv, and (3) a tungsten target and cathode at 6 kv.

The two curves taken at 10 kv were recorded under identical conditions except for the change in the x-ray tube cathode. The two limits are displaced from each other by 3.5 volts. This is exactly what we would expect since the work function for tungsten is 4.52 electron volts, and a reasonable value for the oxide on nickel is one electron volt, which gives 3.5 electron volts as the

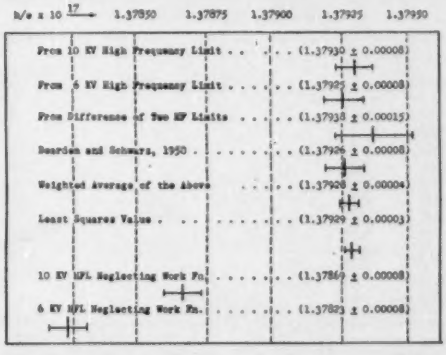
h/e x 10^17
1.37850
1.37875
1.37900
1.37925
1.37950
From 10 KV High Frequency Limit . . . (1.37930 ± 0.00008)
From 6 KV High Frequency Limit . . . (1.37925 ± 0.00008)
From Difference of Two KV Limits . . . (1.37938 ± 0.00015)
Bearden and Schwarz, 1950 . . . (1.37926 ± 0.00008)
Weighted Average of the Above . . . (1.37928 ± 0.00004)
Least Squares Value . . . (1.37929 ± 0.00003)
10 KV HFL Neglecting Work Fn. . . . (1.37869 ± 0.00008)
6 KV HFL Neglecting Work Fn. . . . (1.37823 ± 0.00008)

FIG. 3. Comparison of various values of h/e. *Note added in proof:* A correction to the least-squares work in the following paper yields $h/e = (1.379300 \pm 0.000016) \times 10^{-17}$ erg sec/esu.

difference in energy available for the production of x-rays. This is the most direct proof yet offered for the necessity of making the work function corrections. Additional evidence is shown in the lower part of Fig. 3, where it is to be noted that all of the values corrected for work function are consistent with each other, the least squares, and the difference value, the last of which is independent of whether or not the work function correction is made. The two values for which the work function correction is not made are inconsistent with each other, the least squares value, and the difference value. These results, together with the previous work, appear to disprove completely the contention of Ohlin[4] that the work function energy is not effective in shifting the position of the high frequency limit for the continuous x-ray spectrum.

An examination of the position of the first peak of the high frequency curves shows that its position with respect to the high frequency limit changes with the voltage applied to the x-ray tube. At 6 kv the peak is separated from the high frequency limit by 2.8 v, and at 10 kv by 4.0 v. This unexpected result prevents our using the voltages and wavelength separation of the fine structure peaks of the two high frequency limits as a method of evaluating h/e. Furthermore, it indicates that Nijboer's[5] theory of the fine structure is inadequate and a new theory must be sought.

[4] P. Ohlin, Inaugural Dissertation, Uppsala (1941), Arkiv Mat. Astron. Fysik **27B**, No. 10; **29A**, No. 3; **29B**, No. 4; **31A**, No. 9; **33A**, No. 23.

[5] B. R. A. Nijboer, Physica **12**, 461 (1946).

Three new evaluations of h/e have been made from the curves in Fig. 2. Within the accuracy required, the present method of recording the high frequency limit does not prevent the use of the second derivative method for determining the cut-off position. These positions are indicated on the experimental curves. We have evaluated h/e for the two limits obtained with a pure tungsten cathode at 6 and 10 kv and in addition have evaluated h/e by the voltage and wavelength separation of the same limits. The latter evaluation completely eliminates any correction for work function. These values are indicated in the first part of Fig. 3. In the same figure we have shown the value of Bearden and Schwarz corrected for the new velocity of light, and an average value of h/e as derived from the experiments. This is compared with the least squares value found in the following paper. The last two values in Fig. 3 show the effect of neglecting to make a correction for the cathode work function.

The probable error indicated in Fig. 3 for the present measurements could be reduced to about two-thirds of that shown by a long and tedious recording of x-ray limits. Such an improvement would affect the weighted average only slightly, and the least squares value not at all. The agreement of the present measurements with those of Bearden and Schwarz[1] indicate that the selection of the work function for BaO on nickel in that work was correct. The agreement of these experiments on h/e with the least squares value gives complete confidence in accepting the latter as the best evaluation of this important atomic ratio.

A Re-Evaluation of the Fundamental Atomic Constants

J. A. BEARDEN AND H. M. WATTS
The John Hopkins University, Baltimore, Maryland
(Received August 2, 1950)

A completely new evaluation of the fundamental atomic constants by the method of least squares is presented. A number of new and highly precise experiments have been taken into account, including the measurement of: (1) the velocity of light by an exceptionally ingenious and precise method due to Hansen and Bol, (2) the absolute proton moment, (3) the ratio of magnetic moments of proton and electron, (4) the proton moment in Bohr magnetons, (5) the hyperfine structure separation of ground-state hydrogen, (6) the ratio of cyclotron to precession frequency of the proton, (7) h/mc using annihilation radiation, and (9) h/e from the x-ray high frequency limit with improved precision.

The results of the critical survey of Dorsey on the velocity of light plus the more recent measurements of c are combined to obtain a weighted-mean value: $c=299790.0\pm0.7$ km/sec. The results of the experiments listed above have been combined by several writers to compute α, e/m, and F. All of the published values, including those of certain older experiments have been corrected for the new value of c and combined in a least-squares calculation. The results are presented in a complete table of the fundamental constants and are compared with the experimental values in an isometric consistency chart. Six of the experimental results: F, N, mN, α, e/m, and h/e are found to show excellent agreement with the least-squares values. In particular the new experimental value of $h/e=(1.37928\pm0.00004)\times10^{17}$ erg sec/esu which precipitated the present work agrees well with the least-squares value, $h/e=(1.379300\pm0.000016)\times10^{-17}$ erg-sec/esu.

I. INTRODUCTION

AN effort to assess the recent work on h/e by Bearden and Schwarz[1] and that of the previous paper[2] in terms of the consistency with the present knowledge of the fundamental atomic constants led to the present rather complete analysis. The most complete recent work is the 1947 evaluation of the atomic constants by Dumond and Cohen.[3] Since then a number of very precise experiments have been reported which must also be included in any new evaluation of the constants.

The following new experimental results are of particular significance: (1) the absolute moment of the proton by Thomas, Driscoll, and Hipple,[4] (2) the ratio of proton magnetic moment to electron magnetic moment by Taub, Kusch, and Foley,[5] (3) the proton moment in Bohr magnetons by Gardner and Purcell,[6] and by R. W. Nelson, and Taub, Kusch, and Foley,[5] (4) the hyperfine structure frequency difference between certain magnetic levels of ground state hydrogen by Prodell and Kusch,[7] (5) the ratio of the cyclotron frequency to the spin precession frequency of the proton by Hipple, Sommer, and Thomas,[8] (6) the Compton wavelength of the electron by Dumond, Lind, and Watson,[9] and (7) h/e from the x-ray high frequency limit by Bearden and Schwarz[1] and Bearden, Johnson, and Watts.[2] These results have been combined by Thomas, Driscoll, and Hipple,[4] Bethe and Longmire,[10] Hipple, Sommer, and Thomas,[8] and the present writers to compute e/m, α, F, and h/m, respectively. These quantities and h/e are shown in the column *New experiments* in Table I. The quantity of interest in each case is the normalized probable error of the experiment and its weight which is inversely proportional to the square of the error. In the same table we show the same data for the group of ten experiments which were used in reference 3. On comparing the total weights of the two groups of data, it is apparent that the 1947 experimental data would have a weight of only 13 percent in a new calculation. The need for a new evaluation using the new data is inescapable.

Another factor of primary importance in a reevaluation of the atomic constants is the excellent work of Hansen and Bol[11] on the velocity of light. This work has

TABLE I. Comparison of weights of 1947 experimental results with the weights of more recent data.

Quantity measured	New experiments Error X10⁴	Weight	Experiments prior to 1947 Error X10⁴	Weight
N			0.7	2.0
F	0.31	10.4	1.0	0.9
mN			1.4	0.5
Fe/m			2.1	0.2
e/m	0.26	15.2	2.2	0.2
h/e	0.58	3.0	2.9	0.1
α	0.37	7.5	3.7	0.1
$h/(em)^{\frac{1}{2}}$			5.8	0
h/m	4.12	0.1	12.4	0
e^2/mh			11.8	0
		Total 36.2		Total 4.0

[1] J. A. Bearden and G. Schwarz, Phys. Rev. **79**, 674 (1950).
[2] Bearden, Johnson and Watts, preceding paper.
[3] J. W. Dumond and E. R. Cohen, Revs. Modern Phys. **20**, 82 (1948); J. W. Dumond and E. R. Cohen, Revs. Modern Phys. **21**, 651 (1949).
[4] Thomas, Driscoll, and Hipple, Phys. Rev. **78**, 787 (1950); **75**, 902 (1949); **75**, 992 (1949).
[5] P. Kusch and H. M. Foley, Phys. Rev. **74**, 520 (1948); H. Taub and P. Kusch, Phys. Rev. **75**, 1481 (1949); P. Kusch and H. Taub, Phys. Rev. **75**, 1477 (1949).
[6] J. H. Gardner and E. M. Purcell, Phys. Rev. **76**, 1262 (1949), also E. M. Purcell, private communication concerning the more recent work of R. W. Nelson.
[7] A. G. Prodell and P. Kusch, Phys. Rev. **79**, 1009, (1950).
[8] Hipple, Sommer, and Thomas, Phys. Rev. **76**, 1877 (1949); J. A. Hipple, H. Sommer, and H. Thomas, Phys. Rev. **80**, 487 (1950); private communications; F. Bloch and C. D. Jeffries, Phys. Rev. **80**, 305 (1950).
[9] Dumond, Lind, and Watson, Phys. Rev. **75**, 1226 (1949).
[10] H. A. Bethe and C. Longmire, Phys. Rev. **75**, 306 (1949).
[11] W. W. Hansen and K. Bol, private communication; K. Bol, Phys. Rev. **80**, 298 (1950).

resulted in a value of C differing so greatly from the value of reference 3 that its use as an auxiliary constant would change the results of a least-squares calculation to a considerable extent. We must therefore review carefully the available information on the value of the velocity of light and its influence as an auxiliary constant on the published results of all the experiments used.

II. THE VELOCITY OF LIGHT

It will be recalled that in the least squares evaluation of reference 3, certain auxiliary constants such as: the Rydberg constant, the velocity of light, the conversion from Siegbahn to absolute wavelength, etc. are used. Of the auxiliary constants involved, only the velocity of light appears to deserve a reconsideration.

In 1944 Dorsey made a very careful study[12] of all the significant experiments on the velocity of light up to that time. He reached three particularly interesting conclusions: (1) there is no evidence for a secular change in the velocity of light, (2) all of the work prior to 1934 shluld be dismissed from any calculation of C, and (3) the mean of the 5 best experimental results is 299773 $\pm$10 km/sec. The last conclusion deserves further attention. The five experiments considered in (3) above are the following:

(a) Michelson, Pease, and Pearson reported in 1935 the results of work with a 32-face prismatic mirror using a light path the major part of which is in vacuum. There was no careful search for systematic errors. Result: 299774$\pm$10 km/sec.

(b) Karolus and Mittelstaedt reported in 1928 and 1929 on Kerr Cell measurements, the errors of which were well studied. Result: 299778$\pm$20 km/sec.

(c) Anderson in 1937 reported on Kerr cell experiments and discussed the errors in detail. Result 299771$\pm$15 km/sec.

(d) Anderson in 1941 reported further Kerr cell results: 299776 $\pm$14 km/sec.

(e) Hüttell in 1940 reported on Kerr cell work, but failed to provide adequate data for an assessment of his results. If he is given the benefit of the doubt on several items including the correction for the index of refraction of air, his result is 299768$\pm$10 km/sec.

In the above experiments one notices the interesting point that the three experiments which were most carefully reported claim errors ranging from 14 to 20 km/sec, while the incompletely reported experiments both claim errors of only 10 km/sec. If one were to take these errors literally, the five experiments would have weights of 4, 1, 2, 2, and 4 respectively, which would give as much weight to each of the questioned experiments as to the whole set of the carefully reported experiments. Dorsey compromises by weighting the five experiments equally. The important point to be gained from Dorsey's work is that the error which should properly be assigned to the velocity of light as of 1944 is actually several times that used in the recent evaluations of the atomic constants.

TABLE II. Weighted mean evaluation of the velocity of light, in km/sec.

Worker	Value	Error, km/sec	Weight
Dorsey	299773	10.0	1.0
Essen	92.5	3.0	11.1
Aslakson	92	2.4	17.4
Bergstrand	92.7	2.0	25.0
Hansen and Bol	89.3	0.8	156.3
Weighted mean	(299790.0$\pm$0.7) km/sec		

[12] N. E. Dorsey, *The Velocity of Light* (American Philosophical Society, New Series, 34, Part I, Philadelphia, 1944).

More recently certain additional experiments have been reported:

(f) Essen[13] reported in 1947 and Essen and Gordon-Smith[13] in 1948 on measurements using a microwave cavity resonator. Result: 299793$\pm$9 km/sec. In 1950 Essen reported[14] further results of 299792.5$\pm$3.

(g) Aslakson[15] reported in 1949 the result of measurements using "Shoran" to measure the velocity of radio waves. He reports a result of 299792.3$\pm$2.4 km/sec, although there is perhaps reason to question the smallness of the claimed uncertainties in view of the variations in the velocity of propagation[16] over the long airpaths that he used.

(h) Bergstrand[17, 18] reported in 1948 and 1949 the results of Kerr cell experiments over 4 km and 9 km paths with a result of 299796$\pm$2 km/sec. However, a correction[19] in 1950 corrects that result to 299793$\pm$2 km/sec and presents the result of new measurements as 299792.7$\pm$0.25 km/sec. The error quoted represents only the random error and there is no evidence of an evaluation of the systematic errors. Until further data are available on these experiments we shall adopt as Bergstrand's value 299792.7$\pm$2 km/sec.

(i) Hansen and Bol in unpublished work[11] using a microwave cavity resonator obtain a result of 299789.3$\pm$0.8 km/sec. We shall discuss this experiment further below.

The several results are shown in Table II, utilizing Dorsey's computed result to summarize all of the earlier work.

It is to be noted that again in the period 1944 to 1950, just as in 1934 to 1941, the techniques have improved so greatly as to render data obtained in the prior period of trivial weight. Even if one were arbitrarily to double the claimed errors in all experiments since 1944, the work prior to that time would have a weight of only two percent in the weighted mean value.

The fact that the work of Hansen and Bol is as yet unpublished and that the claimed error is so small necessitated a detailed consideration of their work in the present paper. Dr. Bol has been exceptionally kind in participating in a careful and critical discussion of the experiments performed by the late Professor Hansen and himself at Stanford and permitting the use of his results prior to publication. The experiment consisted in essence of the measurement of the resonant frequency and the length of a high-Q microwave cavity. From the

[13] L. Essen, Nature **159**, 611 (1947). L. Essen and A. C. Gordon-Smith, Proc. Roy. Soc. **A194** (No. 1038), 348 (1948).
[14] L. Essen, Nature **165**, 582 (1950).
[15] Aslakson, Nature **164**, 711 (1949).
[16] R. L. Smith-Rose, Proc. Inst. Radio Engrs. **38**, 16 (1950).
[17] L. E. Bergstrand, Sv. Vetensk. No. **20** (Stockholm) (1948).
[18] E. Bergstrand, Sv. Vetensk. No. **20** (Stockholm) (1949).
[19] E. Bergstrand, Nature **165**, 405 (1950).

two measurements and the theoretical relationship of cavity length to the free space wavelength of the radiation, the velocity of propagation of the radiation can be determined.

The unusual accuracy of the experiment can be attributed largely to several highly ingenious variations on the cavity measurement of c:

(1) The measurement of the resonant frequency in vacuum in both the TE_{013} and the TE_{021} modes in order to suppress the importance of the diameter of the cylindrical cavity. The cavity length is chosen to place the resonant frequencies of the two modes only a few megacycles, out of 3000, apart.

(2) The use of optical flats (silver plated cast iron) for the end plates of the cavity with 3-point suspension of the upper flat on spacing rods whose ends are zones of a sphere of diameter equal to the rod length. This minimizes spacing uncertainties due to skewness of the assembly.

(3) The use of a gap between the cylindrical portion and each end plate of the cavity to suppress undesired modes of oscillation, and the correction of the results for the effect of the gap.

The various sources of error will be discussed in detail in a forthcoming paper by Bol.

The random errors from the various sources are:

(1) Contour variations	<3 in 10^7
(2) Due to error in Q	~ 1 in 10^7
(3) Frequency measurement	<3 in 10^7
(4) Coupling loop	~ 2 in 10^7
(5) Uncertainty in spacing between end-plates	<5 in 10^7.

The most significant known systematic error is the effect of the thin layer of silver sulfides, oxides, etc. on the side walls upon the resonant frequency. The true electrical diameter of the cavity is greater than the mechanical diameter by the skin depth of the walls for the particular mode of oscillation that is excited. The presence of a film of unknown thickness, with a conductivity and dielectric constant differing from that of the adjacent silver will reduce the observed resonant frequency of the cavity. Bol estimates that the value of C will be increased by approximately 0.3 km/sec when this skin effect is properly corrected for, but he prefers to consider the result provisional until experiments have been completed to measure the correction. Bol obtains a provisional value of

$$C = 299789.3 \pm (0.3 \text{ random} + 0.5 \text{ systematic}) \text{ km/sec.}$$

in which he uses a very conservative estimate of the skin effect error. Fortunately a shift in the value of C of the order of magnitude expected as a result of the correction for surface film effect will not affect the output values of the least squares calculation of the fundamental constants.

In the work which follows we shall use the weighted mean value calculated earlier using all of the published data,

$$C = (299790.0 \pm 0.7) \text{ km/sec.}$$

III. FURTHER NEW EXPERIMENTS

The several significant new experiments the results of which we shall use differ remarkably from the experiments of the 1947 work of Dumond and Cohen.[3] In this interval a whole new class of experiments of which the nuclear resonance experiments are characteristic have come to dominate the field of precision measurements. A technique basic to several of the experiments is the accurate measurement of ratios of certain characteristic resonance frequencies by making two measurements in the same homogeneous magnetic field. Thus the absolute value of the field is unimportant, providing the two samples are accurately located (in turn) at the same point in the field.

In the measurements of Hipple and his co-workers[4,5] at the Bureau of Standards, an electromagnet of unusually homogeneous field was constructed and painstakingly calibrated in absolute units. This instrument has already been used to great advantage in the absolute determination of the proton moment which enables the very accurate calculation of e/m and F.

A. Measurement of the Absolute Proton Moment

In recent papers[4] Thomas, Driscoll, and Hipple reported the results of an elaborate and highly accurate measurement of the proton moment in absolute units, using the technique of Purcell, Torrey, and Pound[20] to detect the nuclear resonance. The considerable pains taken to make an accurate absolute measurement of the magnetic field strength resulted in an accuracy an order of magnitude better than that in previous experiments. Their result when corrected for the diamagnetic effect[21] is

$$\gamma_p = (2.675305 \pm 0.00006) \cdot 10^4 \text{ sec}^{-1} \text{ gauss}^{-1}.$$

B. The Proton Moment in Bohr Magnetons and the Ratio of Magnetic Moments of Proton and Electron

There have been two recent accurate determinations of the proton moment in Bohr magnetons. Gardner and Purcell and R. W. Nelson[6] measured the precession frequency of the proton, $\omega_p = \gamma_p H_0$ and the cyclotron frequency of a free electron, $\omega_e = eH_0/mc$ in the same magnetic field. The proton resonance in mineral oil was observed by the method of Bloembergen, Purcell, and Pound[20] at 14.24 Mc/sec, and the electron resonance was observed at 9360 Mc/sec. The 657th harmonic of the proton frequency is compared with the electron frequency to obtain the result:

$$\omega_e/\omega_p = 657.4685 \pm 0.008.$$

A careful search for systematic errors was made and any resultant uncertainties are included in the above error. When the diamagnetic correction[20] of 2.68×10^{-5} the field at the proton is made, one obtains

$$\mu_p = (1.521026 \pm 0.00002) \cdot 10^{-3} \quad \text{Bohr magnetons}$$

in which we have used

$$\omega_e/\omega_p = (eH_0/mc)/\gamma_p H_0 = e/\gamma_p mc, \quad \gamma_p = 2\mu_p/\hbar,$$
$$\omega_e/\omega_p = e\hbar/2\mu_p mc, \quad \mu_p = (\omega_p/\omega_e)(e\hbar/2mc),$$
$$\omega_p/\omega_e = \mu_p/\mu_1.$$

[20] Purcell, Torrey, and Pound, Phys. Rev. **69**, 37 (1946). Bloembergen, Purcell and Pound, Phys. Rev. **73**, 679 (1948).
[21] H. A. Thomas, Phys. Rev. **80**, 901 (1950); N. F. Ramsay, Phys. Rev. **78**, 699 (1950).

TABLE III. Weighted mean evaluation of μ_p.

	Value	Error $\times 10^6$	Weight
Gardner-Purcell	1.521026	0.2	25.0
Kusch-Foley-Taub	1.521057	0.7	2.0
Weighted mean	1.521027	± 0.2	Total 27.0

The other significant determination of μ_p/μ_l, the proton moment in Bohr magnetons is that of Taub and Kusch,[5] in which a carefully planned series of molecular beam magnetic resonance experiments lead in a somewhat indirect manner to the desired experimental value. The experiments consist of:

(1) The measurement of g_p, the g-value of the proton in the NaOH molecule and g_J, the g-value for total electronic angular momentum of ground state caesium and indium, all in the same magnetic field. The g_p is found from the familiar flip-over frequency of the proton, while the g_J are found from the frequencies corresponding to transitions between the hyperfine structure levels of the ground states of the appropriate atoms. This measurement produced accurate values for the ratios

$$g_p/g_{JCs}=(1.51911\pm 0.00003)\cdot 10^{-3}$$

and

$$g_p/g_{JIn}=(4.56877\pm 0.00007)\cdot 10^{-3},$$

where g_{JCs} is the g_J value for Cs^{133} and g_{JIn} is the g_J value for In^{115}.

(2) The measurement of the ratios

$$g_{JCs}/g_{JNa}=1.000134,$$

and

$$g_{JIn}/g_{JNa}=1/3(1.00243),$$

where g_{JNa} is the g_J value of Na^{23}.

(3) The measurement of the g_J values of Li^6, Li^7, Na^{23}, and K^{39} with the result that they are equal to within one part in 40,000. Kusch and Taub conclude that "within the precision of these measurements, the g_J of these atoms is equal to the spin g, g_e. For if perturbations were to affect the value of g_J, they would presumably affect the different atoms by different amounts."

The results of the three experiments of Kusch, Taub, and Foley are then properly combined as follows:

$$(g_p/g_{JNa})_{Cs}=(g_p/g_{JCs})(g_{JCs}/g_{JNa})=1.51931\times 10^{-3}$$

and

$$(g_p/g_{JNa})_{In}=(g_p/g_{JIn})(g_{JIn}/g_{JNa})=1.51923\times 10^{-3},$$

from which

$$(g_p/g_{Na})_{mean}=(1.51927\pm 0.00010)\cdot 10^{-3},$$

where it is to be noted that the first two values are entirely independent in that the transition field which is the essence of the apparatus is different in the two experiments and the field strengths used differed widely.

Next, the experimental result that the g_J of Na is equal to g_s, the spin g of the electron, leads to the result

$$g_p/g_s=(1.51927\pm 0.00010)\cdot 10^{-3}.$$

This value, together with the good agreement of the experimental value of g_s in reference 5 with Schwinger's value as corrected by Karplus and Kroll,[22]

$$g_s=2(1.001145),$$

leads to

$$g_p=(3.04202\pm 0.00015)\cdot 10^{-3}.$$

The proton magnetic moment in Bohr magnetons is then computed from g_p and a diamagnetic correction of 4.7×10^{-5} is added to obtain

$$\mu_p=(1.521057\pm 0.0007)\cdot 10^{-3}\text{ Bohr magnetons.}$$

The Gardner-Purcell value and the Kusch-Foley-Taub value of μ_p are combined in Table III to obtain a weighted mean value.

C. Hyperfine Structure of Hydrogen

Prodell and Kusch have reported[7] on a precise measurement of the hyperfine structure separation of H and D, of which only the former is of interest here. The atomic-beam magnetic resonance method was used to observe the frequency necessary to induce transitions among certain magnetic levels of the hyperfine structure multiplets of ground-state hydrogen in a weak field. The measurement is absolute in that it depends on a fundamental time standard and nothing else. The result is

$$\nu_H=1420.4051\pm 0.006\text{ Mc/sec.}$$

D. Ratio of Proton Cyclotron Frequency to Proton Precession Frequency

Hipple, Sommer, and Thomas[8] have reported the precise measurement of the ratio of the cyclotron frequency of the proton to its nuclear precession frequency. The primary features in this experiment are the measurement of both frequencies in the highly homogeneous magnetic field described in reference 4, plus the development of a new device called the omegatron for the measurement of the cyclotron resonance frequency of the proton. Their result $\omega_p/\omega_c=2.792685\pm 0.00006$ is combined with the result of Bloch and Jeffries,[8] $\omega_p/\omega_c=2.79245\pm 0.00020$ to obtain an uncorrected weighted mean value of $\omega_p/\omega_c=2.792746\pm 0.000056$.

We apply a diamagnetic correction of 7.8×10^{-6} after Thomas[21] to obtain

$$\omega_p/\omega_c=2.792746\pm 0.000056.$$

E. Compton Wavelength of the Electron

Dumond, Lind, and Watson have reported[9] the result of a precision measurement of the wavelength of

[22] J. Schwinger, Phys. Rev. 73, 416 (1948); R. Karplus and N. M. Kroll, Phys. Rev. 77, 536 (1950). The value given is our result using $1/\alpha=137.043$ in the formula of Karplus and Kroll.

annihilation radiation from Cu^{64} using the two-meter focusing curved crystal spectrometer. A careful consideration of all of the instrumental and theoretical effects leads to the published result:

$$h/mc = (0.024271 \pm 0.000010) \cdot 10^{-8} \text{ cm}.$$

It is to be noted that the effect of the initial velocity of the annihilating positron or electron leads to no appreciable average shift of the photon frequency. Instead, the first-order effect is a line-broadening similar to the Doppler effect.

IV. INPUT DATA DERIVED FROM THE NEW EXPERIMENTS

A. Calculation of e/m

The proton precession frequency, ω_p, and the electron cyclotron frequency, ω_e, are given theoretically by

$$\omega_p = \gamma_p H_0, \quad \omega_e = eH_0/m,$$

where γ_p is the gyromagnetic ratio of the proton, and H_0 is the dc magnetic field strength. Therefore

$$e/m = \gamma_p \omega_e/\omega_p$$

and after Thomas, Driscoll, and Hipple[4,5] we have calculated

$$e/m = (1.758912 \pm 0.00005) \cdot 10^7 \text{ emu/g}$$

by using their value of γ_p and the frequency ratio of Gardner and Purcell.[6]

B. Calculation of α

Bethe and Longmire[10] point out that the Fermi hyperfine-structure formula for hydrogen can be modified to include: (1) Breit's relativistic correction, (2) the reduced mass effect, (3) the electromagnetic correction to the electron magnetic moment, (4) the correction for the distributed nature of the proton magnetic moment, and (5) the correction for the distributed nature of the electron magnetic moment. The result is

$$\nu_H = \alpha^2 \left[\frac{16}{3}\left(\frac{\mu_p}{\mu_1}\right) CR_\infty \left(1+\frac{2\alpha^2}{3}\right)\left(1+\frac{m}{M}\right)^{-3} \times \left(1+\frac{\alpha}{2\pi}-\frac{2.97\alpha^2}{\pi^2}\right)\left(1-\frac{(g_p-g_D)\alpha m}{g_p \mu}\right)\left(1-\frac{\alpha^2}{2\pi}\right)\right],$$

where μ_1 is the Bohr magneton, μ is the meson mass, g_D is the deuteron g-factor, and the other quantities have been previously defined.

We use the results quoted in III c, and b, plus E. R. Cohen's* value of R_∞, and ignore the last two factors in obtaining a result

$$1/\alpha = 137.0432 \pm 0.0009.$$

* *Note.*—We are indebted to E. R. Cohen for communicating to us in advance of publication the result of a recent study in which he has obtained $R_\infty = 109737.323 \pm 0.024$ cm^{-1}.

C. Calculation of F

From the relation

$$F = \gamma_p M_p \omega_e/\omega_p$$

and the values of γ_p and ω_e/ω_p quoted in III a, and d, plus the isotopic weight of the proton,[3]

$$M_p = 1.007580 \pm 0.000003,$$

Hipple, Sommer, and Thomas calculate

$$F = 9652.03 \pm 0.3 \text{ emu/g}$$

on the physical scale.

D. Calculation of h/e

When the new value of the velocity of light is used in the formula

$$h/e = (V\lambda/C^2) \cdot 10^8,$$

V being in absolute volts and λ in centimeters, the weighted-mean value of Bearden and Schwarz and of Bearden, Johnson and Watts as computed in reference 2 gives

$$h/e = (1.37928 \pm 0.00004) \times 10^{-17} \text{ erg sec/esu}.$$

E. Compton Wavelength of the Electron, h/mc

We use the result of III e and multiply by C to obtain

$$h/m = 7.2762 \pm 0.0030 \text{ erg sec/g}.$$

V. CORRECTIONS ON OLD INPUT DATA

A careful study of the original references[22–34] was made on the remaining experimental input data of reference 3 which are not being replaced by new input data. The point of this survey was to determine which of the

TABLE IV. Revised values of 1947 data.

Quantity	Value	c-dependence	Corrected value
N	6.02338×10^{23}	none	——
mN	5.48541×10^{-4}	none	——
Fe/m	1.69824×10^{11}	none	*1.69778×10^{11}
$h/(me)^{\frac{1}{2}}$	1.00084×10^{-6}	$c^{-\frac{1}{2}}$	1.000818×10^{-6}
e^2/mh	3.8197×10^{24}	c^{+1}	3.81987×10^{24}

* We have included the correction pointed out in reference 10 to Fe/m to account for the effect of scattering by the atomic nuclei.

[22] J. A. Bearden, J. Appl. Phys. **12**, 395 (1941).
[24] J. A. Bearden, Phys. Rev. **54**, 698 (1938).
[25] F. G. Dunnington, Rev. Modern Phys. **11**, 68 (1939).
[26] C. E. Robinson, Phil. Mag. **22**, 1129 (1936).
[27] Robinson and Clews, Proc. Roy. Soc. London **A176**, 28 (1940).
[28] Robinson and Mayo, Proc. Roy. Soc. London **A173**, 192 (1939).
[29] Drinkwater, Richardson, and Williams, Proc. Roy. Soc. London **A174**, 164 (1940).
[30] W. V. Houston, Phys. Rev. **51**, 446 (1937); Phys. Rev. **30**, 608 (1927).
[31] D. Y. Chu, Phys. Rev. **55**, 175 (1939).
[32] R. C. Williams, Phys. Rev. **54**, 568 (1938).
[33] C. E. Robinson, Phys. Rev. **55**, 423A (1939).
[34] C. D. Shane and F. H. Spedding, Phys. Rev. **47**, 33 (1935).

TABLE V. Equations of condition and associated normalized errors.

Quantity measured	n	a_n	b_n	c_n	ω_n	ϵ_n
N	1	0	1	0	−5.62	0.710
F	2	1	0	0	2.84	0.304
mN	3	−4	5	3	5.11	1.37
Fe/m	4	6	−5	−3	−1.28	2.06
e/m	5	5	−5	−3	−0.909	0.255
h/e	6	−1	1	1	6.79	0.290
α	7	2	−2	−1	2.832	0.065
$h/(me)^{\frac{1}{2}}$	8	1.5	−1.5	−0.5	13.77	5.80
h/m	9	4	−4	−2	1.32	4.12
e^2/mk	10	6	−6	−4	0.41	11.78

Cross Terms:
$\epsilon_{25}^{-2}=\epsilon_{52}^{-2}=+0.0484$,
$\epsilon_{57}^{-2}=\epsilon_{75}^{-2}=-0.00845$

subject experiments used the velocity of light in computing the published values from the experimental data. The results are given in Table IV.

VI. LEAST SQUARES METHOD

The method of least squares has been discussed adequately in numerous texts and journals, of which one of the most readable is *The Calculus of Observations* by Whittaker and Robinson.[35] It is easily shown[3] that all of the experimental quantities for which measured values are given in III and IV can be expressed as products of various powers of F, N, m, and h, and certain auxiliary constants such as c which are known to a high precision. It has been shown that these equations can be reduced through a Taylor expansion to linear equations in terms of deviations from origin values of the variables F, N, m, and h. Further, by virtue of the exceptional precision with which R_∞ is known, the equation for R_∞ can be used to eliminate one of the variables. We follow Dumond and Cohen[3] in eliminating m, so that we will express each experimentally observed quantity in terms of F, N, and h.

As an example, consider the fine-structure constant,

$$\alpha=2\pi e^2/ch,$$

but $F=Ne$, so

$$\alpha=2\pi F^2/chN^2,$$

The linearized equation is given by

$$(\partial\alpha/\partial F)_0(F-F_0)+(\partial\alpha/\partial N)_0(N-N_0)+(\partial\alpha/\partial H)_0(H-H_0)=(V-V_0),$$

where h has been changed to H for convenience of notation, the subscript 0 denotes an origin value chosen close enough to the expected "true" value to render second order terms unimportant, V_0 is the corresponding origin value of α, and v without subscript is the observed value of α. On performing the indicated differentiations and evaluating the derivatives with the origin values, we obtain

$$2V_0\frac{(F-F_0)}{F_0}-2V_0\frac{(N-N_0)}{N_0}-V_0\frac{(H-H_0)}{H_0}=(V-V_0).$$

Divide through by M_0 and use the definitions

$$x=(F-F_0)/F_0,\quad y=(N-N_0)/N_0,\quad z=(H-H_0)/H_0,\quad v=(V-V_0)/V_0,$$

to obtain

$$2x-2y-z-v=0,$$

the desired linear equation of condition for the observable, α.

We will modify the equations of condition to the form

$$a_nX+b_nY+c_nZ+\omega_n=0$$

wherein the three new variables are defined by

$$X=10^4x,\quad Y=10^4y,\quad Z=10^4z.$$

Also we define

$$\omega_n=-10^4v_n,\quad \epsilon_n=10^4e_n,$$

where e_n is the normalized probable error in the experimental determination of the quantity V_n (V_n was simply V in our example). The coefficients of the equations of condition for the ten experimental results discussed in IV and V are given in Table V, using the auxiliary constants listed later in Table VII. All masses are expressed according to the chemical scale of atomic weights.

The values listed for ω_n and ϵ_n are carried beyond the number of significant figures as one effort to minimize accumulation of error due to successive roundings-off.

Before the equations of condition of Table V can be used to obtain the normal equations, the individual equations must be divided by their respective ϵ_n^2's to obtain the weighted equations of condition. In order to obtain the normal equation in the variable X we multiply each weighted equation through by its a_n and add the ten equations so obtained. By a similar process the normal equations in Y and Z are obtained. However, in the present case F and e/m are correlated through their common use of γ_p (see Sec. IV) and α and e/m are correlated through the quantity μ_p/μ_1. The normal equations must therefore be obtained by a more general method due to E. R. Cohen[36] which includes the cross terms listed in Table V in a 10 × 10 error matrix. The resultant normal equations were then solved for X, Y, and Z, and the latter were used to compute F, N, and h.

Since the method of handling correlated variables is complicated and particularly subject to computational errors we sought a different means of solving the problem as a check. A new method was evolved[37] which allowed expressing all of the pertinent observations in

[35] E. T. Whittaker and G. Robinson, *The Calculus of Observations* (Blackie and Son, Ltd., London, 1948).

[36] E. R. Cohen, Phys. Rev. **81**, 162 (1951). We are deeply indebted to J. W. Dumond for pointing out to us the error in principle involved in a solution which ignores this correlation.

[37] J. A. Bearden and H. M. Watts, Phys. Rev. **81**, 160 (1951).

a set of uncorrelated equations of condition. The results of the uncorrelated method were in excellent agreement with those of the correlated method. Owing to the considerable difference in complexity of calculating and checking both the values of the atomic constants and the associated errors, the simpler uncorrelated method was adopted in the remainder of the work.

The least-squares values of F, N, and h, obtained by both methods are shown in Table VI.

TABLE VI. Least-squares values of the base variables.

F	9649.54 emu equiv.$^{-1}$ (Chem.)
N	6.02402×10^{23} (Chem.)
h	6.62363×10^{-27} (erg sec)

All of the other fundamental constants can be computed in terms of these plus the auxiliary constants.

The errors can be computed in the usual way[35] for a

TABLE VII. Least squares adjusted values of the fundamental atomic constants.

F	Faraday	(9649.54±0.18)emu equiv^{-1} (Chem.) (9652.17±0.17) emu equiv^{-1} (Phys.)
N	Avogadro's number	$(6.02402\pm0.00017)\times10^{23}$ (Chem.) $(6.02566\pm0.00016)\times10^{23}$ (Phys.)
h	Planck's constant	$(6.62363\pm0.00016)\times10^{-27}$ erg sec.
m	Electron mass	$(9.10710\pm0.00022)\times10^{-28}$ g
e	Electronic charge	$(4.80217\pm0.00006)\times10^{-10}$ esu $(1.601844\pm0.000021)\times10^{-20}$ emu
h/e		$(1.379300\pm0.000016)\times10^{-17}$ erg sec esu^{-1}
e/m	Specific electronic charge	$(1.758896\pm0.000028)\times10^{7}$ emu g^{-1}
h/m		(7.27304±0.00007) cm^2 sec^{-1}
α	Fine structure constant	$(7.296953\pm0.000037)\times10^{-3}$
α^2		$(5.324552\pm0.000054)\times10^{-5}$
$1/\alpha$		137.0435±0.0007
h/mc	Compton wavelength of electron	$(2.426045\pm0.000025)\times10^{-10}$ cm
$e/4\pi mc$	Zeeman displacement per gauss	$(4.668885\pm0.00008)\times10^{-5}$ cm^{-1} gauss^{-1}
a_0	First Bohr radius	$(0.5291483\pm0.0000024)\times10^{-8}$ cm
a_0'	Separation of electron and proton in the ground state of H^1	$(0.5291342\pm0.0000024)\times10^{-8}$ cm
a_0''	Radius of the electron orbit referred to center of mass for normal H^1	$(0.5294224\pm0.0000024)\times10^{-8}$ cm
$\frac{1}{16}R_H\alpha^2$	Doublet separation in hydrogen	(0.3649900±0.0000037) cm^{-1}
σ	Stefan-Boltzmann constant	$(5.6694\pm0.0011)\times10^{-5}$ erg cm^{-2} deg^{-4} sec^{-1}
k	Boltzmann's constant	$(1.38020\pm0.00007)\times10^{-16}$ erg deg^{-1}
c_1	First radiation constant	$(4.99060\pm0.00012)\times10^{-15}$ erg cm
c_2	Second radiation constant	(1.43870±0.00007) cm deg
$\lambda_{max}T$	Wien displ. law constant	(0.289762±0.000014) cm deg
μ_1	Bohr magneton	$(9.27100\pm0.00017)\times10^{-21}$ erg gauss^{-1}
$(3K/N)^{\frac{1}{2}}$	Multiplier of (Curie const.)$^{\frac{1}{2}}$ to give magnetic moment per molecule	$(2.62173\pm0.00009)\times10^{-20}$ (erg mole deg^{-1})$^{\frac{1}{2}}$
h/k	Atomic specific heat constant	$(4.79903\pm0.00023)\times10^{-11}$ sec deg
μ	Reduced mass of electron in H^1	$(9.10214\pm0.00022)\times10^{-28}$ g
$2m/\hbar^2$	Schrödinger constant for fixed nucleus	$(1.638995\pm0.000045)\times10^{27}$ erg^{-1}
$2\mu/\hbar^2$	Schrödinger constant for the H^1 atom	$(1.638103\pm0.000045)\times10^{27}$ erg^{-1}
mN	Atomic weight of the electron	$(5.486137\pm0.00009)\times10^{-4}$ (Chem.) $(5.487629\pm0.00009)\times10^{-4}$ (Phys.)
λ_0	Wavelength associated with 1 ev	$(12396.32\pm0.16)\times10^{-8}$ cm
M/m	Ratio proton mass to electron mass	(1836.093±0.044)
ν_0	Frequency associated with 1 ev	$(2.418378\pm0.000029)\times10^{14}$ sec^{-1}
E_0	Energy associated with 1 ev	$(1.601844\pm0.000021)\times10^{-12}$ erg
h/e	Potential associated with unit frequency	$(1.379300\pm0.000016)\times10^{-17}$ esu
E_1	Energy associated with unit wave number	$(1.985698\pm0.000048)\times10^{-16}$ erg
v_0	Speed of 1-ev electron	$(5.931098\pm0.000046)\times10^{7}$ cm sec^{-1}
	Conversion factor atomic mass units to Mev 1 amu = 931.128±0.017 Mev	
mC^2	Energy equivalent of electron mass	(0.510969±0.000009) Mev
$(R_0/F)\times10^{-4}$	Energy associated with 1°K	$(8.61632\pm0.00042)\times10^{-5}$ ev
T_0	"Temperature" associated with 1 ev	(11605.9±0.6) deg K
n_0	Loschmidt's number	$(2.68754\pm0.00010)\times10^{19}$ cm^{-3}
	Auxiliary Constants Used	
c	Velocity of light	(299790.0±0.7) km sec^{-1}
R_∞	Rydberg constant for infinite mass	109737.323±0.024 cm^{-1}
R_H	Rydberg constant for H^1 atom	(109677.581±0.008)cm^{-1}
ν_H	Hyperfine structure splitting in ground state H^1	$(1420.4051\pm0.0003)\times10^{6}$ sec.$^{-1}$
	Atomic masses (Physical scale)*	$H^1 = 1.0081283\pm0.0000028$ $M_p = 1.007580\pm0.000003$
R_0	Gas constant per mole	$(8.31436\pm0.00038)\times10^{7}$ erg mole^{-1} deg^{-1}
V_0	Standard volume of perfect gas	(22414.6±0.6) cm^3 mole^{-1}
	Conversion factors NBS Int. units to absolute electrical units 1 NBS ohm $= p$ absolute ohm $\quad p = 1.000495$ 1 NBS v $= pq$ absolute v $\quad pq = 1.000330$ 1 NBS amp $= q$ absolute amp $\quad q = 0.999835$	
λ_0/λ_s	Ratio of grating in Siegbahn scales of wavelength	1.002030±0.000020
d_{20}	Grating space of calcite at 20°C	$(3.03567\pm0.00005)\times10^{-8}$ cm
ρ	Density of calcite at 20°C	(2.71030±0.00003) g cm^{-3}
r	Ratio physical to chemical scale of atomic weights	(1.000272±0.000005)

* K. T. Bainbridge, "Isotopic weights of the fundamental isotopes," Preliminary Report No. 1, National Research Council (June, 1948).

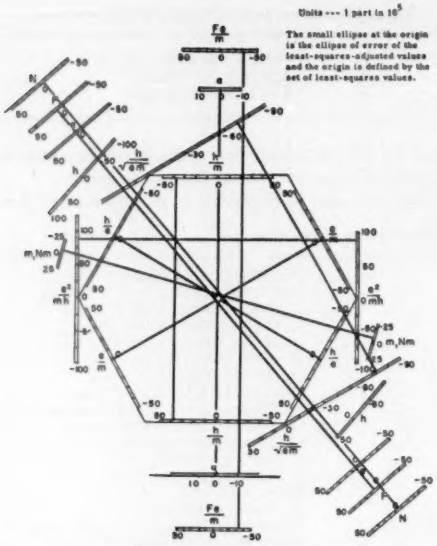
Units --- 1 part in 10^5
The small ellipse at the origin is the ellipse of error of the least-squares-adjusted values and the origin is defined by the set of least-squares values.

FIG. 1. Isometric consistency chart showing deviation of the input data from the least-squares-adjusted values.

function F_n, (we use F_n to denote an output value to distinguish it from ω_n, an input value for the same quantity).

$$F_n(X, Y, Z) = a_n X + b_n Y + c_n Z$$

through use of the relation

$$\sigma^2(F_n) = a_n^2\sigma_{XX}^2 + b_n^2\sigma_{YY}^2 + c_n^2\sigma_{ZZ}^2 + 2a_nb_n\sigma_{XY}^2 + 2a_nc_n\sigma_{XZ}^2 + 2b_nc_n\sigma_{YZ}^2.$$

The normalized errors, σ, are obtained from the characteristic determinant of the normal equations as follows: Let A be the 3×3 characteristic determinant with elements A_{ij}, then

$$\sigma_{ij}^2 = (-)^{i+j}A_{ij}^{-1},$$

where A_{ij}^{-1} is the minor of A_{ij} divided by $\det A$. If the coefficients of the normal equations are arranged in the determinant in the order a_n, b_n, c_n in each row, and the rows represent the normal equations in X, Y, Z in that order, then for i or j in σ_{ij}^2 read 1 for X, 2 for Y, and 3 for Z.

The errors computed thus far are mean errors for an observation of unit weight. In order to convert to probable error for the weight appropriate to a given set of weighted equations of condition, one must multiply the above results by the factor

$$W = 0.6745[(\sum w_i d_i^2)/(s-f)]^{\frac{1}{2}}.$$

The factor 0.6745 arises from the conversion from mean to probable error, s is the number of equations of condition (10 in this case), f is the number of variables (3 in this case), and $\sum w_i d_i^2$ is the sum of the squares of the residuals of the 10 weighted equations of condition obtained by substituting in them the computed least-squares values of the three variables.

On applying these and earlier relationships we obtain finally the set of least-squares adjusted values of the fundamental atomic constants and their errors as shown in Table VII.

The input data of the ten experiments used in the calculations are shown on an isometric consistency chart[38] in Fig. 1. The origin of the chart is the set of least-squares-adjusted values of Table VI, and the normalized deviations from its origin are shown on the appropriate scales in units of 1 part in 10^5. It will be noted that the input values group rather evenly about the origin, but that some deviations of input from output values are in the order of several parts in 10^4. The small ellipse about the origin is the ellipse of error of the output values.

The same situation is again presented in Fig. 2 on a scale ten times as large as that of Fig. 1. It is noted that only six of the ten experimental results agree well enough with the least-squares value to appear on this highly expanded consistency chart. These six, however, agree an order of magnitude better with the output values than did the results of 1947. This means, of course, that the highly refined recent experiments are converging nicely on what we may hope are the true values. Further, the excellent consistency of the results points to an improved recognition, or elimination, of the

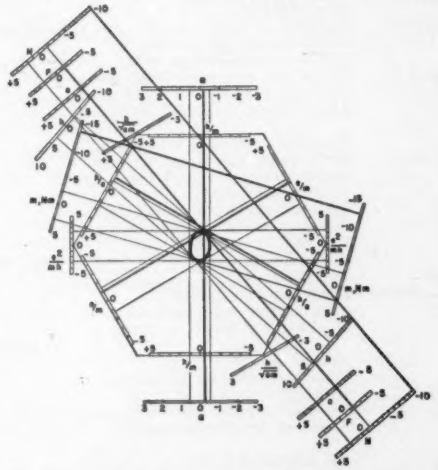

FIG. 2. Isometric chart comparing deviation of experimental values from least-squares-adjusted values with probable errors of latter. (Light lines—probable errors; heavy lines—experimental values; units—1 part in 10^6.) 1. α: Gardner and Purcell; 2. e/m: Hipple, Sommer, and Thomas; 3. mN: Drinkwater, Richardson, and Williams; 4. N: Bearden; 5. h/e: Bearden and Schwarz and Bearden, Johnson, and Watts; 6. F: Hipple, Thomas, and Driscoll.

[38] J. W. Dumond, Phys. Rev. 58, 457 (1940).

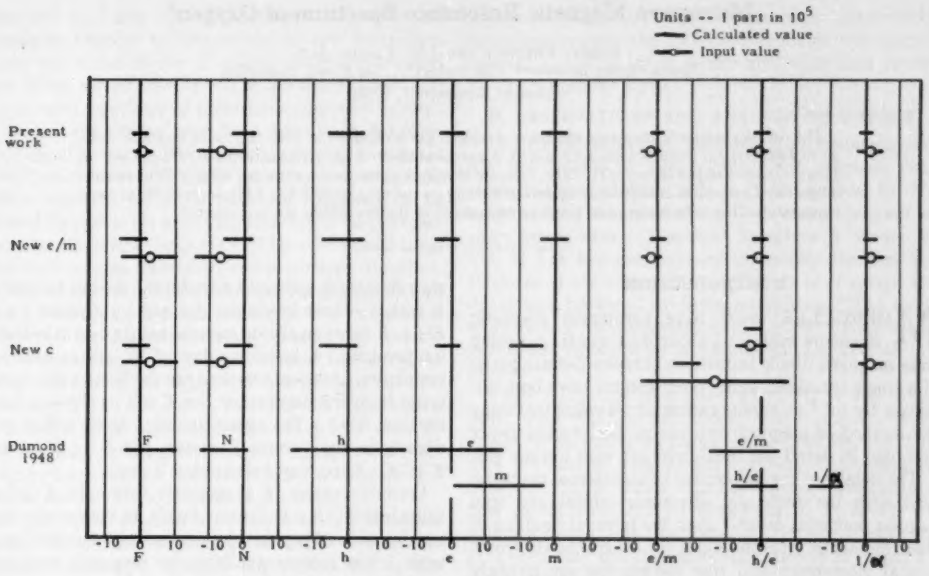

FIG. 3. Comparison of values and errors of several atomic constants.

systematic errors whose persistent presence has necessitated the least-squares approach. The results can be considered to confirm the Hansen and Bol value of c, since a minor change in c distorts Fig. 2 radically.

Figure 3 illustrates the trend in the values and the probable errors of several selected atomic constants since Dumond's calculation in 1948. The present least-squares-adjusted values were arbitrarily used as origins in Fig. 3. Early in 1950 we made a least-squares calculation using the new value of c and other new data available at that time. These results are shown under the heading "New c." It is noted that the probable errors in these results have dropped to about half their prior values and the overlap of input with output values is good. Next the new results[4] on e/m represented such a significant improvement on the error in the input value of e/m that a new calculation was made and the results are shown under the heading "New e/m." Finally, the new experimental value of F obtained by Hipple and his co-workers (see Sec. IV c) necessitated a third calculation, the results of which are given under the heading "Present Work." One sees that the errors have shrunk further and the consistency of input with output values is excellent.**

We acknowledge the invaluable assistance of Drs. Kees Bol, D. E. Kerr, and D. D. King in examining and assessing the experiments of Hansen and Bol. In addition, we thank Messrs. D. Barbieri and H. T. David for advice concerning least squares, and Mr. F. T. Johnson for aid in various parts of the work. We are greatly indebted to Professor T. H. Berlin for critically reviewing the manuscript, and to the Bureau of Ordnance U. S. N. for financial assistance which made this work possible.

** *Note added in proof.*—The original monograph of the present work released last summer has elicited numerous private communications which together with recently published data modify the input values noticeably. In order to prevent obsolescence of the present work we have incorporated these new data. Accordingly, the table of values represents our knowledge of the atomic constants as of December 1, 1950.

Microwave Magnetic Resonance Spectrum of Oxygen*

ROBERT BERINGER AND J. G. CASTLE, JR.†
Sloane Physics Laboratory, Yale University, New Haven, Connecticut
(Received September 7, 1950)

The complex magnetic-resonance spectrum of oxygen gas is observed at 9340 Mc/sec in magnetic fields up to 9000 oersted. Some 40 lines are resolved. A partial analysis of the spectrum is made with the help of Henry's recent Zeeman theory of O_2. Other lines are identified by the temperature dependence of the relative intensities. Line widths are measured by several techniques and range from 0.6 to 4 Mc/sec/mm Hg at room temperature. The temperature and pressure dependence of the line widths are investigated.

I. INTRODUCTION

MOLECULES which have permanent magnetic moments exhibit an absorption spectrum arising from magnetic dipole transitions between Zeeman levels of a single rotational state. Such spectra have been observed by us[1,2] at three-centimeter wavelengths using the method of magnetic resonance. The present paper describes in detail our measurements with oxygen gas.

The details of the interaction of an external magnetic field with the molecular electronic orbital and spin angular momenta depend upon the internal coupling of these momenta. In Hund's case (a), where the electronic orbital momentum and spin momentum are strongly coupled to the internuclear axis and weakly coupled to the nuclear rotation, the external field effectively interacts with their resultant J; at available field intensities the magnetic level displacements are given to fair approximation by simple Zeeman theory.[3] Nitric oxide[1] exemplifies this situation. In extreme case (b) coupling where the electronic spin is very weakly coupled to the orbital and rotational momenta, an external field of low intensity breaks down the coupling and produces the Paschen-Back effect.[3] In both of these extreme situations the spectral interpretation can be made by vector-model considerations; perturbation calculations are only necessary when accurate line positions and intensities are required. Oxygen, in which the spin-rotation coupling is about 2 cm^{-1} is in neither of these simple categories for the conditions of the present experiment. Fields sufficient to separate adjacent magnetic levels by the observing frequency (0.3 cm^{-1}) break down the internal coupling to a considerable degree, but not nearly enough to produce the Paschen-Back regularities.

The ground electronic state of the oxygen molecule is $^3\Sigma$. The angular momenta in zero field approximate case (b) coupling. The rotational states are characterized by K (total angular momentum except for spin) and each K state is split into a triplet by the interaction[4] of K with S. These levels are denoted by J where $J=K$, $K\pm1$. K takes on all odd integral values, and at ordinary temperatures a large number of K states are well populated. (At room temperature the Boltzmann factor, apart from the degeneracy, for $K=17$ is about a tenth that for $K=1$.) The separation of J levels differs only slightly in the various K states; the K to $K+1$ and K to $K-1$ spacings being about 2 cm^{-1}.

On introduction of a magnetic field each K triplet splits into 3 $(2K+1)$ Zeeman levels. In view of the large number of well-populated states several hundred magnetic levels become available for magnetic resonance transitions. At very low fields the M level energy displacements follow Zeeman theory.[3] If these formulas held at fields of a few thousand oersteds, only the magnetic levels of the $K=1$ state would be separated sufficiently to be resonant at our observing frequency. However, at the field strengths employed, the internal coupling breaks down; some observable transitions for high K values are pushed to moderate fields and some of those for low K values are displaced beyond attainable field strengths.

The absence of a simple coupling scheme and the large number of levels involved makes it impossible to analyze the spectrum without the use of an accurate theory. Such a Zeeman theory for O_2 was developed by Schmid, Budó, and Zemplén.[5] Their formulas result by introducing the magnetic field interactions after computing the coupling which leads to the K triplets. These formulas are not sufficiently accurate for use here, and are particularly poor for low K values. Henry[6] has recently computed the positions and intensities of several of our lines by a more exact procedure which includes all of the perturbations at one time. Our agreement with these calculations is quite good and will be discussed in detail in Sec. II.

Henry's calculations are very laborious and have been carried out in detail for only the magnetic levels of the $K=1$ and $K=3$ states. They serve to identify only a few of the observed lines. A partial identification of other lines was made by observing the spectrum at

* Assisted by the ONR.
† DuPont Fellow in Physics (1949–50). This paper presents part of the author's thesis for the degree of Doctor of Philosophy in Yale University.
[1] R. Beringer and J. G. Castle, Jr., Phys. Rev. **78**, 581 (1950) and Phys. Rev. **76**, 868 (1949) for the gas NO.
[2] R. Beringer and J. G. Castle, Jr., Phys. Rev. **75**, 1963 (1949) for O_2 and J. G. Castle, Jr. and R. Beringer, Phys. Rev. **80**, 114 (1950) for NO_2.
[3] G. Herzberg, *Molecular Spectra and Molecular Structure* (Prentice-Hall, Inc., New York, 1939).
[4] See R. Schlapp, Phys. Rev. **51**, 342 (1937), Phys. Rev. **39**, 806 (1932) for a precise theory of the O_2 states in zero external field.
[5] Schmid, Budó, and Zemplén, Z. Physik **103**, 250 (1936).
[6] A. Henry, Phys. Rev. **80**, 396 (1950).

room and at liquid air temperatures. Comparison of intensities permits an estimation of the Boltzmann factor and hence of the K values of the unidentified lines. These measurements will be discussed in Sec. III.

The main experimental procedures employed in most of the present studies have been described.[1] A microwave signal is transmitted through a gas-filled resonant cavity and received with a bolometer. A dc magnetic field is adjusted until the quantum frequency of an allowed transition between magnetic sublevels coincides with the observing frequency. The microwave magnetic field induces transitions and is partially absorbed. A small ac magnetic field modulates the absorption and the microwave power to the bolometer. The modulation is detected by the bolometer and is amplified, usually at the fundamental of the modulation frequency, in which case the output signal *vs* H is essentially the first derivative of the absorption line. The amplified signal is detected in a phase-coherent mixer and used to deflect a long-period galvanometer. The galvanometer readings trace the first derivative of the absorption line contour as the dc magnetic field is varied.

Several minor changes in the apparatus and experimental procedures were made in the course of the present experiments. One of these, detection at the second harmonic of the modulation frequency, is discussed in Sec. IV. Another change is the use of a direct-coupled triode preamplifier. When preceded by a well-shielded input transformer this amplifier had a measured noise voltage at 30 cycle/sec of only twice the Johnson noise of the 400-ohm signal source. Under ideal conditions, the preamplifier improved our minimum detectable signal by a factor ten or more over that described,[1] but this factor was not always realized because of the increased noise contribution from the microwave oscillator. This noise was particularly troublesome when the stabilized oscillator was tightly coupled to the gas-filled cavity and when that cavity had an unusually high Q.

II. OBSERVATIONS AND ANALYSIS BY THEORY

In all of the experiments the observing frequency was 0.31 cm^{-1} (9340 to 9360 Mc/sec); the magnetic field intensities ranged from 3000 to 9000 oersteds. In this range of field intensities about 40 lines are observed at room temperature. A typical spectrum is shown in Fig. 1. The line contours are essentially the first derivatives of the absorption coefficients *vs* H except for distortions produced by finite modulation.[7] The room temperature measurements employed a TM_{011} mode cylindrical cavity with H parallel to the axis of the cavity.

Table I lists the lines observed in Fig. 1 and other runs, their relative intensities,[8] and resonance field values for an observing frequency of 9340 Mc/sec. The lines are labeled with Arabic numbers for purpose of reference. Table I also lists the calculated resonance field values from Henry's work,[6] the K, J, $M \rightarrow M-1$ values for each, and the calculated relative intensities. It is seen that the agreement with theory is generally satisfactory.

The absolute strength of the absorption can be computed in terms of observed quantities by the formulas of reference 1. Expressed as an absorption Q of the transition, the computed strength at resonance is

$$\frac{1}{Q_A} = \frac{2fN\nu\pi\mathfrak{M}^2\mu_0^2}{(2J+1)kT\Delta\nu}$$

for an O_2 line observed in a TM_{011} cavity at frequency ν. Here f is the fraction of all molecules which are in the

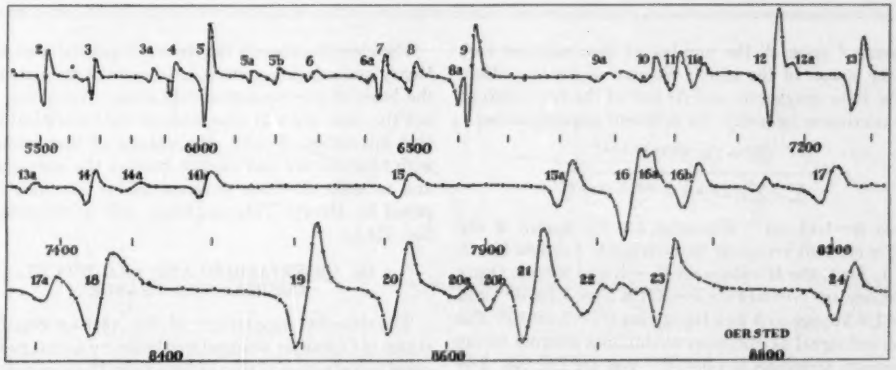

FIG. 1. Magnetic resonance spectrum of O_2 at 300°K. Fixed observing frequency is 9360 Mc/sec, O_2 pressure 4.0 mm Hg, modulation amplitude 8.5 oersted. The ordinate in each of the three traces is the galvanometer position. Lines are numbered to correspond to the text.

[7] These distortions are discussed in reference 1 on p. 584.

[8] The *relative intensity* is here defined as a number proportional to the transition matrix element squared times the population factor of the rotational state involved. It is thus independent of the line width and comes directly from theory. In terms of the observed signal strength: intensity $\propto$ (signal strength)$\Delta\nu$.

TABLE I. Magnetic resonance absorption lines in oxygen at 9340 Mc/sec.

Line No.	Observed Resonance field (oersted)	Observed relative intensity at 300°K	Calculated resonance field (oersted)	Calculated relative intensity at 300°K	Quantum numbers $K, J, M \rightarrow M-1$	Relative $\Delta\nu$
1	4100	—			—	—
2	5527	0.48	5524	0.53	1, 1, 0→−1	0.89
3	5659	0.52				1.4
3a	5845	0.24				1.5
4	5925	0.30				0.78
5	6014	Taken as 1.00	6023	1.00	1, 2, 2→1	Taken as 1.00
5a	6138	0.09				0.9
5b	6190	0.12				0.8
6	6280	0.11				1.2
6a	6406	0.14				1.2
7	6437	0.35				0.82
8	6497	0.36				1.2
8a	6600	0.26				0.6
9	6620	1.1	6634	1.50	1, 2, 1→0	0.99
9a	6884	0.10				1.3
10	6965	0.39				1.1
11	7000	0.29				0.70
11a	7037	0.26				1.1
12	7149	0.92	7170	1.00	1, 2, 0→−1	0.97
12a	7172	0.08				0.6
13	7284	0.39				0.69
13a	7357	0.16				1.3
14	7445	0.22	7448	0.62	3, 2, 0→−1	0.74
14a	7496	0.20				1.8
14b	7585	0.15				0.6
15	7814	0.19				0.82
15a	7962	0.29				0.7
16	8025	0.68				0.76
16a	8038	0.07				0.5
16b	8076	0.25				0.6
17	8196	0.23				0.67
17a	8310	0.11				0.51
18	8352	0.76				0.9
19	8500	0.83	8529	1.24	3, 4, 0→−1	0.70
20	8563	0.48				0.57
20a	8607	0.07				0.5
20b	8626	0.09				0.3
21	8657	0.58				0.55
22	8690	0.18				0.55
23	8745	0.48				0.60
24	8857	0.25				0.48

relevant J state, N the number of molecules per cm^3, $\mathfrak{M}^2$ the square of the matrix element of the transition, μ_0 the Bohr magneton, and $\Delta\nu$ half of the line width at half maximum intensity. To sufficient approximation

$$f=\frac{(2J+1)e^{-BK(K+1)hc/kT}}{\sum_K\sum_J(2J+1)e^{-BK(K+1)hc/kT}},$$

where $B=1.44$ cm^{-1}. Formulas for the square of the matrix element are given in reference 6. For line No. 2, $K=1$, $J=1$, the M values are 0, −1, and $\mathfrak{M}^2=\frac{1}{3}$. Other constants are $f=0.014$ for $T=300°$K, $N=3.2\times10^{16}$, and $\Delta\nu=1.9$ Mc/sec at 1 mm Hg, giving $Q_A=2.2\times10^3$. The observed signal at optimum modulation referred to the bolometer terminals is 1.0×10^{-6} volt for line No. 2 at 300°K. This corresponds to an observed $Q_A=7.2\times10^3$. The disagreement is probably outside of experimental errors in the measured signal strength, apparatus gain, and line width determinations. Other lines also give signal strengths smaller, by a factor three to five, than those calculated from theory.[6]

The identifications of the observed spectral lines using Henry's calculations were in most cases unambiguous on the basis of the resonance field alone. When this was not the case, use was also made of the theoretical relative intensities. Finally, the change in line intensity with temperature was used to confirm the assignments and to make K value assignments for lines not computed by Henry. This procedure will be discussed in Sec. III.

III. OBSERVATIONS AND ANALYSIS BY TEMPERATURE CHANGE

The relative populations of the various rotational states of O_2 can be changed markedly by a change from room temperature to that of liquid air. These population changes are observed as changes in the relative signal strengths[9] of the various lines, and allow the rotational

[9] The signal strength is defined as being proportional to the output galvanometer deflection at optimum modulation and hence proportional to $1/Q_A$. In terms of our definition of intensity: signal strength $\propto$ (intensity)/$\Delta\nu$.

states of the lines to be identified thereby. The procedure is as follows.

The observed signal strength is proportional to $1/Q_A$. For a given gas pressure and temperature, various lines have signal strengths proportional to $\mathfrak{M}^2 f/(2J+1)\Delta\nu$. Experimental evidence shows that $\Delta\nu$ scales with temperature by approximately the same factor for all of the lines, and that $\Delta\nu$ is proportional to the pressure at constant temperature. Since f depends to a good approximation only on K and the temperature, a comparison of sets of relative signal strengths at two known temperatures serves to assign K values. The observed signal strengths and results of such an analysis are given in Table II. It is seen that the K values obtained in this way are in good agreement with those deduced in Table I by correlation with Henry's calculations.

The observations at liquid air temperature required certain apparatus modifications. A circular TE_{111} mode cavity, contained in a Dewar vessel, was used to detect resonance. The cavity was oriented with its axis vertical; two vertical wave guides of thin walled brass supported the cavity from above and carried the microwave power to and from the cavity through circular holes in its top plate. The wave-guide electric fields were parallel to the dc magnetic field of the electromagnet. In this configuration, unlike that for the TM_{011} cavity, the microwave magnetic field in the cavity has components both parallel and perpendicular to the dc magnetic field. Only the perpendicular components contribute to the observed spectrum.

The signal-to-noise ratio was greater for the low temperature observations than for those at room temperature. Lowering the temperature increases the cavity Q, increases the difference in population of adjacent M levels, and decreases the partition function, combining to increase the signal strength for low K lines. In practice, these gains are partially offset by the

TABLE II. Assignment of K values by temperature dependence of the signal strength.

Line No.	Relative signal strength $T=300°K$	$T=78°K$	Assigned K
1	—	0.06	—
2	0.54	0.54	1
3	0.38	0.34	3
3a	0.16	<0.03	⩾9
4	0.39	0.30	3
5	1.0	1.0	1
5a	0.10	<0.05	⩾5
5b	0.14	<0.03	⩾9
6	0.09	0.09	1
6a	0.12	0.05	7
7	0.43	0.23	5
8	0.30	0.12	7
8a	0.44	<0.04	⩾9
9	1.1	1.1	1
9a	0.08	0.06	3 or 5
10	0.30	0.03	9 or 11
11	0.41	0.05	9 or 11
11a	0.24	0.03	9 or 11
12	0.95	0.95	1
12a	0.14	<0.04	⩾7
13	0.57	0.19	7
13a	0.12	0.05	5 or 7
14	0.30	⩾0.21	3 or 5
14a	0.11	<0.03	⩾7
14b	0.25	<0.01	⩾5
15	0.23	0.12	5
15a	0.41	<0.03	⩾11
16	0.89	0.50	5
16a	0.14	<0.07	⩾11
16b	0.41	<0.03	⩾11
17	0.35	0.12	7
17a	0.22	—	—
18	0.85	0.23	7 or 9
19	1.2	0.80	3 or 5
20	0.85	0.17	9
20a	0.14	<0.03	⩾9
20b	0.30	0.03	9 or 11
21	1.0	0.40	7
22	0.33	0.07	9
23	0.80	0.24	7
24	0.52	<0.03	⩾11

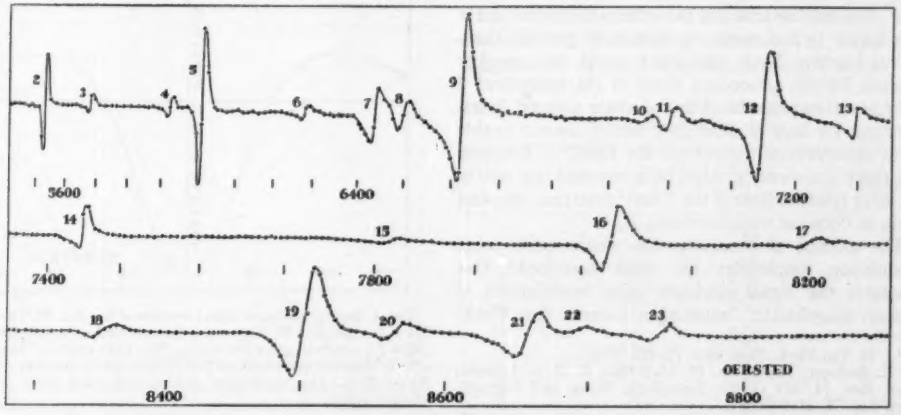

FIG. 2. Magnetic resonance spectrum of O_2 at 85°K. Fixed observing frequency is 9340 Mc/sec, O_2 pressure 3.6 mm Hg, modulation amplitude 4.2 oersted. Ordinates are galvanometer position. Lines are numbered to correspond to the text.

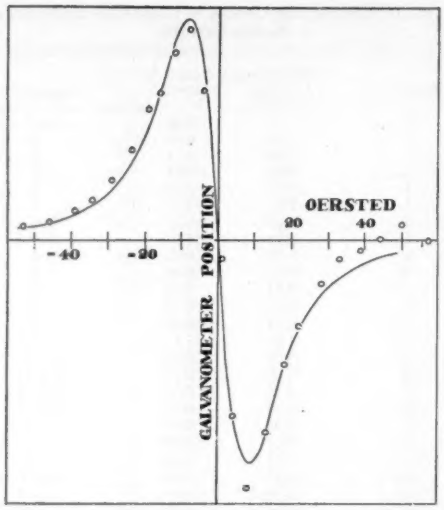

FIG. 3. First harmonic signal of a line at small modulation amplitude. The solid line is the first derivative of a Lorentz line shape with $\Delta H = 14$ oersteds. Points are observed galvanometer positions for line No. 5 at 300°K and 10.1 mm Hg pressure. The ΔH value is not arbitrary but is taken from the measurements of Table III. The modulation amplitude is 3.8 oersteds in the figure.

increased 30-cycle/sec noise of our stabilized oscillators when working into the higher Q cavity. Figure 2 shows a spectrum taken with this apparatus at liquid air temperature. The pronounced changes in relative signal strength referred to above are apparent on comparison of Figs. 1 and 2.

IV. LINE WIDTHS

A considerable part of our effort was concerned with line width measurements. Even the earliest work showed that all of the lines did not have the same width, and it was hoped to find some regularities of possible theoretical interest. Such regularities could also possibly account for the anomalous shape of the unresolved 2 cm^{-1} gas absorption band in O_2, where a single Δv-assignment for lines of different J and K seemed unable to fit observations throughout the band.[10,11] Recently the Duke University group[12] have reported line widths for three resolved lines of the 2 cm^{-1} spectrum, and find them to decrease with increasing K.

The method of obtaining line widths using large modulation amplitudes has been described.[1] One measures the signal contours using modulations of various magnitudes. Assuming a Lorentz-Van Vleck-Weisskopf line shape, the line contours are computed, and graphs of certain parameters of the contours *vs* modulation allow the line widths to be evaluated by extrapolation.

Recent apparatus modifications permit two other methods to be used. Increases in signal-to-noise ratio, largely due to the low noise preamplifier, permit line contours to be observed for low modulations where distortions are negligible. Figure 3 shows such a contour for line No. 5. The solid line is the first derivative of a Lorentz line shape, and is seen to fit the data satisfactorily.

Another method of line width measurement uses the second harmonic signals of the modulated absorption line. Whereas the fundamental frequency signal is most useful for determining the resonance field of a line, since the slope of the contour is greatest at resonance, the second harmonic signals allow more precise line width determinations, their contours having steepest slope near the half-intensity points of the line.

The procedure for deducing the line width from the measurements of modulation-broadened second harmonic contours is similar to that for the fundamental frequency method. One assumes a Lorentz line shape given by

$$\Delta H^2/[(H-H_0)^2+\Delta H^2].$$

The second harmonic signals are then proportional to the Fourier coefficient

$$B_2=\frac{1}{\pi}\int_{-\pi}^{\pi}\frac{\cos 2\omega t\, d(\omega t)}{[(H_1/\Delta H)+(H_m/\Delta H)-(H_m/\Delta H)(1+\cos\omega t)]^2+1},$$

where $H_1=H-H_0+H_m\cos\omega t$. B_2 as a function[13] of H_1 is the observed line contour at frequency 2ω for a

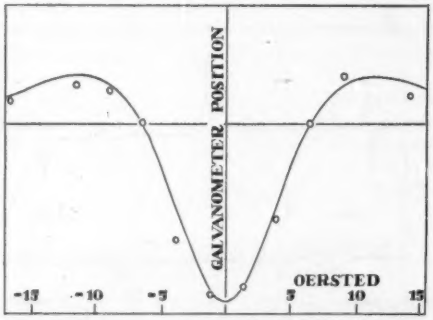

FIG. 4. Second harmonic signal contour of line No. 19. The solid line is the function B_2 plotted for the modulation amplitude used ($H_m = 2.9$ oersteds) and a line width, $\Delta H = 10.7$ oersteds. The circles are the observed galvanometer positions for an O_2 pressure 2.6 mm Hg at 78°K. The modulation distortion is quite small for the contour shown.

[10] J. H. Van Vleck, Phys. Rev. **71**, 413 (1947).

[11] R. Beringer, Phys. Rev. **70**, 53 (1946); H. R. L. Lamont, Phys. Rev. **74**, 353 (1948); Strandberg, Meng, and Ingersoll, Phys. Rev. **75**, 1524 (1949).

[12] Burkhalter, Anderson, Smith, and Gordy, Phys. Rev. **77**, 152 (1950); Phys. Rev. **79**, 224 (1950); and Phys. Rev. **79**, 651 (1950).

[13] Similar integrals are evaluated by W. D. Hershberger, J. Appl. Phys. **19**, 411 (1948).

modulation amplitude H_m at frequency ω. A typical observed contour is shown in Fig. 4. Figure 5 shows the dependence of the intercept (points where $B_2=0$) separation with modulation amplitude as computed from the B_2 coefficients; it is used to determine ΔH from measurements of H_m and the intercept separation.

Our best line width measurements were made with the second harmonic method. Contours such as Fig. 4 were plotted, and the intercept separations found. These were extrapolated to zero modulation using Fig. 5 to determine ΔH.

The magnitude of ΔH depends, among other things, on the field value at which it is observed. Not ΔH, but $\Delta\nu$, the frequency width of the line, is the fundamental quantity in line broadening theory, and the two are related by

$$\Delta\nu=\Delta H\cdot\nu/H,$$

where ν is the fixed observing frequency and H the resonance field of the line. Thus at high fields the lines are intrinsically wider in field strength units. In the discussion which follows the line widths are reduced to $\Delta\nu$-units using the above formula.

The line width measurements were designed to discover the dependence of $\Delta\nu$ on temperature, pressure, and the quantum numbers. Figure 6 shows the observed pressure dependence of a line at 300°K. As might be expected, ΔH, and so $\Delta\nu$, is proportional to pressure for low pressures. Because of overlapping in the spectrum, we were not able to carry out these measurements at pressures greater than a few cm of Hg.

The temperature dependence of $\Delta\nu$ was studied by measuring the line widths of a selected group of strong, isolated lines at room and liquid air temperatures using the second harmonic technique. Table III gives the result of these measurements. It is seen that the line widths at constant pressure increase by an approximately constant factor of 3 for a decrease in temperature

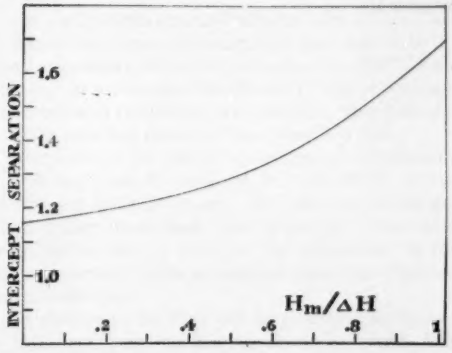

FIG. 5. Curve used to determine ΔH from measurement of the second harmonic line contour. The ordinate is the distance in ΔH units between the intercepts (zero signal points) of the function B_2. These intercept points are the most easily determined parameters of a line broadened by modulation.

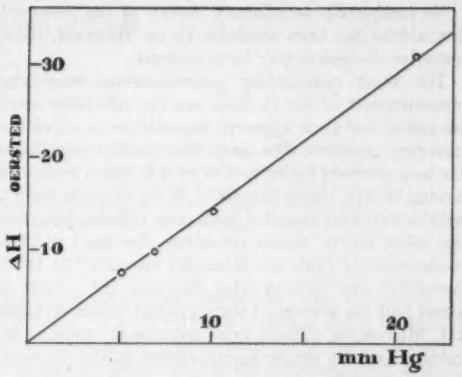

FIG. 6. Variation of width of line No. 5 with pressure at 300°K. ΔH values were determined using the measured intercept separations of second harmonic signal contours.

from 300°K to 85°K. Less precise line-width values were also taken from observed spectra such as Figs. 1 and 2. These are included in Table I in relative units which can be converted to absolute units by use of Table III.

From Table III we may take 2.0 Mc/mm Hg as an average $\Delta\nu$ for $K=1$ lines at 300°K. Converting this to one atmosphere pressure at the same temperature gives 0.051 cm^{-1}. This may be compared with the recent measurement[12] 0.053 cm^{-1} for the width of a $K=3$ line in the 2 cm^{-1} O_2 absorption spectrum and with the value 0.02 cm^{-1} to 0.05 cm^{-1} used to fit the unresolved[11] 2 cm^{-1} spectrum.

Table III and Table I do not show any regular dependence of $\Delta\nu$ with K alone. The spread in $\Delta\nu$ values for various lines from the same K state is as great as the total observed spread. Presumably this is due to a rather strong dependence of $\Delta\nu$ on M as well as the other quantum numbers. There is some evidence in Table I that the minimum $\Delta\nu$ for a given K decreases with increasing K. However, a different and incomplete sample of M values is observed for each K state.

TABLE III. Line widths of strong, isolated lines determined by second harmonic method.

Line No.	Lorentz half-width in Mc/sec at 1 mm Hg $T=300°K$	$T=85°K$	Probable K
2	1.93	5.62	1
3	—	8.65	3
4	1.66	5.08	3
5	2.22	6.23	1
7	1.82	5.14	5
9	—	6.17	1
11	—	4.36	>9
12	2.04	6.27	1
13	1.44	4.50	7
14	—	4.13	3
16	—	4.75	5
17	—	4.42	7
19	—	4.33	3

No completely satisfactory theory of the observed line widths has been available to us. However, some tentative discussion may be of interest.

The most outstanding generalizations from the measurements of the O_2 lines are the relatively small $\Delta\nu$ values and their apparent dependence on all of the quantum numbers. The small line width results from the lack of strong forces such as exist between molecules having electric dipole moments. If we compare the O_2 widths with that expected from pure collision-broadening using kinetic theory constants, the small width is made evident. From the measured viscosity[14] at 15°C, $\Delta\nu = 0.028$ cm^{-1}/atmos. $= 1.1$ Mc/mm Hg, which is about half the average of the measured values of Table III. Microwave collision cross sections for polar molecules exceed the simple kinetic theory values by much larger factors.[15]

The exchange forces which contribute the greater part of the interactions in kinetic theory processes have not been calculated explicitly or applied in theories of microwave pressure broadening. One would expect them to be relatively insensitive to the rotational quantum numbers, and one would expect these forces to provide a relatively constant background contribution to all of the widths. Roughly then, half of the observed width does not arise from specific forces which can be treated with the present theories of pressure broadening.

The remaining contributions to $\Delta\nu$, and presumably those which carry the strong quantum number dependence, may be (a) electric quadrupole interactions, (b) van der Waals forces, or (c) magnetic dipole forces.

It is easily shown that (c) is small compared with (a) and (b) above.

An unpublished manuscript of M. Mizushima[16] proposes that electric quadrupole forces can account for the observed widths in the 2 cm^{-1} spectrum of O_2 and for their K dependence. We agree that these forces do make an important contribution. On modifying the Mizushima theory to the case of the present spectrum we find that the electric quadrupole moment required is of reasonable magnitude.[17] However, the predicted dependence on rotational and magnetic quantum numbers is not exhibited by the measured values.

Margenau has made a preliminary investigation of the possible role of van der Waals forces (i.e., $1/r^6$ forces) in the present spectrum. It appears that this line-width contribution will be about as large as that of the quadrupole forces. The calculated dependence of these forces on the quantum numbers is generally similar to that for the quadrupole forces. Thus no improvement in the quantum number dependence of $\Delta\nu$ is achieved.

There are two well known limiting cases for the temperature dependence of $\Delta\nu$. In pure impact theories $\Delta\nu$ is proportional to the collision frequency and thus to $T^{-\frac{1}{2}}$ for constant pressure. Microwave observations do not follow this law.[15] In pure statistical theories $\Delta\nu$ is proportional to the density of molecules and thus to T^{-1} at constant pressure. The present observations (Table III) lie between these extreme cases, the observed $\Delta\nu$ ratio at constant pressure being 3.0 for a temperature ratio of 3.5. The Mizushima model, a modified impact theory, predicts that $\Delta\nu \propto T^{-\frac{1}{2}}$ at constant pressure. With this law the $\Delta\nu$ ratio for the conditions of Table III would be 2.6. Thus the observations lie midway between a T^{-1} and a $T^{-\frac{1}{2}}$ dependence.

The authors are indebted to Professor Henry Margenau for many discussions of the pressure broadening aspects of this study and for the use of his unpublished calculations. The authors also wish to thank Dr. A. F. Henry for his interest and help in connection with the Zeeman theory of the spectrum.

[14] E. H. Kennard, *Kinetic Theory of Gases* (McGraw-Hill Book Company, Inc., New York, 1938).

[15] W. V. Smith and R. Howard, Phys. Rev. **79**, 132 (1950).

[16] This manuscript was kindly loaned to us by Professor Margenau.

[17] Say 2×10^{-26} esu depending on the state chosen. This is not much larger than Ramsey's value for H_2 [Phys. Rev. **78**, 221 (1950)] but several times that deduced by Smith and Howard (reference 15).

The Band Spectrum of HgIn

R. L. PURBRICK*
University of Wisconsin, Madison, Wisconsin
(Received August 28, 1950)

An examination of the band spectrum of the HgIn molecule has been carried out using the second order of the Wisconsin 21-foot reflection grating. Band systems were obtained with intensity maxima at 4102, 4511, 4994, 5226, 5544, and 5760 angstrom units. The systems at 4102A and 4511A appear to be continuous, but the others have been resolved into bands. Vibrational analyses were made of the 4994A, 5226A, and 5544A systems; but the 5760A bands have not yet been successfully worked into a single square array.

I. INTRODUCTION

WHILE working with the sensitized fluorescence of indium in mercury vapor, Winans, Leitzke, and Davis[1] found that a Tesla discharge through the mercury-indium mixture gave rise to several band systems of the HgIn molecule. The system at 5227A was resolved into bands with heads on the long wavelength side. These early measurements showed the 5227A system, extending from 5270A to 4880A with a second maxima at 4998A, to be made up of bands spaced 11 to 15 angstroms apart. Another system at 5800A was observed to extend from 6390A to 5400A with minima in intensity at four places in this range. Continuous bands at 4132A and 4574A were also found.

The purpose of the present investigation was to make a more detailed examination of the HgIn bands using the second order of the Wisconsin 21-foot reflection grating. The spectra obtained show several new band systems most probably due to HgIn. Two of these new systems at 5760A and 5544A have been resolved into bands, while those at 4350A, 4740A, and 4825A appear to be continuous. A very weak system in the red was also observed, but it has not yet been possible to obtain it with sufficient intensity for detailed examination.

II. APPARATUS AND PROCEDURE

An electrodeless quartz discharge tube with a Tesla coil providing the excitation energy was found to be the most convenient source. After baking at 1000°C for a few days at a pressure of less than 10^{-7} mm of mercury, indium was first distilled into the tube, then mercury, and the tube was sealed off the vacuum system.

The purity of the indium was tested spectroscopically by placing a small sample of it in the lower of two carbon electrodes in an arc. The spectrum of the arc showed lines other than those of indium. These were identified as due to cadmium by comparison of the indium spectrum with a cadmium spectrum obtained in the same way.

In addition to the Tesla coil for producing excitation, a high frequency (60 Mc) oscillator was tried. The oscillator was of the push-pull type and employed two 250TH Eimac tubes. This produced bands of approximately the same intensity as the Tesla coil. Since the Tesla coil is more portable and less liable to require adjustment, it was used for most of the spectra obtained.

It was necessary to heat the discharge tube with an external source to obtain a sufficient pressure of indium vapor in the tube atmosphere to give the HgIn bands. For the first experiments a gas-air flame was used. As the discharge tube became older, the intensity of the mercury hybride bands in its spectrum increased. This was attributed to the diffusion of hydrogen from the flame through the hot quartz. When a furnace was used, this did not occur. The furnace was made with nichrome wire windings and was usually operated at 400 watts. An air space surrounding the nichrome wire prevented excessive local heating and gave long life, as described by Winans and Cram.[2] Small side arms were added to reduce the temperature gradient between the center of the furnace and the outside. Tesla coil leads were introduced through the side arms.

Five different spectrographs were used. Small Hilger quartz and glass spectrographs were used to determine best conditions for excitation. A Bausch and Lomb medium quartz spectrograph was used to obtain all bands on one plate and to determine the purity of the indium. Reflection grating spectrographs of 10- and 21-foot radius were used for greater dispersion. Most of the band head measurements were made on plates taken with the 21-foot grating. The dispersion of the 21-foot instrument is 1.31A per millimeter. The grating is one of 90,000 lines ruled on aluminum by R. W.

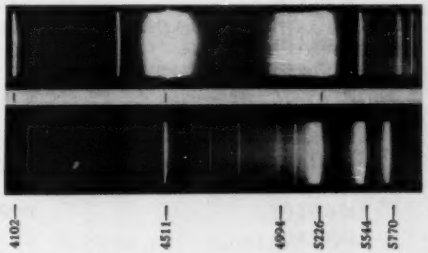

FIG. 1. Glass prism spectrograms of (A) the absorption in yellow region at high mercury pressure and (B) the band systems of HgIn.

* Now at Willamette University, Salem, Oregon.
[1] Winans, Davis, and Leitzke, Phys. Rev. 57, 70 (1940).
[2] J. G. Winans and S. W. Cram, Rev. Sci. Instr. 10, 272 (1939).

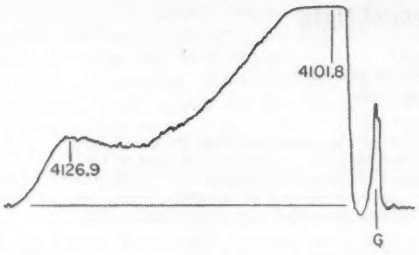

FIG. 2. Microphotometer trace of the 4102A band. A grating ghost of the indium 4102A atomic line appears at (*G*).

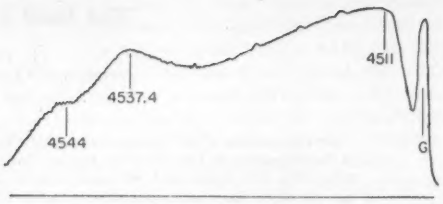

FIG. 3. Microphotometer trace of the 4511A band. A 4511A ghost line occurs at (*G*).

Wood to concentrate energy at wavelength 5500A in the second order.

III. THE BAND SYSTEM

Figure 1 shows two spectrograms of the HgIn band systems made with a small Hilger glass spectrograph. The long wavelength limit or the location of the most intense band of the system has been used to identify each group, with the exception of the two bands attached to the indium resonance lines at 4102A and 4511A. These are identified by the adjacent indium line.

The intensity of any given band system relative to that of the other band systems was found to depend upon the temperature and the mercury pressure in the discharge tube. High temperature and the resulting increase in indium atoms in the tube atmosphere favor the 4511A band, while lower temperature and higher mercury pressure increase the intensity of the 5226A and 4994A systems. In Fig. 1A it was necessary to overexpose the 4511A, 5226A, and 4994A bands to reveal the intensity variations in the region between the mercury yellow lines at 5770A and 5790A and the mercury green line at 5461A. A microphotometer trace

FIG. 4. Grating spectrogram of the 5226A and 4994A systems. Iron comparison lines were superimposed on all grating spectra.

of the negative from which this print was made showed that each of the intensity maxima is in turn made up of several intensity variations. Using a longer discharge tube made it possible to lower the mercury pressure

TABLE I. Square array of the bands of the 5226A system. Estimated relative intensities on a 1 to 10 scale are in brackets after the wave numbers of the band heads.

v' \ v''	0	1	2	3	4	5
0	19,128.3 (10) 19,130.1 (10)	19,076.8 (5)	19,034.7 (1)			
1	19,176.4 (9) 19,177.8 (9)					
2	19.226.2 (8)					
3	19,275.8 (7)		19,179.3 (6)			
4	19,326.8 (7) 19,328.4 (7)	19,275.2 (7)	19,233.2 (7)			
5	19,374.5 (7) 19,376.0 (7)			19,248.8 (6)		
6	19,424.2 (7)			19,297.1 (4)	19,269.5 (2)	
7	19,475.6 (6)					19,308.2 (4)
8	19,522.4 (5)					
9	19,572.8 (4)					
10	19,620.5 (4)		19,528.1 (2)			
11	19,671.4 (4)			19,543.0 (2)		
12	19,722.2 (4)				19,563.3 (2)	
13	19,769.2 (3)					19,605.5 (1)
14	19,819.2 (2)					

TABLE II. Square array of the 4994A bands.

v'' / v'	0		1		2		3
0	20,018.1 (5)	59.6	19,958.5 (4)				
	40.1		41.1				
1	20,058.2 (2)	58.6	19,999.6 (3)				
			40.5				
2			20,040.1 (2)	54.5	19,985.6 (3)	51.8	19,933.8 (1)
					39.3		
3					20,024.9 (1)		

and obtain the spectrogram of Fig. 1B which reveals the 5760A and 5544A systems.

If a pool of mercury and indium is placed at the center of the furnace in the discharge tube, at first the mercury vapor pressure is too great for a discharge. However, when most of the mercury has been boiled off, the discharge spectrum is produced. After the first nine minutes of operation, the band systems at 5760A and 5544A decrease in intensity until after 20 minutes they have almost disappeared. However, the bands at 5226A, 4994A, and 4511A increase slightly in intensity with time. The rapidity with which the 5760A and 5544A systems die out is determined by the temperature. If the temperature is high, they are intense but last for only a short period. If the temperature is lower, the bands are weaker but remain for a much longer time.

The band systems at 4102A, 4511A, 4994A, 5226A, 5544A, and 5760A have been investigated with the 21-foot spectrograph. Exposure times varied from one to fifteen hours. Figure 2 is a microphotometer trace of the 4102A band. It is continuous with an intensity maximum at 4126.9A. It extends to approximately 4133A. The microphotometer trace of the 4511A band in Fig. 3 shows it to be continuous with maxima at 4544A and 4537.4A. The long wavelength limit is at about 4551A.

Spectrograms of the 5226A and 4994A systems are shown in Fig. 4. Tables I and II list the wave numbers and relative intensities of these bands. Figure 5 is a spectrogram of the bands at 5544A. Table III gives their wave numbers. The system at 5760A is shown in Fig. 6; wave numbers are listed in Table IV. This system differs from those at 4994A, 5226A, and 5544A, since it contains bands shaded toward the violet and red, whereas those of the other systems are all shaded toward the violet.

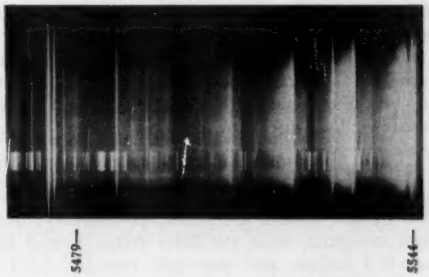

FIG. 5. Grating spectrogram of the more intense bands of the 5544A system. Higher order atomic lines also appear.

The bands at 4350A, 4740A, 4825A, and 6104A were too weak to be investigated with the grating spectrograph. They appear and disappear with the 5760A and 5544A systems. None of the bands attributed to HgIn have been found in absorption.

TABLE III. Square array of the 5544A system.

v'' / v'	0	1	2	3	4	5
	18,031.2 (10)					
0	18,033.5 (10)	17,970.6 (1)				
	(18,038.0) (8)					
		18.077.2 (9)				
1		18,078.8 (9)	18,017.2 (3)	17,958.3 (3)		
		(18,081.4) (3)				
2	18,242.8 (3)		18,123.4 (8)	18,064.4 (4)	18,007.5 (2)	17,951.9 (2)
	18,247.1 (3)					
3		18,288.8 (3)		18,170.8 (6)	18,113.5 (4)	
4			18,334.4 (3)		18,220.1 (4)	18,163.9 (4)
5				18,381.6 (2)		
6					18,430.1 (1)	

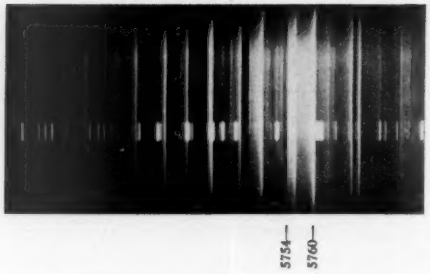

FIG. 6. Grating spectrogram of the 5760A system.

IV. DISCUSSION

A. The 4102A and 4511A Bands

Guernsey[3] and later Watson and Shambon[4] found continuous bands in the arc spectrum of indium which extend to the short wavelength side of the indium resonance lines at 4102A and 4511A. These bands were attributed to semistable molecules of In_2. Thus, it is reasonable to assume that the continuous bands on the long wavelength side of these same indium lines in a mercury-indium discharge spectrum are due to a semistable molecule of HgIn.

Potential curves which account for these bands are shown in Fig. 7. The upper electronic state, formed from excited indium and unexcited mercury, has a slight minimum, while the lower states, formed from unexcited indium and unexcited mercury, have no minima. This explains the maxima on the long wavelength side of the atomic lines and also the absence of an absorption spectrum.

TABLE IV. The wave numbers of the band heads of the 5760A system. (*) denotes bands shaded to the red.

Wave-number cm^{-1}	Intensity	Wave-number cm^{-1}	Intensity
17,275.6	1	17,453.6	1
17,290.5	3	17,457.6	1
17,296.8*	4	17,460.9	7
17,305.8	1	17,481.0	6
17,311.2	2	17,492.0	4
17,325.0*	7	17,506.1*	4
17,330.4	8	17,516.6	5
17,342.7	3	17,551.9	4
17,346.7	4	17,564.3*	1
17,356.3	10	17,587.1	1
17,369.6	9	17,596.7	1
17,374.7*	8	17,610.1	1
17,378.9	4	17,631.1	1
17,382.6	4	17,647.0	1
17,387.4	1	17,665.1	1
17,392.5	9	17,683.8	1
17,401.9*	7	17,697.6	1
17,407.7	8	17,719.6	1
17,414.4	4	17,754.5	1
17,419.5	2	17,782.9	1
17,427.7	8	17,940.9	1
17,430.7*	7		
17,445.0	7		
17,449.3	4		

[3] M. L. Guernsey, Phys. Rev. **46**, 114 (1934).
[4] W. W. Watson and A. Shambon, Phys. Rev. **50**, 607 (1936).

If we assume the coupling between the L_i and S_i of the separated atoms to be strong in comparison with the coupling of the L_i to the internuclear axis of the molecule, the electronic angular momentum, Ω, along the internuclear axis is given by

$$\Omega = M_{J_1} + M_{J_2},$$

where $J_i = L_i + S_i$, J_i = total angular momentum of atom i, L_i = resultant orbital angular momentum of atom i, S_i = resultant spin angular momentum of atom i, and M_{J_i} = component of J_i along the internuclear axis. Hence, for $In(^2P_{1/2})$ and $Hg(^1S_0)$, $\Omega = 1/2$. But for $In(^2P_{3/2})$ and $Hg(^1S_0)$, Ω may be 1/2 or 3/2. The $In(^2P_{3/2})$ and $Hg(^1S_0)$ combination gives two unstable states corresponding to Ω equal to 1/2 and 3/2 and therefore two maxima on the long wavelength side of the indium 4511A line. But the combination $In(^2P_{1/2})$ and $Hg(^1S_0)$ yields only one unstable state and hence one intensity maximum to the long wavelength side of the 4102A line. The upper electronic state with $In(^2S_{1/2})$ and $Hg(^1S_0)$ has only one possible value of Ω, $\Omega = 1/2$.

B. The 5226A and 4994A Systems

The wave number formula for the vibrational structure of a molecule may be written

$$\nu = \nu_{00} + \omega_0' v' - \omega_0' x_0' v'^2 - \omega_0'' v'' + \omega_0'' x_0'' v''^2. \quad (1)$$

The band heads of the 5226A system can be arranged in the square array of Table I and the vibrational constants of Eq. (1) obtained. The constants are given in Table V. The v' progression $v''=0$ can be traced until it meets the 4994A system. Thus, the energy of dissociation of the upper electronic state, D_0', must be greater than 840 cm^{-1}.

An approximate limit for the energy of dissociation of the lower state is given by the formula

$$D_0'' = \omega_0''^2 / 4\omega_0'' x_0''. \quad (2)$$

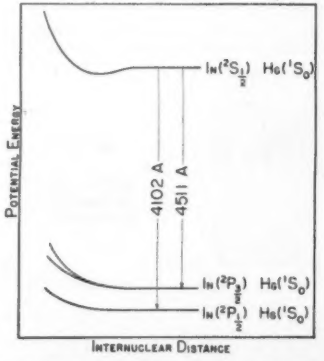

FIG. 7. Electronic states of the 4511A and 4102A bands.

The vibrational constants of Table V give 169 cm^{-1} for D_0'' when substituted in Eq. (2).

Winans[5] found that the majority of mercury lines are not affected by heat; but the 5460A, 4358A, and 4047A lines are weakened, probably from collisions of the first kind which raise excited atoms to higher states. These three mercury lines have $^1S_1$ for their upper state. The 5226A system of HgIn also decreases in intensity at higher temperatures. If this system has an upper electronic state formed from Hg($^3S_1$) and In($^2P_{1/2}$) as shown in Fig. 8, it should decrease in intensity with increase in temperature because of the decrease in the number of mercury atoms in the atomic state from which the upper electronic state is formed. The extent of the band system shows that D_0' is greater than 840 cm^{-1}. This condition is satisfied if the upper electronic state is formed from Hg($^3S_1$) and In($^2P_{1/2}$) and the lower from Hg($^3P_1$) and In($^2P_{1/2}$). When the energy difference between the mercury states, the known value of D_0'', and the wave number of the (0,0) band are used, D_0' is found to be 3980 cm^{-1}. Thus D_0' is greater than 840 cm^{-1} and the upper and lower electronic states very likely dissociate into the assumed atomic states.

Since the 4511A system has excited indium and unexcited mercury for its upper state, higher indium temperatures should increase its intensity because of the greater number of excited indium atoms in the atmosphere of the discharge tube. This corresponds to observation.

The 4994A system is very likely another transition with dissociation products of the upper state the same as for the 5226A system and with lower state dissociation products Hg($^3P_0$) and In($^2P_{1/2}$). Because only a few bands are found in the 4994A system, it is difficult to construct a square array for them, but a possible arrangement is given in Table II.

C. The 5544A System

The band heads of this system can be arranged in the square array of Table III. The (0,0) and (1,1) bands have two sharp heads and one diffuse head (in brackets in Table III). The sharp heads are probably the two R heads of a $^2\Sigma \rightarrow {}^2\Sigma$ transition. The diffuse head is probably the two P branches. The bands of the $\Delta V = -2$ sequence appear to have several heads. Vibrational constants are given in Table V. The energy

TABLE V. Vibrational constants of the 5226A and 5544A systems. Measurements are in cm^{-1}

Band system	5226A	5544A
ν_{00}	19,129	18,032
ω_0'	49.3	105.5
$\omega_0'x_0'$	very small	very small
ω_0''	57.8	62.0
$\omega_0''x_0''$	4.94	0.80

[5] J. G. Winans, Phys. Rev. 39, 745 (1932).

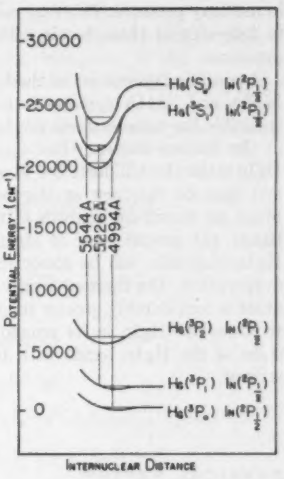

FIG. 8. Possible electronic states of the 4994A, 5226A, and 5544A systems.

of dissociation for the lower electronic state using Eq. (2) is 1201 cm^{-1}.

In Fig. 1 the 5544A system can be seen to extend to the 5226A system; hence, the energy of dissociation of the upper state must be greater than 1097 cm^{-1}. If the upper electronic state of the 5544A system is assumed to be formed from Hg($^1S_0$) and In($^2P_{1/2}$) and the lower one from Hg($^3P_2$) and In($^2P_{1/2}$), D_0' can be obtained from the equation

$$\nu_{00}+D_0' = \text{energy difference between Hg}(^1S_0) \text{ and Hg}(^3P_2)+D_0''$$
$$18{,}032+D_0' = 19{,}885+1201$$
$$D_0' = 3054 \text{ cm}^{-1}.$$

D. The 5760A System

This system, shown in Fig. 6, has a majority of its bands shaded towards the violet; but several strong bands are shaded to the red. A mixture of band shading can often be correlated through the assumption of "tail bands." In the 5760A system the bands shaded to the red might be considered to be tail bands. The stronger bands fall into four distinct groups by virtue of their spacings, shadings, and intensities. These groups may be considered as progressions or as sequences, but they have not been successfully worked into a single square array. Possibly several electronic transitions between multiplet states overlap in this region.

There are several reasons for believing the 5760A and 5544A systems have upper electronic states formed from the same atomic states. Under all conditions of temperature, mercury pressure, and fading with time, they appear and disappear together. If a mercury atomic state lies slightly below the minimum of the upper electronic state of the 5760A and 5544A systems, a quenching of these systems might occur with increase

in mercury pressure. This may account for the decrease in intensity of these bands with increase in mercury pressure.

A possible explanation of the fading with time of the 5760A and 5544A systems is that the molecules responsible for these systems are boiled off the amalgam at the furnace center. After a certain time all of the HgIn molecules will have boiled off leaving only indium and gaseous mercury at the center of the furnace. Since, as shown by analysis of the 4102A and 4511A bands, the ground state of HgIn is very shallow, the HgIn molecules will be dissociated a short time after evaporation. The thermal energy at the 900°C temperature is considerably greater than the energy necessary to dissociate HgIn in its ground state. The fading of some of the HgIn bands with time may thus be described.

The persistence of the 5226A system with time may mean that this system is due to molecules formed in the atmosphere of the discharge tube from excited mercury $^3S_1$ and unexcited indium $^2P_{1/2}$. It should therefore not fade with time. The difference in behavior of 5226A and of 5760A and 5544A may indicate a difference in character of the upper states for these two systems. This difference may be such that the upper state for 5760A and 5544A may not be formed from collisions between excited mercury and other atoms while the upper state for 5226A may be formed from collisions.

It is a pleasure to thank Professor J. G. Winans for suggesting the HgIn problem and for many illuminating discussions. This work was supported in part by the Research Committee of the graduate School from funds supplied by the Wisconsin Alumni Research Foundation.

PHYSICAL REVIEW VOLUME 81, NUMBER 1 JANUARY 1, 1951

Boson Current Corrections to Second Order

D. C. PEASLEE*
Eidgenössische Technische Hochschule, Zürich, Switzerland
(Received April 10, 1950)

The β-matrix formalism is applied to the Schwinger-Tomonaga method of calculating second-order current corrections for particles with spin 0 or 1 in interaction with the electromagnetic field. A rule for eliminating the troublesome "surface terms" is introduced, which makes the general formalism exactly similar to that for the electron. One other complication is the appearance in the results of an operator M which has no counterpart in the electron case; this operator can be handled without difficulty, however.

The second-order current corrections are found to diverge logarithmically for the vector meson, including the corrections to the dipole and quadrupole moments. For the scalar meson, on the other hand, the divergent terms vanish identically because of special relations between the operators. Thus to this order of calculation, the scalar meson like the electron requires only renormalization of the charge and mass, while the same is no longer true of the vector meson.

I. INTRODUCTION

THE necessary modifications in the Schwinger-Tomonaga covariant formulation[1,2] of electrodynamics in going from the case of electrons to that of bosons have been discussed by several authors.[3,4] It is found that for bosons it is necessary to introduce certain additional terms in the current and interaction Hamiltonian in order to make integrable the equations describing the development of the system in space time. These extra terms depend not only on the point under consideration, but also on the orientation of a mathematical surface σ through that point, which is expressed by the unit normal vector n_μ. On physical grounds, this surface dependence cannot appear in any calculated final quantity that is in principle measurable; explicit calculation of the first-order corrections (vacuum polarization and self-mass)[4,5] have shown that the surface-dependent parts finally cancel in the total expression. This has not been done for the higher order calculations, so that the present paper begins with a proof of a similar cancellation in the second-order corrections to the boson current. Generalizing from these examples of first- and second-order cancellation, a simple rule is given for writing expressions correct to any order without explicit introduction of the surface terms.

It is found that the β-matrix formalism of Kemmer[6] is the most convenient means of calculating electrodynamic corrections for boson fields, and is especially suited for expressing the rule for removal of the surface terms. The essential advantage of the formalism is that all expressions for particles of spins 0 and 1 become exactly similar in general structure to the corresponding

* AEC Postdoctoral Fellow.
[1] S. Tomonaga, Prog. Theor. Phys. **1**, 27 (1946).
[2] J. Schwinger, Phys. Rev. **74**, 1439 (1948); **75**, 651 (1949).
[3] S. Kanesawa and S. Tomonaga, Prog. Theor. Phys. **3**, 101 (1948).
[4] M. Neuman and W. H. Furry, Phys. Rev. **76**, 1677 (1949).
[5] R. Jost and J. Rayski, Helv. Phys. Acta **22**, 457 (1949).
[6] N. Kemmer, Proc. Roy. Soc. (London) **173**, 97 (1939).

expressions in the electron case. Therefore Section III contains a summary of the properties and identities of the β-matrices that are useful for electrodynamic calculations.

In Section IV the method is applied to the computation of the second-order current corrections for boson currents, proceeding in the same manner as in the corresponding calculation for the electron case.[7] These corrections include that to the particle's magnetic moment (if one exists, as is the case for the vector but not for the scalar meson). It is found that for the scalar meson a great simplification in the final expression is possible, with the result that there are no divergent terms, as in the corresponding electron calculation, and the only corrections are of type $\Box^2 a j_\mu$. For the vector meson several different types of terms appear in the result, including logarithmically divergent parts corresponding to the magnetic moment and to $\Box^2 j_\mu$; the latter term appears to represent a divergent quadrupole moment. Thus in this case there appears a new type of divergence not to be removed by simple renormalization of charge and mass.

II. THE SURFACE TERMS

The current and interaction operators for boson electrodynamics have already been established in terms of the β-matrix formalism;[4] in the interaction representation[1,2] they become

$$\begin{aligned} H(x) &= \{-ie[\bar\psi(x)\beta_\mu\psi(x)]+(e^2/\hbar c\kappa) \\ &\quad\times[\bar\psi(x)\beta_\mu(1+\beta_N{}^2)\beta_\nu\psi(x)]A_\nu(x)\}A_\mu(x), \\ j_\mu(x) &= -c\delta H/\delta A_\mu = iec[\bar\psi(x)\beta_\mu\psi(x)] \\ &\quad-(e^2/\hbar\kappa)[\bar\psi(x)\{\beta_\nu(1+\beta_N{}^2)\beta_\tau \\ &\quad+\beta_\tau(1+\beta_N{}^2)\beta_\nu\}\psi(x)]A_\tau(x). \end{aligned} \tag{1}$$

Here $\beta_N=\beta_\mu n_\mu$, where n_μ is a unit vector ($n_\mu{}^2=-1$) normal to a space-like surface σ through the point x; from the β-commutation rules it follows that

$$(1+\beta_N{}^2)\beta_\mu(1+\beta_N{}^2)=0. \tag{2}$$

These "surface terms" appear for the following reason: the components of ψ are not all independent, so that the Hamiltonian of the free-particle field can be expressed without containing the redundant components, which are accordingly not affected by changing to the interaction representation.[1] Thus the forms of $j_\mu(x)$ and $H(x)$ in this representation depend on which components of ψ are redundant, which in turn depend on the orientation of the surface σ at the point x. In fact, the independent component of ψ is $-\beta_N{}^2\psi$, the redundant component $(1+\beta_N{}^2)\psi$. In terms of the β-matrix formalism itself, one can say that these surface terms appear because the β's have no inverses.[8]

Of course all physical results must be independent of β_N and the mathematical surface σ. In the first-order calculations (vacuum polarization and self-energy), the $\beta_N{}^2$-terms in j_μ or H are well known to cancel those arising in the following way. It is necessary to evaluate expressions of the type

$$\begin{aligned} &\int_{-\infty}^{\infty}\epsilon(x-x')[j_\mu(x),H(x')]d\omega', \\ &\int_{-\infty}^{\infty}\epsilon(x-x')[H(x),H(x')]d\omega' \end{aligned} \tag{3}$$

using the commutation rules

$$\begin{aligned} [\psi_\sigma(x),\bar\psi_\tau(x')] &= -iS_{\sigma\tau}(x-x') \\ &= -i[\beta_\mu\partial_\mu-\kappa^{-1}\beta_\mu\beta_\nu\partial_\mu\partial_\nu]_{\sigma\tau}\Delta(x-x'), \\ \{\psi_\sigma(x),\bar\psi_\tau(x')\}_0 &= S^1{}_{\sigma\tau}(x-x') \\ &= [\beta_\mu\partial_\mu-\kappa^{-1}\beta_\mu\beta_\nu\partial_\mu\partial_\nu]_{\sigma\tau}\Delta^1(x-x'). \end{aligned} \tag{4}$$

In these expressions, both $\epsilon(x-x')$ and $\Delta(x-x')$ depend on the surface $\sigma(x)$, while $\Delta^1(x-x')$ and $\bar\Delta(x-x')=-\frac{1}{2}\epsilon\Delta$ do not. In the electron case the operators involved in S contain no derivatives higher than the first, so that ϵ commutes with these operators and one has simply $-\frac{1}{2}\epsilon S=\bar S$, where $\bar S$ is defined as S, but with $\bar\Delta$ replacing Δ; thus all dependence on the surface σ is eliminated. In the boson case, however, expressions (4) contain operators $\partial_\mu\partial_\nu$, with which ϵ does not commute; one finds that

$$-\tfrac{1}{2}\epsilon S=\bar S+\beta_N{}^2\kappa^{-1}\delta(x-x'). \tag{5}$$

Thus surface-dependent terms of type $\beta_N{}^2$ also appear in expressions (3); in the first-order calculations these just cancel the $\beta_N{}^2$-terms from (1) leaving a result independent of σ, as expected.

Note, however, that the cancellation of the $\beta_N{}^2$-terms arising from (5) does not mean simply that the resulting expression can be formed by the rule $-\frac{1}{2}\epsilon S=\bar S$. In expressions (1) $\beta_N{}^2$ occurs only in the combination $(1+\beta_N{}^2)$; therefore when the $\beta_N{}^2$-terms cancel, the resulting expression is the same as if the ϵ^2 terms in j_μ and H were entirely neglected and we had put simply

$$-\tfrac{1}{2}\epsilon S=\bar S=\bar S-\kappa^{-1}\delta(x-x'). \tag{6}$$

The argument concerning the $(1+\beta_N{}^2)$ terms holds for all higher order calculations as well; therefore it need merely be proved that the $\beta_N{}^2$-terms cancel to the desired order in e, and the remaining terms must automatically be those resulting from the rule (6).

[7] J. Schwinger, Phys. Rev. **76**, 790 (1949).

[8] This can be seen as follows: from the Lagrangian

$$L=-\bar\psi\beta_\mu\partial_\mu\psi+\partial_\mu\bar\psi\beta_\mu\psi-2\kappa\bar\psi\psi$$

one obtains $\pi=\bar\psi\beta_N$, $\bar\pi=-\beta_N\psi$. To express the free-field Hamiltonian H_0 in terms of $(\pi\bar\pi)$, one must be able to write $\bar\psi=\pi\beta_N{}^{-1}$, $\psi=-\beta_N{}^{-1}\bar\pi$. Such a step is possible with the γ-matrices of the electron, but not with the β-matrices, and $(\pi\bar\pi)$ can be introduced into H_0 only in correspondence to the term $-\bar\psi\beta_N{}^2\psi$. This canonical form leads to correct equations of motion only for the component $-\beta_N{}^2\psi$, and not for the remainder $(1+\beta_N{}^2)\psi$; therefore this H_0 will transform correctly to the interaction representation only the component $-\beta_N{}^2\psi$.

To show that β_N-terms actually do cancel in the second-order calculation, it is necessary to analyze the current operator correct to order e^2, given by the series

$$[j_\mu(x)]=j_\mu(x)+\frac{i}{\hbar c}\int_{-\infty}^{\infty}[-\tfrac{1}{2}\epsilon(\sigma\sigma')][j_\mu(x),H(x')]$$
$$+\left(\frac{i}{\hbar c}\right)^2\int_{-\infty}^{\infty}d\omega'd\omega''[-\tfrac{1}{2}\epsilon(\sigma\sigma')]$$
$$\times[-\tfrac{1}{2}\epsilon(\sigma',\sigma'')][[j_\mu(x),H(x')]H(x'')]+\cdots, \quad (7)$$

where j_μ and H are given by (I) and the renormalization of the infinite self-mass has not yet been introduced. This analysis is performed in detail in Appendix I, and the β_N-terms shown explicitly to cancel.

Generalizing from these lowest order results, one may postulate the following as a general rule for eliminating the surface terms from the Schwinger-Tomonaga formalism:

In electrodynamic calculations for particles of spin 0 and 1 treat the β-matrix formalism exactly as in the corresponding electron case, using throughout only the first-order current and interaction operators,[9]

$$j_\mu=iec\bar\psi\beta_\mu\psi \quad \text{and} \quad H(x)=-ie\bar\psi\beta_\mu\psi A_\mu. \quad \text{(I)}$$

In the resulting expressions then put

$$-\tfrac{1}{2}\epsilon(x-x')S(x-x')\rightarrow\bar S(x-x')$$
$$=\bar S(x-x')-\kappa^{-1}\delta(x-x').$$

The modified function $\bar S$ has the highly recommendable property that it is the four-dimensional Green's function for the original equation of motion:

$$(\beta_\mu\partial_\mu+\kappa)\bar S(x-x')=-\delta(x-x')$$
$$=-\partial_\mu'\bar S(x-x')\beta_\mu+\kappa\bar S(x-x') \quad (8)$$

as can be checked by direct computation, using the commutation rules for the β's. Moreover, $\bar S$ itself does not satisfy this requirement, but instead gives

$$(\beta_\mu\partial_\mu+\kappa)\bar S(x-x')=\kappa^{-1}\beta_\mu\partial_\mu\delta(x-x'). \quad (9)$$

Clearly $\bar S$ will be a much more satisfactory function for calculation than $\bar S$. In Fourier representation,

$$\bar S(x)=(1/2\pi)^4\int e^{ikx}T(k)dk/(k^2+\kappa^2), \quad (10)$$

$$T(k)=i\beta k+\kappa^{-1}(\beta k)^2-\kappa^{-1}(k^2+\kappa^2), \quad (11)$$

where the last term from $T(k)$ gives $-\kappa^{-1}\delta(x)$. Note that for the sake of symmetry we can also write S^1 in a similar form

$$S^1=(1/2\pi)^3\int e^{ikx}T(k)\delta(k^2+\kappa^2)dk, \quad (10a)$$

since $(k^2+\kappa^2)\delta(k^2+\kappa^2)=0$. It may also be of interest to remark that these forms reduce to the usual ones for the electron case if we substitute γ_μ for β_μ, because of the special property that $(\gamma k)^2=k^2$. Hence the forms (10) and (11) are valid for all three cases of spin 0, ½, and 1.

Rule (I) and the associated forms (10) and (11) will be used below to compute the second-order current correction. The application of these techniques to the simpler problem of the self-mass is illustrated in Appendix II. One further remark may be made about the mass renormalization. In grouping the terms obtained from (7), one obtains an expression of the form

$$(ie/\hbar)\int_{-\infty}^{\infty}d\omega'[\bar\psi(x)\beta_\mu\bar S(x-x')\varphi(x')$$
$$+\bar\varphi(x')\bar S(x'-x)\beta_\mu\psi(x)], \quad (12)$$

where

$$\varphi(x)=-\tfrac{1}{2}e^2\int_{-\infty}^{\infty}d\omega'\beta_\nu[\bar D(x-x')S^1(x-x')$$
$$+D^1(x-x')\bar S(x-x')]\beta_\nu\psi(x')$$
$$=\delta mc^2\psi(x) \quad (13)$$

and δmc^2 is the self-energy operator. Therefore to achieve mass renormalization one must replace $\varphi(x)$ by $\varphi(x)-\delta mc^2\psi(x)$ in Eq. (12) in the usual fashion. In the present formalism, however, it is difficult to see how this mass subtraction could be performed in advance (as in the electron case) by inserting into Eq. (7) a term

$$-(i/\hbar c)\int_{-\infty}^{\infty}d\omega'[-\tfrac{1}{2}\epsilon(\sigma\sigma')][j_\mu(x),H_{10}(x')]$$

because there is no obvious way of writing a self-mass operator H_{10} that will not give rise to uncompensated $\beta_N{}^2$-terms from this commutator. The mass renormalization can always be handled in the same way as that of charge, of course, simply by identifying and removing the appropriate terms from the total expression after it has been established.

The application of this rule to the formalism of Feynman[10] is obvious. The corresponding function $K_+(2,1)$ for the meson case is defined by an equation exactly similar to (8) for $\bar S$; and it has already been observed[10] that although the β's have no inverses, the operator $(\beta k-\kappa)$ has a well-behaved inverse, given by

$$(\beta k-\kappa)^{-1}=\left[(\beta k)+\frac{(\beta k)^2}{\kappa}+\frac{\kappa^2-k^2}{\kappa}\right]\frac{1}{k^2-\kappa^2}. \quad \text{(A)}$$

Therefore in this formalism the rule becomes simply:

Proceed exactly as in the electron case, using β_μ in place of γ_μ and the definition (A), and inserting a factor (-1) for each closed meson loop.[5] (IA)

[9] These definitions for j_μ and H will be implicitly assumed throughout the remainder of the present paper.

[10] R. P. Feynman, Phys. Rev. **76**, 749, 769 (1949).

This seems to be somewhat simpler than the corresponding formalism without β-matrices, even for the case of spin 0, because no terms in A^2 appear in the equations of motion and hence there are no new problems in evaluating the matrix elements. In this connection it should be noted that the proof of equivalence[11] of the Feynman and Schwinger-Tomonaga formalisms is independent of the commutation properties of the γ- or β-matrices involved; hence the fact that the "surface terms" never appear in the Feynman treatment provides a basis for assuming that (I) is valid to all orders. Since this was written, the methods of Källen[12] and of Yang and Feldman[12a] have appeared for doing covariant calculations entirely in the Heisenberg representation. Of course no surface terms appear in such treatments, and they provide a general proof of (I) to all orders.

III. PROPERTIES OF THE β-MATRICES

A few identities and properties of the β-matrices may be listed as aids to calculation. Explicit five-rowed (spin 0) and ten-rowed (spin 1) representations have been given by Kemmer.[6] For both spin possibilities the commutation relations are

$$\beta_\lambda\beta_\mu\beta_\nu+\beta_\nu\beta_\mu\beta_\lambda=\beta_\nu\delta_{\mu\lambda}+\beta_\lambda\delta_{\mu\nu}. \tag{14}$$

Sometimes the derived relation is useful

$$\beta_\lambda\beta_\mu\beta_\lambda=\beta_\lambda\delta_{\mu\lambda}\text{ (no summation)}. \tag{14a}$$

The commutation relations must be left in their original form because the β's have no inverses; thus $\beta_\lambda^3=\beta_\lambda$ does not imply $\beta_\lambda^2=1$ as in the electron case. The spin zero case has the additional property that

$$\beta_\lambda\beta_\mu\beta_\nu=0 \quad \text{if} \quad \lambda\neq\mu\neq\nu\neq\lambda. \tag{15}$$

If one defines $\beta p=p_\lambda\beta_\lambda$, where p is any vector, the commutation rules (14) may be put in various forms by multiplying by p_λ, p_μ, p_ν and summing:

$$\begin{gathered}\beta p\beta_\mu\beta_\nu+\beta_\nu\beta_\mu\beta p=\beta_\nu p_\mu+\beta p\delta_{\mu\nu},\\ \beta p\beta p'\beta_\nu+\beta_\nu\beta p'\beta p=\beta_\nu(pp')+\beta p p_\nu',\\ \beta p\beta p'\beta p''+\beta p''\beta p'\beta p=\beta p''(pp')+\beta p(p'p''),\\ \beta p\beta p'\beta p=\beta p(pp')\end{gathered} \tag{16}$$

and so forth.

In performing detailed calculations, one must evaluate expressions of the following types, where a repeated index implies summation:

$$\beta_\nu\beta_\nu=M, \tag{17a}$$

$$\beta_\nu\beta_\mu\beta_\nu=\beta_\mu, \tag{17b}$$

$$\beta_\nu\beta k'\beta_\mu\beta_\nu=-(M-1)\beta_\mu\beta k'+Mk_\mu', \tag{17c}$$

$$\beta_\nu\beta k'\beta k''\beta_\mu\beta_\nu=\beta k''\beta k'\beta_\mu+\beta k''\beta_\mu\beta k'+\beta_\mu(k'k''), \tag{17d}$$

$$\begin{aligned}\beta_\nu\beta k'^2\beta_\mu\beta k''\beta_\nu=&[(\beta k')^2-k'^2][\beta k''\beta_\mu(M-1)-Mk_\mu'']\\ &+\beta k'\beta_\mu\beta k''\beta k',\end{aligned} \tag{17e}$$

$$\begin{aligned}\beta_\nu\beta k'^2\beta_\mu\beta k''^2\beta_\nu=&\beta k'[(k'k'')\beta_\mu-\beta k''\beta_\mu\beta k']\beta k''\\ &+k'^2\beta_\mu k''^2.\end{aligned} \tag{17f}$$

Other equivalent forms of (17) may be found by using (16), and its related forms; the relations equivalent to (17) when β_μ is replaced by (βk) are found by multiplying both sides by k_μ and summing.

Note that when an even number of β's occurs between the pair that is summed over all indices, the matrix M appears in the result. This matrix therefore plays an essential role in all calculations with the β-matrices; and in fact, the final quantities to be computed generally contain this operator. For example, the particle self-energy is of the form

$$\delta mc^2\psi=(A+BM+CM^2)\psi,$$

where A, B, C are (infinite) constants; thus in this case the self-energy δmc^2 is actually an *operator*, not merely a scalar. The operator M and its powers are the only such operators that appear in addition to those found in the electron case. They will also occur in the second-order current corrections.

As an aid to the discussion of the properties of M, we shall present a method for evaluating the traces of various combinations of β's. The method is in principle perfectly straightforward and will apply to any product of β's for either spin 1 or spin 0. It is known that the β_μ's can be given by a "complete" representation which also satisfies the defining relation (14),

$$\beta_\mu{}^c=\tfrac{1}{2}[\gamma_\mu I'+\gamma_\mu' I], \tag{18}$$

where γ_μ, γ_μ' are two sets of commuting Dirac matrices, and I, I' are the corresponding identity matrices. Since the β^c correspond to the compounding of two particles of spin $\frac{1}{2}$, they must contain as reducible parts both the spin 0 and spin 1 representations; and since these are matrices of order 5 and 10, each is contained just once in the 16-rowed β^c. The remaining one-rowed representation must be trivial, with all elements zero. Therefore for any combination $\beta_\lambda\cdots\beta_\tau$ we have

$$Tr\beta_\lambda{}^c\cdots\beta_\tau{}^c=Tr\beta_\lambda{}^0\cdots\beta_\tau{}^0+Tr\beta_\lambda{}^1\cdots\beta_\tau{}^1, \tag{19}$$

where the superscripts c, 0, and 1 refer to the corresponding representations. The left-hand side of (19) is quite straightforward to evaluate with the definition (18); and on the right-hand side it will appear that for the spin 0 case the traces of all combinations have a very simple form by virtue of (15), which can also be evaluated at once. The traces for spin 1 are then found by subtraction according to (19). This method allows the evaluation of any trace for either spin and is in principle elementary.

Consider first the case of spin zero: (15) and (14a) together imply that the combination $\beta_{\mu_1}\beta_{\mu_2}\cdots\beta_{\mu_n}$ vanishes unless

$$\begin{aligned}&\mu_1=\mu_2, \quad \mu_3=\mu_4, \quad \cdots\mu_{n-1}=\mu_n,\\ &\mu_n=\mu_1, \quad \mu_2=\mu_3, \quad \cdots\mu_{n-2}=\mu_{n-1}.\end{aligned} \tag{20}$$

[11] F. J. Dyson, Phys. Rev. **75**, 486 (1949).
[12] Källen, Arkiv. f. Fys. **19**, 187 (1950).
[12a] C. N. Yang and D. Feldman, Phys. Rev. **79**, 972 (1950).

If n is an even number, this means that

$$Tr\beta_{\mu_1}{}^0\cdots\beta_{\mu_n}{}^0=C[\delta_{\mu_1\mu_2}\cdots\delta_{\mu_{n-1}\mu_n}+\delta_{\mu_n\mu_1}\cdots\delta_{\mu_{n-2}\mu_{n-1}}] \quad (n \text{ even}) \quad (21a)$$

where the constant C is the same for both cases (20), since the trace does not depend on the cyclic order of the factors. If n is an odd number, (15) and (14a) imply that the matrix combination vanishes unless somewhere it contains the factor $\beta_\nu{}^3$. But since $\beta_\nu{}^3=\beta_\nu$, the combination is immediately reduced to order $n-2$; and proceeding in this way, one has

$$Tr\beta_{\mu_1}{}^0\cdots\beta_{\mu_n}{}^0=Tr\beta_\nu{}^0 \quad (n \text{ odd}). \quad (21b)$$

One can show immediately that $Tr\beta_\nu{}^0=0$. The trace of any combination is independent of the cyclic order of the factors; and applying (14) and (14a) we have for either spin case

$$Tr\beta_\mu=Tr\sum_\lambda\beta_\lambda\beta_\mu\beta_\lambda=Tr\sum_\lambda\beta_\lambda{}^2\beta_\mu=Tr\sum_\lambda\beta_\mu\beta_\lambda{}^2=Tr\sum(5-\beta_\lambda{}^2)\beta_\mu=Tr5\beta_\mu/2=0. \quad (22)$$

Thus for the spin 0 case, we have

$$Tr\beta_{\mu_1}{}^0\cdots\beta_{\mu_n}{}^0=Tr\beta_\nu{}^0=0 \quad (n \text{ odd}). \quad (21c)$$

From the form (18) it is obvious that the trace also vanishes for odd products of the β^ε, since this is true of the γ's themselves. Therefore by (19) the same is true for spin 1, and it is true in general for both spins that

$$Tr\beta_{\mu_1}\cdots\beta_{\mu_n}=0 \quad (n \text{ odd}). \quad (23)$$

For even products, the constant C is first found by taking $\mu_1=\mu_2=\cdots=\mu_n=\nu$, so that

$$C=\tfrac{1}{2}Tr[\beta_\nu{}^0]^n=\tfrac{1}{2}Tr[\beta_\nu{}^0]^2=\tfrac{1}{8}TrM^0=1 \quad (24)$$

as it will be shown below that $TrM^0=8$. This value of C inserted into (21a) gives the traces of even products for spin 0. Note that in the special case $n=2$, the two δ-terms are the same and hence

$$Tr\beta_\mu{}^0\beta_\nu{}^0=2\delta_{\mu\nu}. \quad (21d)$$

It only remains to determine the traces of even products for spin 1 as described above. For example,

$$\begin{aligned}&Tr\beta_\mu{}^c\beta_\nu{}^c=\tfrac{1}{4}Tr(\gamma_\mu\gamma_\nu I'+\gamma_\mu'\gamma_\nu' I)=2Tr\gamma_\mu\gamma_\nu=8\delta_{\mu\nu},\\&Tr\beta_\mu{}^1\beta_\nu{}^1=Tr\beta_\mu{}^c\beta_\nu{}^c-Tr\beta_\mu{}^0\beta_\nu{}^0=6\delta_{\mu\nu}.\end{aligned} \quad (25)$$

For the four-product, it is necessary to evaluate $Tr\gamma_\mu\gamma_\nu\gamma_\rho\gamma_\sigma$, which can be done by shifting γ_μ stepwise to the right with the commutation rule $\gamma_\mu\gamma_\lambda+\gamma_\lambda\gamma_\mu=2\delta_{\lambda\mu}$ and finally observing that the trace does not depend on the cyclic order so that

$$Tr\gamma_\mu\gamma_\nu\gamma_\rho\gamma_\sigma=4(\delta_{\mu\nu}\delta_{\rho\sigma}-\delta_{\mu\rho}\delta_{\nu\sigma}+\delta_{\mu\sigma}\nu_{\nu\rho}). \quad (26)$$

Thus one obtains

$$\begin{aligned}&Tr\beta_\mu{}^c\beta_\nu{}^c\beta_\rho{}^c\beta_\sigma{}^c=4(\delta_{\mu\nu}\delta_{\rho\sigma}+\delta_{\mu\sigma}\delta_{\nu\rho}),\\&Tr\beta_\mu{}^1\beta_\nu{}^1\beta_\rho{}^1\beta_\sigma{}^1=3(\delta_{\mu\nu}\delta_{\rho\sigma}+\delta_{\mu\sigma}\delta_{\nu\rho}).\end{aligned} \quad (27)$$

Traces of higher products for spin 1 may be obtained by the same procedure with sufficient labor.

Although the matrix M has no direct physical interpretation, its behavior is quite simple to catalog. Its commutation relations are

$$M\beta_\mu+\beta_\mu M=5\beta_\mu \quad (28)$$

from which it follows that for any operator Ω

$$\Omega=\begin{matrix}(5-M)\Omega(\text{odd})\\M\Omega(\text{even})\end{matrix} \quad (28a)$$

according as Ω contains the product of an odd or even number of β's. Similarly.

$$M\beta_\mu M=M(5-M)\beta_\mu=\beta_\mu(5-M)M \quad (28b)$$

or hence the operator $(5M-M^2)$ commutes with any β_μ and therefore with any arbitrary operator Ω. But any matrix commuting with all the matrices of a representation must be a constant; therefore

$$5M-M^2=A. \quad (29)$$

This relation is very useful, for it means that any polynomial in M can be reduced to an expression of the form $(a+bM)$; hence the only essential difference from the electron case is the operator M. Unlike the β_μ's themselves, M is well behaved and has an inverse, obtainable from (29). The most straightforward evaluation of the constant A is by direct construction of M, using the representations given in reference 6. For the five-rowed representation, M is a diagonal matrix with four 1's and one 4; for the ten-rowed, it is diagonal with six 2's and four 3's. Thus

$$A=\begin{Bmatrix}4\\6\end{Bmatrix} \text{ for spin } \begin{Bmatrix}0\\1\end{Bmatrix}. \quad (30)$$

Hence A also satisfies a quadratic equation

$$t^2-10A+24=0 \quad (31)$$

so that any expression can be reduced to first powers in A and M.

From (29) and (30) one obtains the relation used in (24):

$$\begin{aligned}5TrM-TrA=TrM^2=Tr\sum_\lambda\beta_\lambda\beta_\lambda M=Tr\sum\beta_\lambda M\beta_\lambda\\=Tr\sum_\lambda\beta_\lambda\beta_\lambda(5-M)=5TrM/2,\end{aligned} \quad (32)$$

$$TrM^0=\tfrac{8}{5}TrA^0=\tfrac{8}{5}A^0TrI^0=8$$

since the trace of the unit matrix is 5 in the representation for zero spin.

Although higher powers of M can be eliminated through (29), it is not in general possible to eliminate M from the final expressions. There are two special cases, however, when one can put $M\to 5/2$. The forms of $j_\mu(x)$ and $H(x)$ given above are without charge symmetrization and will lead to terms of the type $M\beta_\mu$ in the results. If the charge-symmetrical current and

interaction energy had been used, this term would everywhere be replaced by

$$M\beta_\mu \rightarrow \tfrac{1}{2}(M\beta_\mu+\beta_\mu M)=5\beta_\mu/2. \tag{33}$$

This is the only effect of charge symmetrization, so that rule (33) obviates its use.

For a general operator Ω one cannot simply write

$$\bar\psi(x)M\Omega\psi(x)\rightarrow(5/2)\bar\psi(x)\Omega\psi(x) \tag{34}$$

for a particular point (x). Such an equivalence holds, however, if we are interested only in the expectation value of the operator integrated over the entire four-dimensional volume. To see this, consider the function $(M-5/2)\psi(x)$ which satisfies the equation

$$(\beta_\mu\partial_\mu-\kappa)(M-5/2)\psi(x)=0. \tag{35}$$

But it is also true that

$$(\beta_\mu{}^T\partial_\mu-\kappa)\bar\psi^T(x)=0 \tag{35a}$$

where the superscript T means transposed. Furthermore, it is possible to choose a representation such that β_μ is symmetric, $\beta_\mu=\beta_\mu{}^T$ (as in reference 6, but with $\pm i$ replaced by 1). Therefore

$$\bar\psi^T(x)=b(M-5/2)\psi(x) \tag{35b}$$

where $b\neq0$ is a constant. Now although $\bar\psi\Omega\bar\psi^T$ does not vanish at a particular point (x), the integral goes to zero if the region of integration is made sufficiently large. Therefore, using (35b),

$$\int\bar\psi\Omega\bar\psi^T d\omega\rightarrow 0=b\{\langle\Omega M\rangle-(5/2)\langle\Omega\rangle\}. \tag{36}$$

By using the similar construction with $\bar\psi(x)(M-5/2)$, one obtains

$$\langle\Omega M\rangle=(5/2)\langle\Omega\rangle=\langle M\Omega\rangle \tag{37}$$

for any operator Ω. Thus in certain cases it will be possible to eliminate M entirely from our results—as, for example, in the case of the self-energy δmc^2.

Another operator that appears naturally in the course of calculation is the spin operator,

$$\sigma_{\mu\nu}=-i(\beta_\mu\beta_\nu-\beta_\nu\beta_\mu)=-\sigma_{\nu\mu}. \tag{38}$$

In terms of this operator, the particle current can be decomposed into a convection and a dipole component, in analogy with the Gordon decomposition for the electron case. First note the extremely useful identity[4]

$$\partial_\mu\psi=\beta_\nu\beta_\mu\partial_\nu\psi, \quad \partial_\mu\bar\psi=\partial_\nu\bar\psi\beta_\mu\beta_\nu. \tag{39}$$

This is immediately verified by multiplying with β_μ, and summing over μ, and using (14a). This identity is also essential in developing the Klein-Gordon equation from the original equation of motion $(\beta_\mu\partial_\mu+\kappa)\psi=0$, as may be seen by applying ∂_μ to both sides of (39) and summing over μ. Substitution of (39) into (38) yields

$$\partial_\mu\psi=i\sigma_{\nu\mu}\partial_\nu\psi-\kappa\beta_\mu\psi, \quad \partial_\mu\bar\psi=i\partial_\nu\bar\psi\sigma_{\mu\nu}+\kappa\bar\psi\beta_\mu. \tag{40}$$

Multiplying left and right by $\bar\psi$, ψ, and subtracting, one has the current decomposition

$$(\partial_\mu\bar\psi\psi-\bar\psi\partial_\mu\psi)-i\partial_\nu(\bar\psi\sigma_{\mu\nu}\psi)=2\kappa\bar\psi\beta_\mu\psi=(2\kappa/iec)j_\mu. \tag{41}$$

Similar relations can be obtained by multiplying left and right by $\bar\psi\Omega$, $\Omega\psi$, with Ω any desired operator.

Some useful identities also follow from the consideration of combinations of the operators M, $\sigma_{\mu\nu}$, which commute according to (28a). The operator $M\sigma_{\mu\nu}$ allows the rare opportunity of distinguishing the case of spin 0 from the general formalism; for

$$M\sigma_{\mu\nu}=-i\textstyle\sum_\lambda(\beta_\lambda{}^3\beta_\mu\beta_\nu-\beta_\lambda{}^3\beta_\nu\beta_\mu) \tag{42}$$

and for spin 0, the summand vanishes by (15) unless $\lambda=\mu$, $\lambda=\nu$, or $\mu=\nu$. In the last case $\sigma_{\mu\nu}=0$, so we need only consider the first two instances:

$$\begin{aligned}M\sigma_{\mu\nu}{}^0&=-i[\beta_\mu{}^3\beta_\nu+\beta_\nu{}^3\beta_\mu\beta_\nu\beta_\nu-\beta_\nu{}^3\beta_\mu-\beta_\mu{}^3\beta_\nu\beta_\mu]\\&=-i[\beta_\mu\beta_\nu-\beta_\nu\beta_\mu]=\sigma_{\mu\nu}{}^0\end{aligned} \tag{43}$$

by use of (14a), where here the superscript emphasizes that the identity (13) holds only for spin 0. We can now see that the case distinguished by (13) really represents spin 0, but only in the sense of (37); from these two equations,

$$(5/2)\langle\sigma_{\mu\nu}{}^0\rangle=\langle M\sigma_{\mu\nu}{}^0\rangle=\langle\sigma_{\mu\nu}{}^0\rangle=0. \tag{44}$$

One cannot write $\bar\psi\sigma_{\mu\nu}{}^0\psi=0$ at any point (x).

A second identity specific to the case of spin 0 may be obtained with the help of the first, and depends on the fact that if we multiply Eq. (40) by the operator $(M-1)$, the terms containing $\sigma_{\mu\nu}$ will vanish. For example, multiply left and right by $\bar\psi(M-1)$ and $(M-1)\psi$ and subtract, obtaining with the help of (28)

$$\partial_\mu\bar\psi(M-1)\psi-\bar\psi(M-1)\partial_\mu\psi=3\kappa\bar\psi\beta_\mu\psi. \tag{45}$$

Now replace μ in Eqs. (40) by a dummy index α, multiply left and right by $\partial_\alpha\bar\psi\beta_\mu(M-1)$ and $(M-1)\beta_\mu\partial_\alpha\psi$ and add, summing over α:

$$3\partial_\alpha\bar\psi\beta_\mu\partial_\alpha\psi=\kappa[\bar\psi(4-M)\partial_\mu\psi-\partial_\mu\bar\psi(4-M)\psi]. \tag{46}$$

The terms in M can be eliminated by subtraction of (46) from (45); then by use of relation (41) and the fact that $(\Box^2-\kappa^2)(\psi,\bar\psi)=0$, the identity is obtained in its final form,

$$\partial_\nu(\bar\psi\sigma_{\mu\nu}{}^0\psi)=\frac{i}{2\kappa}\Box^2(\bar\psi\beta_\mu\psi)=\frac{1}{2ec\kappa}\Box^2 j_\mu \tag{47}$$

where again the superscript indicates that it is valid only for spin 0.

IV. SECOND-ORDER CURRENT CORRECTION

Using rule (I), we obtain as in the electron case[7] the second-order current correction

$$\delta j_\mu^{(2)}=-\frac{i}{\hbar c^2}\int_{-\infty}^{\infty}d\omega'\left[-\frac{\epsilon}{2}(x-x')\right][j_\mu(x),\, j_\nu(x')]_0\delta A_\nu(x')$$
$$+\frac{ie}{2\hbar}[\bar\psi(x)\beta_\mu\chi(x)+\bar\chi(x)\beta_\mu\psi(x)]$$
$$-\frac{ie^2}{2\hbar}\int_{-\infty}^{\infty}d\omega'd\omega''\bar\psi(x')$$
$$\times K_\mu^{(1)}(x'-x,\,x-x'')\psi(x''),\quad(48)$$

where the first term contains the charge renormalization, with δA_ν given by (A.11); the second involves the mass renormalization, with

$$\chi(x)=\int_{-\infty}^{\infty}d\omega'\bar S(x-x')[\varphi(x')-\delta mc^2\psi(x')],\quad(49)$$

where $\varphi(x)$ is given by the expression (13); and the third term is the actual second-order correction from which the first-order infinities of charge and mass have been removed, in which

$$K_\mu^{(1)}(y,\,z)=\beta_\nu[\bar S(y)\beta_\mu S^1(z)\bar D(y+z)$$
$$+S^1(y)\beta_\mu\bar S(z)\bar D(y+z)$$
$$+\bar S(y)\beta_\mu\bar S(z)D^1(y+z)]\beta_\nu.\quad(50)$$

Consider first the second term in (48). In the electron case it was possible to evaluate (49) by constructing a suitable $\psi_{x+\delta x}(x)$ and passing to the limit $\delta\kappa\to0$. In the present case, however, $\varphi(x)$ and δmc^2 are not simple scalars, but contain also the operator M [Eq. (29) reduces higher powers]; and it must be shown that this circumstance does not alter the procedure. Equations (8) and (35) yield, after an integration by parts

$$\int_{-\infty}^{\infty}\bar S(x-x')(M-5/2)\psi(x')d\omega'$$
$$=\frac{1}{\kappa}\int_{-\infty}^{\infty}d\omega'[\partial_\mu'S(x-x')\beta_\mu-\delta(x-x')](M-5/2)\psi(x')$$
$$=-\int_{-\infty}^{\infty}d\omega'\bar S(x-x')(M-5/2)\psi(x')d\omega'$$
$$-\kappa^{-1}(M-5/2)\psi(x)$$
$$=-(2\kappa)^{-1}(M-5/2)\psi(x).\quad(51)$$

Therefore the divergent integral

$$\int_{-\infty}^{\infty}d\omega'\bar S(x-x')M\psi(x')$$

is identical with the divergent integral obtained by putting $M\to5/2$, except for a finite residual term $-\frac{1}{2}\kappa(M-5/2)\psi(x)$. This residual term is the same for corresponding parts of $\varphi(x)$ and $\delta mc^2\psi(x)$ and hence cancels from $\chi(x)$. Therefore the same construction can be used as in the electron case, provided that we eventually put $M\to5/2$; but this is already assured by the symmetrical form of (48) with respect to β_μ and $\chi(x)$, so that the rule finally becomes

to evaluate $\chi(x)$, proceed exactly as in the electron case with no additional prescriptions. (II)

The second term of (48) can thus be written in a form similar to the third, but with a kernel $K_\mu^{(2)}$ given in Fourier representation by

$$K_\mu^{(2)}(x'-x,\,x-x'')$$
$$=\frac{1}{(2\pi)^8}\int dp''dp'\exp[ip'(x'-x)]$$
$$\times\exp[ip''(x-x')]B_\mu^{(2)}(p',\,p''),\quad(52)$$

where

$$B_\mu^{(2)}(p',\,p'')=\beta_\mu G(p'')+G(p')\beta_\mu,\quad(53a)$$

$$G(p)=\frac{1}{2\kappa(2\pi)^2}\int dk\,p_\lambda\frac{\partial}{\partial p_\lambda}$$
$$\times\left\{\beta_\nu T(p-k)\beta_\nu\left[\frac{\delta(a)}{b}+\frac{\delta(b)}{a}\right]\right\},\quad(53b)$$

$$a=(p-k)^2+\kappa^2,\quad b=k^2\quad(53c)$$

with T as in Eq. (11). To evaluate $G(p)$, first sum over ν in accordance with (17), and express the δ-function combination as in (C.2). The δ-function argument is then made a function of k^2 alone by the substitution[13] $k\to k+up$; after this the operation $p_\lambda\partial/\partial p_\lambda$ is carried out, neglecting odd powers of k. One obtains

$$G(p)=\frac{1}{2\kappa(2\pi)^2}\int dk\int_0^1du\left\{\left[i\beta p_0+\frac{2}{\kappa}(1-M)(\beta p_0)^2\right]\delta'(x)\right.$$
$$-2p^2(u^2-u)\left[i\beta p_0+\frac{1}{\kappa}(1-M)\right.$$
$$\left.\left.\times[(\beta p_0)^2+(\beta k)^2-M\kappa^2]\right]\delta''(x)\right\},$$
$$p_0=p(1-u),\quad x=k^2-p^2(u^2-u)+\kappa^2u.\quad(54)$$

Now $G(p)$ will finally be incorporated in a form of the type $\int d\omega'\exp[ip(x-x')]G(p)\psi(x')$; integrating by parts with respect to $d\omega'$ and using the (interaction-free) equations of motion for the wave function $\psi(x')$, one has the following equivalences for $G(p)$: $\beta p\to i\kappa$,

[13] Strictly speaking, the result of this step is ambiguous, since the integral does not converge. The ambiguity is decided by adopting a standard convention. See article immediately following.

$(\beta p)^2 \to p^2 \to -\kappa^2$. The symmetry of the δ-functions in k also implies that $k_\mu k_\nu = \frac{1}{4}k^2\delta_{\mu\nu}$, $(\beta k)^2 = \frac{1}{4}k^2 M$. With these substitutions, the variable p entirely vanishes from $G(p)$, and one is left with integrals $\int dk \int_0^1 du$ of integrands $\delta''(k^2+\kappa^2u^2)$, $k^2\delta''(k^2+\kappa^2u^2)$ and $\delta'(k^2+\kappa^2u^2)$. The first is convergent, but the last two are logarithmically divergent; the second is transformed into the third by the convention (C.9),

$$\int dk k^2 \delta''(k^2+\kappa^2u^2) = -2\int dk \delta'(k^2+\kappa^2u^2).$$

The divergent and convergent elements of this last integral are separated by integration by parts with respect to u:

$$\int_0^1 du f(u)\delta'(k^2+\kappa^2u^2) = F(1)\delta'(k^2+\kappa^2) - 2\kappa^2\int_0^1 udu F(u)\delta''(k^2+\kappa^2u^2), \quad (55a)$$

$$F(u) = \int_0^u f(x)dx, \quad (55b)$$

where the first term of (55a) gives a logarithmic divergence on integration $\int dk$, and the second term converges. Note that the lower limit of integration in (55b) must be zero, because the form (55a) depends explicitly on the fact that $F(0)=0$.

Using the evaluations (C.14) for the integrals over $\int dk$ in (55a), we have

$$G(p) = \frac{\pi}{2(2\pi)^3}\left\{\left[\ln\frac{p+p_0}{k} - 1\right]\tfrac{1}{2}(A-7) + \frac{1}{18}(5A+34) - 4\left[1+\ln\frac{\kappa}{2k_0}\right]\right\}. \quad (56)$$

The first logarithmic term in (56) represents a real divergence; the second is an "infrared catastrophe," where k_0 is an invariant minimum wave number. This term comes from a more careful consideration (C.16) of the meaning of $\int dk \int_0^1 du \delta''(k^2+\kappa^2u^2)$. It is only an apparent divergence, since it will be exactly canceled by a similar effect from any means used to measure the current to second order.

The next step is to evaluate the kernel $K_\mu^{(1)}$, the Fourier transform of which is

$$B_\mu^{(1)}(p', p'') = \frac{1}{(2\pi)^3}\int dk\left\{\beta_\nu T(p'-k)\beta_\mu T(p''-k)\beta_\nu \times\left[\frac{\delta(a)}{bc}+\frac{\delta(b)}{ac}+\frac{\delta(c)}{ab}\right]\right\}, \quad (57)$$

$$a=(p'-k)^2+\kappa^2, \quad b=(p''-k)^2+\kappa^2, \quad c=k^2. \quad (57a)$$

The δ-function combination is reduced as in (C.6) to the integral over a single δ''-function; since $K_\mu^{(1)}$ will be applied in an integral over $\bar\psi(x')$, $\psi(x'')$, we may suppose an integration by parts and put $p'^2, p''^2 \to -\kappa^2$ in $B_\mu^{(1)}$ and the δ''-function. The argument of the δ''-function is finally made symmetrical in k by the transformation

$$k \to k + \tfrac{1}{2}u\{p'+p'') + (p'-p'')v\} \quad (58)$$

and the entire δ''-function becomes

$$\int_{-1}^1 \tfrac{1}{2}dv \int_0^1 udu\delta''(k^2+\lambda^2u^2), \quad (59)$$

$$\lambda^2 = \kappa^2\left[1+\frac{(p'-p'')^2}{4\kappa^2}(1-v^2)\right]. \quad (59a)$$

The chief task is now to reduce the various β-matrix products in

$$\beta_\nu T(p'-k)\beta_\mu T(p''-k)\beta_\nu. \quad (60)$$

Because the δ''-function has been made a function of k^2 alone, it is only necessary to retain even powers of k in performing this reduction. Of course the substitution (58) must also be made in (60). It is algebraically more convenient, however, to perform first the β-matrix reduction on the k^4, k^2, and k^0 terms in (60), and then in the final result make the equivalent substitutions

$$\begin{aligned} p' &\to p'[1-\tfrac{1}{2}u(1+v)] + p''[-\tfrac{1}{2}u(1-v)], \\ p'' &\to p'[-\tfrac{1}{2}u(1+v)] + p''[1-\tfrac{1}{2}u(1-v)] \end{aligned} \quad (61)$$

before performing the integrals on k, u, and v.

Consider first the k^4 terms, which have the form

$$\kappa^{-2}\beta_\nu[(\beta k)^2 - k^2]\beta_\mu[(\beta k)-k^2]\beta_\nu. \quad (62)$$

But by (16),

$$\begin{aligned} (\beta k)^2\beta_\mu(\beta k)^2 = \beta k(\beta k\beta_\mu\beta k)\beta k = (\beta k)^3 k_\mu = k^2 k_\mu(\beta k), \\ \beta_\mu(\beta k)^2 + (\beta k)^2\beta_\mu = k^2\beta_\mu + k_\mu(\beta k) \end{aligned} \quad (63)$$

so that (62) vanishes identically. Therefore there are no k^4 terms and hence no quadratic divergences for either spin case.

To obtain the k^2 terms, it is simplest to put $k' = p'-k$, $k'' = p''-k$ and perform the β-matrix reduction, subsequently picking out the k^2 parts. Performing the sum over ν in (60), one has

$$\begin{aligned} &\kappa^{-2}\{(\beta k')^2\beta_\mu(\beta k'')^2 - k_\mu'\beta k'(\beta k'')^2 \\ &\qquad - (\beta k')^2\beta k'' k_\mu'' + (k'k'')\beta k'\beta_\mu\beta k''\} \\ &+ (i/\kappa)\{(M-1)\beta_\mu\beta k'(\beta k'')^2 + (\beta k')^2\beta k''\beta_\mu(M-1) \\ &\qquad - M(\beta k'')^2 k_\mu' - (\beta k')^2 M k_\mu'' \\ &\qquad + \beta k''\beta k'\beta_\mu\beta k'' + \beta k'\beta_\mu\beta k''\beta k'\} \\ &- \{\beta k' k_\mu' + \beta k'' k_\mu'' - (\beta k')^2\beta_\mu - \beta_\mu(\beta k'')^2 \\ &\qquad + \beta_\mu\beta k''\beta k' + \beta k''\beta k'\beta_\mu - (k'k'')\beta_\mu\} \\ &- i\kappa\{M(k_\mu' + k_\mu'') - (M-1)\beta_\mu\beta k' \\ &\qquad - (M-1)\beta k''\beta_\mu\} + \kappa^2\{\beta_\mu\}. \end{aligned} \quad (64)$$

Each member of the first group in (64) gives six terms of k^2 type on substituting $k' = p'-k$, $k'' = p''-k$; each member of the second group gives three k^2 terms, each member of the third group gives one; and none are ob-

tained from the last two terms. In selecting out the k^2 terms, the symmetry rules are used that $k_\mu k_\nu = \frac{1}{4}k^2\delta_{\mu\nu}$, $(\beta k)^2 = \frac{1}{4}k^2 M$. Next, the substitution (61) is made, and most of the p', p'' eliminated from the result by the following rule: since $K_\mu^{(1)}$ will operate on $\psi(x'')$ to the right, $\bar{\psi}(x')$ to the left, we can put

$$i\kappa \leftarrow \beta p', \quad \beta p'' \rightarrow i\kappa, \tag{65a}$$

the direction of the arrows indicating that this substitution is permissible only when $\beta p'$ (or $\beta p''$) stands at the extreme left (right) of the term in which it is found. If this is not the case, one has the associated rules which are the equivalent of (39) in momentum space:

$$\begin{gathered} p_\mu' \leftarrow \beta_\mu \beta p', \quad \beta p'' \beta_\mu \rightarrow p_\mu'', \\ (p'p'') \leftarrow \beta p'' \beta p' \rightarrow (p'p''). \end{gathered} \tag{65b}$$

Any other forms, such as $M\beta p'$, $\beta p'' M$, or $\beta p'' \beta_\mu \beta p'$ must be changed by means of the commutation rules to equivalent forms with $\beta p'$ and $\beta p''$ on the extreme left and right before applying (65). It is important to note that the transformation (61) must be made *before* applying (65).

The reductions (65) will not entirely remove p', p'' from (60), but will leave terms of the type $(p'p'')$ and $(p_\mu' + p_\mu'')$. These can be cast into customary form by the use of the identities

$$\begin{aligned} (p'p'') &= \tfrac{1}{2}[p'^2 + p''^2 - (p'-p'')^2] \\ &= -\kappa^2 - \tfrac{1}{2}(p'-p'')^2, \end{aligned} \tag{66a}$$

$$i\kappa(p_\mu' + p_\mu'')\Omega = -\kappa(p_\nu' - p_\nu'')\Omega\sigma_{\mu\nu} - \kappa^2(\Omega\beta_\mu + \beta_\mu\Omega), \tag{66b}$$

where Ω is any operator (in particular M) that commutes with $\sigma_{\mu\nu}$. The identity (66b) is the Fourier inverse of the current decomposition (41), with the addition of the operator Ω. One further simplification is achieved by noting that all integrals over v are even in that variable, so that all odd powers of v can be dropped from the result. After all this substitution and reduction one finds that the k^2 terms from (60) may be written in the form $k^2 f_\mu(u, v)/4\kappa^2$, where

$$\begin{aligned} f_\mu(u, v) = f_\mu(u) &= 2\kappa^2\beta_\mu[(5-A) + u(A-4)] \\ &\quad + (p'-p'')^2\beta_\mu(7u/4 - 1) \\ &\quad - \kappa(p_\nu' - p_\nu'')\sigma_{\mu\nu}[2 + (9/2 - A)u + M(3u-4)]. \end{aligned} \tag{67}$$

In this case it happens that $f_\mu(u, v)$ is independent of v, since only odd powers would have occurred, and these have been dropped.

The k^0 part of (60) is obtained from (64) by putting $k' \rightarrow p'$, $k'' \rightarrow p''$, making substitution (61), (65) in order and dropping odd powers of v. In this way one obtains

$$B_\mu^{(1)} = \frac{1}{(2\pi)^3}\int_{-1}^{1}\frac{dv}{2}\int_0^1 u\,du\int dk \times\left[\frac{k^2}{4\kappa^2}f_\mu(u) + g_\mu(u, v)\right]\delta''(k^2 + \lambda^2 u^2), \tag{68}$$

where

$$\begin{aligned} g_\mu(u, v) = {} & \kappa^2\beta_\mu\left[\left(-2u + \frac{19}{4}u^2 - \frac{3}{2}u^3\right) + v^2\left(\frac{5}{4}u^2 - u^3\right)\right] + i\kappa(p_\mu' + p_\mu'')\left[\left(-2u + \frac{13}{4}u^2 - \frac{3}{2}u^3\right) + v^2\left(-\frac{5}{4}u^2 + u^3\right)\right] \\ & + i\kappa(p_\mu' + p_\mu'')M\left[\frac{1}{4}u^2 + v^2\left(\frac{3}{4}u^2 - \frac{1}{2}u^3\right)\right] + (p'p'')\beta_\mu\left[\left(-4 + 6u - 5u^2 + \frac{7}{4}u^3\right) + v^2\left(u^2 - \frac{3}{4}u^2\right)\right] \\ & + i\frac{p'p''}{\kappa}(p_\mu' p_\nu'')[\tfrac{1}{4}(u^3 - Mu^2)(1-v^2)] + \frac{(p'p'')^2}{\kappa^2}\beta_\mu[\tfrac{1}{4}(u^2 - u^2)(1-v^2)] \end{aligned} \tag{69}$$

and the substitutions (66) remain to be made.

The term $k^2\delta''(k^2 + \lambda^2 u^2)$ contains a logarithmic divergence and is equivalent (C.9) to $-2\delta''(k^2 + \lambda^2 u^2)$. To separate the divergent and convergent parts of

$$\int_{-1}^{1}dv\int_0^1 du\int dk[u f_\mu(u)]\delta''(k^2 + \lambda^2 u^2)$$

perform first the partial integration with respect to u as in (55); the second term of (55a) is then convergent when integrated over dk and dv. For the first term of (55a), however, a second partial integration with respect to v is necessary:

$$\begin{aligned} &\int_{-1}^{1}\tfrac{1}{2}\delta'(k^2 + \lambda^2)dv \\ &\quad = \delta'(k^2 + \kappa^2) + \frac{(p'-p'')^2}{4\kappa^2}\int_{-1}^{1}v^2 dv\,\delta''(k^2 + \lambda^2), \end{aligned} \tag{70}$$

where the second term converges when integrated over dk.

The δ-function integrals are evaluated as in (C.12), and (C.14). From (67) to (69) it is clear that

$$B_\mu^{(1)}(p', p'') = B_\mu^{(1)}(p'-p'') = B_\mu^{(1)}(p);$$

when this kernel is inserted in a form like (52) for $K_\mu^{(1)}$ and $K_\mu^{(1)}$ in turn inserted in (48), it is seen that the factor p_ν in B_μ is equivalent to $-i\partial/\partial x_\nu = -i\partial_\nu$ operating on the final expression as a function of x; likewise $p^2 \rightarrow -\Box^2$, again operating on the coordinate x. Using this fact and collecting and evaluating (68), (56), (52) and (48), we have at last

$$\begin{aligned} (4\pi/\alpha)\delta j_\mu^{(2)}(x) = {} & N j_\mu(x) + Q_1 j_\mu(x) + Q_2 m_\mu(x) \\ & + Q_3 m_\mu'(x) + R_1 j_\mu(x) + R_2 m_\mu(x) + R_3 m_\mu'(x), \end{aligned} \tag{71}$$

where

$$N=\left\{\frac{PP_0}{\kappa^2}-\ln\frac{P+P_0}{\kappa}\right\}(4/3)(4-A)$$
$$+\left\{\ln\frac{P+P_0}{\kappa}-1\right\}\left[\tfrac{1}{3}(4-A)(\Box/\kappa)^2-\tfrac{2}{3}\right]$$
$$-\{\tfrac{1}{6}(\Box/\kappa)^2F_2+\tfrac{1}{8}(A-4)(\Box/\kappa)^4(F_2-\tfrac{1}{3}F_3)\},$$
$$Q_1=\left\{\ln\frac{P+P_0}{\kappa}-1\right\}\frac{1}{12}\left(\frac{\Box}{\kappa}\right)^2$$
$$Q_2=\left[\ln\frac{P+P_0}{\kappa}-1\right](\tfrac{3}{4}A-5),$$
$$Q_3=2\left[\ln\frac{P+P_0}{\kappa}-1\right],$$
$$R_1=\left\{-\frac{7}{2}[1+F_0]+\frac{\Box^2}{\kappa^2}\left[-\frac{1}{18}+\frac{1}{48}\left(-107F_0\right.\right.\right.$$
$$\left.\left.+(4A-25)F_2\right)\right]+\frac{1}{96}\frac{\Box^4}{\kappa^4}[-F_0+3F_1]$$
$$\left.+\left[4\left(1+\ln\frac{\kappa}{2k_0}\right)-4\left(1-\frac{1}{2}\frac{\Box^2}{\kappa^2}\right)G_0\right]\right\},$$
$$R_2=\left\{\left[\frac{2A}{9}-2+\frac{1}{12}(23F_0+5F_1)\right]\right.$$
$$\left.-\frac{1}{12}\frac{\Box^2}{\kappa^2}[F_0+(14-2A)F_1]\right\},$$
$$R_3=\left\{\frac{1}{6}[8-3F_0-F_1]+\frac{1}{8}\frac{\Box^2}{\kappa^2}[F_0+3F_1]\right\}$$

(71a)

and

$$m_\mu(x)=-\frac{ec}{2\kappa}\partial_\nu[\bar\psi(x)\sigma_{\mu\nu}\psi(x)],$$
$$m_\mu'(x)=-\frac{ec}{2\kappa}\partial_\nu[\bar\psi(x)M\sigma_{\mu\nu}\psi(x)].$$

(72)

The operations Fm_μ, etc., are defined to mean

$$Fm_\mu\equiv\int dw'F(x-x')m_\mu(x'),\tag{73}$$

with

$$F_n(x),\,G_n(x)=\frac{1}{(2\pi)^4}\int_0^1 v^{2n}dv\int d\rho\frac{e^{ipx}(F,\,G)}{1+[\rho^2(1-v^2)/4\kappa^2]},\tag{74}$$

$$F=1,\,G=1+\ln\frac{\lambda}{2k_0}=\left(1+\ln\frac{\kappa}{2k_0}\right)+\frac{1}{2}\ln\left[1+\frac{p^2}{\kappa^2}(1-v^2)\right].$$

The function $G_n(x)$ involves an infrared divergence.

The term N in (71) corresponds to the vacuum polarization term in (48), as has already been computed in reference 4, for example. The expression in (71) differs not only in the notation but also somewhat in the numerical constants.[13] The terms Q in (71) represent logarithmic divergences not contained either in the vacuum polarization nor the self-energy effects, and which are peculiar to the present calculation. It is noteworthy that these divergent terms contain nothing proportional to the original $j_\mu(x)$ itself; although both $K_\mu^{(1)}$ and $K_\mu^{(2)}$ contain such terms, they just cancel on combination. The terms R in (71) are finite corrections.

For the vector meson, the divergences Q in (71) include both the dipole moment $m_\mu(x)$ and a term $\kappa^{-2}\Box^2 j_\mu(x)$, which can be shown to involve the quadrupole moment of the particle. Unlike the electron case, therefore, the first correction to the dipole and quadrupole moments is divergent; and a particle of spin 1 possesses no higher intrinsic moment. In the case of spin 0, there are no intrinsic moments, and the divergences cannot be so physically interpreted; on closer inspection, however, it turns out that the divergent terms vanish identically just for spin 0. The divergent terms Q in (71) are proportional to

$$\frac{1}{12}\frac{\Box^2}{\kappa^2}j_\mu-\frac{ec}{\kappa}\partial_\nu\left[\bar\psi\left(\frac{5}{2}-\frac{A}{3}M\right)\sigma_{\mu\nu}\psi\right],\tag{75}$$

but on insertion of $A^0=4$ and the special identities (43) and (47), the expression (75) vanishes identically. Therefore for the scalar meson, as for the electron, no new divergences appear in the $\delta j_\mu^{(2)}$ calculation outside of charge renormalization and the self-energy.

For the scalar meson, one can also eliminate m_μ and m_μ' from the finite terms in (71) by the use of the identities (43) and (47). The resulting form is not particularly instructive; but it should be stressed that the possibility of such a reduction makes the scalar meson appear, from the point of view of the β-matrix formalism, as a special pathological case. In this special case certain highly characteristic terms may be absent, as in the vanishing of the divergence associated with (75). Therefore in making electrodynamic calculations to compare the effect of Fermi-Dirac *versus* Bose-Einstein statistics, one is tempted to suggest that the vector meson should be regarded as the typical example of a boson field, and that the scalar meson is somewhat atypical.

V. SUMMARY AND CONCLUSIONS

The β-matrix formalism has been shown to be adequate to handle second-order electrodynamic calculations for particles of spin 0 and 1. Furthermore, the expression in terms of these matrices of the "surface terms" in the current and interaction operators leads naturally to the definition of a function $\bar S$ such that the effects of the surface terms are automatically accounted

for, and the entire formalism can be treated exactly as for electron electrodynamics.

In calculation with the β-matrices it is found that a certain matrix M plays a fundamental role, and that effects calculated to any order will contain this operator in addition to the usual ones found in the electron case. The operator M, however, is well behaved and has simple properties, and in most cases of interest can be replaced in the final result by $M\to 5/2$. Higher powers of M serve only to distinguish between the cases of spin 0 and 1, and introduce no new physical considerations.

As a specific example of the techniques described, the second-order correction to the current operator is computed, and is found to contain logarithmically divergent terms in $\Box^2 j_\mu$ and $\partial_\nu(\bar\psi\sigma_{\mu\nu}\psi)$ but none in j_μ itself. For the scalar meson these infinite terms vanish identically by virtue of special identities for this case, so that no new divergences appear beyond those of first-order charge and mass renormalization, just as in the electron case. For the vector meson, however, the infinite terms remain, and represent a divergence of the dipole and quadrupole moments not comprehended in the ordinary vacuum polarization and self-energy effects.

The author wishes to express his sincere thanks to Professor W. Pauli for suggesting this problem and its significance, and for much kind and illuminating criticism, and to Professor P. Scherrer for the hospitality and congenial atmosphere of the Physikalisches Institut. He also wishes to thank Professor W. Heitler for commenting on the manuscript.

APPENDIX I

In this section it is shown explicitly that the surface terms cancel at least to order e^3 in the expression for the corrected $j_\mu(x)$. Consider Eq. (7): to order e^3 the $\beta_N{}^2$-terms from $j_\mu(x)$ cancel those from the second members of (7), as has already been found in computing the vacuum polarization. The e^3 terms come only from the second and third member of (7)—if the series were extended to higher orders, it would contain only e^4 and higher terms. Since the result must be independent of the orientations of σ, σ', and σ'', we can choose these surfaces all to be plane parallel, so that $\beta_N{}^2=\beta_{N'}{}^2=\beta_{N''}{}^2$.

The e^3 terms from the second member of (7) are

$$-\frac{e^3}{\hbar^2 c\kappa}\int_{-\infty}^{\infty}d\omega'[-\tfrac{1}{2}\epsilon(\sigma\sigma')][[\bar\psi(x)\beta_\mu\psi(x),\bar\psi(x')\{\beta_\lambda(1+\beta_N{}^2)\beta_\nu\}\times\psi(x')A_\lambda(x')A_\nu(x')]+[\bar\psi(x)\{\beta_\mu(1+\beta_N{}^2)\beta_\nu+\beta_\nu(1+\beta_N{}^2)\beta_\mu\}\times\psi(x)A_\nu(x),\bar\psi(x')\beta_\lambda\psi(x')A_\lambda(x')]]. \quad (A.1)$$

In all such expressions involving commutators we must include the vacuum expectation values of any bilinear forms, in case these happen to be non-vanishing. For $\bar\psi\beta_\mu\psi$, the vacuum expectation value is 0, so that no change occurs for these terms. The other bilinear forms in Eq. (1) do not have vanishing vacuum expectations; again, however, these vacuum terms will cancel when the original bilinear form is contained in a commutator. The vacuum expectation terms must be explicitly included only in case the original bilinear form occurs in an anticommutator. Making this modification, and using the facts that

$$[\psi A,\psi' A']=\tfrac{1}{2}\{\psi,\psi'\}[A,A']+\tfrac{1}{2}[\psi,\psi']\{A,A'\} \quad (A.2)$$

and for any operators Ω, Ω',

$$[\bar\psi\Omega\psi,\bar\psi\Omega'\psi']=\bar\psi(x)\Omega S(x-x')\Omega'\psi(x')+\bar\psi(x')\Omega' S(x-x')\Omega\psi(x'),$$
$$[\bar\psi\Omega\psi,\bar\psi\Omega'\psi']_1=\bar\psi(x)\Omega S^1(x-x')\Omega'\psi(x')+\bar\psi(x')\Omega' S^1(x-x')\Omega\psi(x'), \quad (A.3)$$

and writing

$$[A_\lambda(x')A_\nu(x)]_0=\tfrac{1}{2}\{A_\lambda(x'),A_\nu(x)\}_0=\tfrac{1}{2}\hbar c D^1(x'-x)\delta_{\lambda\nu},$$
$$[A_\lambda(x),A_\nu(x')]=i\hbar c D(x-x')\delta_{\lambda\nu}, \quad (A.4)$$

one obtains for (A.1)

$$\frac{ie^3}{2\hbar\kappa}\int_{-\infty}^{\infty}[-\tfrac{1}{2}\epsilon(\sigma\sigma')]d\omega'\{D^1(x'-x')G_{\mu\nu\nu}(x,x')+D^1(x-x')[G_{\nu\mu\nu}(x,x')+G_{\nu\nu\mu}(x,x')]-D(x-x')[G_{\nu\mu\nu}{}^1(x,x')+G_{\nu\nu\mu}{}^1(x,x')]-2D(x-x')[\bar\psi(x)\{\beta_\mu(1+\beta_N{}^2)\beta_\nu+\beta_\nu(1+\beta_N{}^2)\beta_\mu\psi(x)]_0\bar\psi(x')\beta_\nu\psi(x')\}, \quad (A.5)$$

where

$$G_{\mu\nu\lambda}(x,x')=\bar\psi(x)\beta_\mu S(x-x')\beta_\nu(1+\beta_N{}^2)\beta_\lambda\psi(x')+\bar\psi(x')\beta_\lambda(1+\beta_N{}^2)\beta_\nu S(x-x')\beta_\mu\psi(x) \quad (A.6)$$

and likewise for G^1 with S^1 replacing S. The last term in (A.5) is due to the inclusion of a vacuum expectation value, as discussed above.

The e^3 terms from the third member of (7) are

$$\frac{e^3}{\hbar^2 c}\int_{-\infty}^{\infty}d\omega'd\omega''[-\tfrac{1}{2}\epsilon(\sigma\sigma')][-\tfrac{1}{2}\epsilon(\sigma'\sigma'')]\times[A_\nu(x')(\bar\psi(x)\beta_\mu S(x-x')\beta_\nu\psi(x')+\bar\psi(x')\beta_\nu S(x-x')\beta_\mu\psi(x)),\times A_\lambda(x'')\bar\psi(x'')\beta_\lambda\psi(x'')]. \quad (A.7)$$

With the help of (A.2) and (A.4) the commutator becomes, exactly as in the electron case,

$$(\hbar c/2i)D^1(x'-x'')[H_{\mu\nu\nu}(x,x',x'')-H_{\nu\mu\nu}(x',x,x'')]-(\hbar c/2i)D(x'-x'')[H_{\mu\nu\nu}(x,x',x'')-H_{\nu\mu\nu}(x',x,x'')]+(\hbar/ec)D(x'-x'')[j_\mu(x),j_\nu(x')]_0\bar\psi(x'')\beta_\nu\psi(x'') \quad (A.8)$$

where

$$H_{\mu\nu\lambda}(x,x',x'')=\bar\psi(x)\beta_\mu S(x-x')\beta_\nu S(x'-x'')\beta_\lambda\psi(x'')+\bar\psi(x'')\beta_\lambda S(x''-x')\beta_\nu S(x'-x)\beta_\mu\psi(x) \quad (A.9)$$

and $H_{\mu\nu\lambda}{}^1$ is defined in the same way only with $S^1(x'-x'')$ substituted for $S(x'-x'')$ the first term of (A.9), and $-S^1(x''-x')$ for $S(x''-x')$ in the second term.

The last term in (A.8) also results from the inclusion of a vacuum expectation value; when combined with the last term from (A.5), it yields

$$-\frac{e^2}{\hbar\kappa}\bar\psi(x)\{\beta_\mu(1+\beta_N{}^2)\beta_\nu+\beta_\nu(1+\beta_N{}^2)\beta_\mu\}\psi(x)\delta A_\nu(x)+\frac{i}{\hbar c}\int_{-\infty}^{\infty}[-\tfrac{1}{2}\epsilon(\sigma,\sigma')][j_\mu(x),H(x')]d\omega' \quad (A.10)$$

where

$$H(x')=-j_\nu(x')\delta A_\nu(x')/c,$$
$$\delta A_\nu(x)=(1/c)\int_{-\infty}^{\infty}\bar D(x-x')j_\nu(x'). \quad (A.11)$$

This is just the expression to order e^3 for the polarization of the vacuum by an electromagnetic field δA_ν, which is produced by the particle current itself. It therefore represents just the ordinary charge renormalization, for which the surface terms are well known to cancel.

Next consider the second term of (A.9) and the third term of (A.5); using relation (5) and the fact that $S(x-x')$ is an odd function, one immediately sees that the $\beta_N{}^2$-parts of these two terms cancel, leaving a residual term formed in accordance with rule (6). Since these expressions are linear in S and hence $\beta_N{}^2$, the cancellation occurs in exactly the same manner as for the simple mass and charge renormalizations.

The first member of (A.8) and first two of (A.5), however, involve terms in both $\beta_N{}^2$ and $\beta_N{}^4$. Consider first the terms in

β_N^2: since

$$[\epsilon(\sigma\sigma')-\epsilon(\sigma\sigma'')][\epsilon(\sigma'\sigma'')]=\epsilon(\sigma\sigma')\epsilon(\sigma\sigma'')-1 \quad (A.12)$$

and

$$\int_{-\infty}^{\infty}d\omega'd\omega''\bar{\psi}(x')\beta_\mu S(x'-x)\beta_\mu S(x-x'')\beta_\nu\psi(x'')=0 \quad (A.13)$$

because there are no real, first-order transitions, the first term of (A.9) can be written

$$-\frac{ie^2}{2\hbar}\int_{-\infty}^{\infty}d\omega'd\omega''D^1(x'-x'')\{[-\tfrac{1}{2}\epsilon(\sigma\sigma')][-\tfrac{1}{2}\epsilon(\sigma'\sigma'')]$$
$$\times[\bar{\psi}(x)\beta_\mu S(x-x')\beta_\nu S(x'-x'')\beta_\nu\psi(x'')$$
$$+\bar{\psi}(x'')\beta_\nu S(x''-x')\beta_\nu S(x'-x)\beta_\mu\psi(x)]+[-\tfrac{1}{2}\epsilon(\sigma\sigma')]$$
$$\times[-\tfrac{1}{2}\epsilon(\sigma\sigma'')][\bar{\psi}(x')\beta_\nu S(x-x')$$
$$\times\beta_\mu S(x-x'')\beta_\nu\psi(x'')]. \quad (A.14)$$

When the corresponding ϵ and S are combined according to (5), the resulting first-order terms in β_N^2 just cancel those from the first two terms of expression (A.5).

There remain finally the quadratic terms in β_N^2 from both (A.5) and (A.9):

$$\frac{ie^2}{2\hbar\kappa^2}\int_{-\infty}^{\infty}d\omega'D^1(x-x')\delta(x-x')[\bar{\psi}(x)\{\beta_\mu\beta_N{}^2\beta_\nu(1+\beta_N{}^2)\beta_\nu$$
$$+\beta_\mu(1+\beta_N{}^2)\beta_\nu\beta_N{}^2\beta_\nu-\beta_\mu\beta_N{}^2\beta_\nu\beta_N{}^2\beta_\nu\}\psi(x')]$$
$$+\{2\text{ permutations of }\mu,\nu\} \quad (A.15)$$

but the factor in brackets is just

$$\beta_\mu[\beta_N{}^2\beta_\nu+\beta_\nu\beta_N{}^2+\beta_N{}^2\beta_\nu\beta_N{}^2]\beta_\nu=-\beta_\mu\beta_\nu\beta_\nu, \quad (A.16)$$

by virtue of (2) and likewise for the two permutations of μ, ν. Therefore all the β_N's have canceled, and the residual terms of type (A.16) are just those to be obtained by application of rule (6), as must necessarily be the case.

APPENDIX II

As an example of the present methods in application to a first-order correction, consider the meson self-energy. The interaction energy correct to order e^2 is contained in the terms

$$\delta H^{(1)}(x)=\frac{i}{\hbar c}\int_{-\infty}^{\infty}d\omega'[-\tfrac{1}{2}\epsilon(\sigma\sigma')][H(x),H(x')]+\cdots. \quad (B.1)$$

Using rule (I) and evaluating for the case of one real meson and no real photons

$$\delta H^{(1)}(x)=\delta mc^2$$
$$=-\frac{e^2}{2}\frac{1}{(2\pi)^4}\int d\omega'\int dp\exp[ip(x-x')]H(p), \quad (B.2)$$

$$H(p)=\frac{1}{(2\pi)^3}\int dk\beta_\nu T(p-k)\beta_\nu\left[\frac{\delta(a)}{b}+\frac{\delta(b)}{a}\right], \quad (B.3)$$
$$a=(p-k)^2+\kappa^2,\quad b=k^2.$$

To evaluate $H(p)$, combine the δ-functions as in (C.2), and make the resulting δ'-function symmetrical in k by the substitution $k\to k+up$. Then reduce $\beta_\nu T(p-k)\beta_\nu$ by summing over ν, extracting the terms even in k according to $k_\mu k_\nu=\frac{1}{4}k^2\delta_{\mu\nu}$, $(\beta k)^2=\frac{1}{4}k^2M$; next make the substitution $p\to p_0=p(1-u)$ and finally apply the rule $\beta p\to i\kappa$, $(\beta p)^2\to p^2\to-\kappa^2$. Then one has

$$H(p)=\frac{\kappa}{(2\pi)^3}\int dk\int_0^1 du[(1-3u+u^2)+M(2u-u^2)$$
$$-(k^2/4\kappa^2)(M-M^2)]\delta'(k^2+\kappa^2u^2). \quad (B.4)$$

The terms with $\delta'(k^2+\kappa^2u^2)$ give rise to a logarithmic divergence, which is separated by partial integration as in (55). The term $k^2\delta'(k^2+\kappa^2u^2)$ is equivalent to $-2\delta(k^2+\kappa^2u^2)$ by (C.9), and produces a quadratic plus a logarithmic divergence. These are again separated out by partial integration:

$$\int_0^1 duf(u)\delta(k^2+\kappa^2u^2)=F(1)\delta(k^2+\kappa^2)$$
$$-2\kappa^2\int_0^1 duuF(u)\delta'(k^2+\kappa^2u^2). \quad (B.5)$$

Where the partial integration is repeated for the second term of (B.5). Using the evaluations (C.12), (C.14), one has

$$\left(\frac{4\pi}{\alpha}\right)\frac{\delta m}{m}=(4M-A)\frac{PP_0}{\kappa^2}+\frac{1}{3}(A+5)\ln\frac{P+P_0}{\kappa}$$
$$+\frac{1}{18}(8A+19-42M). \quad (B.6)$$

This mass-correction naturally contains the operator M in contrast to that for the electron, which is a pure scalar. In general, however, we are interested only in the expectation value of the operator δmc^2, in which case it is permissible to take $M\to 5/2$, according to (39). The numerical discrepancy between (B.6) and the results of reference 6 apparently arises from different treatments of the divergent integrals.[12]

APPENDIX III

A collection is made here of various properties and relations between the δ-functions which are useful in the present calculations.

Using the fact that $a\delta(a)=b\delta(b)=0$, and multiplying by $(a-b)/(a-b)=1$, we have

$$\frac{\delta(a)}{b}+\frac{\delta(b)}{a}=\frac{1}{a-b}[\delta(a)-\delta(b)]=-\int_0^1 du\delta'[b+(a-b)u]. \quad (C.1)$$

In particular, if $a=(k-p)^2+\kappa^2$, $b=k^2$ one obtains

$$\frac{\delta[(k-p)^2+\kappa^2]}{k^2}+\frac{\delta(k^2)}{(k-p)^2+\kappa^2}=$$
$$-\int_0^1 du\delta'[k^2+(-2kp+p^2+\kappa^2)u]. \quad (C.2)$$

In application the right-hand side of (C.2) can generally be simplified by putting $p^2\to-\kappa^2$; and it may be symmetrized with respect to k by the transformation $k\to k+up$.

Note that in any formula such as (C.1) the range of integration can be shifted when convenient from (0, 1) to (−1, 1) by the substitution $u=\frac{1}{2}(1+v)$. For example, if $a=k'^2+\kappa^2$, $b=k''^2+\kappa^2$,

$$\frac{\delta(k'^2+\kappa^2)}{(k'^2+\kappa^2)}+\frac{\delta(k''^2+\kappa^2)}{k'^2+\kappa^2}$$
$$=-\frac{1}{2}\int_{-1}^1 dv\delta'\left[\frac{k'^2+k''^2}{2}+\kappa^2+\left(\frac{k'^2-k''^2}{2}\right)v\right], \quad (C.3)$$

where the right-hand side can be symmetrized by substituting $k'\to\frac{1}{2}k(1-v)+p$, $k''\to\frac{1}{2}k(1-v)-p$.

By observing the even nature of δ and the odd nature of δ' and placing $a\to-a$, we obtain from (C.1) the related identity

$$\frac{\delta(a)}{b}-\frac{\delta(b)}{a}=\frac{1}{2}\int_{-1}^1 dv\delta'\left[\left(\frac{a-b}{2}\right)+\left(\frac{a+b}{2}\right)v\right]. \quad (C.4)$$

More generally, one may show by partial integration with respect to v that

$$f\frac{\delta(a)}{b}+g\frac{\delta(b)}{a}$$
$$=-\frac{1}{2}\int_{-1}^1 dv\delta'\left[\left(\frac{a+b}{2}\right)+\left(\frac{a-b}{2}\right)v\right]\left[\left(\frac{f+g}{2}\right)+\left(\frac{f-g}{2}\right)v\right]$$
$$-\frac{1}{2}\left(\frac{f-g}{a-b}\right)\int_{-1}^1 dv\delta\left[\left(\frac{a+b}{2}\right)+\left(\frac{a-b}{2}\right)v\right], \quad (C.5)$$

where f and g are any functions of a and b.

The sum of three δ-functions may be treated similarly by applying the above decomposition in two stages:

$$\frac{\delta(a)}{bc}+\frac{\delta(b)}{ac}+\frac{\delta(c)}{ab}=\frac{1}{a-b}\left[\frac{\delta(b)-\delta(c)}{b-c}-\frac{\delta(a)-\delta(c)}{a-c}\right]$$
$$-\frac{1}{2}\int_0^1 udu\int_{-1}^1 dv\delta''\left[c+\left(\frac{a+b}{2}-c\right)u+\frac{a-b}{2}uv\right]. \quad (C.6)$$

In particular, if $a=(p'-k)^2+\kappa^2$, $b=(p''-k)^2+\kappa^2$, $c=k^2$, and we can put p'^2, $p''^2\to-\kappa^2$, the integrand of (C.6) becomes

$$k^2-uk[(p'+p'')+(p'-p'')v] \tag{C.7}$$

which can be symmetrized in k by the substitution

$$k\to k+\tfrac{1}{2}u[(p'+p'')+(p'-p'')v].$$

Another general set of relations between the δ-functions and its derivatives is obtained from the relation $x\delta(x)=0$ by differentiating n times, whence

$$\delta^n(x)=-n\delta^{n-1}(x)/x. \tag{C.8}$$

This relation is, however, not unambiguous and must be used with care. For example, consider the integral of the four-dimensional δ-function:

$$\int dkk^2\delta^{n+2}(k^2+\kappa^2)=\frac{1}{2}\int dkk_\nu\frac{\partial}{\partial k_\nu}\delta^n(k^2+\kappa^2)$$
$$=-2\int dkk\delta^n(k^2+\kappa^2)=-2I_n(\kappa^2). \tag{C.9}$$

But from application of (C.8),

$$\int dkk^2\delta^{n+1}(k^2+\kappa^2)=-(n+1)I_n(\kappa^2)-\kappa^2I_{n+1}(\kappa^2). \tag{C.10}$$

If the integral I_n is convergent, we have $I_{n+1}(x)=dI_n(x)/dx$ so that the condition for compatibility of (C.9) and (C.10) is

$$\begin{aligned}-2I_n(x)&=-(n+1)I_n(x)-xdI_n/dx,\\ I_n(x)&=C_n/x^{n-1},\end{aligned} \tag{C.11}$$

where there is only one independent constant among all the C_n for convergent I_n and integral n. Where I_n is not convergent, however ($n\leq1$), it is not legitimate to write the condition (C.11), and a literal evaluation of (C.9) and (C.10) in terms of standard divergent expressions leads to different results. In this case it is possible to argue[13] that the rule (C.9) is heuristically more satisfactory than (C.10), and this convention has been adopted throughout the present study.

To evaluate I_n, consider the invariant, three-dimensional form

$$I_0(\kappa^2)=\int dk\int_{-\infty}^{\infty}dk_0\delta(k^2+\kappa^2-k_0^2)=\int dk\int_0^\infty\frac{dx}{x^{\frac{1}{2}}}\delta(k^2+\kappa^2-x)$$
$$=\int\frac{dk}{(k^2+\kappa^2)^{\frac{1}{2}}}=2\pi\left[PP_0-\kappa^2\ln\frac{P+P_0}{\kappa}\right], \tag{C.12}$$

where $P_0^2=P^2+\kappa^2$ and the limit $P\to\infty$ is always understood. If P is momentarily regarded as finite, one may take derivatives with respect to κ^2 for any value of n, so that

$$I_n(\kappa^2)=4\pi(-1)^n\left[\frac{1}{2}\frac{3}{2}\cdots\frac{(2n-1)}{2}\right]\int_0^P\frac{x^2dx}{(x^2+\kappa^2)^{n+\frac{1}{2}}}, \tag{C.13}$$

where the last is a one-dimensional integral. Note that this last definition should also hold for negative or fractional values of n. Some particular values are

$$I_1=-2\pi\left[\ln\frac{P+P_0}{\kappa}-1\right],\quad I_2=\pi/\kappa^2,\quad I_3=-\pi/\kappa^4,\quad\cdots. \tag{C.14}$$

Finally, consider the form encountered in the text,

$$J=\int dk\int_0^1 udu\delta''(k^2+\kappa^2u)\to\frac{\pi}{\kappa^2}\int_0^1\frac{du}{u} \tag{C.15}$$

an unidentified logarithmic divergence if the k integration is performed first. If, however, the u integration is performed first, one has with (C.14)

$$J=\frac{1}{2\pi^2}\int dk[\delta'(k^2+\kappa^2)-\delta'(k^2)]$$
$$=-\frac{\pi}{\kappa^2}\left[\ln\frac{P+P_0}{\kappa}-\ln\frac{2P}{\kappa}\right]_{P\to0}^{P\to\infty}. \tag{C.16}$$

This expression converges to zero at the upper limit; the divergence comes from the lower limit and is hence a type of "infrared catastrophe." The first term of (C.16) becomes unity as $P\to0$, but for the second we must define a minimum wave number k_0 and adopt the convention that displays this infrared effect,

$$J\to(\pi/\kappa^2)[1+\ln(\kappa/2k_0)]. \tag{C.17}$$

Infinite Integrals in Quantum Electrodynamics

D. C. PEASLEE*
Eidgenössische Technische Hochschule, Zürich, Switzerland
(Received June 16, 1950)

A numerical discrepancy in the results of various authors for the same divergent calculation is traced to differences in the treatment of divergent integrals. The difference is exhibited explicitly, and a standard convention suggested that corresponds to the regularization procedure of Pauli and Villars. Alternative methods of evaluation are criticized on this basis.

I. INTRODUCTION

IN three recent papers on boson electrodynamics, denoted as **A**,[1] **B**,[2] and **C**,[3] respectively, equivalent methods have been used for treating the same problems; in particular, the vacuum polarization and self-energy. Although complete agreement exists regarding the degree of the divergences encountered, there is considerable variation in the numerical coefficients obtained by different authors. This variation is presumably due to the use of different methods for the evaluation of divergent integrals. It therefore seems appropriate to compare these methods explicitly and to suggest a standard convention on the basis of this comparison.

The actual convention to be suggested rests on the principle that divergent integrals should be handled in all possible respects as if they were convergent, so that if convergent expressions are ultimately found to replace the present divergent ones, they can be inserted into the present computations with a minimum of readjustment. This principle has already been invoked in the regularization methods of Pauli and Villars;[4] in the present note, however, the auxiliary masses are not introduced explicitly, but certain formal rules are advocated for the treatment of divergent expressions. Since the divergent expressions are ambiguous, these formal rules cannot be justified in themselves, but must always presuppose an implicit regularizing procedure. An example of the equivalence between the present rules and regularization is given below.

The considerations given here are exactly similar for the Schwinger and Feynman schemes of calculation, except that in the former the functions involved in the infinite integrals are $\delta(k^2+\kappa^2)$ and its derivatives δ^n, while in the latter the functions concerned are $1/(k^2+\kappa^2)$ and its derivatives. A parallel discussion can be made for both systems by defining the general function

$$G_n(k^2+\kappa^2)=\delta^n(k^2+\kappa^2) \quad \text{or} \quad =(-)^n n!/(k^2+\kappa^2)^{n+1}. \tag{1}$$

This function has the general properties that [**C**, Eq. (C.8)]

$$xG_n(x)=-nG_{n-1}(x), \quad \text{and} \quad dG_n(x)/dx=G_{n+1}(x) \tag{2}$$

at least in those cases where the integral $\int G_n dk$ is convergent.

The first point concerns the change of variables

$$k_\mu \rightarrow k_\mu+up_\mu \tag{3}$$

which must be introduced into integrals of the form

$$\int_0^1 du \int dk f(k, p) G_n[k^2-2ukp+u(p^2+\kappa^2)] \tag{4}$$

in order to exploit the symmetry in k of the resulting argument of G_n. The integrals (4) can be expressed in the identical form

$$\int_0^1 du \int dk[1+D]g(k+up; p) \tag{5}$$

where $g(k; p)$ is the integrand of (4) and

$$D=-up_\mu\frac{\partial}{\partial k_\mu}+\frac{1}{2}u^2p_\mu p_\lambda\frac{\partial^2}{\partial k_\mu \partial k_\lambda}-\cdots. \tag{6}$$

Now if the integral $\int g dk$ is absolutely convergent, the operator D contributes nothing, since each term of it vanishes on integration by parts. If, however, $\int g dk$ is not absolutely convergent, the lowest order terms of D will be ambiguous and yield finite (or infinite) values or zero, depending on the order in which the k integrations are performed. The number of these ambiguous terms is limited, extending only up to that order n at which $\int[\partial^n g/\partial k^n]dk$ is first absolutely convergent. The authors of **B** assign non-vanishing values to all these ambiguous terms.

The ambiguous terms have generally been neglected in calculation, the tacit procedure being to make the present theory as much like a convergent one as possible. Under such conditions the operator D can be neglected in making the substitution (3), since all its contributions would vanish. This is the same argument as is used to draw the conclusion that

$$\int k_\mu G^n(k^2+\kappa^2)dk=0, \tag{7}$$

whether the integral converges or not. Of course, terms of types (6) and (7) always vanish on regularization.

A second, similar type of ambiguity occurs in

* AEC Postdoctoral Fellow.
[1] M. Neuman and W. H. Furry, Phys. Rev. **76**, 1677 (1949).
[2] T. Kinoshita and Y. Nambu, Prog. Theor. Phys. (to be published). I wish to thank these authors for the opportunity of seeing their manuscript before publication.
[3] D. C. Peaslee, Phys. Rev. **80**, 94 (1950), preceding paper.
[4] W. Pauli and F. Villars, Revs. Modern Phys. **21**, 434 (1949).

evaluating integrals of the type

$$\int k^2 G_n(k^2+\kappa^2)dk. \tag{8}$$

Such integrals can be evaluated in two ways:

$$\int k^2 G_n = \int (k^2+\kappa^2)G_n - \kappa^2 \int G_n$$

$$= -n\int G_{n-1} - \kappa^2 \int G_n \tag{9a}$$

$$\int k^2 G_n = \frac{1}{2}\int k_\mu \partial G_{n-1}/\partial k_\mu = -2\int G_{n-1}. \tag{9b}$$

Strictly speaking, these equations are justified only provided all of the integrals are convergent, in which case (9a) and (9b) are exactly equivalent [**C**, Eq. (C.9) to (C.11)]. If the integrals are not convergent, (9a) involves an illegitimate extension of (2), and (9b) an illegitimate integration by parts.[5] It is not surprising, therefore, that for the logarithmic divergences ($n=1$), (9a) and (9b) differ by a finite term; and for $n=0$, not even the coefficients of the leading (quadratic) divergence are the same, but differ by a factor of 2. This explains the different numerical coefficients in **A**, **B**, and **C** for the divergences in δm and δe (vacuum polarization); the method (9a) was used in **B** and apparently in **A**, while (9b) was used in **C**.

An argument similar to that above can be made in favor of (9b). In a convergent or regularized theory the functions G_n would be replaced by convergent functions R_n, for which (9b) would certainly be correct; on the other hand, (9a) depends on the fact that $(k^2+\kappa^2)G_n = -nG_{n-1}$, a property special to the G_n and not to be expected from the R_n. The practical inconvenience associated with (9a) may be imagined as follows. Suppose a divergent expression is computed with (9a) and the remainder terms $-\kappa^2 \int G_n$ combined with other similar terms in the numerical result; then if a convergent theory becomes available, it is not sufficient merely to correct the divergences in the previous result, but the terms $-\kappa^2 \int G_n$ must be sought out and explicitly subtracted. Thus convention (9a) not only makes extra labor in any divergent calculation, but this work must be undone again in converting to any convergent form. The same argument of course applies to terms arising from the operator D.

This point may be illustrated by explicit introduction of the regularizing procedure. For convenience, suppose the k-space to be only two-dimensional, and consider

$$\int \frac{k^2 d^2k}{(k^2+\kappa^2)^2} = \int \frac{d^2k}{(k^2+\kappa^2)} - \kappa^2 \int \frac{d^2k}{(k^2+\kappa^2)^2} \tag{10a}$$

$$= \int \frac{d^2k}{(k^2+\kappa^2)} - \pi \tag{10a'}$$

$$= \frac{1}{2}\int d^2k\, k_\mu \frac{\partial}{\partial k_\mu}\left(\frac{1}{k^2+\kappa^2}\right) = \int \frac{d^2k}{(k^2+\kappa^2)}. \tag{10b}$$

The contradiction between (10a) or (10a′) and (10b) corresponds to that between (9a) and (9b). Now if a regulator of mass κ_0 is introduced,

$$\int \frac{k^2 d^2k}{(k^2+\kappa^2)^2} \to \int k^2 d^2k \left[\frac{1}{(k^2+\kappa^2)^2} - \frac{1}{(k^2+\kappa_0^2)^2}\right]$$

$$= 2\pi \ln\frac{\kappa_0}{\kappa} \tag{11}$$

$$\int \frac{d^2k}{k^2+\kappa^2} \to \int d^2k \left[\frac{1}{k^2+\kappa^2} - \frac{1}{k^2+\kappa_0^2}\right] = 2\pi \ln\frac{\kappa_0}{\kappa}. \tag{12}$$

Thus (10b) is verified exactly, but there is still a remainder term $-\pi$ in (10a′). It must now be recalled that this factor came from the integral

$$-\kappa^2 \int \frac{d^2k}{(k^2+\kappa^2)^2};$$

this must also be regularized, so that

$$\kappa^2 \int \frac{d^2k}{(k^2+\kappa^2)^2} \to \kappa^2 \int \frac{d^2k}{(k^2+\kappa^2)^2} - \kappa_0^2 \int \frac{d^2k}{(k^2+\kappa_0^2)^2} = 0. \tag{13}$$

Thus regularization, if consistently carried out, also removes the factor $-\pi$ from (10a′) and makes it equivalent to (10b). The whole awkward procedure of inserting $-\pi$ and removing it again is avoided by the use of (10b) or (9b), as discussed in the preceding paragraph.

In order to avoid a confusing but superficial inconsistency of numerical results in present divergent calculations, some convention is desirable; and from the preceding arguments it is suggested that (a) terms of type D be always neglected when making transformations of type (1), regardless of convergence; (b) convention (9b) be adopted in preference to (9a) whenever the integrals are divergent so that the two are not equivalent.

The ambiguities in divergent integrals of this sort have been made the basis of a proposal[6] for the elimination of some of the divergences. Specifically, it is observed that

$$\int d^4k\,\delta(k^2) = \frac{1}{2\pi}\int d^4k \int_{-\infty}^{\infty} d\alpha \exp(i\alpha k^2)$$

$$(=)\frac{1}{2\pi}\int_{-\infty}^{\infty} d\alpha \int d^4k \exp(i\alpha k^2) = \frac{\pi i}{2}\int_{-\infty}^{\infty} \frac{d\alpha}{\alpha|\alpha|} = 0 \tag{14}$$

[5] J. Schwinger, Phys. Rev. **76**, 790 (1949).

[6] J. McConnell, Nature **164**, 218 (1949).

because of the odd nature of the last integrand; the ambiguity arises in the exchange of orders of integration, indicated by (=). It may then be suggested that this procedure, if generally followed, would eliminate all quadratic divergences from quantum electrodynamics, rendering them not only finite but zero. This rule can be criticized in the same way as above; namely, it depends [like (9a)] on a particular algebraic property of the divergent function, and would almost certainly not be true if a physically correct convergent function stood in its place. That is, a convergent theory would be expected to replace divergences by finite, but nonzero quantities; and if numerical results are obtained with the present theory by setting divergences equal to zero, then in the event of a convergent theory the calculation must be repeated to rediscover the originally divergent terms. Finally, it is clear that the situation with (14) is even less satisfactory than with (9a); for (9a) holds for all divergent functions (but presumably not for convergent functions, if they existed), while (14) must be specially modified to suit each type of divergent function. For example, the prescription (14) for use with $\delta(k^2)$ does not hold for the corresponding Feynman function $1/k^2$; in this case one has

$$\int d^4k\frac{1}{k^2}=-\frac{i}{2}\int d^4k\int_{-\infty}^{\infty}\exp(ia k^2)\frac{\alpha}{|\alpha|}$$

$$(=)-\frac{i}{2}\int_{-\infty}^{\infty}\frac{\alpha}{|\alpha|}d\alpha\int d^4k\exp(ia k^2)=\frac{\pi^2}{2}\int_{-\infty}^{\infty}\frac{d\alpha}{|\alpha|^2} \quad (15)$$

the last expression being quadratically divergent, as expected.

The author wishes to thank Professors Pauli and Heitler for helpful advice and criticism.

PHYSICAL REVIEW VOLUME 81, NUMBER 1 JANUARY 1, 1951

Formative Time Lags of Spark Breakdown in Air in Uniform Fields at Low Overvoltages*

L. H. Fisher and B. Bederson†
Department of Physics, College of Engineering, New York University, University Heights, New York
(Received June 12, 1950)

An attempt has been made to establish the region of validity of the streamer and Townsend mechanisms of spark breakdown in air by measurements of the formative time lag of the breakdown process.

Formative time lags were measured in a uniform field for overvoltages of a few percent down to as close to threshold as possible. Such measurements have been carried out as a function of pressure (atmospheric to a few cm of Hg) and plate separation (0.3 to 1.4 cm). For pressures greater than 200 mm Hg, the formative time lags very close to threshold are of the order of 100 μsec and longer. These times are orders of magnitude longer than those previously reported. For all pressures studied, the time lags decrease as the percent overvoltage (percent o.v.) increases, until at about two percent above threshold, the formative times are of the order of 1 μsec. The time lag *vs* percent o.v. curve is independent of pressure from atmospheric down to 200 mm Hg. At a given percent o.v., the time lags increase linearly with plate separation. Changing the approach voltage from two to four kv below breakdown does not affect the results appreciably. The number of initiating electrons at the cathode has been varied by a factor of about seven, and this again does not materially alter the results.

The long time lags and their dependence on pressure and percent o.v. cannot be explained by secondary emission of electrons from the cathode by positive ion bombardment. The proper explanation is the enhancement of field intensified ionization due to field distortion acting in conjunction with a photoelectric secondary process. The experiment demands an extension of the streamer concept of breakdown, and makes very questionable the role of positive ion bombardment of the cathode in spark breakdown for the pressures and plate separations studied. No transition region for change of streamer to Townsend breakdown was found.

I. INTRODUCTION

THE theory of spark breakdown has undergone radical changes in the last ten years.[1–4] Until 1946 it was commonly believed that in air,[5] the Townsend mechanism of breakdown is valid below values of the product of pressure[6] (p) and plate separation (δ) of 200 mm×cm, and that above this value of $p\delta$, the breakdown proceeds by the streamer mechanism. How-

* Supported by the ONR and the Research Corporation. For preliminary reports of this work, see L. H. Fisher and B. Bederson, Brookhaven Gas Discharge Conference, October, 1948; Phys. Rev. 75, 1324, 1615 (1949); Pittsburgh Gaseous Electronics Conference, November, 1949; Phys. Rev. 78, 331 (1950).

† Now at Massachusetts Institute of Technology, Cambridge, Massachusetts.

[1] L. B. Loeb, *Fundamental Processes of Electrical Discharge Through Gases* (John Wiley and Sons, Inc., New York, 1939).

[2] J. M. Meek, Phys. Rev. 57, 722 (1940).

[3] L. B. Loeb and J. M. Meek, *The Mechanism of the Electric Spark* (Stanford University Press, Stanford University, California, 1941).

[4] H. Raether, Arch. Elektrotech. 34, 49 (1940); Z. Physik 117, 375, 524 (1941); Ergeb. exakt. Naturw. 22, 73 (1949).

[5] Unless otherwise noted, all statements in this paper refer to air.

[6] Raether takes the value of this product as 1000 mm×cm, see reference 4.

ever,[7] on the basis of an analysis of Meek's equation for calculating sparking potentials, it was pointed out that the transition of Townsend to streamer mechanism may depend not on the product $p\delta$ but rather on the values of p and δ separately. It appeared impossible to study the transition by means of sparking potentials. A more hopeful approach seemed to lie in the study of formative time lags of spark breakdown.[8,9]

The formative time lag is defined as the time necessary for a potential difference to be maintained across a gap before it breaks down, provided a primary source of ionization is present. From mobility measurements it is known that at the sparking potential the positive ion requires about 18 μsec to cross a one-centimeter gap at atmospheric pressure. In 1936, Schade[10] measured formative time lags for the glow discharge in neon at very low pressures. He found time lags between 10 μsec and 0.1 sec. Schade could not measure times shorter than 10 μsec with his equipment, a circumstance of great importance in the subsequent theoretical development of the field. But even earlier, and continuing up to the present[11] there had been observed a formative time lag of spark breakdown in air near atmospheric pressure so short that the positive ions formed in the gap could not possibly have had time to cross the gap. These times have been found to be of the order of 0.1 μsec, some observers reporting formative times as short as 10^{-3} μsec. Thus, the Townsend theory was shown to be inadequate at pressures near atmospheric and the streamer theory of Loeb and Meek,[2,3] and Raether[4] was developed for this pressure region. The general impression, with the enormous prestige of the Townsend theory and the confirming work of Schade, was that the Townsend theory applies at small values of $p\delta$ (where the time lags were found to be long), and that the streamer theory applies at large $p\delta$ (where the time lags were found to be short).

The work reported here was undertaken to determine the transition region.

II. APPARATUS AND EXPERIMENTAL PROCEDURE

The ionization chamber used in this study was previously employed by Sanders[12] and Posin[13] for measurements of the first Townsend coefficient in air and nitrogen respectively. The chamber was later modified to its present form[14] when it was used to measure sparking potentials in air. The chamber was originally constructed with the aid of a grant in support of Sanders' research by the National Research Council. A description of the chamber may be found in the original papers.[12,14] The levelling and polishing of the electrodes, the measurement of electrode separation, the admitting and drying of the air, and the measurement of pressure were carried out as described previously.[14] All pressures have been corrected to 22°C.

In order to avoid the measurement of statistical time lags, the cathode was illuminated with ultraviolet light from a dc quartz mercury arc. The light was focused by a quartz lens and passed through a quartz window in the side of the chamber. To determine the photoelectric current i_0 emitted at the cathode, the gas amplified current i was measured with a voltage across the gap of about 10 percent below the sparking potential V_s. An electrometer was used to measure the resulting potential drop V across a resistor R inserted in series with the gap. Thus $V=i_0e^{\alpha\delta}R$, where α is the first Townsend coefficient as given by Sanders.[12] Hence the number of electrons n_0 leaving the cathode per second is given by

$$n_0=V/(1.6\times10^{-19}Re^{\alpha\delta}), \qquad (1)$$

where all electrical quantities are in practical units. The irradiation was adjusted so that at least several electrons were emitted each microsecond, and was large enough in nearly all cases to prevent statistical variations in the time lags yet small enough to prevent distortion of the electric field. The ultraviolet lamp was on continuously during a set of measurements. No elaborate provisions were made for stabilizing the dc voltage for the mercury arc, since the experimental data were found to be very insensitive to small changes in n_0.

In order to determine the formative time lags, an approach voltage $V_0(V_0<V_s)$ is applied across the gap. Then, at some time, an additional voltage V_1 (the pulse voltage) is applied, where $V_0+V_1>V_s$. The time that V_0+V_1 must be maintained before the gap breaks down is the formative time lag.

TABLE I. Resistances in megohms and capacity in microfarads (unless otherwise noted.)

R_1	0.7 Ω	R_{10}	20
R_2	0.1	R_{11}	2000 Ω
R_3	1	R_{12}	25 Ω
R_4	20	R_{13}	1
R_5	1	R_{14}	1
R_6	100	R_{15}	1
R_7	1000 Ω	R_{16}	1
R_8	1000 Ω	R_{17}	1
R_9	3300 Ω		
C_1	0.25	C_7	0.01
C_2	0.25	C_8	0.01
C_3	0.25	C_9	50 mmfd
C_4	0.25	C_{10}	16
C_5	0.25	C_{11}	1000 mmfd
C_6	0.25	C_{12}	1000 mmfd

[7] L. H. Fisher, Phys. Rev. **69**, 530 (1946); L. B. Loeb, Proc. Phys. Soc. (London) **60**, 561 (1948).

[8] For a detailed description of the background leading to this research, see L. H. Fisher, Elec. Eng. **69**, 613 (1950).

[9] A somewhat parallel experimental program was undertaken by B. Gänger, Arch. Elektrotech. **39**, 508 (1949).

[10] R. Schade, Z. Physik **104**, 487 (1937).

[11] See for example P. O. Pedersen, Ann. Physik **71**, 317 (1923); W. Rogowski, Arch. Elektrotech. **20**, 99 (1928); H. J. White, Phys. Rev. **49**, 507 (1936); R. R. Wilson, Phys. Rev. **50**, 1082 (1936); M. Newman, Phys. Rev. **52**, 652 (1937); R. C. Fletcher, Phys. Rev. **76**, 1501 (1949). The results of these and other authors have been summarized in reference 1, p. 441 and by R. Strigel, *Elektrische Stossfestigkeit* (Verlag. Julius Springer, Berlin, 1939).

[12] F. H. Sanders, Phys. Rev. **41**, 667 (1932).

[13] D. Q. Posin, Phys. Rev. **50**, 650 (1936).

[14] L. H. Fisher, Phys. Rev. **72**, 423 (1947).

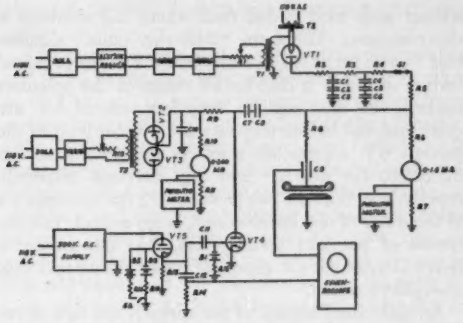

FIG. 1. Circuit diagram. Values of circuit elements are given in Table I.

The circuit diagram of the electronic apparatus is shown in Fig. 1. The values of the circuit elements are given in Table I.

The V_0 power supply is shown in the upper section of the diagram. V_0 is measured by R_6, a bank of five 20-megohm high accuracy wire wound resistors. The absolute value of R_6 is not known, but comparison of sparking potential measurements with those made at Berkeley[14] in the same chamber with precision Taylor resistors indicates that the value of R_6 is known to within one percent. (The present experiment requires relative rather than absolute accuracy.) The ripple in V_0 was measured as 0.1 v at 20 kv. The voltage regulation is satisfactory, the voltage remaining fixed to within several volts over many minutes.

The V_1 power supply (shown in the center section of Fig. 1) is capable of delivering from 0 to 5 kv, with a maximum ripple of about 0.2 v. The trigger circuit is shown in the bottom section of the diagram.

The delay between the application of the sweep trigger pulse and the start of the sweep is about 0.1 μsec. When VT_5 fires, VT_4 also fires forcing the potential of the high voltage electrode of the spark gap to fall by an amount equal to the value of V_1 minus the voltage drop in VT_4 while firing. The voltage across the gap becomes essentially equal to V_0+V_1 in a time determined by the time constant of R_5 and the gap capacity. The capacity of the gap (with the low voltage electrode connected to the chamber) has been measured as 190 mmfd at $\delta=1$ cm. Thus, the time constant for the rise of the pulse (assuming VT_4 breaks down instantaneously) is 0.19 μsec; with $\delta=0.3$ cm (the smallest electrode separation studied) the time constant is 0.4 μsec. Actually, the time of breakdown of VT_4 is of the order of 0.5 μsec, so that the time for the pulse to reach its full value across the electrodes ranges from about 0.6 to 1.0 μsec, depending on electrode separation. Because of the long times observed in the experiment this rise time can be neglected. The time constant of the pulse decay circuit is 0.2 sec. Since the present equipment was not used to measure times longer than 100 μsec, the pulse decay time is unimportant.

A signal from the pulse across the chamber is picked up on the vertical deflection plates of the synchroscope. The delay of several tenths of a microsecond in the breakdown of VT_4 is always sufficient to make the start of the pulse visible. When the spark gap breaks down, a sharp break is seen on the synchroscope trace. Normally, the spark signal has too high an amplitude to be seen. A typical trace is shown in Fig. 2. The dotted part of the signal is due to the spark current and can be seen only when V_s is small.

The synchroscope has four sweeps; by using the various sweeps, times from about 0.5 μsec to 100 μsec can be measured. The sweeps were calibrated against a crystal oscillator.

After the chamber was filled with air, approximately fifty sparks were passed with the V_0 supply in order to season the plates.[8,14] After these sparks passed, V_s assumed a value which at any given time was very definite, but which increased slightly, perhaps by a few tenths of one percent, as the measurements were carried out. This small gradual rise is probably due to the warming up of R_6. At any given time, V_s was reproducible to within 2 or 3 v.

After determination of V_s, a value of V_0 exactly 2 kv below V_s was applied. As V_s changed, V_0 was adjusted so as to maintain V_s-V_0 at 2 kv. (This procedure was justified by the consistent results obtained.) V_1 was then applied, and the time lag was read by visual observation.

The overvoltage ΔV is defined by $\Delta V=V_0+V_1-V_s-V'$, where V' is a correction due to the loss of part of V_1 in the circuit. The percent o.v. is defined as $100\,\Delta V/V_s$.

At a selected value of ΔV and p, about 10 measurements of the formative time lag were made. These measurements constitute a run. Runs were made for various percent o.v. from about two to as close to zero as possible. The entire procedure thus far described constitutes a series, and such series were carried out at various pressures and plate distances. Measurements were then carried out to study the effect of increasing the ultraviolet illumination; the effect of changing V_0 such that V_s-V_0 was 4 kv was also determined.

Before each measurement in a run, both V_0 and V_1 were checked by potentiometer. V_s was determined at the start of a run, several times during the run, and at the end of the run. In calculating the data, it was

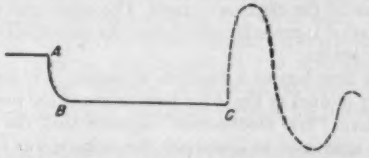

FIG. 2. Typical synchroscope trace. A—Start of pulse; AB—pulse rise; C—beginning of spark; BC—time lag in inches.

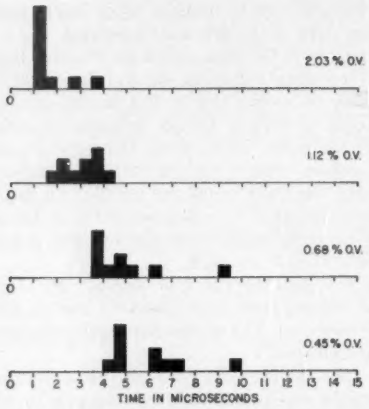

FIG. 3. Typical time lag distribution for four runs. $p = 532$ mm Hg, $\delta = 1$ cm. One square block represents one measurement.

assumed that if V_s increased, it increased linearly with the number of sparks passed.

Correction for the losses in V_1 due to the drop in VT_4 and to capacity division was made by assuming that for a given V_0, the lowest value of V_1 which gives consistent failures corresponds to $\Delta V = 0$. The value of V' thus obtained agrees to within a few percent with the losses as calculated from the known steady-state voltage drop in VT_4 and the measured capacities of the circuit.

III. EXPERIMENTAL RESULTS

All time lags reported represent the average of the individual measurements of a run. The minimum time lag in a run was usually about half of the average time lag, while the maximum time lag in a run was about twice the average time lag. The spread in the time lags in a run increases approximately linearly with the average time lag of the run. Figure 3 shows a typical distribution for four runs at various percent o.v. When the average time lag is of the order of tens of microseconds, the spread is as large as the time lag itself. However, in not a single case was an abnormally short time lag observed. That is, no single measurement gave a time lag which was less than about 40 percent of the average time lag. Thus the measurements represent formative time lags. The fluctuations of the formative time lags cannot be explained by the lack of initiating primary electrons. A part, but not all, of the fluctuations are due to the electronic errors. The other part of the fluctuation is probably inherent in the statistical nature of the spark.

The time lags as a function of percent o.v. for $\delta = 1$ cm are plotted in Fig. 4 for four values of the pressure. The term "low illumination" signifies that the ultraviolet light used to illuminate the cathode was filtered through several thicknesses of copper screen to reduce its intensity. The primary current obtained when the screens were used varied from about 1.3 to about 6 electrons/μsec. The term "2000-volt pulse" signifies that V_0 was set at exactly 2 kv below V_s. The principal feature of Fig. 4 is that for all values of the pressures studied, the time lags for very low percent o.v. are quite long and indeed may increase without limit as the percent o.v. approaches zero. As the percent o.v. is increased, the average time lags decrease extremely rapidly, and at about two percent o.v., the time lags are of the order of one microsecond, in agreement with the results of previous investigators. The measurements below two percent o.v. represent essentially a previously unexplored region.

An additional feature of the curve is the lack of dependence of the time lags on pressure to within the experimental accuracy of the apparatus.[15] For the four values of pressure for which the lags are plotted in Fig. 4, the time lags for a given percent o.v. are approximately the same. If pressures below several hundred mm Hg were included in the graph, the time lags would follow the curve of Fig. 4 until the percent o.v. reaches

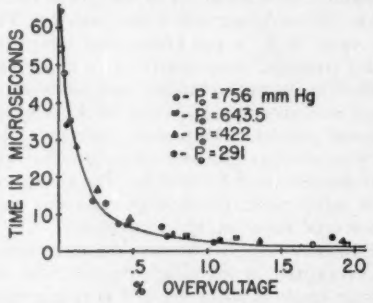

FIG. 4. Time lag *vs* percent o.v., $\delta = 1$ cm. Low illumination, 2000-volt pulse.

a few tenths of one percent. As the percent o.v. is decreased below this value, the time lags do not increase as rapidly as the curve in Fig. 4. The departure from the curve at small percent o.v. becomes more pronounced as the pressure is lowered. These shorter time lags for low pressures at overvoltages of a fraction of a percent may be instrumental. (There is an error in V_1 of several volts and for low pressures this error becomes an appreciable percentage of V_s, while for high pressures this error is only a few hundredths of a percent of V_s.)

Figure 5 contains the data of Fig. 4 with the addition of data for $\delta = 1.4$, 0.6, and 0.3 cm. Here again, there is no dependence of the time lags on pressure. It is seen, however, that the average time lags for a given percent o.v. increase with increasing gap separation. Figure 6 shows three sections of Fig. 5 for 0.05, 0.1, and 0.2 percent o.v. It is seen that for a given percent o.v., the

[15] It is interesting to note that Gänger (reference 9) who studied formative time lags in air in the range from about four to several hundred percent o.v., also found no marked pressure dependence over the range of one atmosphere to 25 mm of Hg.

time lags increase linearly with increasing plate separation.

To determine the possible effects of the illumination and of V_0 on the time lags, additional data were taken at $\delta=1$ cm and at various pressures. First, the copper screens were removed from the path of the ultraviolet light. The primary current then ranged from 18 to 20 electrons/μsec. The time lag curve is identical with that shown in Fig. 4 to within the experimental error. It can thus be stated that for an average primary current of between 3 and 20 electrons/μsec, the time lags are independent of the illumination. Second, the effect of V_0 was investigated at low illumination by changing V_0 from two to four kv below breakdown, and again to within the experimental accuracy, the data are identical with those shown in Fig. 4.

To determine the reproducibility of the measurements, duplicate data were obtained at various pressures for $\delta=1$ cm (low illumination, $V_s-V_0=2$ kv)

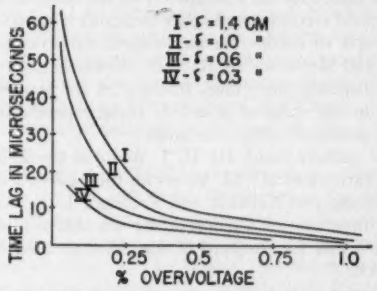

FIG. 5. Time lag *vs* percent o.v. for four values of plate separation. Curves represent average of data taken at all pressures between atmospheric and about 200 mm Hg. Low illumination, 2000-volt pulse.

after the entire experiment was completed. The resulting data again coincide with the results shown in Fig. 4.

There is an error introduced because of the electronic apparatus, such as the ripple in V_0 and V_1, the uncertainty in the magnitude of V_1, and the rise time and decay of V_1. An upper limit of 5 v can be set for the cumulative error of all these factors. Since this error is essentially independent of V_0, the accuracy of the data depends on the pressure. Thus at atmospheric pressure and $\delta=1$ cm, the lower limit of quantitatively reliable data is 0.017 percent o.v., while for a pressure of 20 mm Hg, this lower limit is about 0.3 percent o.v.

IV. DISCUSSION OF RESULTS

The existence of long time lags at low percent o.v. indicates that (for the experimental conditions studied) the motion of positive ions plays an important role in the breakdown process. The fact that the time lags decrease continuously and smoothly as the percent o.v. is increased indicates that the role of the positive ions gradually decreases in importance as the field strength

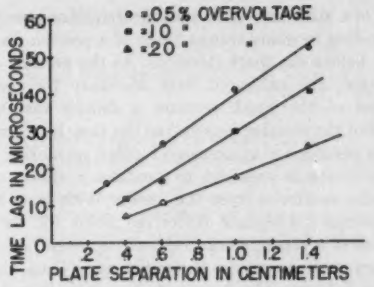

FIG. 6. Time lag *vs* plate separation for three values of percent o.v. Curves represent average of data taken at all pressures between atmospheric and about 200 mm Hg. Low illumination, 2000-volt pulse.

increases, until finally the time lags become so short that the positive ions may be considered to remain stationary throughout the formative time of breakdown.

One can try to account for the results on the basis of the Townsend discharge mechanism, in which secondary electrons are liberated from the cathode by positive ion bombardment. However, for the Townsend mechanism, even at very high overvoltages the time lags should still be in the microsecond region. Since the time lags decrease much more rapidly with increasing percent o.v. than can be explained by the variation of the positive ion velocity, the role of the positive ions is not the emission of secondary electrons from the cathode.

The second possibility for explaining the role of the positive ions in producing the spark is based on the fact that the positive ions aid the spark formation by producing a distorted field in the gap.[16] Electrons produced in the cathode region subsequent to the first avalanche multiply more intensely than in the undistorted field provided α/p increases more rapidly than linearly with E/p, the ratio of field strength to pressure. These newly created electrons may be produced by a secondary mechanism (the most probable ones being photoionization in the gas and photoelectric emission at the cathode) or by the constant primary electron current produced by illumination of the cathode. As the positive ions, originally created in the anode region, move toward the cathode, the field strength in the cathode region increases more and more rapidly with time. Thus, owing to the curvature of the α/p *vs* E/p curve, the quantity $\exp(\int_0^s \alpha dx)$, which represents the number of ion pairs produced by an electron originating near the cathode, increases with time. If conditions in the gap are not satisfactory for the formation of a spark when the first primary electron has crossed the gap, it is possible that as the positive ions created in the first avalanche approach the cathode, subsequent avalanches may produce the charge densities necessary for the develop-

[16] For a discussion of the effect of space charge falsification of the second Townsend coefficient, see Varney, White, Loeb, and Posin, Phys. Rev. 48, 818 (1935).

ment of a streamer. With such a mechanism, times corresponding to many transit times of a positive ion may occur before the spark develops. As the percent o.v. is increased, the enhanced field necessary for the production of the spark requires a shorter distance of travel of the positive ions and so the time lag decreases. As the percent o.v. is increased further, no motion of the positive ions is required to produce a spark, and a streamer emanates from the anode. With even higher overvoltages, adequate distortion fields for the production of a streamer can be built up even before the primary electron crosses the entire gap. Thus, the distortion field provides a smooth transition from formative times long compared to the positive ion transit time to times comparable to the electron transit time.

The method whereby sufficient initiating electrons are supplied to maintain the pre-spark current is now considered further. It can be shown[17] that if, under the assumption of a primary current with no secondary mechanism, the field strength in the cathode region as a function of time is derived for times less than the transit time of a positive ion (assuming no diffusion and a parabolic dependence of α/p on E/p), and if one assumes that a spark occurs when this distortion field reaches a critical value, fair agreement with the experimental data is obtained. However, if such a mechanism is valid, it is necessary to assume that all the primary electrons are emitted from a small region on the cathode. This is unlikely, since the spark rarely occurred at the same cathode spot twice in succession. Furthermore, no dependence of the time lag on illumination was observed, whereas such a mechanism would depend strongly on the magnitude of i_0. Better agreement with the experimental data is obtained by assuming a secondary mechanism involving photo-emission at the cathode by photons produced in the avalanche.[17]

It is believed, therefore, that two processes acting together produce the observed long time lags at low overvoltages. These are (1) a suitable secondary mechanism (most probably photo-emission at the cathode) to maintain and perhaps increase the pre-spark current and (2) space charge distortion due to the large number of positive ions in the gap. It should be noted that such a space charge mechanism can explain the long time lags obtained for low as well as high pressures. Indeed, in view of the fact that even at the lowest pressures studied (several cm of Hg) the time lags for overvoltages of a few percent are as short as those obtained for the higher pressures, it is clear that the classical Townsend theory, hitherto assumed valid for the product $p\delta$ less than several hundred mm Hg, is inadequate.

The search for the transition from the streamer to the Townsend mechanism of spark breakdown has revealed no simple dichotomy in mechanisms as envisaged by Loeb and Meek, and by Raether; the mechanism of the spark depends much more strongly on the percent o.v. than on the value of p and δ. These experiments are being continued with other gases.[18]

The authors thank Dr. H. J. White of the Research Corporation and Mr. M. Menes for their aid in developing the electronic circuit, and Professor L. B. Loeb of the University of California for his interest in the problem and for the loan of the chamber used in the research.

[17] To be published.

[18] G. A. Kachickas and L. H. Fisher, Phys. Rev. **79**, 232 (1950).

On Bound States and Scattering in Positron Theory

W. H. FURRY
*Department of Physics, Harvard University, Cambridge, Massachusetts**
(Received July 18, 1950)

The use of bound-state wave functions in calculations in positron theory is justified by the introduction of a new representation, in a certain sense intermediate between the Heisenberg and interaction representations. In the bound-state representation the definition of a stable vacuum state is possible only for a restricted class of external fields. Some attention is given to the problem of vacuum polarization, and it is shown that a very simple procedure accomplishes the charge renormalization with sufficient accuracy to be of use in certain scattering problems. The application to the scattering of radiation is discussed in some detail, in order to show the relation between the different points of view that may be adopted in problems of the coherent scattering by a bound electron and the "Delbrück scattering" by virtual electron pairs.

I. INTRODUCTION

IN the early days of the Dirac theory of the electron, strong evidence for the importance of the states with negative energy was found in the theory of scattering of radiation. A very significant part of the scattering had to be ascribed to "intermediate states" in which the electron's energy was negative. Such states indeed provided all of the scattering of light of longer wavelengths ($h\nu \ll mc^2$) by free electrons. In the nonrelativistic theory this scattering came from the term $(e^2A^2/2mc^2)\psi$ in the Schrödinger equation and was called by Dirac "true scattering."

Dirac's suggestion that the negative energy states are "filled up," which is the underlying idea of the present positron theory, was seen to contradict the idea of negative energy intermediate states. It was pointed out, however, by Dirac[1] and by Waller[2] that the same result for the scattering could still be obtained. Instead of intermediate states with the electron's energy negative, one has to consider intermediate states in which a pair is present in addition to the original electron, the electron of the pair being in its final state. The transition to the final state of the system then occurs with the annihilation of the positron and the original electron. The contribution to the probability amplitude for scattering is just equal to that calculated earlier by using negative energy intermediate states.

During the development of positron theory stimulated by the experimental discovery of the positron, it was realized that the possibility of intermediate states with a pair present has another connection with scattering. An electromagnetic field alone can scatter light by processes in which electrons appear only virtually, in such intermediate states. The possibility of this kind of coherent scattering by the Coulomb field of a nucleus was pointed out by Delbrück,[3] and results inferred from incomplete calculations by the Born approximation were published by Kemmer and Ludwig[4] and by Achieser and Pomerantchuk.[5]

More recently Halpern and Hall[6] have raised questions about scattering in positron theory and have suggested that, when bound states of the electron are involved, the conclusions of Dirac and Waller require modification. Particularly in the case of coherent scattering by a bound electron, the usual idea of an intermediate state with a pair present cannot be used: the electron of the pair would be created in its final state, but this state is the same as the initial state and is already occupied. On the other hand, the presence of the electron in a bound state will affect the possibility of some of the transitions involved in the Delbrück scattering. The question as to whether the interaction of electrons in an atom has such an effect that Waller's results would have to be modified has been considered by Arnous; in a brief note[7] based on extensive calculations he concludes that such a modification is not required. In the present situation, in which various questions have been raised but only brief notes have been published, it appears that a general discussion of the relations of incoherent and coherent scattering, Delbrück scattering, and vacuum polarization may be of interest.

The writer has been particularly concerned to consider these matters in connection with the general question of bound states in positron theory. It has usually been taken for granted that calculations in positron theory could be based on either free-electron wave functions or on the wave functions of a bound electron in a given field, as might be convenient. Complete but rather involved proofs of the equivalence of the two methods for a number of important cases were given by Furry and Oppenheimer.[8] It afterward[9] ap-

* This paper was written while the writer was a guest at the Institute for Theoretical Physics, Copenhagen, Denmark. I wish to express my appreciation to Professor Niels Bohr and his colleagues for their very kind hospitality, and to the John Simon Guggenheim Memorial Foundation for the grant of a Fellowship.

[1] P. A. M. Dirac, Proc. Roy. Soc. **126A**, 360 (1930).
[2] I. Waller, Z. Physik **61**, 837 (1930).
[3] M. Delbrück, Z. Physik **84**, 144 (1933).
[4] N. Kemmer and G. Ludwig, Helv. Phys. Acta **10**, 182 (1937).
[5] A. Achieser and I. Pomerantchuk, Physik. Z. Sowjetunion **11**, 478 (1937).
[6] O. Halpern and H. Hall, Phys. Rev. **75**, 910, 1322A (1949).
[7] E. Arnous, Phys. Rev. **77**, 149 (1950).
[8] W. H. Furry and J. R. Oppenheimer, Phys. Rev. **45**, 245 (1934).
[9] W. H. Furry and J. R. Oppenheimer Phys. Rev. **45**, 343 (1934).

peared possible to dispense with such proofs by remarking that the simple subtraction procedure of primitive positron theory could have no effect on the validity of the usual transformation theory. It turned out, however, that the simple subtraction procedure was neither so harmless nor so adequate as at first supposed, since it gave rise to difficulties with the Lorentz- and gauge-transformation properties of the theory. Moreover, there are clearly differences between the free-particle and bound-particle methods in regard to the phenomena of vacuum polarization. Thus it seems desirable to reconsider the question of the bound-particle method from the point of view of Schwinger's reformulation of the theory, in which the invariance properties are kept manifest and no subtraction procedure such as those of early positron theories is used. Such a reconsideration not only provides for the usual cases of interest a derivation that is rigorous without being excessively involved; it also provides a framework for the treatment of exceptional cases that may arise.

The section immediately following is, accordingly, devoted to a development of the bound-state method as a modification of Schwinger's method of the interaction representation. This is accomplished by a canonical transformation, and the various formulas of the theory are obtained in the resulting bound-state representation. The third section is concerned with the problem of vacuum polarization as it appears in the bound-state representation, and with charge-renormalization. In its present context the task of renormalization has a difficult aspect and is dealt with in a rather crude and summary fashion; the procedure followed is adequate for the treatment of scattering of light with $h\nu \ll mc^2$ by an electron moving in the field of one or more arbitrary small sources and also for scattering with an arbitrary value of $h\nu$ if the field is a Coulomb field. The last section contains the application to scattering and a discussion of the physical meaning of the result.

II. THE BOUND-STATE REPRESENTATION

We proceed to introduce a representation in which the action on the electrons and positrons of a classically prescribed external field with potentials $A_\mu^{(e)}(x)$ is included in the equations of motion of the wave function ψ and its adjoint $\psi^\dagger$, but the interaction between the particles and the dynamical electromagnetic field is taken into account in the dependence of the Schrödinger functional $\Psi'[\sigma]$ on the space-like surface σ. This is a modified type of interaction representation, differing from the standard interaction representation in that bound states of the one-electron problem, rather than free-particle states, provide the bases for the construction of the wave function operators ψ and $\psi^\dagger$.

The arguments used are for the most part closely analogous to those of Sec. 2 of Schwinger's first paper[10] on quantum electrodynamics, and much detail can, accordingly, be omitted here. The notation is that of Schwinger's paper, which is referred to as I.

The equation of motion and supplementary condition for the Schrödinger functional $\Psi[\sigma]$ of the interaction representation can be taken in the forms

$$ih c\delta\Psi[\sigma]/\delta\sigma(x) = \{-(1/c)j_\mu(x)[A_\mu(x)+A_\mu^{(e)}(x)]\}\Psi[\sigma], \quad (1)$$

$$\left\{[\partial A_\mu(x')/\partial x_\mu']-(1/c)\times\int_\sigma D(x'-x)j_\mu(x)d\sigma_\mu\right\}\Psi[\sigma]=0. \quad (2)$$

It is here conveniently assumed that the classically prescribed potentials $A_\mu^{(e)}$ satisfy

$$\partial A_\mu^{(e)}/\partial x_\mu=0. \quad (3)$$

It has been shown by Schwinger[11] that these equations are related by a canonical transformation to a perhaps more naturally accepted set in which the classically prescribed quantities are the source-currents $j_\mu^{(e)}(x)$ instead of the potentials $A_\mu^{(e)}(x)$.

We now make the canonical transformation

$$\Psi[\sigma]=V[\sigma]\Psi'[\sigma], \quad (4)$$

where $V[\sigma]$ is taken to satisfy the equation

$$ih c\delta V[\sigma]/\delta\sigma(x)=-(1/c)j_\mu(x)A_\mu^{(e)}(x)V[\sigma] \quad (5)$$

and commutes with $A_\mu(x)$. The new equation of motion and supplementary condition are found to be

$$ih c\delta\Psi'[\sigma]/\delta\sigma(x)=-(1/c)\mathbf{j}_\mu(x)A_\mu(x)\Psi'[\sigma], \quad (6)$$

$$\left\{[\partial A_\mu(x')/\partial x_\mu']-(1/c)\times\int_\sigma D(x'-x)\mathbf{j}_\mu(x)d\sigma_\mu\right\}\Psi'[\sigma]=0, \quad (7)$$

where

$$\mathbf{j}_\mu(x)=V^{-1}[\sigma]j_\mu(x)V[\sigma]=-(iec/2)[\psi_\alpha,\psi_\beta^\dagger](\gamma_\mu)_{\beta\alpha} \quad (8)$$

with

$$\psi(x)=V^{-1}[\sigma]\psi(x)V[\sigma],\quad \psi^\dagger(x)=V^{-1}[\sigma]\psi^\dagger(x)V[\sigma]. \quad (9)$$

Here the point x lies on the surface σ.

In obtaining the equations of motion of ψ and $\psi^\dagger$ we shall depart from exact analogy with the procedure of I. It has been widely recognized that the argument of I lacks generality in that it is restricted to cases in which the operator occurring in the equation of motion of the transformation matrix—Eq. (5), or (I, 2.5)—does not contain derivatives. This condition is of course satisfied in the case of I and in our present case, though not in meson theories. It has been pointed out, however, by

[10] J. Schwinger, Phys. Rev. **74**, 1439 (1948), referred to in the text as I.

[11] J. Schwinger, Phys. Rev. **76**, 790 (1949).

Belinfante[12] that, even in the case of **I**, the equation (**I**, 2.9) used in obtaining the new equations of motion of the operators is not of really general validity. We here set up an equation not subject to this objection.

It is proved in **I** that the validity of an equation of the form of (5) (or (**I**, 2.5)) has as a consequence that the transformed quantity

$$\mathbf{F}(x)=V^{-1}[\sigma]F(x)V[\sigma], \tag{10}$$

like the original quantity $F(x)$, depends only on x and not on the particular choice of space-like surface σ containing x; this result actually depends on the absence of derivatives in the operator appearing in Eq. (5) (or (**I**, 2.15)). It follows that derivatives of $\mathbf{F}(x)$ can be calculated from

$$\partial\mathbf{F}/\partial x_\nu=\lim_{a\to 0}(1/a)$$
$$\times\{V^{-1}[(\sigma')_{\nu a}]F(x_\mu+\delta_{\mu\nu}a)V[(\sigma')_{\nu a}]$$
$$-V^{-1}[\sigma]F(x)V[\sigma]\}, \tag{11}$$

where $(\sigma')_{\nu a}$ is the surface obtained by displacing σ rigidly by the amount a in the direction of x_ν. The change in $V[\sigma]$ produced by such a displacement is

$$\delta V[\sigma]=V[(\sigma')_{\nu a}]-V[\sigma]$$
$$=a\int_\sigma\{\delta V[\sigma]/\delta\sigma(x')\}d\sigma_\nu'+O(a^2)$$
$$=(ia/\hbar c^2)\int_\sigma j_\mu(x')A_\mu^{(e)}(x')V[\sigma]d\sigma_\nu'+O(a^2).$$

We find that

$$\partial\mathbf{F}/\partial x_\nu=V^{-1}[\sigma]\Big\{(\partial F/\partial x_\nu)+(i/\hbar c^2)$$
$$\times\int_\sigma[F(x),j_\mu(x')A_\mu(x')]d\sigma_\nu'\Big\}V[\sigma]. \tag{12}$$

This equation differs from an exact analogue of Eq. (**I**, 2.9) essentially by the interchange of the arguments x and x' in the integrand. It is generally valid as a consequence of Eqs. (5) and (10), whereas Eq. (**I**, 2.9) gives incorrect results[12] in some cases in which $F(x)$ contains derivatives.

From Eqs. (9) and (12) and the equations of motion and commutation relations of the operators ψ, $\psi^\dagger$ in the interaction representation, the equations of motion of ψ, $\psi^\dagger$ are readily obtained. The argument resembles in a general way that of Eqs (**I**, 2.13–16) and gives the results

$$\{\gamma_\mu[(\partial/\partial x_\mu)-(ieA_\mu^{(e)}/\hbar c)]+\kappa_0\}\psi=0, \tag{13}$$
$$[(\partial/\partial x_\mu)+(ieA_\mu^{(e)}/\hbar c)]\psi^\dagger\gamma_\mu-\kappa_0\psi^\dagger=0. \tag{14}$$

[12] F. J. Belinfante, Phys. Rev. **76**, 66 (1949), especially footnotes 5 and 23.

The energy-momentum four-vector of the fields ψ and A_μ, taken apart from their mutual interaction, may be written P_μ^B, where the superscript emphasizes that ψ satisfies Eq. (13) for bound electrons. The expression for P_μ^B is formally the same as is given in Eqs. (**I**, 1.55) and (**I**, 1.26), with ψ, $\psi^\dagger$ replacing ψ, $\psi^\dagger$. The property of a time-like component of this vector as a displacement operator is used in the definition of the vacuum state.[13] The complete energy-momentum four-vector, including the effects of interaction, is

$$P_\mu[\sigma]=P_\mu^B+(1/c^2)\int_\sigma \mathbf{j}_\nu A_\mu d\sigma_\nu. \tag{15}$$

In establishing these facts it is convenient to use the transformation from the constant state-functional Φ of the Heisenberg representation to the functional $\Psi'[\sigma]$:

$$\Psi'[\sigma]=R[\sigma]\Phi, \tag{16}$$
$$ihc\delta R[\sigma]/\delta\sigma(x)=-(1/c)\mathbf{j}_\mu A_\mu R[\sigma]. \tag{17}$$

The consistency of these relations with Eqs. (1)–(5) is readily established. The argument leading to Eq. (15) is then similar to that of Eqs. (**I**, 2.45–52); the use of an equation analogous to Eq. (12), rather than to (**I**, 2.9), removes the need for a doubtful step like that in (**I**, 2.51).

The commutation relations of the operators ψ and $\psi^\dagger$ are not the same as those of the operators ψ, $\psi^\dagger$ of the interaction representation. It is through the difference in the commutation relations that the effects of the external potentials $A_\mu^{(e)}$ appear in subsequent calculations. The physical reason for the difference in the commutation relations is that ψ and $\psi^\dagger$ contain the effects of the external field, as shown in Eqs. (13) and (14). Formally, it is seen that the commutation relations of ψ, $\psi^\dagger$ at points x and x' are not the same as those of ψ, $\psi^\dagger$ because in the transformation of Eq. (9) one has in general to use different surfaces σ, σ' for the points x, x': thus, the transformation is not a mere similarity transformation.

In the construction of the commutation relations of ψ, $\psi^\dagger$ it is convenient to start with the special case in which x and x' are on the same surface σ, so that the transformation is just one of similarity. Here and in following calculations we need consider only plane surfaces σ, with $x_4=ict=$ constant. For $t=t'$, then, the relations for ψ, $\psi^\dagger$ are the same as those for ψ, $\psi^\dagger$, and we have

$$\{\psi_\alpha(x),\psi_\beta^*(x')\}=\delta_{\alpha\beta}\delta(\mathbf{r}-\mathbf{r}'),\qquad t=t', \tag{18}$$
$$\{\psi_\alpha(x),\psi_\beta(x')\}=\{\psi_\alpha^*(x),\psi_\beta^*(x')\}=0,\quad t=t'. \tag{19}$$

The operator ψ for time $t=0$ can be expanded in terms of any complete orthonormal set of functions of the position $\mathbf{r}$; for convenience we use the notation of the dis-

[13] J. Schwinger, Phys. Rev. **75**, 651 (1949). Here particularly Sec. 1. Referred to in the text as **II**.

crete case:

$$\psi_\alpha(\mathbf{r};0)=\sum_{(s)} a_{(s)}\psi_{(s)\alpha}(\mathbf{r});$$
$$\psi_\alpha^*(\mathbf{r};0)=\sum_{(s)} a_{(s)}^*\psi_{(s)\alpha}^*(\mathbf{r}). \quad (20)$$

The coefficients $a_{(s)}$, $a_{(s)}^*$ are operators; from Eqs. (18)–(20) it follows that

$$\{a_{(r)}, a_{(s)}^*\}=\delta_{(r)(s)}; \quad \{a_{(r)}, a_{(s)}\}=\{a_{(r)}^*, a_{(s)}^*\}=0. \quad (21)$$

Since $a_{(s)}$, $a_{(s)}^*$ are independent of $\mathbf{r}$, it is natural to take them independent of t also; we then set

$$\psi_\alpha(\mathbf{r};t)=\sum_{(s)} a_{(s)}\psi_{(s)\alpha}(\mathbf{r};t);$$
$$\psi_\alpha^*(\mathbf{r};t)=\sum_{(s)} a_{(s)}^*\psi_{(s)\alpha}^*(\mathbf{r};t) \quad (22)$$

with the time-dependences of $\psi_{(s)}$ and $\psi_{(s)}^*=\psi_{(s)}^\dagger\gamma_4$ given by Eqs. (13) and (14). From these equations it follows that

$$(\partial/\partial x_\nu)\psi_{(r)}^\dagger\gamma_\nu\psi_{(s)}=0, \quad (23)$$

and thus by the usual argument that the orthonormal property of the functions $\psi_{(s)}$ persists in time; accordingly, the use of $a_{(s)}$, $a_{(s)}^*$ independent of time is consistent with the general validity of Eqs. (18) and (19). Then from Eqs. (21) and (22) we have in general

$$\{\psi_\alpha(x), \psi_\beta^\dagger(x')\}=\sum_{(s)} \psi_{(s)\alpha}(x)\psi_{(s)\beta}^\dagger(x'), \quad (24)$$

$$\{\psi_\alpha(x), \psi_\beta(x')\}=\{\psi_\alpha^\dagger(x), \psi_\beta^\dagger(x')\}=0. \quad (25)$$

The sum appearing on the right-hand side of Eq. (24) is a generalization of Schwinger's function $S(x-x')$, as changed by the effect of the external field $A_\mu^{(s)}$:

$$\sum_{(s)} \psi_{(s)\alpha}(x)\psi_{(s)\beta}^\dagger(x') \rightarrow -iS_{\alpha\beta}(x-x') \text{ for } A_\mu^{(s)}\rightarrow 0. \quad (26)$$

The sum also plays the same role as the function $S(x-x')$ in solving the boundary-value problem of the equations of motion; in analogy to Eqs. (I, 2.23) and (I, 2.27) we have

$$\psi(\mathbf{r};t)=\int \sum_{(s)} \psi_{(s)}(\mathbf{r};t)\psi_{(s)}^\dagger(\mathbf{r}';t')\gamma_4\psi(\mathbf{r}';t')d\nu', \quad (27)$$

$$\psi^\dagger(\mathbf{r};t)=\int d\nu'\psi^\dagger(\mathbf{r}';t')\gamma_4\sum_{(s)} \psi_{(s)}(\mathbf{r}';t')\psi_{(s)}^\dagger(\mathbf{r};t). \quad (28)$$

In the bound-state representation a gauge-transformation may affect either the external potentials $A_\mu^{(s)}$, the dynamical potentials A_μ, or both. The transformation equations are

$$A_\mu^{(s)}\rightarrow A_\mu^{(s)}-\partial\Lambda^{(s)}/\partial x_\mu,$$
$$\psi\rightarrow\exp(-ie\Lambda^{(s)}/\hbar c)\psi,$$
$$\psi^\dagger\rightarrow\exp(ie\Lambda^{(s)}/\hbar c)\psi^\dagger \quad (29)$$

and

$$A_\mu\rightarrow A_\mu-\partial\Lambda/\partial x_\mu, \quad \Psi'[\sigma]\rightarrow e^{-iG[\sigma]}\Psi'[\sigma] \quad (30)$$

with

$$G[\sigma]=(1/\hbar c^2)\int_\sigma \mathbf{j}_\mu(x)\Lambda(x)d\sigma_\mu. \quad (31)$$

The proof of invariance under the latter transformation is entirely analogous to Schwinger's discussion, Eqs. (I, 2.39–43). The essential lemma, Eq. (I, 2.34), follows readily, for the sufficient case of plane surfaces, from Eqs. (24)–(28).

Charge-conjugate wave functions ψ', $\psi^{\dagger\prime}$ can be defined by the usual relations

$$\psi'(x)=C\psi^\dagger(x), \quad \psi^{\dagger\prime}(x)=C^{-1}\psi(x), \quad (32)$$

with

$$C^{-1}\gamma_\mu C=-\gamma_\mu^T. \quad (33)$$

The matrix C commutes with $V[\sigma]$, so that the relation to the operators of the interaction representation is

$$\psi'=V^{-1}[\sigma]\psi' V[\sigma], \quad \psi^{\dagger\prime}=V^{-1}[\sigma]\psi^{\dagger\prime}V[\sigma]. \quad (34)$$

The equations of motion of the charge-conjugate operators differ from Eqs. (13) and (14) by a change of sign of the factor e, and their commutation relations differ from those of the original operators in a corresponding way. The lack of absolute symmetry between ψ and ψ' brought about by the external field has physical consequences, among them vacuum polarization (following section).

The definition of the vacuum state given by Schwinger in his second paper[13] on quantum electrodynamics can reasonably be used in the bound-state representation only for certain kinds of external fields. Already from the possibility of gauge transformations of the type (29), which do not exist in the interaction representation, it is seen that the separation of the operators ψ and $\psi^\dagger$ into parts,

$$\psi=\psi^{(+)}+\psi^{(-)}, \quad \psi^\dagger=\psi^{\dagger(+)}+\psi^{\dagger(-)}, \quad (35)$$

containing respectively the positive-frequency and negative-frequency parts of the time-dependences, can have no absolute significance. A natural physical meaning can be given to this separation only if there is a gap in the spectrum of the time dependences of the operators. Such a gap can be expected to have width about 2 mc², in the energy scale. As a reasonable choice[14] of the gauge $\Lambda^{(s)}$ we take such potentials $A_\mu^{(s)}$ that the location of the gap is about the same for $\psi^\dagger$ as for ψ, whereupon it can be expected that zero frequency falls about the middle of the gap. The vacuum state with Schrödinger functional Ψ_0' is then defined by

$$\psi^{(+)}(x)\Psi_0'=0, \quad \psi^{\dagger(+)}(x)\Psi_0'=0. \quad (36)$$

The energy of the vacuum state is then lower than that of any other state by about the amount mc². The fact that the definition of a stable vacuum state is possible for only a restricted class of fields was pointed out in the early days of positron theory.[15]

[14] Of course, this is by no means a unique specification of the gauge. Moreover, while convenient in that it makes possible the definition of the vacuum state as that of minimum energy, the restriction is not necessary: for example, the fact that the addition of a large constant to the scalar potential puts a premium on states having large net charge has a natural and clear physical meaning.

[15] Reference 8, p. 255.

We must from now on restrict our attention to fields for which this procedure is available. Having chosen some suitable gauge for any particular given field, we can choose the basic sets of functions $\psi_{(s)}$ so that the sequence of labels (s) can be divided into two separate lists, written s and σ, such that

$$\psi^{(+)}=\sum_s a_s\psi_s; \quad \psi^{(-)}=\sum_\sigma a_\sigma\psi_\sigma. \tag{37}$$

It then follows that

$$\psi^{\dagger(+)}=\sum_\sigma a_\sigma^*\psi_\sigma^\dagger; \quad \psi^{\dagger(-)}=\sum_s a_s^*\psi_s^\dagger. \tag{38}$$

The states s are positive energy states of the electron in the given field; the states σ, negative energy states.

The way in which the interpretation of the operators $a_{(s)}$, $a_{(s)}^*$ presents itself naturally in the bound-state representation is shown in the following section, in connection with the evaluation of vacuum expectation values.

III. POLARIZATION OF THE VACUUM: RENORMALIZATION

The current four-vector, Eq. (8), can be written in either of two equivalent forms:

$$\begin{aligned}\mathbf{j}_\mu&=-(iec/2)[\psi_\alpha,\psi_\beta^\dagger](\gamma_\mu)_{\beta\alpha}\\&=(iec/2)[\psi_\alpha',\psi_\beta^{\dagger\prime}](\gamma_\mu)_{\beta\alpha}.\end{aligned} \tag{39}$$

Because of the differences in the behavior of ψ and ψ', it does not follow, as it did in the interaction representation (Eq. (II, 1.72))[16] that the vacuum expectation value $\langle\mathbf{j}_\mu(x)\rangle_0$ must vanish; it can only be concluded that, if an expansion in powers of e can be used, the series for $\langle\mathbf{j}_\mu(x)\rangle_0$ contains only terms with the even powers.

The formal evaluation of $\langle\mathbf{j}_\mu(x)\rangle_0$ in terms of the definition of the vacuum state, Eq. (36), involves just the algebraic steps used by Schwinger, Eqs. (II, 1.66–67). The result is

$$\langle\mathbf{j}_\mu(x)\rangle_0=-(iec/2)\langle\{[\psi_\alpha^{(+)}-\psi_\alpha^{(-)}),\psi_\beta^\dagger]\}_0(\gamma_\mu)_{\beta\alpha}. \tag{40}$$

Because the condition (36) holds for every point x, we can conclude from Eqs. (36)–(38) that

$$a_s\Psi_0'=0, \quad a_\sigma^*\Psi_0'=0. \tag{41}$$

From this and Eq. (21) we find that

$$\begin{aligned}&\langle a_{(r)}^*a_{(s)}\rangle_0=\langle a_{(s)}a_{(r)}^*\rangle_0=0, \quad (r)\neq(s),\\&\langle a_s^*a_s\rangle_0=\langle a_\sigma a_\sigma^*\rangle_0=0,\\&\langle a_sa_s^*\rangle_0=\langle a_\sigma^*a_\sigma\rangle_0=1.\end{aligned} \tag{42}$$

If the operators $a_{(s)}$, $a_{(s)}^*$ are given their original interpretation[17] for a many-electron theory, these formulas (42) correspond to the original Dirac suggestion that the vacuum has all negative energy states filled. It is to be noted, however, that Eq. (42) follows, without any special assumption, simply from the definition of the vacuum state as the state which in a definite physical sense has minimum energy, and that the formulas hold in the bound-state representation as well as in the free-particle or interaction representation.

States $a_s^*\Psi_0'$ and $a_\sigma\Psi_0'$ have energies higher than that of the state Ψ_0' by at least about mc^2; on the other hand $a_sa_s^*\Psi_0'=a_\sigma^*a_\sigma\Psi_0'=\Psi_0'$. The interpretation of these facts is that the operators a_s^* and a_σ refer to the creation of an electron and a positron, respectively, while a_s and a_σ^* are the corresponding destruction operators. That the effect of these operators on the charge agrees with this interpretation follows from arguments of a familiar kind, given for instance by Schwinger in Eqs. (II, 3.54–55).[18] The construction of corresponding arguments in the bound-state representation, by the use of Eqs. (24)–(28), presents no difficulty.

From Eqs. (40) and (42) we find that

$$\langle\mathbf{j}_\mu(x)\rangle_0=-(iec/2)\{\textstyle\sum_s\psi_s^\dagger\gamma_\mu\psi_s-\sum_\sigma\psi_\sigma^\dagger\gamma_\mu\psi_\sigma\}. \tag{43}$$

These sums are divergent. The possibility of obtaining a definite result by making active use of the postulate that the theory is gauge invariant is illustrated in the work of Schwinger.[19] Another way to make the result definite is to use a program of modifying the formulas and then obtaining the value in a suitable limit, a procedure known as "regularization."[20] The result contains in order e^2 a logarithmically divergent but gauge-invariant term, whose removal must be accomplished by charge-renormalization; that is, by its being regarded as physically indistinguishable from the classically prescribed current $j_\mu^{(s)}=-c\partial^2A_\mu^{(s)}/\partial x_\nu^2$. We shall not attempt a generalization of these methods for application to Eq. (43), but shall only show, in order e^2, how the use of the Born approximation to evaluate $\langle\mathbf{j}_\mu(x)\rangle_0$ leads to the results already known in the interaction representation. We shall then concern ourselves with the problem of effecting the renormalization.

Before proceeding to show the calculation in Born approximation we must remark on the actual content of Eq. (43) and its relation to other quantities that have been calculated. To the order e^2, the expression given here contains the whole of the vacuum polarization. In higher orders part of the polarization comes from interaction between the electron-positron field and the dynamical field A_μ. This part is not included in the present expression; it has been studied in the approximation e^4 by Jost and Luttinger,[21] who find that there is also in this order a logarithmically divergent gauge-invariant term that requires removal by charge-renormalization. The higher order contributions that are included in Eq. (43) are non-linear in $A_\mu^{(s)}$, being of orders $e^4(A_\mu^{(s)})^3$, $e^6(A_\mu^{(s)})^5$, $\cdots$. These terms have been

[16] The symbol II is used to refer to Schwinger's second paper, reference 13.

[17] P. Jordan and E. Wigner, Z. Phys. 47, 631 (1928); W. Pauli, *Handb. d. Physik* 24/1, p. 199.

[18] Through a misprint Eq. (II, 3.54) has in the integrand a square bracket which should be a curly bracket (anticommutator).

[19] Reference 16, Sec. 2; also reference 11, Appendix.

[20] W. Pauli and F. Villars, Rev. Modern Phys. 21, 434 (1949).

[21] R. Jost and J. M. Luttinger, Helv. Phys. Acta 23, 201 (1950).

studied by Källén,[22] who finds that in order $e^4(A_\mu^{(e)})^3$ there are divergences completely removable by "realistic regularization," and that in higher orders there are no divergences. It should be remarked that Eq. (43) is a valid expression for this part of the vacuum polarization also in cases in which the Born approximation is not admissible, although the actual evaluation without use of the Born approximation could be expected to be very laborious.

In order to apply the Born approximation to the evaluation of $\langle \mathbf{j}_\mu(x)\rangle_0$ as given in Eq. (43), we expand $\psi_{(e)}$ and $\psi_{(e)}^\dagger$ in powers of the charge e:

$$\begin{aligned}\psi_{(e)}&=\psi_{(e)}+e\psi_e^{(1)}+\cdots,\\ \psi_{(e)}^\dagger&=\psi_{(e)}^\dagger+e\psi_e^{\dagger(1)}+\cdots.\end{aligned}\tag{44}$$

The term of order e in $\langle \mathbf{j}_\mu(x)\rangle_0$ is obtained by replacing $\psi_{(e)}$, $\psi_{(e)}^\dagger$ by the free-particle functions $\psi_{(e)}$, $\psi_{(e)}^\dagger$, and this term vanishes, as shown by Schwinger in Eqs. (II, 1.72–73). The term of order e^2 is

$$\begin{aligned}\langle \mathbf{j}_\mu(x)\rangle_0^{(2)}=-(ie^2c/2)\{&\textstyle\sum_s(\psi_s^\dagger\gamma_\mu\psi_s^{(1)}+\psi_s^{\dagger(1)}\gamma_\mu\psi_s)\\ &-\textstyle\sum_\sigma(\psi_\sigma^\dagger\gamma_\mu\psi_\sigma^{(1)}+\psi_\sigma^{\dagger(1)}\gamma_\mu\psi_\sigma)\}.\end{aligned}\tag{45}$$

The function $\psi_{(e)}^{(1)}$ is the solution of the inhomogeneous equation

$$[(\gamma_\mu\partial/\partial x_\mu)+\kappa_0]\psi_{(e)}^{(1)}=(i/\hbar c)\gamma_\nu A_\nu^{(e)}\psi_{(e)}\tag{46}$$

given by the expression

$$\begin{aligned}\psi_{(e)}^{(1)}(x)=&-(i/\hbar c)\\ &\times\int\bar S(x-x')\gamma_\nu A_\nu^{(e)}(x')\psi_{(e)}(x')d\omega',\end{aligned}\tag{47}$$

where the function[23]

$$\bar S(x-x')=[(\gamma_\mu\partial/\partial x_\mu)-\kappa_0]\bar\Delta(x-x')\tag{48}$$

satisfies the condition (Eq. (II, A.6)),

$$[(\gamma_\mu\partial/\partial x_\mu)+\kappa_0]\bar S(x)=-\delta(x_1)\delta(x_2)\delta(x_3)\delta(x_4).\tag{49}$$

On substituting Eq. (47) and the corresponding formula for $\psi_{(e)}^{\dagger(1)}=\psi_{(e)}^{(1)*}\gamma_4$ into Eq. (45), we see that the result depends on a sum whose value is

$$\textstyle\sum_s\psi_s(x)\psi_s^\dagger(x')-\sum_\sigma\psi_\sigma(x)\psi_\sigma^\dagger(x')=-S^{(1)}(x-x').\tag{50}$$

That this sum of products of *free-particle* functions has the value given can be seen by comparing Eqs. (39) and (43) with Eq. (II, 1.68). The value of $\langle \mathbf{j}_\mu(x)\rangle_0^{(2)}$ is found to be

$$\begin{aligned}\langle \mathbf{j}_\mu(x)\rangle_0^{(2)}=(e^2/\hbar)\int d\omega' Tr\{&S^{(1)}(x'-x)\gamma_\mu\bar S(x-x')\gamma_\nu\\ &+\bar S(x'-x)\gamma_\mu S^{(1)}(x-x')\gamma_\nu\}A_\nu^{(e)}(x').\end{aligned}\tag{51}$$

This is identical with Schwinger's expression given by Eqs. (II, 2.19) and (II, 2.10).

The expression (43) for $\langle \mathbf{j}_\mu(x)\rangle_0$ contains entangled in it the logarithmically infinite part, proportional to $j_\mu^{(e)}(x)$, which must be removed by renormalization, and other parts, finite and not just proportional to $j_\mu^{(e)}(x)$, which are regarded as having physical meaning. The task of disentangling these parts is a complicated one, and is scarcely to be undertaken at all except with the use of the Born approximation. We shall be content here to point out that for some purposes, to be illustrated by the application to scattering, the disentangling is not required.

The structure of $\langle \mathbf{j}_\mu\rangle_0$ can be symbolized by writing

$$\langle \mathbf{j}_\mu\rangle_0=J_\mu^{\log}+J_\mu',\tag{52}$$

where $J_\mu^{\log}$ is to be removed by renormalization. For any field from finite sources in the finite region of space the remaining part J_μ' satisfies

$$\int J_\mu' dv=0.\tag{53}$$

For a point source, or a source of dimensions small compared with $\hbar/mc$ the extent of the distribution of J_μ' is of the order of $\hbar/mc$. If there are a number of such sources separated from each other by distances large compared with $\hbar/mc$, Eq. (53) holds also with the integral extended over a suitable region around any single source. The emission, absorption, and scattering of radiation depend on quantities

$$\int \mathbf{j}_\mu e^{i\mathbf{k}\cdot\mathbf{r}}dv.\tag{54}$$

If $A_\mu^{(e)}$ is due to well-separated small sources, the contribution from J_μ' to such quantities can be calculated from a sum of integrals over regions of extent about $\hbar/mc$ around the separate sources. For light of long wavelength, $|\mathbf{k}|\ll mc/\hbar$, the exponential factor in each integral is essentially constant; thus by Eq. (53) all the integrals vanish, and J_μ' does not contribute to the scattering. In this case the renormalization is accomplished with sufficient accuracy by simply replacing $\mathbf{j}_\mu(x)$ with $\mathbf{j}_\mu(x)-\langle \mathbf{j}_\mu(x)\rangle_0$. For light of shorter wavelength the contribution of J_μ' to integrals such as Eq. (54) may not be negligible, and may have to be taken into account as a part of the Delbrück scattering.

For the case of the Coulomb field of a stationary charge, and indeed for any *truly static*[24] spherically symmetrical electric field, the contribution of J_μ' is zero for all wavelengths. Because of the transverse character of light waves, only the space-components of j_μ need be considered. By symmetry the direction of the vector $\mathbf{J}'$ is radial. In a static field the functions $\psi_{(e)}$ have strictly harmonic time-dependences, so that $\mathbf{J}'$ is constant in time. It is then zero, since a nonvanishing value would

[22] G. Källén, Helv. Phys. Acta **22**, 637 (1949).

[23] The choice of this particular solution of Eq. (49), which has a certain symmetry as between past and future, corresponds to the fact that the field $A_\mu^{(e)}$, belonging to the class specified at the end of Sec. II, is incapable of producing real pairs: see reference 13, pp. 659–660. A calculation like the present one, but approached from a different point of view, has just been published by G. Källén, Arkiv för Fysik **2**, 187 (1950).

[24] A field produced by screening is, of course, static only to a certain approximation.

mean nonconservation of charge. (J_4', on the other hand, is not zero.) Thus, for the Coulomb field the procedure we shall use gives correct results for the scattering at all frequencies, and there is no Delbrück scattering apart from that calculated in the next section.

According to Eqs. (39) and (22) the original expression for the current is

$$\mathbf{j}_\mu(x)=(iec/2)$$
$$\times\sum_{(r)(s)}\psi_{(s)}^\dagger(x)\gamma_\mu\psi_{(r)}^\dagger(x)(a_{(s)}^*a_{(r)}-a_{(r)}a_{(s)}^*). \quad (55)$$

From this and Eq. (43) we get as the expression for the approximately renormalized current to be used in the calculations of the next section:

$$\mathbf{j}_\mu(x)-\langle\mathbf{j}_\mu(x)\rangle_0=(iec/2)\sum_{(r)(s)}\psi_{(s)}^\dagger(x)\gamma_\mu\psi_{(r)}(x)$$
$$\times[a_{(s)}^*a_{(r)}-a_{(r)}a_{(s)}^*+\delta_{(r)(s)+}-\delta_{(r)(s)-}]. \quad (56)$$

Here $\delta_{(r)(s)+}$ equals 1 or 0, according as (r) and (s) do or do not take identical values belonging to the list s of positive energy states, and $\delta_{(r)(s)-}$ has an analogous definition. Then by Eq. (21)

$$\mathbf{j}_\mu(x)-\langle\mathbf{j}_\mu(x)\rangle_0$$
$$=iec\sum_{(r)(s)}\psi_{(s)}^\dagger(x)\gamma_\mu\psi_{(r)}^\dagger(x)(a_{(s)}^*a_{(r)}-\delta_{(r)(s)-}). \quad (57)$$

In calculating it is convenient to write the factor $(a_{(s)}^*a_{(r)}-\delta_{(r)(s)-})$ as a single term. The way of doing this depends on whether (s) takes a positive-energy value s or a negative-energy value σ, and also on whether (r) takes a value r or a value ρ. The four possibilities are

$$a_{(s)}^*a_{(r)}-\delta_{(r)(s)-}=\begin{cases}a_s^*a_r\\ a_s^*a_\rho\\ a_\sigma^*a_r\\ -a_\rho a_\sigma^*\end{cases}. \quad (58)$$

The expressions written in Eqs. (57) and (58) are formally the same as those obtained by the simple subtraction procedure of primitive positron theory.[25] The meaning of these expressions and the status assigned to them are, however, entirely different from what they were in the earlier version. In primitive positron theory such formulas were to be applied only to free-particle states, or states defined in an "even" field in the sense of Schrödinger;[26] here they are written for particle states defined in any field that permits a reasonable definition of the vacuum state of the system. In primitive positron theory the formulas were obtained by a postulated subtraction procedure, and were originally believed to be definitively correct; the introduction of more elaborate subtraction procedures[27] removed some inconsistencies, but genuine consistency and adequacy were not achieved by the subtraction methods.[28] In the present argument the expressions in question are obtained as an approximation to the results of a physically reasonable process of renormalization, and there are strong reasons[29] to believe in the general consistency of the method. The expressions given represent only a crude way of estimating the results of renormalization; but we have been able to designate a class of cases for which they should be adequate, and a definite theoretical basis exists for improving them.

[25] For example, reference 8, pp. 250–251.
[26] E. Schrödinger, Berl. Ber., Jahrgang 1931, p. 63; W. Pauli, *Handb. d. Physik* 24/1, p. 229.
[27] W. Heisenberg, Z. Phys. 90, 209 (1934).

IV. APPLICATION TO SCATTERING

When the formula (57) is used as an approximately correct expression for the renormalized current, the second-order term of the S-matrix[30] is written in the form

$$(-ie/\hbar)^2\int_{-\infty}^{\infty}dt\int_{-\infty}^{t}dt'\int\int dvdv'$$
$$\times\sum_{(m)(n)(r)(s)}\psi_{(n)}^\dagger(x)\gamma_\kappa\psi_{(r)}(x)A_\kappa(x)$$
$$\cdot\psi_{(s)}^\dagger(x')\gamma_\lambda\psi_{(m)}(x')A_\lambda(x')$$
$$\cdot\{a_{(n)}^*a_{(r)}-\delta_{(n)(r)-}\}\{a_{(s)}^*a_{(m)}-\delta_{(s)(m)-}\}. \quad (59)$$

The quantities $a_{(l)}^*$, $a_{(l)}$ are operators affecting the occupation numbers of the various bound states of electrons and positrons, and the potentials A_μ contain linear combinations of operators affecting the number of photons.[31] The expression (59) thus comprises a list of various second-order processes of interaction between the particles and radiation, and indicates how the corresponding probability amplitudes are to be calculated. The calculation for any particular kind of transition is to be performed according to the ordinary method of Dirac for time-dependent perturbations;[32] when the customary use is made of states having harmonic time-dependence, the integration over dt secures conservation of energy and the integration over dt' leads to the usual expression of second-order perturbation theory, with an energy-difference in the denominator.

The expression (59) contains not only an account of scattering, double emission, and double absorption of radiation, but also of the interaction of particles, and of self-energies and the electromagnetic shift of energy-levels. It is not to be used as a basis for calculating these latter effects, however; the approximate way in which the effects of charge-renormalization have been taken into account is adapted primarily only to the problems of scattering, emission and absorption. This type of problem is obtained by choosing in the operators $A_\kappa(x)$

[28] R. Serber, Phys. Rev. 49, 545 (1936).
[29] F. J. Dyson, Phys. Rev. 75, 1736 (1949).
[30] F. J. Dyson, Phys. Rev. 75, 486 (1949), especially p. 489.
[31] G. Wentzel, *Quantum Theory of Fields* (Interscience Publishers, Inc., New York, 1949), Chapter IV.
[32] P. A. M. Dirac, *Principles of Quantum Mechanics* (Oxford University Press, 1947), third edition, pp. 172–180.

and $A_\lambda(x')$ terms corresponding to the emission and/or absorption of two distinct photons.

In order to list the various processes it is convenient to separate the expression (59) into its two-particle, one-particle, and vacuum parts. To do this we need consider only the last two factors of the expression, and for each the transcription shown in Eq. (58) can be used. There are then $4\times4=16$ kinds of terms to be considered. The two-particle part is obtained by arranging the four factors so that all creation operators are to the left, and annihilation operators to the right: this assures that the process involves only transitions of existing particles and/or creation of new particles. One-particle parts contain only two factors a and/or a^*, with creation operators to the left, annihilation to the right. Such parts describe two successive transitions of an existing particle, or else two-step pair production or annihilation; the subscripts on a δ-symbol indicate the intermediate state of a particle. Vacuum parts contain no factors a or a^*, and involve particles only virtually; subscripts on δ-symbols indicate the states of particles appearing in the intermediate state of the system.

It suffices to illustrate the process of separation for the kind of term containing the greatest variety of parts:

$$a_\nu^*a_\tau a_\sigma^*a_\mu=a_\sigma^*a_\nu^*a_\tau a_\mu+a_\nu^*a_\mu\delta_{\tau\sigma}$$
$$=a_\sigma^*a_\mu a_\nu^*a_\tau-a_\sigma^*a_\tau\delta_{\mu\nu}-a_\mu a_\nu^*\delta_{\tau\sigma}+\delta_{\mu\nu}\delta_{\tau\sigma} \quad (60)$$

(a_σ^* and a_μ are operators of creation).

The two-particle parts need not be listed in detail. They describe processes of transition of two distinct existing particles, double pair production, double pair annihilation, pair production or annihilation accompanied by transition of a particle not belonging to the pair, or destruction of a pair and creation of another pair.

The one-particle parts comprise the following:

Two-step pair production: $a_n^*a_\mu\delta_{\tau\sigma}+a_\mu a_\sigma^*\delta_{\mu\nu}$, (61)

Two-step pair annihilation: $a_\nu^*a_m\delta_{\tau\sigma}+a_\tau a_\sigma^*\delta_{\mu\nu}$, (62)

Scattering by an electron: $a_n^*a_m\delta_{\tau\sigma}-a_\sigma^*a_\tau\delta_{\mu\nu}$, (63)

Scattering by a positron: $a_\mu a_\sigma^*\delta_{\mu\nu}-a_\mu a_\nu^*\delta_{\tau\sigma}$. (64)

The single vacuum term is:

Delbrück scattering: $\delta_{\mu\nu}\delta_{\tau\sigma}$. (65)

The first term of the expression (63) gives to the probability amplitude for scattering a contribution that corresponds to the picture of the electron passing through the intermediate state $s=r$. In the original Dirac theory of the electron, with negative energy intermediate states allowed, the other term would be $a_n^*a_m\delta_{\rho\sigma}$. The positron-theoretic expression (63) contains instead the term $-a_\sigma^*a_\tau\delta_{\mu\nu}$, indicating a process in which the intermediate state contains a pair. Since the subscripts are mere summation indices, and since we have free choice as to which factor $A_\kappa(x)$, $A_\lambda(x')$ corresponds to which photon—the sum over both choices being taken at the end—the result of the space-integrations in Eq. (59) is the same, apart from sign, for the two theories. The difference in sign visible in the second term of Eq. (63) can be said, in the language of Dirac's suggestion of "filled-up" states, to come from the exchange of the original electron with an electron from the negative energy states. When the time integrations are performed, a second difference of sign is found: in the "filled-state" picture of the positron theory, the transition from a negative-energy state to the final state of the electron occurs first instead of last, and thus the difference of energies of initial and intermediate states has the opposite sign; this energy difference appears in the denominator because of the integration over dt'. Thus, there are in all two changes of sign that cancel each other, and the result of positron theory is identical with that of one-electron theory.[33]

The second term of the expression (63) contains no reference to the non-identity or identity of the states r and s; it contributes just as well to a process in which the electron remains in the state $r=s$ as to one in which the electron changes from state r to another state s. Thus, this expression gives in the positron theory the same result for the scattering as would be found in a one-electron theory, independently of whether the scattering is coherent or incoherent.

It is clear then that the use of the expression (63) leads to a calculation of the scattering of an electron in which the exclusion principle is ignored in intermediate states. The same is true of the use of Eq. (65) to calculate the Delbrück scattering; the expression gives always the same coherent scattering by creation and destruction of all possible virtual pairs, making no reference to whether any states are actually occupied or not.

On the other hand it is certainly correct also to make any calculation of scattering according to the concrete picture of the Dirac method of variation of parameters, considering just the changes in time of the probability amplitudes of different states of the system; indeed the expression (59), as it stands, simply instructs us to do just this in any given case. From this point of view intermediate states are treated on the same basis as initial or final states of the system, the only difference being that their energy is not the same. Thus, it must also be correct to use the exclusion principle in the intermediate states.

There is no contradiction between the two ways of proceeding because the only thing physically observable is the total coherent scattering. In a case in which an electron is present in a state s_1, the use of the exclusion principle in intermediate states requires us to omit the

[33] The occurrence of the two compensating changes of sign was not mentioned by Dirac (reference 1) or Waller (reference 2), and appears not to have been noted in the literature until as late as 1942: H. I. Bhabha and D. Basu, Proc. Indian Acad. Sci. **15A**, 461 (1942).

contribution to the coherent scattering which would be given by $s=r=s_1$ in the second term of Eq. (63); but it also requires us to omit the contribution from Eq. (65) with $s=r=s_1$. Since in this case $a_{s1}^* a_{s1}=1=\delta_{s1s1}$ and the two terms have opposite signs, the method that ignores the exclusion principle in intermediate states differs from the other method only by the insertion of two terms whose sum is zero.

In order to take account of the exclusion principle in the general case with particles originally present in an arbitrary number of states,[34] one must replace[35] the last terms of Eqs. (63) and (64) by the following expressions:

$$-a_s^* a_r \delta_{\mu\nu} \rightarrow -a_s^* a_r (1-\delta_{r_2})\delta_{\mu\nu}(1-a_\mu a_\nu^*),$$
$$-a_\mu a_\nu^* \delta_{rs} \rightarrow -a_\mu a_\nu^* (1-\delta_{\mu\nu})\delta_{rs}(1-a_s^* a_r)$$

and also the expression (65) by

$$\delta_{\mu\nu}\delta_{rs}(1-a_s^* a_r)(1-a_\mu a_\nu^*).$$

The sum of the new expressions is not identical with the sum of those given first, but the discrepancy is precisely accounted for by replacing the first term (two-particle part) in the right-hand member of Eq. (60) as follows:

$$a_s^* a_\mu a_\nu^* a_r \rightarrow a_s^* a_\mu a_\nu^* a_r (1-\delta_{\mu\nu})(1-\delta_{rs}).$$

This is just the change required to apply the exclusion principle to the intermediate state of the process in question: the pair (μ, s) is to be produced *provided* there is already present a pair (ν, r), which is thereupon annihilated.

All available evidence indicates that the Delbrück scattering given by Eq. (65), which is the same whether or not actual electrons are present, is very small. Using the Born approximation, Kemmer and Ludwig[4] give for the scattering cross section of a Coulomb field for long wavelengths

$$\sigma \approx \text{const.}\cdot (Z/137)^4 (h/mc\lambda)^4 (e^2/mc^2)^2, \quad \lambda \gg h/mc. \quad (66)$$

Here the numerical constant factor is probably quite small. Achieser and Pomerantchuk[5] give this result, and also a result for short wavelengths:

$$\sigma \approx \text{const.}\cdot (Z/137)^4 (\lambda mc/h)^2 \ln(h/mc\lambda)\cdot (e^2/mc^2)^2, \quad \lambda \ll h/mc. \quad (67)$$

From these results it can be surmised that the maximum cross section should occur at $\lambda \approx h/mc$ and that even for the largest values of Z it is very small compared to the Thomson cross section $(8\pi/3)(e^2/mc^2)^2$.

Particularly at long wavelengths one is inclined to doubt the validity of the calculation by the Born approximation, which certainly is inadequate for the bound states. An accurate calculation, however, would be extremely laborious. It is thus of some interest to examine a nonrelativistic formula that approximates the effect of bound states and of ionized states in which the electron's speed is not large. The "true scattering" term $(e^2A^2/2mc^2)\psi$ in the Schrödinger equation gives an effect equivalent to that of the transitions between all negative energy levels and any given positive energy state of not too high energy. To get the Delbrück scattering we must sum over all positive energy states. Then, if $\mathbf{k}$, $\mathbf{k}'$ are the propagation vectors of the incident and scattered radiation, the probability amplitude is in this approximation proportional to

$$\sum_n \int \psi_n^*(\mathbf{r}) \exp\{i(\mathbf{k}-\mathbf{k}')\cdot\mathbf{r}\}\psi_n(\mathbf{r})\,dv. \quad (68)$$

The sum is taken over the states of the non-relativistic problem of the electron in the given field.

The expression (68) is a divergent one, but can reasonably be given a meaning by modification in two respects. One modification is the rather usual one of inserting a factor $e^{-\beta r}$ in the integrand and taking the limit $\beta \rightarrow 0+$ at the end of the calculation. The other modification is based on the fact that this nonrelativistic approximation is not valid for the states in which the momentum of the electron is large; for such states, indeed, the relativistic Born approximation is more suitable. One can allow only the states with not too large momentum their full importance by replacing the Schrödinger function $\psi_n(\mathbf{r})$ with an average value,

$$\psi_n(\mathbf{r}) \rightarrow (3/4\pi b^3)\int_{r'>b} \psi_n(\mathbf{r}+\mathbf{r}')\,dv' \quad (69)$$

over a sphere whose radius b is of the order of the Compton wavelength. When these modifications are made and the formula

$$\sum_n \psi_n^*(\mathbf{r})\psi_n(\mathbf{r}'') = \delta(\mathbf{r}-\mathbf{r}'') \quad (70)$$

is used, the expression (68) becomes

$$(3/4\pi b^3)\lim_{\beta\rightarrow 0+}\int \exp\{i(\mathbf{k}-\mathbf{k}')\cdot\mathbf{r}-\beta r\}\,dv = 0. \quad (71)$$

This result indicates that the contribution to the Delbrück scattering from positive energy states in the nonrelativistic region, including bound states, is very small.

The calculations of scattering given by Waller[2] correspond in the language of the positron theory to the complete neglect of Delbrück scattering and the use of the expression (63) to calculate the scattering by an electron. The name "scattering by an electron" is thus given to the whole effect occasioned by the electron's presence, without regard to the details of a picture of successive transitions.

On purely mathematical grounds there is nothing to

[34] In the many-particle case the field $A_\mu^{(e)}$ could be suitably chosen to take approximate account of the interaction of the particles. Arnous (reference 7) considers interactions rather from the point of view of the Born approximation.

[35] Such modifications could also be made in other terms to show the effect of using the exclusion principle in intermediate states; but we here concern ourselves only with the terms relating to the pair intermediate states for scattering, about which questions have been raised. These terms all come from the single primitive term that is the left-hand member of Eq. (60).

choose between the procedure of applying the exclusion principle in intermediate states and that of ignoring it for such states; both yield the same total numerical results. The former procedure appears as the natural one when an individual scattering problem is approached by the traditional method of variation of parameters. The latter procedure, on the other hand, corresponds to a simple algorithm for the systematic analysis of the S-matrix, and to a direct and simple statement as to the cause of the scattering.

PHYSICAL REVIEW VOLUME 81, NUMBER 1 JANUARY 1, 1951

The Mobility of Electrons in Diamond

CLIFFORD C. KLICK* AND ROBERT J. MAURER†
Carnegie Institute of Technology, Pittsburgh, Pennsylvania
(Received July 17, 1950)

The mobility of electrons in diamond has been measured by means of the Hall effect. In agreement with the theory of Seitz, the mobility is inversely proportional to the three-halves power of the absolute temperature. The measured room temperature value of the mobility is 900 cm²/volt-sec as compared with the theoretical estimate of 156 cm²/volt-sec.

I. INTRODUCTION

A THEORY of the scattering of electrons by lattice vibrations in nonpolar crystals has been given by Seitz,[1] which predicts that, for a nondegenerate electron gas, the electronic mobility and mean free path vary as $T^{-\frac{3}{2}}$ and T^{-1}, respectively. The experimental data on silicon[2] and germanium[3] are in excellent agreement with the theoretical prediction of the absolute magnitude of the mobility and its temperature dependence.

Diamond is a typical nonpolar crystal and, because of its successful use as a crystal counter, the problem of the electronic mobility in it is of considerable interest. Seitz has estimated the room temperature mobility of diamond to be approximately 156 cm²/volt-sec. The measurements of the Hall effect of Lenz[4] yield a room temperature mobility of about 200 cm²/volt-sec. On the basis of admittedly scanty evidence, Lenz concluded, however, that the mobility was probably independent of temperature.

Some time ago[5] we reported a value of 900 cm²/volt-sec for the room temperature electronic mobility in diamond and a temperature variation in agreement with Seitz. The purpose of the present paper is to present in detail the Hall effect measurements on which these conclusions were based.

The theory and technique of measurement of the Hall effect are well known.[6,7] The electronic mobility, μ, may be defined in terms of the electronic conductivity, σ, by the equation,

$$\sigma = ne\mu, \tag{1}$$

where n is the concentration of free electrons and e is the charge of an electron. The elementary theory[8] of a nondegenerate electron gas subjected to mutually perpendicular electric and magnetic fields results in the following equation for the mobility of the electrons:

$$\mu = (8/3\pi)(c/H)(E_h/E_a), \tag{2}$$

where E_h is the Hall field developed in the crystal when the applied electric and magnetic fields are E_a and H, respectively. The measured Hall and applied potentials are related to their respective fields by the equations $V_h = E_h t$ and $V_a = E_a L$. The length of the specimen measured parallel to the applied field is L, and t is the width of the specimen between the Hall electrodes.

The mobility and mean free path, l, are simply related by the equation,

$$\mu = 4el/3(2\pi mkT)^{\frac{1}{2}}, \tag{3}$$

where m is the electronic mass and k is Boltzmann's constant.

II. EXPERIMENTAL

The intrinsic conductivity of diamond at room temperature and below is too small to permit the measurement of the Hall effect. Upon absorption of ultraviolet and visible radiation, diamond exhibits a photo-conductivity which has been the subject of numerous investigations.[9–11] Photocurrents of the order of 10^{-10}

* Now at the Naval Research Laboratory, Washington, D. C.
† Now at the University of Illinois, Urbana, Illinois.
[1] F. Seitz, Phys. Rev. **73**, 549 (1948).
[2] G. L. Pearson and J. Bardeen, Phys. Rev. **75**, 865 (1949).
[3] K. Lark-Horovitz, Report NDRC 14-585, OSRD Contract OEMsr-36, 1945, unpublished.
[4] H. Lenz, Ann. Physik **83**, 941 (1927).
[5] C. C. Klick and R. J. Maurer, Phys. Rev. **76**, 179 (1949).
[6] F. Seitz, *Modern Theory of Solids* (McGraw-Hill Book Company, Inc., 1940) p. 192.
[7] A. H. Wilson, *Semi-conductors and Metals* (Cambridge University Press, 1939), p. 95.
[8] H. Fröhlich, *Elektronentheorie der Metalle*, (Verlag. Julius Springer, Berlin, 1936) p. 220.
[9] B. Gudden and R. Pohl, Z. Physik **20**, 14 (1924).
[10] Robertson, Fox, and Martin, Proc. Roy. Soc. (London) **157**, 579 (1936).
[11] Sec. Symposium on the Structure and Properties of Diamond, Proc. Indian Acad. Sci. 24A (1946).

amp were produced in the diamond used in the present investigation by absorption of the radiation from a high pressure mercury arc. The incident radiation was limited to the wavelength region from 3000 to 6200A by filters. The diamond was completely opaque to radiation of wavelength less than 2900A.

The diamond was mounted inside a vacuum cryostat which is illustrated in Fig. 1(*a*). It was supported on a vertical plate, *P*, which was fastened to the bottom of the liquid air reservoir, *Q*. This reservoir was suspended and thermally insulated from a second liquid air reservoir, *R*, to which was attached the radiation shield, *O*. German silver tubes were used to support the reservoirs and introduce the liquid air.

The diamond was a plate 0.22 cm thick. The length of the diamond between electrodes was 0.58 cm and the width of the plate at the Hall electrode was 0.35 cm. The maximum width of the diamond was 0.42 cm. A flat face of the diamond was fixed to a piece of polystyrene, $\frac{1}{16}$-inch thick, by means of polystyrene cement. The polystyrene sheet *S* was fastened to the vertical metal plate, *P*. A sketch of the mounted diamond is shown in Fig. 1(*b*). Aquadag current electrodes were painted on the diamond, *D*, and electrical contact made to them by spring brass electrodes. One of these brass electrodes was clamped to the plate, *P*, in order to cool the diamond effectively. The junction of a copper-constantan thermocouple, *T*, was placed in contact with this brass electrode in order to determine the temperature of the diamond. The second spring electrode was soldered to an insulated wire, which was wound upon the liquid air reservoirs to prevent heat loss from the diamond. The electrical leads were brought out of the top of the cryostat through individual Kovar-glass seals.

One Hall electrode, *H*, was used in a circuit originated by Evans.[12] The Hall electrode was a line of Aquadag on one face of the crystal. A thin wire of spring brass, one end of which was imbedded in the polystyrene plate, was pressed against the Aquadag electrode. A thin constantan wire, soldered to the spring brass wire, served as a lead to the electrometer. Polystyrene beads were used to insulate the constantan lead wire, which was brought out of the cryostat top through a double Kovar-glass seal, the outer seal serving as a guard ring. To eliminate a.c. pick-up and insulation problems, the electrometer tube and circuit elements, which were connected to ground through a high impedance, were mounted in a brass can which was an integral part of the cryostat top.

The temperature of the diamond was controlled by providing interchangeable brass and copper spacers between the reservoir, *Q*, and the vertical plate, *P*. In addition, the plate, *P*, and the radiation shield, *O*, had insulated heating elements wrapped on them.

The interior parts of the cryostat were suspended from a top plate which rested on a rubber gasket to provide a vacuum-tight seal to the outer jacket. The lower portion of the outer jacket, which surrounded the diamond, was in the form of a rectangular box, $3''\times3''\times\frac{3}{4}''$, which was placed between the poles of the electromagnet. A quartz window, waxed to the cryostat wall, allowed radiation to fall upon the diamond through a hole in the radiation shield. The cryostat was evacuated by a mechanical pump and the pressure determined with a thermocouple gauge.

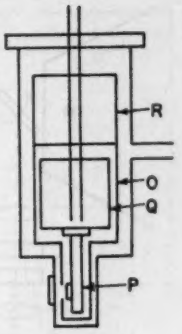

(a)

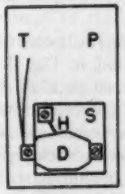

(b)

FIG. 1. Low temperature cryostat.

The optical system is illustrated in Fig. 2. The glass lenses, *L*, allowed the arc, *S*, to be placed well outside the field of the electromagnet, *M*. The rhodium surfaced mirror, *R*, was used to reflect the radiation, through a right angle, to the diamond, *D*. The diamond was uniformly illuminated by focusing the image of the rather broad arc upon it. The light source was a 100-watt H4 General Electric mercury arc operated from a voltage regulator. The glass lenses and filters, *F*, removed radiation of wavelength less than 3000A in order to avoid possible surface photo-emission from the electrodes. The work of Gudden and Pohl indicates that irradiation of diamond with red or infrared light during exposure to ultraviolet radiation results in an enhanced photocurrent. Since this enhanced current may be due to mobile "holes," which would affect the Hall measurements, a one-centimeter thick water cell and Corning No. 4308 filter were used to eliminate radiation of wavelengths greater than 6200A.

A block diagram of the circuit used for the measure-

[12] J. Evans, Phys. Rev. 57, 47 (1940).

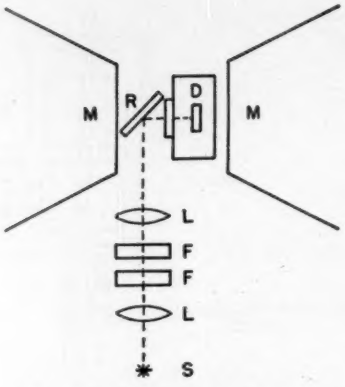

FIG. 2. Optics for illumination of diamond.

ment of the Hall potential and photo-conductive current is illustrated in Fig. 3. In this circuit, originated by Evans,[12] a single Hall electrode is used; and the measured Hall potential difference is one-half that given by the conventional two-electrode circuit, which is inconvenient for use with high resistance materials. With the diamond, *D*, illuminated, the photocurrent was measured with the high sensitivity ammeter circuit, *A*. This was a battery operated amplifier using a single VX-41 Victoreen tube and a grid resistance of 10^9 ohms. The sensitivity of the circuit was 10^{-12} amp/mm deflection of the output galvanometer. The variable tap, *T*, was adjusted so that the high impedance electrometer circuit, *E*, indicated that the Hall electrode was at ground potential. After application of the magnetic field, the change in potential of the Hall electrode was compensated by the potentiometer, *P*. The voltmeter, *V*, then gave the Hall potential difference.

To reduce a.c. pick-up it was necessary to by-pass all resistors with condensers and to choose with care the proper position for grounding the circuit. The lead from the Hall electrode to the electrometer circuit was shielded by the cryostat jacket. The high impedance electrometer circuit was used only as a null instrument, so that exact calibration was unnecessary. The electrometer consisted of a three-stage battery operated voltage amplifier with an over-all gain of about 40. The effective input impedance of the first stage was raised to better than 10^{13} ohms without increase of the time constant by the use of negative feedback. This large input impedance was necessary because of the high resistance of the diamond.

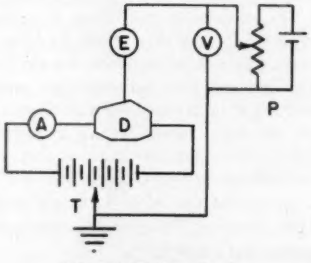

FIG. 3. Hall effect circuit.

The electromagnet had five-inch diameter pole pieces, which tapered to a diameter of three inches at the gap. The magnetomotive force was supplied by two coils, each possessing 30,000 turns of small diameter wire and a resistance of 3200 ohms. The maximum magnetic field strength was 5150 oersteds, which was obtained with a coil current of 226 ma. The power supplied to the magnetic coils was current regulated. The emf generated in a small coil placed in the magnet gap and rotated by a synchronous motor was used to determine the dependence of the magnetic field strength upon the magnet coil current.

III. RESULTS

A test of the proportionality between Hall potential and magnetic field strength is shown in Fig. 4. The magnetic field was proportional to the magnet coil current, which is used as the independent variable in plotting this data. The potential difference applied to the diamond during this test was 370 volts and the illumination yielded a constant photocurrent of 2×10^{-10} amp.

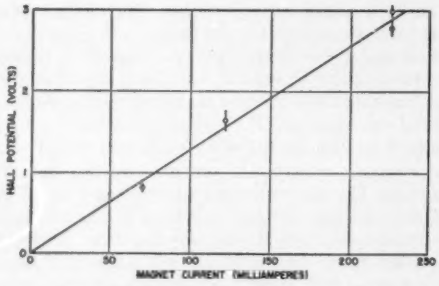

FIG. 4. Hall potential *versus* magnet current.

Within the precision of measurement the Hall potential was found to be proportional to the magnetic field strength. Each point plotted in Fig. 4 (and succeeding graphs) is the average of eight readings with the magnetic field reversed between each pair of readings. In agreement with theory, the magnitude of the Hall voltage was found to be independent of the magnetic field direction, and the sign of the Hall potential changed upon reversal of the magnetic field direction. The relative directions of the applied electric field, magnetic field, and Hall potential were such as to indicate that the photocurrent resulted from a displacement of negatively charged particles.

The Hall potential should be independent of the

magnitude of the photocurrent when the magnetic field strength and applied potential are held constant. The results obtained with a potential of 370 volts applied to the diamond and a magnetic field of 2780 oersteds are shown in Fig. 5. The results of Lenz[4] are indicated, for comparison, by the crosses of Fig. 6. The photocurrent was varied by changing the intensity of illumination. It is to be observed that in each case the Hall potential decreased and went to zero for small photocurrents but was constant for currents greater than a minimum value which was about 100 times greater in Lenz' work than it was in the present experiment.

It appears probable that the decrease of the Hall potential at small photocurrents is due to the finite input resistance of the electrometers. The data of Fig. 5 are consistent with an electrometer input resistance of about 2×10^{13} ohms, a reasonable value. In making this calculation the resistance of the diamond was taken as the ratio of the applied voltage to the photocurrent. The solid curve of Fig. 6, was calculated with the assumption that the leakage resistance of Lenz' electrometer was 1.8×10^{12} ohms, indicating rather inferior insulation.

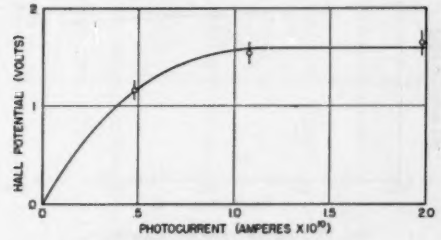

FIG. 5. Hall potential *versus* photocurrent.

The data of Fig. 7 show the linear dependence of the Hall potential upon the applied potential with constant magnetic field and illumination. The reversal in sign of the Hall potential with reversal of the applied potential is also illustrated. In these experiments the magnitude of the magnetic field was 5150 oersteds and the maximum photocurrent 3×10^{-10} amp. Potentials larger than 600 volts could not be applied to the crystal because of insulation difficulties.

A similar experiment was not performed by Lenz. Figure 8 illustrates his data (solid curve) on Hall potential *versus* applied potential with the photocurrent maintained constant by proper adjustment of the illumination. In this case, the crystal resistance increases as the voltage is raised. The saturation of the solid curve does not seem to be due, however, to electrometer leakage as has been postulated to explain the data of Figs. 5 and 6. The dashed curve of Fig. 8 was calculated for infinite electrometer resistance on the assumption that the solid curve was taken with an electrometer having a resistance of 1.8×10^{12} ohms.

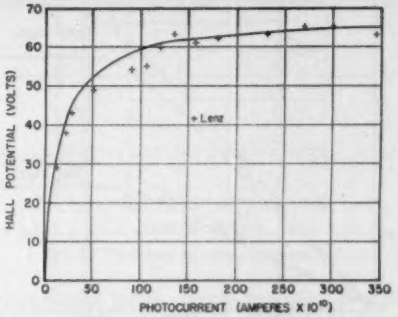

FIG. 6. Hall potential *versus* photocurrent (measurements of H. Lenz).

Although the saturation of Lenz' curves at large potentials is unexplained, the linear form of the curves at moderate potentials indicates that it is possible to define a mobility in this region.

The passage of photocurrent through the diamond resulted in the development of space charge. The photocurrent exhibited a rapid initial decrease, which was accompanied by a change in the potential of the Hall electrode. The rate of change of the potential decreased with time and finally became negligibly small. In a typical experiment, at room temperature, the total applied potential was 225 volts. After a lapse of several minutes the photocurrent reached a steady value and the potential difference between the Hall electrode and the anode was 25 volts with zero applied magnetic field. At 100°K, with the same total potential difference between cathode and anode, the equilibrium Hall electrode potential was 15 volts negative with respect to the anode.

The equilibrium potential distribution inside the

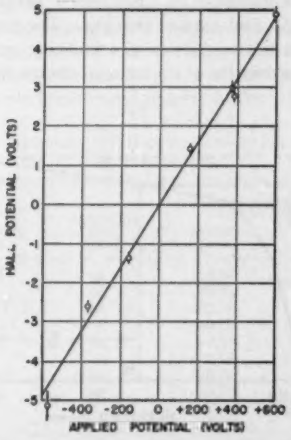

FIG. 7. Hall potential *versus* applied potential.

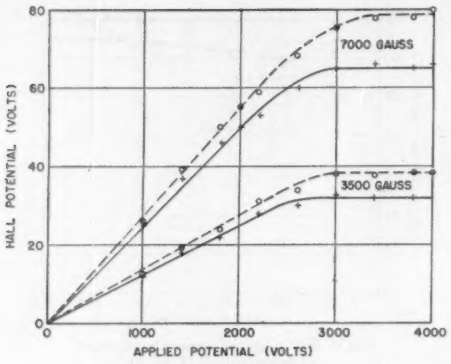

FIG. 8. Hall potential *versus* applied potential (measurements of H. Lenz).

crystal appears to be similar to that sketched in Fig. 9, with a rapid drop in potential near the cathode. This cathode fall in potential implies a positive space charge adjacent to the cathode. A possible explanation is that electrons cannot enter the crystal from the cathode and that the removal of photo-electrons by the applied field leaves this region of the crystal with a positive space charge of immobile "holes."

In the treatment of the experimental data, the internal electric field has been taken as $E_a=(V_0-V'')/S$ where V'' is the potential difference between anode and the Hall electrode in zero magnetic field. The distance between the parallel planes containing the anode interface and the Hall electrode is S.

The polarization, defined as (V'/V_0) (Fig. 9) changed slightly but detectably with temperature. Figure 10 is a temperature-polarization curve.

The preliminary observations which have been discussed indicated that the measured Hall potential behaved satisfactorily as a function of magnetic field, photocurrent, and applied potential. The greatest uncertainty in the calculation of a mobility undoubtedly lies in the estimation of the internal electric field, which

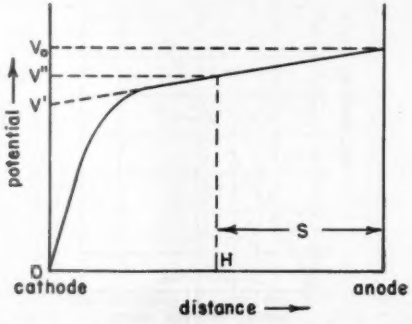

FIG. 9. Probable potential distribution within diamond.

differs from that calculated from the applied potential because of polarization. The results, as a function of temperature are shown in Fig. 11, where the logarithm of the mobility is plotted as a function of the logarithm of temperature. The solid line has the theoretical slope. In these experiments a magnetic field of 2780 oersteds and an applied potential of 265 volts were used. The photocurrent was approximately 7×10^{-10} amp. While the consistency of the data leaves much to be desired, it is clear that an inverse $\frac{3}{2}$-power dependence of the mobility on the temperature is a much better representation than either an inverse first- or second-power dependence. The room temperature value of the mobility is 900 ± 50 cm²/volt-sec.

The present data yield a room temperature mobility of about 200 cm²/volt-sec if the effect of polarization is neglected. There seems to be no justification, however, for this procedure.

The same data which were used to calculate the mobility may be used to compute the mean free path by means of Eq. (3). At room temperature, the mean free path is 6.5×10^{-6} cm.

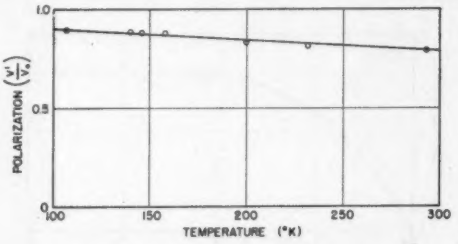

FIG. 10. Polarization *versus* temperature.

Pearlstein, who has investigated the rise time of the voltage pulses produced in diamond under gamma-irradiation, has reported[13] that the room temperature electronic mobility of diamond is greater than 1500 cm²/volt-sec. More recently, he has increased his estimate[14] of the minimum mobility to 4000 cm²/volt-sec. It is not immediately evident why our results of the Hall measurements and those of Pearlstein differ so widely; but it is possible that we have overestimated the internal applied field, E_a, because of the presence of an unsuspected abrupt change in potential near the anode.

IV. ADDITIONAL OBSERVATIONS

McKay[15] has reported that positive holes in diamond, produced by electron bombardment, are mobile. Gudden and Pohl[9] have also observed that the simultaneous illumination of diamond with ultraviolet and infrared radiation results in an enhanced photocurrent,

[13] E. Pearlstein and R. B. Sutton, Phys. Rev. **79**, 217 (1950).
[14] E. Pearlstein, private communication.
[15] K. McKay, Phys. Rev. **74**, 1606 (1948).

which they interpret as being caused by the freeing of positive charges by the long wavelength radiation. High intensities of red and infrared radiation appear to be necessary for the observation of this effect. The diamond used in the present investigation was illuminated simultaneously with radiation from the filtered mercury arc, as previously described, and radiation from a 100-watt tungsten lamp, filtered to remove wavelengths below 5500A. The enhancement of the photocurrent by the radiation from the tungsten lamp was 0.5 percent.

As shown in Fig. 12, the photocurrent excited in the diamond by constant illumination was practically independent of temperature. Lenz found, however, that at 100°K the photocurrent had decreased to 15 percent of its room temperature value. He also noted that the polarization, which was 20 percent at room temperature, increased to 85 percent at 100°K. In the present

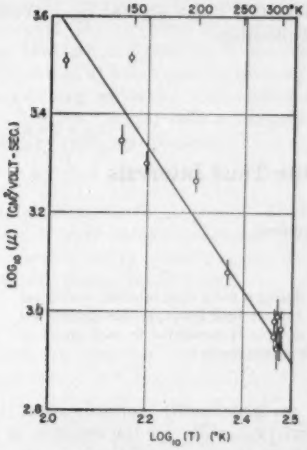

FIG. 11. Mobility *versus* temperature.

work, the polarization was found to be large (Fig. 10) but, like the photocurrent, practically independent of temperature. The difference between our results and those of Lenz appears to be due to the difference in the nature of the exciting radiation. Lenz used the full radiation of the mercury arc as transmitted by quartz. The diamond used in the present experiments, when illuminated in this manner, exhibited a photocurrent which at 100°K had decreased to 22 percent of its room temperature value.

When the diamond was illuminated with the full radiation of the mercury arc, a pronounced asymmetry in the Hall potential was also observed, the magnitude of the potential depending on the relative directions of the applied electric and magnetic fields. This effect is illustrated by the data of Table I. In Table I are shown typical sets of Hall potential data, taken at 100°K with the diamond excited by unfiltered radiation and by

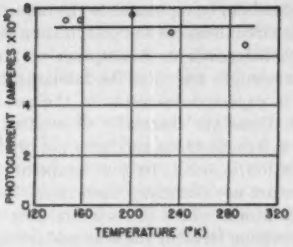

FIG. 12. Photocurrent *versus* temperature.

radiation filtered in the manner previously described. At room temperature the asymmetry in the Hall potential, as measured with unfiltered radiation, was even larger than at 100°K. When the diamond was excited with unfiltered radiation, the Hall potential assumed a maximum value when the relative direction of the electric and magnetic fields was such as to give the Hall electrode a negative charge. Lenz does not report any asymmetry in the magnitude of the Hall potential, possibly because he used the conventional two-electrode Hall circuit rather than the single Hall electrode used in the present experiments.

The observed asymmetry in the Hall potential may be due to surface photo-emission from the Hall electrode which is produced by the short wavelength radiation of the unfiltered mercury arc. A photocurrent of 10^{-13} amp from the diamond electrodes was observed when unfiltered radiation was used, but the fraction of the current which originated at the Hall electrode was not determined. The photo-conductive process in diamond does appear, however, to depend on the wavelength of the exciting radiation, as evidenced by the behavior of the polarization, the photocurrent, and their temperature dependence. A possible explanation is as follows. The fundamental optical absorption band of diamond begins at 2250A. The long wavelength tail of this band, which may extend into the visible region of the spectrum, is undoubtedly due to impurities. Absorption of radiation in the impurity tail of the fundamental band frees electrons from impurity atoms; the positive

TABLE I. Asymmetry of Hall potential under full radiation of the mercury arc.

Magnetic field direction	Magnetic field turned	Change in potential of Hall probe (volts) filtered radiation	unfiltered radiation
Forward	on	+0.94	+0.71
	off	−0.82	−0.63
Reversed	on	−0.58	−1.47
	off	+0.70	+1.52
Forward	on	+0.88	+0.68
	off	−0.62	−0.72
Reversed	on	−0.62	−1.51
	off	+0.70	+1.50
	Average	0.73	

holes are immobile, being bound to the impurity atoms. Under these circumstances the polarization is large and temperature independent. Absorption of radiation in the long wavelength region of the fundamental absorption band is expected to result in the production of excitons. If these are thermally dissociated at room temperature, free electrons and holes are produced, and the polarization is small. At low temperatures, where the excitons are not thermally dissociated, they wander to impurity atoms where dissociation does occur, the electron becoming free but the hole remaining bound to the impurity atom. Under these conditions of excitation, as the temperature is reduced, the polarization increases.

The dissociation energy of an exciton can be estimated from the relation[16]

$$E_n = -\pi^2 m e^4/\mu^4 h^2 n^2 \qquad (4)$$

by taking $n=1$. The index of refraction, μ, of diamond is 2.42 and $E_1 \simeq 0.2$ ev. The lifetime of the exciton is given by

$$\tau = \tau_0 \exp(+E_1/kT). \qquad (5)$$

Estimating $\tau_0 \simeq 10^{-12}$ sec, one obtains $\tau(100°\text{K}) \simeq 10^{-2}$ sec and $\tau(300°\text{K}) \simeq 10^{-9}$ sec. If the cross section for collision with an impurity atom is taken to be 10^{-14} cm^2, the concentration of impurity atoms of the order of 10^{17} cm^{-3}, and the velocity of the exciton as 10^5 cm/sec, then at 100°K an exciton will make a million collisions with impurity atoms during its thermal lifetime. At room temperature, the corresponding number of collisions is less than unity. The behavior of the exciton is therefore in agreement with the preceeding interpretation.

The authors wish to thank Professor Frederick Seitz for advice and his suggestion of this problem. The work was partially supported by the Office of Naval Research. One of us (C.C.K.) was assisted by a Westinghouse Research Fellowship.

[16] F. Seitz, Phys. Rev. **76**, 1376 (1949).

PHYSICAL REVIEW VOLUME 81, NUMBER 1 JANUARY 1, 1951

Relativistic Quantum Theory for Finite Time Intervals

E. C. G. STUECKELBERG*
University of Geneva, Geneva, Switzerland
(Received August 11, 1950)

If transition probabilities are evaluated for transitions occuring during a finite time interval, additional divergencies occur different from those commonly encountered for infinite time intervals. The expressions obtained can however be made convergent, if an indeterminacy of time is attributed to each epoch of observation. The method is applied to the emission of a photon by a free electron.

I. INTRODUCTION

THE convergent results in the relativistic quantum theory of elementary particles, which have been recently obtained by different authors,[1] apply only to time periods of infinite duration between two observations. If one tries to evaluate transition probabilities for processes which are localized in space-time by a *sharply defined boundary* (for example two time-like hypersurfaces specifying an initial and final observation), one obtains divergent results. These divergences arise from regions near the boundary, where processes occur without conservation of the momentum-energy component normal to the hypersurface. However, we show here that one can obtain convergent results if *diffuse boundaries* are introduced. We show in Sec. I that this generalization is possible without affecting the unitarity and causality of the array of probability amplitude forming the S-matrix. In Sec. III, we evaluate, in second-order approximation, the time-independent probability for the emission of a photon by an electron.

Time, with these unsharp limits, no longer appears as a *parameter*, t, whose values $t=t'$ and $t=t''$ are fixed for the two limits of the *period of evolution*, $t''-t'=2T$, during which the photon emission takes place. The initial and final epochs themselves, $t \cong t'$ and $t \cong t''$, are now of finite duration, $\Delta t'$ and $\Delta t''$, and must be given in terms of *two probability amplitudes for time*, $f'(t)$ and $f''(t)$, describing the precision with which t' and t'' have been determined. In the probability $dw(\omega)$ that an electron has emitted a photon of frequency between ω and $\omega+d\omega$ during the period considered, the Fourier transforms, $g'(\omega)$ and $g''(\omega)$, of the two probability amplitudes figure as convergence factors for the integral.[2] We have:

$$dw(\omega) = d\omega(|g''|^2 + |g'|^2)(\omega)n(\omega) \equiv dw''(\omega) + dw'(\omega). \qquad (1)$$

* Work supported by the Swiss Atomic Energy Commission.

[1] S. Tomonaga, Progr. Theor. Phys. **1**, No. 2, 27 (1946); J. Schwinger, Phys. Rev. **74**, 1439 (1948); **75**, 651 (1949); **76**, 790 (1949); R. P. Feynman, Phys. Rev. **76**, 749, 769 (1949); F. Dyson, Phys. Rev. **75**, 486, 1736 (1949).

[2] To $g'(\omega)=\exp(i\omega t')$; $g''(\omega)=\exp(i\omega t'')$ correspond the epochs $f'(t)=\delta(t-t')$ and $f''(t)=\delta(t-t'')$ of sharply determined time values, for which the integral of Eq. (1) diverges.

$g'(\omega)$ and $g''(\omega)$ are normalized to $|g'(0)|=|g''(0)|=1$. Their absolute squares are time independent. We are thus led to think of (1) as the sum of two probabilities for processes which take place *only during the epochs of the initial and of the final observations*. Furthermore, these processes show no conservation of energy: ω is the surplus energy in the final state over that in the initial state. This excess energy can be interpreted as having been furnished by the measuring apparatus during either of the two epochs of observation. Then $|g'(\omega)|^2$ and $|g''(\omega)|^2$ indicate the probability that such an energy is available.

II. THE CONVERGENCE CONDITIONS FOR PROBABILITY AMPLITUDES

We describe a process taking place in a given space-time (x-space) region, V, as the *annihilation of momentum-energy* out of the *incoming* matter or radiation waves and the *creation of momentum-energy* into the *outgoing* waves. We represent the incoming waves of electrons, positrons and photons by the wave packets $u'(x)$, $v'(x)$ and $\varphi'(x)$ with a positive frequency spectrum and the outgoing waves by their conjugate complex $u''^{\dagger}(x)$, $v''^{\dagger}(x)$ and $\varphi''^{\dagger}(x)$ with a negative frequency spectrum. The particular packets

$$u_{A}'(x)=(2\pi)^{-\frac{3}{2}}\pi_{A}(k'n')\exp(ik'x) \tag{2}$$

are plane electron waves. A packet (2) represents a quantum of sharply defined *momentum-energy* k', lying in the *momentum-energy space* (p-space) on the hypersurface of rest mass κ, $p=k'$, where

$$k'^{4}=+(\kappa^2+|\mathbf{k}'|^2)^{\frac{1}{2}} \tag{3}$$

n' numbers the two spin orientations, π^{A} in (3) is normalized to $\pi_{A}^{\dagger\prime\prime}\pi'^{A}=2\kappa i\delta(n''/n')$ for electrons. For photons of rest mass[3] μ we write $p=l'$ and number their polarizations by $n'=1, 2, 3$ (normalization $\pi_{\alpha}^{\dagger\prime\prime}\pi'^{\alpha}=\delta(n''/n')$). Then the nth order contribution to the probability amplitude of a process is the n-fold space-time integral over V:

$$\epsilon^{n}S_{n}[V](u''\cdots\varphi''\cdots/u'\cdots)$$

$$=i\epsilon^{n}\int dx''V(x'')\cdots\int dy''V(y'')\cdots\int dxV(x)\cdots$$

$$\times\int dx'V(x')\cdots u_{A}''^{\dagger}(x'')\cdots\varphi_{\alpha}''^{\dagger}(y'')\cdots$$

$$\times\Delta_{B\cdots}^{(c)A\cdots\alpha\cdots}(x''-y'',\cdots x''-x,$$

$$\cdots x''-x',\cdots)u'^{B}(x')\cdots. \tag{4}$$

For sharply defined boundaries, $V(x')$ is a *discontinuous function*, with the two values 0 or 1 for events x' outside or inside V. The causal[4] function, $\Delta^{(c)A\cdots}(x''-y'',\cdots)$ is a covariant function of the $n-1$ relative displacements of the n events. It is contragradient in its indices to the vector, $\alpha\cdots\beta\cdots$, or spinor, $A\cdots B\cdots$, indices of the packets.

Let us now see how the *generalization to a continuous real function* $V(x)$ related to the time uncertainties of the initial and final observation epochs is possible without affecting the unitarity of the theory or changing the causal function $\Delta^{(c)}$. The unitarity of the S-matrix corresponding to (4) implies that the hermitian part of S_n is determined in terms of the S_m for $m<n$. Therefore S_1 is antihermitian and is given in terms of a single space-time integral of the hermitian interaction energy density and the real function $V(x)$. In electrodynamics the typical element is:

$$\epsilon S_{1}[V](u''\varphi''/u')$$

$$=i\epsilon 2^{-\frac{1}{2}}\int dxV(x)(\varphi_{\alpha}''^{\dagger}u''^{\dagger}\gamma^{\alpha}u')(x). \tag{5}$$

In terms of this S_1, we *define* the hermitian part of S_2 by means of the unitarity relation. We obtain for this part expressions of the type (4) (with $n=2$), where $i\Delta^{(c)}$ is replaced by non-causal functions $-\frac{1}{2}(\Delta^{(+)}+\Delta^{(-)})$. The anti-Hermitian part of S_2 is then determined in terms of a causality correction $i\Delta^{(c)}$, such that the sum of the hermitian and antihermitian parts gives $i\Delta^{(c)}$. The higher order approximations are obtained in exactly the same way. This procedure shows that the unitarity and the causality of the S-matrix are independent of the particular form given to $V(x)$, as long as it is a real function.

In order to find the convergence conditions of (4), we transform it into p-space. The transformed integral is $n-1$ fold. If m is the total number of incoming and outgoing packets, then

$$\epsilon^{n}S_{n}[V](k''n'',\cdots l'',\cdots/k'n',\cdots)$$

$$=i\epsilon^{n}(2\pi)^{\frac{1}{2}n-\frac{1}{2}m}\int dp\cdots\int dq\cdots\int dr\cdots$$

$$\times V(k''-p-q-r-\cdots)\cdots V(l''+p)\cdots$$

$$\times V(0+q)\cdots V(-k'+r)\cdots\pi_{A}''^{\dagger}\cdots\pi_{\alpha}''^{\dagger}\cdots$$

$$\times\Delta_{B\cdots}^{(c)A\cdots\alpha\cdots}(p,\cdots q,\cdots r,\cdots)\pi'^{B}\cdots. \tag{6}$$

This formula involves the Fourier transforms of $V(x)$ and $\Delta^{(c)}$. We shall use the same letters to describe these functions in both x- and p-spaces. We see at once that the existence of the Fourier transform of the causal

[3] In order to avoid the difficulties connected with zero rest mass photons, we suppose the photon to have a finite rest mass, small compared to that of the electron.

[4] By the term "causal" we imply that $\Delta^{(c)}$ in Eq. (4) is a network of causal functions $\Delta^{(c)}(x-y)$ [given in Eq. (9)] describing an outgoing wave at y and an incoming wave at x, if x is later than y (the "creation at y" precedes the "annihilation at x"), and *vice versa* if y is later than x. See Stueckelberg and Rivier, Phys. Rev. 74, 218 (1948); Helv. Phys. Acta 23, 215 (1950); 23, supp. III, 236 (1930).

function $\Delta^{(a)}(p, \cdots)$ is a *necessary condition for the convergence of the amplitude* S_n. For the particular case $V(p)=\delta(p)$ one obtains the usual result:

$$\epsilon^n S_n[\infty](k''n''\cdots l''\cdots/k'n'\cdots)$$
$$=i\epsilon^n(2\pi)^{4n-1}\delta(-k''-l''-\cdots+k'+\cdots)$$
$$\times\pi_A''\uparrow\cdots\pi_\alpha''\uparrow\cdots$$
$$\times\Delta^{(a)A\cdots\alpha\cdots}{}_{B\cdots}(-l'', \cdots 0, \cdots k', \cdots)\pi'^B\cdots, \quad (7)$$

which is commonly used to define transition probabilities for a region V extending over "infinite" physical space-time.

III. PHOTON EMISSION BY A FREE ELECTRON

In the second approximation of quantum electrodynamics, the probability amplitude of an electron-electron transition inside of V is

$$\epsilon^2 S_2[V](u''/u')$$
$$=\epsilon^2\int dxV(x)\int dyV(y)u''\uparrow(x)$$
$$\times(\gamma\partial\Delta_2{}^{(a)}+\kappa\Delta_1{}^{(a)})(x-y)u'(y)$$
$$\equiv\delta(u''/u')(-\tfrac{1}{2}W(u')+\tfrac{1}{2}C(u')-i\Phi(u')). \quad (8)$$

Its Hermitian and anti-Hermitian parts correspond to the separation of the two scalar, causal functions into real and imaginary parts according to:

$$i\Delta^{(a)}=-\tfrac{1}{4}(\Delta^{(+)}+\Delta^{(-)})+i\Delta^{(a)}. \quad (9)$$

$\Delta^{(\pm)}$ are functions involving only definite frequencies larger than the sum of the two rest masses κ and μ.

$$\Delta^{(-)}(-p)=\Delta^{(+)}(p)=\begin{Bmatrix}0\\ 2\Delta^{(1)}(p^2)\end{Bmatrix} \text{ for } p^4\lesseqgtr 0, \quad (10)$$

$$\Delta^{(1)}(p^2)=0 \text{ for } -p^2<(\kappa+\mu)^2. \quad (11)$$

$\Delta^{(a)}$ is the causality correction, defined in terms of $\Delta^{(1)}$ by the following differential equation

$$\left(-\frac{d}{d(p^2)}\right)^n\Delta^{(a)}(p^2)=\frac{n!}{2\pi}\int_0^\infty d(z)^2\frac{\Delta^{(1)}(-z^2)}{(p^2+z^2)^{n+1}} \quad (12)$$

for the lowest n, for which the principal value converges.[5]

Let us now recall briefly the physical meaning of the three parts in Eq. (8) due to $\Delta^{(\pm)}$ and $\Delta^{(a)}$ in (9):

(1) $W(u')$ is a *decrease of the probability* of observing only an emerging electron u'', due to the process of photon emission (in which case we should observe the outgoing waves u'' and φ'').

(2) $C(u')$ is an *increase of this probability*, due to the diminution of the probability for the spontaneous process of three quantum creation (photon, electron and positron), when the electron state u' is occupied.

(3) $\Phi(u')$ is a phase change, different for different wave packets, and giving rise to a *change of the dispersion law for electron waves* [i.e., differing from (2)].

We evaluate these quantities for the space-time region V bounded by two time-like hyperplanes $\cong t'$ and $\cong t''$ defined by the amplitudes $f'(t)$ and $f''(t)$. In terms of the Fourier transforms, normalized to $|g'(0)|=|g''(0)|=1$, the transform $V(p)$ in (6) (Appendix I) is

$$V(p)=\delta(\mathbf{p})i(2\pi\omega)^{-1}(g'-g'')(\omega), \omega=p^4. \quad (13)$$

Omitting the δ-symbol in (8) (because it is evidently diagonal in the momentum and spin space of the electron), we have the following p-space representation of $S_2[V]$ in terms of W, C and Φ:

$$W(k')=\int_{-\infty}^{+\infty}d\omega|g''-g'|^2(\omega)\frac{(2\pi)^3\epsilon^2}{k'^4\omega^2}$$
$$\times(k'p\Delta_2{}^{(+)}+\kappa^2\Delta_1{}^{(+)})(p), \quad (14)$$
$$\mathbf{p}=\mathbf{k}'; \quad p^4=k'^4+\omega. \quad (14a)$$

C is the same expression involving $-\Delta^{(-)}$ instead of $\Delta^{(+)}$, and in the phase $\Phi(u')$, $4\Delta^{(a)}$ has to be substituted for $\Delta^{(+)}$. In the limit, where the period $2T=t''-t'$ between the two epochs t'' and t' is long with respect to their indeterminacies $\Delta t''$ and $\Delta t'$, a frequency ω_0 may be defined

$$2T\gg\omega_0{}^{-1}\gg\Delta t'', \Delta t' \quad (15)$$

allowing in the integrand of (14) the substitution:

$$\omega^{-2}|g''-g'|^2(\omega)=\begin{cases}\omega^{-2}(2\sin\omega T)^2, \text{ for } \omega^2<\omega_0{}^2 & (16)\\ \omega^{-2}(|g''|^2+|g'|^2)(\omega), \text{ for } \omega^2>\omega_0{}^2. & (17)\end{cases}$$

If the intergrand is different from zero for $\omega=0$, W, C, and Φ consist of a *time proportional* part plus a *time independent* part.

In our particular case, we obtain a time proportional part for the phase alone. Its form, $2T\Delta\kappa^2(2k'^4)^{-1}$, shows that the dispersion law Eq. (2) is affected in the form of a rest mass change $\Delta\kappa^2$. The value of the invariant $\Delta\kappa^2$ is undetermined on account of the arbitrary constants in the definition of $\Delta^{(a)}$ in (12). The integrand of the time-independent probability (14) decomposes, on account of (17), into the two contributions due to the two limits of the region V. The four vector, p, is the momentum-energy in the electron+photon state. The substitution of $2\Delta^{(1)}$ for $\omega\ll\kappa=k'^4$ (Appendix II) gives the following expression for the low frequency

[5] The integration of (12) introduces a finite series of terms of the type $a_0+a_1p^2+\cdots+a_{n-1}(p^2)^{n-1}$ with n arbitrary constants. A detailed discussion of this arbitrariness will be published in the *Helvetica Physica Acta*.

probability spectrum to find a photon within ω and $\omega+d\omega$ created at $t\cong t'$.

$$dw'(\omega)=d\omega\,|g'(\omega)|^2\frac{\epsilon^2}{(2\pi)^3}\frac{(\omega^2-\mu^2)^{\frac{1}{2}}}{\omega^2\mu^2}. \tag{18}$$

This expression may be compared to the frequency spectrum of the total energy of a spherically symmetric classical radiation field $\chi^a(x)$ of longitudinal photons ($n'=3$). Writing $\omega=l'^4$, the total energy is in such a case:

$$P^4=\int d\sigma(l')l'^4\sum_{n'=1}^{3}(b^\dagger b)(l'n')$$

$$=\int d\omega 4\pi\omega(\omega^2-\mu^2)^{\frac{1}{2}}(b^\dagger b)(l3). \tag{19}$$

$b^\dagger$ and b are the coefficients of the field $\sqrt{2}\chi^a(x)$, developed in terms of plane wave packets $\varphi'^a(x)$ and their conjugates of the form (2) with the three polarizations n' normalized to $\pi_a''^\dagger\pi'^a=\delta(n''/n')$.

We now determine χ^a from the condition at $t=t'$

$$\chi(x')=0;\quad \chi^4(x')=-\frac{\epsilon}{4\pi}\frac{\exp(-\mu|\mathbf{x}'|)}{|\mathbf{x}'|}+\frac{\epsilon}{\mu^2}\delta(\mathbf{x}');$$
$$\partial_4\chi(x')=-\frac{\epsilon}{\mu^2}\operatorname{grad}\delta(\mathbf{x}');\quad \partial_4\chi^4(x')=0. \tag{20}$$

At $t=t'$, this field compensates the static field everywhere except "inside" of the point particle. We find

$$b^\dagger b(l3)=\frac{1}{2}\frac{\epsilon^2}{(2\pi)^3}\frac{\omega^2-\mu^2}{\omega^2\mu^2}. \tag{21}$$

Comparing (18) with (19) and (21), we see that the classical radiation field corresponding to $dw'(\omega)$ compensates the field of the point charge ϵ, except within a sphere with a radius of the order of $\Delta t'$. The energy density of the total field (static+radiation) is strictly zero outside of this sphere.

IV. CONCLUSIONS

These arguments show, that the introduction of a finite period of evolution in current quantum electrodynamics produces no difficulty of convergence, if diffuse time boundaries are used.

It is also interesting to note that the emission of a photon by a free electron has a simple classical analog. The *photon field* expectation values correspond to a *classical* radiation field, which compensates (or "interferes away") the point electron's static field at the epoch of observation $t\cong t'$ everywhere, except within a small sphere with a radius of the order of the indeterminacy $\Delta t'$ of the time measurement.

APPENDIX I

If we wish to interpret the S-matrix as an operator operating on a state vector ψ, the state vector refers not to a time like hypersurface as in the Tomonaga-Schwinger theory, but to a time-like layer. We may describe such a layer by a real function $F(x)$, which has the values one or zero for events x lying in the future or in the past of the layer. The region V will then be given in terms of the two layers

$$V(x)=F'(x)-F''(x) \tag{I.1}$$

and the S-matrix transforms according to

$$\psi[F'']=S[V]\psi[F'] \tag{I.2}$$

the initial state into the final state. The probability amplitude for the time measurement is the gradient of $F(x)$:

$$f_a'(x)=\partial_a F'(x). \tag{I.3}$$

It reduces to a function of time alone in the case considered in Section III.

$$\mathfrak{f}'(x)=0;\quad f_4'(x)=f'(t)=(2\pi)^{-1}\int_{-\infty}^{+\infty}d\omega e^{-i\omega t}g'(\omega). \tag{I.4}$$

The Fourier transforms of $V(x)$ is then given by (13).

APPENDIX II

In terms of the invariant functions of given rest mass

$$D_\kappa^{(+)}(x)=(2\pi)^{-3}\int d\sigma(k)e^{ikx};\quad d\sigma(k)=(k^4)^{-1}(dk)^3 \tag{II.1}$$

the $\Delta^{(+)}$-functions in (8) are

$$\Delta_1^{(+)}(x)=-\tfrac{1}{2}D_\kappa^{(+)}(x)D_\mu^{(+)}(x)=-\tfrac{1}{2}\Delta^{(+)}(x), \tag{II.2}$$

$$\partial_a\Delta_2^{(+)}(x)=-\tfrac{1}{2}\partial_a D_\kappa^{(+)}(x)\cdot D_\mu^{(+)}(x)-(1/2\mu^2)\times\partial_\beta D_\kappa^{(+)}(x)\cdot\partial^\beta\partial_a D_\mu^{(+)}(x). \tag{II.3}$$

From the divergence of (II.3), we can explicitly evaluate the Fourier transforms for $p^4>0$ and their limiting values for $\mathbf{p}=0$, $p^4=\kappa+\omega$ and $\omega\ll\kappa$:

$$\Delta^{(+)}(p)=2\Delta^{(1)}(p^2)=(2\pi)^{-3}(-p^2)^{-1}[(p^2+(\kappa+\mu)^2)(p^2+(\kappa-\mu)^2)]^{\frac{1}{2}}$$
$$\cong(2\pi)^{-3}\kappa^{-1}[2(\omega^2-\mu^2)^{\frac{1}{2}}+\sim\kappa^{-1}]. \tag{II.4}$$

$$\Delta_2^{(+)}(p)=2\Delta_2^{(1)}(p^2)=-\tfrac{1}{2}(-p^2)^{-1}(-p^2+\kappa^2+\mu^{-2}(p^2+\kappa^2)^2-2\mu^2)\Delta^{(1)}(p^2)$$
$$\cong-(\tfrac{1}{2}+\tfrac{1}{2}\mu^{-2}\omega^2+\sim\kappa^{-1})2\Delta^{(1)}(p^2). \tag{II.5}$$

From these approximations, the expression

$$2(k'p\Delta_2^{(1)}+\kappa^2\Delta_1^{(1)})(p^2)\cong(2\pi)^{-3}\kappa(\mu^{-2}(\omega^2-\mu^2)^{\frac{1}{2}}+\sim\kappa^{-1}) \tag{II.6}$$

is obtained, leading from (14) to (18).

On the Quantization of Angular Momenta in Heavy Nuclei

AAGE BOHR
*Department of Physics, Columbia University, New York, New York**
(Received May 31, 1950)

The individual particle model of nuclear structure fails to account for the observed large nuclear quadrupole moments. It is possible, however, to allow for the existence of the quadrupole moments, and still retain the essential features of the individual particle model, by assuming the average field in which the nucleons move to deviate from spherical symmetry. The assumptions underlying such an asymmetric nuclear model are discussed; this model implies, in particular, a quantization of angular momenta in analogy with molecular structure. The asymmetric model appears to account better than the extreme single particle model for empirical data regarding nuclear magnetic moments.

I. INTRODUCTION

THE individual particle model, which describes the stationary state of a nucleus in terms of the motion of the individual nucleons in an average nuclear field, has accounted successfully for a large number of nuclear properties.[1] In the simplest form of this model the nucleons are assumed to move in a field of spherical symmetry and the quantization of angular momenta is similar as in atomic structures.

This extreme model meets with the difficulty, however, that nuclei are found to have very large electric quadrupole moments. Even in the case of nuclei with one particle more or one particle less than the number required for closed shells, the quadrupole moments are, in general, several times larger than can reasonably be attributed to a single particle.[2]

This circumstance has a direct bearing on the problem of the quantization of angular momenta in the nucleus, quite apart from what other modifications of the model may be necessary. In fact, while the extreme single particle model, in the case of odd nuclei, assumes the total angular momentum of the nucleus to be possessed by the single odd particle, the magnitude of the quadrupole moments, in certain cases, demands that at least 20 or 30 nucleons somehow share the nuclear angular momentum.

Little is known regarding the coupling of angular momenta in heavy nuclei, and we may have to do with complicated coupling schemes. However, it is possible to allow for the existence of the large quadrupole moments, and still retain many essential features of the individual particle model by assuming that the average nuclear field in which the nucleons move deviates from spherical symmetry.

This model involves certain assumptions regarding the dynamical properties of the nucleus and has a number of direct implications regarding nuclear moments which form the subject of the present paper.

A model of this type has recently been considered independently by J. Rainwater,[3] who found it possible to account for the order of magnitude of the quadrupole moments by estimating the nuclear deformation produced by the centrifugal pressure of the odd particle. The following considerations, however, are largely independent of the origin of the nuclear deformations responsible for the large quadrupole moments.

II. THE ASYMMETRIC NUCLEAR MODEL

The model of the asymmetric nucleus suggests an analogy with molecular structure, in which the electrons move in average force fields which deviate from spherical symmetry. As is well known, the possibility of a simplified treatment of molecular states is based on the fact that the masses of the nuclei are very large compared with the mass of the electron. Consequently the motion of the nuclei, their vibration and rotation, only adiabatically influences the electronic motion, whose frequencies are very large compared to those characteristic of the nuclear motion.

The model of a nucleon moving in an average field of a deformed nucleus assumes, in a similar manner, that the shape and orientation of the nucleus is approximately fixed over time intervals comparable with the periods of the single particle motion. In contrast with the molecular case, there are here no heavy particles to provide the necessary rigidity of the structure. However, nuclear matter appears to have some of the properties of coherent matter which makes it capable of types of motion for which the effective mass is large as compared with the mass of a single nucleon.

Thus it is generally assumed that nuclei may vibrate under the influence of surface tension, and since such oscillations involve the whole nuclear mass, the shape of the nucleus will change very slowly compared with the single particle motion. Moreover, the magnitude of the quadrupole moments implies that in general a large number of nucleons are involved in the deformation of the nucleus, and therefore suggests that the frequencies associated with the rotation of the deformed nucleus

* On leave from the Institute for Theoretical Physics, Copenhagen, Denmark.

[1] M. G. Mayer, Phys. Rev. **78**, 16, 22 (1950). These articles contain references to previous literature regarding the individual particle model. E. Feenberg, Phys. Rev. **77**, 771 (1950).

[2] Townes, Foley, and Low, Phys. Rev. **76**, 1415 (1949).

[3] J. Rainwater, Phys. Rev. **79**, 432 (1950). I am indebted to Dr. Rainwater for informing me of his results prior to publication.

may be considered to be small compared with single particle frequencies.

It may be noted that the nucleus is not assumed to rotate like a rigid structure; this assumption would imply the existence of very closely spaced rotational energy levels in heavy nuclei, and such levels have not been observed. It seems quite possible that a rotation of the nucleus involves the motion of only a fraction of the nuclear particles, due to an incomplete rigidity of the nuclear structure, or due to exchange effects of the type considered by Teller and Wheeler.[4] The effective moment of inertia to be associated with the rotation may thus be considerably smaller than that of the whole nucleus. The rotational level spacing, although small compared with that of a single nucleon, may therefore still be compatible with the absence of very low lying nuclear excited states.

In the analysis of nuclear stationary states we may now first consider the motion of a nucleon in the approximately fixed field produced by the core of the nucleus. In a non-central field the angular momentum of the particle will not be a constant, but for cylindrical symmetry will precess around the symmetry axis of the nucleus. If this precession takes place rapidly compared with nuclear rotation (a point to be considered in more detail in Sec. III), the component of the nucleon angular momentum along the symmetry axis will be a constant of the motion. In analogy with the case of diatomic molecules, we designate this quantity by Ω which may take the values $j, j-1, \cdots, \frac{1}{2}$, where j is the magnitude of the single particle angular momentum.

Next, we must consider the motion of the nuclear core, its vibration and rotation. For our purpose the rotation is of particular significance. Even in the ground state, the nuclear axis will not stay fixed in space, but will undergo a precession around the total nuclear angular momentum vector. This motion, which is like that of a symmetrical top, may be characterized by the quantum numbers I, M, and K, representing, respectively, the magnitude of the total angular momentum, its projection on a fixed axis in space, and its projection on the nuclear symmetry axis. For the ground state, it is to be expected that $I=K=\Omega$ in which case the nuclear rotation energy is smallest.

The value of Ω corresponding to the lowest single particle state will depend on the couplings involved; but at any rate, for nuclei with one particle more or one particle less than required for a closed shell, the value $\Omega=j$ seems probable. In fact, in the two cases mentioned, the signs of the quadrupole moments show that the nuclear shape is of the type of an oblate and prolate spheroid respectively. In both cases therefore, the state of maximum Ω will be energetically favored.

Assuming $\Omega=j$, we have $I=j$ for the ground state. Thus the modification of the single particle model here considered need not impair the success of the model in predicting nuclear spins.

[4] E. Teller and J. A. Wheeler, Phys. Rev. 53, 778 (1938).

III. COUPLING OF ANGULAR MOMENTA AND DETERMINATION OF MAGNETIC MOMENTS

In a more detailed classification of nuclear states, which is required for the evaluation of magnetic moments in particular, it is necessary to compare the strengths of the couplings between the various angular momentum vectors of the nucleus.

In the first place, the coupling between the orbital and spin angular momenta, $\mathbf{l}$ and $\mathbf{s}$, of the single particle, can be characterized by the frequency ν_{ls} with which the two vectors precess around each other. In the second place, the coupling of $\mathbf{l}$ to the nuclear axis may be described by the precession frequency ν_{lA} of $\mathbf{l}$ around the axis. Finally, it will be convenient to introduce the frequency ν_{AI} with which the axis precesses around $\mathbf{I}$.

We consider first the case $\nu_{AI}>\nu_{lA}$, in which the coupling of the nucleon motion to the nuclear axis is weak. In this case, the single particle angular momentum and the rotation $\mathbf{R}$ of the nuclear core must first be quantized separately. For the ground state, R must be assumed to be zero and thus we have again essentially the extreme single particle model which does not allow for the existence of large quadrupole moments. We shall therefore assume $\nu_{AI}<\nu_{lA}$, which seems justifiable since, for the nuclear deformations in question, one expects values for $h\nu_{lA}$ of the order[5] of one Mev.

For $\nu_{AI}<\nu_{lA}$, a number of different cases arise, depending on the magnitude of the spin-orbit coupling:

(A). If the spin-orbit coupling is weak ($\nu_{ls}<\nu_{AI}$), the vector $\mathbf{l}$, but not $\mathbf{s}$, is coupled to the nuclear axis. The resultant of $\mathbf{l}$ and $\mathbf{R}$ forms a total orbital angular momentum $\mathbf{L}$ which is to be compounded with $\mathbf{s}$ by simple vector addition. For the lowest nuclear rotational state, the total orbital g-factor g_L will deviate only slightly from the single-particle value g_l, and the magnetic moment of the nucleus will therefore be close to the single particle value.

(B). For $\nu_{ls}>\nu_{AI}$, the total angular momentum of the single particle is coupled to the nuclear axis along which it has the component Ω. Assuming $\Omega=I$, one finds for the resultant nuclear g-factor:

$$g_I=g_\Omega\frac{I}{I+1}+g_R\frac{1}{I+1}, \tag{1}$$

where g_Ω and g_R are the g-factors associated with the angular momenta Ω and R. For g_R it seems most plausible to assume a value of about Z/A, although deviations from this value may occur, since only a fraction of the nucleons is expected to take part in the nuclear rotation. The value of g_Ω will depend on the relative magnitude of ν_{ls} and ν_{lA}.

(B_1). For $\nu_{ls}<\nu_{lA}$, the vector $\mathbf{l}$ is first coupled to the nuclear axis and, due to the spin-orbit coupling,

the spin moment is subsequently quantized along the axis with a component $\pm\frac{1}{2}$. Consequently, we have:

$$Ig_0=\pm\tfrac{1}{2}g_s+(I\mp\tfrac{1}{2})g_l \qquad (2)$$

corresponding to the two possible types of states for a given I.

(B_2). If $\nu_{ls}>\nu_{LA}$, the vectors **l** and **s** must first be compounded to a resultant **j**, which is then coupled to the axis; in this case,

$$g_0=g_j \qquad (3)$$

where g_j is the Landé factor for l-s coupling.

In all three cases, A, B_1 and B_2, the model allows for the existence of large quadrupole moments. However, it should be noted that the quadrupole moment Q referred to fixed axes in space, for the substate $M=I$, will be smaller than the intrinsic nuclear quadrupole moment Q_0, defined with respect to the axis of the nucleus.

In the case A one thus finds:

$$Q=Q_0\frac{I-1}{I+1}\frac{2I-1}{2I+1} \quad (I=L+\tfrac{1}{2}) \qquad (4)$$

and

$$Q=Q_0\frac{I}{I+1}\frac{2I-1}{2I+3} \quad (I=L-\tfrac{1}{2}) \qquad (5)$$

whereas the cases B always lead to expression (5).

For small values of I, the ratio Q/Q_0 may be quite small; for $I=3/2$, the expressions (4) and (5) give values of 1/10 and 1/5 respectively.

The formulas given in the present section can be derived immediately from the vector model for compounding angular momenta, and from simple considerations regarding the motion of the symmetrical top. Wave functions corresponding to the different coupling cases can also be constructed, as regards their angular and spin dependence, in complete analogy to molecular wave functions.

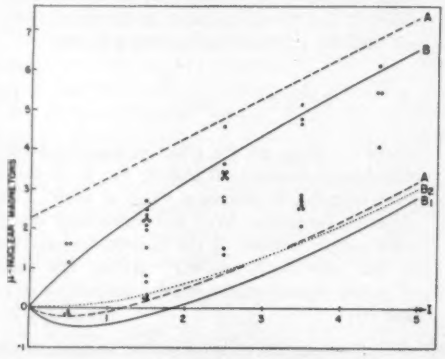

FIG. 1. Magnetic moments of odd proton nuclei.

IV. INTERMEDIATE COUPLING CASES

In Figs. 1 and 2, the magnetic moments of the odd nuclei are given.[5] Only nuclei with mass-number greater than 20 are included, since the models here discussed can only be assumed to have relevance for fairly heavy nuclei. The curves A represent the moments derived from the extreme single particle model (the Schmidt limits). As mentioned above, these values do not differ appreciably from those expected in coupling case A. The curves corresponding to the cases B_1 and B_2 are also shown in the figures, for a value of g_R of 0.45. For parallel **l** and **s** the expressions (2) and (3) lead to the same value for the magnetic moment.

It was one of the first outstanding successes of the single particle model that it accounted, in a general way, for the dependence of the moments on the value of I. Nevertheless, it is a major defect of the model that it fails to explain why the moments do not coincide with the values corresponding to pure single particle states, but lie in between the values for the two states possible for a given value of I.

This difficulty is especially conspicuous for nuclei having one particle more or one particle less than is required for a closed shell. In fact, the moments of these nuclei show no general tendency to approach the pure single particle values.

Since the two states in question have opposite parity, and therefore do not combine by means of conventional types of nuclear interaction, it is possible to alter the magnetic moments only by exciting additional particles. Such configuration perturbations would, however, have to be so strong that the single particle model would represent only a crude approximation. Moreover, it seems to be difficult to explain on this basis why the moments fall in between the two single particle values, rather than deviate more irregularly from these values.

The situation is essentially modified by the introduction of an asymmetric nuclear core. A large number of states now become possible for a given value of I. Thus, in the coupling case B the particular states considered in Sec. III were characterized by $\Omega=I$, and by the largest possible component of the single particle angular momentum along the nuclear axis. If these two restraining conditions are not imposed, it is possible to construct states having a wide range of moment values.

These values lie between definite limits. In fact, for a given value of the total orbital g-factor, g_L, the moment is uniquely determined by the component of the intrinsic spin along the axis of space-quantization. For the substate, $M=I$, the average value of this spin component S_z satisfies the condition $-\frac{1}{2}I/(I+1)<\bar{S}_z<+\frac{1}{2}$. Since the difference between g_L and g_l is usually

[5] The data are taken from a compilation of moments by H. L. Poss, published by Brookhaven National Laboratory, October 1949, supplemented by a few more recent moment determinations published in Phys. Rev.

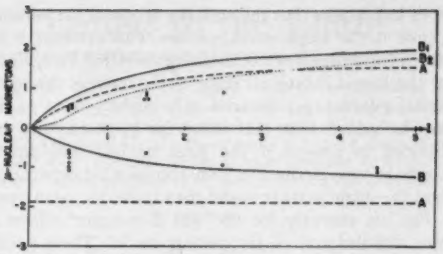

FIG. 2. Magnetic moments of odd neutron nuclei.

of minor importance, the moment is therefore confined within the limiting values A.

If the nucleus can be represented to a high approximation by one of the simple coupling cases discussed in Sec. III, the ground state would seem to have the quantum numbers which were assumed in that section, and which lead to the moment values given by the curves in Figs. 1 and 2. Not only is this choice of quantum numbers suggested by energetic considerations, but it is also required to make the nuclear spin equal to the single particle angular momentum.

However, when some of the characteristic frequencies introduced in Sec. III are comparable in magnitude, we have to do with mixed coupling types. The nuclear ground state will then no longer be a pure state in either of the representations A, B_1 or B_2, but will instead correspond to a mixture of states. Consequently the magnetic moments will, in general, fall in between the limiting values.

As an illustration, we may consider the particularly simple nuclei which have a single particle in addition to the number required for closed shells; e.g., $_{83}Bi^{209}$, and $_{51}Sb^{123}$. According to the shell model, which assumes that a strong spin-orbit coupling is a determining factor for the order of nuclear levels, these nuclei have $j=l-\frac{1}{2}$ and should be represented by the coupling case B_2. Nevertheless, the moments are found to lie very far from the predicted pure state values.

The influence of an asymmetric core implies, however, a coupling case intermediate between B_2 and B_1. The single particle state in question, having $\Omega=l-\frac{1}{2}$, will no longer be a pure $j=l-\frac{1}{2}$ state, but will have an admixture of $j=l+\frac{1}{2}$. The negative sign of the quadrupole moment, for the nuclei in question, indicates that the asymmetry favors states with large components of $\mathbf{l}$ along the nuclear axis. In this case, the magnetic moment for the state in question increases with increasing ν_{lA}. For $\nu_{lA}\gg\nu_{ls}$, the moment actually approaches the opposite limit B, corresponding to a spin-component of $+\frac{1}{2}$ along the nuclear axis. In order to account for the observed moments, comparable values of ν_{lA} and ν_{ls} are required. This appears to be consistent with the evidence[1] for a spin-orbit coupling of the order of 2 Mev for large values of l.

A detailed estimate of such perturbations is made difficult by the fact that a large asymmetry of the core will affect the ordering of the single particle levels to such an extent that the nuclei considered can no longer simply be characterized as having a single particle in addition to closed shells. Of course, this circumstance need not interfere with the explanation of the particular stability of the closed shell nuclei themselves, since these nuclei may be of spherical form.

If the deviation of the moments from the limiting values is ascribed to perturbations of the type considered, one would expect that nuclei having a j-value larger than that of any neighboring single particle level will have moments close to the pure state values. The known magnetic moments of nuclei of this type are given in Table I. There actually appears to be a rather close agreement with the values μ_B, predicted for the coupling case B. For comparison, the moments μ_A, corresponding to the extreme single particle model, are also listed. This model is not in good agreement with the empirical moments of these nuclei.

As regards the deviations of the moments from the μ_B-values, it must be noted that the moments depend to some extent on the value of g_R. As already mentioned, this value may vary from nucleus to nucleus, and a certain spread of the moments is to be expected. Moreover, even the simple nuclei considered will not represent completely pure states. In particular, the asymmetry of the core implies that l is not an exact quantum number. States of higher l, but with the same value of Ω, will therefore be admixed to some extent.

As an additional indication of the influence of the nuclear asymmetry on the magnetic moments, it may be noted that the following empirical rule seems to hold: of two isotopes, which differ by 2 neutrons and have the same value of I, the nucleus with the numerically smallest quadrupole moment has a magnetic moment closest to the pure state value.[6] Examples are

TABLE I. Magnetic moments of selected nuclei.

Nucleus	I	μ_{obs}	μ_B	μ_A
$_{12}Mg^{25}$	5/2	−0.96	−1.04	−1.91
$_{13}Al^{27}$	5/2	3.64	3.74	4.79
$_{21}Sc^{45}$	7/2	4.75	4.86	5.79
$_{23}V^{51}$	7/2	5.14	4.86	5.79
$_{27}Co^{59}$	7/2	4.64	4.86	5.79
$_{36}Kr^{83}$	9/2	−0.97	−1.19	−1.91
$_{38}Sr^{87}$	9/2	−1.1	−1.19	−1.91
$_{41}Cb^{93}$	9/2	6.17	5.92	6.79
$_{49}In^{113}$	9/2	5.46	5.92	6.79
$_{49}In^{115}$	9/2	5.47	5.92	6.79

[6] This rule is somewhat different from the one suggested by W. Gordy (Phys. Rev. 76, 139 (1949)). In many cases the two rules coincide but, although the evidence is not conclusive, Gordy's rule appears not to hold for the Cu-isotopes (P. Brix, Zeits. f. Physik 126, 725 (1949)).

the isotopes of Cl, Cu, Ga, Br, Eu, and Re. The only known exception is In, whose isotopes, however, have almost identical moments.

V. CONCLUDING REMARKS

The most adequate coupling cases to represent nuclear states may be expected to vary from nucleus to nucleus depending, in particular, on the quadrupole moment and the value of the single particle angular momentum.

As regards the question of predominant coupling types, some information can be obtained from Figs. 1 and 2.

In the first instance, a large part of the moments for small values of I fall outside the curves B_2. Apart from the case $I=\frac{1}{2}$ with parallel $\mathbf{l}$ and $\mathbf{s}$, it appears, however, that practically all moments of heavy nuclei lie within the limits B_1, although these limits are considerably narrower than the A curves. In view of the uncertainty of g_R, the only definite exception is the moment of Pr^{141} ($I=5/2$), which lies very close to the A-limit.

It is not surprising that the moments for $I=\frac{1}{2}$ with parallel $\mathbf{l}$ and $\mathbf{s}$ tend to fall outside the B curves. In fact, just in this particular case, the projection of $\mathbf{l}$ on the nuclear axis vanishes (Σ states in molecular terminology). There is thus no net spin-orbit coupling, and the coupling of $\mathbf{s}$ to an axis of the nucleus is presumably very weak. Consequently, an approach to the model A is to be expected.

Evidence regarding the structure of nuclear magnetic moments has been obtained from a study of the anomalies in atomic hyperfine structures caused by the finite size of the nucleus.[7,8] The analysis of such effects has given indications that the orbital g-factor of the nucleus is close to the single particle value. This evidence is in agreement with all of the models considered here, since for the lowest rotational state of the nucleus the total orbital g-factor, g_L, deviates only slightly from g_l. It may be added that this value for g_L would not be obtained in general if the large nuclear quadrupole moments were ascribed to more complicated departures from the single particle model than those discussed here.

The hfs anomaly for the odd K-isotopes[8] allows a more detailed test of the nuclear model. These nuclei contain 19 protons, one less than the number 20 required for closed shells, and are therefore expected to be well represented by the model of a single particle moving in an asymmetric nuclear core. Assuming a coupling case between B_1 and B_2, the nuclear wave functions can be determined from the empirical values of the moments. An estimate of the hfs anomaly on this basis[9] gives a result in close agreement with the observed value.

In many respects it thus appears that the modifications of the extreme single particle model, which are necessary in order to allow for the large quadrupole moments, at the same time improve the agreement of the model with empirical data on nuclear magnetic moments.

The writer is indebted to Columbia University for a fellowship enabling him to take part in research work in the Physics Department, and wishes to acknowledge the benefit of stimulating discussions with Professors I. I. Rabi, J. L. Rainwater, and C. H. Townes on the topics of the present paper.

[7] A. Bohr and V. Weisskopf, Phys. Rev. **77**, 94 (1950).
[8] Ochs, Logan, and Kusch, Phys. Rev. **78**, 184 (1950).
[9] A. Bohr, Phys. Rev. (to be published).

Letters to the Editor

PUBLICATION of brief reports of important discoveries in physics may be secured by addressing them to this department. The closing date for this department is five weeks prior to the date of issue. No proof will be sent to the authors. The Board of Editors does not hold itself responsible for the opinions expressed by the correspondents. Communications should not exceed 600 words in length.

Total Neutron Cross Sections of Several Nuclei at 14 Mev*

ALBERT H. LASDAY
Department of Physics, Carnegie Institute of Technology, Pittsburgh, Pennsylvania
November 7, 1950

THE total neutron cross sections of polyethylene (for hydrogen), beryllium, carbon, titanium,[1] vanadium,[1] zirconium,[1] and lead were obtained from a good geometry transmission measurement using neutrons from the University of Pittsburgh cyclotron, made available through the courtesy of Dr. A. J. Allen. Neutrons in the energy range of 13 to 15 Mev were detected by allowing the neutron beam to impinge on a polyethylene radiator and then detecting recoil protons by passing them through a proportional counter telescope[2] made up of four counters in a triple coincidence, anticoincidence arrangement. Suitable aluminum absorbers were placed between the polyethylene foil and the front counter of the telescope and between the last two counters in order to determine the lower and upper energy limits, respectively, of the sensitive range of the counter telescope. The mean neutron energy was 13.9 Mev.

The samples whose neutron transmissions were measured were placed midway between the cyclotron target and the polyethylene foil of the neutron detector. The largest sample subtended a plane angle of 5° at the detector. Hence, it was necessary to correct each observed cross section for the effect of neutrons scattered elastically into the detector from the sample. This correction was calculated using the method of McMillan and Sewell.[3] Table I lists the observed cross sections, the elastic scattering corrections, and the corrected cross sections. The errors due to counting fluctuations are considered to be much greater than any others inherent in the method used, since the measured transmissions were corrected by measurement of stray neutrons scattered into the detector from the surroundings. Hence, the standard deviations listed with the corrected cross sections were calculated only on the basis of counting statistics.[4] The last column of Table I lists nuclear radii calculated from the corrected cross sections by the relation:

$$\sigma_t = 2\pi R^2.$$

The nuclear radii obtained from the present experiment are compared with those of Amaldi, *et al.*,[5] also measured at 14 Mev, in Fig. 1. The best fit to the data of Amaldi, *et al.*, is given by the straight line:

$$R = (1.3 + 1.37A^{\frac{1}{3}}) \times 10^{-13} \text{ cm},$$

which is plotted on Fig. 1. The carbon, titanium, and vanadium cross sections agree very well with the straight line. The beryllium radius is anomalously high; however, the beryllium cross section agrees well with the beryllium curve in Adair's[6] recent compilation of neutron cross sections. Interpolation of his curve of the beryllium cross section as a function of energy between 4 Mev and 40 Mev gives a value of the beryllium cross section at 14 Mev of about 1¼ barns. The measured value from the present experiment is 1.41±0.11 barns.

The zirconium and lead radii are apparently significantly smaller than the notion of constant nuclear density leads one to expect. Amaldi, *et al.*, also give a small value of the lead radius (9.00±0.13 $\times 10^{-13}$ cm). Furthermore, it is worth noting that the titanium, vanadium, and zirconium cross sections were all measured as part of one continuous data run, as were polyethylene and lead. It is concluded that the anomalously small zirconium and lead radii are indications of closed shell structure[7] of $_{40}Zr^{90}$ (48 percent abundant isotope) with 50 neutrons, and of $_{82}Pb^{208}$ (52 percent abundant isotope) with 126 neutrons or 82 protons.

TABLE I. Neutron total cross sections and nuclear radii.

Scatterer	Observed cross sect. (barns)	Scattering correction (% of obs.)	Corrected cross sect. (barns)	Standard deviation (barns)	Radius (10^{-13} cm)
Poly[a]	2.73	1.8	2.78	±0.09	···
H[a]	···	···	0.77	±0.04	···
Be	1.39	1.4	1.41	±0.11	4.73±0.21
C	1.23	0.8	1.24	±0.06	4.44±0.11
Ti	2.22	0.9	2.24	±0.29	5.98±0.36
V	2.49	1.2	2.52	±0.24	6.33±0.30
Zr	2.34	1.3	2.37	±0.35	6.14±0.45
Pb	4.80	3.5	4.97	±0.27	8.90±0.23

[a] The formula $(CH_2)_n$ was used for polyethylene in order to compute the hydrogen cross section: $\sigma_H = \frac{1}{2}(\sigma_{poly} - \sigma_C)$.

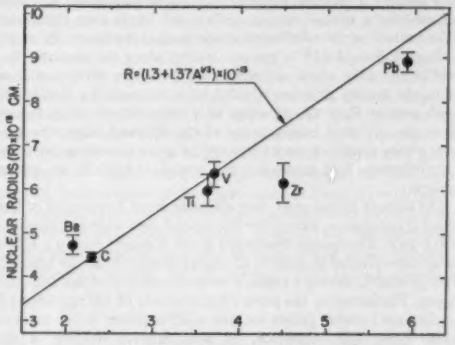

FIG. 1. Nuclear radius as a function of cube root of mass number. The straight line $R = (1.3 + 1.37A^{\frac{1}{3}}) \times 10^{-13}$ cm represents the best fit to the data of Amaldi, *et al.* The plotted points are calculated from the cross sections of the present experiment by the relation: $\sigma_t = 2\pi R^2$.

I wish to express my appreciation and thanks to Professor E. C. Creutz for suggesting this problem and for his continuing interest and advice.

* This work was supported in part by the ONR.
[1] High purity samples very kindly loaned by the Argonne National Laboratory of the AEC.
[2] E. M. Baldwin, to be published.
[3] E. M. McMillan and D. C. Sewell, U. S. AEC publication MDDC-1538, unpublished.
[4] M. E. Rose and M. M. Shapiro, Phys. Rev. **74**, 1853 (1948).
[5] Amaldi, Bocciarelli, Cacciapuoti, and Trabacchi, Nuovo Cimento **3**, 203 (1943).
[6] R. K. Adair, Revs. Modern Phys. **22**, 257 (1950).
[7] M. G. Mayer, Phys. Rev. **74**, 235 (1948).

Mobilities of Electrons in High Electric Fields

E. J. RYDER AND W. SHOCKLEY
Bell Telephone Laboratories, Murray Hill, New Jersey
November 2, 1950

IN ordinary theories of electrical conductivity it is supposed that the electric field is so small that the energy given to the electrons can be transferred to the lattice with no great alteration in the energy distribution of the electrons. In the case of electrical breakdown such changes are considered, but the equilibrium

situation in a given electric field is not readily observed. By using pulse techniques and special experimental precautions, it has been possible to observe steady-state changes in the mobility of electrons in germanium samples.

As has been discussed in several publications,[1] the resistance of n-type germanium samples under relatively low field conditions can be modulated by hole emission from the end electrode. In the experiments which are being reported, precautions have been taken to minimize such modulation. Figure 1 shows the type of

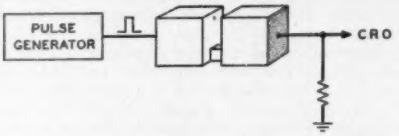

FIG. 1. Schematic diagram of germanium sample and its associated electrical circuit.

sample used and its associated electrical circuit. The resistance of the germanium arises from a small filament which is left after a large portion of the cross section of a block of germanium has been removed by a special cutting technique.[2] Large area electrodes make contact on the relatively massive ends of the block. Although fields as high as 4×10^4 v/cm are applied along the filament, the field at the ends never exceeds about 10 v/cm. With such low fields, the transit time for injected holes to reach the filament is much greater than the duration of a pulse. Hence they do not affect the observed conductivity of the filament. Also, the surfaces of the specimen were prepared to be as smooth as possible, since otherwise hole generation and attendant modulation appear to occur.

The voltage pulses used were obtained from a generator of low internal impedance, were quite flat-topped, and were of a duration of 0.1 μsec. The energy dissipated in the filament during a single pulse corresponded at most to an energy density of 2×10^7 ergs/cc. This produced, during a pulse, a temperature rise of less than one degree. Furthermore, the pulse repetition rate of 100 pps afforded ample time between pulses for this heat to diffuse to the massive ends. There was, therefore, no accumulative heating of the filament.

Current density—electric field characteristics for a typical n-type germanium sample are shown in Fig. 2. Similar characteristics, though not quite so marked, have been obtained with p-type germanium. It is seen that ohmic behavior exists up to a field of about 6×10^2 v/cm, beyond which there is a gradual transition approaching constant current. For fields below 2×10^4 v/cm the number of carriers is considered to remain constant. The constant resistivity portion of the characteristics corresponds, then, to regions of constant mobility. The essentially constant current portion, on the other hand, corresponds to a range in which the mobility varies as E^{-1}, and in which the drift velocity is constant and of the order of 10^7 cm/sec. Beyond a field of 2×10^4 v/cm the current pulses are no longer flat-topped, and it is believed that hole injection or generation occurs. With less carefully prepared surfaces similar increases in the number of carriers are evident at lower fields.

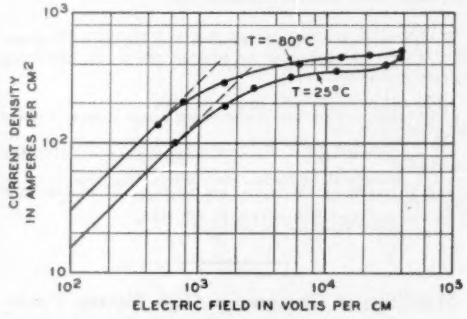

FIG. 2. Current density—electric field characteristic for a typical n-type germanium sample.

A theoretical analysis shows that if energy losses are due to acoustical phonons, the critical field at which Ohm's law should fail is about $c/\mu \doteq 150$ v/cm, where c is the velocity of longitudinal acoustic waves and μ the low field mobility. However, if energy losses due to "optical" modes[3] dominate, the critical field may be higher and a limiting drift velocity of about $(h\nu/m)^{\frac{1}{2}} \doteq 10^7$ cm/sec will arise, in good agreement with that observed. The data appear to represent the cumulative effect of both acoustical and optical scattering. At lower temperatures the acoustical modes should be the more important and a drift velocity $\doteq (c\mu E)^{\frac{1}{2}}$ is predicted. The apparent importance of the optical modes furnishes further evidence that the "effective mass" is not isotropic.[4]

[1] Bray, Lark-Horovitz, and Smith, Phys. Rev. **74**, 1218 (1948). E. J. Ryder and W. Shockley, Phys. Rev. **75**, 310 (1949).
[2] W. L. Bond, Phys. Rev. **78**, 646 (1950).
[3] F. Seitz, Phys. Rev. **73**, 549 (1948). J. Bardeen, Phys. Rev. **79**, 216 (1950).
[4] Pearson, Haynes, and Shockley, Phys. Rev. **78**, 295 (1950).

Experimental Evidence for the Three-Photon Annihilation of an Electron-Positron Pair*

J. A. RICHT
Yale University, New Haven, Connecticut‡
November 6, 1950

A DEVELOPMENT of recent origin in pair theory is the theoretical discovery of selection rules governing the annihilation of electron-positron pairs.[1-3] Calculations of the relative frequency of occurrence of the three-photon annihilation process as compared with the two-photon process have been made by Ore and Powell,[4] who obtain 1/370, and by Lifshitz,[5] who obtains 1/235.

The three-photon annihilation radiation was detected with three scintillation counters arranged symmetrically about the source of radiation and connected in triple coincidence. The coincidence circuit resolving time was 5×10^{-7} sec without genuine coincidence loss.

Cu^{64}, enclosed by aluminum of sufficient thickness to stop all particle radiation, was used as the source of annihilation radiation. Of all the positron emitters considered Cu^{64} was found to satisfy best the conditions imposed on the choice of source. All of the work reported was done with spectroscopically pure copper obtained from the Johnson-Matthey Company, Ltd., London.[6] Turnings from the copper rod, made with a carboloy tool, were sent to Oak Ridge for irradiation with slow neutrons.

Anthracene and naphthalene crystals were used. The maximum efficiencies attained were 8.5 percent for the anthracene crystals and 6.5 percent for the naphthalene crystals for 0.51 Mev photons. In each case the efficiency was about one-half the maximum attainable, as calculated from the Klein-Nishina formula. The range of solid angles used in separate runs extended from 0.534 to 0.740 steradian. Initial singles rates extended from 1.94×10^3/sec to 2.62×10^3/sec. The runs varied in duration from a minimum of 7 to a maximum of 15 hours.

Chief emphasis was placed on the measurement of the ratio of the cross sections. Two supporting experiments were also carried out. In one, measurements were made with the source out of the plane of the counter crystals; and, in the other, lead absorption

measurements were made on the three-photon annihilation radiation.

The ratio of the cross sections for the two-photon and three-photon annihilation processes, respectively, was obtained from the expression,

$$\sigma_2/\sigma_3 = N_2 f_3(\epsilon_{0.33})^3/N_3 f_2(\epsilon_{0.51})^6,$$

where N_2 and N_3 are the genuine doubles and genuine triples per single, respectively; f_3 is the fraction of all three photon sets intercepted by the three counters; f_2 is the fraction of all two-photon sets intercepted by two symmetrically spaced counters; $\epsilon_{0.33}$ and $\epsilon_{0.51}$ are the intrinsic efficiencies of the detectors for 0.33-Mev and 0.51-Mev photons, respectively.

Random accidentals arising from the two-photon annihilation process accounted for the largest portion of the spurious triples rate. The total triples rate was also corrected for accidentals of the second kind and those spurious triples arising as a result of the scattering of the two-photon annihilation radiation in the aluminum converter. The effect on the spurious triples rate of bremsstrahlung radiation emitted by the positron in slowing down was considered and found to be negligible.

Care was taken to eliminate spurious triples arising from counter-to-counter scattering. The sides of the crystals as well as the photo-multipliers were protected by $\frac{1}{16}$-in. lead sheet. In addition, a baffle system of $\frac{1}{4}$-in. lead sheet was arranged so that one counter could not "see" another counter.

Aluminum foil of such thickness as to stop even the most energetic electron recoil from the aluminum converter was put on the face of each crystal.

When equal weights were assigned to fourteen separate runs, the mean of the ratio of the cross sections was found to be

$$\sigma_2/\sigma_3 = (2.0 \pm 0.4) \times 10^3, \quad \epsilon_{0.33} = \epsilon_{0.51};$$
$$\sigma_2/\sigma_3 = (3.3 \pm 0.7) \times 10^3, \quad \epsilon_{0.33} = 1.18\epsilon_{0.51},$$

depending on the assumption made concerning the efficiency of the detector for 0.33-Mev gamma-radiation relative to the efficiency for the 0.51-Mev radiation, the latter being determined by coincidence-counting of the two-photon annihilation radiation.

There are two reasonable assumptions for extrapolation of the value to $\epsilon_{0.33}$ from the measured efficiency $\epsilon_{0.51}$. In the first, $\epsilon_{0.33} = 1.18\epsilon_{0.51}$, the efficiency varies directly as the Compton cross section, Compton scattering being the only process of importance for light materials in this energy range. In the second assumption, $\epsilon_{0.33} = \epsilon_{0.51}$, the increased "absorption" for the 0.33-Mev gamma-rays is compensated for by the greater ease with which the larger pulses from the 0.51-Mev gamma-radiation are detected.

Positive results were also obtained in the auxiliary experiments. The number of genuine triple coincidences obtained with the source out of the plane of the crystals was zero within the error of the experiment. The absorption experiment gave evidence that the three-photon annihilation radiation was softer than the two-photon annihilation radiation.

Work is continuing on the problem. The measurements are to be repeated with more efficient detectors and with a coincident circuit having a resolving time $<5\times10^{-9}$ sec. As an additional check on the existence of the effect it is planned to use Na^{22} as a source of positrons and to measure the quadruple coincidence rate in four counters.

I wish to thank Professor C. G. Montgomery for his constant encouragement and interest in this investigation. I am also indebted to Dr. Aadne Ore for valuable discussions.

* Part of a dissertation presented to the faculty of the Graduate School of Yale University in candidacy for the degree of Doctor of Philosophy.
† AEC Predoctoral Fellow (1948–1949), present address: Knolls Atomic Power Laboratory, General Electric Company, Schenectady, New York.
‡ Assisted by the joint program of the ONR and AEC.
[1] J. A. Wheeler, Ann. N. Y. Acad. Sci. **48**, 219 (1946).
[2] J. Pirenne, Thesis, University of Paris (1944). Chapter III. See also Arch. sci. phys. et nat. **28**, 273 (1946), and **29**, 121 (1947).
[3] I. Pomeranchuk, Doklady Akad. Nauk S.S.S.R. **60**, No. 2, 213 (1948).
[4] A. Ore and J. L. Powell, Phys. Rev. **75**, 1696 (1949).
[5] E. M. Lifshitz, Doklady Akad. Nauk S.S.S.R. **60**, No. 2, 211 (1948).
[6] We are indebted to Professor C. T. Lane for this copper.

Detection of X-Rays by Means of NaI(Tl) Scintillation Counters*

H. I. West, Jr., W. E. Meyerhof, and R. Hofstadter
Stanford University, Stanford, California
November 6, 1950

In connection with proposed research on nuclear isomerism we have been interested in investigating the possibility of detecting individual x-ray quanta by means of scintillation detectors. Using NaI(Tl) crystals[1] with uncooled RCA 5819 photo-multiplier tubes, we have been able to detect individual x-ray quanta in the range of 5- to 80-kev energy with an efficiency approaching 100 percent. X-rays of 2-kev energy have been detected with an efficiency between 50 and 80 percent.

The x-rays used in this experiment were produced as follows. In the range of 15 to 80 kev by monochromatizing x-rays from an Mo target with a Bragg single-crystal spectrometer; in the range of 5 to 20 kev by using the fluorescent radiation of various elements excited by Mo x-rays; at 2 kev by using the continuous radiation from a V target, filtered by the Be window of the x-ray tube and the oil covering the NaI crystal.

The NaI crystals were cleaved under oil into $\frac{1}{2}$ in. to $\frac{1}{4}$ in. parallelopipeds and used according to a technique previously described.[1] A thin (0.0005 in.) Al reflector was set over the crystal. In the detection of low energy x-rays a hole was cut into the reflector to allow the entrance of the x-rays.

With this arrangement we have found, from the widths of the pulse height distributions, 1.0 to 1.5 photo-electrons emitted from the photo-cathode of the 5819 tube for each kilo-electron-volt dissipated in the crystal. This figure agrees with previous estimates.[1] With 8-kev fluorescent x-rays from Cu, for example, we have observed the pulse height distribution shown in Fig. 1a, the width of which corresponds to approximately 12 photo-electrons on the average from the photo-cathode. Since all of the x-rays are absorbed in the crystal and since there seem to be hardly any pulses of zero pulse height, we can be quite sure that each 8-kev x-ray quantum results in a detectable pulse and hence the detection efficiency is close to 100 percent. This follows also from

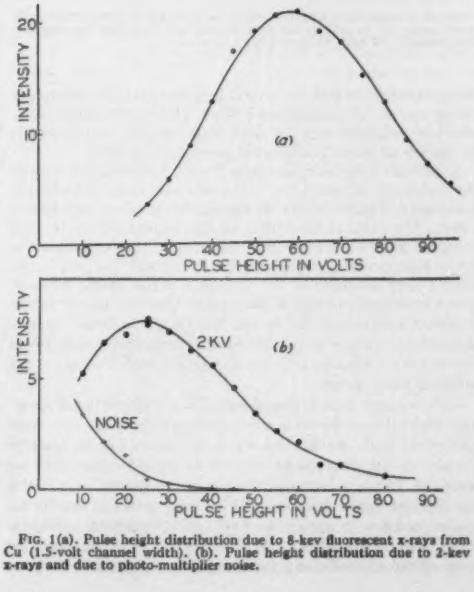

FIG. 1(a). Pulse height distribution due to 8-kev fluorescent x-rays from Cu (1.5-volt channel width). (b). Pulse height distribution due to 2-kev x-rays and due to photo-multiplier noise.

statistical considerations. With 2-kev x-rays the pulse height distribution shown in Fig. 1b was obtained, on which we have plotted also the noise pulse height distribution. The interpretation of this curve in terms of detection efficiency must await further calculations and measurements, but rough considerations indicate a detection efficiency of greater than 50 and less than 80 percent. This high detection efficiency of NaI(Tl) crystals for low energy x-rays sees to differ markedly from the sharp drop in the detection efficiency of anthracene crystals for low energy electrons[3] (<15 kev). Part of the latter effect may perhaps be due to a low light-collection efficiency in that experiment.

The average pulse height, which we identified with the peak pulse height for all energies except for 2 kev, varied linearly (within the experimental error) with the x-ray energy from 2 to 411 kev. For the measurement at 411 kev we used the gamma-ray[3] from Au^{198}. The linearity test was made in three different overlapping energy ranges, indicated by (a), (b), and (c) in Fig. 2. In each energy range different pulse height distributions were measured with a definite photo-multiplier tube voltage—about 700 volts for (a) and (b) and 800 volts for (c). One particular crystal was used

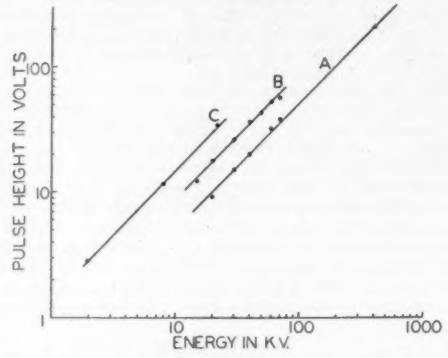

FIG. 2. Average pulse height (normalized to a gain of 1000) *vs.* incident x-ray energy for three different experimental arrangements, showing the proportionality of NaI(Tl) from 2 kev to 411 kev.

during one day, so that the crystal surface would not deteriorate during one set of measurements. The pulse height distributions were not measured with the same amplifier gain, but in Fig. 2 the gain of all points is arbitrarily normalized to 1000.

At incident x-ray energies above 33 kev, the binding energy of the K-electrons in iodine, two peaks were seen in the pulse height distribution. Figure 3 shows the distribution obtained with 44-kev x-rays. The peak at the higher energy corresponds to the full energy of the incident x-ray: both the iodine photo-electron and the iodine K x-ray energy are absorbed in the crystal. The peak at the lower energy is caused by the occasional escape of the iodine K x-rays from the front face of the crystal. That this interpretation is correct is demonstrated by the fact that at different energies of the incident x-rays (above 33 kev) the energy difference between the two peaks remains constant and approximately equal to the iodine K x-ray energy.

This "escape" peak is also observed in gas proportional counters,[4] where it is of the same order of magnitude as the main peak and where both the K_α and K_β escape peaks can be resolved because of the much larger number of pulse-forming electrons available. In the present case the escape probability is at most $\frac{1}{3}$ for incident x-rays just above 33 kev and decreases rapidly for higher energies, in agreement with rough theoretical considerations. This escape of the iodine K x-rays will, of course, lower the over-all detection efficiency for the incident x-rays unless the pulse

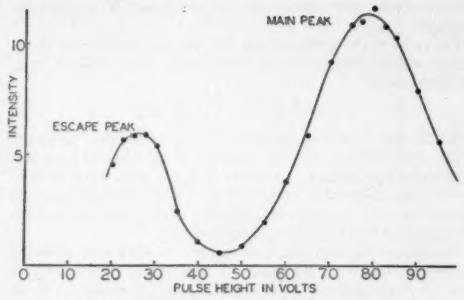

FIG. 3. Pulse height distribution due to 44-kev x-rays, showing small peak due to escape of I K-x-rays.

height discriminator bias is made low enough to detect the lower energy peak. We have also placed additional crystals close to the detector crystal and have observed the capture of most of the escaping radiation.

These and other experiments will be described elsewhere in the near future. We wish to thank Dr. J. A. McIntyre, Mr. W. Anderson, and Mr. L. Rieser for their help with this work.

* This work was supported by the joint program of the ONR and AEC.
[1] R. Hofstadter and J. A. McIntyre, Nucleonics **7**, No. 3, 32 (1950).
[2] W. J. Ramler and M. S. Friedman, Rev. Sci. Instr. **21**, 784 (1950).
[3] J. W. M. DuMond, Cal. Inst. Tech., Report No. 3, March 30, 1948, unpublished.
[4] S. C. Curran, *et al.*, Phil. Mag. **40**, 929 (1949), and earlier; D. West and P. Rothwell, Phil. Mag. **41**, 873 (1950).

Binding Energy of the Triton*

ROBERT L. PEASE† AND HERMAN FESHBACH
Department of Physics and Laboratory for Nuclear Science and Engineering, Massachusetts Institute of Technology, Cambridge, Massachusetts
October 25, 1950

AS is well known, low energy two-body nuclear data can be described satisfactorily in terms of a shape-independent approximation.[1] On the other hand, predictions of high energy $n-p$ scattering data and of the triton binding energy depend on the assumed shape of the interaction potential. We have investigated in a limited way the dependence of the binding energy of H^3 on the range of the tensor force part of such a potential.

A nuclear interaction potential, consisting of central and tensor terms, was assumed as given below:

$$V(r)=-V_0\{[1-\tfrac{1}{2}g+\tfrac{1}{2}g(\boldsymbol{\sigma}_1\cdot\boldsymbol{\sigma}_2)]\exp(-r/r_0)/r/r_0 + \Gamma S_{12}\exp(-r/r_t)/r/r_t\}.$$

It has met with success in describing low energy scattering processes and in accounting for the properties of the deuteron. Singlet and triplet wells can be obtained from such a potential, and charge independence of nuclear forces can be preserved.[2]

Calculations have been carried out to determine more accurately the shape of this well by using, instead of scattering data, the experimental value of the binding energy of H^3 to set the range of tensor forces. Whereas scattering data are in general insensitive to variations in tensor range, the binding energy may be expected to be reasonably sensitive.

The central force range r_0 was obtained from singlet scattering data, primarily on $p-p$ scattering. The constant g was fixed by consideration of the difference between singlet and triplet well depths in $n-p$ scattering. From r_0 and assumed values of r_t, the constants Γ and V_0 were set by use of two-body data, and an upper limit to the triton binding energy was computed by the Ritz method.

The linear variation function first used contained four terms (one S state and three D states). Its flexibility was then increased by using, instead of one S state, a linear combination of two S states of the form

$$A_{s1}\exp[-\tfrac{1}{2}\lambda_1(r_1+r_2+\rho)]+A_{s2}\exp[-\tfrac{1}{2}\lambda_2(r_1+r_2+\rho)],$$

where r_1, r_2, and ρ are, respectively, $n-p$, $n-p$, and $n-n$ separations. This caused a drop in calculated binding energy of several percent. A similar procedure applied to the two most important D states produced negligible improvement.

An approximate value of the relativistic correction to the kinetic energy was computed, and a set of values of $E(H^3)$ *vs* r_t obtained, from which suitable results could be found by interpolation. Table I indicates the values of the phenomenological

TABLE I. Values of the phenomenological constants.

$E=$	7.65	8.50	Mev
$r_0=$	1.184	1.184	$\times10^{-13}$ cm (assumed)
$r_t\simeq$	1.58	1.67	$\times10^{-13}$ cm
$\Gamma\simeq$	0.69	0.54	
$V_0\simeq$	42.7	46.1	Mev
$g\simeq$	−0.044	−0.004	

constants corresponding to respective variationally computed binding energies of 7.65 and 8.50 Mev, representing (corrected) upper bounds of 90 percent and 100 percent of the triton binding energy. One notes that, for the second case in particular, g can be placed approximately equal to zero, so that singlet and triplet central potentials become identical, and the number of required constants is reduced.

Equivalent $n-p$ triplet scattering ranges were also computed, and were respectively 1.72 and 1.73×10^{-13} cm, in excellent agreement with the latest determinations.[3] The respective Coulomb energies for He^3 were 0.99 and 1.02 Mev, higher than the experimental value[4] of 0.77 Mev. The possible compensatory effect of magnetic moment interaction is being investigated. Work on increasing further the flexibility of the wave functions, by multiplication by power series in suitable combinations of interparticle distances, is also in progress.

* The work described was supported in part by the joint program of the ONR and AEC.

† Now at the University of New Hampshire, Durham, New Hampshire (Department of Mathematics).

[1] J. M. Blatt and J. D. Jackson, Phys. Rev. **76**, 18 (1949).
[2] H. Feshbach and J. Schwinger, unpublished.
[3] Hughes, Burgy, and Ringo, Phys. Rev. **77**, 291 (1950).
[4] Tollestrup, Jenkins, Fowler, and Lauritsen, Phys. Rev. **75**, 1947 (1949).

Beta-Spectrum of As^{77}

ERLING N. JENSEN, R. T. NICHOLS, AND J. CLEMENT
*Institute for Atomic Research and Department of Physics, Iowa State College, Ames, Iowa**

November 7, 1950

STEINBERG and Engelkemeier[1] found a maximum energy of 0.8 Mev for the beta-rays[2] of 40-hr As^{77} on the basis of the half-thickness value in aluminum. Mandeville, *et al.*,[3] state that the beta-rays of As^{77} have a range of 0.192 g/cm² in aluminum. This corresponds to a maximum energy[4] of 0.56 Mev.

A source of As^{77} was made available to us through the courtesy of Mr. W. J. Heiman and Dr. A. F. Voigt of this laboratory. The As^{77} was separated chemically from a germanium dioxide sample which had been wrapped with cadmium foil and bombarded with neutrons in the pile of the Argonne National Laboratory. The radiations from As^{77} were examined with a thin lens beta-ray spectrometer.[5] The As^{77}, in the form of arsenic trisulfide, was deposited on a Formvar-polystyrene film having a surface density of about 40 μg/cm². In order to obtain a reasonable counting rate a rather thick source of about 0.8 mg/cm² was required.

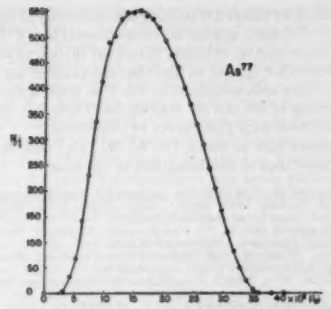

FIG. 1. The beta-spectrum of As^{77}. N is the counting rate and I is the current in the spectrometer coil. The data have not been corrected for counter window absorption.

The beta-spectrum is shown in Fig. 1. The data have not been corrected for window absorption. The allowed Kurie plot is shown in Fig. 2. By the method of least squares, using the points with $W>1.65\ mc^2$, the maximum energy is found to be 2.330 mc^2, giving a maximum kinetic energy of 0.679±0.004 Mev. The deviations of the points from the straight line, at $W<1.65\ mc^2$, are thought to be due to the rather thick source required. No internal conversion lines were observed. A search was made for photo-electron lines using a lead foil, but none were found. However, the source was very weak and therefore the evidence is not conclusive.

Using a half-life[6] of 38 hr the ft value is calculated to be 4.7×10^6. According to the nuclear shell model,[7] a regular filling of the levels would give a $f_{5/2}$ state to the As^{77} nucleus and a $g_{9/2}$ state to the Se^{77} nucleus. This gives a spin change of two units with a change in parity. This would be a first forbidden transition in which the correction factor $a=(W_0-W)^2+\lambda(W^2-1)$ is appropriate,[8] and $\log(ft)$ should have a value[9] between 8 and 9. This is contrary to the experimental evidence presented in this paper.

The experimental data[10–12] on the spin of Se^{77} are conflicting, but there is some evidence[10,12] that the spin is $\frac{1}{2}$. This would give the Se^{77} nucleus a $p_{1/2}$ state. A $p_{1/2}$ level for 43 neutrons is explained by Mayer[7] on the basis that the greater pairing energy causes the $g_{9/2}$ state to fill in pairs. Experimentally it is found that all elements with odd Z from 29 to 35 inclusive have a spin[13] of 3/2 with a $p_{3/2}$ state.[7] This suggests that As^{77} may perhaps have a $p_{3/2}$ state. This assignment is again explained on the basis that a greater pairing energy causes the $f_{5/2}$ state to fill in pairs. With the assignments of $p_{1/2}$ and $p_{3/2}$ for Se^{77} and As^{77}, respectively, this gives a transition in which the spin change is one unit with no change in

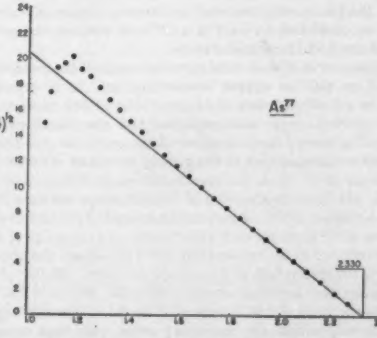

FIG. 2. The allowed Kurie plot of the As^{77} beta-spectrum.

parity. This is an allowed transition and according to Nordheim's[9] rule number 3 should, in general, have values of log (ft) from 4.8 to 5.5. The experimental evidence presented in this paper indicate that the transition is allowed and that the value of log (ft) is 5.7. With the above spin assignments this is in good agreement with the predictions of the nuclear shell model. These spin assignments are in agreement with those given by Nordheim.[14]

The authors wish to thank Dr. W. W. Pratt and Mr. R. Lane for their assistance in obtaining part of the data.

* Contribution No. 128 from the Institute for Atomic Research and Department of Physics, Iowa State College, Ames, Iowa. Work was performed in the Ames Laboratory of the AEC.

[1] E. P. Steinberg and D. W. Engelkemeier, Plutonium Project Report CC-2310, p. 31 (January, 1945), unpublished.
[2] Steinberg, Winsberg, and Engelkemeier, Plutonium Project Report CC-2379, p. 5 (November, 1944), unpublished.
[3] Mandeville, Woo, Scherb, Keighton, and Shapiro, Phys. Rev. **75**, 1528 (1949).
[4] L. E. Glendenin, Nucleonics **2**, No. 1, 12 (1948).
[5] Jensen, Laslett, and Pratt, Phys. Rev. **75**, 458 (1949).
[6] W. J. Heiman, private communication.
[7] M. G. Mayer, Phys. Rev. **78**, 16 (1950).
[8] Laslett, Jensen, and Paskin, Phys. Rev. **79**, 412 (1950).
[9] L. W. Nordheim, Phys. Rev. **78**, 294 (1950).
[10] Strandberg, Wentink, and Hill, Phys. Rev. **75**, 827 (1949).
[11] J. E. Mack and O. H. Arroe, Phys. Rev. **76**, 173 (1949).
[12] Geschwind, Minden, and Townes, Phys. Rev. **78**, 174 (1950).
[13] J. E. Mack, Revs. Modern Phys. **22**, 64 (1950).
[14] L. W. Nordheim, *Tables for β-Decay Systematics*, distributed privately.

On the Existence of a One-Mev Energy Level in C^{13}

MARY BLUNDELL AND J. ROTBLAT
Physics Department, St. Bartholomew's Hospital Medical College, London, England
November 9, 1950

THERE has been considerable discussion recently in the literature concerning the existence of an energy state of C^{13} at 0.8 to 1.0 Mev. A level at 0.8 Mev was first reported to be observed in the $B^{10}(\alpha, p)$ reaction; more recently it was observed by Roy,[1] using polonium α-particles. On the other hand, Creagan,[2] using α-particles produced in the cyclotron, failed to observe such a level. The $C^{13}(d, p)$ reaction was studied in detail by Heydenburg, *et al.*,[3] and by Buechner, *et al.*,[4] the latter using magnetic analysis; but neither of them found any evidence of a C^{13} level in this region. Quite recently, however, Boyer[5] and Berlman[6] claim to have observed a level at 1 Mev in a $C^{13}(d, p)$ reaction, using deuterons of 10 and 14 Mev.

We have made a detailed search for this level in the course of a study of energy states of C^{13}, which will be published elsewhere. The levels were excited using 8-Mev deuterons from the Liverpool cyclotron, and the protons corresponding to the various states of excitation of C^{13} were observed by means of photographic emulsions. The target used was acetylene at a pressure of 10 cm, and care was taken to eliminate contaminations. Although large areas of the plates were scanned and several angles of emission studied, we could find no trace of a C^{13} level between the ground state and the 3.11-Mev excited state.

The observation of such level by other workers can possibly be explained as due to oxygen contamination. It is extremely difficult to get rid of traces of oxygen; even in our experiments, where a gaseous target was employed and the emulsions were evacuated for several hours to drive off the water, we still observe some tracks corresponding to the ground state and the 0.88-Mev excited state of O^{17}, from the reaction $O^{16}(d, p)$. This can be seen in Fig. 1, which shows a section of the histogram obtained at an angle of emission of 75°. Between the ground state and first excited state of C^{13} there are only a few tracks, and almost all of them can be attributed to the two states of O^{17} if we assume the presence of oxygen contamination at a pressure of $\frac{1}{4}$ mm. Similar results were obtained for angles of emission 40°, 60°, 90°, and 120°; in each case the ratio of the numbers of tracks of the two oxygen groups agrees, within the statistical error, with that expected from the angular distribution of the protons from the $O^{16}(d, p)$

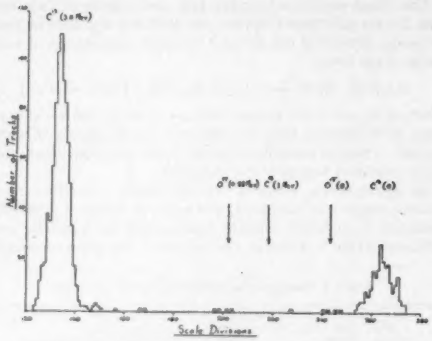

FIG. 1. Section of histogram of protons emitted at an angle 75°. One division = 1.73 microns.

reaction.[7] The position of the supposed 1-Mev level is also indicated on Fig. 1. At larger angles of emission the group of protons corresponding to such a level will fall nearer the 0.88-Mev oxygen group which can, therefore, easily be mistaken for it. We conclude that if a C^{13} level exists in the region of 1 Mev, its probability of excitation in a (d, p) reaction is at least 200 times lower than that corresponding to the ground state.

[1] R. R. Roy, Phys. Rev. **75**, 1775 (1949).
[2] R. J. Creagan, Phys. Rev. **76**, 1769 (1949).
[3] Heydenburg, Inglis, Whitehead, and Hafner, Phys. Rev. **75**, 1147 (1949).
[4] Buechner, Strait, Sperduto, and Malm, Phys. Rev. **76**, 1543 (1949).
[5] K. Boyer, Phys. Rev. **78**, 345 (1950).
[6] I. B. Berlman, Phys. Rev. **79**, 411 (1950).
[7] Burrows, Gibson, and Rotblat, Phys. Rev. **80**, 1094 (1950).

The Ratio of Electrons to Mesons 1100 Feet Underground*

C. A. RANDALL AND W. E. HAZEN
Randall Laboratory of Physics, University of Michigan, Ann Arbor, Michigan
November 14, 1950

THERE have been experiments that apparently contradict the usual assumption that cosmic-ray energy is carried underground primarily by μ-mesons.[1] The present experiments on the absorption of the hard and soft radiation and on the nature of the soft radiation were designed to test whether or not there really are any contradictions with the assumption of μ-mesons. The results on absorption in large thicknesses of lead and cloud-chamber observations,[2] both of which support the assumption of μ-mesons, have been reported previously.

The radiation emerging from a salt layer ~150 cm thick that was 700 cm above the apparatus in a salt mine at a depth of 8.5×10^4 g/cm^2 was measured by coincidences between two trays of G-M counters. (Three trays were used in the auxiliary experiment to determine the effect of local radiation.) The low energy cosmic-ray particles were identified as electrons by comparison of the absorptions by lead and by carbon, and their energy distribution was determined from their range distribution in carbon.

The coincidence rates were converted to flux of particles through the apparatus by making small corrections for side showers, knock-on electrons produced in the material near the counters or in the counter walls, multiple events through the trays, and coincidences produced by gamma-rays from radioactive materials. Auxiliary experiments gave the data required for making the corrections.

The meson flux was subtracted from the total flux in order

to obtain the flux of electrons. The ratio of electron to meson flux is shown in Fig. 1. If the meson spectrum is independent of zenith angle, the electron to meson ratio is independent of zenith angle and the ratio of electron to meson flux through the entire apparatus is the same as the ratio of electron to meson intensity at a given angle. Since the meson energy spectrum underground is probably a function of zenith angle and since Wilson's data[3] give information concerning intensities near the vertical, we should compare vertical intensities of electrons and mesons. This was done for the case of electrons with energy greater than 3 Mev as follows. From the flux determinations for six different tray separations, all with 15 cm of lead absorber, the zenith angle distribution of meson intensity was obtained for angles near the vertical. If we assume that the distribution has the form

$$I(\theta) = I_v \cos^n\theta,$$

the constants have the values

$$I_v = 2.17 \pm 0.02 \times 10^{-6} \text{ sec}^{-1} \text{ sterad}^{-1} \text{ cm}^{-1}$$
$$n = 2.8 \pm 0.1.$$

Similarly, the distribution for electrons of energy greater than 3 Mev has the constants

$$I_v = 0.92 \pm 0.06 \times 10^{-6} \text{ sec}^{-1} \text{ sterad}^{-1} \text{ cm}^{-2}$$
$$n = 1.4 \pm 0.3.$$

The meson vertical intensity was subtracted from the total vertical intensity to give the electron vertical intensity for $E > 3$ Mev. The intensity distribution for electrons of $E > 3$ Mev is an average for electrons of many energies. The higher energy electrons preserve the original direction of the parent mesons and thus may have an angular distribution more nearly like the mesons. (If the meson spectrum is independent of zenith angle, the high energy electrons have the same angular distribution as the mesons.) At any rate, we obtain upper or lower limits for the spectrum of electrons from the vertical by assuming, respectively, that the angular distribution of all electrons is the same as for the mesons or that it is the same as the average value for all electrons with $E > 3$ Mev. The limiting values are shown in Fig. 1.

The number of electron secondaries to be expected has been calculated using the method of Williams.[4] This number depends on the local meson spectrum, which can be obtained, at least approximately, from Wilson's data for intensities at depths greater than the present observation depth.[3] The knock-on contribution does not depend critically on the assumed local meson spectrum and is shown in Fig. 1. On the other hand, the radiation contribution to secondary photons and thence to secondary electrons does depend strongly on the local meson spectrum. If we use a meson spectrum based on Wilson's data and on the assumption that the radiation losses are small enough so that they can simply be added to the collision losses, the contribution to the secondary electrons by radiation by mesons of spin one-half is about equal to the knock-on contribution at low electron energies and becomes greater than the knock-on contribution at high electron energies.

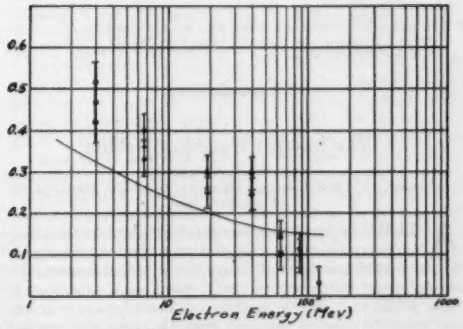

FIG. 1. The integral spectrum for electrons in terms of number of electrons per meson. The curve is the expected contribution by knock-on electrons and their progeny. The inclusion of the contribution by radiation would roughly double the height of the curve at low energies. The experimental points are believed to represent upper and lower limits.

Although the measured number of electrons is somewhat less than predicted, we believe that the uncertainty in the local meson spectrum accounts for the discrepancy and that there is no reason to believe that the penetrating component does not consist mostly of μ mesons. The experiment was made possible by the cooperation of the management of the International Salt Company and of the personnel at the Detroit mine.

* The research was aided by the joint program of the ONR and the AEC.
[1] J. Barnothy and M. Forro, Phys. Rev. **74**, 1300 (1948).
[2] L. Tiffany and W. Hazen, Phys. Rev. **77**, 849 (1950); Randall, Sherman, and Hazen, Phys. Rev. **79**, 905 (1950).
[3] V. C. Wilson, Phys. Rev. **53**, 377 (1938).
[4] E. J. Williams, Proc. Camb. Phil. Soc. **36**, 183 (1940).

An Investigation of the 2943-cm^{-1} Line of the Solar Spectrum*

W. M. BENESCH, F. P. ELDY, AND J. T. ELDER
Johns Hopkins University, Baltimore, Maryland
November 6, 1950

MIDWAY between the -7 and the -8 lines of the ν_3 fundamental band of methane lies an interesting line which has been detected by several investigators.[1-3] Mohler and Pierce[2] measured the wavelength of this line very accurately and attributed the absorption to silicon and magnesium in the sun. Subsequently, Migeotte[4] cast doubt on this assignment by showing that the line did not appear in solar spectra taken at his laboratory in the Swiss Alps. More recently, spectra of highly humid atmosphere obtained at this laboratory during the past summer with a searchlight source failed to reveal this line, although a number of normally weaker water lines were evident.[5] Earlier unpublished[6] work by one of us had indicated the possible intrusion of extraneous lines of methane into this region as well as the sensitivity of the 2943-cm^{-1} line to the insertion of methane into the solar beam. Because of other absorption in the atmosphere in this region, however, this evidence was inconclusive; it appeared advisable, therefore, to obtain a pure spectrum of methane of sufficient concentration to indicate whether or not this was a weak methane line.

Dr. Shirleigh Silverman, of the Applied Physics Laboratory, Johns Hopkins University at Silver Spring, kindly offered the use of his high resolution vacuum spectrograph to obtain this spectrum. The region of the P-branch of this methane band was scanned with a short cell filled with chemically pure methane at atmospheric pressure. Between the -7 and -8 lines of the band of the 2943-cm^{-1} line appeared clearly; with the cell filled with air this line, as well as the -7 and -8 lines, vanished. We conclude from this that the 2943-cm^{-1} line is definitely due to methane.

Among the other main methane lines occurred occasional weak absorption which bore a resemblance to the "background" lines of the early methane spectrum of Nielsen and Nielsen.[7] Although these authors did not identify them definitely with methane, the agreement between many of their lines and ours indicates that this indeed may be their origin, perhaps owing to nearby combination or overtone bands. It is planned to study these weaker lines in more detail in the near future.

The advice and assistance of Dr. John Strong, Dr. Silverman, and Mr. Robert Stanley are gratefully acknowledged.

* Supported in part by ONR funds.
[1] Migeotte, Astrophys. J. **107**, 400 (1948).
[2] Mohler and Pierce, Astron. Soc. Pacific, **61**, 221 (1949).
[3] Benesch, Strong, and Benedict, ONR Progress Report, August 1, 1950.
[4] Talk at Ohio State Symposium on Molecular Spectroscopy, June, 1950.
[5] Benesch, Elder, and Strong, ONR Progress Report, September 15, 1950.
[6] Solar spectra recorded by W. Benesch, October, 1949.
[7] Nielsen and Nielsen, Phys. Rev. **48**, 864 (1935).

Luminescent Efficiency of Organic Solutions and Crystals

PETER D. JOHNSON AND FERD E. WILLIAMS
General Electric Research Laboratory, Schenectady, New York
November 8, 1950

IN a recent paper[1] a theory of luminescent efficiency has been proposed and applied to data on inorganic phosphors. Because the formulation is quite general, it can be used to interpret recent data[2-4] on luminescent organic solutions and crystals excited by gamma-rays. The excitation energy may be absorbed (I) directly by the luminescent molecules, or (II) by the solvent molecules which may (A) transfer the energy to the luminescent molecules or (B) lose the energy by radiationless processes. The luminescent molecules or "activators" lose the energy by (a) nonconcentration dependent radiationless processes, (b) radiationless processes resulting from interactions with nearby unexcited activators, and (c) emission.

The data of Kallman and Furst comprise mainly low activator concentrations; therefore (I) is insignificant. Also, (a) affects the absolute energy efficiency but not the concentration dependence of luminescence. Therefore, it is possible to apply the explicit expression for efficiency, η, as a function of gross activator concentration C:

$$\eta = C(1-C)^z/[C+(\sigma/\sigma')(1-C)], \tag{1}$$

where z is the number of positions surrounding a given activator which if occupied by a second activator molecule quench luminescence, (b), and σ/σ' is the ratio of probabilities of processes (B) to (A) with unit concentrations of solvent and activator, respectively. Figure 1 shows the data of Kallman and Furst[2] and the

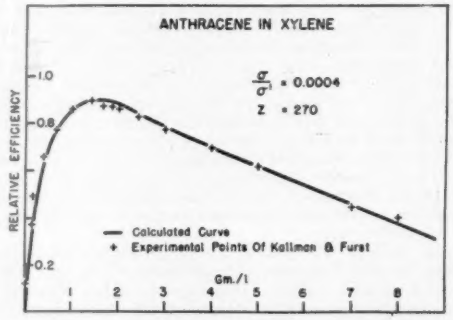

FIG. 1. Efficiency *vs.* activator concentration of anthracene in xylene.

calculated curve for anthracene in xylene. z is 270, indicating an interaction sufficient to quench luminescence between activators separated by three molecular diameters. That σ/σ' is only 0.0004 demonstrates that (A) is favored over (B), transfer of excitation energy occurring over as many as five solvent molecular diameters. The same values of z and σ/σ' are obtained from data[3] on carbazole in xylene. This is not surprising in view of the chemical similarity of anthracene and carbazole.

The situation is different for naphthalene in xylene as shown by the data of Ageno, Chiozzotto, and Querzoli.[3] At high molecular concentrations of naphthalene, there is no evidence of a decrease in luminescent output; therefore, (b) is inoperative and z is zero. Also, at the high activator concentrations involved, (I) is important. The efficiency may be expressed as a linear combination of the efficiencies of the two excitation mechanisms (I) and (II):

$$\eta = f_{\mathrm{I}}\eta_{\mathrm{I}} + (1-f_{\mathrm{I}})\eta_{\mathrm{II}}. \tag{2}$$

The ratio, κ, of capture cross sections of activator and solvent for

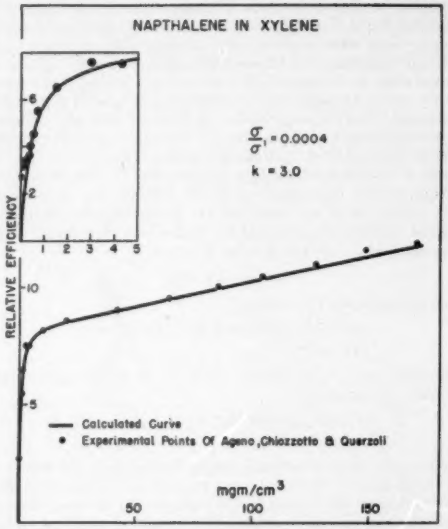

FIG. 2. Efficiency *vs.* activator concentration of naphthalene in xylene.

gamma-rays is approximately equal to the ratio of densities of napthalene and xylene. Equation 2 becomes:

$$\eta = \left[\frac{\kappa C}{C(\kappa-1)+1}\right]\cdot k + \left[\frac{(1-C)}{C(\kappa-1)+1}\right]\cdot\left[\frac{C}{C+(\sigma/\sigma')(1-C)}\right]. \tag{3}$$

Figure 2 demonstrates the agreement of Eq. (3) and the data[3] of Ageno, *et al.* The value of σ/σ' appears to be characteristic of xylene. The relative probabilities of (a) and (c) and of (I) and (II) determine k. That there is no interaction to quench luminescence is probably related to the chemical stability of naphthalene.

Equation (11) of reference 1 predicts that the temperature dependence of luminescent efficiency should be greater at lower activator concentration because of a higher activation energy for (b). Also, this activation energy should change less rapidly with concentration at lower concentrations. Both predictions are in agreement with the data of Liebson and Farrar[4] on the temperature dependence of luminescence of mixtures of naphthalene and anthracene.

[1] P. D. Johnson and F. E. Williams, J. Chem. Phys. **18**, 1477 (1950).
[2] H. Kallman and M. Furst, Phys. Rev. **79**, 857 (1950).
[3] Ageno, Chiozzotto, and Querzoli, Phys. Rev. **79**, 720 (1950).
[4] S. H. Liebson and R. J. Farrar, Phys. Rev. **79**, 733 (1950).

The Isotopic Weight of Helium

KENNETH T. BAINBRIDGE
Department of Physics, Harvard University, Cambridge, Massachusetts
November 7, 1950

A TABLE of isotopic weights obtained by the combination of nuclear reaction Q values and mass spectrograph doublets has been published by Tollestrup, Fowler, and Lauritsen.[1] It is the purpose of this letter to show (1) that a more satisfactory isotopic weight scale can be based on a different approach, in which the value for He^4 is obtained from the mass spectrographic ($2D^2-He^4$) doublet,[2-4] and (2) that apparent gross errors which exist in the Q values can reasonably be attributed to the values associated with the $Li^7(p,\alpha)He^4$ and $Li^6(d,\alpha)He^4$ reactions.

Table I of reference 1 should be utilized to obtain the Q values

needed in the discussion which follows. The reactions of column 1 of Table I should be numered in sequence. The "as measured" Q values in column 2 are the input values in Mev from which the mass equivalents in milli-mass units are secured by multiplying by the usual conversion factor 1.074.

The mass difference $(2D^2-He^4)$ can be obtained from disintegration data alone by the combination in "cycles" of Q values from reactions from which all atoms other than D and He have been eliminated by subtraction of identities.[5] One such cycle utilizing n, H^1, D^2, He^3, He^4, Li^6, and Li^7 yields

$$(2D^2-He^4)=0.025522\pm0.000045\text{MU}=(Q_1+Q_4+Q_{10}+Q_{13}-Q_9)\times1.074. \quad (a)$$

A second cycle involving H^1, D^2, He^4, Li^7, Be^8, and Be^9 yields

$$(2D^2-He^4)=0.025536\pm0.000039\text{MU}=(Q_{13}+Q_{21}-Q_{15}-Q_{18})\times1.074. \quad (b)$$

A third cycle which includes H^1, D^2, He^4, Li^8, Be^8, and Be^9 yields

$$(2D^2-He^4)=0.025431\pm0.000042\text{MU}=(Q_{11}+Q_{19}-Q_{15}-Q_{18})\times1.074. \quad (c)$$

These three cycles are sufficient for the argument. If (a), (b), and (c) are combined, the result would be represented approximately by 0.02550 ± 0.000023.

In the case of the four measurements of the $(2D^2-He^4)$ doublet by four different instruments, the values (in MU) are 0.02551 ± 0.00008;[6] 0.02561 ± 0.00004;[7] 0.025604 ± 0.000009;[8] 0.025612 ± 0.000008.[4] The recent measurements of Nier and Ewald may be weighted equally to give

$$0.025608\pm0.000006=(2D^2-He^4). \quad (d)$$

The differences between this value and those given by Eqs. (a), (b), and (c) are 12 to 30 times the probable errors of the Ewald-Nier measurement and 2 to 4 times the probable errors of the combined Q values of Eqs. (a), (b), and (c). Q_{11} and Q_{12} naturally come under suspicion as they represent the only Q values obtained from range-energy measurements, while all other Q values are from electrostatic or magnetic deflection studies.[1] Also, Q_{11} should equal $Q_{10}+Q_{13}$; and the fact that the probable errors do not overlap, $Q_{11}-Q_{10}-Q_{13}>\epsilon_{11}+\epsilon_{10+13}$, has indicated that Q_{13} or Q_{11} or both may be away from their true values by more than the assigned probable errors. Equations (a), (b), and (c), considered with the Ewald-Nier value for $(2D^2-He^4)$, Eq. (d), furnish a strong indication that Q_{13} and Q_{11} are *both* too small, where hitherto only one or the other of these values or their difference has been under suspicion. An error of the magnitude indicated above in the mass spectrograph result of Ewald would correspond to an error in the doublet separation of $\frac{1}{4}$ the width of a line or an error in the dispersion of $\sim\frac{1}{4}$ percent. An examination of Ewald's remarkable spectra shows how remote is the possibility of any error of that magnitude. Equivalent possibilities in Nier's excellent work are equally unlikely.

The magnitudes and assigned probable errors of the Q values other than Q_{11} and Q_{13} make it appear that the difficulties lie with Q_{11} and Q_{13} in the disagreement between the mass spectrograph and the disintegration mass scales. The source of the possible errors in Q_{11} and Q_{13} might be in the range energy curve.

However, as is well known, the measurement of Q_{13} for the reaction $Li^7(p,\alpha)He^4$ is essentially a measurement of the small range difference between the alpha particles from the Li^7 reaction and the alpha-particles of ThC′. The energy of the latter has been measured with very high precision by Briggs,[7] and Rosenblum and Dupouy.[8] Also, indirect checks of several kinds exist for the ThC′ measurements. The only reasonable change in Q_{11} from the ThC′ experiments is associated with the change in $2\epsilon/M$ for alpha-particles to conform to the weight of helium given below. There is no significant change in Q_{13} from this consideration. A detailed survey emphasizes that the $Li^7(p\alpha)He^4$ and $Li^6(d\alpha)He^4$ reaction Q values should be brought to the same high order of accuracy as is obtained by deflection methods for the other Q values listed in Table I of reference 1.

A mass scale for H^1, D^2, He^4, C^{12}, and O^{16} obtained chiefly from doublet measurements is appended. The input data also includes the important results of Bell and Elliott[9,10] for Q_1 for $H^1(n\gamma)D^2$, and Taschek, *et al.*,[11] and others[12] for $n-H^1$ combined to give $2H^1-D^2=1.555\pm0.006\times10^{-3}$ MU. This is averaged with Roberts and Nier's[13] measurement $1.549\pm0.006\times10^{-3}$ MU.

The baic mass-spectrographic doublets are as follows:

$$(H^1)_2-D^2=15.52\pm0.04\times10^{-4}\text{ MU}^{9,11,13}$$
$$(D^2)_3-\tfrac{1}{4}C^{12}=422.28\pm0.19\times10^{-4}\text{ MU}^{10}$$
$$C^{12}+(H^1)_4-0=364.5\pm0.22\times10^{-4}\text{ MU}^{10}.$$

The corresponding mass scale is as follows:

$$n=1.0089785;\quad H^1=1.0081386;\quad D^2=2.0147252;$$
$$\underset{38}{}\quad\underset{32}{}\quad\underset{57}{}$$
$$He^4=4.003842;\quad C^{12}=12.003895.$$
$$\underset{13}{}\quad\underset{19}{\phantom{C^{12}=12.003895.}}$$

A complete table of isotopic weights derived from both reaction Q-values and mass spectrograph doublets is in preparation for the Nuclear Science Series of the National Research Council.

[1] Tollestrup, Fowler, and Lauritsen, Phys. Rev. **78**, 372 (1950).
[2] K. T. Bainbridge and E. B. Jordan, Phys. Rev. **51**, 384 (1937).
[3] H. Ewald, Z. Naturforsch. **5**, 1 (1950).
[4] I am indebted to Professor A. O. Nier for this information, which is one of many doublet measurements in process of publication in a paper to appear in the *Physical Review*.
[5] W. Braunbek, Z. Physik **107**, 1 (1937).
[6] F. W. Aston, Nature **135**, 541 (1935).
[7] G. H. Briggs, Proc. Roy. Soc. **A157**, 183 (1936).
[8] S. Rosenblum and G. Dupouy, Compt. rend. **194**, 1919 (1932).
[9] R. E. Bell and L. G. Elliott, Phys. Rev. **79**, 282 (1950).
[10] K. T. Bainbridge, Seventh Solvay Chemistry Congress, R. Stoops, Brussels, 1948.
[11] Taschek, Argo, Hemmendinger, and Jarvis, Phys. Rev. **76**, 325 (1949).
[12] W. B. Lewis, Report DR 12, Natural Research Council, Canada, December 30, 1949.
[13] T. R. Roberts and A. O. Nier, Phys. Rev. **77**, 746 (1950).

The Perfect Diamagnetism of Free Electrons with Application to Superconductivity

M. F. M. Osborne
Naval Research Laboratory, Washington, D. C.

November 6, 1950

CALCULATIONS have been made on the Fermi-Dirac statistics of free charged particles in a uniform magnetic field in a *finite* box, and of free particles in a magnetic field which decays exponentially from the applied field at the surface of the box. Particular attention is paid to using $\psi=0$ rather than ψ periodic as the boundary condition on the walls of the box.

Considering the first problem above, it follows from the rigorous application of this boundary condition to a finite cylinder of dimensions R, L_0, with H along the axis, that the total number of particles and the energy $U-MH$ at absolute zero are, for an orbit radius smaller than the dimensions of specimen: $\alpha=kch/eH$,

$$N=(Vk^3/6\pi^2)[1+(3\pi/8R)\alpha+(2/5R^2)\alpha^2]$$
$$U-MH=(k^5V/20m\pi^2)[1+(5\pi/12R)\alpha+(10/21R^2)\alpha^2].$$

Here, $k=(2m\zeta)^{\frac{1}{2}}/\hbar$, where ζ is the energy of the highest occupied state.

The last two terms in brackets correspond to orbits whose centers are just outside (<orbit radius) the specimen[1] (with periodic boundary conditions, these would be counted in the adjoining "big cell"), and orbits which encircle the origin.[2] These extra terms vanish in the limit $V\to\infty$, N/V finite, so that they depend on the size and the shape of the specimen. For macroscopic specimens they still make a large contribution to the magnetic moment, shown in Fig. 1.

If one assumes that Fig. 1 gives M as a function of $H_{\text{effective}}$ and uses the relation $H_{\text{eff}}=H_{\text{appl}}+4\pi M(H_{\text{eff}})$ to obtain $H_{\text{appl}}=f(H_{\text{eff}})$, and then $M=f(H_{\text{appl}})$, one obtains Fig. 2, curve (1), which indicates almost perfect diamagnetism up to a critical field and then a triple-valued transition (similar to the condensation of a Van der

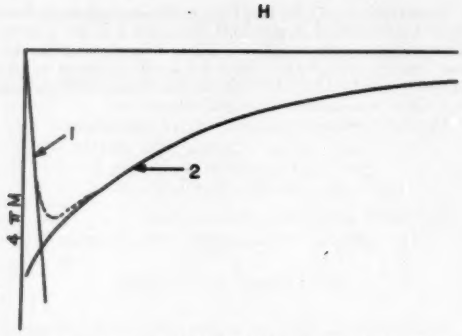

FIG. 1. Magnetization *vs.* field. (1) Orbit radius greater than the specimen dimension (perturbation calculation of plane wave functions). (2) Orbit radius smaller than the specimen dimensions.

Waals gas) to a nondiamagnetic state. This behavior is provisionally identified with the perfectly diamagnetic behavior of a superconductor, which will hold for all specimens of reasonable macroscopic dimensions. If the validity of the above idealized analysis is admitted, the remaining problem is not to explain why some materials *are* perfectly diamagnetic, but rather to explain why most real materials and specimen sizes are *not* perfectly diamagnetic, except a few known superconductors over a very restricted range of field and temperature.

It follows from the above calculation that for fields which are not too large an applied field will be almost completely expelled from the box, leaving some small residual effective field ϵ. But since H must be continuous at the surface of the box, there must be a small layer there where the field rises rapidly from the small internal effective value ϵ to the external applied value. We can take as our second problem the limiting case in which the field is expelled completely except for a thin magnetic layer to provide continuity of H. The solution of this problem is given by curve (2) in Fig. 2. The wave functions are of two classes: (1) plane waves slightly modulated in amplitude and phase at the boundary, and (2) unidirectional waves which creep along the boundary. These unidirectional waves give the major contribution to the curve (2) of Fig. 2. There are no creeping quantum states if $H<\hbar c/k\epsilon\lambda^3$. λ is the penetration depth.

Evidently a completely consistent solution of the problem under

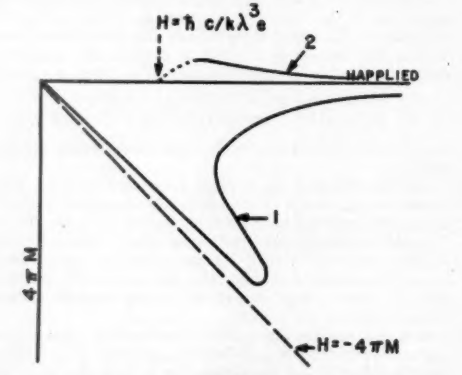

FIG. 2. Magnetization *vs.* applied field (1) H_{interior} uniform. (2) $H_{\text{interior}}=H_{\text{applied}}\exp(-y/\lambda)$, $y=0$ on surface.

discussion would be intermediate between the two cases above, but it seems evident that strong diamagnetism for not too large fields will certainly dominate the situation. Self-consistency can be achieved in another way. One compares $\mathbf{J}=-(c/4\pi\lambda^2)\mathbf{A}$ (London's equation) where $\mathbf{A}$ is the given vector potential with the quantum mechanical current

$$\mathbf{J}=(\hbar e/2mi)(\psi^*\nabla\psi-\psi\nabla\psi^*)-(e^2/mc)\mathbf{A}\psi\psi^*,$$

using the ψ's calculated in the presence of this $\mathbf{A}$. If the criterion for the absence of the creeping states is met, then the quantum mechanical current, $\mathbf{J}$ is of order $-\mathbf{A}$. This supports the original conjecture of London.[3]

It is a pleasure to acknowledge the benefit of numerous discussions of this problem with R. D. Meyers and the members of the cryogenics group of the Naval Research Laboratory.

[1] L. Landau, Z. Physik 64, 629 (1930).
[2] C. G. Darwin, Proc. Camb. Phil. Soc. 27, 37 (1931).
[3] F. London, Nature 140, 793, 834 (1937).

On the Determination of Reduced Widths from the One-Level Dispersion Formula

R. G. THOMAS*
Kellogg Radiation Laboratory, California Institute of Technology, Pasadena, California
October 16, 1950

THE intention of this note is to point out that a common approximation used in applying the one-level nuclear dispersion formula to the determination of reduced level widths may be unjustified in the case of broad levels, which are numerous in light nuclei.

The one-level dispersion formula as given by Eq. (57) of the paper of Wigner and Eisenbud[1] for the λth energy level is

$$\sigma^{ss'}=\frac{\pi}{(2js+1)k_s^2}\sum_{ii'}\frac{(2J+1)\Gamma_{\lambda si}\Gamma_{\lambda s'i'}}{(E_\lambda+\Delta_\lambda-E)^2+\frac{1}{4}\Gamma_\lambda^2}, \tag{1}$$

and according to Eqs. (58a) and (58b), in their notation,

$$\tfrac{1}{2}\Gamma_{\lambda si}=(B_{si}\gamma_{\lambda si})^2/(1+C_{si}^2), \quad \Gamma_\lambda=\Sigma_{si}\Gamma_{\lambda si};$$
$$\Delta_\lambda=\Sigma\Delta_{\lambda si}; \quad \Delta_{\lambda si}=\tfrac{1}{2}C_{si}\Gamma_{\lambda si};$$

i is the relative orbital momentum of the pair of particles s; B and C are related to the value and derivative of the extra nuclear wave functions at the nuclear radius a_s. The common approximation in applying these formulas to the determination of reduced level widths, $\gamma_{\lambda si}^2$, is to neglect the variation of the level shift, Δ_λ, with respect to the energy of the incident particle, with the result that Γ_λ is interpreted as the observed level width. It is not hard to calculate this variation, and it will be shown to be important in some cases. In the notation of Yost, Wheeler, and Breit[2] the regular solution to the wave equation in the region external to the nucleus is $F(x)$ and the irregular solution is $G(x)$, the argument x being equal to kr; then

$$\Delta_{\lambda si}=-(\gamma_{\lambda si}^2/a_s)(g_{si}+i), \quad \text{where} \tag{2}$$
$$g_{si}=[d\ln(F_{si}^2+G_{si}^2)^{\frac{1}{2}}/d\ln x]_{x=ka_s}.$$

By expanding Δ_λ linearly with respect to energy about the resonance, usually a good approximation, the one-level formula may be written as

$$\sigma^{ss'}=\frac{\pi}{(2js+1)k_s^2}\sum_{ii'}\frac{(2J+1)\Gamma'_{\lambda si}\Gamma'_{\lambda s'i'}}{(E-E_r)^2+\frac{1}{4}\Gamma_\lambda'^2}, \tag{3}$$

where the primed widths, which may be called the observed widths, are

$$\Gamma'_{\lambda si}=\Gamma_{\lambda si}[1+\Sigma_{si}(\gamma_{\lambda si}^2/a_s)(dg_{si}/dE)_{E=E_r}]^{-1}; \tag{4}$$

E_r is the observed resonance energy and satisfies the equation

$$E_\lambda+\Delta_\lambda(E_r)-E_r=0. \tag{5}$$

The same consideration applies to the dispersion theory of Feshbach, Peaslee, and Weisskopf.[3] All of the Γ's in expressions

(42) and (43) of reference 3 should be primed; in the notation of their paper, with the exception of g which is defined in Eq. (2) above; and with F^2+G^2 now equal to the $|v|^2$ of their paper, we have

$$\Gamma_n'^{(\rho)}=-(2x/|v|^2)[(df_0/dE)-(dg/dE)]^{-1}E=E_r,$$
$$\Gamma_a'^{(\rho)}=-2k[(df_0/dE)-(dg/dE)]^{-1}E=E_r; \quad (6)$$

$a^{-1}f_0$ is the real part of the logarithmic derivative of the wave function at the nuclear surface. The unprimed Γ's of expressions (41) and (12) remain unchanged.

An example where this correction is important is the 456-kev resonance in the $C^{13}(p,\gamma)$ reaction. The quantity dg/dE, which can be obtained from Breit's tables,[3,4] is here actually larger than df_0/dE; the sign of dg/dE is such that Γ is about $2\frac{1}{2}$ times larger than the observed width, Γ'. With this correction the reduced width, γ^2, becomes about equal to $\hbar^2/Ma$, M is the reduced mass (the exact value of γ^2 is sensitive to the value of the nuclear radius that is used). This reduced width $\hbar^2/Ma$ is equal to that given by Eq. (64) of reference 1 for a square well interaction and likewise the limiting value given by Eq. (44) of this same reference. This is an indication that the s-wave $C^{13}+p$ interaction can be treated as a simple one-body problem. The reduced width of the low energy neutron s-wave scattering by C^{13} is also equally large. This width is determined by fitting a one-level dispersion curve, including s-potential scattering, to the neutron scattering data up to 2 Mev, where scattering from higher partial waves becomes important. The scattering length in the low energy region is positive, and the bound state associated with it is the 3.10-Mev level of C^{13}. The correspondence of this bound level with the 456-kev resonance level of N^{13} has been pointed out.[5] In showing this correspondence it is necessary to consider this correction given by Eq. (4). A detailed report on the s-wave proton and neutron interaction with C^{13} will be forthcoming.

In applying the one-level dispersion theory at energies considerably off resonance, formulas (1) above or (38) and (39) of reference 3 should be used rather than the approximate expression (3); that is, f_0 may be a linear function of E (basic assumption of the one-level formula) over a wider range of energies than g.

In the case of s-wave neutron reactions, g is zero so that there is no correction. For higher partial waves dg/dE can be calculated from the penetrability factors $|v|^2$ given by Eqs. (45a) of reference 3; in the case of p neutrons $Edg/dE=(ka)^2[1+(ka)^2]^{-2}$. For example, if the resonance at 1.2 Mev in the scattering of neutrons by He^4 is p-wave, then $dg/dE=0.16$ Mev^{-1}. Supposing $\gamma^2=\hbar^2/Ma$, a being taken as $2.5\cdot10^{-13}$ cm, then the observed width at resonance would be $\Gamma'=0.76$ Mev. Were γ^2 infinite, the observed width would be only 1.2 Mev.

An exact criterion for the application of this correction cannot be given. It is probably not negligible for resonances for which $\gamma^2\gtrsim\hbar^2/10Ma$ (s-neutron resonances, of course, being excepted).

The writer is grateful for the discussion and suggestions of Professor R. F. Christy.

* AEC Predoctoral Fellow.
[1] E. P. Wigner and L. Eisenbud, Phys. Rev. **72**, 29 (1947).
[2] Yost, Wheeler, and Breit, Phys. Rev. **49**, 174 (1936).
[3] Feshbach, Peaslee, and Weisskopf, Phys. Rev. **71**, 145 (1947).
[4] Bloch, Hull, Broyles, Bouricius, Freeman, and Breit, *Coulomb Functions for Reactions of Protons and Alpha-Particle with the Lighter Nuclei*, Yale University (unpublished).
[5] R. G. Thomas, Phys. Rev. **80**, 136, 138 (1950), and J. B. Ehrman, private communication.

The Hall Coefficient of Semiconductors

H. JONES
Imperial College, London, England
November 6, 1950

IN a recent letter Johnson and Lark-Horowitz[1] have given an expression for the Hall coefficient of a semi-conductor which takes into account both thermal and impurity scattering of electrons in the conduction band. This theory is based on the following assumptions. (1) The mean free path for thermal scattering, l_1, is independent of the velocity of the electrons, and the mean free path for impurity scattering, l_2, is proportional to the fourth power of the velocity. The actual mean free path l is thus given by

$$l=l_1l_2/(l_1+l_2). \quad (1)$$

(2) It is assumed that the resistivity ρ can be expressed as the sum of the resistivity ρ_T due to thermal scattering alone plus the resistivity ρ_I due to impurity scattering alone; i.e.,

$$\rho=\rho_T+\rho_I. \quad (2)$$

The Hall coefficient R is then given by the equation

$$R/(1/ne)=(\sqrt{\pi}/48)(\rho/\rho_1)^2\int_0^\infty x^{9/2}e^{-x}dx/(1+\theta x^2)^3, \quad (3)$$

where, as a result of Eq. (2), θ is set equal to $\frac{1}{6}[(\rho/\rho_1)-1]$. This theory, however, appears to be not entirely satisfactory, for assumption (2) is not consistent with Eq. (1), which leads directly to Eq. (3). If the resistivity is determined from Eq. (1), it is easy to show that the Hall coefficient can be expressed as a function of ρ_1/ρ by Eq. (3) and the equation,

$$\rho_1/\rho=\tfrac{1}{2}\int_0^\infty x^2e^{-x}dx/(1+\theta x^2), \quad (4)$$

in terms of the parameter $\theta=\rho_T/6\rho_1$, which is now no longer equal to $\frac{1}{6}[(\rho/\rho_1)-1]$.

Figure (1) shows $R/(1/ne)$ as a function of ρ_1/ρ as determined

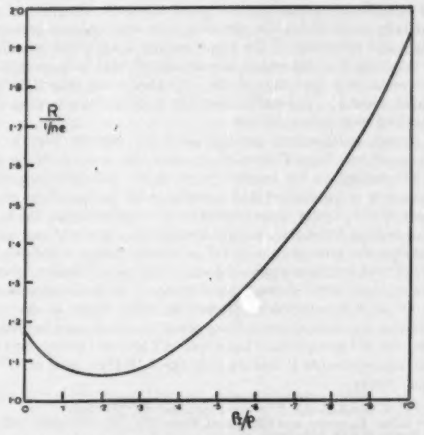

FIG. 1. Variation of the Hall coefficient R with the ratio of the resistance due to impurity scattering to total resistance; n is the number of electrons per cc.

from Eqs. (3) and (4). The integral of Eq. (4) can be expressed in finite terms, but Eq. (3) must be evaluated numerically. It will be noticed that, except at the end points, the values of $R/(1/ne)$ lie higher than those given by Johnson and Lark-Horowitz [Fig. 1, of reference 1]. A consequence of this is that the mobilities as given by these authors in a later letter,[2] should be generally reduced; e.g., by a factor of 1.8 at $\rho_1/\rho=0.2$ and by a factor of 2.0 at $\rho_1/\rho=0.5$. The discrepancy between the original values of the mobilities and the higher values found by Pearson, *et al.*,[3] would not, therefore, appear to be removed in the manner suggested.

From Eq. (4) it is easy to find the ratio $\rho/(\rho_T+\rho_I)$. It reaches a maximum value of approximately 1.43 at ρ_1/ρ in the neighborhood of 0.30.

[1] V. A. Johnson and K. Lark-Horowitz, Phys. Rev. **79**, 176 (1950).
[2] V. A. Johnson and K. Lark-Horowitz, Phys. Rev. **79**, 409 (1950).
[3] G. L. Pearson, Phys. Rev. **76**, 179 (1949).

γ-Rays from the Decay of N^{16}

C. H. MILLAR, G. A. BARTHOLOMEW, AND B. B. KINSEY
Atomic Energy Project, National Research Council of Canada, Chalk River, Ontario, Canada
November 6, 1950

SOMMERS and Sherr[1] observed that γ-radiation of about 6 Mev is emitted in the β-decay of N^{16}; and more recently, Millar, Cameron, and Glicksman[2] have demonstrated that this radiation consists of at least two components. Since a direct and accurate measurement of these γ-rays is of interest in connection with the levels of O^{16}, we have studied them with the aid of a pair spectrometer.

The N^{16} is produced in the cooling water from the Chalk River pile by the fast neutron reaction $O^{16}(n, p)N^{16}$. Since the half-life of this isotope is only 7.35 sec, it was necessary to maintain a continuous flow of the active water through a reservoir in front of the spectrometer.

In a survey of the γ-ray spectrum between 5.8 and 9.8 Mev only two γ-rays were found. These have energies of 6.133±0.011 and 7.10±0.02 Mev, which are in good agreement with the values 6.136±0.030 and 7.111±0.030 Mev recently reported by Chao, Tollestrup, Fowler, and Lauritsen[3] for the energies of two of the excited states of O^{16}. The ratio of the intensity of the 7.10-Mev γ-ray to that of the 6.133-Mev γ-ray is 0.08±0.02.

No definite evidence was obtained for a γ-ray with an energy corresponding to that of the 6.91 Mev excited state of O^{16}. Since we determine the energy of a γ-ray by measuring the end point of its coincidence spectrum, the most energetic component of a partially resolved doublet can always be observed and measured, while the existence of the lower energy component is difficult to establish. For this reason, a γ-ray of 6.91 Mev with an intensity not much less than that of the 7.10-Mev γ-ray might have escaped detection, especially since the coincidence counting rates obtained were extremely low.

Recent independent measurements by Barnes, French, and Devons,[4] and Arnold[5] have shown that the γ-ray emitting level of O^{16} excited by the bombardment of F^{19} with 340-kev protons has a spin of 3 units and is of opposite parity to that of the ground state of O^{16}. Under these conditions of bombardment, the 6.133-Mev level of O^{16} is the one most frequently produced,[6] and assuming that the ground state of O^{16} is of even parity, it follows that the excited level has a spin of 3 and odd parity. Bleuler, Scherrer, Walter, and Zünti[7] showed that β-decay of N^{16} to the ground state of O^{16} is a first-forbidden transition, while decay to the γ-ray emitting levels is allowed. From these results it may be deduced that the N^{16} ground state has a spin of 2 and odd parity, and from our measurements it follows that the 7.10-Mev level of O^{16} has odd parity.

[1] H. S. Sommers and R. Sherr, Phys. Rev. **69**, 21 (1946).
[2] Millar, Cameron, and Glicksman, Phys. Rev. **77**, 742 (1950), and Can. J. Research **A28**, 475 (1950).
[3] Chao, Tollestrup, Fowler, and Lauritsen, Phys. Rev. **79**, 108 (1950).
[4] Barnes, French, and Devons, Nature **166**, 145 (1950).
[5] W. R. Arnold, Phys. Rev. **80**, 34 (1950).
[6] W. E. Burcham and J. M. Freeman, Phys. Rev. **73**, 1756 (1949).
[7] Bleuler, Scherrer, Walter and Zünti, Helv. Phys. Acta. **20**, 96 (1947).

Precise Determination of the $Li^7(p, \alpha)He^4$ and $Be^9(d, \alpha)Li^7$ Q-Values*

WARD WHALING† AND C. W. LI
Kellogg Radiation Laboratory, California Institute of Technology, Pasadena, California
October 26, 1950

A MAGNETIC spectrograph of the double-focusing 180° sector type has recently been constructed in this laboratory and used to measure the energy released in the $Li^7(p, \alpha)He^4$ reaction. This 16-in. spectrograph follows closely the design of the 10.5-in. instrument used previously but has an extended energy range and a larger aperture (0.007 steradian). The angle θ between the direction of the proton beam incident on the target and the direction in which alpha particles leaving the target enter the spectrograph was measured by two independent methods: (1) by the ratio of the energies of monoenergetic protons elastically scattered from Be and Ta targets; (2) by means of a stop with a narrow slit in it which could be rotated about the target to intercept first the incident protons and then the particles entering the spectrograph. The angle through which the slit turned was read from a dividing head fixed to it. Both methods agree within 0.1° and show the angle of observation to be 89.3°; we assign a probable error of 0.2°.

Both thick and thin targets of lithium, evaporated in vacuum on copper backings, were used. Figure 1 shows typical thin and thick target spectra, together with the alpha-spectrum from ThC′ source located in the target position. The energy scale is fixed by the peak in the ThC′ curve. For the thick target curve the energy of the alphas coming from the surface of the target was taken to be that of a point at 54 percent of the maximum thick target yield, indicated by the arrow in the figure. This value was chosen by consideration of the shape of the curve obtained by folding the spectrograph window into the spectrum for infinite resolution. For the thin target the peak in the curve shows the energy of the alpha-particles, which must be corrected for the finite target thickness. This correction was made by adding to the peak energy one-half the thickness of the target measured in units of alpha-particle energy.

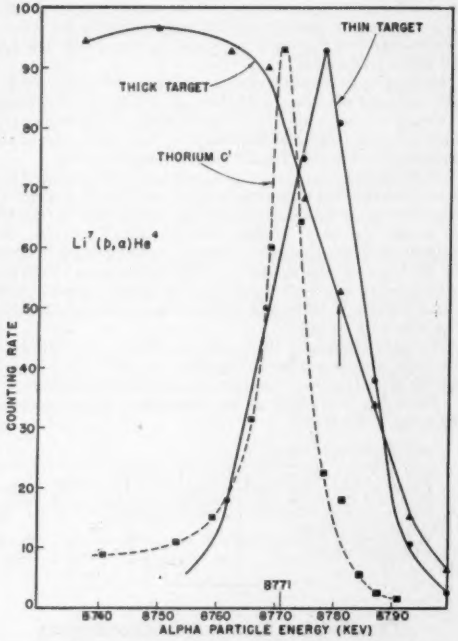

FIG. 1. Typical thin and thick target spectra of α-particles from $Li^7(p, \alpha)He^4$. Bombarding energy 336 kev. Angle of observation 89.3°. Energy scale fixed by peak in ThC′ spectrum.

The proton bombarding energy was held constant to within 0.1 percent with an electrostatic analyzer. Three determinations of Q were made at a bombarding energy of 1008 kev using H^+ ions and eight at 336 kev using HHH^+ ions. At the lower bombarding

energy the Li alpha-particle energy is very close to that of the ThC′ alpha-particles, and by calibration of the fluxmeter with the ThC′ alphas, errors that might arise from inaccuracies in the field measurement are avoided. The values of Q at these two energies agreed to within 3 kev and have been averaged to give the final value of 17.338±0.011 Mev. The 11-kev uncertainty is the probable error in Q arising from various experimental factors, of which the largest, ΔQ=7.5 kev, is due to the 0.2° probable error in θ.

During a run the magnetic field was monitored continuously with a fluxmeter previously described[1] and controlled by varying the magnet current manually. To check on the stability of the fluxmeter the ThC′ spectrum was observed both before and after each Li run. The ThC′ source, prepared by the capture of recoils from the decay of thoron on a highly polished aluminum electrode, 1/16 in. in diameter, was mounted on the target holder so that it could be moved quickly into the target position without disturbing the apparatus. The energy of the alpha-particles from ThC′ is given by Briggs[2] as 8.7759±0.0009 Mev. The energy of the alphas from our source will be less than this because the ThC′ atoms are imbedded in the source backing as a result of the recoil of the ThB nucleus into the source. After the method given by Rutherford[3] we calculate the range of the ThB recoil to be 0.136 mm air equivalent, and estimate the average alpha-energy loss in the source to be 4.4 kev, with a probable error of 25 percent. The peak in the ThC′ spectrum thus represents an energy of 8.7715±0.0020 Mev.

The observed energy of the alpha-particles has been corrected for the energy loss of incident and emitted particles in the surface layers of carbon and oxygen that appear on the target surface during bombardment. The way in which these layers build up on a clean Li surface as a function of the bombarding charge was first determined, by measurement of the thickness of the layers by observing the protons elastically scattered from them. Then the surface layer on each target used was estimated from its total bombardment. The thickness of both C and O layers together usually amounted to about 1 kev (for 336-kev protons, measured normal to the surface), which requires a 4-kev correction to the measured Q-value.

Our value of Q is higher than the previously accepted value of 17.280±0.030 Mev, determined from range measurements.[4] This discrepancy may be accounted for in part by the surface layers or possibly to an error in the measurement of θ, which seems difficult to know accurately in the earlier experiment. This new value is in excellent agreement with a similar magnetic measurement by Buechner,[5] whose value is 17.340±0.014 Mev.

For this value of Q one can calculate the mass of the α-particle from the mass of the deuteron and the Q values of the three reactions: (1) $Be^9(d,\alpha)Li^7$, (2) $Be^9(p,d)Be^8$, (3) $Be^9(\alpha)He^4$. Q_2 and Q_3 have been measured previously with a magnetic spectrograph.[6] We have checked the value of Q_1 listed in reference 6 following exactly the procedure described above for the $Li^7(p,\alpha)\alpha$ reaction. The average of 6 determinations with both thick and thin Be targets is 7.151±0.010 Mev in good agreement with Buechner's value[5] of 7.150±0.008. Using 2.226±0.003 Mev for the binding energy[7] and 2.014723 for the mass of the deuterium, and the "adopted" values of Q_2 and Q_3 listed in reference 6, we find for the He^4 mass 4.003840±0.000018, where the error is the root square average of the probable errors in the Q-values entering in the calculation including an 0.004-mmu error in the deuteron mass. Ewald's[8] recent mass spectroscopic measurement of the He^4 mass from the $2D-He^4$ doublet also gives the value 4.003840±0.000012, based on a D^2 mass of 2.014722±0.000006.

* Assisted by the joint program of the ONR and AEC.
† AEC Post-Doctoral Fellow.
[1] C. C. Lauritsen and T. Lauritsen, Rev. Sci. Instr. 19, 916 (1948).
[2] Holloway and Livingston, Phys. Rev. 54, 18 (1938).
[3] Rutherford, Chadwick, and Ellis, *Radiations from Radioactive Substances* (Macmillan Company, 1930), p. 155.
[4] N. R. Smith, Phys. Rev. 56, 548 (1939).
[5] W. W. Buechner, private communication.
[6] Tollestrup, Fowler, and Lauritsen, Phys. Rev. 78, 372 (1950).
[7] Mobley and Laubenstein, Phys. Rev. 80, 309 (1950).
[8] H. Ewald, Z. Naturforsch. 5A, No. 1, 5 (1950).

The Inverse Voltage Characteristic of a Point Contact on *n*-Type Germanium

LLOYD P. HUNTER
Westinghouse Research Laboratories, East Pittsburgh, Pennsylvania
November 10, 1950

THE purpose of this letter is to suggest a qualitative picture of the effect of self-heating on the inverse voltage characteristic of a point contact. The typical inverse voltage characteristic of n-type germanium shown in Fig. 1 has never been satisfactorily explained in detail. Benzer[1] and others have reported that the form of the high voltage breakdown portion depends strongly on temperature. The low voltage portion has not been well accounted for by the diffusion and diode theories[2] of rectification, but seems to be explained by the theory of Aigrain.[3]

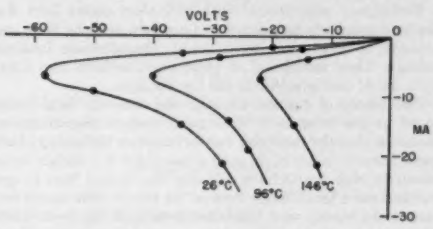

FIG. 1. Typical inverse voltage characteristic for n-type germanium point contacts.

The high voltage breakdown portion may be explained entirely on the basis of self-heating if one assumes: (1) that the isothermal characteristics are straight lines (as shown in Fig. 2); (2) that Newton's law of cooling holds, so that the difference between the temperature immediately beneath the point and the ambient temperature is directly proportional to the power dissipated; (3) that the conductivity of the isothermal characteristic shows a thermal activation energy of the order of one electron volt; then one can generate a thermal equilibrium characteristic as follows. In Fig. 2, the isothermal characteristics are laid out from the origin as straight lines. The one representing the ambient temperature being assumed, and the others calculated using the activation energy (0.76 ev in this example). On top of these isothermal characteristics are drawn several hyperbolas of constant

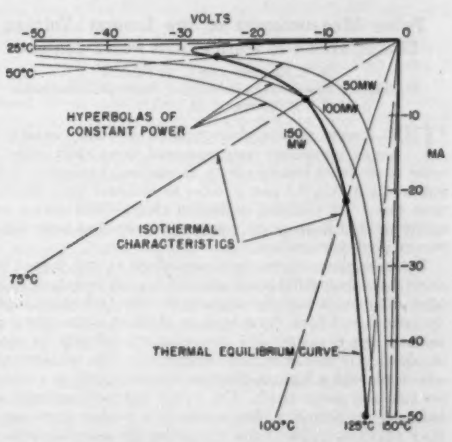

FIG. 2. Method of generating a thermal equilibrium characteristic.

power dissipated, using increments of power proportional to the increments of temperature used in laying out the isothermal characteristics. The desired thermal equilibrium characteristic can now be drawn through the intersection points of the isothermal characteristics and their respective hyperbolas.

It can be seen that this thermal equilibrium characteristic qualitatively resembles the measured characteristic of Fig. 1. If one increases the ambient temperature, i.e., starts out along a higher temperature isothermal characteristic, it is easy to see that the temperature dependence found is also qualitatively that shown in Fig. 1.

Preliminary experiments[4] with very short pulses have shown the isothermal characteristics to be nearly straight lines out to voltages of more than twice the dc characteristic breakdown voltage. These isothermal or pulse characteristics also coincide with the dc characteristic at the low voltages.

The theory of Aigrain[3] explains the relatively large currents found at low voltages in some point contact characteristics by assuming that the rectifying barrier is not on the surface, but lies some distance below it. In such a case there is a surface layer of relatively high conductivity allowing the current lines to spread out and use a much larger area of the barrier than would be the case if the barrier were immediately beneath the point contact. This model, when considered in connection with the effects of heating, would require that the surface layer immediately beneath the point would be heated first as the current is increased. If the bulk resistivity of this layer is considerably below the intrinsic resistivity at the ambient temperature, its resistance should increase until the intrinsic range is reached at some elevated temperature. This behavior would result in the thermal equilibrium curve showing a greater resistance than the ambient isothermal curve for a small range of intermediate currents. Such a behavior has been found[5] for contacts which show relatively high currents at low voltages.

The physical assumption of Aigrain seems to be capable of explaining the observed behavior in this case even though such an assumption seems impossible for very high inverse resistances, since in such cases it requires surface layers of thickness considerably less than the mean free path of a current carrier in germanium.

[1] S. Benzer, J. Appl. Phys. **20**, 804 (1949).
[2] Torrey and Whitmer, *Crystal Rectifiers* (McGraw-Hill Book Company, Inc., New York, 1948), p. 78.
[3] P. Aigrain, Compt. rend. **230**, 62 (1950).
[4] A. I. Bennett and L. P. Hunter, Phys. Rev., following letter.
[5] Figure 1 of reference 4.

Pulse Measurement of the Inverse Voltage Characteristic of Germanium Point Contacts

A. I. Bennett and L. P. Hunter
Westinghouse Research Laboratories, East Pittsburgh, Pennsylvania
November 10, 1950

THE inverse voltage characteristics of point contacts on *n*-type germanium were measured using short pulses in order to eliminate heating effects. It was found necessary to use pulses of less than 0.5 μsec in order to eliminate these effects in most cases. The resulting isothermal characteristic curves were nearly straight lines out to voltages of more than twice the dc inverse breakdown voltage.

The germanium crystals used were single crystals lapped to a thickness of about 0.015 in and soldered to a relatively large copper block. The crystal and the copper block were both maintained in the temperature bath. Because of the thinness of the crystal and the large area in contact with the copper, it is felt that the crystal remained very nearly at bath temperature. The measurements were made with a basic oscilloscope, consisting only of a cathode ray tube and power supply. The crystal and probe assembly was hung on the deflection plate connections so that there was no more than two inches of line connecting the assembly with the deflection plates themselves. This arrangement eliminated most

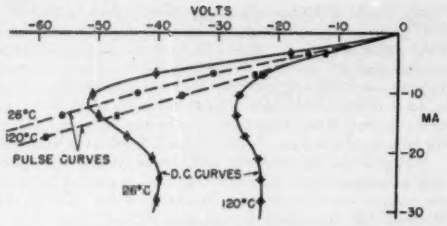

FIG. 1. Pulsed and dc inverse characteristics.

of the reactive effects, and the small amount of reactance remaining was tuned out with a variable condenser across the current measuring resistor.

In order to get stable and reproducible operation, the point contacts were formed by momentarily running them at a high inverse current (several times the current used in the measurements). This resulted in lower resistance contacts than would otherwise have been obtained.

A typical set of results are shown in Fig. 1. It should be noted that at room temperature the dc or thermal equilibrium curve lies above the pulse or isothermal curve for intermediate values of current. However, when the temperature is raised, it is seen that this effect disappears near that temperature where the bulk resistivity reaches a maximum just before the intrinsic range is reached.

We will consider first the nearly linear isothermal characteristics in terms of the theory of Aigrain.[1] For moderate voltages Aigrain gives the formula

$$V=(Ri_s/2\pi)[1-(i/i_s)+(i/i_s)\ln(i/i_s)] \quad (1)$$

for the inverse voltage characteristic neglecting thermal effects. Since $i_s \sim 10^{-7}$ amp, and since $i \sim 10^{-3}$ amp, the unity in Eq. (1) can be neglected and this becomes

$$V=(Ri/2\pi)[\ln(i/i_s)-1]. \quad (2)$$

Since the ratio $i/i_s > 10^4$, the logarithm is nearly constant, so that we have essentially a linear characteristic of slope $R[\ln(i/i_s)-1]/2\pi$. The temperature dependance should be that of R, which in turn is that of the bulk resistivity of the surface layer. The temperature dependence of i_s is that of the intrinsic conductivity so that, unless the logarithm were quite large, it would contribute to the over-all temperature dependence. In the case of the results shown in Fig. 1, the temperature is uniform for the pulse curves but not for the dc curves. This means that in the low current region of the dc curve we might expect the Aigrain surface layer to heat up immediately beneath the probe, while the temperature of the barrier is not appreciably increased above ambient. If this is the case, we should expect the dc curve to exhibit somewhat higher resistance values at low currents than the pulsed curve for the same low ambient temperature, since at moderately low temperatures the resistivity of the surface layer should have a positive temperature coefficient. As the ambient temperature of the pulsed curves is increased, however, we need not necessarily expect their resistance to increase even at first, since in this case the temperature of the barrier region and the surface layer are the same and the temperature dependence of R may be balanced or overcome by the temperature dependence of i_s.

In conclusion it would seem that since there are two regions at different temperatures represented by two temperature dependent constants (i_s and R), it is very difficult to generate the thermal equilibrium curve (dc characteristic) quantitatively from the isothermal curves (pulsed chtracteristics) by the method of Hunter.[2] It does appear, however, that qualitatively such a relation exists between the two sets of curves, and that back voltage breakdown is really a self-heating effect.

[1] P. Aigrain, Compt. rend. **230**, 62, 194 (1950).
[2] L. P. Hunter, Phys. Rev., preceding letter.

Latent Image Fading in Nuclear Emulsions

ARTHUR BEISER
Department of Physics, New York University, University Heights, New York
November 10, 1950

THE magnitude of the regression of the latent image produced by charged particles incident on a nuclear emulsion is, in general, a function of the emulsion characteristics, the flux, kind, and energy of the particles, and of the time and conditions of storage in the interval between irradiation and development. This effect is much more marked in nuclear emulsions than in optical-type emulsions because of the extremely small size of the silver speck development centers in the former, which is caused by inefficiency in the photolytic process when the time of exposure of the halide grains is very short. This occurs in traversal by a radiation particle, where it will be in the vicinity of a halide grain for a time of the order of 10^{-14} sec. Since latent image regression is a surface phenomenon of the specks, the smaller ones will be affected to a proportionally greater extent, accounting for the relative instability of nuclear emulsion latent images.

Investigations by Lauda[1] and Mather[2] demonstrate a reduction of about 90 percent in the fading of the latent image after pre-development storage in an evacuated chamber. This indicates that the dominant agent involved is a constituent of the atmosphere, with the known susceptibility of the silver specks to oxidizing agents suggesting the oxygen and water vapor present as causative factors. This is corroborated by studies[3] of the variation of fading with storage in atmospheres of oxygen, nitrogen, and air, and with water vapor added to the above. The fading rate was found to be greatest in oxygen and least in nitrogen, with the addition of water vapor greatly increasing the fading rate in all cases. The temperature of storage will influence the rate of latent image oxidation, and may also act in connection with a purely thermal regression process[4] that could account for part of the 10 percent residual fading observed even after vacuum storage.

To obtain a relation between the magnitude of the regression and the time of storage, the fading rate under a constant set of conditions may be considered proportional to the number of development centers present at any time. In integrated form this gives the expression

$$(N_0-N)/N_0=1-\exp(-ct),$$

where N_0 is the initial number of centers present after irradiation, N the number after a time t, and c a constant dependent on the size of the silver specks and on the storage conditions. For nuclear emulsions the density D after development will, to a good approximation, be proportional to N. Thus, the fading coefficient will be given by

$$(D_0-D)/D_0=1-\exp(-ct), \qquad (1)$$

with D_0 being the density produced upon immediate development. $(D_0-D)/D_0$ is plotted in Fig. 1 as a function of t for various values of c, in good agreement with the experimental values given by Yagoda and Kaplan[5] for two storage conditions.

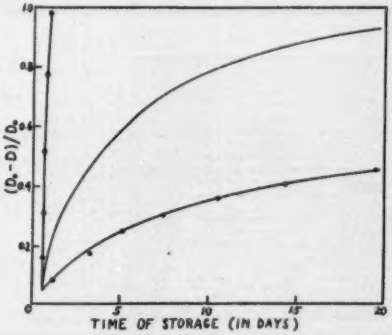

FIG. 1. The variation of fading with time of storage for various values of c.

The variation of the fading index c with temperature and humidity may be determined from a consideration of the effect of temperature on the velocity of a gas-solid reaction. Combining the Arrhenius relation

$$dN/dt=A\exp(-E/RT),$$

where T is the absolute tempertture and A, E, and R constants, and the empirical Freundlich adsorption isotherm

$$dN/dt=kC^n,$$

where C is the concentration of the gas and n a fraction whose value lies between 0 and 1, gives for c in this case

$$c=k_1H^n\exp(-k_2/T),$$

where H is the absolute humidity. For storage in air the oxygen concentration varies to a negligible extent and therefore can be included in k_1. Since for reactions of this kind $n\sim\frac{1}{2}$,

$$c=k_1H^{\frac{1}{2}}\exp(-k_2/T). \qquad (2)$$

Equations (1) and (2) are adequate to describe the major part of fading phenomena in nuclear emulsions.

[1] J. Lauda, Sitzber. Akad. Wiss. Wien, Abt. IIa **145**, 707 (1936).
[2] K. B. Mather, Phys. Rev. **76**, 486 (1949).
[3] Albouy and Faraggi, Report of Conference on Fundamental Mechanisms of Photographic Sensitivity. Part III, ONRL-66-50, 4 (1950), unpublished.
[4] A. Beiser, Phys. Rev. **80**, 112 (1950).
[5] H. Yagoda and N. Kaplan, Phys. Rev. **73**, 634 (1948).

Decay of the Hydrogen Discharge*

JOHN M. RICHARDSON† AND R. B. HOLT
Department of Physics, Harvard University, Cambridge, Massachusetts
November 13, 1950

THE decay of the electrodeless hydrogen discharge has been studied by the previously described techniques[1] of electron density, optical spectrographic, and optical light intensity measurements as a function of time after termination of the exciting fields. The electron density is measured by the shift of resonance of a microwave cavity due to the presence of free electrons, and this measurement has been improved by the technique of sweeping the exploring microwave signal through resonance in a few microseconds rather than depending upon the decay transient of the discharge to plot a resonance indication. Pressures studied varied from 1.0 to 19.8 mm Hg; times from 35 to 3500 μsec; and electron densities from 5×10^7 to 5×10^9 electrons/cm^3.

The character of the decay curves for electron density indicates that two-body recombination of electrons occurs from about 7 mm Hg to 20 mm Hg, and that the recombination coefficient, α, defined by the relation $dn/dt=-\alpha n^2$, where n is the electron concentration, is constant within experimental error at 6.2×10^{-6} cm^3/electron-sec. Measurements at the lower pressures indicate that ambipolar diffusion predominates. The decay curve is taken to be represented by Biondi's expression.[2]

$$n/(1+\alpha\tau n)=[n_0/(1+\alpha\tau n_0)]\exp[-(t-t\alpha)/\tau]$$

and by the use of three experimental points, τ is extracted without the necessity of assuming the behavior of α at low pressures. At the same time, α is determined, provided the distribution of electrons within the cavity can be assigned with certainty. The use of τ enables $D_a p=\Lambda^2 p/\tau$ to be calculated at the constant value 600 cm^2-mm Hg/sec for pressures in the range 1 to 3 mm Hg, where D_a is the ambipolar diffusion coefficient, p the pressure, and Λ the characteristic diffusion length. In this range α is observed to rise from 2×10^{-6} cm^3/electron-sec toward the above value at 7 mm Hg.

Spectrographic examination of the discharge under excitation shows most of the energy to be in the molecular spectrum of hydrogen, including the ultraviolet continuum associated with the

$1s\sigma 2s\sigma^3\Sigma_g \rightarrow 1s\sigma 2p\sigma^3\Sigma_u$ transition, with atomic lines also visible. Decay of the molecular spectrum is so rapid that it cannot be photographed within the 10–15-μsec resolution of our shutter. The light at times from 0–600 μsec is continuous in character, having a maximum at about 4250A and cutting off at about 3400A; and is thus not identifiable with the molecular continuum. Changes in spectral distribution and absolute intensity are observed in passing from quartz to Pyrex containers.

Estimates to within a factor of 2 or 3 (by means of a calibrated 1P28 photo-tube) of the absolute energy lying in the band of the 1P28 per disappearing electron lead to results which (a) are less than 1/500 of the available energy (ionization potential) per recombining electron, and (b) vary widely with time instead of remaining constant. These and other results lead to the conclusion that the light associated with the hydrogen afterglow arises from the container walls, and that nonradiatiative volume recombination accounts for the removal of electrons. A possible mechanism is

$$H_3^+ + e \rightarrow H + H + \text{K.E.},$$

with the $1s\sigma 2p\sigma^3\Sigma_u$ or similar state as the final state of the molecule.

* This research was supported in part by the ONR.
† AEC Predoctoral Fellow.
[1] Holt, Richardson, Howland, and McClure, Phys. Rev. **77**, 239 (1950).
[2] M. A. Biondi, Phys. Rev. **79**, 733 (1950).

Californium Isotopes from Bombardment of Uranium with Carbon Ions*

A. Ghiorso, S. G. Thompson, K. Street, Jr., and G. T. Seaborg
Radiation Laboratory and Department of Chemistry, University of California, Berkeley, California
November 8, 1950

THE recent production and identification[1] of isotopes of elements with atomic numbers up to six higher than the target element through bombardment with approximately 120-Mev carbon (+6) ions made it seem worth while to apply this technique to the transuranium region.

Accordingly, small pieces of natural uranium metal (about 0.5 mil thick and 2.5 cm by 0.6 cm area) were irradiated in the internal carbon ion beam in the Berkeley 60-inch cyclotron. Following the irradiations, the uranium was dissolved in dilute hydrochloric acid containing hydrogen peroxide and a transplutonium fraction was isolated through the use of lanthanum fluoride and lanthanum hydroxide precipitation steps followed by the ion exchange adsorption column procedure, in which concentrated hydrochloric acid is used to separate the tripositive actinide elements from the rare earth elements.[2]

The transplutonium fractions in hydrochloric acid were evaporated as weightless films on platinum plates which were placed in the ionization chamber of the 48-channel pulse analyzer apparatus in order to measure the yield and energies of any alpha-particles which might be present. In the best experiment at about one hour after the end of the 90-min bombardment, some 50 disintegrations per minute of the distinctive 7.15±0.05-Mev alpha-particles[3] of Cf^{244} were observed to be present and to decay with the 45-min half-life. The Cf^{244} was presumably formed by the reaction $U^{238}(C^{13}, 6n)$.

After the decay of the alpha-particles due to Cf^{244}, about five disintegrations per minute of alpha-particles with 6.75±0.05-Mev energy were observed and this alpha-radioactivity decayed with a half-life of about 35 hours. In subsequent experiments involving the use of an ion exchange method[4] to separate the individual actinides from each other, both the ~45-min and ~35-hour activities were found together in the chemical fraction corresponding to the new element californium. A consideration of the systematics of alpha-radioactivity[5] leads us to the view that this 35-hour period is due to the new isotope Cf^{246} formed by the reaction $U^{238}(C^{13}, 4n)$. The measured half-life agrees with the expected alpha half-life for the observed energy for an even-even isotope of the element with atomic number 98.

It is not possible at this time to obtain a good estimate of the intensity of the carbon ion beam. Therefore, the cross sections for the reactions given above cannot be calculated. However, it is interesting to note that the indicated yields for the (C, 6n) and (C, 4n) reactions are comparable.

If the mass assignment of the new 35-hour activity to Cf^{246} is correct, these new data give a better idea as to the slope of the alpha-energy *vs* mass number line for californium, which in turn makes it possible to make better predictions of the radioactive properties of the nuclides in this region.

We wish to express our appreciation to Professor J. G. Hamilton, J. F. Miller, G. B. Rossi, T. M. Putnam, Jr., M. T. Webb, and the operating crew of the 60-inch cyclotron in the Crocker Laboratory for their help in the carbon ion bombardments. We would also like to thank Mr. E. K. Hulet for his help in the chemical separations.

* This work was performed under the auspices of the U. S. AEC.
[1] Miller, Hamilton, Putnam, Haymond, and Rossi, Phys. Rev. **80**, 486 (1950).
[2] K. Street, Jr. and G. T. Seaborg, J. Am. Chem. Soc. **72**, 2790 (1950).
[3] Thompson, Street, Jr., Ghiorso, and Seaborg, Phys. Rev. **78**, 298 (1950).
[4] Thompson, Street, Jr., Ghiorso, and Seaborg, Phys. Rev. **80**, 792 (1950).
[5] Perlman, Ghiorso, and Seaborg, Phys. Rev. **77**, 26 (1950).

Thresholds of Photo-Neutron Reactions*

R. Sher, J. Halpern, and W. E. Stephens
Randal Morgan Laboratory of Physics, University of Pennsylvania Philadelphia, Pennsylvania
November 6, 1950

NEUTRON yields as functions of the maximum energy of the bremsstrahlung output of the University of Pennsylvania betatron have been measured for several substances in the energy region from threshold to 22 Mev. The samples, of the order of 50 grams of high purity materials, were inserted in a block of paraffin 9 in×9 in×20 in, in which was also placed a $B^{10}F_3$ counter (Fig. 1). Shielding against background neutrons was obtained by surrounding the apparatus with sheet cadmium, then with about 4 inches of paraffin mixed with B_4C, then with about 1 foot of additional paraffin. The samples were ¾-in diameter cylinders. The collimated x-ray beam was about ⅝ in diameter and irradiated the samples axially. The distance from sample to betatron target was 8.5 feet. The counter was parallel to the beam and about one inch away.

In order to avoid counting pile-up due to the x-ray pulse, and also to avoid being bothered by transient effects on the counting system due to the x-ray burst and auxiliary betatron pulses, only those neutrons were counted which, having been delayed in the paraffin, entered the counter some time after each burst of x-rays. This was done by constructing an electronic gate signal which was delayed from each x-ray burst by about 30 μsec, and whose dura-

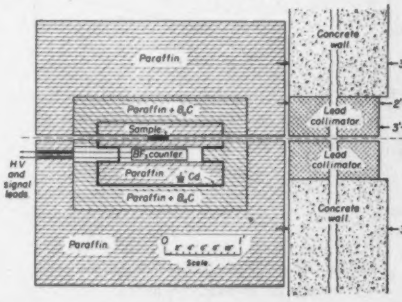

FIG. 1. Schematic diagram of the experimental arrangement (side view).

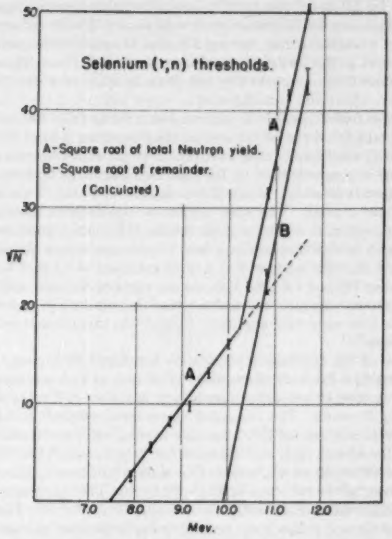

FIG. 2. Square root of neutron yield vs energy. This graph is a typical case in which two thresholds are present: Se^{77} (7.5 Mev) and $Se^{(?)}$ (9.9 Mev).

tion was about 300 μsec. (The time between x-ray pulses was 5550 μsec.) The gate was "counted" in coincidence with the pulses from the BF_3 chamber; thus, only those neutrons which fell within the gated interval were recorded.

The maximum energy of the x-ray beam was varied by expanding the electron beam in the betatron at any desired value of the magnetic field, using circuits similar to those described by Katz, *et al.*[1] The energy scale was calibrated using the deuterium photodisintegration threshold at 2.23 Mev, the $Cu^{65}(\gamma, n)Cu^{64}$ threshold at 10.9 Mev, and the $C^{12}(\gamma, n)C^{11}$ threshold at 18.7 Mev.

Thresholds were determined by plotting the square root of the neutron yield as a function of energy in the region around threshold.[2] The resulting graphs are of two kinds: those in which one straight line is obtained, characteristic of substances containing contributions of only one isotope, and those in which one or more abrupt increases in slope occur, corresponding to the additional contributions of isotopes with higher thresholds (Fig. 2). In this case the yields corresponding to the lower thresholds were extrapolated and subtracted from the total yield, and the higher thresholds obtained by plotting the square root of the remainder.

TABLE I. Photo-neutron thresholds.

Parent isotope	Threshold (Mev)*	Parent isotope	Threshold (Mev)*
$_5B^{10}$	7.6	$_{38}Sr^{88}$	10.9
$_5B^{11}$	11.1	$_{41}Nb^{93}$	8.7
$_{11}Na^{23}$	12.6	$_{46}Pd^{105}$	7.2
$_{12}Mg^{25}$	7.1	$_{46}Pd^{?}$	8.8
$_{12}Mg^{26}$	10.1 ±1.0	$_{52}Te^{125}$	6.8
$_{14}Si^{29}$	8.4	$_{52}Te^{?}$	8.8
$_{16}S^{34}(?)$	10.8	$_{55}Cs^{133}$	9.0
$_{21}Ti^{49}$	8.7	$_{56}Ba^{137}$	7.1
$_{22}Ti^{50}(?)$	11.6	$_{56}Ba^{138}(?)$	8.7
$_{23}V^{51}$	10.8 ±0.5	$_{57}La^{139}$	8.8
$_{24}Cr^{52}$	7.5	$_{58}Ce^{?}$	6.7
$_{24}Cr^{53}$	11.6 ±0.4	$_{58}Ce^{?}$	8.7
$_{27}Co^{59}$	10.0	$_{74}W^{186}$	6.0
$_{28}Ni^{61}(?)$	7.5	$_{74}W^{?}$	7.1
$_{34}Se^{77}$	7.5	$_{74}W^{?}$	9.5
$_{38}Sr^{87}$	7.2 ±0.5		

* ±0.3 Mev unless otherwise indicated.

The advantage of detecting neutrons rather than residual radioactivities is, of course, the possibility of finding (γ, n) processes whose products are either stable or have very long or very short half-lives. One also may obtain by this method neutrons generated by other processes such as $(\gamma, 2n)$, (γ, np), etc. The thresholds for these reactions generally lie considerably higher than (γ, n) thresholds, however, and so their presence will have no effect on the present results, but will be advantageous in interpreting the total yield data. On the other hand, the identification of some of the isotopes becomes more doubtful. For a nucleus of even Z, the lowest threshold was assumed to be that of the isotope of highest odd A. Higher thresholds were occasionally assigned on the basis of isotopic abundance; in such substances as Pd, Te, and W, there are several even A isotopes of almost equal abundance and identification was not possible.

The results are listed in Table I. The experimental errors are ±0.3 Mev unless otherwise indicated.

In addition to the new thresholds listed in the table, more than twenty thresholds were observed which had been previously reported.[2-4] These agreed with the earlier results within experimental error.

The yield data will permit a detailed study of the cross sections of photo-neutron processes and their variation with energy; this work and more complete details about the experiment will be reported at a later date.

* Assisted by the joint program of the AEC and ONR.

[1] Katz, McNamara, Forsyth, Haslam, and Johns, Can. J. Research **A28**, 113 (1950).

[2] McElhinney, Hansen, Becker, Duffield, and Diven, Phys. Rev. **75**, 542 (1949).

[3] Hansen, Duffield, Knight, Diven, and Palersky, Phys. Rev. **76**, 578 (1949).

[4] W. E. Ogle and R. E. England, Phys. Rev. **78**, 63 (1950); Ogle, Brown, and Carson, Phys. Rev. **78**, 63 (1950); G. C. Baldwin and H. W. Koch, Phys. Rev. **67**, 1 (1945).

Kramers' Theorem and Nuclear Effects in Paramagnetic Absorption*

C. KIKUCHI†
Brookhaven National Laboratory, Upton, New York
November 6, 1950

SHORTLY after the discovery of the hfs in solids by Penrose,[1] Pryce[2] pointed out a relationship between ΔH, the hfs component separation for the cobalt ion, and θ, the angle between the crystalline axis and the applied magnetic field. Later Ingram[3] showed that this same relation applies to the copper ion. It occurred to us, therefore, to investigate the conditions under which Pryce's relation would be valid. We should like to point out that his relation is a consequence of Kramers' theorem,[4] when the effect of the nuclear magnetic moment is taken into account to the first approximation.

Let ψ_1 and ψ_2 be the wave functions of a doubly degenerate electron ground state of a paramagnetic ion. In the presence of a magnetic field, the degeneracy will be removed and the wave functions of the two states become

$$f_1=[g_\perp \sin\theta\psi_1+(g-g_\parallel\cos\theta)\psi_2]/[2g(g-g_\parallel\cos\theta)]^{\frac{1}{2}}, \quad (1)$$

$$f_{-1}=[-(g-g_\parallel\cos\theta)\psi_1+g_\perp\sin\theta\psi_2]/[2g(g-g_\parallel\cos\theta)]^{\frac{1}{2}}, \quad (2)$$

corresponding to the magnetic energies $\frac{1}{2}\mu_B gH$ and $-\frac{1}{2}\mu_B gH$. Here g is given by $(g_\parallel^2\cos^2\theta+g_\perp^2\sin^2\theta)^{\frac{1}{2}}$. The quantities $g_\parallel$ and $g_\perp$ will depend, of course, on the particular ion and the crystalline electric field; but the form of the wave functions as given above will be the same for any ion. The invariance requirement leads to the following expression for the nuclear interaction potential:

$$V=a_1\mathbf{L}\cdot\mathbf{I}+a_2[(3\mathbf{I}\cdot\mathbf{r}\mathbf{S}\cdot\mathbf{r}/r^2)-(\mathbf{I}\cdot\mathbf{S})]+a_3\mathbf{I}\cdot\mathbf{S}. \quad (3)$$

If J is a good quantum number, the above interaction potential can be expressed in the form $a_J\mathbf{I}\cdot\mathbf{J}$. In addition, there is the term

representing the interaction of the nuclear magnetic moment with the external magnetic field. The diagonal elements of Eq. (3) can be written

$$(1, m|V|1, m) = -(2, m|V|2, m) = Am,$$

where $m = I, I-1, \cdots -I$. This follows from a relation pointed out by Kramers. The wave functions, (1) and (2) then yield

$$(\pm\tfrac{1}{2}, m|V|\pm\tfrac{1}{2}, m) = \pm Am g_{11}\cos\theta/g$$

and, for the off-diagonal elements

$$(\pm\tfrac{1}{2}, m+1|V|\pm\tfrac{1}{2}, m) = (g_\perp \sin\theta/2g)B[I(I+1)-m(m+1)]^{\frac{1}{2}}.$$

The eigenvalues are

$$E(\tfrac{1}{2}, m) = \tfrac{1}{2}g\mu_B H + [(\tfrac{1}{2}\Delta\nu_{11}g_{11}/g+\gamma H)^2\cos^2\theta+(\tfrac{1}{2}\Delta\nu_\perp g_\perp/g+\gamma H)^2\sin^2\theta]^{\frac{1}{2}}$$

$$E(-\tfrac{1}{2}, m) = -\tfrac{1}{2}g\mu_B H - [(-\tfrac{1}{2}\Delta\nu_{11}g_{11}/g+\gamma H)^2\cos^2\theta+[(-\tfrac{1}{2}\Delta\nu_\perp g_\perp/g)+\gamma H]^2\sin^2\theta]^{\frac{1}{2}}.$$

In the above result, $\frac{1}{2}\Delta\nu_{11}$ and $\frac{1}{2}\Delta\nu_\perp$ were substituted for A and B, since these quantities can be identified with one-half of the experimentally observed hfs component separation for parallel and perpendicular fields. For allowed transitions, $\Delta m = 0$, and assuming γH is small compared to $\Delta\nu_{11}$ and $\Delta\nu_\perp$, the energy separation for levels between which transitions are allowed, then, is

$$E(\tfrac{1}{2}, m)-E(-\tfrac{1}{2}, m) = \mu_B g H_m + (m/g)(\Delta\nu_{11}{}^2 g_{11}{}^2\cos^2\theta+\Delta\nu_\perp{}^2 g_\perp{}^2\sin^2\theta)^{\frac{1}{2}}.$$

This gives

$$\mu_B{}^2 g^4(\Delta H)^2 = \Delta\nu_\perp{}^2 g_\perp{}^2+(\Delta\nu_{11}{}^2 g_{11}{}^2-\Delta\nu_\perp{}^2 g_\perp{}^2)\cos^2\theta,$$

where ΔH is the separation between adjacent hfs components in magnetic field units. A similar relation, in a different form, has been given by Pryce.

It is a pleasure to acknowledge the continued interest and the stimulating discussions with Dr. V. W. Cohen of Brookhaven National Laboratory and E. F. Carr of Michigan State College.

* Research carried out under contract with AEC.
† Permanent address: Michigan State College, East Lansing, Michigan.
[1] Penrose, Gorter, Abragam, and Pryce, Nature **163**, 992 (1949).
[2] Bleaney, Ingram, and Pryce, Nature **164**, 116 (1949).
[3] D. J. E. Ingram, Proc. Phys. Soc. (London) **A62**, 664 (1949).
[4] H. A. Kramers, Proc. Akad. Amat. **35**, 1272 (1932).

Nuclear Spin Relaxation Times in Single Crystals of LiF

R. V. POUND
Department of Physics, Harvard University, Cambridge, Massachusetts
November 1, 1950

THE relaxation times of nuclear spins in crystals are usually of the order of seconds or fractions of a second at room temperatures. Such short times may be caused by paramagnetic impurities,[1] internal lattice jumps,[2] or by direct spin-lattice interaction through the nuclear electric quadrupole moment.[3] In lithium nitrate a relaxation time of the order of an hour has been observed.[2] To see whether such a time would be found in sufficiently pure LiF, single crystals of LiF were obtained from the Harshaw Chemical Company and from the Optivac Company. These crystals, $\frac{1}{2}''$ diameter by $\frac{1}{2}''$ long, were used in two associated novel experiments to be reported shortly.[4,5] As background for these, some preliminary, rather qualitative, results obtained for relaxation times and the effects of x-ray produced color centers are reported here.

The relaxation times were measured by observation of a magnetization curve either after insertion in the 6376-gauss permanent magnet or after r-f saturation. An r-f spectrometer,[6] held at low level, was set at the frequency of maximum deflection of the recorder for short periods at regular time intervals. The amplitudes of the recorded deflections gave points on the exponential magnetization curve, little net disturbance of the spin system resulting from the sampling.

In the Harshaw crystals the relaxation times were found to be 5 min for Li^7 and 2 min for F^{19}. Evidently paramagnetic impurity is still present for otherwise one would expect the F^{19} to have the longer relaxation time, having no electric quadrupole moment. The times in the Optivac crystal were 2 min for Li^7 and 45 sec for F^{19}, apparently magnetically less pure in spite of a reportedly greater ultraviolet transparency.

It was found possible to remove the crystals from the magnet (residual field of the earth) and return them after a brief interval with only small loss in magnetization. A study of the dependence of the loss of magnetization on the time held out of the field revealed an exponential decay with a time constant of about 15 sec in the Harshaw crystals. The spin system is evidently adiabatically demagnetized to a temperature (about 1°K) determined by the spin-spin interaction, and a relaxation process allows the lattice to heat the spin system with a time constant of 15 sec. In zero field, the F^{19} and Li^7 spin systems are coupled together and thus both showed the same relaxation time. The reasonably large value of this time suggested and made feasible the experiments referred to above.[4,5]

Two of the Harshaw crystals were irradiated with x-rays. One was irradiated on each of two sides for 30 min, at $\frac{1}{4}''$ from the beryllium window of a molybdenum target, Machlett A-2 tube, run at 40 kv, 20 mamp. The relaxation times were reduced[7] to 1½ min for Li^7 and 30 sec for F^{19}. The other crystal was irradiated on the ends for 40 min each at 5 cm from the target of an AEG-50 tube run at 40 kv, 40 mamp, and on four sides, 10 min each, 3 cm from the target of the tube[8] run at 40 kv, 50 mamp. The resulting relaxation times were about 30 sec for Li^7 and 10 sec for F^{19}. The first crystal showed yellow spots near the x-ray source and the second a uniform yellow coloration about 2 mm deep, presumably F' centers. It is suggested that such effects on relaxation times provide a simple means for study of the properties of color centers, using a theory along the lines proposed by Bloembergen, if the paramagnetic relaxation time of the F-centers were known. A double resonance experiment involving saturation of the F-centers by a microwave signal, while using the nuclear resonance as a thermometer, is planned.

[1] N. Bloembergen, Physica **15**, 386 (1949).
[2] A. Sachs, Thesis, Harvard University (1949); E. H. Turner, Thesis, Harvard University (1949); R. Newman, J. Chem. Phys. **18**, 669 (1950).
[3] R. V. Pound, Phys. Rev. **79**, 685 (1950).
[4] N. F. Ramsey and R. V. Pound, "Nuclear audiofrequency spectroscopy by resonant heating of the nuclear spin system" (to be published).
[5] E. M. Purcell and R. V. Pound, "A nuclear spin system at negative temperature" (to be published).
[6] R. V. Pound and W. D. Knight, Rev. Sci. Instr. **21**, 219 (1950).
[7] The author wishes to thank Professor K. T. Bainbridge for providing this irradiation.
[8] The author wishes to thank Dr. H. D. Doolittle and the Machlett Laboratories for providing this irradiation.

Hall Coefficient and Resistivity of Evaporated Bismuth Layers

W. F. LEVERTON AND A. J. DEKKER
University of British Columbia, Vancouver, Canada
November 6, 1950

FILMS of bismuth 0.2 to 1.3 microns in thickness were prepared by distillation of 99.8 percent pure bismuth in a Vycor glass apparatus similar to the Pyrex apparatus we described recently.[1] During evaporation, the bismuth was heated to 750–850°C, the rate of condensation varied from 30 to 210 $\mu g/cm^2/min$.

The Hall coefficient, R, was measured at 20°C by an ac method.[1] R did not depend on the current density but varied with the magnetic field H according to an equation of the form,

$$R(H) = R_0 - bH^2. \quad (1)$$

Measured values of R for each sample fitted a curve of this type within the experimental error (1 percent) for magnetic fields from 1.5 to 12 kgauss. However, the constants R_0 and b varied from sample to sample; the average values were $R_0 = +0.89$ c.g.s.m. and $b = 1.0\times10^{-9}$ c.g.s.m./(gauss)^2 with mean deviations of 4 and 10 percent, respectively.

Annealing at 260°C in carbon dioxide reduced R_0 and b; after annealing, $R_0=0.71$ c.g.s.m. and $b=0.84\times10^{-9}$ c.g.s.m/(gauss)[2] with mean deviations of 6 and 8 percent, respectively.

Heaps[2] found $R=+1$ c.g.s.m. for single crystals with H parallel to the trigonal crystal axis. We found no report of Hall coefficient measurements for thin layers of bismuth.

The resistivity ρ was measured at 293 and 77°K. $\rho_{293}=1.09\times10^{-4}$ ohm-cm perpendicular to the trigonal crystal axis.

For our samples the temperature coefficient of resistivity was negative. ρ_{77}/ρ_{293} decreased from 3.1 at 0.2 microns to 1.7 at 1.3 microns. This is in contrast to the positive temperature coefficient observed by Kaye[3] for single crystals.

Annealing had no appreciable effect on the resistivity.

The influence of a magnetic field on the resistivity was measured at 293°K for fields up to 12 kgauss (H perpendicular to plane of bismuth film). For each sample the resistivity increased with increasing H according to an equation of the form,

$$\rho(H)=\rho_{293}+aH^2, \tag{2}$$

where ρ_{293} is the field free resistivity and a is a constant. The increase in ρ due to a field of 12 kgauss varied from 7 percent for the thinnest sample up to 22 percent for the thickest one. Annealing had no effect on the constant a.

Measurements with H parallel to the plane of the sample indicated that the increase in ρ was about twice as great as with H perpendicular to the sample. This result is in agreement with measurements on single crystals by Kaye,[3] assuming that our layers are polycrystalline with the trigonal axis perpendicular to the backing, as found by Lane.[4]

According to a theory by Jones,[5] R should be independent of H for pure bismuth; i.e., for equal numbers of electrons and holes. Equation (1) corresponds, according to the theory, to bismuth alloyed with tetravalent impurities which act as electron acceptors. A relation of the same type as Eq. (2) holds for pure bismuth and for bismuth alloys, provided the impurity content is small, the temperature is high, and H is sufficiently small.

These arguments, applied to our results, do not necessarily mean that tetravalent impurities are responsible for the observed effects. A relation similar to Eq. (1) would be found if a number of the free electrons were trapped in surface states (this effect may be appreciable for evaporated layers because of the small size of the crystallites). Electron trapping can also account qualitatively for the dependence of ρ on the sample thickness, the negative temperature coefficient of ρ, and the decrease in R_0 and b on annealing.

To check the suggested interpretation, experiments are being carried out on films distilled from spectroscopically pure bismuth.

[1] W. F. Leverton and A. J. Dekker, Phys. Rev. **80**, 735 (1950).
[2] C. W. Heaps, Phys. Rev. **30**, 61 (1927).
[3] G. W. Kaye, Proc. Roy. Soc. **170A**, 561 (1939).
[4] C. T. Lane, Phys. Rev. **48**, 193 (1935).
[5] H. Jones, Proc. Roy. Soc. **155A**, 653 (1936).

The Electric Quadrupole Moment of Li^6

N. A. Schuster and G. E. Pake
Physics Department, Washington University,[6] St. Louis, Missouri
November 6, 1950

QUADRUPOLE splitting of the Li^6 and Li^7 magnetic resonances has been obtained from a natural single crystal of $LiAl(SiO_3)_2$ (spodumene). The apparatus used is a recording radio-frequency spectrometer consisting of an r-f oscillator, an untuned r-f amplifier, a detector, an audio amplifier, and a phase-sensitive detector to be described in detail elsewhere.

The crystal, about 40 mm×9 mm×10 mm, was placed in the r-f coil of the oscillator tank, the coil itself residing in the gap of a permanent magnet which produces a constant magnetic induction in the neighborhood of 7312 gauss. The Li^7 resonance occurs near 12.10 Mc sec^{-1} in this field. The resonance of the Li^6 nucleus, which is presumably present in this crystal in its natural abundance of 7.39 percent, falls near 4.58 Mc sec^{-1}.

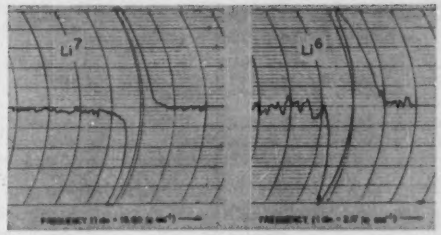

FIG. 1. Lithium nuclear magnetic resonances in a single crystal of $LiAl(SiO_3)_2$ at a crystal orientation giving essentially zero quadrupole splitting. The center of the Li^7 resonance occurs at approximately 12.097 Mc sec^{-1} and the center of the Li^6 resonance occurs at approximately 4.582 Mc sec^{-1}.

The mounting of the crystal permitted it to be turned about its c-axis, and the Li^7 resonance was observed as a function of crystal orientation in order to find the maximum and minimum (zero) quadrupole splittings. The crystal was then set at one of these orientations and left untouched while both Li^7 and Li^6 resonances were recorded. Simply for purposes of comparison, Fig. 1 shows both resonances for the crystal orientation giving minimum splitting. Maximum splittings, which permit experimental evaluation of the magnitude of the ratio of the quadrupole moments, appear in Fig. 2. The Li^6 resonance in this figure is one of several recorded at this crystal setting.

The nuclear quadrupole interaction splits the magnetic resonance spectrum of a nucleus with spin $I>\frac{1}{2}$ into $2I$ components, which spread over a frequency range[1]

$$\Delta\nu=(3eQ/2Ih)(\partial E_z/\partial z)_0, \tag{1}$$

where e is the proton charge, Q is the nuclear quadrupole moment, and $(\partial E_z/\partial z)_0$ is a component of the gradient of the crystalline electric field, evaluated for present purposes at the lattice site of a lithium nucleus. In accordance with Eq. (1), the ratio of the quadrupole moments is

$$|Q_6/Q_7|=\Delta\nu_6 I_6/\Delta\nu_7 I_7. \tag{2}$$

The spins of Li^6 and Li^7 are previously known to be 1 and $\frac{3}{2}$. The number of quadrupole components found for each resonance in Fig. 2 incidentally confirms these values.

The centers of the satellite lines of the Li^7 resonance in Fig. 2 are separated by 66.4±0.6 kc $sec^{-1}=\Delta\nu_7$. For the less completely resolved Li^6 resonances, absorption curves were obtained by direct integration, by means of a planimeter, of the experimentally measured derivative. The result of integrating the Li^6 derivative of Fig. 2 is shown in Fig. 3. Curves such as this were analyzed by recognizing that the symmetry properties of the two component absorption curves require the midpoint C of the center line AB of the resultant curve to lie on both of the component quadrupole

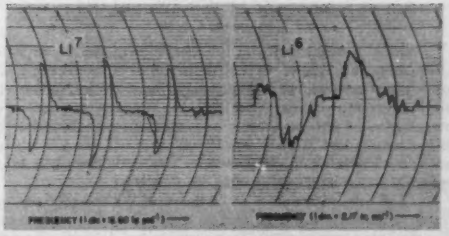

FIG. 2. Lithium nuclear resonances in a single crystal of $LiAl(SiO_3)_2$ showing the maximum quadrupole splitting obtainable with the crystal c-axis perpendicular to the external magnetic field.

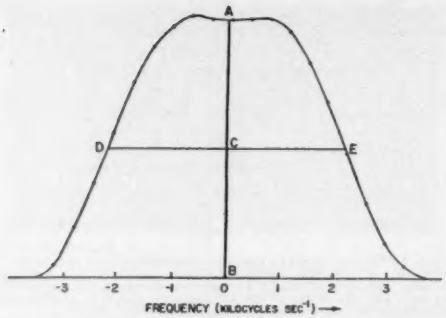

FIG. 3. Li^8 absorption curve obtained by integrating the resonance of Fig. 2, showing construction lines used in arriving at the splitting of the incompletely resolved pair of quadrupole component lines.

curves. Therefore, the midpoints of the segments DC and CE are separated by the frequency $\Delta\nu_Q$, once one is satisfied that ordinates at D and E of the resultant curve originate solely from one quadrupole component and are not influenced by a tail of the other component line, and it follows that $DE=2\Delta\nu_Q$. Each of the three Li^8 resonances analyzed in this way gave values which depended to some extent upon whether attempts were made to correct for slight zero-drift of the spectrometer. Averages of these values for each of the three resonances were, respectively, 2.20, 2.35, and 2.34 kc sec^{-1}. All individual determinations of $\Delta\nu_Q$ fall within the limits 2.30±0.15 kc sec^{-1}, which value may be used in Eq. (2) to find $|Q_b/Q_l|=(2.3\pm0.2)\times10^{-2}$. The quoted error is roughly twice the usual statistical probable error, and the ratio is significantly below the upper limit of 4.4×10^{-2} arrived at by Kusch.[2]

The value of $(\partial E_z/\partial z)_0$ is not known for this crystal; and $Q_l=2\times10^{-26}$ cm^2, as obtained by Kusch,[2] must be used to evaluate the magnitude of Q_b. The result, $|Q_b|=4.6\times10^{-28}$ cm^2, is about one-sixth as large as the quadrupole moment of the deuteron, 2.73×10^{-27} cm^2.

Attempts are being made in this laboratory to improve the accuracy of the ratio $|Q_b/Q_l|$ by utilizing higher frequencies to increase signal-to-noise and by efforts to eliminate possible magnetic field inhomogeneities which may prevent more complete resolution of the Li^8 resonance. Such increased accuracy may be of doubtful value, however, so long as the magnitude of Q_l is known to but one significant figure.

We wish to thank Mr. Werner G. Zinn for assistance in assembling parts of the spectrometer.

* Assisted by the joint program of the ONR and AEC.

[1] R. V. Pound, Phys. Rev. 79, 685 (1950).
[2] P. Kusch, Phys. Rev. 75, 887 (1949).
[3] P. Kusch. Phys. Rev. 76, 138 (1949).

Beta-Activity of Potassium

C. F. G. DELANEY
Physical Laboratory, Trinity College, Dublin, Ireland
November 6, 1950

EARLY measurements on the specific beta-activity of potassium gave values ranging from 20 to 50 betas/sec/gm of ordinary potassium, while later results have tended to converge on a figure near 31 betas/sec/gm. As, however, two recent determinations[1,2] put the activity as low as 28.3±1.0 betas/sec/gm of potassium, and 318±10 betas/min/gm of KI, (i.e., 22.5 betas/sec/gm of potassium), respectively, the work described below, which favors a larger value, may be of interest.

A G-M tube with a mica end window of thickness 9.6 mg/cm^2, cathode diameter 2 inches, and an argon-alcohol filling was used for the beta-measurements. Its geometry was determined using a modification of the usual Ra(E+F) calibration technique. Ra(E+F) sources were obtained by spontaneous deposition on nickel from a solution of Ra(D+E+F) in N/10 HCl, and the subsequent growth in the alpha-activity of the RaF was measured using Ilford 50μ nuclear plates, type C2. For a source placed directly in contact with a plate the counting efficiency is 50 percent, since alpha-particle backscattering is negligible. Consequently, by exposing a plate to a source for a suitable time and finding the average number of tracks per microscope field, the absolute activity can be determined knowing merely the diameters of the microscope field (2.875×10^{-2} cm), and that of the source, (4.50 cm). In practice the exposure time was chosen to give the convenient number of about 15 tracks per field, and varied between 3 and 8 hours. Exposures were made at two-day intervals for at least twenty days, and the growth of the RaF thus followed absolutely. The amount of RaE present at any time could then be deduced, and from the observed beta-activity the counter geometry found.

The mean of four independent determinations by this method, corrected empirically for window absorption of the RaE beta particles, is 35.6 percent. This figure is too large by a factor of about 1.5 on account of beta backscattering; but since nickel of sufficient thickness to give saturation backscattering was used as backing for all sources, both RaE and KCl, this factor need not be considered further.

The actual count/sec/gm of KCl, extrapolated to zero thickness was 5.39. Taking into consideration the geometry as found above, the potassium content of KCl, and the window absorption of the K^{40} beta-particles, this corresponds to a figure of 32.0±3 betas/sec/gm of ordinary potassium.

Some counts were also made on KBr of different origin to ensure that no radioactive contamination was present in the KCl.

The only factor uncorrected for in the above calculations appears to be the self-scattering present in the KCl sources, but absent in the almost weightless RaE sources. This can,[3] under adverse conditions, introduce an error of up to 8 percent; but since with the arrangement used the sources were quite close to the counter window (7.1 mm away), the effect is not likely to be large.

The thickness of aluminum required to reduce the intensity of the K^{40} beta-rays by half was also investigated, and found to be 69.5±2 mg/cm^2, a logarithmic plot being linear down to 200 mg/cm^2.

A more detailed account of the work will be published later. The author is indebted to Professor J. H. J. Poole for advice on this problem.

[1] G. A. Sawyer and M. L. Wiedenbeck, Phys. Rev. 79, 490 (1950).
[2] Smaller, May, and Freedman, Phys. Rev. 79, 940 (1950).
[3] B. P. Burtt, Nucleonics 5, 28 (August, 1949).

Remarks on Relativistic Quantum Mechanics

K. V. ROBERTS
King's College, Cambridge, England, and H. H. Wills Physical Laboratory, University of Bristol, England
November 7, 1950

IN two letters[1] we have described a classical approach to the interaction representation of Tomonaga and Schwinger, based on the classical field dynamics of Weiss.[2] Unfortunately these letters were of necessity extremely condensed, and they also contained serious errors. The theory has since been developed in detail, and considerably extended;[3] but, although the first section is now in the press,[4] some time must elapse before a complete discussion can be published. It therefore seems pertinent to give a brief summary of the results. The notation has been defined in I and II.

A covariant and formally consistent scheme of quantum field dynamics is obtained by first extending the classical theory of Weiss, and then quantizing it by a generalization of the usual rules. In the Heisenberg picture the operators ξ depend on an arbitrary parametrized space-like surface σ, and vary according to the Eqs. $II(1)$; in the alternative Schrödinger picture the state vector $\Psi[\sigma]$ depends on σ, and varies according to $II(4)$. The interaction representation is a particular case of the general

scheme, and lies between these two pictures; it has as its classical analog a covariant perturbation theory in which the canonical variables $\varphi^{\mathrm{in}}(\sigma,\tau)$, $\pi_a^{\mathrm{in}}(\sigma,\tau)$ depend on two surfaces σ and τ. It may be proved that the whole scheme is covariant and formally consistent for a quite arbitrary set of interacting Bose or Fermi fields, and a separate proof for each particular set is not needed.

A remarkable feature is that although the theory must be stated in Hamiltonian form, according to the general rules of quantum mechanics, the S-matrix and other quantities can be shown to involve only the Lagrangian. This suggests that one might look for a new kind of quantum mechanics, in which the Lagrangian replaces the Hamiltonian functions.

The more important results are as follows:

(a) There is a simple rule[4] for writing down the interaction Hamiltonian function $\mathcal{H}^I$, and the correct order for the operators is uniquely defined. $\mathcal{H}^I$ contains the interaction Lagrangian $\mathcal{L}^I$, and may also contain a number of surface-dependent terms.

(b) The Schrödinger equations $II(4)$, and the corresponding equations of the interaction representation, are always integrable.

(c) Parametrization is not needed in the interaction representation, because the interaction Hamiltonian functions h_s^I are identically zero. (This was not made clear in II. The paragraph leading to Eq. $II(5)$ should be ignored.)

(d) In the Heisenberg picture, or in the interaction representation, it is always possible to construct a set of field operators $\varphi^{\mathrm{in}}(x)$, independent of the surfaces, and satisfying a set of field equations which can be written in Lagrangian form.

(e) There is a simple rule for writing down the invariant commutation rules of the interaction representation, and the Feynman function, from the free Lagrangian $\mathcal{L}^I$.

(f) The Dyson S-matrix is

$$S=1+\sum_{n=1}^{\infty}\left(\frac{1}{i\hbar}\right)^n\frac{1}{n!}\int_{-\infty}^{\infty}dx^{(1)}\cdots \times\int_{-\infty}^{\infty}dx^{(n)}P[\mathcal{H}^I(x^{(1)})\cdots\mathcal{H}^I(x^{(n)})]. \quad (1)$$

It must be defined with the help of an arbitrary 1-parameter set of non-parametrized space-like surfaces $\sigma(\rho)$, and the choice of this set may affect the expression (1) in two distinct ways; through the ordering of the operators in the P-bracket, and through the surface-dependent terms in $\mathcal{H}^I$. These effects always cancel each other, and the correct result is obtained by retaining only the interaction Lagrangian $\mathcal{L}^I$ in (1), and dropping all the surface-dependent terms which arise from coalescence of the vertices.[6] Hence there is a 1−1 correspondence between the vertices of Feynman-Dyson graphs and the terms of $\mathcal{L}^I$, while the factors for the lines are determined by $\mathcal{L}^I$.

Schwinger's method of canonical transformations[7] can also be expressed in Lagrangian form. Several authors[8] have discussed the cancellation of surface-dependent terms for particular sets of fields, but the real importance of the Lagrangian seems to have been overlooked. It is significant that the present scheme does not lead directly to the Feynman-Dyson graphs, which are multiply-connected and have multiple vertices. One can either use the interaction representation and obtain the expression (1), in Hamiltonian form, or use the Heisenberg picture and solve the Lagrangian equations by iteration. The second method avoids the surface-dependent terms, but leads to simply-connected graphs with multiple vertices, or 'trees'. In either case the general proof of (d) is difficult. One is led to enquire whether any mathematical scheme exists which involves graphs of the Feynman-Dyson type. Such a scheme might provide the basis for a Lagrangian theory of quantum mechanics.

[1] K. V. Roberts, Phys. Rev. 77, 146 (1950). Designated as I and II, respectively.
[4] P. R. Weiss, Proc. Roy. Soc. 169, 102 (1938).
[6] Dissertation submitted for the Ph.D. degree, Cambridge, 1950.
[6] Proc. Roy. Soc. (to be published).
[6] P. T. Matthews, Phys. Rev. 75, 1270 (1949).
[6] P. T. Matthews, Phys. Rev. 76, 684 (1949).
[7] J. Schwinger, Phys. Rev. 75, 651 (1949).
[8] P. T. Matthews, reference 6, F. J. Belinfante, Phys. Rev. 76, 66 (1949). C. N. Yang and D. Feldman, Phys. Rev. 79, 972 (1950), and other authors.

Dirac's Equation in a Riemann Space with an Asymmetrical Metric*

M. EL NADI
Faculty of Science, Fouad I. University, Cairo, Egypt
February 17, 1950

IT has been shown[1] that the equations of motion of a charged particle in an electromagnetic field take the form of a geodesic curve in the 4-dimensional continuum described by the metric

$$g_{\mu\nu}dx^\mu dx^\nu+2f_\mu dx^\mu ds-ds^2=0, \quad (\mu,\nu=1,2,3,4). \quad (1)$$

The covariant vector, f_μ, is connected with the electromagnetic 4-vector potential, κ_μ, through the relation

$$f_\mu=(e/m_0c^2)\kappa_\mu, \quad (2)$$

where e is the charge of the particle, m_0 is its rest mass, and c is the velocity of light. We shall assume that Eq. (1) can be linearized as follows

$$(\gamma_\mu dx^\mu+i\gamma_4 ds)(\gamma_\nu dx^\nu+i\gamma_4 ds)=0, \quad (3)$$

where γ_μ and γ_4 are matrix operators defined by the relations,

$$\begin{aligned}&\gamma_\mu\gamma_\nu+\gamma_\nu\gamma_\mu=2g_{\mu\nu},\\ &i(\gamma_\mu\gamma_4+\gamma_4\gamma_\mu)=2f_\mu, \quad \gamma_4^2=1,\end{aligned} \quad (4)$$

which can be combined into the simple form

$$\gamma_i\gamma_k+\gamma_k\gamma_i=2\gamma_{ik}. \quad (5)$$

Here the Latin letters $i, k, \cdots$ run from 1 to 5, while Greek letters $\mu, \nu, \cdots$ run from 1 to 4. We have assumed in Eq. (5) that

$$\gamma_{\mu\nu}=g_{\mu\nu}, \quad \gamma_{\mu 4}=\gamma_{4\mu}=-if_\mu, \quad \gamma_{44}=\gamma_4^2=1. \quad (6)$$

On introduction of $dx^4=ids$, and use of the notation in Eq. (6), we see that Eq. (1) takes the form

$$\gamma_{ik}dx^i dx^k=0. \quad (7)$$

Similarly, Eq. (3) gives rise to the relation

$$\gamma_m dx^m=0 \quad \text{or} \quad \gamma_m dx^m/ds=0. \quad (8)$$

We shall now consider the 5-dimensional space defined by the metric (7). If A_μ is an ordinary 4-vector and C_m is the corresponding vector in our 5-dimensional space,[2] we can easily deduce the following relations:

$$\begin{aligned}&C_\mu=A_\mu, \quad C_4=R^2(\text{scalar}),\\ &C^4=R+if_\mu C^\mu, \quad C^\nu=A^\nu+iRf^\nu-f^\nu f_\nu C^\nu.\end{aligned} \quad (9)$$

We shall use Eq. (9) in establishing the relation between the 5-vector, γ^i, and the corresponding 4-vector, α^μ, defined by the conditions

$$\begin{aligned}&\alpha_\mu\alpha_\nu+\alpha_\nu\alpha_\mu=2g_{\mu\nu},\\ &\alpha^\mu\alpha^\nu+\alpha^\nu\alpha^\mu=2g^{\mu\nu}, \quad \alpha^\mu\alpha_\nu+\alpha_\nu\alpha^\mu=2g_\nu^\mu,\end{aligned} \quad (10)$$

where $g_\nu^\mu=0$ if $\mu\neq\nu$, $=1$ if $\mu=\nu$.

Since $\gamma_{44}=\gamma_4^2=1$, we deduce that the scalar, R, which occurs in the equations relating γ^i to α^μ, must be equal to unity. Thus, we conclude from Eq. (9) that

$$\gamma^4=1+if_\mu\gamma^\mu, \quad \gamma^\nu=\alpha^\nu+if^\nu-f^\nu f_\nu\alpha^\nu, \quad (11)$$

neglecting higher powers of f^ν.

If the momentum vector in the 5-space is defined by

$$\pi^i=m_0cdx^i/ds,$$

Eq. (8) can be written in the form

$$\gamma_i\pi^i=\gamma^i\pi_i=0, \quad (12)$$

and with the use of the familiar operator substitution

$$\pi_i\rightarrow-i\hbar\partial/\partial x^i,$$

this becomes

$$\gamma^i\partial\psi/\partial x^i=0. \quad (13)$$

This is the required form of the Dirac equation related to the metric (1). It can be written in the explicit form, from (11),

$$\begin{aligned}&[\alpha^\nu(\partial\psi/\partial x^\nu)+(im_0c/\hbar)\psi]+[if^\mu(\partial\psi/\partial x^\mu)-(m_0c/\hbar)f_\mu\alpha^\mu\psi]\\ &-[f^\mu f_\nu\alpha^\nu(\partial\psi/\partial x^\mu)+(im_0c/\hbar)f_\mu f^\mu\psi]=0.\end{aligned} \quad (14)$$

The first bracket in Eq. (14) contains the usual form of Dirac's equation in four dimensions. Using Eq. (2) and replacing $-i\hbar\partial\psi/\partial x^\sigma$ by π_σ, we can write the expression contained in the second bracket in the form,

$$-(e/c)\kappa_\mu\alpha^\mu\psi-(e/m_0\hbar c^2)\kappa^\mu\pi_\mu\psi.$$

These are the expressions for the relativistic and nonrelativistic terms of the interaction with the electromagnetic field. Similarly, the terms in the third bracket in Eq. (4), which represent the second-order interaction terms, can be written in the form

$$(ie^2/m_0\hbar c^3)[(1/m_0c)(\kappa^\sigma\pi_\sigma)(\kappa_\tau\alpha^\tau)+\kappa_\sigma\kappa^\sigma]\psi.$$

* Revised manuscript received November 6, 1950.

[1] G. Randers, Phys. Rev. 59, 195 (1941). A Mosharrafa, Phil. Mag. 39, 728 (1948).
[2] H. T. Flint, Phil. Mag. 29, 417 (1940).

A New Formulation of the Least-Squares Calculation of Atomic Constants

J. A. Bearden and H. M. Watts
Department of Physics, Johns Hopkins University, Baltimore, Maryland

November 16, 1950

In a recent report[1] we published the results of a least-squares calculation of the atomic constants in which we used the base variables F, N, and h to express all of the experimentally observed quantities. Dumond has pointed out[2] that certain experimental quantities in our least-squares adjustment were correlated (both F and e/m involve γ_p in reference 1), and we have corrected our work in a later paper[3] by a method originated by Cohen.[4] The possibility that some other set of variables might provide a more direct (and possibly more accurate) approach is obvious, and the following is the result of the successful pursuit of this idea.

When we weight the various pertinent experimental results (see references 1 and 3) inversely as the square of the probable errors, we find that four experiments carry 98 percent of the weight of any new calculation. They are (1) ω_p/ω_e by Gardner and Purcell,[5] (2) ω_p/ω_e by Hipple, Sommer, and Thomas[6,7] and by Bloch and Jeffries,[8] (3) γ_p by Thomas, Driscoll, and Hipple,[9] and (4) h/e by Bearden, Johnson, and Watts.[10] We accordingly consider what variables are needed to express these observables. Recall the following relations:

Bohr magneton,

$$\mu_1=\tfrac{1}{2}\hbar e/m, \tag{1}$$

nuclear magneton,

$$\mu_2=\tfrac{1}{2}\hbar e/M, \tag{2}$$

gyromagnetic ratio,

$$\gamma_p=\mu_p/\tfrac{1}{2}\hbar, \tag{3}$$

proton magnetic moment in Bohr magnetons,

$$\mu_p'=\mu_p/(\tfrac{1}{2}\hbar e/m), \tag{4}$$

proton magnetic moment in nuclear magnetons,

$$\mu_p''=\mu_p/(\tfrac{1}{2}\hbar e/M), \tag{5}$$

isotopic mass of proton,

$$M_p=MN, \tag{6}$$

where e is in emu, μ_p is the absolute proton magnetic moment, N is Avogadro's number, $\omega_p/\omega_e=\gamma_pH_0/H_0(e/m)=\mu_p/\frac{1}{2}\hbar(e/m)=\mu_p'$, and $\omega_p/\omega_e=\gamma_pH_0/H_0(e/M)=\mu_p''$. We divide Eq. (5) by Eq. (6) and collect the pertinent equations:

$$\begin{aligned}\mu_p'&=4\pi m\mu_p/he\\ \mu_p''/M_p&=4\pi\mu_p/Nhe\\ \gamma_p&=4\pi\mu_p/h\\ h/e&=h/e.\end{aligned} \tag{7}$$

We find that the four observed quantities can be expressed in terms of five variables. However, m can be eliminated[11] by the relation,

$$m=R_\infty ch^3/2\pi^2e_1^4, \tag{8}$$

leaving four variables (e_1 denotes e in esu). Next, we recall that Fermi's hyperfine structure formula can be written

$$\Delta\nu_H=\alpha^2[(16/3)CR_\infty\mu_p'\mu_e'AB], \tag{9}$$

wherein: μ_e' = electron magnetic moment in Bohr magnetons,
A = relativistic correction factor,
B = reduced mass correction factor.

Making use of the relation,

$$\alpha=2\pi e_1^2/hc, \tag{10}$$

we find

$$\mu_p'=3\Delta\nu_Hh^2C/64\pi^3R_\infty\mu_e'ABe_1^4. \tag{11}$$

Use Eqs. (1) and (8) in Eq. (11) to convert to μ_p

$$\mu_p=(3\Delta\nu_H/128\pi R_\infty^2\mu_e'AB)e, \tag{12}$$

Next we make use of the fact that all of the quantities in the parenthesis in Eq. (12) are known to within 1 ppm. The corrections A and B are known accurately because they are small-order corrections involving precisely known constants, μ_e' is now known[12] to the fourth order in e, and $\Delta\nu_H$ is now known[13] to within ±2 parts in 10^7. We can therefore treat the quantity in the parenthesis as an exact number and replace μ_p in Eq. (7) by a constant times e. Our observational equations then become

$$\begin{aligned}\mu_p'&=k_1h^3/e^4\\ \mu_p''/M_p&=k_2/Nh\\ \gamma_p&=k_3e/h\\ h/e&=h/e\end{aligned} \tag{13}$$

which involve only the three variables N, h, and e. (It is to be noted that all of the observational equations representing the older experiments listed in references 1 and 3 can also be expressed in terms of these same new variables.)

The best data now available for the several quantities of Eq. (13) are listed in Table I. All of the quantities involving magnetic moment contain the latest diamagnetic correction; μ_p'' and γ_p being corrected by Thomas[7] by a fractional amount of 28.1×10^{-6}, and μ_p' being corrected as suggested by Purcell[5] by Ramsey's[14] fractional amount of 27×10^{-6}. We use Cohen's[3] new value of R_∞. The value given for μ_e' is calculated from Karplus and Kroll's[12] formula,

$$\mu_e'=1+(\alpha/2\pi)-2.97\alpha^2/\pi^2, \tag{14}$$

using $\alpha=1/137.043$.

TABLE I. Experimental data and auxiliary constants.

Experimental data	Auxiliary constants
$\mu_p'=1.521026\times10^{-3}(\pm13$ ppm)	$\Delta\nu_H=1.4204051\times10^9(\pm0.2$ ppm)
$\mu_p''=2.792746(\pm20$ ppm)	$R_\infty=109737.3235(\pm0.1$ ppm)
$\Delta_p=2.675305\times10^4(\pm22$ ppm)	$C=2.997900\times10^{10}$ $(\pm2.3$ ppm)
$h/e=1.37928\times10^{-17}(\pm29$ ppm)	$M_p=1.007580(\pm3$ ppm)
	$r=1.000272(\pm5$ ppm)
	$\mu_e'=1.001145(\pm1$ ppm)
	$A=1.0000799(\pm1$ ppm)
	$B=0.9983680(\pm1$ ppm)

An interesting incidental result of formula (12) is that γ_p now becomes a measurement of h/e and μ_p' becomes a measurement of h/m, as is seen in Eq. (13). The given values of the constants yield the result:

$$h/e=(1.379300\pm0.000016)\times10^{-17}\text{ erg sec/esu},$$

which is in satisfactory agreement with the x-ray value.

The data of Table I and the relations of Eq. (13) were used in the normal least-squares adjustment of uncorrelated data to obtain results which compared precisely with the results[3] of the more complex method of Cohen.[4]

It is interesting to note that the accurate new experiments have reduced the errors of the least-squares computed atomic constants so drastically that r, the ratio of the physical to the chemical scale

of atomic weights, and even Bol's new and precise value of the velocity of light are noticeable sources of error in the calculation.

[1] J. A. Bearden and H. M. Watts, Johns Hopkins University Radiation Laboratory Report, July 31, 1950, unpublished.
[2] J. W. DuMond, private communication.
[3] J. A. Bearden and H. M. Watts, Phys. Rev. 81, 73 (1951).
[4] E. R. Cohen, Phys. Rev. 81, 162 (1951).
[5] J. H. Gardner and E. M. Purcell, Phys. Rev. 76, 1262 (1949), and more recent results by R. W. Nelson communicated privately to us by E. M. Purcell.
[6] Hipple, Sommer, and Thomas, Phys. Rev. 76, 1877 (1949), results communicated privately by J. A. Hipple.
[7] H. A. Thomas, Phys. Rev. 80, 901 (1950).
[8] F. Bloch and C. D. Jeffries, Phys. Rev. 80, 305 (1950).
[9] Thomas, Driscoll, and Hipple, Phys. Rev. 78, 787 (1950).
[10] Bearden, Johnson, and Watts, Phys. Rev. 81, 70 (1951).
[11] J. W. DuMond and E. R. Cohen, Revs. Modern Phys. 20, 82 (1948).
[12] R. Karplus and N. M. Kroll, Phys. Rev. 77, 536 (1950).
[13] A. G. Prodell and P. Kusch, Phys. Rev. 79, 1009 (1950).
[14] N. F. Ramsay, Phys. Rev. 78, 699 (1950).

Revised Dielectric Parameters of Alkali and Halide Ions

SHEPARD ROBERTS
General Electric Research Laboratory, Schenectady, New York
October 9, 1950

IN a previous publication[1] a classical model of a polarizable ion was suggested which was consistent with the experimental data for dielectric constants, indices of refraction, and infrared absorption frequencies of all the alkali-halide crystals. The ionic model was defined by three linear stiffness coefficients or "springs" between the nucleus, the electron cloud, and the external boundary. An alternative set of parameters to describe the same model was comprised of an effective nuclear charge Ae, a nuclear compliance or polarizability B, and an electronic compliance C.

The dielectric polarizability α_D of a single ion in a crystal was written A^2B+C and the optical polarizability α_g of an isolated "gaseous" ion was $(A-1)^2B+C$ for alkali ions or $(A+1)^2B+C$ for halides. The polarizability per ion pair at optical frequencies in a crystal was somewhat less, namely:

$$\alpha_s=[(A_1+A_2)^2/(1/B_1)+(1/B_2)]+C_1+C_2\cong C_1+C_2, \quad (1)$$

where the subscripts 1 and 2 refer to the alkali and halide ions, respectively.

Tentative values of the parameters A, B, and C were given in which B and C for lithium had been arbitrarily set equal to zero. It is now possible to choose more definite values for the parameters of lithium which lead to a new set of values for the other ions as shown in Table I. The dielectric constants, etc., calculated from the new ionic parameters are identical with those calculated from the original values. The table also gives values of the dielectric polarizability α_D and the electronic polarizability of free ions α_g.

The new values are chosen so as to fulfill the following conditions for lithium: (1) $\alpha_g=0.4A^3$, in accord with the calculations of Pauling;[2] (2) $\alpha_D=11.7$, in agreement with the author's previous results;[1] (3) the ratios of the respective stiffness coefficients of lithium are to compare systematically to those of the other alkali ions.

In spite of the vagueness of the last condition, the resulting values are quite well defined. It turns out that the stiffness coefficient "b" between the nucleus and the boundary is in every case negative. This coefficient will indeed have to be negative if the actual forces between the nucleus and the neighboring ions are predominantly electrostatic, since it is axiomatic in classical mechanics and electrostatics that a charged particle cannot be supported at rest in stable equilibrium by purely electrostatic forces.

TABLE I. Revised ionic parameters (all but A are in cubic angstroms).

	A	B	C	α_D	α_g
Li	1.108	9.3	0.28	11.7	0.4
Na	1.234	10.7	3.40	19.7	4.0
K	1.291	17.4	12.39	41.4	13.9
Rb	1.449	19.2	17.00	57.3	20.9
Cs	1.215	25.3	34.14	71.5	35.3
F	−0.780	25.9	10.04	25.8	11.3
Cl	−0.645	66.3	35.22	62.8	43.6
Br	−0.627	78.1	50.32	81.0	61.2
I	−0.568	99.9	77.14	109.4	95.8

As an extreme illustration, suppose that we take away all the electrons and consider the motion of a lone nucleus of charge pe inside a spherical conducting boundary of radius R. The electrostatic force on such a particle displaced a distance X from the center is

$$F_x=+p^2e^2X/4\pi\epsilon_0R^3=-bX$$

or

$$b=-p^2e^2/4\pi\epsilon_0R^3, \quad (2)$$

where ϵ_0 is the permittivity of free space. Equation (2) gives values of b which are of the right order of magnitude if R is chosen to be about three times the usual ionic radius. This would correspond to a reasonable average distance between the nucleus and other particles with which it has a strong electrostatic interaction.

The electronic polarizabilities of free ions are given roughly by the formula $\alpha_g=2.9R^{4.7}$, where R and α_g are given in angstrom units. The polarizabilities of noble gas atoms satisfy the same equation if Pauling's "univalent" radii are substituted for R.

[1] S. Roberts, Phys. Rev. 77, 258 (1950).
[2] L. Pauling, Proc. Roy. Soc. (London) A114, 181 (1927).
[3] S. Roberts, Phys. Rev. 76, 1215 (1949).

2^{L-1}-Magnetic 2^L-Electric Interference Terms in γ-γ-Angular Correlations

STUART P. LLOYD
Department of Physics, University of Illinois, Urbana, Illinois
November 17, 1950

IT is the purpose of this note to point out that the relative phases of the reduced (magnetic quantum number independent) matrix elements for the simultaneous emission of a magnetic 2^{L-1}-pole quantum and an electric 2^L-pole quantum in a transition between eigenstates of angular momentum are determined almost completely by the time-reversal properties[1] of the emitting system. In the notation of Ling and Falkoff,[2] the quantities α and β can both be made real by choice of nuclear phases, so that the phase angle δ can have only the value 0° or 180°. Which of these two applies would have to be determined from a more detailed model of the nucleus.

The reduced matrix elements in question are:

$$\beta_l=(j\|e_l\|j')=\Sigma_{mm'n}(-1)^{j-m+n}(jj'-mm'|jj'l-n)\times(jm|e_l{}^n|j'm') \quad (1a)$$

for electric 2^l-pole transitions;

$$\alpha_l=(j\|m_l\|j')=\Sigma_{mm'n}(-1)^{j-m+n}(jj'-mm'|jj'l-n)\times(jm|m_l{}^n|j'm') \quad (1b)$$

for magnetic 2^l-pole transitions between levels $j'\to j$. The matrix elements for the individual components of $j'\to j$ are[3]

$$(jm|e_l{}^n|j'm')=-ik^{-1}[l(l+1)]^{-\frac{1}{2}}\int\mathbf{j}(\mathbf{r})\cdot\nabla\mathbf{x}(\mathbf{r}\times\nabla) f_l(kr)Y_l{}^n(\mathbf{r})d\tau \quad (2a)$$

$$(jm|m_l{}^n|j'm')=-[l(l+1)]^{-\frac{1}{2}}\int\mathbf{j}(\mathbf{r})\cdot\mathbf{r}\times\nabla f_l(kr)Y_l{}^n(\mathbf{r})d\tau, \quad (2b)$$

where $f_l(x)=(8\pi^3/x)^{\frac{1}{2}}J_{l+\frac{1}{2}}(x)$, $Y_l{}^n(\mathbf{r})$ is the Condon and Shortley[4] spherical harmonic, and

$$\mathbf{j}(\mathbf{r})=\Sigma_i\int\Psi_j{}^{m}(X)^\dagger\mathbf{j}_i(\mathbf{r})\Psi_{j'}{}^{m'}(X)d_iX. \quad (3)$$

In Eq. (3), X is the set of nuclear coordinates; $\Psi_{j'}{}^{m'}(X)$, $\Psi_j{}^m(X)$ are the initial and final nuclear state functions; and the integral is over all nuclear coordinates except the coordinate $\mathbf{r}$ of the ith nuclear particle. The dimensionless current operator $\mathbf{j}_i(\mathbf{r})$ has the form $\mathbf{j}_i(\mathbf{r})=(\mathbf{v}_i/c)$ for a positively charged elementary particle. The normalization is such that R quanta/sec of frequency

$\nu=(ck/2\pi)$ are emitted in the transition, where

$$R=\nu(e^2/hc)\sum_{l=1}^{\infty}[|(j\|a_l\|j')|^2+|(j\|m_l\|j')|^2]/[(2l+1)(2j'+1)].$$

For any wave function Ψ, the "time-reversed" wave function[1] is $K\Psi=U\Psi^*$, where U is a hermitian unitary operator ($U=1$ for spinless nucleons, $U=\sigma_y$ for spin$=\frac{1}{2}$ nucleon). K is not a linear operator. If the nuclear level j has no other degeneracies than that of the magnetic quantum number, it can be shown that

$$K\Psi_j^m(X)=U\Psi_j^m(X)^*=\kappa_j(-1)^{j-m}\Psi_j^{-m}(X), \tag{4}$$

where κ_j is a phase factor of modulus unity which depends on the choice of nuclear phase. The property $Kj\Psi=-jK\Psi$, (all Ψ), which can be written in the form

$$U\mathbf{j}_l(\mathbf{r})^*U=-\mathbf{j}_l(\mathbf{r}), \tag{5}$$

expresses the fact that the current changes sign under reversal of the direction of time.

Combination of Eqs. (1) to (5) and use of the following identity for the vector-addition coefficients,

$$(jj'-mm'|jj'l-n)=(-1)^{l+j'-1}(jj'm-m'|jj'ln),$$

obtained from Wigner's formula,[6] shows that

$$\beta_l^*=\kappa_j^*\kappa_{j'}(-1)^l\beta_l \tag{6a}$$

$$\alpha_l^*=\kappa_j^*\kappa_{j'}(-1)^{l+1}\alpha_l. \tag{6b}$$

Assuming that the nuclear levels have definite parities, the nonvanishing β_l will be those for which l is even (odd) and the nonvanishing α_l will be those for which l is odd (even), so that the phase factors in (6a) and (6b) are the same; by proper choice of phase for the levels j' and j the nonvanishing α_l and β_l may be made real for all l. Only the signs and magnitudes of α_l and β_l are left undetermined by these considerations. The relative phases cannot be used as arbitrary parameters to fit the data.

I wish to thank Professor John Blatt for stimulating discussions on time-reversal and on the multipole radiation moments.

[1] E. Wigner, Nachr. Ges. Wiss. Göttingen, Math.-Physik. Klasse, p. 546 (1932).
[2] D. S. Ling, Jr., and D. L. Falkoff, Phys. Rev. **76**, 1639 (1949).
[3] These multipole radiation matrix elements have been obtained by Weisskopf and Blatt and independently by the author; the derivations are as yet unpublished.
[4] E. U. Condon and G. H. Shortley, *The Theory of Atomic Spectra* (Cambridge University Press, 1935), pp. 50–54.
[5] Reference 4, p. 75.

Nonindependent Observational Equations in the Theory of Least Squares

E. Richard Cohen
Atomic Energy Research Department, North American Aviation, Inc., Downey, California
October 13, 1950

In recent years several very precise measurements have been performed which yield information on the values of the fundamental physical constants e, m, h, N, respectively the charge and mass of the electron, Planck's constant, and Avogadro's number. The recent measurements, such as those by (1) Hipple, Sommer, and Thomas,[1] (2) Thomas, Driscoll and Hipple,[2] (3) Gardner and Purcell,[3] (4) Taub and Kusch,[4] and (5) Nafe and Nelson[5] are unfortunately not as direct determinations of functions of e, m, h, N as one is accustomed to in direct measurements of h/e or e/m. For example, item (4) can be combined with item (5) to obtain e^2/h, with item (1) to obtain Nm, and with item (2) to obtain e/m. This clearly implies that the errors in the numerical values obtained for e^2/h, Nm, and e/m are not independent; and, therefore, the usual least squares analysis to determine an unbiased set of "best values" of the atomic constants must be modified so that it properly takes into consideration the nonindependence of the data.

In the usual application of the theory of least squares the implicit assumption is made that if $P_i(\epsilon_i)$ is the probability of obtaining an error ϵ_i in the measurement of the ith quantity, then the probability $P(\epsilon_1, \epsilon_2, \epsilon_3, \cdots \epsilon_n)$ of obtaining simultaneously the errors $\epsilon_1, \epsilon_2, \cdots \epsilon_n$ in the least squares fitted set of quantities is just equal to $P_1(\epsilon_1)\cdot P_2(\epsilon_2)\cdots P_n(\epsilon_n)$. Such a situation is possible only if the errors are unrelated. The observational equations are usually written in a linearized form as

$$a_ix+b_iy+\cdots+f_iw=s_i+\epsilon_i, \tag{1}$$

where x, y, $\cdots w$ are the variables to be fitted, a_i, b_i, $\cdots f_i$ are known coefficients, s_i is the observed quantity, and ϵ_i its (unknown) error. The method of least squares is based on the criterion of finding values of the variables which have the highest probability of being correct. When these errors are independent, this leads to the conditions that

$$\Sigma_i p_i\epsilon_i^2=\Sigma_i p_i(a_ix+b_iy+\cdots+f_iw-s_i)^2=\text{minimum}. \tag{2}$$

The "weight" p_i of each equation is given as $1/\sigma_i^2$, the reciprocal of the mean square deviation of s_i.

In many cases (such as the one that prompts this note) it may be inconvenient to cast the observational equations into the above independent form. If such is the case, let the equations be written instead as

$$A_ix+B_iy+C_iz+\cdots+F_iw=S_i+E_i, \tag{3}$$

in which the quantities S_i are not the results of single observations, but are each compounded from several observed quantities which may be involved in more than one S_i. (The case in which S_i is compounded from several observed quantities, none of which, however, appears in any of the other S_j, is considered in Whittaker and Robinson;[6] but the more general case seems to have been neglected.) If we write S_i as functions of the independent variables s_j, we have $dS_i=\Sigma_j\alpha_i^j ds_j$ (i.e., $E_i=\Sigma_j\alpha_i^j\epsilon_j$). If the "weights" associated with the s_j are $p_j=\sigma_j^{-2}$, we can define a weight matrix π_{ik} which is the inverse of the error matrix $\rho_{ik}=\Sigma_j\alpha_i^j\alpha_k^j\sigma_j^2$. Equation (2) is then replaced by the quadratic form

$$\Sigma_{ik}\pi_{ik}(A_ix+B_iy+C_iz+\cdots+F_iw-S_i)\times(A_kx+B_ky+\cdots+F_kw-S_k), \tag{4}$$

which leads to "normal" equations with coefficients of a generalized form. A typical coefficient would be $\Sigma_{ik}\pi_{ik}A_iB_k$ in place of the coefficient $\Sigma_i p_ia_ib_i$ associated with the quadratic form of Eq. (2).

[1] Hipple, Sommer, and Thomas, Phys. Rev. **76**, 1877 (1949).
[2] Thomas, Driscoll and Hipple, Phys. Rev. **75**, 902, 992 (1949).
[3] J. H. Gardner and E. N. Purcell, Phys. Rev. **76**, 1262 (1949).
[4] H. Taub and P. Kusch, Phys. Rev. **75**, 1481 (1949).
[5] J. E. Nafe and E. B. Nelson, Phys. Rev. **73**, 718 (1948).
[6] E. T. Whittaker and G. Robinson, *The Calculus of Observations* (Blackie and Son, Ltd., London, 1948).

On the Angular Correlation Theorem

B. A. Lippmann
Nucleonics Division, Naval Research Laboratory, Washington, D. C.
November 9, 1950

In the theory of the angular correlation between successive particles emitted by a system undergoing a double transition, among states of definite total angular momentum, the following theorem appears. If the z axis of quantization is along the direction of emission of one of the particles, the probability of the double transition is given by the product of the probabilities of each of the two successive transitions, summed over those intermediate states that are degenerate in the magnetic quantum number. Interference terms are absent.

This property of the double transition, first employed by Hamilton[1] for $\gamma-\gamma$-emission, was verified for a number of other particular cases by Falkoff and Uhlenbeck.[2] Recently, Lloyd[3] has given a general proof for arbitrary decay particles by applying group-theoretical arguments to second-order perturbation theory.

According to the physical interpretation of the quantum-mechanical formalism, however, the probability of a transition from an initial to a final state, via a set of intermediate states, contains interference terms only when it is not possible to measure the system in the intermediate state; if the experiment is inherently capable of specifying the particular intermediate state the

system passes through, the classical law of compounding independent probabilities holds and no interference terms occur. This characteristic of quantum mechanics can be applied to the angular correlation theorem as follows.

The experiment is designed to emphasize precise angular information; hence, a plane wave representation of the emitted particles is appropriate. But then the description of the process of emission of the first (second) particle is invariant under rotations about the direction of emission. Taking the z axis along this direction, the total magnetic quantum number, as well as that of the emitted particle alone, are each constants of the motion. Thus, for this special choice of the z axis, the magnetic quantum number of the emitted particle may be measured without disturbing the process; and the known value of the initial (final) state magnetic quantum number then fixes the intermediate state uniquely. *The special choice of the z axis therefore makes possible*[4] *a determination of the intermediate state* and the theorem follows.

From this point of view, detection of the first particle means that the system has been left in a (potentially) known angular momentum state with its z axis aligned along the direction of emission. To explain the occurrence of angular correlation, we note that the second particle now has a probability of emission distributed in angle according to the known relations between angular distribution and change in angular momentum.

I am indebted to Dr. M. H. Johnson for valuable comments.

[1] D. R. Hamilton, Phys. Rev. **58**, 122 (1940).
[2] D. L. Falkoff and G. E. Uhlenbeck, Phys. Rev. **79**, 323 (1950).
[3] S. P. Lloyd, Phys. Rev. **80**, 118 (1950).
[4] Only the *possibility* need be present in the apparatus. The experimenter's decision regarding how he will utilize the potentialities of the apparatus is unessential.

Crystals for the Scintillation Geiger Counter*

H. O. Albrecht and C. E. Mandeville
Bartol Research Foundation of the Franklin Institute, Swarthmore, Pennsylvania
November 16, 1950

In four previous communications,[1,2] the writers have discussed the detection in photo-sensitive Geiger counters of short-lived fluorescent pulses of ultraviolet light from phosphors irradiated by nuclear particles. A considerable number of ultraviolet scintillators have already been reported,[3] but the list has now been extended. Some newly examined ultraviolet emitters are given in Table I.

Table I. Ultraviolet scintillators.

Scintillators (listed in order of response)	Particles detected with the photo-sensitive Geiger counter
CaF_2 (activators unidentified)	α, β, γ
Al_2O_3 artificial white sapphire	α
Al_2O_3 ignited powder, chemically pure	α
Pentamethylbenzene	α
Hexaethylbenzene	α
B_2O_3 (glass, rare earth activated)	α
$CaHPO_4$—Ag	α
SrF_2 (activators unidentified)	α
BaF_2 (activators unidentified)	α
NaI—Tl	α

The detection of scintillations from alpha particles on NaI—Tl suggests the possible use of this phosphor to obtain a highly efficient gamma-ray counter.

Of the above mentioned scintillators, fluorite appears for the moment to be the most promising. Six natural varieties of fluorite obtained from Ward's Natural Science Establishment, Rochester, responded in varying degrees to alpha-particles. Commercially prepared CaF_2 has proven to be the most efficient ultraviolet scintillator to date. Although the activator is unknown, PbF_2 has been used as a scavenger in the purification process. Preliminary quantitative analyses indicate the presence of a slight amount of heavy metal.

The availability of efficient ultraviolet scintillators brings to mind the possibility of developing photo-multipliers with photocathode response peaked in the ultraviolet, thus further reducing the thermionic background in the tube.

* Assisted by the joint program of the ONR and AEC.
[1] C. E. Mandeville and H. O. Albrecht, Phys. Rev. **79**, 1010 (1950); **80**, 117 (1950); **80**, 300 (1950).
[2] C. E. Mandeville and H. O. Albrecht, Phys. Rev. **80**, 299 (1950).

PHYSICAL REVIEW VOLUME 81, NUMBER 1 JANUARY 1, 1951

Proceedings of the American Physical Society

Minutes of the Meeting of the Ohio Section at Heidelberg College, Tiffin, Ohio, November 4, 1950

The regular autumn meeting of The Ohio Section of The American Physical Society was held at Heidelberg College, Tiffin, Ohio, on Saturday, November 4. Approximately 85 were in attendance. Abstracts of nine contributed papers appear below; a tenth paper was presented which contained remarks on "International Interest in Physics" by W. R. Pyle of Wilmington College. The invited paper was: "Ultrasonics as a Tool for Research" by Dr. William J. Price, Acting Head of Physics Department, U. S. A. F. Institute of Technology, Wright Field, Dayton. Owing to pressure of work, Professor F. L. Berger insisted that his resignation from the office of Vice-chairman of the Ohio Section be accepted. This was done with regret and Dr. F. G. Tucker of Oberlin College was elected to serve in this place.

Leon E. Smith, *Secretary*
Ohio Section of
The American Physical Society

The Background Texture in X-Ray Diffraction Patterns of Annealed Metals. Norman P. Goss, *Mayfield Research Laboratory*.—The presence or absence of background textures in the x-ray diffraction patterns is a sensitive test for completeness of recrystallization. Background texture has also been observed in single crystals of mica. Some metals and alloys recrystallize completely in a few seconds at temperature. Others fail to recrystallize even though heated for extended periods of time. A number of x-ray diffraction patterns will be shown to illustrate these textures.

Physics in Norway. LEONARD O. OLSEN, *Case Institute of Technology.*—A brief description will be given of experiences as a Fulbright Visiting Professor in Physics at the University of Oslo, Oslo, Norway during the spring semester of 1950. These experiences are concerned with physics teaching and research at the principal universities of Norway. The role of the Norwegian government in physical research will also be described.

A Universal Spectroscopic Source Unit. ERNEST YEAGER, JOHN YEAGER, AND WILLIAM WOLFE, *Western Reserve University.*—A universal spectroscopic source unit has been designed and constructed for general emission work with particular emphasis on sensitivity, reproducibility, and versatility. Four distinct types of spectroscopic sources have been incorporated: (1) a high voltage, condensed ac spark with an air-blast control gap, (2) a high voltage (5000 v) ac arc, (3) a low voltage dc arc which is spark ignited, and (4) a combination source in which either ac or dc arcs are discharged simultaneously with the high voltage ac spark through the analytical gap. The latter source unit appears to combine the sensitivity of the arc with the stability of the spark. Oscillograms and spectrograms are presented to indicate the characteristics of each type of discharge. Elaborate control circuits permit the operator to set up four different source conditions at one time and to select any for immediate use by means of a single switch.

Electron Secondaries of Mesons Found Underground.* C. A. RANDALL,† *University of Michigan.*—Measurements of intensity and angular distribution of mesons carrying cosmic-ray energy into a salt mine at a depth of 1100 feet, and measurements of the energy spectrum, intensity and angular distribution of the electron secondaries of the mesons have now been completed. Preliminary results have been reported.[1] The differential energy spectrum of the secondary electrons has the form, $1/E$. Final results of the experiment will be given for both carbon and lead absorbers in the mine. Their interpretation, based upon the coulomb interaction of mesons with matter, will be discussed.

* Assisted by the joint program of the ONR and AEC.
† Now at Ohio State University, Athens, Ohio.
[1] C. A. Randall, Phys. Rev. **78**, 320 (1950).

The Multiplicity of Neutrons Produced by Cosmic-Ray Mu-Mesons Stopping in Lead.* MARSHALL F. CROUCH,† *Washington University.*—The nature of the mu-meson capture process in lead has been investigated by studying the number of neutrons emitted by the excited lead nucleus. Working under 2000 g cm^{-2} of earth and limestone and 144 g cm^{-2} of lead, events were studied in which a single charged particle penetrated a counter telescope and stopped in an 86 g cm^{-2} lead absorber, with one or more delayed coincident neutron counts from an array of $B^{10}F_3$ counters in a paraffin moderator placed below the absorber. A paraffin barrier was interposed below the lead filter to discriminate against nuclear interactions produced in the filter. The mean multiplicity of neutrons per stopped meson as found to be $\bar{m}=1.90\pm0.24$ and the mean squared multiplicity $\bar{m}^2=6.9\pm1.8$. The expected multiplicity assuming the lead nucleus receives 100-Mev excitation is 6 or 7,[1] while the low excitation theory of Tiomno and Wheeler[2] leads to an expected multiplicity of about unity.

* Assisted by the joint program of the ONR and AEC.
† Now at Case Institute of Technology, Cleveland, Ohio.
[1] Y. Fujimoto and Y. Yamaguchi, Prog. Theor. Phys. **4**, 468 (1949).
[2] J. Tiomno and J. A. Wheeler, Revs. Modern Phys. **21**, 153 (1949).

High Current Low Voltage X-Ray Tube. JACK A. SOULES, *The Ohio State University.*—Preliminary tests have been made on a low voltage, high current x-ray source for use in the 5 to 15A region. An electron gun developed by O. Heil is used to deliver up to 500 ma in a sharply collimated electron beam. An inhomogeneous magnetic field bends the beam through 90° and produces a sharp line focus on the target, 2 mm wide and 15 mm long. Target currents up to 60 ma were actually obtained at voltages up to 6000 v. The tube is mounted integrally with the high vacuum spectrometer to eliminate the problem of a thin window. The demountable cathode and target assemblies are sealed in place with moulded rubber gaskets. At elevated temperature and pressure these gaskets were found to evolve an oil plasticizer which quickly poisoned the cathode and made it impossible to obtain the 500 ma emission of which the gun is capable. A second tube has been built of glass and copper using ground joints. The electron beam is focused by an axial magnetic field and produces a circular focal spot. Tests on this arrangement are to be made in the near future. This work was supported by the ONR and the OSU Development Fund, under the direction of Dr. C. H. Shaw. It is a part of a program of research in soft x-ray spectroscopy of the solid state.

A Report on Some Studies of Friction. CHARLES A. MANEY, *Defiance College.*—Results of several experiments on sliding friction are presented with some of the difficulties and uncertainties pointed out.

A Report on Audio Oscillators with Demonstration. RICHARD H. HOWE, *Denison University.*—Various types of audio oscillators will be briefly reviewed. A simplified rc-type oscillator circuit with amplifier and square wave generator suitable for use in lecture demonstrations and electronics laboratory will be described in detail and demonstrated.

Demonstration of Phase Difference Using Voltmeters. FRANKLIN MILLER, JR., *Kenyon College.*—A simple phase-shift oscillator has been constructed which gives reliable oscillation with a period of about 10 seconds. Sinusoidal voltage variations of amplitude up to 100 volts are produced in the network which constitutes the feed-back path in the oscillator. Three 20,000 ohm/volt voltmeters are connected at appropriate points to render visible the oscillations, which differ in phase by about 60°. Some basic principles of oscillators, attenuated waves, and ac networks are thus demonstrated in a direct way, since voltage variations are presented by means of a familiar instrument, the voltmeter.